Synthetic studies toward [18F]-fluorination of solid-supported silyl ethers

Louise Bergsjø Sand

Thesis for the degree of Philosophiae Doctor (PhD)
University of Bergen, Norway
2023

UNIVERSITY OF BERGEN

Synthetic studies toward [18F]-fluorination of solid-supported silyl ethers

Louise Bergsjø Sand

Thesis for the degree of Philosophiae Doctor (PhD)
at the University of Bergen

Date of defense: 25.05.2023

Year: 2023

Title: Synthetic studies toward [18F]-fluorination of solid-supported silyl ethers

Name: Louise Bergsjø Sand

Print: Skipnes Kommunikasjon / University of Bergen

«Have no fear of perfection;

you'll never reach it»

– Marie Curie

Scientific environment

This dissertation was submitted 2023-02-24, as part of the fulfilment for the degree of Philosophiae Doctor (PhD) at the University of Bergen (UiB), department of Chemistry. The work was supervised by Professor Bengt Erik Haug (Department of Chemistry, UiB), Dr. Ole Heine Kvernenes (PET centre, Haukeland University Hospital) and Prof. Emmet McCormack (K2, Haukeland University Hospital). The thesis is based on synthetic studies carried out at the department during the period August 2017-October 2022 which includes a maternity leave for 1.5 years. The radiochemistry was performed at the PET-centre at Haukeland University Hospital in 2022-2023. The work was financed by the University of Bergen and Trond Mohn Stiftelse (TMS).

UNIVERSITY OF BERGEN

Acknowledgements

First and foremost, I would like to express my sincere gratitude to my supervisor, Prof. Bengt Erik Haug, for assigning me this project and for his excellent supervision and guidance throughout the project. It was mainly because of the enjoyable experience of taking part in the Haug group that I returned to academia after finishing my master thesis. A huge thanks is also addressed to my co-supervisor, Dr. Ole Heine Kvernenes, for his contributions with the hot fluorinations at the PET center, and for revisions of the written work.

Additionally, I would like to show my appreciation to Dr. Bjarte Holmelid and Assoc. Prof. Nils-Åge Frøystein for technical support in HRMS and NMR analyses. I am also grateful to Dr. Markus Baumann, who was able to prepare the DOTA-GzmB analogue while I was in maternity leave.

I would not have been able to finish this project without friends and colleagues at work, both in the Haug group and others. You have enriched these past seven years by sharing the ups and downs of being a PhD-student, helping me to make lemonade when PhD-life gave me lemons. Frida, Illimar and Beate, you are my biggest sources of inspiration and I want to express my admiration and gratefulness for having you around during most of my time at the Chemistry Department. Sharing an office with Illimar, after I was "promoted" to the 3rd floor, was a boost of energy sorely needed at the time. Also, Eirin, Sara, Ludvik, and Nina – I want to thank you for enriching these years through sharing knowledge, travels, dinners, teaching duties and numerous enjoyable lunches. I would also like to thank Jan, who in record time became a good colleague, and friend, for our many laughs and games of SET in the office, and also for taking the time to read parts of my thesis.

Furthermore, I want to thank my friends and family, for always being there and for cheering me on in the process, even though most of you (until recently) lived on the other side of the country. And last, but definitely not least, a huge gratitude to my husband Erlend, for always having my back and rooting for me to achieve my goals. And thanks to Julie, a daily reminder that life comprises so much more than work.

Abstract

Molecular imaging is defined as the visualization of *in vivo* biological processes at the molecular or cellular level. It requires the use of imaging probes and can provide anatomic as well as functional information. Molecular imaging includes radiotracer imaging/nuclear medicine, magnetic resonance (MR) imaging, MR spectroscopy, optical imaging and ultrasound.

The most sensitive molecular imaging techniques are the radionuclide-based positron emission tomography (PET) and single photon emission computed tomography (SPECT) imaging modalities, which offer non-invasive and quantitative images that can be used to investigate biological processes, such as metabolism and receptor expression in tissues. Anything from biomacromolecules to small molecules and nanoparticles can be utilized as radiolabeled tracers, depending on the imaging target and the kinetics of the process under investigation.

In this work, we aimed at developing a new method for ^{18}F-radiolabeling of peptides or other biologically relevant molecules, as well as preparing relevant peptide-based tracers for PET-imaging.

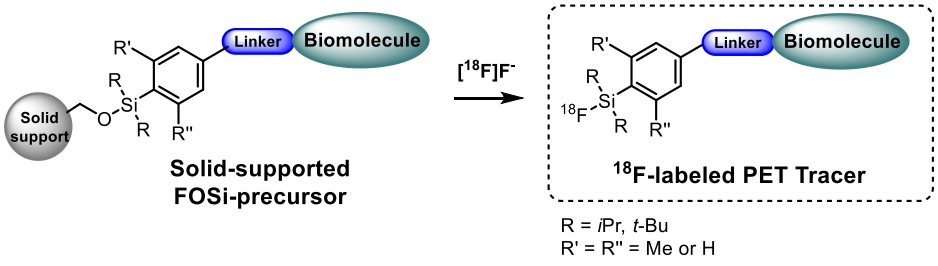

Figure 1. Fluoride-mediated breaking of oxygen-silicon bonds (FOSi-method) for radiolabeling.

We have expanded the field of radiofluorinated organosilicons, by immobilizing precursors onto a solid support, using an O-Si linker that can be cleaved by $^{18}F^-$ to release the ^{18}F-radiolabeled tracer without the need for HPLC purification to separate the product from unreacted material or unlabeled tracer (Figure 1).

A wide variety of silyl ethers have been prepared to investigate the use of this new method for radiotracer production. Synthesis of silanes and chlorosilanes with various substitution patterns has laid the foundation for further hydrolytic stability-studies and exploration of fluorination conditions. Constructing the Si-O bond was challenging for bulky di-*tert*-butyl-substituted analogues, while for diisopropyl-substituted analogues, silyl ethers with various functionality on the benzene ring (azide, aldehyde, ethers) could readily be prepared. One silyl-ether analogue was immobilized on a solid support, and fluorinations of both non-immobilized and immobilized precursors were successful. The immobilized precursor was also subjected to hot fluorination at the PET-center, where we obtained promising results. Further studies of the reaction conditions are required to fully elucidate the potential of the FOSi-method.

Three peptide-based tracers constituting a Granzyme B (GzmB) binding peptide sequence (β-Ala-Gly-Gly-Ile-Glu-Phe-Asp-H), which can be used to monitor activation of the immune system, linked to different chelators that can coordinate to metallic radioisotopes, have been prepared in this work. NOTA-GzmB, NODAGA-GzmB and DOTA-GzmB will be radiolabeled with ^{68}Ga and potentially ^{64}Cu, and further studied by our collaborators in Tromsø.

Sammendrag

Molekylær avbildning er definert som visualisering av *in vivo* biologiske prosesser på molekylært- eller cellulært nivå. Dette krever bruk av prober og kan gi anatomisk samt funksjonell informasjon. Molekylær avbildning inkluderer radiotracer-avbildning/nukleær medisin, magnetisk resonanstomografi (MR), MR spektroskopi, optisk avbildning og ultralyd.

De mest sensitive molekylære avbildningsteknikkene er de radionuklide-baserte positron emisjons tomografi (PET) og singel foton emisjons-computertomografi (SPECT), som tilbyr noninvasiv avbildning samt kvantitative bilder som kan benyttes for å undersøke biologiske prosesser, som metabolisme og reseptoruttrykking i vev. Alt fra biomakromolekyler til små molekyler og nanopartikler kan brukes som radiomerkede tracere, avhengig av avbildningsformålet og kinetikken til prosessen som studeres.

Vår målsetting i dette arbeidet har vært å utvikle en ny metode for ^{18}F-radiomerking av peptider og andre biologisk relevante molekyler, samt å fremstille peptidbaserte tracere for PET-avbildning.

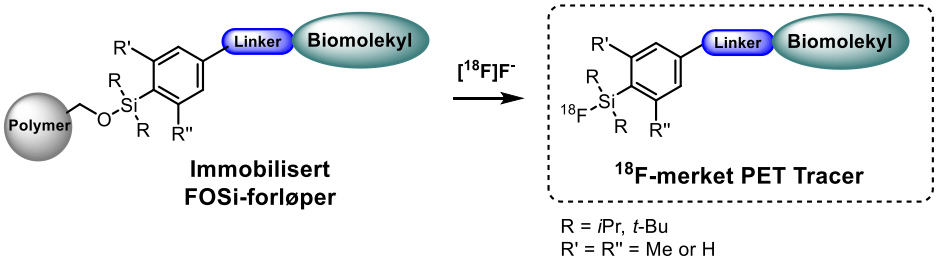

Figur 1. Radiomerking ved fluormediert kløyving av oksygen-silisium bindinger (FOSi-metoden).

Vi har hatt et ønske om å utvide feltet for ^{18}F-radiofluorering av organosilisium-forbindelser ved å immobilisere forløpere på fast-fase via en O-Si binding som kan kløyves med $^{18}F^{-}$. Dette kan potensielt anvendes for produksjon av radiotracere uten behov for HPLC-opprensing for å separere radiomerket produkt fra ureagert startmateriale eller umerket tracer (Figur 1).

I dette arbeidet har en rekke ulike silyletere blitt fremstilt for å undersøke FOSi-metoden. Syntese av silaner og klorsilaner med ulike substitusjons-mønstre har lagt grunnlaget for videre stabilitetsstudier og utforskning av fluoreringsbetingelser. Tillagingen av Si-O bindinger var utfordrende for de sterisk hindrede di-*tert*-butylanalogene, mens for diisopropylanalogene ble det laget silyletere med variert funksjonalitet på den aromatiske ringen (azid, aldehyd, etere). Én silyleteranalog ble immobilisert på fast-fase og fluoreringer av både ikke-immobilisert og immobilisert forløper var vellykket. Utprøving av ^{18}F-fluorering av fast-faseforløperen på PET-senteret ga lovende resultater. Videre studier av reaksjonsbetingelser er nødvendig for å kunne belyse det fulle potensialet til FOSi-metoden.

Tre peptidbaserte tracere ble syntetisert, bestående av en Granzyme B bindende peptidsekvens, som kan brukes til å observere aktiveringen av immunsystemet, bundet til ulike kelatorer som koordineres til metalliske radioisotoper. NOTA-GzmB, NODAGA-GzmB og DOTA-GzmB ble laget fra samme peptidaldehyd-sekvens (β-Ala-Gly-Gly-Ile-Glu-Phe-Asp-H), men med ulik kelator-konjugasjon. De tre forløperne skal radiomerkes med ^{68}Ga, og potensielt ^{64}Cu, og studeres videre av våre samarbeidspartnere i Tromsø.

Contents

Abbreviations

DBU	1,8-Diazabicyclo[5.4.0]undec-7-ene
DIPEA	*N*,*N*-diisopropylethylamine
i-Pr_2SiHCl	Diisopropylchlorosilane
DMP	Dess-Martin periodinane
DOTA	2,2′,2″,2‴-(1,4,7,10-Tetraazacyclododecane-1,4,7,10-tetrayl)tetraacetic acid
DPPA	Diphenylphosphoryl azide
$DTBSiCl_2$	Di-*tert*-butyldichlorosilane
DTBSiHCl	Di-*tert*-butylchlorosilane
FDG	Fluorodeoxyglucose
FOSi	Fluoride-mediated breaking of Oxygen-Silicon bonds
GzmB	Granzyme B
HCTU	*O*-(1H-6-Chlorobenzotriazole-1-yl)-1,1,3,3-tetramethyl-uronium hexafluorophosphate
IE	Ion-exchange
K[2.2.2]	Kryptofix[2.2.2] or 4,7,13,16,21,24-Hexaoxa-1,10-diazabicyclo[8.8.8]hexacosane
mAbs	Monoclonal antibodies
NODAGA	2-(4,7-Bis(carboxymethyl)-1,4,7-triazonan-1-yl)pentanedioic acid
NOTA	2,2′,2″-(1,4,7-Triazacyclononane-1,4,7-triyl)triacetic acid
PPTS	Pyridinium *para*-toluenesulfonate
PTSA	*para*-Toluenesulfonic acid
RCP	Radiochemical purity
RCY	Radiochemical yield
SA	Specific activity
SiFA	Silicon-fluoride acceptor
SPE	Solid-phase extraction
SPPS	Solid-phase peptide synthesis

TBAF	Tetrabutylammonium fluoride
TCICA	Trichloroisocyanuric acid
TRT	Targeted radionuclide therapy

1. Introduction

1.1 Molecular imaging

Molecular imaging is a constantly growing, biomedical research discipline that enables the visualization, characterization, and quantification of biologic processes taking place at the cellular and subcellular levels within living organisms, including patients. In the field of medicine, there are several ways of imaging biological processes within the body, such as X-ray computed tomography (CT), magnetic resonance (MR) imaging, MR spectroscopy, optical imaging, and ultrasound. Within nuclear medicine, imaging involves the use of radiotracers, which are defined as specific radiolabeled molecules used to monitor processes within the body without perturbing the system, and providing biological information in a living system.[1] In other words, a radiotracer or radiolabel, is a chemical compound in which one or more atoms have been replaced by radioactive isotopes. Tracing the radioactive decay of these isotopes can be used to explore the mechanism of biochemical processes, by tracing the path that the radioisotope follows from reactants to products.[2]

Nuclear medicine provides sensitive functional imaging techniques and highly specific therapeutic applications by utilizing radionuclides. In the decades following Marie and Pierre Curie's discovery of radium in 1898, the radiochemistry field experienced a rapid development.[3] In the 1920s, George de Hevesy, considered as "the father of nuclear medicine", experimented with the application of radioactive isotopes in the form of tracers and described the radiotracer principle, which underpins the use of radionuclides to investigate the behavior of stable atoms and molecules. The tracer principle states that radiopharmaceuticals can participate in biological processes but have no pharmacological effect owing to the small dose. In this way, radiopharmaceuticals facilitate the imaging of healthy and pathological processes without interfering with them.[4] The amount of radiopharmaceutical administered to a patient is just sufficient to obtain the required information, and the radiation dose received is medically negligible. The non-invasive nature of this technology, combined

with the ability to observe an organ functioning from outside the body, renders this technique a powerful diagnostic tool.[3]

For studying local biochemical reactions and their kinetics, particularly in diagnosis of cancer, the use of positron emission tomography (PET) and single-photon emission computed tomography (SPECT) have become hugely accessible and widely used. A multitude of pathologically upregulated physiological processes allows for differentiation of tumors from healthy tissue. These processes provide a vast array of molecular targets, allowing *in vivo* detection and functional characterization of tumors using suitable imaging probes (radiotracers).

Diagnostic radiopharmaceuticals can be used to examine several processes, such as blood flow to the brain as well as liver, lungs, heart, or kidney function, bone growth assessment and tumor detection. Another important use is to predict the effects of surgery and assess various types of treatment, including cancer therapy.[4] Imaging modalities have historically been divided into two general categories: structural (anatomical) and functional (physiological). Structural imaging modalities include CT, MRI and ultrasound, while functional imaging modalities include PET and SPECT.[4] One of the most influential recent developments in the methodology of radionuclide imaging is multi-modality imaging, which is a combination of nuclear medicine and radiology, such as PET-CT,[5,6] SPECT-CT[7,8] and most recently PET-MRI,[9-11] have gained widespread application. It not only offers more accurate diagnosis, it also facilitates personalized therapy and aids in getting better understanding of the underlying pathological processes.[12] Such multi-functional molecular imaging could overcome the limitations of using a single technique, and provide a better insight and more detailed information about a particular disease or biological procesess.[13]

Positron emission tomography

Positron emission tomography (PET) is an imaging technique that complements MR and CT imaging. Its non-invasive modality allows visualization and quantification of a wide variety of physiological and biochemical processes or specific low-density protein targets. It is used to visualize metabolic processes, such as blood flow, glucose consumption, fatty acid metabolism as well as detection and quantification of cell

surface receptors in target tissues.[14] In PET, a radionuclide is bound to a pharmacologically significant molecule which is administered to the patient. According to its designed pharmacological properties, it accumulates in certain regions of the body, and a PET scanner is used to pin-point its localization through its β^+-decay.[15]

Positron-emitting radionuclides are a requirement for PET. In the decaying nuclide (N), a proton (Z) is converted to a neutron, thereby simultaneously emitting a positron (β^+) (Equation 1a). As the counter particle to the electron (e^-), the positron will almost instantaneously annihilate with an electron producing energy in the form of two gamma-photons (γ) with 511 keV each (Equation 1b).[15,16]

$$1)\ {}^{A}_{Z}N_N \rightarrow {}^{A}_{Z-1}Y_{N+1} + \beta^+$$
$$2)\ \beta^+ + e^- \rightarrow 2 \times \gamma\ (511\ \text{keV})$$

Equation 1. a) Decay of the β^+-particle from a radioactive nuclide (N).
b) Annihilation of the β^+ and e^- to create two γ-rays (511 keV each).

The two photons will travel in parallel but in opposite direction and is detected by a PET-scanner, which is composed of multiple gamma cameras organized in a circular array around the body to form a three-dimensional image (Figure 2).[16]

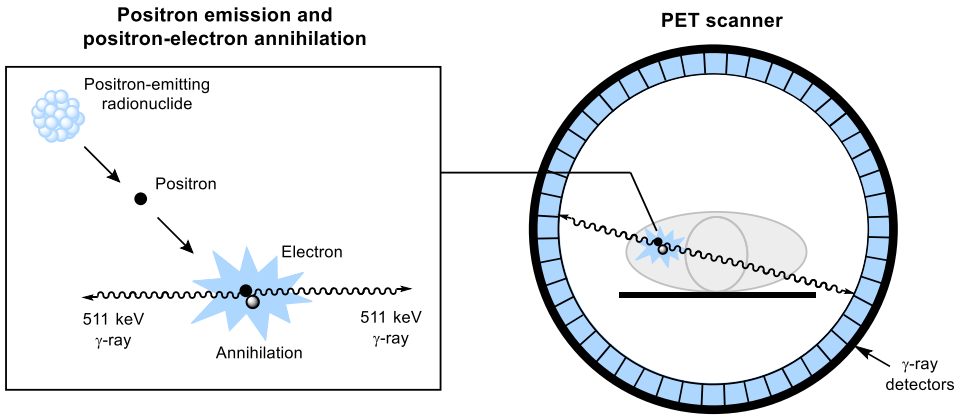

Figure 2. Schematic presentation of the principle of PET with the positron emission annihilation event and detection by a PET-scanner.[2]

The positioning of the gamma cameras allows for a full-body scan, capturing and pinpointing annihilation events occurring within the patient's body to ensure very accurate diagnosis and localization of e.g., a tumor.

The currently most frequently used radiotracer in PET imaging is [^{18}F]fluorodeoxyglucose ([^{18}F]FDG), a glucose analogue with the positron-emitting radionuclide ^{18}F substituted for the hydroxyl group at the C-2 position in the glucose molecule (Figure 3).

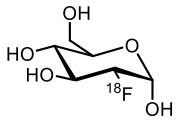

[^{18}F]FDG

Figure 3. [^{18}F]Fluorodeoxyglucose

[^{18}F]FDG is readily incorporated into the cell through glucose transporters, and then phosphorylated by hexokinase to [^{18}F]FDG-6-phosphate, which becomes trapped within the cell.[17] It is a good indicator of cell metabolism and it has found widespread use for PET studies in oncology, neuroscience and cardiology.[18] However, [^{18}F]FDG has several disadvantages such as high uptake in the brain, kidney, bladder and in the gut, the latter due to gut bacteria. This results in high background radiation which lowers the image quality, especially in the brain and abdominal area. In addition, it is also sub-optimal for tumors with slower glucose uptake.[19] Therefore, new, more specific tracers are being developed to overcome the limitations of [^{18}F]FDG.

1.2 Tracers for nuclear medicine

1.2.1 Radionuclides in nuclear medicine

The radioactive half-life, emission profile and chemistry of the radionuclide are all important considerations when radiolabeling a receptor-binding or physiologically relevant molecule. The biological half-life of the tracer must be considered, and it should ideally be paired with radionuclides of similar physical half-lives.[4]

Some of the most commonly used radionuclides in PET, SPECT and therapy and their characteristics are summarized in Table 1.

Table 1. Radioisotopes commonly used in nuclear medicine[4]

Isotope	Half-life	Decay mode (%)	Production method	Application
^{11}C	20.4 min	β^+ (100)	Cyclotron	Imaging (PET)
^{13}N	9.97 min	β^+ (100)	Cyclotron	Imaging (PET)
^{15}O	2.1 min	β^+ (100)	Cyclotron	Imaging (PET)
Halogens				
^{18}F	110 min	β^+ (97), EC (3)	Cyclotron	Imaging (PET)
^{123}I	13.2 h	EC (100), γ	Cyclotron	Imaging (SPECT)
^{124}I	100.3 h	β^+ (23), EC (77)	Cyclotron	Imaging (PET)
^{131}I	192.5 h	β^- (100), γ	Reactor	Therapy
Metals				
^{64}Cu	12.7 h	β^+ (19), β^- (40), EC (41)	Cyclotron	Imaging (PET); therapy
^{67}Ga	78.3 h	EC (100), γ	Cyclotron	Imaging (SPECT)
^{68}Ga	67.7 min	β^+ (89), EC (11)	Generator	Imaging (PET)
^{89}Zr	78.4 h	β^+ (23), EC (77)	Cyclotron	Imaging (PET)
^{86}Y	14.7 h	β^+ (33), EC (67)	Cyclotron	Imaging (PET)
^{90}Y	64.1 h	β^- (100)	Generator	Therapy
^{99m}Tc	6.0 h	IT (100), γ	Generator	Imaging (SPECT)
^{111}In	67.2 h	EC (100), Auger, γ	Cyclotron	Imaging (SPECT); therapy
^{177}Lu	159.5 h	β^- (100), γ	Reactor	Imaging (SPECT); therapy
^{223}Ra	273.6 h	α (100)	Reactor	Therapy
^{225}Ac	240.0 h	α (100)	Generator	Therapy

β^+ positron emission, *$\beta-$* electron emission, *EC* electron capture, *γ* gamma emission, *IT* internal transition

The invention of the cyclotron in 1929 enabled large-scale production of positron-emitting nuclides. Short-lived positron-emitters such as the most commonly employed ^{18}F ($t_{1/2}$ = 109.8 min) and ^{11}C ($t_{1/2}$ = 20.4 min) are routinely produced at most nuclear-medicine centers on a daily basis.[18,3] In recent time, other PET nuclides have been gaining increasing interest, in particular ^{68}Ga ($t_{1/2}$ = 68 min), which can be obtained from a generator system. For metal radioisotopes, such as ^{68}Ga, ^{64}Cu, ^{90}Y, ^{177}L, etc. a chelating group capable of coordinating the metal ion and attaching it to the receptor-targeting moiety is required. Therefore, the use of these nuclides is limited to biomolecules such as large peptides or proteins, antibodies, aptamers and others where the introduction of a chelator group, which often require a linker group, is tolerated without compromising its pharmacological properties.[20]

^{18}F is currently the most frequently used radionuclide for PET imaging and it has several advantages, one of which is its relatively long half-life of about 110 minutes, allowing more complex radio-syntheses.[21] Also, ^{18}F has widespread use and established production methods (cyclotron). Chemically, fluorine is similar in size to the hydrogen-atom. The van der Waal's radii of hydrogen and fluorine are 1.20 and 1.35 Å, respectively, thus the introduction of ^{18}F in place of H induces only a slight steric perturbation. Another favorable feature is the strong carbon-fluorine bond (440 kJ/mol), making it less likely to be metabolized and release free $^{18}F^-$, which would accumulate in the bone. In addition, the radionuclide has a relatively low β^+-energy of 0.635 MeV, which gives high-resolution images and less radiation burden to patients.[13,16,18]

As previously mentioned, [^{18}F]FDG has been, and still is, the work-horse of most PET-centers worldwide. However, there are also other ^{18}F-labeled tracers in use, such as [^{18}F]NaF, the simplest form of ^{18}F-labeled radiopharmaceutical. It was found to be taken up by the bone and dentine structures in *in vitro* studies as early as 1940,[22] and it has been in clinical use since the 1960s.[18] 6-[^{18}F]Fluoro-L-DOPA ([^{18}F]FDOPA) is the second-most commonly used ^{18}F-labeled PET pharmaceutical and is the PET tracer of choice for studies of the dopaminergic system, particularly for studies of changes in the presynaptic dopaminergic nerve terminals in Parkinson's disease (Figure 4).[18,23] [^{18}F]Fluoromisonidazole ([^{18}F]FMISO), consisting of a 2-nitroimidazole moiety radiolabeled with ^{18}F, was synthesized and recognized as a hypoxia imaging tracer in the 1980s,[24,25] and is still the most widely used marker for hypoxic tissue (Figure 4).[26,27]

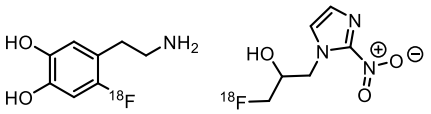

[^{18}F]FDOPA **[^{18}F]FMISO**

Figure 4. Structures of commonly used ^{18}F-labeled tracers.

In addition to the use of radioisotopes for diagnostic purposes (PET and SPECT), targeted radionuclide therapy (TRT) is a growing field that has enabled the development of highly specific and individually tailored treatments for cancer patients. Radionuclide-labeled molecules (α-, β^-- and Auger electron-emission) are designed to

deliver therapeutic doses of ionizing radiation to specific disease sites (e.g. tumors) with high specificity, destroying cells within short distance.[28] α-Emitters have a shorter range in tissue (<5 μm) than β^--emitters (<2 mm), on the other hand they do have higher linear energy transfer (LET), approximately 80 keV/μm, and are capable of damaging DNA both directly and indirectly via the production of reactive oxygen species. β^--emitters, in contrast, have low LET values between 0.2-2 keV/μm. Particles of both high and low LET values can be useful for radiotherapy depending on the nature of the disease, for example, TRT of leukemia and lymphoma typically require lower energy particles than TRT of solid tumors.[4] Some examples of therapeutic use of radionuclides are Azedra® (^{131}I-MIBG), Xofigo® ([^{223}Ra]$RaCl_2$), Pluvicto™ (^{177}Lu-PSMA) and Lutathera® (^{177}Lu-DOTATATE). Theranostic radiopharmaceuticals is also an evolving concept within nuclear medicine, constituting a combination of both therapy and diagnosis. These tracers can usually be labeled with two different types of radionuclides: therapeutic particle-emitting nuclides and diagnostic β^+- or γ-emitting). Although, there are also examples of radionuclides (e.g. ^{177}Lu) which serves a dual purpose by emitting both particles and photons, allowing both therapy and diagnostics simultaneously.[29] Theranostic modalities can have three different anti-cancer strategies: targeting the tumor itself, targeting the tumor immune microenvironment or targeting the peripheral immune system to activate immune cells that invade the tumor.[30]

1.2.2 Targeting vectors

A variety of targeting mechanisms have been used to deliver diagnostic and, increasingly, therapeutic radionuclides to specific organs, tissues, or cells within the human body. To ensure effective delivery to the target site, the radionuclide needs to be tightly bound to a vector that displays a high affinity for the cell or tissue to be studied. Examples of radiopharmaceutical vectors, that will be explained further in the following sections, include small molecules, peptides, antibodies and nanoparticles.

Small molecules

From its discovery in the 1970s[31] until the mid-2000s, PET imaging was dominated by [^{18}F]FDG used in imaging of cancer. Only a few other PET radiotracers received FDA approval during this early period ([^{18}F]NaF, [^{13}N]NH_3, and [^{82}Rb]$RbCl_2$).[32] From the mid-2000s to the present day, the PET landscape has changed radically. In the last decade, numerous new small-molecule PET radiotracers have been approved (Figure 5).

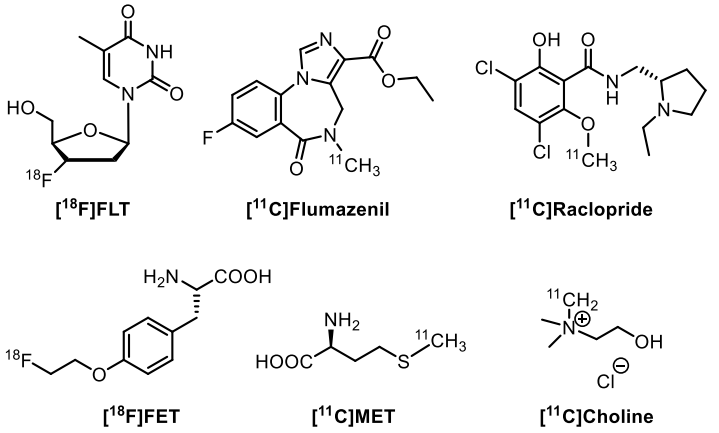

Figure 5. Small molecule radiopharmaceuticals used for diagnostic purposes.

Even though [^{18}F]FDG remains the most commonly used, the availability of new radiotracers has led to a revolution in the imaging environment. In addition to [^{18}F]FDOPA and [^{18}F]FMISO, mentioned in the previous section, some examples of clinically utilized tracers are the ^{18}F-labeled thymidine derivate 3-deoxy-3'-[^{18}F]fluorothymidine ([^{18}F]FLT), used for imaging of cell proliferation of tumors with increased thymidine kinase-1 (TK1) levels,[33] as well as the amino-acid derivate *O*-(2-[^{18}F]Fluoroethyl)-L-tyrosine ([^{18}F]FET) used for imaging of brain tumors displaying minimal uptake in healthy brain cells.[18]

^{11}C-labeled compound [^{11}C]Raclopride is a selective antagonist on D_2 dopamine receptors and is used in the diagnosis of movement disorders, particularly for Huntington's disease. Furthermore, radiolabeled raclopride is used to determine the efficacy and neurotoxicity of dopaminergic drugs.[34] [^{11}C]Flumazenil is a selective

benzodiazepine receptor antagonist, labeled with ^{11}C to visualize the distribution of γ-aminobutyric acid type A (GABAA) receptors in neuroimaging.[35] L-[*S*-Methyl-^{11}C]Methionine ([^{11}C]-MET) is an amino-acid analogue used for monitoring uptake of methionine in tumors. The methionine uptake has not been fully understood, although it is considered to be taken up in large quantities due to high proliferation rate in neoplasms.[36] Choline is the precursor to neurotransmitter acetylcholine, and the radiolabeled analogue [^{11}C]Choline was initially used to examine patients suffering from with Alzheimer's disease,[37] but no pharmacokinetic pattern was found. In later years, the tracer was successfully used in brain cancer, as well as prostate cancer imaging.[38,39]

There remains some debate over what constitutes a *small molecule*. Medicinal chemists usually refer to drug molecules with molecular weight (MW) below ≤500–550 Da that are compliant with the Lipinski rules.[40] In contrast, molecular biologists on the other hand often use the term to refer to species that aid the regulation of biological processes or species that are able to diffuse across cell membranes, or generally refer to molecules with an MW ≤900 Da.[32] In some cases, a peptide is by definition considered a small molecule, but it is useful to distinguish between small molecules and peptide-based targeting vectors, primarily because of the different biological behavior of most small molecules and peptides.

In general, peptides and small molecules both have advantageous and disadvantageous features as the basis for tracers, as summarized in Table 2.

Table 2. Peptides vs. small molecules, advantages and disadvantages[41]

Peptides	Small molecules
Advantages:	*Advantages*:
• High potency • High selectivity • Broad range of targets • Easy to modify • Low toxicity • Low accumulation in tissue • High chemical and biological diversity	• High oral bioavailability • Metabolic stability • High number of pharmacologic targets • Small dimensions
Disadvantages:	*Disadvantages:*
• Poor metabolic stability • Poor membrane permeability • Poor oral availability • Rapid clearance • Sometimes poor solubility	• High toxicity • Main side effects • Potentially low solubility • Lower selectivity • High production costs

For instance, the physicochemical properties, like overall polarity of the molecule and the potentially high number of hydrogen-bond donors (HBD) and hydrogen-bond acceptors (HBA), distinguish peptides from small molecules, providing them with high receptor-binding affinity. Small molecules usually exhibit high metabolic stability, whilst peptides display poorer metabolic stability. Peptides are generally more selective, and a broad range of targets for peptide-based ligands, i.e. a peptide-based molecule that binds reversibly or irreversibly to another (macro) molecule, are available.[41]

Peptide ligands

Many human cancer cells over-express peptide receptors on their surfaces, which could be used as molecular targets for diagnosis and therapy. Peptide-based radiopharmaceuticals (Figure 6) typically contains the following components: a peptide acting as the targeting entity, a linker, a radionuclide-bearing moiety, and a radionuclide. The linker is sometimes an optional component of a radiopharmaceutical that is incorporated to facilitate the conjugation of the targeting peptide and the radionuclide-bearing moiety, and/or improve its pharmacokinetics such as increasing metabolic stability or manipulating biodistribution.[42-45] The linker can also be used as

a spacer to distance bulky portions of a radiopharmaceutical, such as chelators, to reduce steric interference and maintaining high binding affinity.[46] The radionuclide-bearing moiety (like chelators) is not necessary for all radionuclides, e.g. when the radionuclide is covalently bound to the peptide.

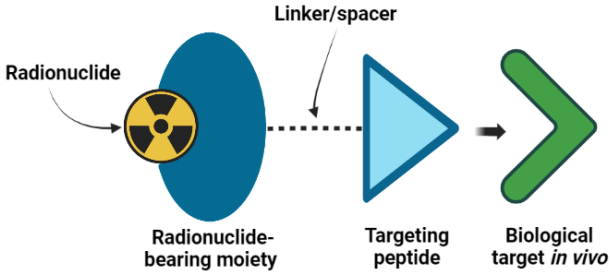

Figure 6. Structural components of peptide-based radiopharmaceuticals.[47]

Peptide ligands as radiotracers are of increasing interest in the field of nuclear imaging and therapy, mainly because of the many advantages of peptides, such as relatively low molecular weight (typically between 5 to 100 amino acids in length, ~0.5–10 kDa).[4] Compared to antibodies, bioactive peptides and peptide hormones, offer high target uptake and rapid blood clearance. Peptides have increased capillary permeability, which allows for more efficient penetration into target tissue compared to other macromolecules.[48-52] In addition, the well-established principle of solid-phase peptide synthesis (SPPS) provides easy access to a wide range of peptides (Scheme 1).[53]

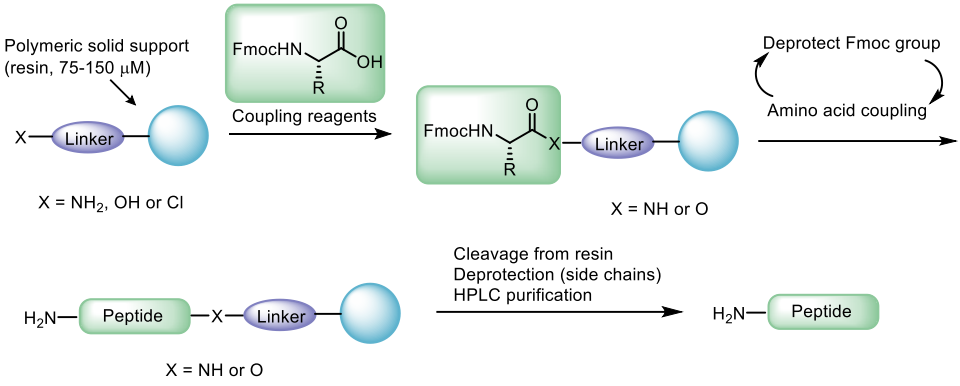

Scheme 1. Principles of Fmoc-based solid phase peptide synthesis (SPPS).

The basic principle has been further developed and automated. Modern SPPS relies on the attachment of the first amino acid to a linker group, which is covalently attached to

a polymeric material. The coupling of each amino acid is performed using a large excess of reagents in order to drive the reaction to completion. Immobilization of the growing peptide chain allows easy removal of excess reagents by simple filtration.

The history of radiolabeled peptides goes back to the 1980s when Reubi and co-workers[54] discovered that somatostatin receptors had an extraordinarily high density in pituitary tumors, which was a breakthrough for radiolabeled somatostatin analogues. The first study of radiolabeled peptides in humans were published by Krenning *et al.*[55] in 1989, using a ^{123}I-radioiodinated somatostatin analogue in patients with endocrine-related carcinomas. A few examples of peptides and their receptors over-expressed on human cancer cells and their respective developed ligand peptides are listed in Table 3.

Table 3. Oncological targets for radiolabeled peptides.[52]

Receptor target	**Base peptides**
Chemokine receptor (CXCR4)	CPCR4/AcTZ14011
Cholecystokinin/gastrin receptor (CCK1R, CCK2R)	Cholecystokinin (CCK) analogues, Gastrin analogues
Extracellular tumor pH	pH (low) insertion peptide (pHLIP)
Gastrin-releasing peptide receptor (GRPR)	Bombesin (BBN), Gastrin releasing peptide (GRP) analogues
Glucagon-like peptide-1 receptor (GLP1R)	GLP-1 analogues/Exendin
Integrin receptors (α_v, β_3, $\alpha_v\beta_6$, others)	Arginyl-glycyl-aspartic acid (RGD) peptides
Matrix metalloproteinase (MMP-2, MMP-9)	Activatable cell-penetrating peptides (ACPP)
Melanocortin 1 receptor (MC1R)	α-Melanocyte-stimulating hormone (α-MSH)
Neuropeptide Y receptors (NPYR)	Neuropeptide Y (NPY)
Neurotensin receptor (NT1, others)	Neurotensin (NT)
Somatostatin receptors (SSTR2, others)	Somatostatin analogues, ocreotide
Vasoactive intestinal peptide receptor (VIPR1)	Vasoactive intestinal peptide (VIP) analogues

One of the many advantages of peptides is the ease of modification of the peptide sequence. Optimization of binding affinity to the receptor binding site, optimization of the chelator/linker that separates the radionuclide and the peptide, and increasing the plasma half-life are some of the objectives for modifying peptides.[19,48,52] Modifications

to the peptide sequence can be either N-terminal, internal or C-terminal. Internal modifications can be performed by use of more stable D-amino acids or pseudo-peptide bonds, by inclusion of amino alcohols and insertion of unnatural amino acids, or by post-translational modifications.[48,56] Further modifications include the addition of spacers, typically small, flexible linkers, such as polyethylene glycol (PEG) linkers (called PEGylation)[57], that reduces steric hindrance at the binding sites of the peptide. Chain cyclization such as disulfide-bridging of the peptide chain, can stabilize the peptide conformation, increase bioactivity, and improve enzyme stability.[58] N- or C-terminal modifications, like acetylation[59,60] at the N-terminal remove the positive charge and mimic natural proteins, and can increase peptide stability by preventing N-terminal degradation, in some cases. Amidation[61] of the C-terminal neutralizes negative charges, which hinders enzyme degradation, mimicking native proteins, and in some cases, remove hydrogen bonding at the C-terminal of the peptides which may interfere with the assays. Further, C-terminal peptide aldehydes are used to achieve covalent binding to both serine and cysteine proteases.[62,63]

Compared to antibodies and proteins, small peptides distribute more uniformly and penetrate tissues more readily. Their small size gives them pharmacokinetic advantages including short time between injection and binding equilibrium. Furthermore, peptides are generally excreted rapidly from the systemic circulation, which is an important characteristic of a useful tracer for establishing a target to non-target signal. However, too rapid metabolism and excretion can result in a peptide tracer that cannot accumulate at the target site. This can be solved by modification of the peptide by e.g. PEGylation.[47]

Radiolabeled peptides (P) are injected intravenously into the patient and distributed in the whole body (Figure 7).[52] For peptide-receptor targeting peptides, there is an over-expression of the corresponding peptide receptor (P-R) on cancer cells, and in most cases, the radiolabeled peptide can be preferentially internalized in these cells, leading to accumulation of radioactivity in the tumor. A whole-body PET-scan detects the radioactivity accumulated in the tumor, whereas remaining radioactivity in the body will be rapidly cleared through the kidneys.

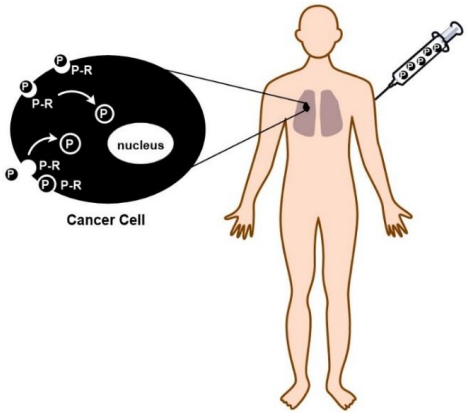

Figure 7. Principle of internalization of receptor-targeted radiolabeling using peptides. Adapted from Reubi *et al*.[52]

In the expanding field of nuclear medicine, peptide-based radiopharmaceuticals have gained particular interest due to their many advantages, mentioned previously. New, radiolabeled peptide-based tracers are developed at a rapid pace, and a few examples of radiolabeled, receptor-targeting peptides are shown in Figure 8.

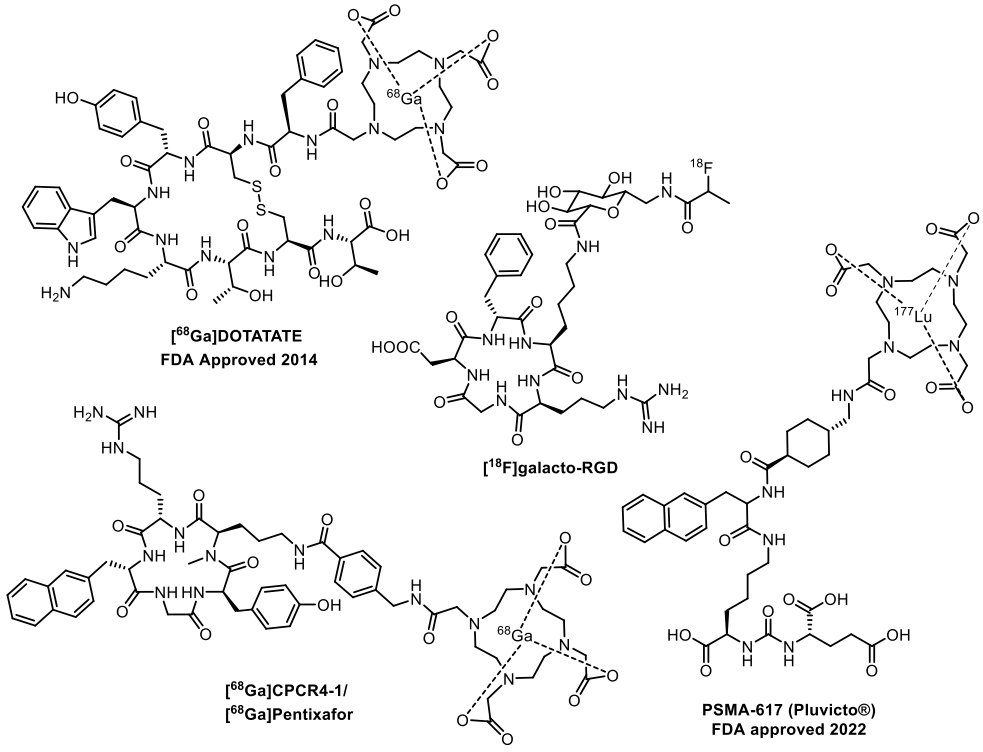

Figure 8. Some examples of peptides used as cancer targeting agents.

The somatostatin receptor (SSTR) targeting peptide [^{68}Ga]DOTATATE (NETSPOT^{TM}) was the first peptide radiopharmaceutical for PET to be approved by the FDA in 2014.[64] Prostate-specific membrane antigen (PSMA) is over-expressed on the surface of prostate cancer cells, and various PSMA-targeting ligands have been developed, both for diagnostic and therapeutic purposes. Most recently, small molecular inhibitors of PSMA have been introduced to recognize the enzymatic site and have been developed for clinical studies, whereof PSMA-11 (Illuccix®/Locametz®), PSMA-617 (Pluvicto®) and ^{18}F-DCFPyl (Pylarify®/ Piflufolastat®) recently received FDA approval.[65] The tripeptide RGD-motif, which binds to $\alpha_v\beta_3$-integrins, is also well-established in the field of peptide-receptor targeting. [^{18}F]Galacto-RGD was the first in its class of tracers to be investigated in humans and showed good potential in imaging of tumors. However, this tracer requires a multistep synthesis and 200-min preparation time. [^{18}F]Galacto-RGD has, nonetheless, laid the groundwork for further development of even simpler synthetic routes to radiolabeled integrin-targeting tracers.[64,66] The chemokine receptor (CXCR4) targeting radiopeptide [^{68}Ga]CPCR4-1/[^{68}Ga]Pentixafor was first synthesized in 2011 by Demmer *et al*.[67] and has been found to display comparable or superior imaging characteristics in comparison to [^{18}F]FDG for localizing lesions. Analogues of this radioligand, [^{177}Lu]Pentixafor and [^{90}Y]Pentixafor, bearing the alpha-emitting radionuclides ^{177}Lu and ^{90}Y were synthesized and used in cancer treatment. Both therapeutic agents are safe and well tolerated and display no acute adverse non-hematologic effects.[68-70] Another interesting receptor-binding peptide is a Granzyme B inhibitor, and this will be further explained in the next section.

Granzyme B

Cancer immunotherapy has represented a significant advance in cancer therapy and is an immensely growing subject in oncology.[71,72] Cancer immunotherapy can be described as the artificial stimulation of the immune system to treat cancer by improving the immune system's natural ability to fight the disease.

While cancer immunotherapy can produce dramatic responses, only a minority of patients respond to this form of treatment.[71,73,74] Therefore, reliable response biomarkers are needed to distinguish responders from non-responders, allowing treatment termination for those who do not benefit and must suffer unnecessary side effects, along with the opportunity for alternative therapeutic strategies. Immunotherapy is often associated with severe immune-related adverse events (hepatitis, colitis, and even death), and it is therefore of particular importance to predict which patients will benefit from the treatment. Recently, an enzyme which is part of our immune system, granzyme B (GzmB), has been extensively studied for its role in the adaptive immune response in the context of cancer immunotherapy. It plays an important role as a predictive biomarker for response to immunotherapy.[75]

Granzymes are serine proteases released into defective cells by T-lymphocytes and natural killer (NK) cells as part of our immune response. They induce apoptosis (programmed cell death) in the target cell, thus eliminating cells that have become cancerous or are infected with viruses or bacteria.[76,77] GzmB functions in conjunction with perforin in pore formation in the membranes of cells marked for destruction. Detection of GzmB release by actively engaged immune cells is useful in the cancer treatment and provides insight into the mechanism responsible for immune-mediated cell death. Therefore, GzmB-specific PET-imaging agents are being developed to achieve early differentiation between responders and non-responders.[71,75]

A GzmB peptidomimetic inhibitor based on a GzmB substrate has been identified (Figure 9).[71,73,74] The tetrapeptide “Ile-Glu-Phe-Asp” has been well characterized as a preferred murine GzmB substrate, and previous evidence has shown that modification of the C-terminal aspartate residue with an aldehyde moiety creates an electrophilic trap, potently inhibiting GzmB with a K_i of 80 nM through covalent-bond formation between the aldehyde and the enzyme active-site serine residue.[78,79]

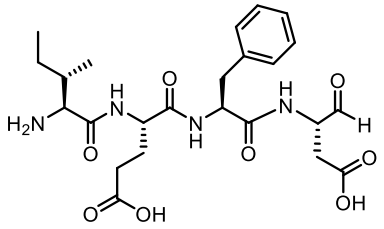

Figure 9. GzmB peptidomimetic inhibitor.

Larimer *et al.*[71] reported a PET-imaging agent, NOTA-GzmB, capable of detecting the release of GzmB by actively-engaged immune cells (Figure 10). This imaging agent allows repeated non-invasive and systemic interrogation of the tumoral response to cancer immunotherapy and provides insight into a major biochemical mechanism responsible for immune-mediated cell death.

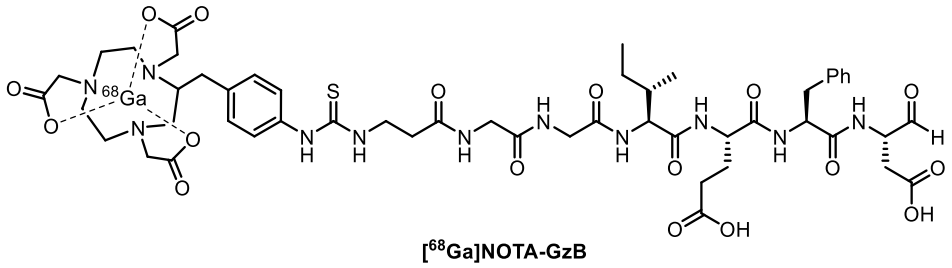

Figure 10. PET imaging agent [^{68}Ga]NOTA-GzmB.[71]

To generate the PET-imaging construct, a small, flexible linker (β-Ala-Gly-Gly) was used to bridge the peptide and the radiometal chelator 2-[4,7-bis(carboxymethyl)-1,4,7-triazonan-1-yl]acetic acid (NOTA). Through this, Larimer and co-workers[71] have provided a preclinical proof-of-concept for the use of GzmB as an early biomarker for tumors responding to immunotherapy.

Monoclonal antibodies and proteins

In the 1970s, the use of radiolabeled monoclonal antibodies (mAbs) was established in cancer staging of malignant tumors.[80] The use of radioimmunodetection for staging of cancer was largely abandoned in the 1980s as the approval and widespread use of [^{18}F]FDG constituted a more generally applicable diagnostic tool than antibodies or their fragments. A great improvement to this approach was given by the invention of the hybridoma technology proposed in 1975 by Köhler and Milstein[81] permitting

production of uniform mAbs with defined specificity and affinity to tumor-associated antigens. Due to their specificity, affinity and serum stability, mAbs have become increasingly applied as novel therapeutics against a variety of diseases.[30] Due to their unique properties, mAbs are also exploited in molecular imaging. Dammes *et al*.[30] summarized the use of mAbs in molecular imaging strategies and their theranostic potential, concluding that mAb-targeted imaging is used for a variety of purposes, for instance to monitor disease progression and to predict response to a specific therapeutic agent.

In addition to mAbs, radiolabeled proteins have recently been advanced as a viable alternative to small-molecule PET tracers, offering high-contrast imaging of expression of therapeutic molecular targets in tumors shortly after injection. This allows for non-invasive determination of a target-expression level and selection of patients for targeted therapies. Radiolabeled proteins hold great promise to play an important role in development and implementation of personalized targeted treatment of malignant tumors.[80]

1.3 Radiolabeling strategies

The radionuclide should in general be incorporated into the tracer at the latest possible stage, and the radiolabeling step needs to be rapid, efficient and provide the radiopharmaceutical in high radiochemical yield and purity. Depending on the type of radionuclide and the method used to design the unlabeled probe, the three main radiolabeling principles that are commonly used include nucleophilic substitution, metal chelation and isotope exchange, which will be detailed below.[82,83]

1.3.1 Nucleophilic substitution

The most commonly used radionuclide in nuclear medicine, ^{18}F, is produced by a cyclotron, and must quickly be incorporated into the molecule of interest after production due to its short half-life. Normally, the introduction of ^{18}F into aliphatic molecules is accomplished using no-carrier-added (n.c.a.) approach, where [^{18}F]fluoride reacts in an S_N2 reaction with a precursor containing a good leaving group

(e.g., Br, I, OMs, OTs, OTf, NR_3^+). This method usually produces radiotracers with high specific activity (SA). One of the challenges associated with this labeling procedure is the challenging removal of water traces, which is necessary to remove the hydration shell surrounding the fluoride anion. In addition, polar organic solvents (MeCN, DMF, DMSO) are typically used with a cryptand (Kryptofix[2.2.2], Figure 11) as a phase-transfer catalyst and as a ligand for the cation to facilitate charge separation of cation and fluoride, to produce what is referred to as "naked fluoride".

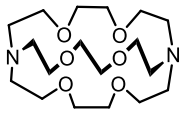

Figure 11. Cryptand Kryptofix[2.2.2]/K[2.2.2]

In these cases, the unlabeled probe and the radiolabeled probe have different chemical properties, as in the case of [^{18}F]FDG, in which a hydroxyl-group is exchanged into an ^{18}F atom in the deoxyglucose molecule (Scheme 2). The most common way of synthesizing the work-horse PET tracer ([^{18}F]FDG) at PET centers world-wide, is by using potassium fluoride in acetonitrile, with potassium carbonate as a base and Kryptofix[2.2.2] as a chelator carrying the counter-ion of fluoride.[84]

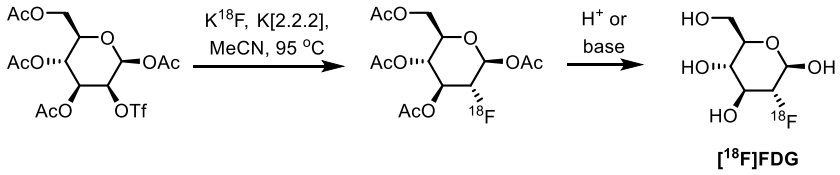

Scheme 2. Conventional radiosynthesis of [^{18}F]FDG.[84]

1.3.2 Metal chelation

As for nucleophilic substitution, metal chelation also introduces a foreign element, a radionuclide (such as ^{68}Ga, ^{99m}Tc, ^{64}Cu and ^{111}In), into an organic compound, by using a chelating group. Multiple atoms (such as O, N and S) in the chelating agent donate electron pair(s) to the foreign metal atom to form coordinate bonds (Figure 12).

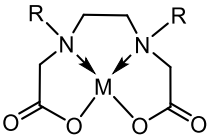

Figure 12. Generalized chelation complex.

Certain peptides and macromolecules, such as mAbs, can be labeled with radiometals based on metal chelation, however this requires the prior conjugation of a bifunctional chelate (BFC) to the peptide or protein, followed by chelation of the radiometal. In that way, the radiometal is not directly incorporated into the peptide or protein molecule. Some of the most common BFCs used to radiolabel peptides and other macromolecules are shown in Figure 13.[85]

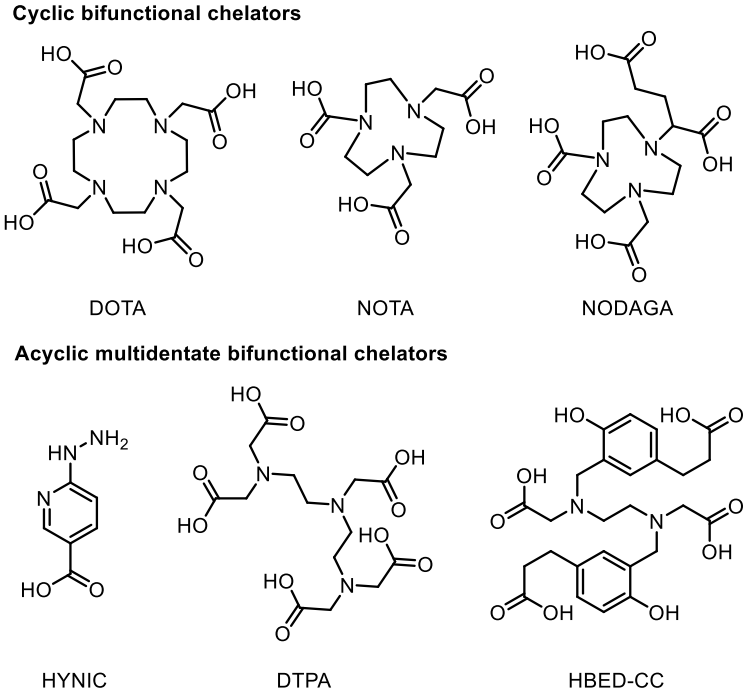

Figure 13. Basic structures of the most common BFCs used to radiolabel peptides.[85]

Another chelating strategy for introducing the PET-radionuclide ^{18}F into tracers is the $Al^{18}F$-chelating method developed by McBride *et al.*,[86,87] which is based on the strong interaction of fluorine to aluminum. The $Al^{18}F$-complex can be captured by a chelator as shown in Scheme 3, which allows a simple ^{18}F-fluorination of many targeting molecules (e.g., small molecules, peptides, and proteins).

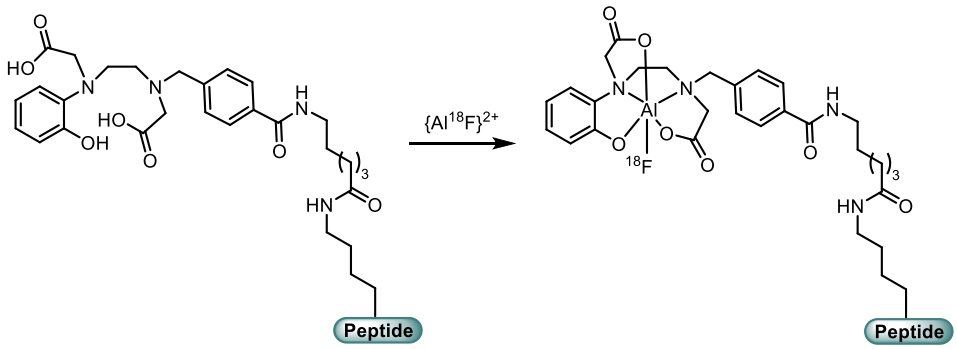

Scheme 3. Radiolabeling of a peptide with $Al^{18}F$-chelation, reported by Cleeren *et al.*[88]

1.3.3 Isotope exchange

An alternative approach for radiolabeling is by isotope exchange (IE). In this case, the tracer is prepared by direct exchange (isotope substitution) of one or more stable atoms of an element in a molecule with one or more nuclides of a radioisotope of the same element (Scheme 4).[89,90] The radiolabeled and the unlabeled molecule are chemically identical and will show the same *in vivo* pharmacokinetic and pharmacodynamic characteristics. This way of radiolabeling is generally used to prepare radio-iodinated radiopharmaceuticals in which stable ^{127}I atoms are replaced by radioactive ^{123}I or ^{124}I atoms. The same strategy has been employed on some ^{11}C-labeled radiotracers as well. In recent years, this strategy was expanded to ^{18}F-labeling, which will be further explained in section 1.3.4.[91-96]

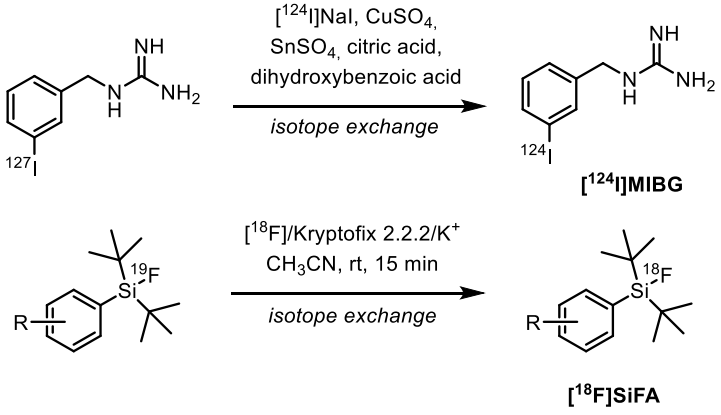

Scheme 4. Isotope exchange as a way of radiolabeling.

Recently, another approach for fast radiolabeling by IE was published by Zheng *et al*.,[97] utilizing sulfur fluoride exchange (SuFEx), as shown in Scheme 5. They reported the radiolabeling of 25 structurally and functionally diverse aryl fluorosulfates and achieved excellent RCYs (83-100%) and high molar activity (280 GBq μmol^{-1}) at room temperature for 30 s reaction time. The method did not require HPLC purification, only filtration through a solid-phase cartridge extraction (SPE)-cartridge.

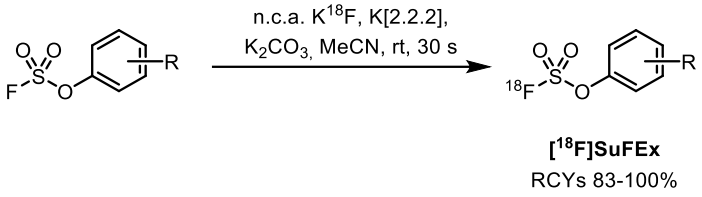

Scheme 5. [^{18}F]SuFEx of aryl fluorosulfates published by Zheng *et al.*[97]

1.3.4 Radiofluorination of organosilicon compunds

The use of compounds containing Si-F bond in radiochemistry has been explored since 1958,[98] with *in vivo* studies reported as early as in the 1970s.[99] The Si-F bond was considered as an alternative to C-F bonds due to its increased bond strength (565 kJ/mol for Si-F versus 485 kJ/mol for C-F).[100] The first use of [^{18}F]fluorosilanes as labeling synthons was proposed in 1985 by Rosenthal *et al*.[100] who treated chlorotrimethylsilane with n.c.a. $^{18}F^-$ in aqueous acetonitrile isolating the corresponding [^{18}F]fluorosilane in 65% yield. However, *in vivo* evaluation revealed fast hydrolysis of the compound combined with high radioactivity uptake in bone, which made it unsuitable as a labeling synthon.

In the past decades, fluorosilanes have gained interest by several research groups, as potential labeling synthons.[101-103] A new method for ^{18}F-radiolabeling of peptides, where silicon's affinity to fluorine is utilized, has been described by Wängler and co-workers (Scheme 6).[91] This protocol is based on IE, where ^{19}F bound to silicon is exchanged with ^{18}F in a process denoted the silicon-fluoride acceptor (SiFA) method.[104]

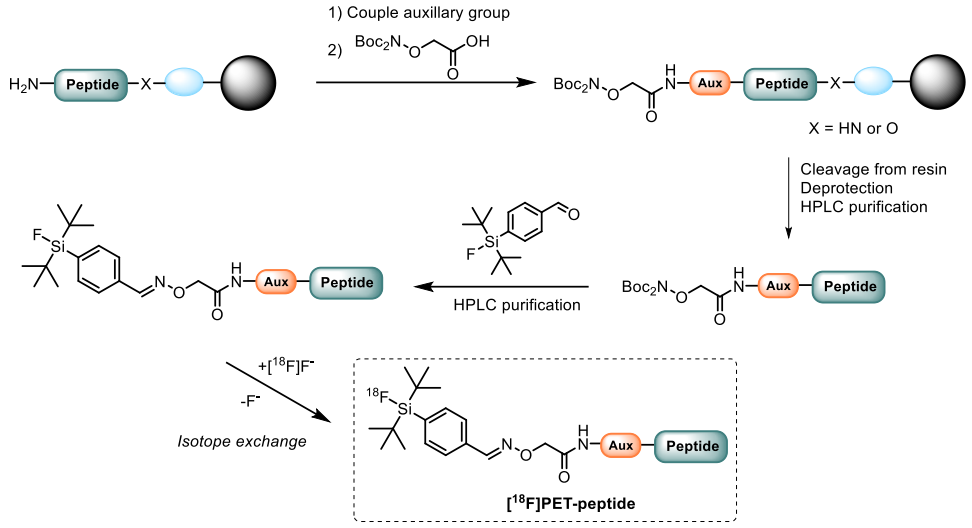

Scheme 6. Principle of IE by the silicon-fluoride acceptor (SiFA) method by Wängler *et al.*[96]

An advantage of the SiFA-method is the elimination of chromatographic purification of the reaction mixture, as the only difference between the starting material and the product is the number of neutrons in their fluorine atoms. A disadvantage of the method may be low SA, i.e., amount of radiation that can be achieved per mol of product. If the IE-step is sub optimal, the product will be contaminated with cold tracer, which will have the same pharmacodynamic properties as the hot tracer and competes for receptor interaction.

Contemporary to the development of the SiFA-method, the group of Ametamey[105-107] explored labeling of organosilanes as well, but instead of IE, they utilized the strong Si-F bond and its formation through substitution from silanes and silyl ethers. This leaving-group methodology currently constitutes one of the two extensively exploited strategies towards [^{18}F]SiFAs. Both approaches have shown to deliver [^{18}F]-labeled biomolecules in high RCYs and SAs, although important distinctions exist between the two methods, summarized in Figure 14.[108]

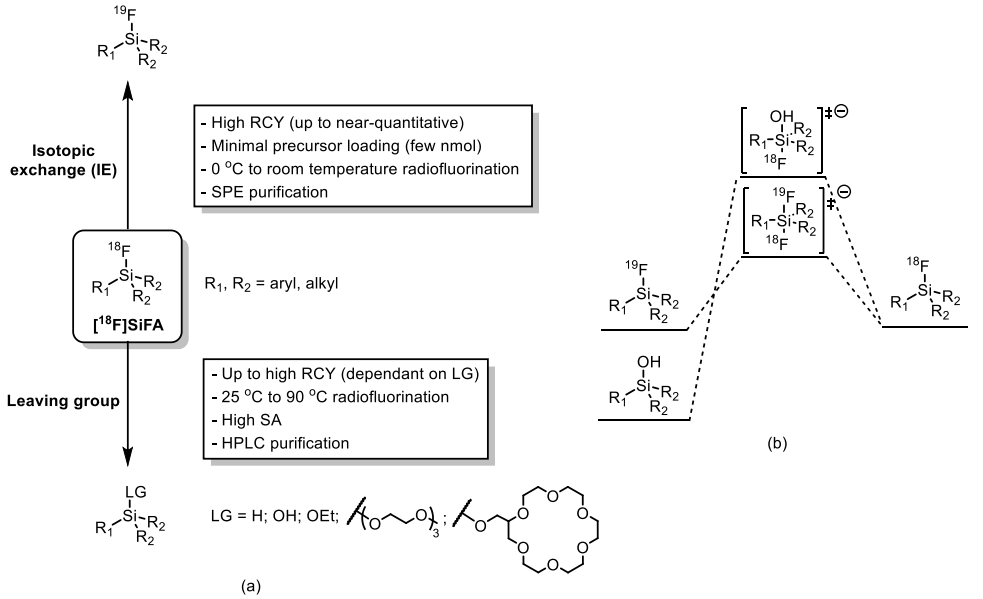

Figure 14. a: Approaches towards [^{18}F]SiFA compounds for PET, either by IE or the leaving group strategy. b: Comparison of simplified reaction coordinated for IE and leaving group radiofluorination in MeCN. Adapted from Bernhard-Gautier *et al.*[108]

Isotope exchange typically proceeds at room temperature or below, while the leaving group approach requires elevated temperatures, which may be detrimental when direct labeling of biomolecules is considered. An additional important distinction between IE and the leaving group method relates to purification techniques. Since the IE involves chemically identical entities and proceeds under mild conditions that do not lead to side products, HPLC purification can often be avoided, and purification can be limited to SPE. However, the ^{19}F-^{18}F IE method often suffers from low SA and hence low radiochemical yield due to the presence of inseparable ^{19}F radioisomer.[94]

In contrast, HPLC purification constitutes a prerequisite of the leaving-group approach as chemically distinct precursors and ^{18}F-radiolabeled products must be carefully separated. In this regard, the method we are developing in this work combines the advantages of the leaving-group strategy, while avoiding the HPLC-purification.

In a study performed by Al-Huniti *et al.*,[109] the leaving-group strategy was combined with the nucleophile-assisting leaving group (NALG) strategy to generate potassium-chelating SiFA-based leaving groups (Scheme 7, Strategy B). Unfortunately, this

strategy provided quite low RCYs because of low solubility of n.c.a. $K^{18}F$ in the reaction media. This strategy was explored further, and in 2017 the same researchers published a strategy for novel bifunctional phase-transfer agents to promote rapid fluorination at silicon, named crown ether nucleophilic catalysts (CENCs), which are 18-crown-6 derivatives containing a side-arm and a hydroxyl group (Scheme 7, Strategy C).[110] They achieved rapid fluorinations due to the entropic advantage of localizing the fluoride anion nucleophile near the Si atom. Only diisopropylaryl-substituted silyl ethers were used as precursors, which have demonstrated lower hydrolytic stability than the more sterically-substituted analogues with di-*tert*-butyl groups (more on this in section 3.3) was reported.

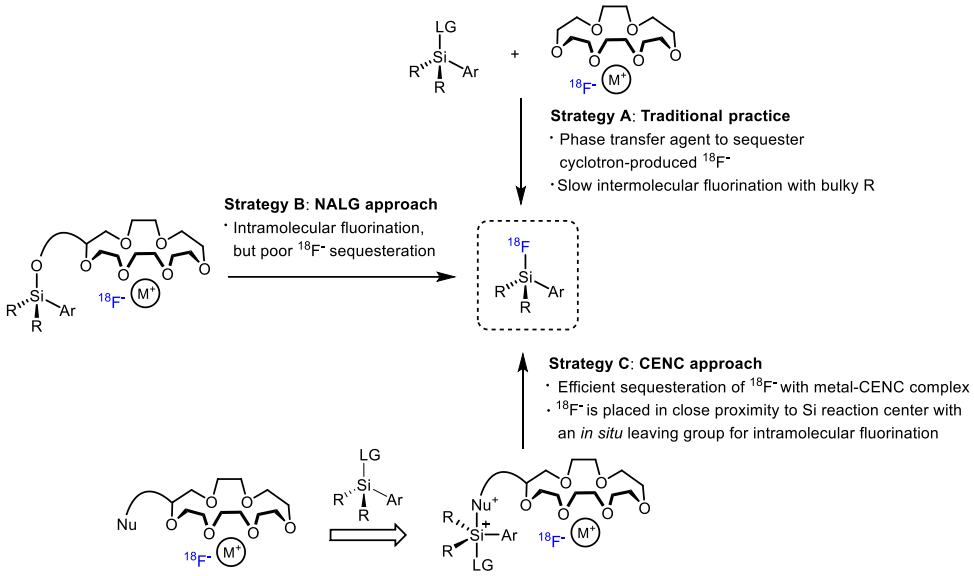

Scheme 7. Strategies for radiofluorination using phase-transfer agents inter- and intramolecularly. Adapted from Jana *et al.*[110]

A number of research groups have worked on the use of organosilicons within the field of radiolabeling.[96,105,111-118] Reports in the literature include development of building blocks for PET-imaging using click-chemistry,[111-113,119] ^{18}F-radiolabeled silicon-based nitroimidazoles,[120] silylated L-amino acids and synthesis of peptide derivatives for labeling,[114] silyl *N*-methyl imidazoles as a tool for fluorination of biomolecule,[121] silicon-labeled amino acid suitable for late stage fluorination,[115] 4-*N*-acyl and 4-*N*-aryl

gemcitabine analogues with SiFA[113] and labeling of peptides via heteroaromatic SiFAs.[117]

1.3.5 Solid-phase radiolabeling

Since the concept of solid-phase chemistry was introduced in the 1960s by R. B. Merrifield,[53] it has been of increasing interest, especially for synthesis of peptides used in drug development. To date there have not been many attempts at utilizing the advantages of solid-phase chemistry in radiolabeling, although there are recent advances in this field, which will be further explained in this section.

In the early 2000s, Sutcliffe-Goulden and co-workers investigated into radiolabeling by attaching small-molecules onto peptides bound to a solid-support prior to cleavage of the peptides from the resin (Scheme 8).[122-124] Radiolabeling of compounds with more than one acylable functional group can lead to complex mixtures of products, however, shown by the work by Sutcliffe-Goulden and co-workers,[124] peptides can be labeled regioselectively on solid-phase.

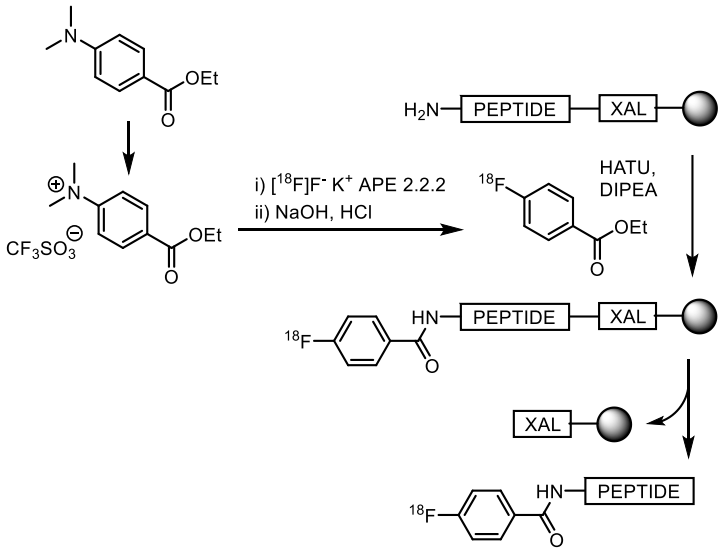

Scheme 8. Solid-supported synthesis of ^{18}F-labeled peptides, proposed by Sutcliffe-Goulden *et al.*[123]

Brown *et al.*[125] presented a reliable route for synthesis of a solid support that liberated protected [^{18}F]FDG in high radiochemical yield upon treatment with $^{18}F^-$ ions (Scheme 9). They attached the FDG-precursor to the solid support through a sulfonate

linker that allows specific cleavage of the radiotracer into solution by using the [^{18}F]fluoride ion. Any precursor present at the end of the reaction would remain attached to the resin, permitting purification by simple filtration, avoiding the presence of excess reactive triflate in the deprotection step. Following removal of the protecting groups, the ^{18}F-tracer could be purified by ion-exchange chromatography leaving pure product ready for administration.

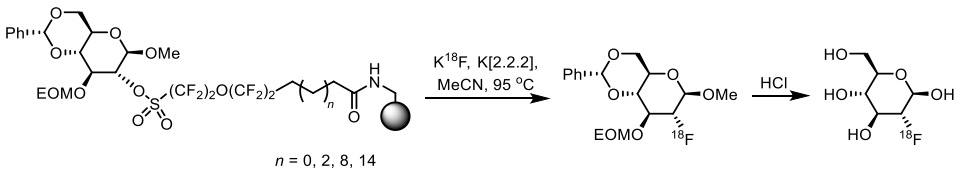

Scheme 9. Solid-phase synthesis of [^{18}F]FDG reported by Brown *et al.*[125]

The most recent addition to the solid-supported radiolabeling field was published in 2022 by Steffann and co-workers.[126] They introduced a new radiolabeling strategy involving fluorination-mediated release of the tracer from the solid-support by cleaving a Si-C bond, as shown in Scheme 10.

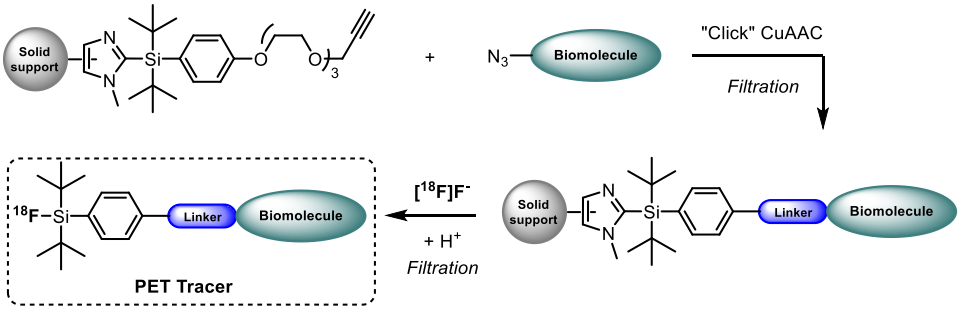

Scheme 10. Strategy for solid-phase radiolabeling presented by Steffann *et al.*[126]

They were able to achieve fully automated production of ^{18}F-labeled bioconjugates using heterogenous precursors obtained by anchoring imidazole-di-*tert*-butyl-arylsilanes to a polystyrene resin. The RCY was reported to be up to 19% and good to excellent RCP could be obtained through a simple filtration using an SPE-cartridge. By eliminating the HPLC-step, this methodology is highly promising for the development of ^{18}F-fluorination kits for automated syntheses of PET tracers. This

publication underlines the relevance of the approach we are aiming for in our work, showing that fluorination of polymer-supported precursors might be part of the future of radiolabeling.

1.4 Aims

The aims of this work have been twofold:

1 Tracers for immuno-PET imaging

We aimed at designing new targets for studying immune cells. The PET-tracers will contain the GzmB-specific peptide aldehyde-sequence and include chelators for radioactive metals, such as ^{68}Ga or ^{64}Cu (Figure 15). The synthesis of NOTA-GzmB was reported in 2017 by Larimer *et al.*,[71] and the GzmB tracer will be synthesized to have a reference for further studies. DOTA-GzmB and NODAGA-GzmB will also be synthesized to explore the effect of different chelators. Biological studies will be performed by our collaborators in Tromsø.

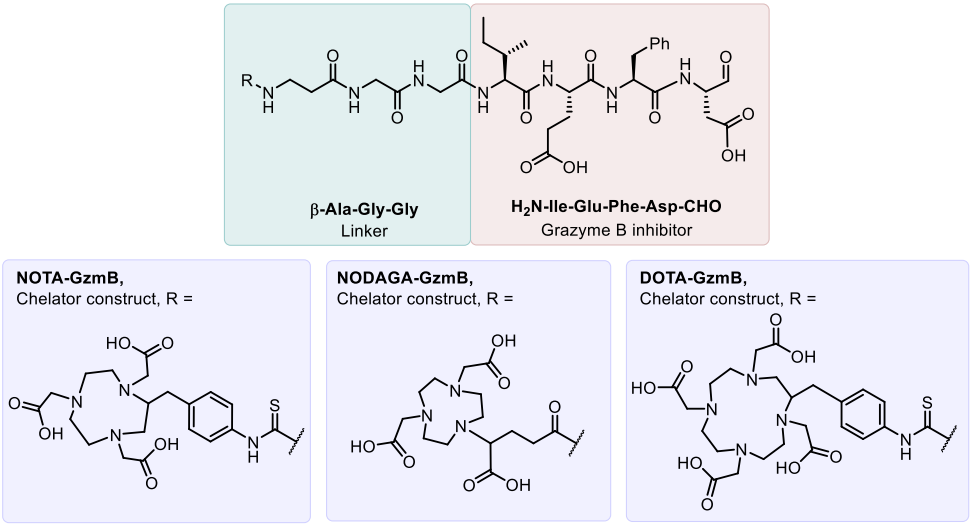

Figure 15. Granzyme B-specific PET-tracers with different chelating groups.

2 Method-development: ^{18}F-radiolabeling of receptor-targeting ligands

We aimed at developing a new method for radiolabeling peptides by introducing ^{18}F at a late stage (Scheme 11). Silyl ethers are used as protecting groups in organic chemistry and are typically cleaved by a fluoride source. This concept could be utilized to introduce a F-Si bond into a tracer by breaking an O-Si bond, hence the method is named fluoride-mediated breaking of oxygen-silicon bonds (FOSi). The objective has been to supplement the field of radiolabeling by developing a solid-supported method, as an alternative to the IE-reaction in the SiFA-strategy by Wängler and co-workers.[96] The only substance released from the solid support will be the radiofluorinated peptide and purification could be achieved by simple filtration.

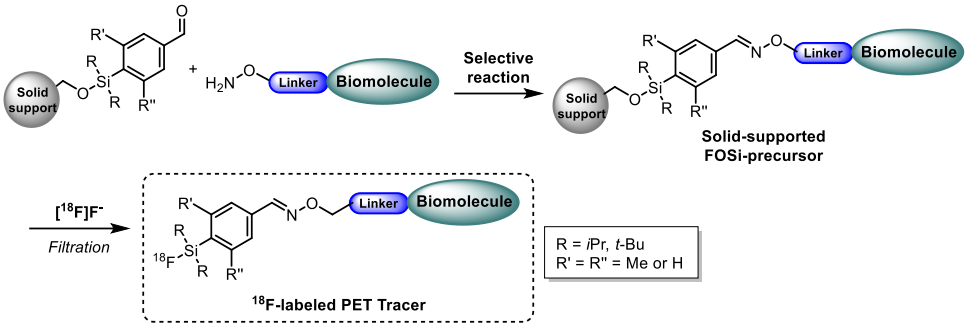

Scheme 11. Overview of the FOSi-method.

The FOSi-construct is connected to a polymer resin, a solid support, through a linker which can be altered to feature different couplings to the resin (Figure 16). The silyl ether is built from a primary alcohol and a silane, where the silane can have many different substitution patterns. The silane is attached to a receptor-binding peptide or other biomolecule through a linker, where different click-type reactions can be explored.

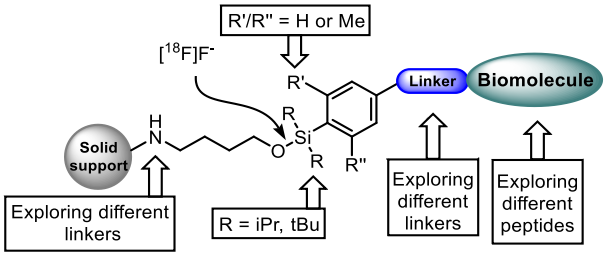

Figure 16. Possible modifications to the FOSi-construct.

2. Granzyme B – immuno PET

The aim of this part of the work was to prepare GzmB-specific PET imaging constructs bearing chelators for either ^{68}Ga or ^{64}Cu. These peptides will be further used to investigate immune-cell activation in animals that have undergone radiation therapy in a study led by our collaborators in Tromsø.

The GzmB-binding sequence was first identified by Thornberry *et al.*[127] in 1997, as the tetrapeptide sequence Ile-Glu-Pro-Asp (IEPD). It has been reported that human GzmB cleaves optimally after the tetrapeptide IEPD, whereas mouse GzmB has somewhat different peptide specificity, preferring to cleave after IEFD.[128,129] GzmB is a relevant and important biological target, used to enhance our understanding of the human immune system, and being able to diagnose and monitor inflammatory diseases (e.g. arthritis or inflammatory bowel diseases, among others)[130-132] as well as being able to observe immune response to cancer therapy.[71,73,74,133] This has been done in a range of ways, e.g. inhibitors, PET imaging probes and optical reporters.[71,134,135] Recently, the first chemiluminescence probe for *in vivo* imaging of GzmB activity released from NK cells was reported by Scott *et al.*[136] In 2022, the same group published a report on GzmB-targeting fluorescent probes,[137] and by molecular dynamic simulations they also encountered a probe consisting of six amino acids (IEPDAL) that binds to a previously unreachable binding pocket, indicating that the field of GzmB targeting is continuously growing.

The preparation of PET-imaging tracer NOTA-GzmB has previously been described by the Larimer-group[71] (presented in section 1.2.2, Figure 10), although in their paper the structure and the name reported did not match, as they have drawn the linker as a Gly-Gly-Gly construct (also written once in the text), yet they have presented the structure of the PET-tracer construct under "synthesis" with β-Ala-Gly-Gly as a linker. The reasoning for using β-Ala instead of Gly as the N-terminal amino acid in the sequence, stems from the reported side-reaction of isothiocyanates with α-amino acids.[138] Also, we found their synthesis protocol incomplete, only stating that

NOTA-GzmB was “synthesized using standard Fmoc chemistry” and the material that was produced was not fully characterized by either MS or NMR analyses.

Studies comparing peptide, peptidomimetic or antibody bioconjugates with different chelators reveal that the choice of chelator is critical, as it influences the radiolabeling of the biomarker, targeting and pharmacokinetics.[139-143] Chelating groups for the most common radionuclides, was discussed in the introduction (Section 1.3.2). The NODAGA chelating group is a derivative of NOTA, displaying similar denticity to the NOTA, with functionalization on the carbon between the carboxyl and the nitrogen of the ring. NODAGA has reported enhanced chelating effect to ^{68}Ga.[85] DOTA is still the most widely used chelator for this radionuclide, even though it is well known that the ^{64}Cu-DOTA complex has only modest *in vivo* stability, likely because of its commercial availability, FDA approval, and mild labeling conditions.[139]

We set out to re-synthesize NOTA-GzmB for further studies of immune response by our collaborators in Tromsø. Preparing GzmB tracers with alternative chelating groups was also of interest, and NODAGA-GzmB and DOTA-GzmB were selected, as shown in Figure 17.

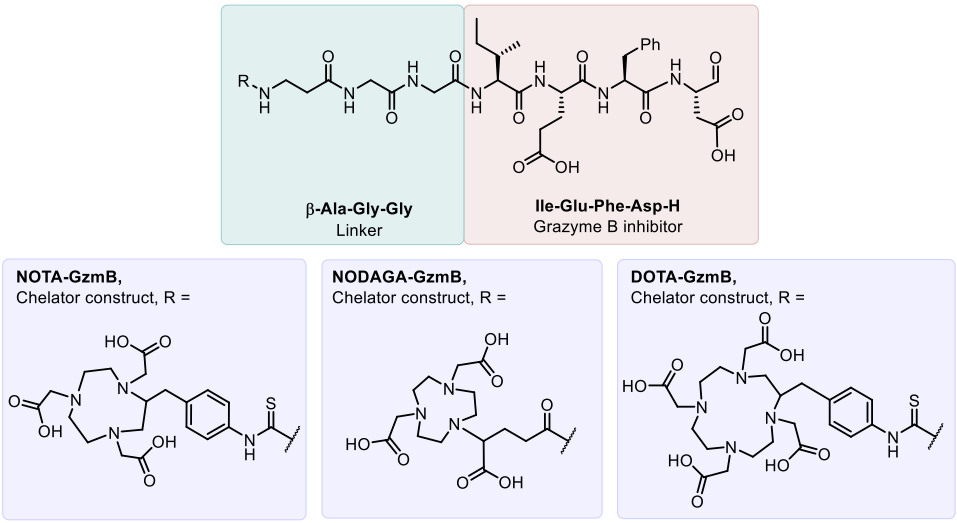

Figure 17. Structures of NOTA-GzmB, NODAGA-GzmB and DOTA-GzmB.

The PET tracer analogue NODAGA-GzmB has a similar composition as NOTA-GzmB with the same peptide aldehyde backbone (H_2N-AβGGIEFD-H) and three carboxylic

acids on the chelator construct for conjugation to ^{68}Ga. We aimed at developing NODAGA-GzmB as an alternative to NOTA-GzmB, to study the different *in vivo* stability of the radio conjugation and the receptor-binding differences between the two tracers. NODAGA was conjugated to the peptide sequence through an amide, whilst the NOTA chelator was conjugated through a benzylic thiourea moiety.

The synthesis of DOTA-GzmB was part of the planned work for this thesis, though it was performed by former member of the Haug-group, Dr. Markus Baumann, due to my maternity leave. DOTA-GzmB also consists of the same backbone as NOTA-GzmB, and the chelating construct has the same thiourea linkage to the peptide. The DOTA-analogue has one extra carboxylic acid for radiometal conjugation, and is the most widely used chelating group for ^{64}Cu, which is why we were interested in this analogue.[139,144]

Synthesis of NOTA-GzmB, NODAGA-GzmB and DOTA-GzmB

The structure of the PET-imaging construct NOTA-GzmB consists of the GzmB binding motif (H_2N-Ile-Glu-Phe-Asp-H), a linker (β-Ala-Gly-Gly), which is connected to the chelating group NOTA through a thiourea moiety. This ensures selective conjugation of the amino group of the linker and the chelating group.

The classical methods for preparing peptide aldehydes, such as oxidation of a peptide alcohol[145] (Scheme 12A), reduction of a peptide Weinreb amide[146,147] (Scheme 12B) or step-wise or fragment synthesis using a protected pre-formed aldehyde[148-152] (Scheme 12C), can be lengthy and time-consuming.

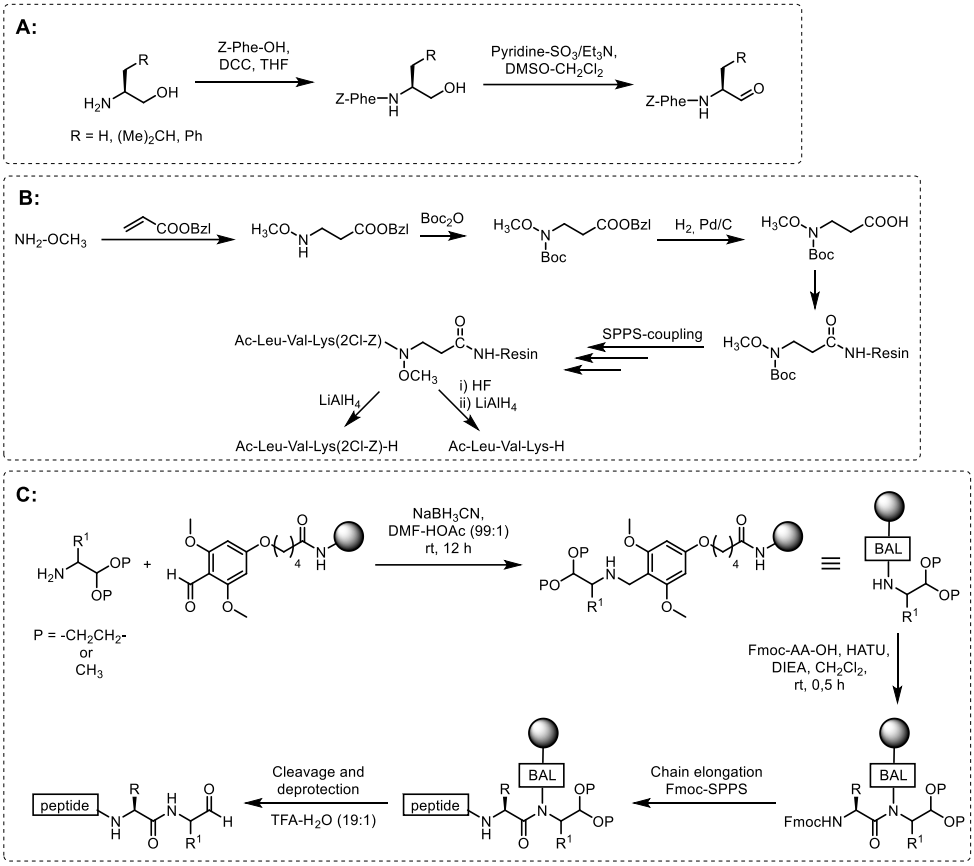

Scheme 12. A: Oxidation of a peptide alcohol to attain peptide aldehydes, reported by Woo *et al.*[145] B: Example of reduction of peptide Weinreb amide, reported by Fehrentz *et al.*[147] C: Example of peptide aldehyde synthesis from amino acetals anchored to a backbone amide linker (BAL). Reported by Kappel, *et al.*[152, 153]

All the examples presented above are both laborious and costly, and they involve multiple steps towards the desired peptide aldehyde. To our advantage, NovaBioChem produces pre-loaded aldehyde resins as a simple and convenient alternative. We set out to prepare the unlabeled GzmB PET tracer by constructing the peptide sequence (H_2N-AβGGIEFD-H) using the H-Asp(OtBu)-H NovaSyn® TG resin, where the aspartic aldehyde has been converted into an oxazolidine and then Boc-protected, which avoids side-reactions. The peptide sequence AβGGIEF was loaded on the resin by standard Fmoc-based peptide synthesis where amino-acid couplings were performed using HCTU and DIPEA with DMF as solvent and 20% piperidine in DMF

to facilitate Fmoc-deprotections. The peptide was prepared using a Biotage Initiator+ Alstra automated microwave assisted peptide synthesizer (Scheme 13).

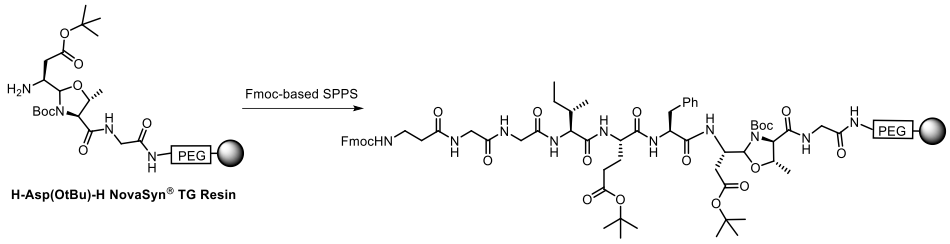

Scheme 13. Solid-phase synthesis of Granzyme B binding motif with β-Ala-Gly-Gly linker.

With the resin-bound peptide aldehyde at hand, we proceeded to conjugate the chelator groups to the N-terminal amino group. The chelator groups *p*-NCS-Bn-NOTA and *p*-NCS-Bn-DOTA were conjugated to the peptide aldehyde using DIPEA in DMSO at rt as shown Scheme 14.

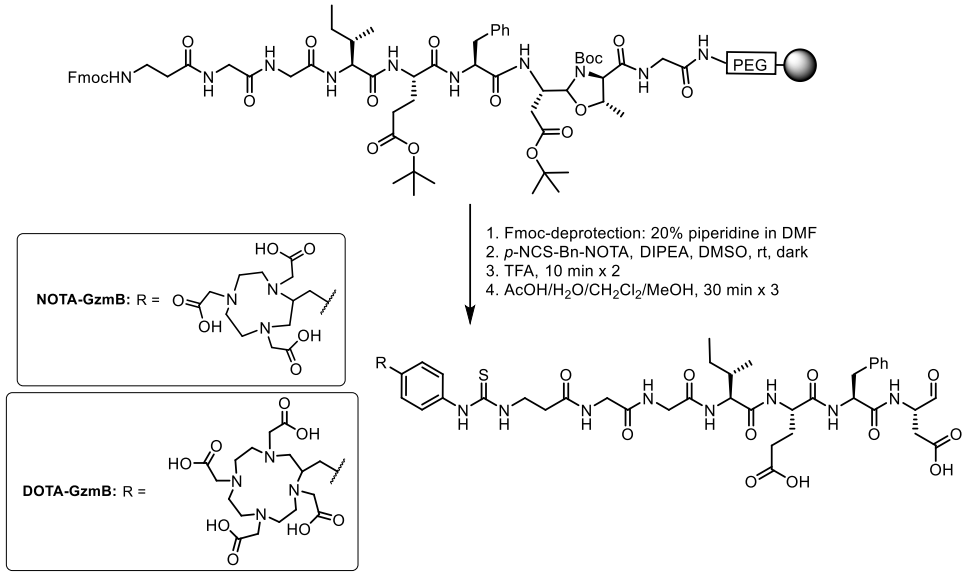

Scheme 14. Conjugation of NOTA-SCN and DOTA-SCN to resin-bound peptide.

Cleavage from the resin and side-chain deprotection was carried out in two steps whereby side-chain protecting groups were removed by treatment with anhydrous TFA, and then cleavage from the resin was carried out by treatment with AcOH/water/CH_2Cl_2/MeOH (10:5:63:21). Results of the syntheses are summarized in Table 4 on page 50.

For preparation of NODAGA-GzmB, the same peptide aldehyde was employed. Coupling of NODAGA-tris-*t*Bu ester was performed in two steps, with initial Fmoc-deprotection followed by a standard peptide coupling of NODAGA-tris-*t*Bu ester and the peptide chain (Scheme 15). The NODAGA-tris-*t*Bu ester contains *tert*-butyl protection groups on all the chelating side-arms, to ensure that the coupling takes place in the correct position. *tert*-Butyl protection groups are generally cleaved under acidic conditions (TFA), and the two-step cleavage from resin, as performed for the NOTA and DOTA analogues, was attempted (Scheme 15).

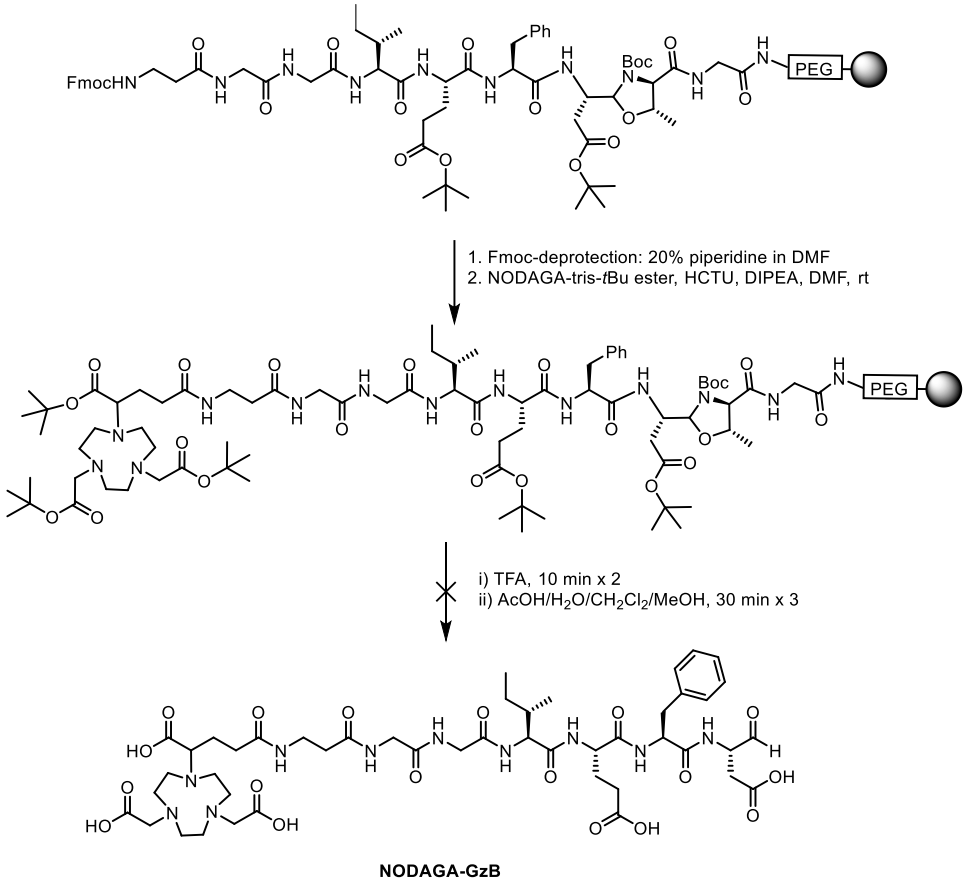

Scheme 15. Fmoc-deprotection followed by coupling of the NODAGA-chelator construct. Cleavage of *t*Bu-protection groups was not successful.

We expected to find the mass of NODAGA-GzmB ($[M+H]^+ = 1049.2$), though this was not observed in the LRMS spectrum after cleavage (Figure 18). There were three signals that were quite predominant in the spectrum, *m/z* 1161.5, 1217.5 and 1245.5, where the first two correspond to NODAGA-GzmB with two and three *tert*-butyl-groups still present (*m/z* calcd for $[M+t\text{Bu}+H]^+$ 1105.5; $[M+2t\text{Bu}+H]^+$: 1161.5; $[M+3t\text{Bu}+H]^+$: 1217.5).

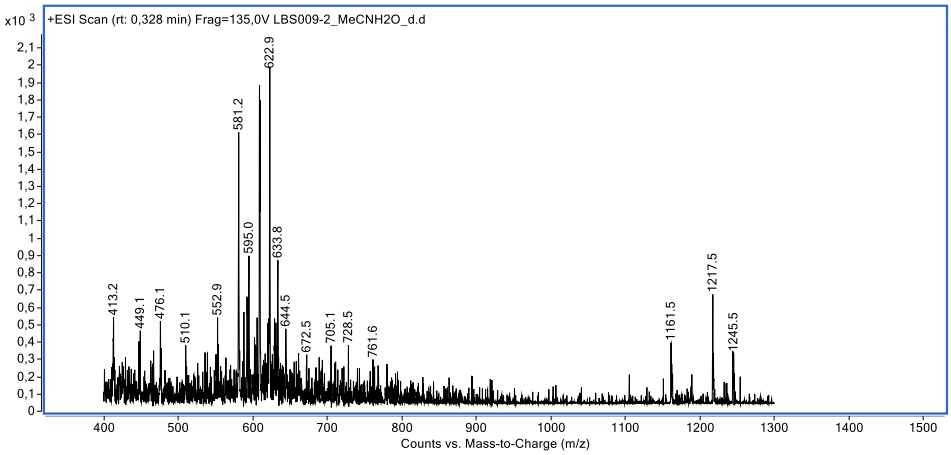

Figure 18. LRMS spectrum after first cleavage of NODAGA-GzmB from resin.

Once the fragments were identified as signals corresponding to uncomplete deprotection of NODAGA-GzmB, we extended the deprotection step to 3 h. We additionally tested to submit the material that had been treated with TFA for 10 minutes prior to cleavage from the resin in the subsequent step to another round of prolonged (3 h) TFA-treatment. These experiments gave similar results, and both provided fully deprotected NODAGA-GzmB (Scheme 16). Longer reaction times (>4 h) with TFA resulted in decomposition of the resin.

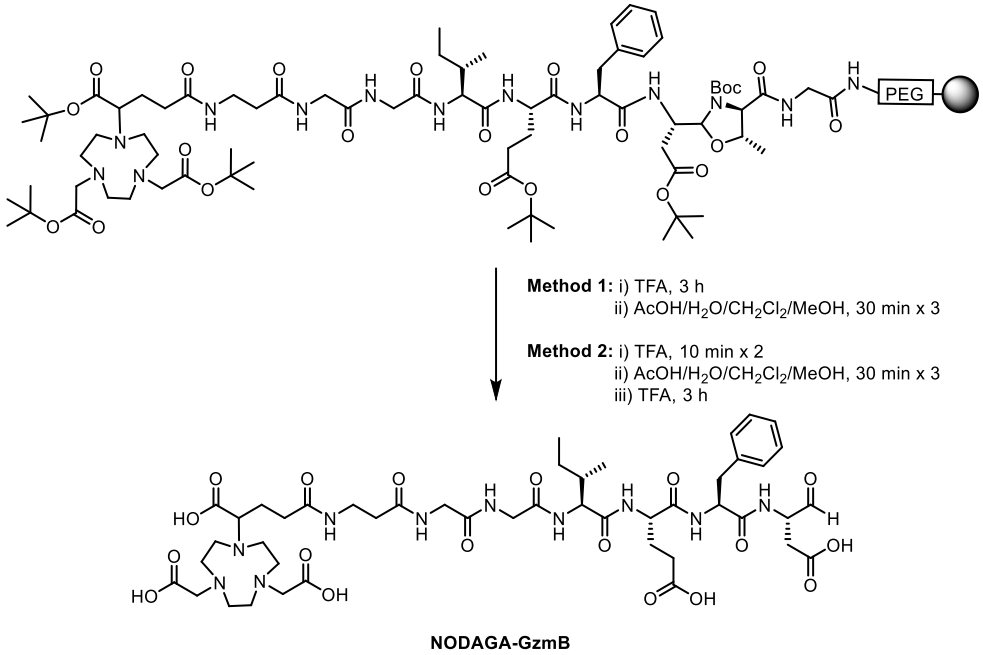

Scheme 16. Cleavage conditions for NODAGA-*GzmB*.

NODAGA-GzmB was successfully synthesized in high purity. Results from the synthesis is shown in Table 4 below.

Table 4. Results from synthesis of NOTA-, NODAGA- and DOTA-GzmB.

Compound	MS $[M+H]^+$ (calcd)	MS $[M+H]^+$ (found)[a]	HPLC purity [a]	Amount
NOTA-GzmB	1142.4	1142.4	97.6%	3.3 mg
NODAGA-GzmB	1049.3	1049.4	95.2%	1.5 mg
DOTA-GzmB	1243.5	1243.3	91.0%	0.99 mg

[a]Analytical data presented in the Appendix

^{1}H NMR analyses of the NOTA-GzmB and NODAGA-GzmB tracers revealed that the materials most likely contain two diastereoisomers, as two distinct aldehyde signals could be observed (Figure 19). The analytical HPLC of both compounds (see Appendix), however, shows that the isomers were inseparable.

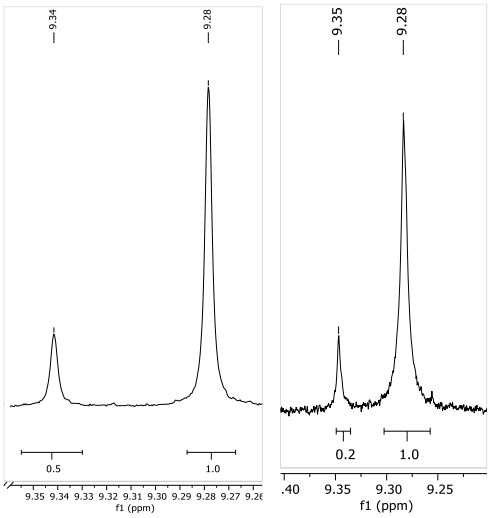

Figure 19. ^{1}H NMR of the aldehyde signals of NOTA-GzmB (left) and NODAGA-GzmB (right).

In summary, NOTA-GzmB was successfully re-synthesized, while NODAGA-GzmB and DOTA-GzmB are new analogues that have not been prepared previously. Syntheses of the NOTA- and DOTA-analogues were performed in the same manner as reported by Larimer *et al.*[71] Synthesis of the NODAGA-analogue required prolonged reaction time for complete deprotection of the multiple *t*Bu-protection groups. If the studies that are to be performed in Tromsø using these tracers are successful, further possibilities for optimization of the GzmB PET tracers will be explored.

3. Development of the FOSi-method – radiolabeling tracers for PET

3.1 Overview of the proposed FOSi-method

We set out to develop a new method for effective and selective radiofluorination of peptides and other receptor-binding biomolecules based on the principle that the silicon-fluoride bond is stronger than the silicon-oxygen bond, and that it can be selectively cleaved by a fluoride ion. We envisioned that a precursor bound to a solid support would allow for modification on-resin before cleavage, and that a selective cleavage should lead to release of the ^{18}F-labeled precursor from the resin, without other contaminations (Scheme 17).

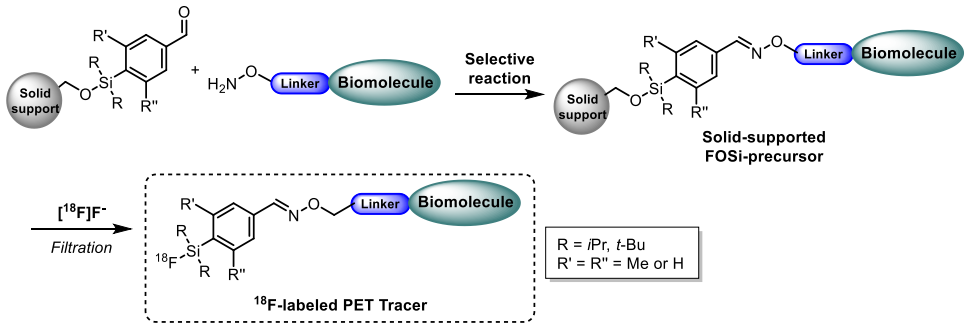

Scheme 17. Overview of the concept of the FOSi-method.

The FOSi-method is based on the tracers that have been reported by Wängler, Schirrmacher and co-workers[92-96] around ten years ago, which is detailed in Section 1.3.4. The SiFA-construct "SIFA-A" (Figure 20) is a key intermediate for their work, and our work started out by targeting silyl ether analogues of this motif.

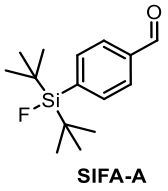

Figure 20. The building-block of the SiFA-strategy, published by Wängler *et al.*[96]

In addition to the aldehyde functionality proposed by the Wängler-group that allows for a selective reaction with an aminooxy-group on the peptide-chain, other functional

groups were investigated in this project, such as the interesting click-reaction between azides and alkynes, known as the Huisgen-Sharpless reaction.[154, 155] Different substitution patterns on the silane and the aryl substituent on the silane have been found to influence the stability and rate of reaction and are important factors that were considered in the development of the FOSi-strategy. Also, various linkers to the resin and different types of peptides can potentially be explored and some examples of the possibilities of modification is shown in Figure 21. The method allows for attachment to a wide variety of receptor-targeting biomolecules through selective linkage to the functional group on the aryl ring.

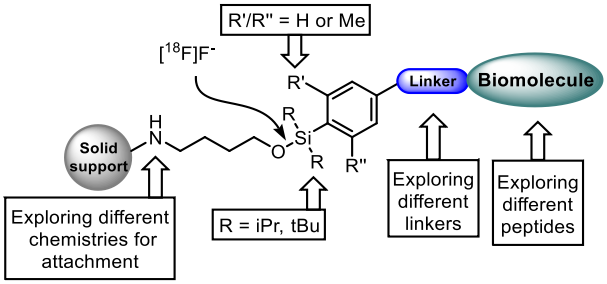

Figure 21. Variations of the FOSi-construct.

The foundation for this method is synthesis – and cleavage – of the silicon-oxygen bond, and the effort toward preparing the required building blocks, the linking of these and the initial results from testing of the FOSi-method is presented in the following sections.

3.2 Silanes, chlorosilanes and silyl ethers

Organosilanes are organometallic compounds containing a C-Si bond. They are absent in nature, but they are of great interest in synthetic organic chemistry. The carbon-silicon bond is longer and weaker than the carbon-carbon bond, whilst the strength of the Si-O bond is strikingly high.* Of particular importance is the known lability of silyl ethers in the presence of fluoride ions. The remarkable strength of the Si-F sigma bond

* Average bond lengths and strengths (at 273 K): C-Si bond: 1.89 Å, 318 kJ/mol; C-C bond: 1.54 Å, 334 kJ/mol; Si-O bond: 1.63 Å, 531 kJ/mol. See reference 156.

(808 kJ/mol, 1.60 Å)[156] allows for preparation of highly stable fluorosilanes, which we are aiming for in this work.

Preparation of silyl ethers typically require silanes or chlorosilanes as starting materials. Arylsilanes are usually obtained by reacting aryl-based Grignard reagents with simple chlorosilanes (Scheme 18A), or by lithiation of halogenated aryl components by use of a butyllithium reagent and then introducing the desired chlorosilane (Scheme 18B).

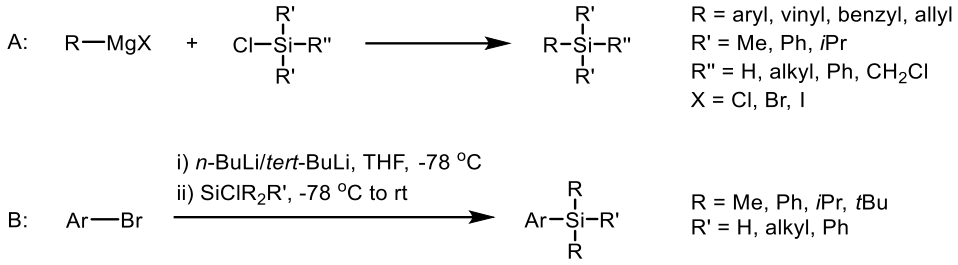

Scheme 18. A: Grignard-reaction for preparation of arylsilanes. B: Lithiation of halogenated aryls followed by reaction with chlorosilane to form desired arylsilane.

Silanes are typically transformed to silyl ethers by dehydrogenative coupling (Scheme 19). In this case, a substituted silane is reacted with an alcohol, and although thermodynamically quite favorable, this reaction requires a catalyst to take place at convenient rates, and many transition-metal based catalysts have been reported to mediate the process,[157-160] as well as different bases (NaOH, K_2CO_3, *t*BuOK)[161-163] and Lewis acids ($B(C_6F_5)_3$).[164] Some of these protocols suffer from one or more disadvantages, such as poor functional-group tolerance, slow rates with bulky (desirable) silanes and tertiary alcohols, the need for rigorously anaerobic and water-free conditions, and the lack of a commercially available catalysts.

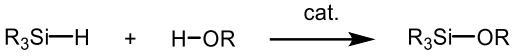

Scheme 19. General dehydrogenative coupling of silanes and alcohols to form silyl ethers.

The most common way to form silyl ethers is by reacting a substituted chlorosilane with an alcohol in the presence of imidazole in DMF as shown in Scheme 20, initially reported by Corey *et al.*[165] in 1972 and later modified in various directions.[166-169]

Substituted chlorosilanes can be prepared by chlorinating the corresponding silanes by various chlorinating protocols,[170-174] but are also in many cases commercially available. For silyl-protection groups with simple substitution patterns, such as TMS, TES, TIPS and TBDMS, the required silyl triflates are commercially available and allow for effective synthesis of silyl ethers from alcohols.[175]

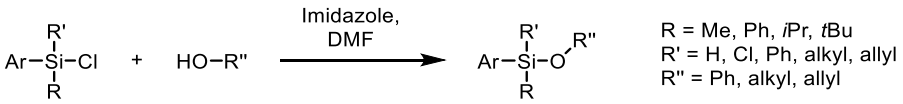

Scheme 20. Preparation of silyl ethers, reported by Corey *et al.*[165]

Silyl ethers are frequently used as protecting groups for alcohols, and both trialkyl- and alkylaryl-silyl ethers are known. Their stability toward acidic and basic conditions depends both on the substituents on the silicon atom and the nature of the alcohol to be protected, and span a range of 10^5 order of magnitude. Thus, in multistep organic syntheses, two or more different silyl protecting groups can be used simultaneously, and be removed selectively at different synthetic stages.[168] Also, the lability of silyl ethers towards fluoride sources allows for orthogonal cleavage of protection groups. By using a fluoride source, such as tetrabutylammonium fluoride (TBAF), the protection group is cleaved and removed by extraction. In the FOSi-labeling strategy, the fluorosilane produced in the deprotection reaction is of interest, opposed to the alcohol which is usually acquired in these reactions (Scheme 21).

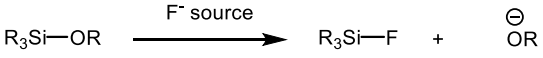

Scheme 21. Cleavage of silyl ethers by a fluoride source.

The stability of fluorosilanes varies considerably, depending on steric and electronic effects of the substituents on the silicon atom, as discussed in the next section.

3.3 Hydrolytic stability

High degree of radiodefluorination of ^{18}F-based tracers results in high background uptake and accumulation of free $^{18}F^-$ in the skeleton, which is why one of the important

parameters that needs to be addressed in the development of the FOSi-precursors is the tracer stability *in vitro* and *in vivo*.[176] The stability of a ^{18}F-radiolabeled tracer *in vivo* is highly dependent on how fluoride is attached to the precursor. This section will give insight into the hydrolytic stability of the Si-F bond, and how it is influenced by the surrounding substituents.

In the past 20 years, fluorosilanes have been studied extensively, by several research groups, as potential labeling synthons.[101,103,177] In 2000, Walsh and co-workers[178] attempted to stabilize the Si-F bond by introducing bulky substituents such as phenyl and *tert*-butyl groups and found that bulky substituents on the silicon atom reduces the hydrolysis of the Si-F bond. Furthermore, Choudhry and Blower[103] investigated the influence of different sized alkyl groups (Me, Ph, *tert*-Bu) and their combinations on fluorosilane stability, and found that *tert*-butyldiphenyl[^{18}F]fluorosilane ([^{18}F]**3**) contained the most stable Si-F-bond. Schirrmacher *et al*.[91] reported the syntheses of substituted [^{18}F]organofluorosilanes [^{18}F]**1**-**3** using organochlorosilanes as labeling precursors. The three [^{18}F]fluorosilanes (Figure 22) evaluated showed different *in vitro* stability in human serum and *in vivo* stability in rats. Only [^{18}F]**3** was stable in both human serum and *in vivo*, indicated by low radioactivity uptake in the bone, suggesting it was the most promising starting point for ^{18}F-radiolabeling purposes.

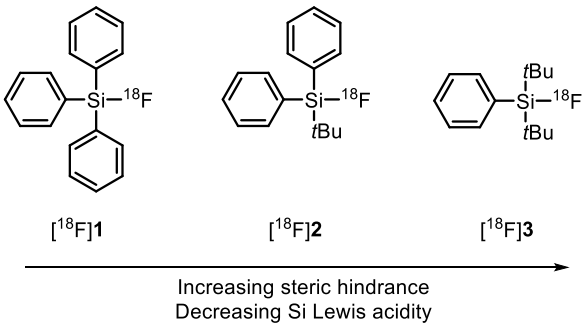

Figure 22. [^{18}F]fluorosilanes evaluated for *in vitro* and *in vivo* stability and radioactivity uptake in the bone.

These results created the foundation for the well-established "silicon-fluoride acceptor" (SiFA)-method published later by Wängler, Schirrmacher *et al.*,[92-94] explained in more detail in Section 1.3.4. At the same time, Ametamey *et al.*[105-107]

reported on the evaluation of hydrolytic stability of variously substituted fluorosilanes and alternative functionalization of the side chain on the aryl substituent, confirming the importance of sterically demanding substituents (Scheme 22). Their labeling strategy targets direct fluorination of silanes and silanols as opposed to isotope exchange on fluorosilanes coined by Wängler and co-workers.

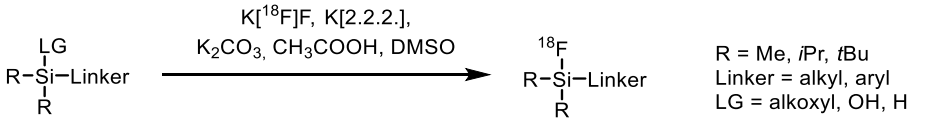

Scheme 22. Direct radiofluorination of silanes, hydrosilanes and silyl ethers reported by Ametamey *et al.*[105]

The research group also proposed a viable mechanistic explanation for the hydrolysis of organofluorosilanes (Scheme 23). The reaction proceeds in a classic S_N2 reaction, and most likely leads to inverted structure, according to the calculations by Höhne *et al*.[107] The pathway proposed by the group is in accordance with the known mechanism of nucleophilic substitution at the silicon atom, which is believed to proceed via a pentacoordinate intermediate.

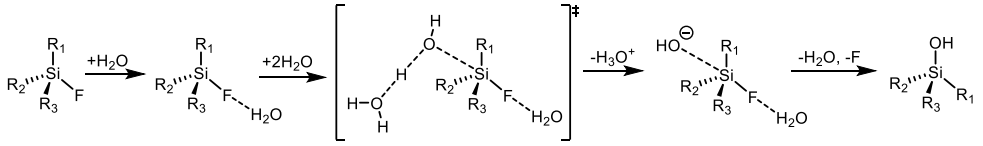

Scheme 23. Proposed S_N2 mechanism of the hydrolysis reaction for the organofluorosilanes, by Höhne *et al.*[107]

The stability trend for fluorosilanes strongly correlates with the steric bulk of the substituents on silicon, in combination with the reduced silicon Lewis acidity in the presence of *tert*-butyl substituents. Unfortunately, this substitution pattern comes at the price of a significant increase in lipophilicity which, when chemically linked to biomolecules, may significantly impact metabolism and biodistribution, generating unspecific uptake and leading to poor PET-imaging quality. If the lipophilicity of the administrated compounds is too high, accumulation in the liver can make them unavailable for binding to their intended binding site. For brain imaging, passive transport of radiotracers across the blood-brain barrier is required and only compounds with a certain degree of lipophilicity can into the brain.[179,180] This issue has been

addressed through development of lipophilicity-reducing auxiliaries. In 2015, Niedermoser *et al.*[181] found that the [^{18}F]SiFA*lin*-modified TATE (Figure 23) exhibited high binding affinities to somatostatin receptor–positive tumor cells (1.88-14.82 nM). The most potent compound demonstrated comparable pharmacokinetics and an even slightly higher absolute tumor accumulation level in *ex vivo* biodistribution studies as well as higher tumor standardized uptake values in PET/CT imaging than ^{68}Ga-DOTATATE *in vivo*. The radioactivity uptake in non-tumor tissue was, however, higher than for [^{68}Ga]DOTATATE. The automated process for the manufacturing of [^{18}F]SiFA*lin*-TATE has been developed to make the tracer routinely accessible for use in clinical neuroendocrine tumor diagnosis.[181-184]

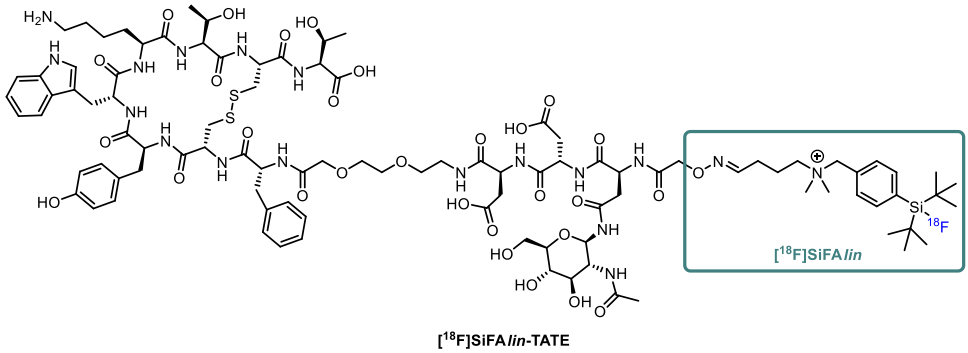

Figure 23. Somatostatin-receptor binding [^{18}F]SiFA*lin*-TATE, modified to accommodate high lipophilicity.[181]

The presence of bulky *tert*-butyl groups, combined with an aryl-linker moiety, results in remarkable stability whereas for tracers with smaller alkyl substituents a progressive enhancement in the hydrolysis rate is observed as the substituents become smaller. Increased steric hindrance around the silicon atom makes it more difficult to bring about radiofluorination. Existing techniques for fluorination of organosilicon compounds require forcing conditions to afford reasonable yields including high temperatures and very polar solvents. Even though the di-*tert*-butyl-substituted fluorosilanes have superior hydrolytic stability, analogues containing two isopropyl substituents on the silicon atom have been investigated by multiple research groups, as an alternative to the sterically demanding *tert*-butyl groups.[105-107,110,113-115] In a study of hydrolytic stability reported by Mu *et al.*[107], diisopropyl analogues were found to have

moderate hydrolytic stability (Figure 24). Introduction of one or two methyl groups on the aryl substituent, in the *ortho*-position to the silyl substituent, increased hydrolytic stability dramatically ($t_{1/2}$ > 300 h). The isopropyl substituent is less hydrophobic than the *tert*-butyl substituent,[185] which could be a favorable characteristic in the search for less lipophilic precursors. It should be noted that additional methyl groups on the aryl substituent in turn increases the lipophilicity of the molecule, though this does not affect the Lewis acidity of the Si atom to the same extent. It should be emphasized that these studies are only performed in buffer solution, and as such may not necessarily translate to the behavior *in vivo*.

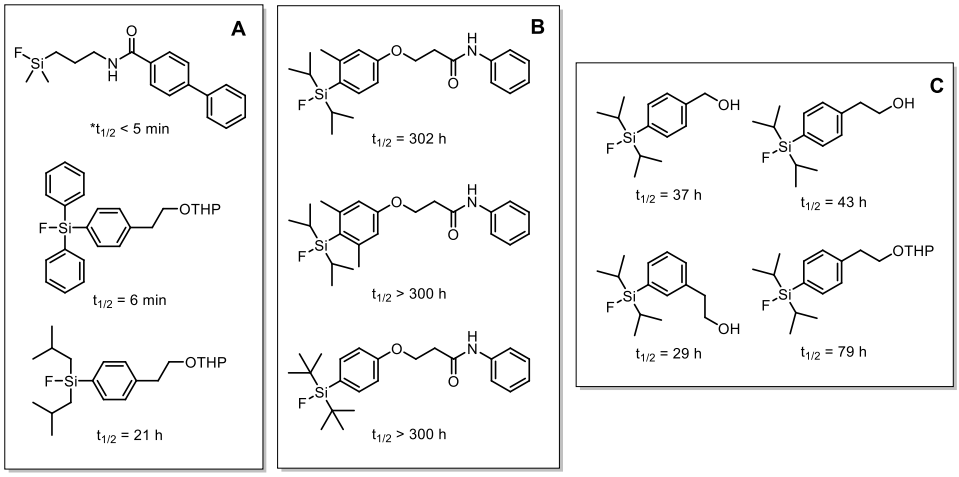

Figure 24. A: Fluorosilanes with very low hydrolytic stability. The compound bearing two iso-butyl groups exhibits a relatively high stability towards hydrolysis. B: Silicon building blocks with highest hydrolytic stability. C: Influence of the substituent on the aryl moiety on hydrolytic stability. (*$t_{1/2}$: hydrolytic half-life).[107]

Upon subjecting di-*tert*-butyl substituted fluorosilanes to phosphate buffer (pH 7.4) for up to 10 days, Rugeri *et al.*[114] studied the hydrolytic stability of fluorosilylated dipeptides, where the di-*tert*-butyl-substituted analogue showed excellent hydrolytic stability (only traces of free fluoride ion observed after 10 d), whilst the diisopropyl-substituted analogue released 40% of the F^- within 5 min, and then the amount of F^- increased steadily over time (>60% hydrolyzed within 13 h). Most SiFA analogues to date have demonstrated desirable *in vitro* and *in vivo* stability, with a few examples of *in vivo* defluorination reported to date.[120,186,187]

3.4 Synthesis of silanes and silyl ethers

As starting point for the FOSi-method, we decided to target the same products produced through the SiFA process, where the aldehyde-containing di-*tert*-butyl-substituted silane **5** would be a key intermediate. In the following sections, the efforts toward preparation of both di-*tert*-butyl and diisopropyl-substituted silanes and silyl ethers will be presented.

Synthesis of di-tert-butyl-substituted silanes and chlorosilanes

Silane **5** was the first building block required for silyl-ether formation. The di-*tert*-butylphenyl-substituted silane (**5**) containing an aldehyde in the *para*-position was prepared as described by Rugeri *et al.*[114] using di-*tert*-butylchlorosilane (DTBSiHCl) as the silylating reagent (Scheme 24). Desired silane **5** was prepared in 62% yield, isolated as a mixture with *n*-butylated side-product **6** (ratio **5**/**6**, 9:1).

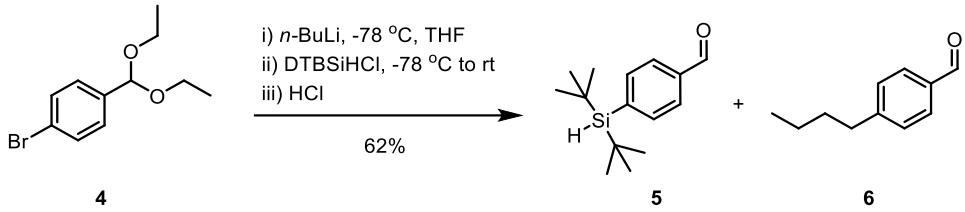

Scheme 24. Preparation of silane **5**.

To avoid *n*-butylation, use of *tert*-butyllithium (*tert*-BuLi) was investigated, though this only resulted in isolation of several impure fractions after flash chromatography and *n*-BuLi was therefore used in further reactions.

We assumed that the chlorosilane **7**, or a protected version of **7**, would be suitable compounds for further reaction with an alcohol to install the Si-O bond. Chlorination of silane **5** was carried out following a procedure published by Savela *et al.*[170], as shown in Scheme 25. This was not successful in providing **7**, and we suspect that the aldehyde was reduced by iron(III) as the aldehyde signal was not present in the crude mixture ^{1}H NMR-analysis. The chlorinating protocol was not applicable with aldehyde functionality present, though protected aldehydes or other functional groups are potential starting points.

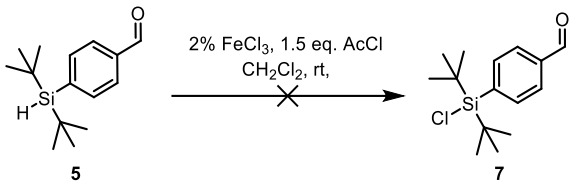

Scheme 25. Unsuccessful synthesis of chlorosilane **7**.

An obvious solution to this would be to use the diethyl acetal analogue of **5**, as the unprotected aldehyde could cause complications in further reactions toward the silyl ether. Similar reaction conditions and work-up, except for the hydrolysis step, were applied to the same starting material as before. However, the acetal was hydrolyzed, even with slightly basic conditions in the work-up (Scheme 26).

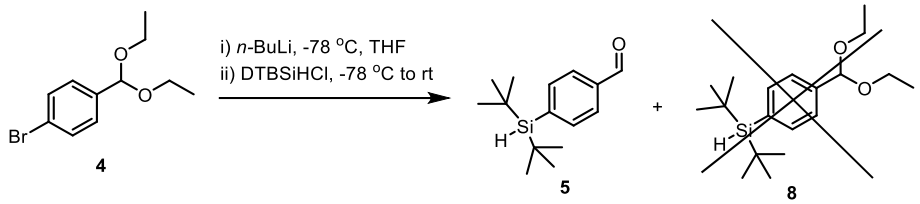

Scheme 26. Silylation of **4** in attempt to prepare acetal **8**.

We then turned to cyclic acetal-protected **9**, as cyclic acetals are generally more stable towards hydrolysis.[188,189] Compound **9** was lithiated and reacted with DTBSiHCl in the same manner as linear-acetal protected **4** and silane **10** could be isolated in 41% yield after flash chromatography (Scheme 27).

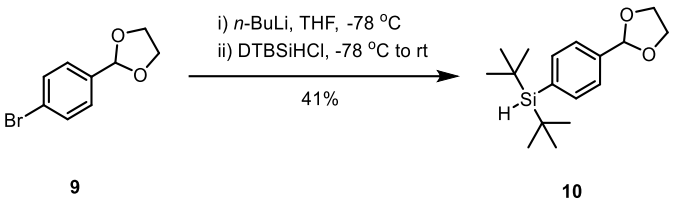

Scheme 27. Preparation of acetal protected compound **10**.

As mentioned above, the lithiation step using *n*-BuLi, in most cases, produced *n*-butylated side-products with similar R_f-values as both the starting material and the desired product. Bailey *et al.*[190] reported that the extent of *n*-butylation is highly dependent on the solvent system used. A mixed solvent system of THF and heptane was preferred to limit the formation of the *n*-butylated side-product. As we had

anhydrous hexane available from the in-house SDS solvent purification system, this was used as substitute for heptane, and solvent systems hexane/THF 99:1, hexane/THF 9:1 and hexane/THF 1:1 was employed for synthesis of silane **5**. The poor solubility of the starting materials (**4** and **9**) in hexane provided lower yields and more complex reaction mixtures, which were difficult to purify. The ^{1}H NMR spectrum in Figure 25 displays three signals in the aldehyde-proton region (around 10 ppm), and also more than one *tert*-butyl signal around 1 ppm.

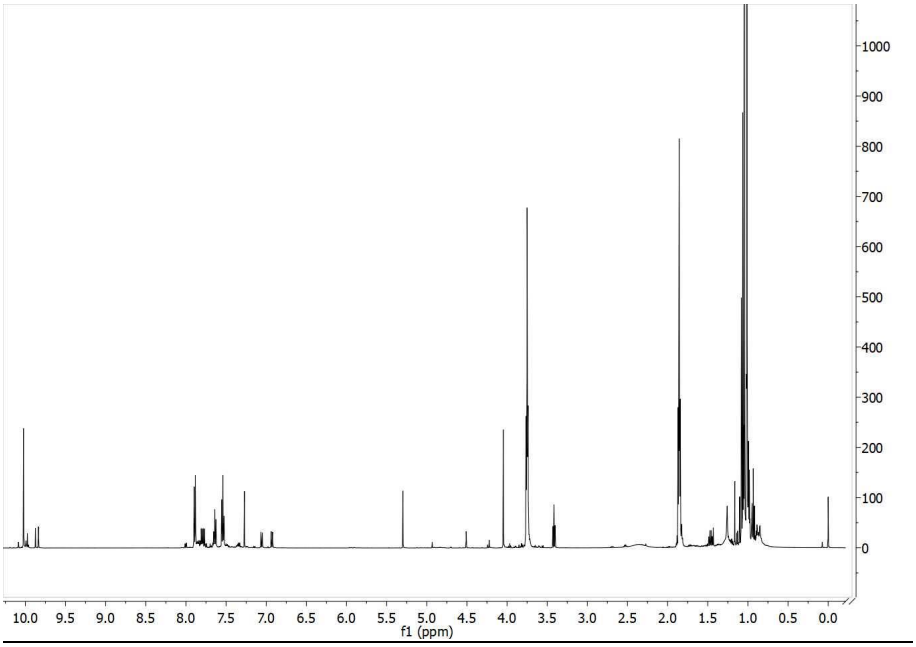

Figure 25. ^{1}H NMR spectrum of crude product for synthesis of **5**.

An alternative route to desired chlorosilane **7** was tested, which involved using di-*tert*-butyldichlorosilane (DTBSiCl$_2$) as the electrophile instead of DTBSiHCl after the lithiation. The reaction that seemed best suited was an adapted version of the protocol published by Schirrmacher *et al.*[91] in 2006, where an arylbromide was lithiated and then reacted with di-*tert*-butyldifluorosilane. We therefore submitted **9** to the same conditions, except DTBSiCl$_2$ was used as the silylating reagent (Scheme 28). The reaction was successful, and the cyclic acetal remained intact. The only work-up conducted was evaporating the solvent and then re-dissolving the residue in hexane/ethyl acetate. This work-up procedure worked well for the cyclic acetal, though

it was unsuccessful for the linear acetal. Compound **11** was not purified by flash chromatography as we suspected that the chlorosilane would not be stable on silica gel. Once again, *n*-butylated side-product **12** constituted approximately 30% of the product-mixture. The reaction resulted in 100% conversion of starting material, but compound **11** could not be separated from the *n*-butylated side-product **12** (ratio **11**/**12**, 7:3) and the product mixture was used directly in the next reaction.

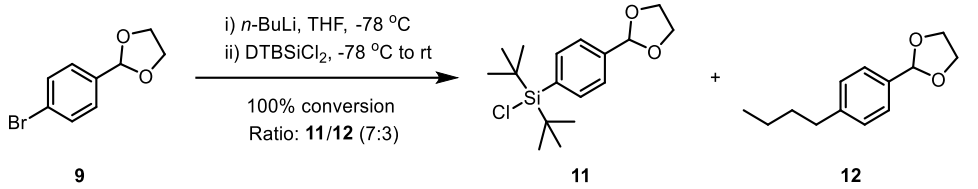

Scheme 28. Preparation of chlorosilane **11**.

The hexane/THF (99:1) solvent system was also applied in this reaction (Scheme 29), nevertheless, it only resulted in 16% conversion of starting material (**9**) based on NMR. The use of hexane/THF 9:1, however, resulted in 100% conversion of the starting material (Scheme 29). There was unfortunately still $DTBSiCl_2$ present in the crude mixture, which turned out to be a problem in the upcoming reaction. In hindsight, this crude mixture should have been purified by flash chromatography, as the highly substituted chlorosilane **11** presumably would not undergo hydrolysis on silica gel.

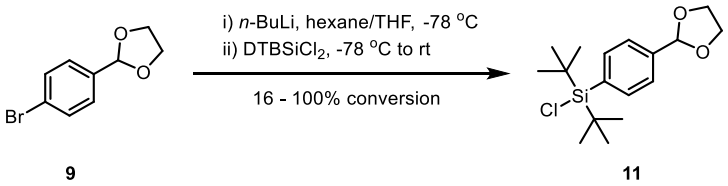

Scheme 29. Different solvent systems tested for preparation of acetal-protected aldehyde **11**.

Further, cyclic acetal **11** was submitted to hydrolysis conditions by employing a procedure described for a corresponding di-*tert*-butyl-substituted fluorosilane by Wängler *et al.*[96] This was not successful and resulted in a complex mixture (Scheme 30).

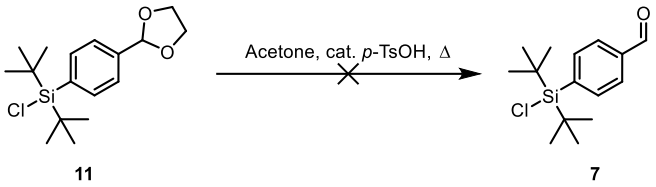

Scheme 30. Unsuccessful synthesis of chlorosilane **7**.

Trying to avoid the *n*-butylated side product, we looked in a different direction and decided to apply the Grignard reaction (Scheme 31) through modification of a procedure published by Abdelbagi *et al*.[191]

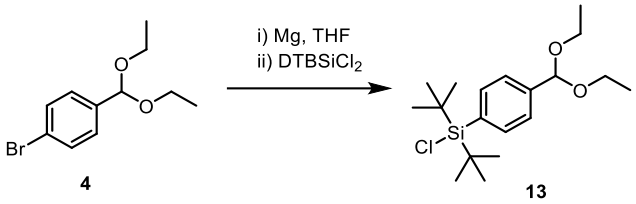

Scheme 31. Grignard procedure for preparation of chlorosilane **13**.

Activating the magnesium was somewhat troublesome, and the yields were lower than for the halogen-exchange reactions, but crude product ^{1}H NMR revealed that mostly **13** had been formed in the reaction (Figure 26).

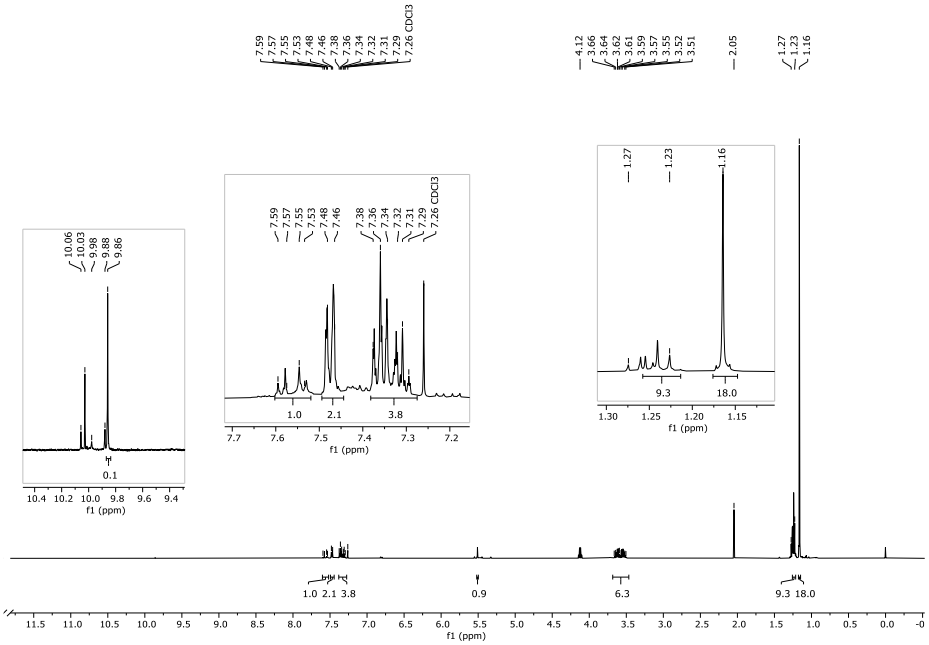

Figure 26. ^{1}H NMR spectrum of crude mixture after Grignard reaction to compound **13**.

Signals at approximately 10 ppm were identified, implying that aldehydes were present indicating some hydrolysis even before purification. We also attempted this procedure for preparation of silane **8**, using DTBSiHCl as electrophile. In this case, hydrolysis of the acetal was observed, even under basic aqueous work-up, as multiple aldehyde signals were present in the ^{1}H NMR spectrum (Figure 27). Due to the lability of the acetal, this strategy was abandoned.

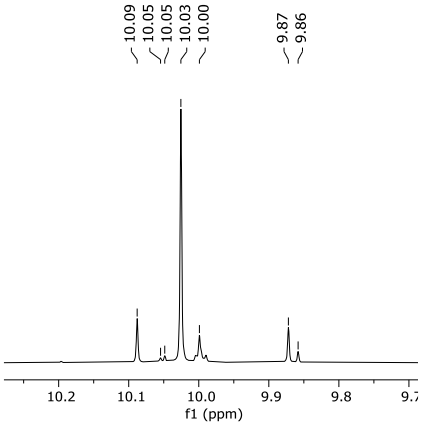

Figure 27. ^{1}H NMR spectrum showing the aldehyde-proton region of crude mixture after Grignard synthesis of compound **8**.

As the syntheses of aldehyde FOSi-precursors were troublesome, we looked at other possible starting points. The selective reaction between an alkyne and an azide was found appropriate for this project, where instead of an aldehyde, an alkyne would be present on the aryl substituent. Motifs such as **14** or **15** would be excellent candidates for this route (Figure 28).

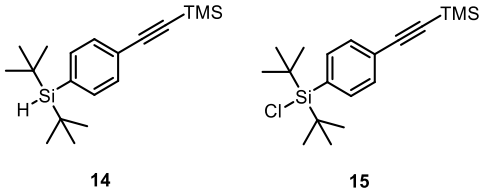

14 **15**

Figure 28. Possible alkyne FOSi-precursors.

The initial strategy to obtain silane **14** and chlorosilane **15** started out by submitting trimethylsilyl (TMS)-protected **16** to the same lithium-halogen exchange strategy as for the aldehydes (Scheme 32), and subsequently adding DTBSiHCl or $DTBSiCl_2$. We chose TMS as protection group for the alkyne as this could be cleaved under conditions

that are not suspected to affect the silyl-ether moiety which is to be installed in the next step. This gave 100% conversion of starting material, though the crude product contained multiple components, all being highly non-polar, and co-eluting with R_f-values around 0.6, even when 100% hexane was used as eluent. This resulted in unsuccessful attempts at purification by flash chromatography, and the product could not be isolated.

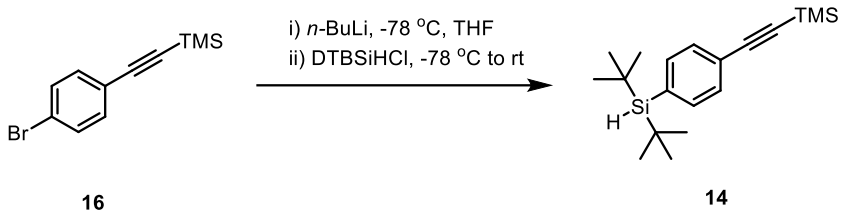

Scheme 32. Preparation of **14** via the lithium-halogen exchange protocol.

^{1}H NMR analysis of the crude mixture displays only one compound, containing a *tert*-butyl-proton signal at 1.01 ppm and a TMS-proton signal at 0.25 ppm (Figure 29). It appeared to us that some of the fractions from flash chromatography previously thought to be impure, could in fact be mixtures of the TMS-protected alkyne and the desilylated alkyne, which gave rise to two quite similar signals in the spectrum (Figure 29).

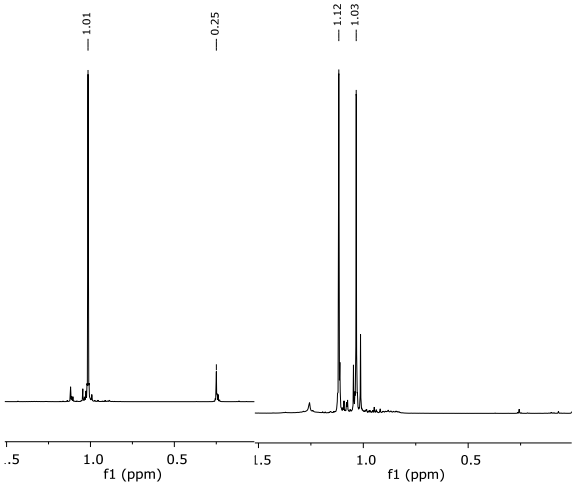

Figure 29. Left: crude mixture of **14**. Right: fraction 1 after flash of **14**.

Protection of the alkyne was nonetheless required to proceed to silylation of alcohols. Alternatively, more sterically hindered and more stable protection groups for alkynes,

such as triisopropylsilyl (TIPS) or *tert*-butyldimetylsilyl (TBDMS) could have been employed, although this might not result in selective deprotection of the alkyne once the desired silyl ether is present. The same reaction conditions were employed to prepare chlorosilane **15** (Scheme 33). Again, starting from **16** conducting the lithium-halogen exchange reaction and adding $DTBSiCl_2$ in the next step**,** yielded the desired product.

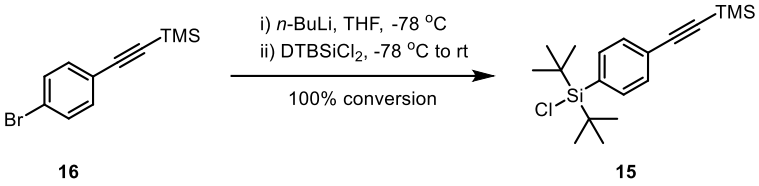

16 **15**

Scheme 33. Preparation of chlorosilane **15** via the BuLi-approach.

^{1}H NMR of the crude product (Figure 30) indicated that the reaction was successful, as the only up-field signals observed were TMS-protons at 0.25 ppm and di-*tert*-butyl protons at 1.16 ppm. However, the aromatic region of the spectrum revealed that there was more than one compound present. *n*-Butylation, which was observed to a great extent in the aldehyde-precursor, was not observed in this reaction. Only traces of the *n*-butylated side product could be identified in ^{1}H NMR analysis of the crude product.

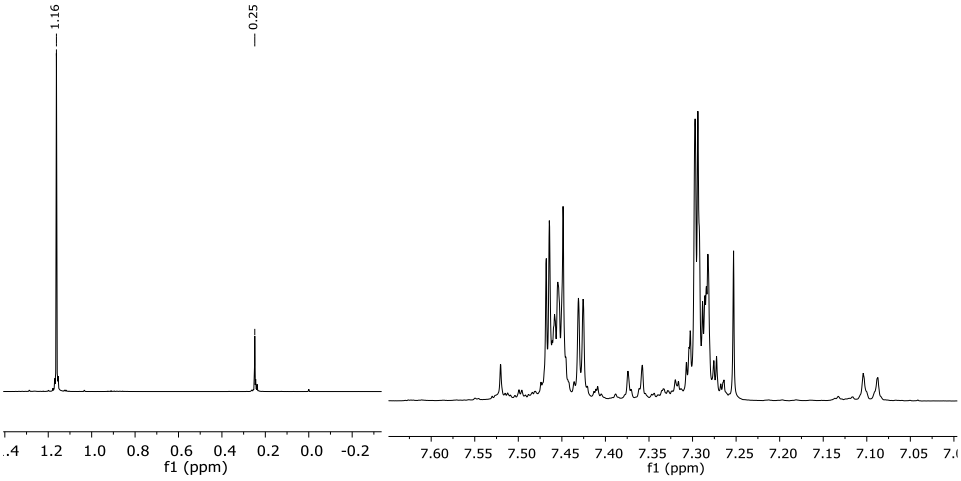

Figure 30. ^{1}H NMR of the crude product after work-up. Left: TMS- and di-*tert*-butyl protons. Right: Aromatic region.

Even with the impurities in the aromatic region, the crude product was used further without purification because of the suspected instability of the chlorosilanes on silica gel. We reasoned that the crude mixture most likely contained only one chlorosilane which could react with an alcohol in the next step, and the impurities could be removed at a later stage. Purification of alkyne precursors was not as simple as for the aldehyde precursors. Flash chromatography was difficult to conduct as the compounds in the crude mixture had almost identical retention time, even in 100% hexane.

The Grignard reaction was also performed on **16** as presented in Scheme 34, and the results were similar as for the BuLi-reaction with a comparable crude product ^{1}H-NMR spectrum.

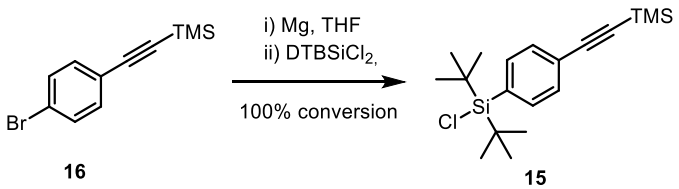

Scheme 34. Synthesis of **15** via the Grignard reaction.

The lithium-halogen exchange reaction was also tested without TMS-protection of the alkyne, this only resulted in a mixture of multisilylated products (Scheme 35). This was not entirely unexpected, due to the acidity of the terminal-alkyne proton.

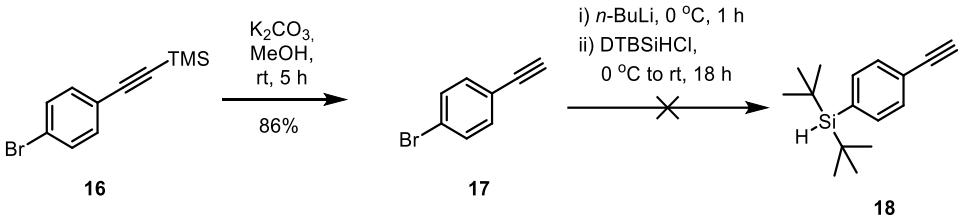

Scheme 35. Unsuccessful attempt to prepare **29** from unprotected alkyne **30**.

Since the crude alkyne-containing silane was challenging to purify, and the aldehyde silane **5** had been successfully obtained, the conversion of the aldehyde to the alkyne was a potential option. Seyferth-Gilbert homologation is a base-promoted reaction of dimethyl (diazomethyl)phosphonate with aldehydes and aryl ketones at low temperatures to give alkynes. The Bestmann-Ohira modification using dimethyl 1-diazo-2-oxopropylphosphonate (**20**) allows the conversion of base-labile substrates

such as enolizable aldehydes, which could undergo aldol condensation under the Seyferth-Gilbert conditions due to the use of stronger base (KO*t*Bu). The Bestmann-Ohira-modified reaction[192] is an excellent way of converting aldehydes to alkynes, by utilizing Bestmann-Ohira reagent **20** and potassium carbonate in methanol. Reagent **20** was prepared from dimethyl (2-oxopropyl)phosphonate (**19**) as described by Pietruszka and Wiit[193] (Scheme 36).

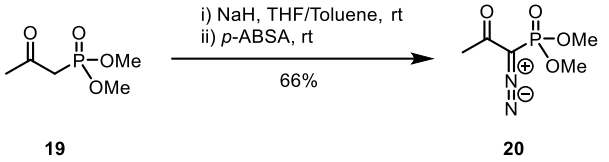

Scheme 36. Preparation of the Bestmann-Ohira reagent (**20**).

Aldehyde **5** was alkynylated by reaction with **20** in anhydrous MeOH and K_2CO_3 as base, as shown in Scheme 37 below. This reaction was easily monitored by TLC-analysis, and purification by flash chromatography was uncomplicated, as the aldehyde and the alkyne had very different R_f-values (100% hexane), and compound **18** was isolated in good yield.

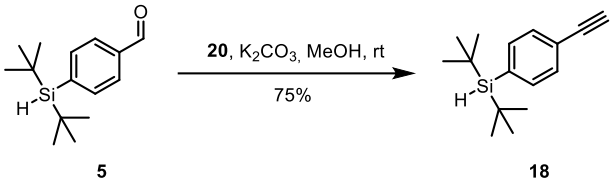

Scheme 37. Ohira-Bestmann reaction from aldehyde **5** to alkyne **18**.

We also wanted to investigate azides as potential functionality on the precursor. This would provide flexibility as to which building block contains which functionality for the triazole linkage. In this case, it is necessary for the peptide (or other ligand) to be modified to contain a terminal alkyne.

The first step towards the azide, was synthesis of benzylic alcohol **22** from 4-bromobenzyl alcohol (**21**) (Scheme 38). Sternson *et al.*[194] reported a procedure for the corresponding diisopropyl-substituted analogue, in three steps, which commenced with deprotonation of the benzylic alcohol by NaH, followed by lithiation by *n*-BuLi and then subsequently adding diisopropylchlorosilane (*i*-Pr_2SiHCl). We performed a similar reaction, exchanging the silylating agent with DTBSiHCl, but this resulted in

formation of several side products and caused difficulties in purification of the crude product and the yield was therefore quite low (20%).

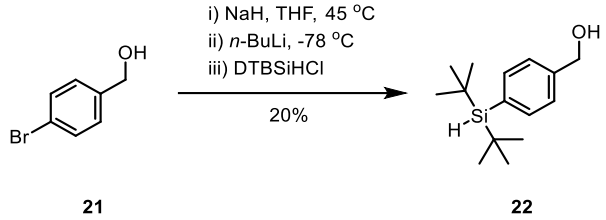

21 **22**

Scheme 38. Synthesis of benzyl alcohol silane **22**.

An alternative route to this molecule was investigated, by protecting the alcohol with a tetrahydropyranyl (THP) group and then performing the lithium-bromine exchange reaction. This has been reported for a diisopropyl-substituted analogue, with an approximate yield of 80% over three steps.[110] Benzylic alcohol **21** was reacted with dihydropyran (DHP) using pyridinium *para*-toluenesulfonate (PPTS). The THP-protected alcohol **23** was then lithiated in a halogen-lithium exchange reaction and subsequently reacted with DTBSiHCl to give silane **24.** Deprotection of the THP-protection group was achieved by use of *para*-toluenesulfonic acid (PTSA) to give silane **32** in only 22% yield over 3 steps (Scheme 39). As the pathway involved multiple steps and no increase in yield, this strategy was abandoned.

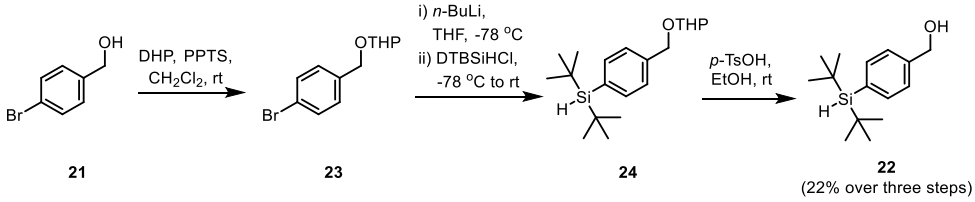

21 **23** **24** **22**
(22% over three steps)

Scheme 39. Preparation of compound **22** through THP-protection of the alcohol.

Chen *et al*.[195] also reported on the reaction from benzylic alcohol **21** to a diisopropyl-substituted silane, although they used an excess of *n*-BuLi to deprotonate the benzylic alcohol simultaneously as the lithiation, in good yield (73%). Both NaH and *n*-BuLi are strong bases, so eliminating one step in this key procedure is time efficient. The procedure was attempted with varying conditions for the di-*tert*-butyl-substituted silane (**22**), yielding up to 37% (Table 5, entry 2), almost double of what had been obtained previously.

Table 5. Syntheses of silane **22** with aim to increase the yield.

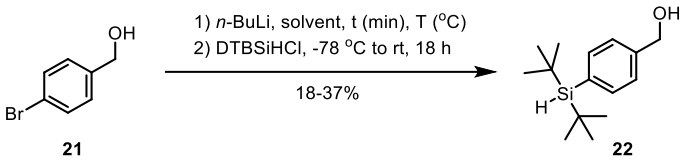

21 **22**

***n*-BuLi (eq.)**	**Addition of *n*-BuLi (x min)**	**Scale (mmol)**	**Solvent**	**T (°C)**	**t (min)**	**Result (%[a])**
2.5	15	5.3	THF	-78	60	22
2.5	2	5.6	THF	-78	60	37
2.2	2	8.2	THF	-78	60	18
2.0	10	1.5	THF	0	20	5 or more compounds
2.0	2	1.5	THF/ hexane (1:1)	-78	40	4 or more compounds
2.0	2	1.5	THF	-78	40	3 compounds

[a]Isolated yields

To obtain the azide, alcohol **22** was treated with 1,8-diazobicyclo[5.4.0]undec-7-ene (DBU) and diphenylphosporyl azide (DPPA) in DMF as reported by James *et al*.,[112] as shown in Scheme 40. This reaction led to full conversion after stirring overnight, and after aqueous work-up no further purification was required.

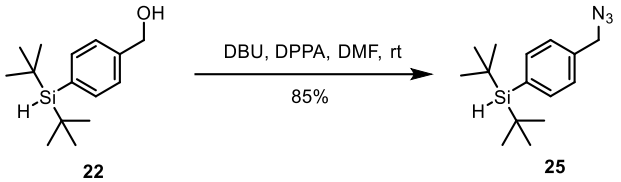

22 **25**

Scheme 40. Preparation of azide **25** from alcohol **22**.

With the various silane and chlorosilane building blocks at hand, silyl-ether formation was next. We reasoned that it would be best to form the Si-O bond before attaching the precursor to a resin to have control over the conversion from Si-H or Si-Cl to Si-O. Different approaches to make Si-O bonds are described in the following sections.

Silylation of alcohols (silyl ether formation)

Silyl-ether formation from di-*tert*-butyl silanes or di-*tert*-butyl chlorosilanes with alcohol **27** or **29** proved to be difficult and a summary of the conditions tested can be found in Table 6 on page 75.

Our first attempt at preparing the Si-O bond in this project was by following a procedure described by Mirza-Aghayan *et al.*[157] (Table 6, entry 1, 2 and 3), providing a fast and simple strategy for Si-O-compounds from silanes using a palladium catalyst. In their protocol, only benzyl alcohol, 1-decanol and 2-octanol were reported as starting alcohols. We aim at preparing analogues with functional groups for selective coupling to the resin, in this case alkyne **27**, which could potentially react under the given conditions. We were, however, not able to obtain silyl ether **26** (Scheme 41), and mostly starting material was identified upon ^{1}H NMR analysis of the crude mixture.

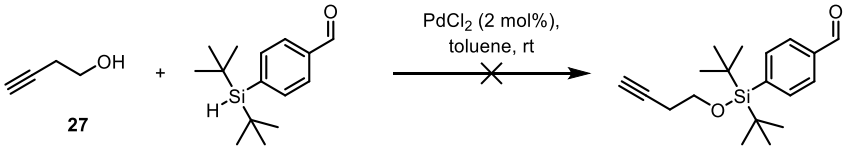

Scheme 41. Palladium-catalyzed reaction between **5** and **27**.

Toutov *et al.*[161] reported a procedure of dehydrogenative coupling for preparation of silyl ethers from benzylic alcohols catalyzed by NaOH (Scheme 42).

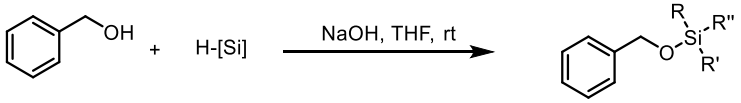

H-[Si] = Et_3SiH, Ph_2MeSiH, $(t\text{-}Bu)_2H_2$, $(i\text{-}Pr)_3SiH$, $t\text{-}BuMe_2SiH$

Scheme 42. Base-induced reaction between substituted silanes and benzyl alcohol, reported by Toutov *et al.*[161]

In our hands, no conversion of starting material was observed under these conditions (Table 6, entry 4, 5 and 6). Similar results were observed with other bases such as K_2CO_3[162], KO*t*Bu[163] and TEA[196, 197] (Table 6, entry 7, 8, 9 and 10). Other Si-O coupling procedures were investigated, starting with the conditions described by Porto *et al.*[169] using chlorosilane **11** and alcohol **27** as starting materials (Scheme 43; Table 6, entry 11 and 12).

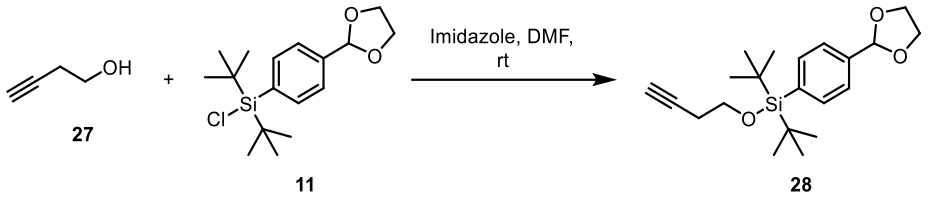

Scheme 43. Attempted silylation of **11**.

This resulted in three different compounds, indicated by ^{1}H NMR analysis of the crude product mixture (Figure 31). The *n*-butylated side-product (**12**) that could not be separated from the starting material was present as expected. There seemed to be two compounds containing an alkyne-moiety present (potentially **27** and **28**), indicated by the presence of two signals from terminal-alkyne protons (triplets at 2.61 and 2.45 ppm). In retrospect, this result seems quite interesting, however, purification by flash chromatography was not conducted at this point and the compounds in the crude mixture were not characterized further.

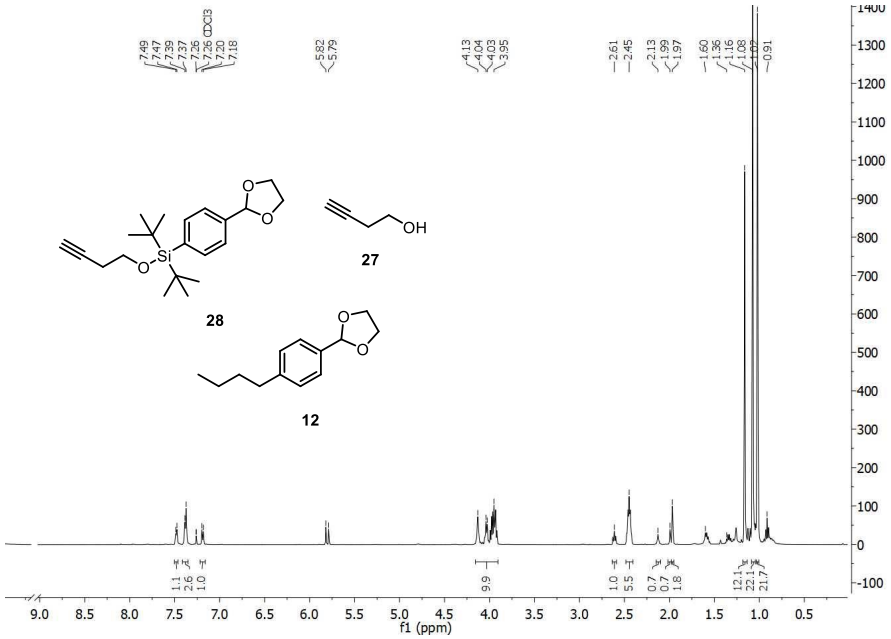

Figure 31. ^{1}H NMR-spectrum of product mixture after reaction between **11** and **27**.

Bartoszewicz *et al.*[168] reported on a similar procedure, using *N*-Me-Imidazole and I_2 to promote silyl-ether formation. Unfortunately, no conversion was observed following this procedure (Table 6, entry 13).

Thus far, preparation of silyl ethers required for our planned studies was mostly disappointingly unsuccessful. A summary of the various conditions tested for silyl ether formation is shown in Table 6. It is apparent that the sterically hindered silanes and chlorosilanes are not readily reacting with alcohols, possibly due to the steric hindrance imposed by the substituents on silicon. We have not encountered any reports on preparation of silyl ethers with the substitution pattern we are aiming for (di-*tert*-butylaryl), other than for methoxy-silyl ethers.[114]

Table 6. O-Si bonds from di-*tert*-butyl silanes and chlorosilanes.

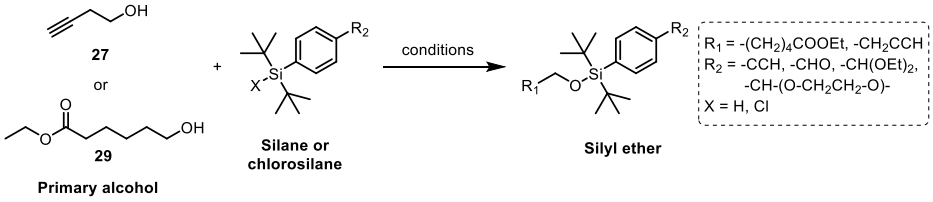

Entry	Conditions	X	R_2	Alc.	Result
1	$PdCl_2$, toluene, rt	H	-CHO	**27**	Reduction of aldehyde
2	$PdCl_2$, toluene, rt	H	-CH-(O-CH_2CH_2-O)-	**27**	Complex crude
3	$PdCl_2$, toluene, rt	H	-C≡C-H	**29**	Complex crude
4	NaOH, THF/DMF, 65 ºC	H	-CHO	**27**	3 compounds in crude
5	NaOH, THF/DMF, 65 ºC	H	-CH-(O-CH_2CH_2-O)-	**29**	Hydrosilane formation
6	NaOH, THF/DMF, 65 ºC	H	-C≡C-H	**29**	No conversion
7	KOtBu, THF/DMF[a], rt	H	-CH-(O-CH_2CH_2-O)-	**27**	No conversion
8	K_2CO_3, THF/DMF, 60 ºC	H	-C≡C-H	**29**	No conversion
9	TEA, CH_2Cl_2, 0 ºC to rt	Cl	-CH-(O-CH_2CH_2-O)-	**27**	Complex crude
10	TEA, CH_2Cl_2, 0 ºC to rt	Cl	-C≡C-TMS	**29**	Complex crude
11	Imidazole, DMF, rt	Cl	-CH-(O-CH_2CH_2-O)-	**27**	Complex crude, some product?
12	Imidazole, DMF, rt	Cl	-C≡C-TMS	**29**	No trace of product after purification
13	*N*-Methyl-imidazole, I_2, CH_2Cl_2/THF, rt	Cl	-C≡C-TMS	**29**	No conversion

[a] DMSO was added after 48h

Palladium-catalyzed silylation of alcohol

Rugeri, *et al.*[114] reported a reaction where an alkene was reduced by hydrogen by a palladium-catalyst in methanol, where the methoxysilane was reported as the only product in 99% yield (Scheme 44).

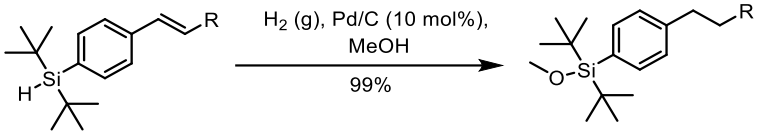

Scheme 44. Silylation reported by Rugeri *et al.*[114]

Inspired by this report, we attempted to prepare silyl ethers using different palladium catalysts, summarized in Table 7. Our first attempt at silyl-ether formation using palladium catalysts was performed as described by Rugeri *et al.*[114], using azide **25** and alcohol **29** in the presence of Pd/C as catalyst, yet no reaction was observed in this case (Table 7, entry 1). An attempt at silylating **25** with benzaldehyde using $Pd(OAc)_2$ as catalyst, was performed.[159] These conditions resulted in no conversion of starting material (Table 7, entry 2). Further, a silylation protocol was performed using methanol as the alcohol source (and solvent), with $PdCl_2$ as catalyst, as described by Mirza-Aghayan *et al.*[157] These conditions were, however, not compatible with the azide, as ^{1}H-NMR analysis indicated that an aldehyde was formed in the reaction, and there were multiple other compounds present in the mixture (Table 7, entry 3).

Table 7. Palladium-catalyzed silylation of alcohols.

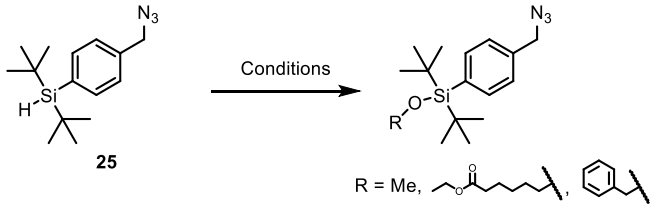

Entry	Reagent	Catalyst	Solvent	Result
1	**29**	Pd/C	THF	no reaction
2	Benzaldehyde	$Pd(OAc)_2$	DMF	no reaction
3	MeOH	$PdCl_2$	-	oxidation of azide

At this point, all attempts at making the Si-O bond had resulted in no or very low yields and complex reaction mixtures. We decided to abandon the di-*tert*-butyl-substituted analogues, and shift focus to the precursor containing a diisopropyl-substituted silane instead. Our method then deviates from the core SiFA-structure reported by Wängler *et al.* which we aimed at, though several research groups have employed the SiFA-construct with less sterically hindered silyl groups.[105,113]

Diisopropyl-substituted silanes

To circumvent the obstacles we had encountered with the di-*tert*-butyl substituted silanes and chlorosilanes due to the steric hindrance and bulkiness of the substituents, we decided to prepare diisopropyl analogues as FOSi-precursors. Based on available starting materials, some suggested analogues with remote functionalities for coupling to a peptide or other type of ligand are shown in Scheme 45, below.

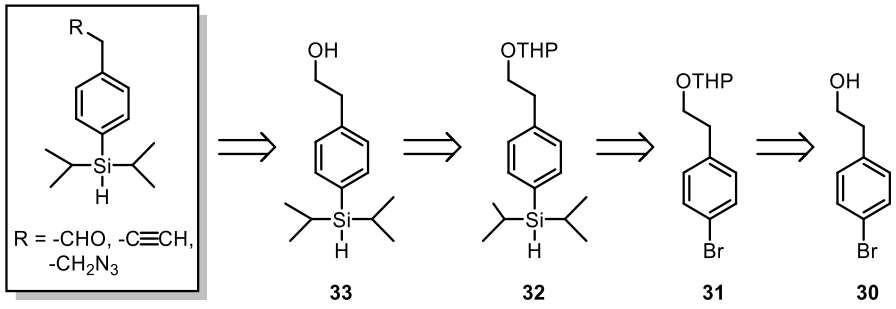

Scheme 45. Retrosynthetic approach to the diisopropyl-substituted silane analogues with remote functionalities.

We also looked at a possible retrosynthetic approach to some diisopropyl-substituted silane analogues with an additional oxygen linker, shown in Scheme 46 below. Looking towards analogues of remote functionalization and an oxygen linker can also allow for further investigations into reactivity of the different silyl ethers upon fluorination and hydrolytic stabilities of fluorosilanes due to the substitution pattern on the aromatic ring.

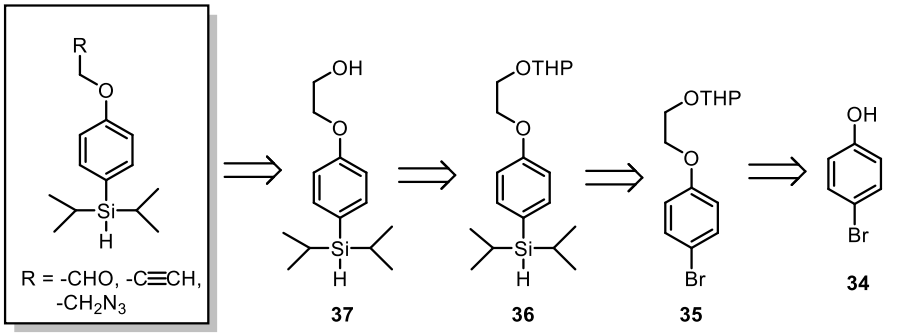

Scheme 46. Retrosynthetic approach to the diisopropyl-substituted silane analogues with oxygen-linker and remote functionalities.

Remote functionalization

Diisopropyl-substituted FOSi-precursors with various substituents in the *para*-position on the benzene ring were prepared based on the procedures reported by Mu *et al.*,[105] and on our previous experiences from the di-*tert*-butylsilyl analogues.

The first step towards compound **33** involved THP-protection of commercially available 2-(4-bromophenyl)ethan-1-ol (**30**) by DHP using PPTS as shown in Scheme 47. The THP-protected alcohol **31** was then lithiated in a halogen-lithium exchange reaction and subsequently reacted with *i*-Pr_2SiHCl to give silane **32.** THP-protected compound **32** was deprotected by using PTSA in EtOH, to give silane **33** in 31% yield over 3 steps, contaminated by *n*-butylated side-product (ratio **33**/**38**, 65:35).

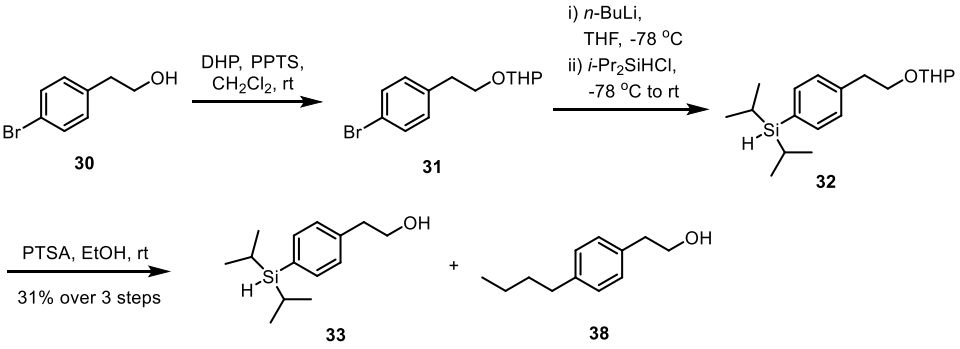

Scheme 47. Preparation of silane **33** from compound **30** over three steps.

Remote functionalization with oxygen linker

The first step towards compound **37** involved a Williamson ether synthesis between commercially available 4-bromophenol (**34**) and 2-(2-bromoethoxy)tetrahydro-2*H*-pyran (**39**) (Scheme 48). The ether synthesis was conducted with an excess of bromine **39** (1.5 eq.), which resulted in contamination of the product mixture (**35**/**39**; 85/15), based on integration of the ^{1}H NMR signals. Next, lithium-halogen exchange followed by electrophilic attack by *i*-Pr$_2$SiHCl gave **36**, which was taken to the next step without purification. Deprotection by PPTS in methanol afforded silane **37** in decent yield (55%) over two steps.

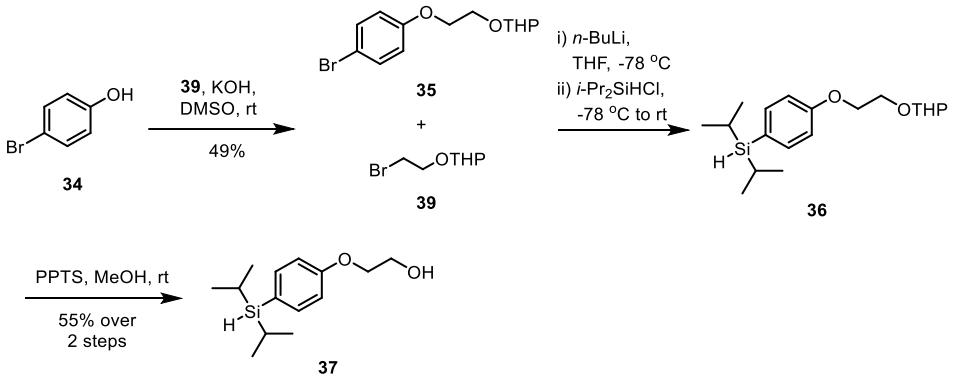

Scheme 48. Preparation of silane **37** from 4-bromophenol (**34**).

The next step was oxidation of the alcohol, which was attempted for compound **37**, by using Dess-Martin periodinane (DMP) without success (Scheme 49).

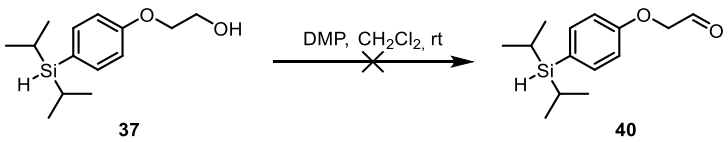

Scheme 49. Unsuccessful synthesis of aldehyde **40**.

^{1}H-NMR analysis of the crude product (Figure 32), revealed the presence of an aldehyde (signal at 9.87 ppm), although only in very small amounts. Also, for the characteristic diisopropyl-signals (two doublets around 1.5-0.8 ppm) multiple signals were observed, thus this approach was not pursued further at the time.

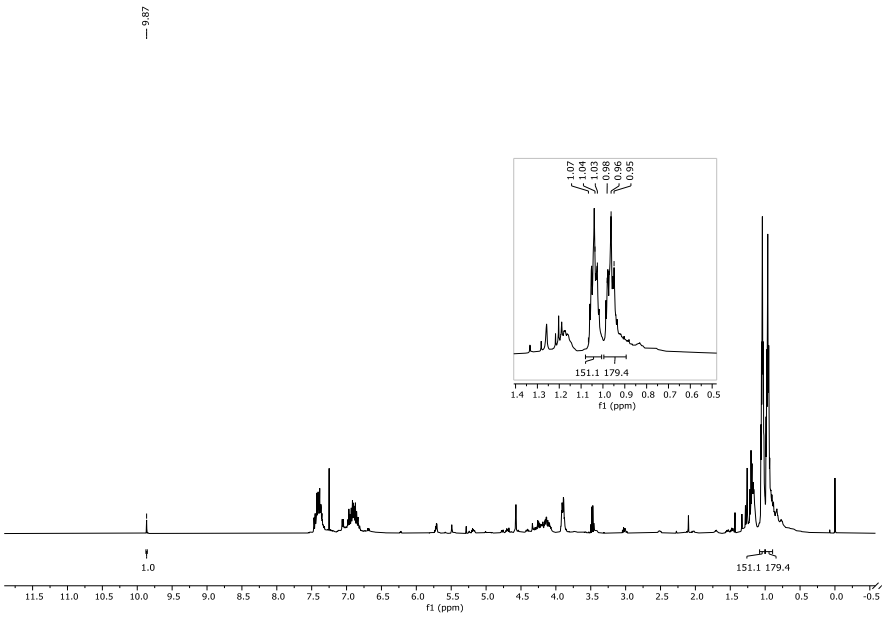

Figure 32. ^{1}H NMR of crude mixture after oxidation of **37**.

As we had encountered some difficulties transforming the functional groups of the silanes with remote functionality, an alternative was to prepare compounds with a benzylic aldehyde or azide instead.

Diisopropyl-substituted precursors modified in the benzylic position

Synthesis of diisopropyl-substituted silane **41** proved to be one of the key syntheses in this work as it provided a valuable building block towards different varieties of FOSi-precursors. Compound **41** was obtained through a lithium-bromine exchange reaction using 2.5 eq. of *n*-BuLi to ensure deprotonation of the alcohol at the same time as the bromine is exchanged (Scheme 50). Different work-up protocols and reaction times were explored, based on previous reports,[105,107,110,114] and we found that one hour reaction time for the lithiation was sufficient, and the silylation step required an overnight reaction using 1.2 eq. of *i*-Pr_2SiHCl. This reaction usually provided yields around 61-86% after purification by flash chromatography. Variation in yield can be explained by the exploration of different cooling baths to achieve −78 ºC, where the N_2/acetone-bath was superior in keeping the desired temperature throughout the first step.

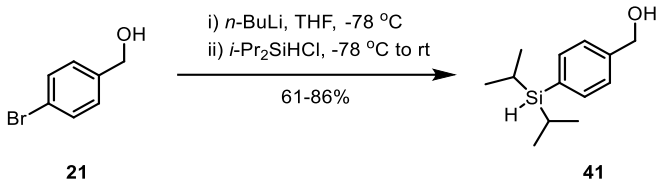

21 **41**

Scheme 50. Synthesis of silane **41** from 4-bromobenzalcohol (**21**).

Silane **41** was used further to prepare silane **42** by treatment with DBU and DPPA in DMF as reported by James *et al.*[112] (Scheme 51). This reaction led to full conversion after stirring overnight. The product could be extracted with pentane to give 60% yield or subjected to an aqueous work-up followed by purification by flash chromatography to give **42** in 77% yield.

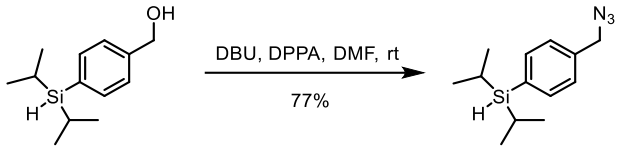

41 **42**

Scheme 51. Synthesis of silane **42**.

In 2017, Jana *et al.*[110] reported a procedure for direct chlorination of 4-(diisopropyl-silyl)benzaldehyde (**43**) using trichloroisocyanuric acid (TCICA) followed by reaction with methanol in the presence of imidazole to give 4-(diisopropyl(methoxy)silyl)-benzaldehyde (**44**) in good yield, as shown in Scheme 52.

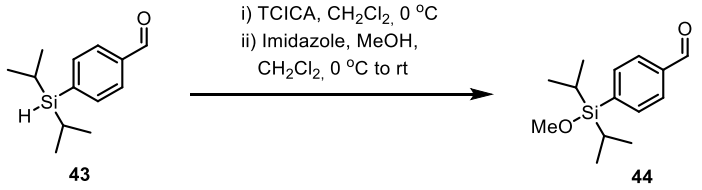

43 **44**

Scheme 52. Procedure published by Jana *et al.*[110]

Ohkubo and co-workers[198] published a similar protocol in 2009, with an azide as benzylic functionality, using 1,3-dichloro-5,5-dimethylhydantoin as chlorinating agent. They reported a two-step *in situ* process, with no work-up between the chlorination and the silylation step.

Inspired by the protocols of Ohkubo *et al.*[198] and Jana *et al.*[110] we prepared compound **45** using TCICA as chlorinating agent in the first step, and subsequently

adding imidazole and ethyl 6-hydroxyhexanoate (**29**) in the second step. Silyl ether **45** was isolated in good yield (78%), as shown in Scheme 53. These reactions are very sensitive to water and strictly anhydrous conditions are required, as the formation of hydroxysilane (Si-OH) competes with silyl-ether formation (Si-OR) if there is any water present.

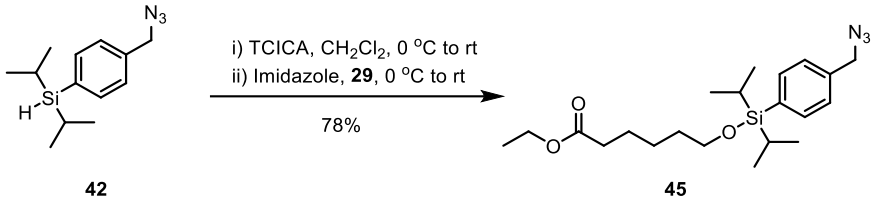

42 **45**

Scheme 53. Synthesis of silyl ether **45** in subsequent two steps.

The first silyl ether to be used for further development of the FOSi-method had been prepared. The ester functionality will in turn be hydrolyzed and attached to an amine-resin, whilst the azide will be reacted with an alkyne moiety on a biologically active molecule in a so-called click-chemistry reaction.

Since we were interested in having an aldehyde group in the molecule from the start, we also wanted to make the diisopropyl-substituted aldehyde analogues in the same manner. Several different approaches were tested to obtain benzylic aldehyde **43**. To start, preparation of the acetal-protected aldehyde **46** was attempted in the same way as for the di-*tert*-butyl-substituted silanes, resulting in 35% yield of **46**, contaminated with the *n*-butylated side-product after purification (**46**/**47**; 7:3) (Scheme 54). This strategy was dismissed.

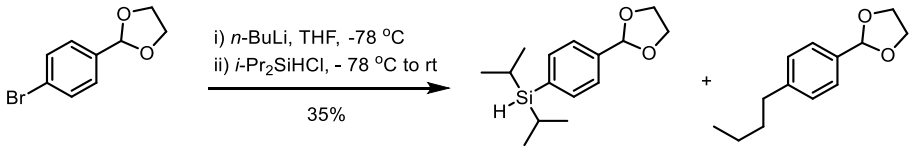

9 **46** **47**

Scheme 54. Synthesis of acetal protected aldehyde **46**.

Since benzylic alcohol **41** already had been prepared, oxidation of this compound was an apparent strategy. Use of DMP was as the oxidizing agent successfully gave aldehyde **43** in the first attempt, but this could not be reproduced (Scheme 55). All

further attempts at this reaction only gave crude mixtures containing multiple compounds which were difficult to separate.

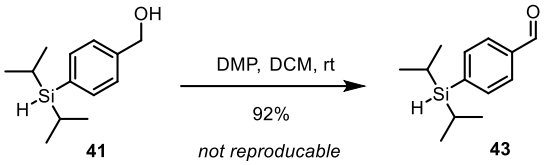

Scheme 55. Non-reproduceable oxidation of benzylic alcohol **41**.

Instead, aldehyde **43** was prepared from alcohol **41** in excellent yield using manganese(IV)dioxide as oxidizing agent, as described by Chen *et al*.[195] and Jana *et al.*[110] (Scheme 56). Simply passing the reaction mixture through a pad of Celite was sufficient to provide **43** in high purity.

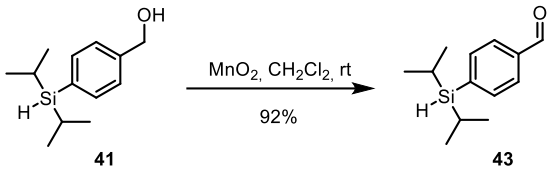

Scheme 56. Oxidation of alcohol **41** to aldehyde **43**.

As we had tested the Bestmann-Ohira modification of the Seyferth-Gilbert homologation reaction, for the di-*tert*-butyl substituted analogues with success, we wanted to try this for the diisopropyl-substituted silane as well, to get access to alkyne **48** (Scheme 57). This did not provide the desired result, as the base K_2CO_3 acted as a dehydrogenative coupling-catalyst in the silyl-ether formation between **41** and methanol, giving methoxysilane **49** as the main product.

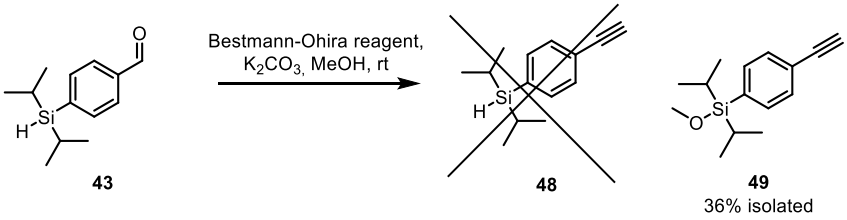

Scheme 57. Ohira-Bestmann reaction resulting in compound **49**.

Continuing with aldehyde **43** from the MnO_2-oxidation, silyl ether **50** was prepared using similar conditions as for azide analogue **45**. Chlorination by TCICA in the first

step followed by subsequent reaction with 3-butyn-1-ol (**27**) and imidazole gave the desired silyl ether **50** in 58% yield (Scheme 58).

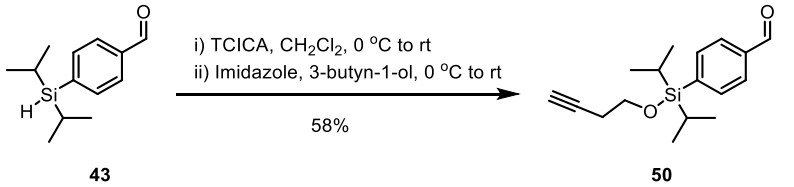

Scheme 58. Synthesis of silyl ether **50**.

Revisiting the di-tert-butyl analogues

Having had success preparing diisopropyl-silyl ethers, we looked back at the di-*tert*-butyl analogues, to see if we could prepare these highly sterically-hindered silyl ethers. Results of the attempted alcohol silylations of the di-*tert*-butyl analogues are summarized in Table 8 on page 86.

Since methoxysilane **49** was produced in the presence of K_2CO_3 and MeOH, similar conditions were applied to di-*tert*-butyl-substituted analogue **25** as well, yet no reaction was observed. Addition of DMF and heating to 60 ºC led to some conversion of starting material (Scheme 59; Table 8, entry 1), however, the hydroxysilane was the major product. We did not attempt this reaction using alcohol **29** (or similar) due to the low yield with MeOH.

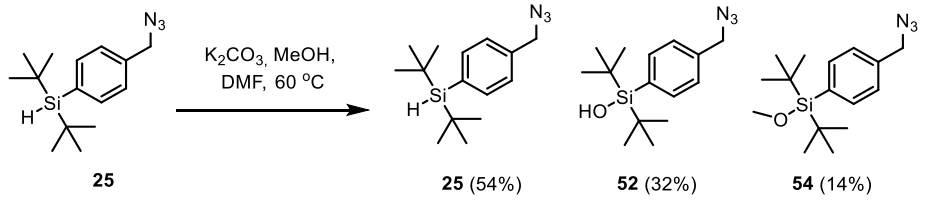

Scheme 59. Base-catalyzed reaction between **25** and MeOH.

We then turned to using TCICA toward preparing a di-*tert*-butyl-substituted silyl ether based on the successful results from the diisopropyl-substituted analogues. We wanted to establish if the Si-O bond formation was possible using MeOH as the alcohol source, and this gave a mixture of hydroxysilane **52** (60%) and methoxysilane **54** (40%) (Scheme 60; Table 8, entry 3).

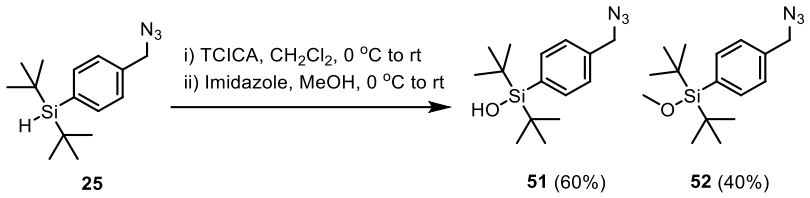

Scheme 60. Silylation of **25** by MeOH.

Encouraged by these results, we continued with the same conditions using alcohol **29** and silane **25** (Scheme 61; Table 8, entry 3). Unfortunately, target compound **53** could not be obtained, instead, chlorosilane **51** and hydrolyzed starting material were isolated in 62% and 38% yield, respectively.

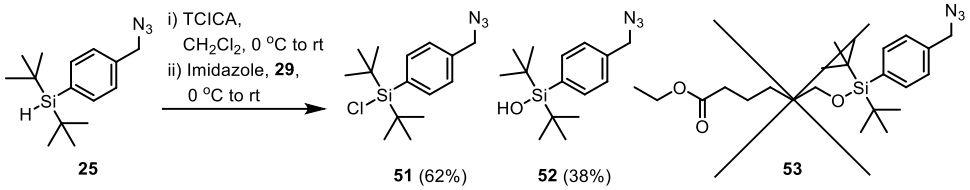

Scheme 61. Attempt at silylation of compound **25**.

The isolated chlorosilane **51** was then submitted to the reaction conditions that had been attempted previously (Table 6, entry 13), as shown in Scheme 62 below. The desired silyl ether **53** was not obtained in this reaction either, only hydroxysilane **52** (isolated in 50% yield) and unreacted **51** were present in the crude mixture (Table 8, entry 2).

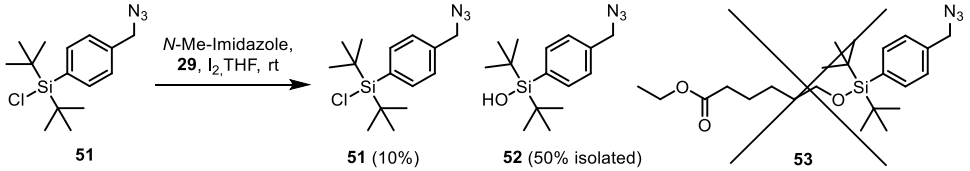

Scheme 62. Attempt at preparing **53** from chlorosilane **51**.

Next, silane **25** was submitted to chlorination using TCICA in CH_2Cl_2 and further reacted with alcohol **29**, imidazole and DMF while heating to 40 ºC overnight in the second step (Scheme 63; Table 8, entry 5). Silyl ether **53** was obtained in 13% yield. Heating to 60 ºC for another 18 h did not improve the yields further.

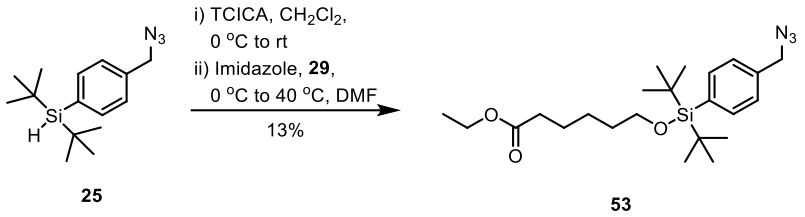

Scheme 63. Preparation of compound **53**.

Table 8. Attempted silyl-ether formations with azide precursor.

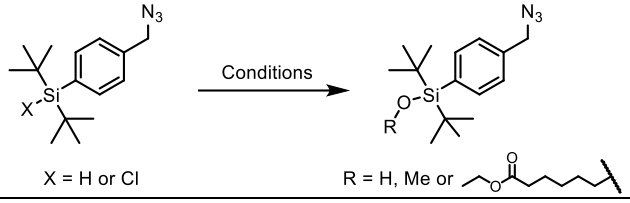

Entry	Si-X	Reagent (equiv.)	Base	Solvent	Yield[c] Si-X/Si-OH/Si-OR (%)
1	Si-H[a]	MeOH (10)	K_2CO_3	-	56/33/11
2	Si-Cl	**29** (2)	*N*-Me-Im, I_2	THF	10/90/0
3	Si-Cl	MeOH (10)	Imidazole	CH_2Cl_2/DMF	0/60/40
4	Si-Cl	**29** (2)	Imidazole	CH_2Cl_2/DMF	0/100/0
5	Si-Cl[b]	**29** (10)	Imidazole	CH_2Cl_2/DMF	50/25/25

All reactions: overnight, under argon, at rt unless otherwise noted.
[a] Added 100 mg NaOH and stirred overnight at 60 ºC.
[b] Stirred overnight at 40 ºC
[c] Not isolated yields. Based on ^{1}H NMR integration.

These results showed that silyl-ether formation of bulky di-*tert*-butyl analogues was possible, though it was challenging to obtain the desired product with the relevant alcohol **29**, as just a minor presence of water competes with the alcohol and hydrolyzes the silane. Dry conditions are crucial for the outcome, and it seems from these results that chlorosilanes are the most promising starting point compared to silanes.

Synthesis of di-tert-butyl aldehyde precursor

Preparation of the aldehyde-functionalized silyl ether, that was supposed to be the starting point of this work, had proven to be quite challenging to achieve using protected aldehydes. Utilizing benzylic alcohol **22** as the starting point, oxidation by manganese(IV)oxide to aldehyde **5** was obtained (Scheme 64), in the same way as for the diisopropyl analogue.

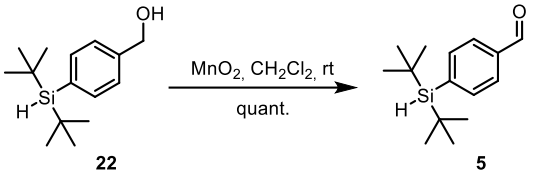

Scheme 64. Oxidation of compound **22** to aldehyde **5**.

Reacting aldehyde **5** further with 3-butyn-1-ol (**27**) to achieve desired silyl ether **26** was attempted once, yet only the hydrolyzed product could be isolated (Scheme 65). We could potentially have changed the alcohol to MeOH or ethyl 6-hydroxyhexanoate (**29**) to see if this would affect reactivity, but we decided to abandon this approach.

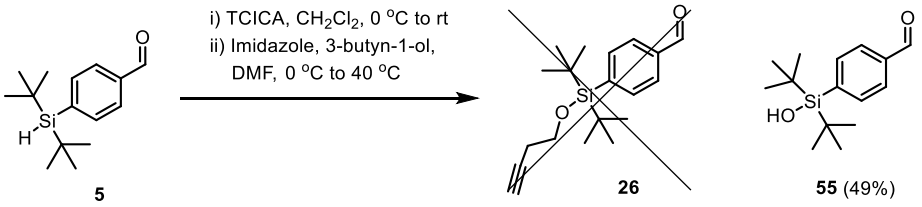

Scheme 65. Unsuccessful synthesis of compound **26**.

Synthesis of mono- and dimethyl-phenyl-substituted analogues

At this point we had successfully prepared silyl ether **53**, but only in very low yield (13%). Since the hydrolytic stability of fluorosilanes seemingly is related to the substitution pattern next to the silane on the aryl substituent (Section 3.3), we decided to shift focus, and pursue analogues with one or two methyl groups in the *ortho*-position to the silane in order to make a complete library of differently substituted silyl ethers.

At first, we sought a simple construct to test fluorination under cold conditions, and reasoned that an ester substituent on the aryl substituent could be a fitting start. Ester **56** is commercially available, and we proposed a simple route to prepare precursor **58** (alternative 1), and a second route to prepare the azide and aldehyde functionality we had already established synthetic protocols for. The proposed synthetic route from **56** to **58**, a very simple construct to test fluorination without too much modification, is shown in Scheme 66 (Alt 1). Another alternative (Scheme 66, Alt 2) was reduction of

the ester (**56**) and further oxidation to aldehyde and/or making the azide, as for the non-methyl analogues.

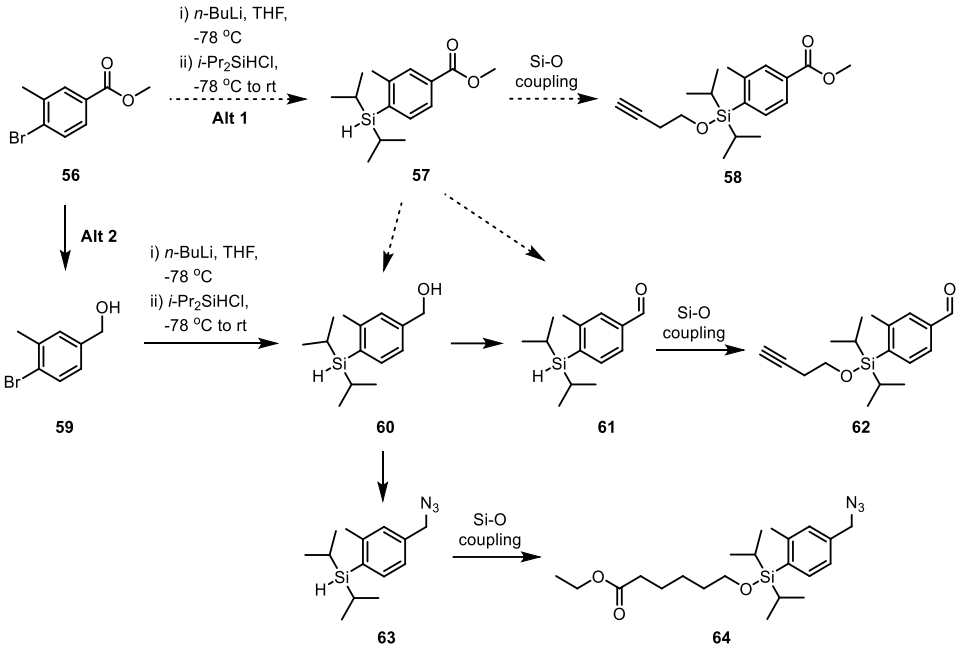

Scheme 66. Proposed synthetic route to FOSi-precursors **58**, **62** and **64**.

We hypothesized that the lithiation reaction would be difficult with an ester present (**56**), and one attempt at preparing silane **57** directly from **56** also failed. We then moved to alternative 2, to retrieve silane **60**. Benzylic alcohol **59** was not commercially available and had to be prepared from ester **56** (Scheme 67). We initially planned to use $LiAlH_4$, which is the most common reducing agent from esters to alcohols, but this was not available in the lab at the time, thus $NaBH_4$ was used instead. Reduction of esters and similar functional groups using $NaBH_4$ is described as relatively difficult, however, the reactivity of sodium borohydride can be enhanced by carrying out the reaction in the presence of certain additives. For example, addition of iodine to $NaBH_4$ in THF provides H_3B-THF, which is useful for hydroborations, reduction of esters[199] and various others functional groups.[200] The $ZnCl_2$-$NaBH_4$ reagent system also exhibits powerful reducing properties in the presence of tertiary amine and provides another example of esters reductions.[201] In 1984 Soai and co-workers[202] published a procedure where esters were reduced by sodium borohydride

in a mixed solvent system where they studied the effect of slow addition of methanol. This was also reported by Boechat *et al.*[203] in 2004, with consistently high yields for multiple substrates. The latter procedure was tested for the reduction of ester **56** to give benzylic alcohol **59** in excellent yield.

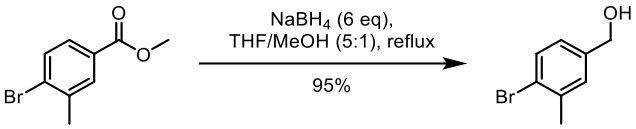

56 **59**

Scheme 67. Reduction of ester **56** to alcohol **59** using sodium borohydride.

After reducing the ester, the previously developed procedure for preparing silyl ethers was performed and successfully yielded silyl ether **64** (Scheme 68).

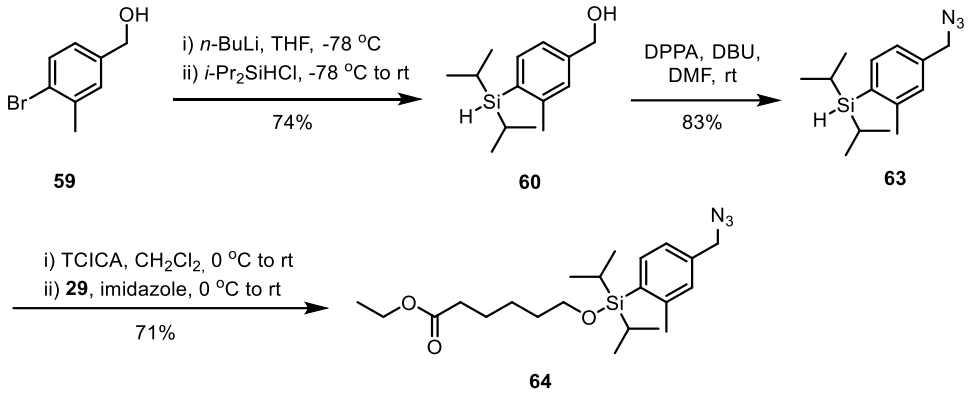

59 **60** **63**

64

Scheme 68. Synthesis of mono-methyl *o*-substituted silyl ether **64** in three steps.

During characterization of silane **60**, it became evident that is was poorly ionizable using ESI-HRMS, thus the analysis had to be carried out using GC-HRMS(EI+). The diisopropyl-containing silanes and silyl ethers displayed a characteristic fragmentation pattern in these analyses, as depicted in Scheme **69**.

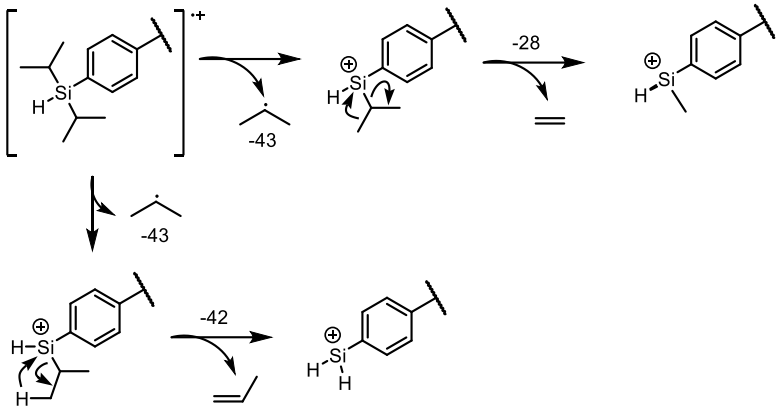

Scheme 69. Proposed GC-MS fragmentation of diisopropyl-substituted silanes and silyl ethers.

The proposed GC-MS fragmentation pattern is represented by example of compound **60** in Figure 33.

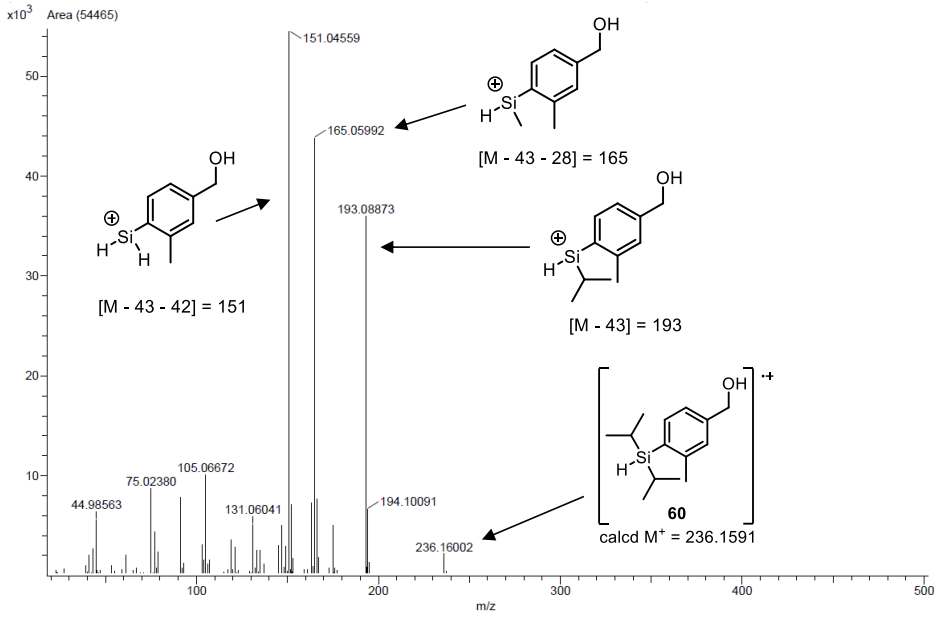

Figure 33. Example of GC-MS fragmentation of diisopropyl-substituted **60**.

Benzyl alcohol **65**, which was required for the preparation of silyl ether analogues with two *ortho*-methyl groups, and for silyl ether bearing an azide group, was carried out as shown in Scheme 70.

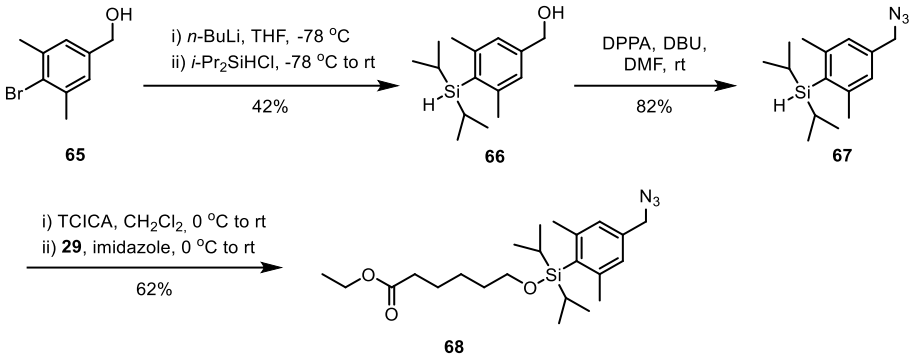

Scheme 70. Synthesis of di-methyl *o*-substituted silyl ether **68**.

Since we had silanes **60** and **66** at hand, we also prepared the aldehyde-containing silyl ethers with mono- and di-methyl substitution, compounds **69** and **70**, over two steps as shown in Scheme 71.

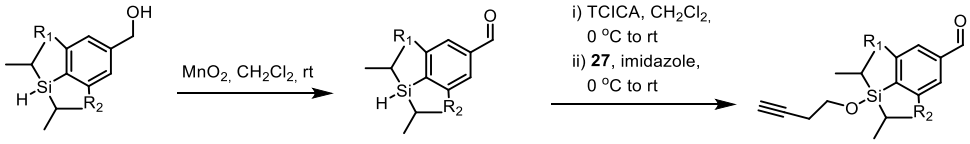

60: R_1 = Me, R_2 = H
66: R_1 = Me, R_2 = Me

61: R_1 = Me, R_2 = H, 90%
62: R_1 = Me, R_2 = Me, 84%

69: R_1 = Me, R_2 = H, 70%
70: R_1 = Me, R_2 = Me, 68%

Scheme 71. Synthesis of **69** and **70**.

A new, simple structure for test-fluorination

After preparing analogues with relevant functionalization, we decided that a very simple construct of these silanes would be an efficient way of testing fluorination without too much functionality in place. Therefore, silanes **75** and **76** were prepared, as shown in Scheme 72 below.

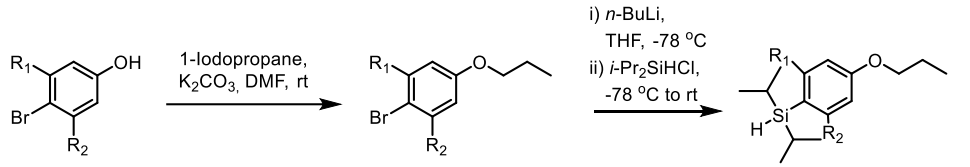

71: R_1 = Me, R_2 = H
72: R_1 = Me, R_2 = Me

73: R_1 = Me, R_2 = H, 93%
74: R_1 = Me, R_2 = Me, 93%

75: R_1 = Me, R_2 = H, 97%
76: R_1 = Me, R_2 = Me, 95%

Scheme 72. Synthesis of mono- and di-methyl *o*-substituted silanes **75** and **76**.

Direct synthesis of di-*tert*-butylchlorosilane **78** was also attempted as shown in Scheme 73. This was unsuccessful, and the main product was the *n*-butylated side-product **79**.

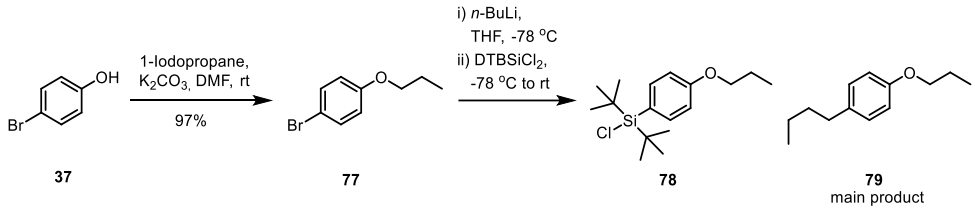

Scheme 73. Attempt at direct preparation of chlorosilane **78**.

Silyl-ether formation turned out to be troublesome in the next step, as both the ether-oxygen and the methyl groups are *ortho-para* directing, resulting in chlorination of the aromatic ring as well as chlorination of the silane by TCICA, resulting in low yield of **80** and no trace of **81** (Scheme 74).

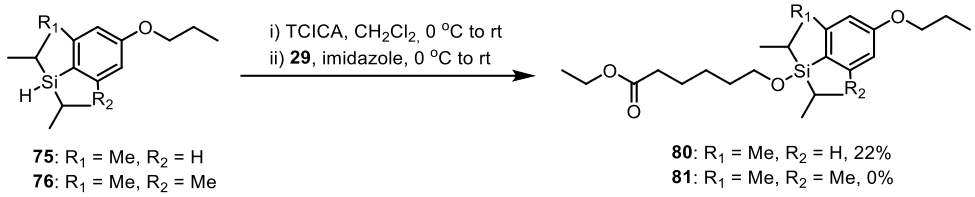

Scheme 74. Synthesis of silyl ethers **80** and **81**, resulting in low yield of **80** and no trace of **81**.

Another synthetic pathway to the di-methyl *ortho*-substituted silyl ether (**81**) was by applying basic conditions in a dehydrogenation reaction. This was attempted for silyl ether **81** following the procedure by Grajewska *et al.*[204], though no product was observed after several days of stirring (Scheme 75).

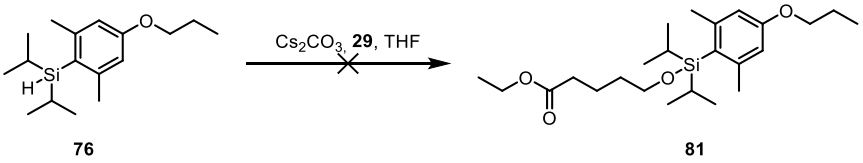

Scheme 75. Unsuccessful synthesis of silyl ether **79.**

Successful synthesis of mono-methyl *ortho*-substituted analogue **80** allowed for the initial fluorination experiments, i.e. breaking of the Si-O bond, which is discussed further in section 3.5.

Mono- and di-methyl substituted diisopropyl analogues with remote functionalization

In order to show that these ether-linked analogues could be functionalized further, we also prepared analogues containing a primary alcohol (Scheme 76) that we envisioned could be further converted to the required functional group for attachment to a peptide or other ligand.

These silanes were prepared based on reports by Mu *et al.*[105] with various substitution patterns. The first step towards compound **86** and **87** involved a Williamson ether synthesis between commercially available 3-methyl-4-bromophenol (**71**) and 3,5-dimethyl-4-bromophenol (**72**) and THP-protected alcohol **39**, followed by purification by flash chromatography. Next, lithium-halogen exchange followed by nucleophilic attack by *i*-Pr_2SiHCl to afford **84** and **85**, which was taken to the next step without purification. Deprotection by either PTSA (mono-methyl) or PPTS (di-methyl) in ethanol afforded silanes **86** and **87** in decent yields over two steps (Scheme 76). When attempting to deprotect the THP-protected alcohol **85** with 1 eq. PTSA in ethanol, desilylation was observed as well as deprotection of the alcohol. Therefore, a less acidic catalyst, PPTS, was utilized for this analogue.

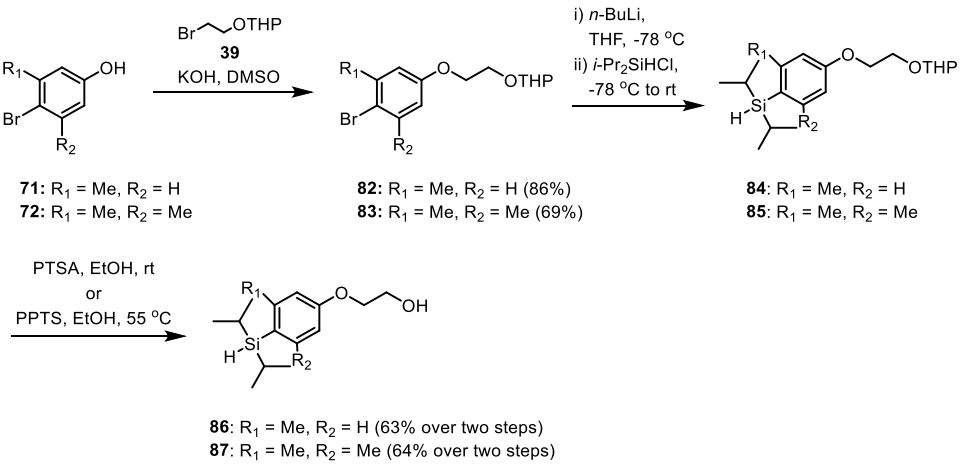

Scheme 76. Synthesis of functionalized analogues **86** and **87**.

As the synthesis of the di-methyl *ortho*-substituted silyl ether **81** was troublesome, we decided to not pursue this molecule and instead pursued model compounds without the handle to attach peptides or other ligands.

Benzene analogues

Diisopropyl analogues without a handle were prepared using the same reaction conditions as for previous analogues (Scheme 77). The aim of making these analogues was to have reference compounds to test fluorination conditions with no interference from other functional groups. Synthesis of compounds **94**, **95** and **96** was achieved in good yields over two steps.

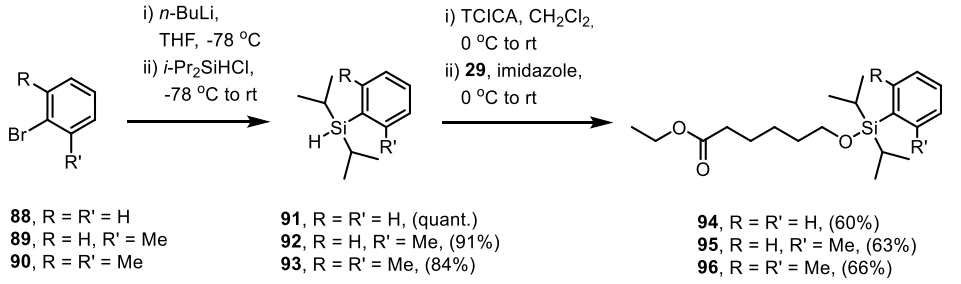

Scheme 77. Synthesis of benzene-analogues **94**, **95** and **96**.

The di-*tert*-butyl-benzene analogue (**98**) was also prepared as shown in Scheme 78, though in lower yield than for the diisopropyl-substituted silyl ethers.

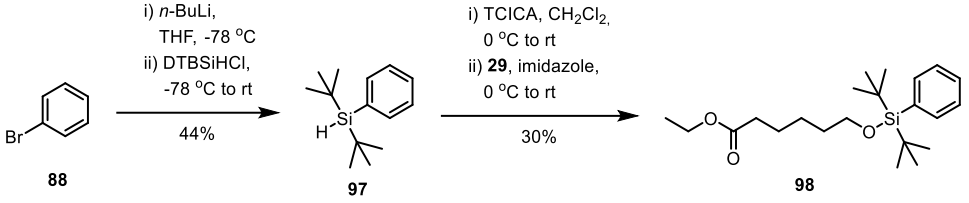

Scheme 78. Synthesis of di-*tert*-butyl-substituted analogue **98**.

These non-functionalized analogues were used for exploration of fluorination conditions, discussed further in section 3.5.

Summary of synthesized silyl ethers

Many different silyl ethers have been prepared, some with possibilities for further coupling, and some with less functionalization which were synthesized mainly to test and develop the FOSi-method. An overview of silyl ethers prepared in this work is shown in Figure 34 below.

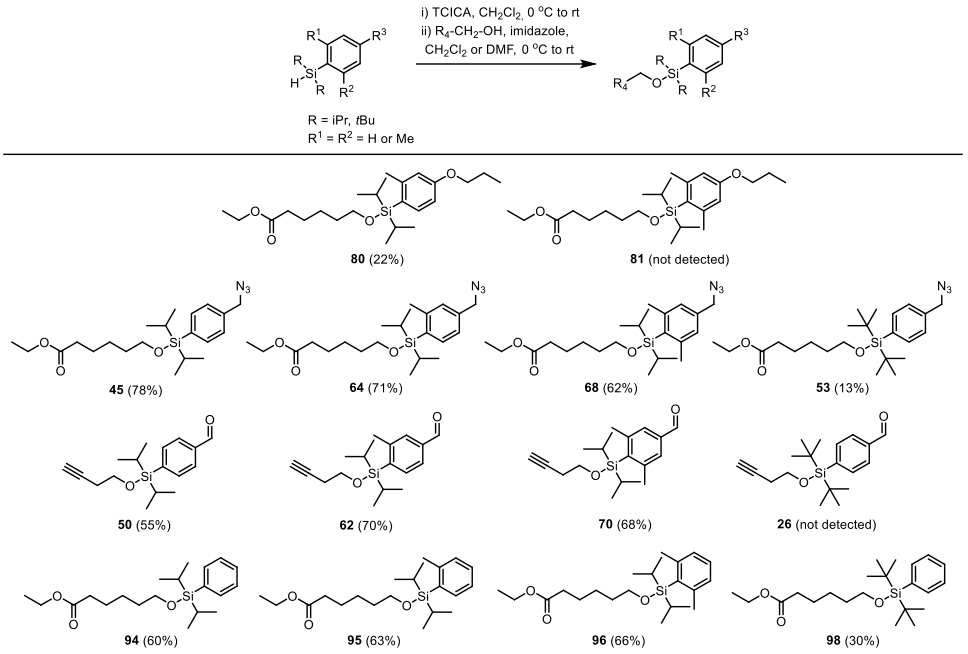

Figure 34. Overview of silyl ethers prepared in this work.

3.5 Fluorination of silyl ethers

Synthesis and fluorination of FOSi-precursor 1

For cold off-resin testing, to follow Si-O bond-cleavage easier than on-resin, both ends of the previously described diisopropyl-substituted silyl ethers were modified accordingly to simulate "peptide-like" behavior. For this purpose, ester **45** was hydrolyzed and the resulting carboxylic acid **99** was coupled to glycinamide (**100**) before the azide was reacted with propiolamide (**102**) in a Huisgen-Sharpless reaction to give FOSi-precursor 1 (**103**).

The first attempt at ester hydrolysis of compound **45** was conducted as described by Baumann *et al.*,[205] although after multiple additions of lithium hydroxide, no reaction

was observed and the starting material was recovered. Changing to sodium hydroxide as base and using a mixture of CH_2Cl_2 and MeOH as solvent, conditions reported by Theodorou *et al.*,[206] gave full conversion of ester **45** to carboxylic acid **99** (Scheme 79).

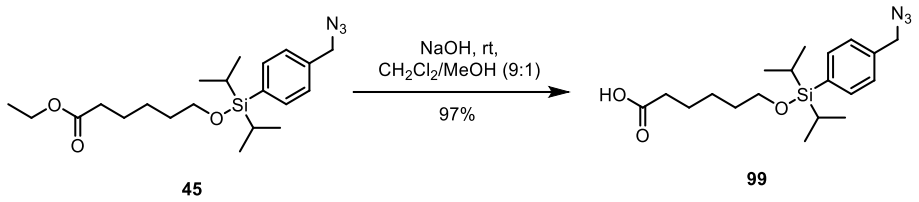

Scheme 79. Hydrolysis of ester **45**.

Next, glycinamide (**100**) was coupled to the carboxylic acid under standard coupling conditions in good yield and finally the copper-catalyzed Huisgen-Sharpless cycloaddition step was performed as described by Harmsen *et al.*[207] with slightly adjusted conditions (Scheme 80). The last step was performed with ascorbic acid and sodium carbonate, with CH_2Cl_2/H_2O as solvent system, which provided the desired triazole **103** in 14% yield over the six steps. This synthetic pathway currently requires four purifications by flash chromatography.

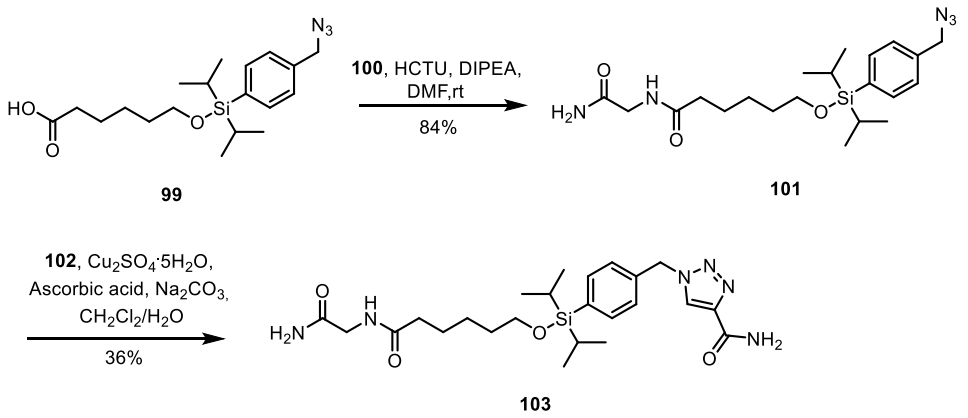

Scheme 80. Synthesis of FOSi-precursor 1 (**103**).

Fluorination of the FOSi-precursor 1 (**103**) was tested by using TBAF in THF (Scheme 81). Stirring at room temperature resulted in full conversion of starting material based on TLC-analysis after 30 min.

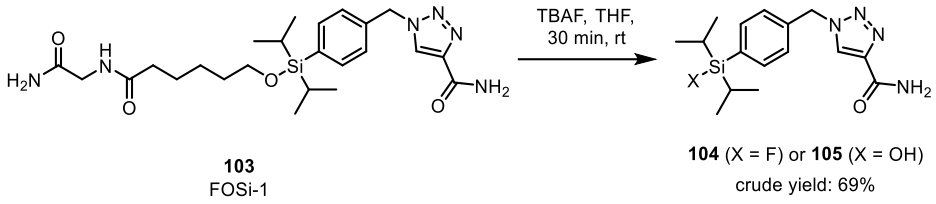

Scheme 81. Fluorination by TBAF in THF.

We speculate that fluorosilane **104** was most likely produced in the reaction, but it could have been converted to Si-OH (confirmed by ^{1}H NMR broad singlet signal at 2.64 ppm, Figure 35) during aqueous work-up, or in the NMR-solvent.

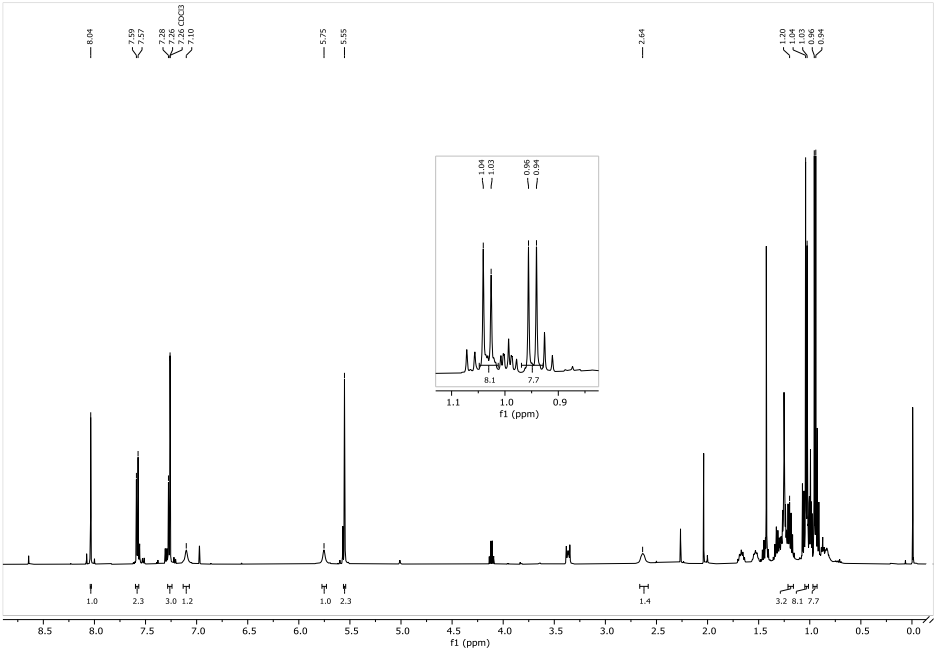

Figure 35. ^{1}H NMR spectrum after fluorination of FOSi-precursor 1 (**103**).

Presence of hydroxysilane **105** ($[M+H]^+$ = 333.2, $[M+Na]^+$ = 355.2) was confirmed by LRMS-analysis (Figure 36).

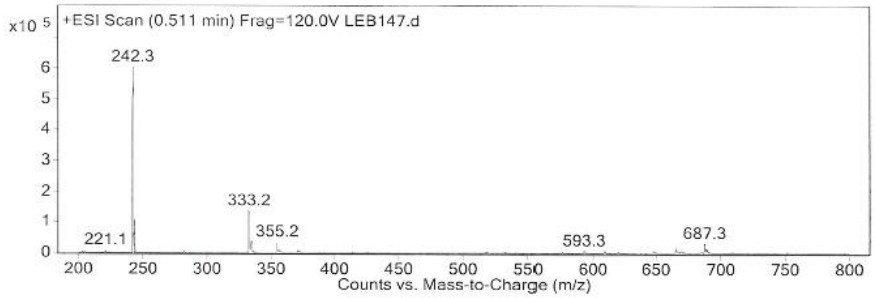

Figure 36. LRMS of crude mixture after fluorination of **103** with TBAF; TBAF: $[M+H]^+$ = 242.3; **104** (Si-F): $[M+H]^+$ = 335.2; **105** (Si-OH): $[M+H]^+$ = 333.2, $[M+Na]^+$ = 355.2

Synthesis and fluorination of modified FOSi-precursor 2

To prepare FOSi-precursor 2 (**111**) aldehyde-substituted silyl ether **50** was attached to an aminooxy-component **108** to simulate a peptide, which was prepared from compound **106** and benzylamine (**107**) in two subsequent steps. The first step towards compound **108** involved a standard coupling reaction using HCTU and DIPEA in DMF, subsequent deprotection of the Boc-group gave desired building block **108** in 67% yield (Scheme 82).

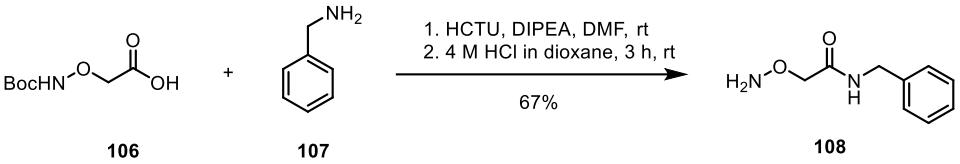

Scheme 82. Coupling compound **106** to benzylamine (**107**) to attain compound **108**.

Aldehyde **50** and the aminooxy-component **108** were then dissolved in CH_2Cl_2 with pyridine as base, as described by Gantt *et al.*,[208] to form oxime **109** in good yield (Scheme 83). The last step entailed connecting alkyne **109** to azidobenzene (**110**) in a cycloaddition reaction. The conditions were adjusted during the course of the reaction, and the solvent system was changed in order to get a better conversion (from CH_2Cl_2 to *tert*-butanol) following a procedure by Rostovtsev *et al.*,[155] which eventually resulted in full conversion of starting material to form FOSi-precursor 2 (**111**). The low yield can be explained by a suboptimal flash chromatography, where the product remained on the silica column due to use of inappropriate solvent system, which can be improved in future attempts.

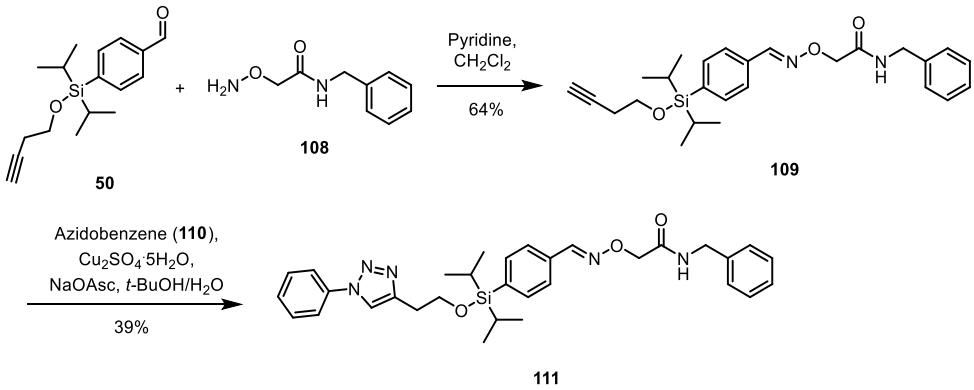

Scheme 83. Synthesis of FOSi-precursor 2 (**111**).

Fluorination of FOSi-precursor 2 (**111**) was performed, using KF and Kryptofix[2.2.2], as shown in Scheme 84. Stirring at room temperature for 45 minutes resulted in full conversion of starting material based on TLC-analysis.

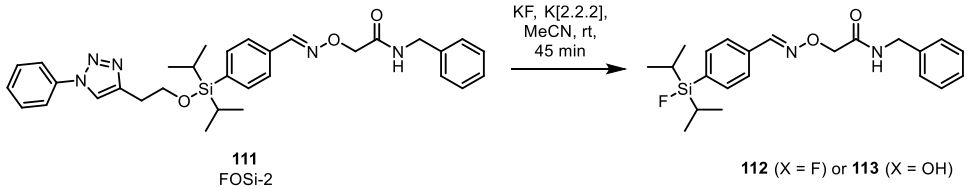

Scheme 84. Fluorination of **111**, using KF as fluoride source.

The crude mixture was filtered through an SPE-cartridge, then directly dissolved in $CDCl_3$ to perform NMR-analysis. The tube was left at rt overnight and then MS was performed. The NMR-spectrum (Figure 37) confirms there is only one diisopropyl-containing compound present, and that the Si-O bond has been cleaved. It was nevertheless difficult to confirm whether it is fluorosilane (**112**) or hydroxysilane (**113**).

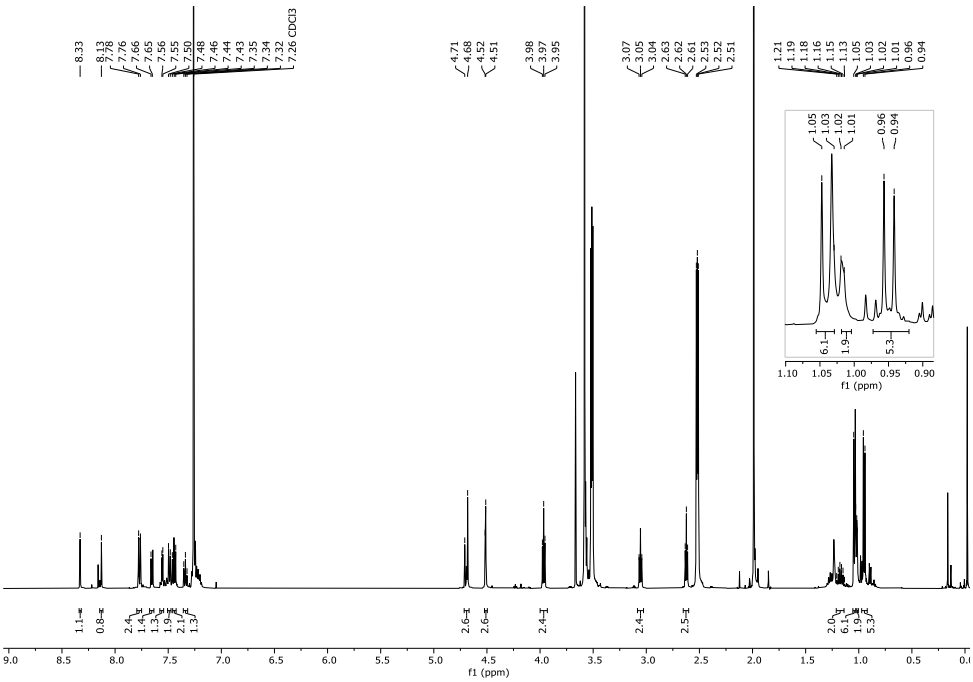

Figure 37. ^{1}H NMR spectrum after fluorination of **111** with KF/K222, and filtering through SPE-cartridge.

The MS-analysis mostly displays ionized Kryptofix[2.2.2] ([M+H]$^{+}$ = 377.3, [M+Na]$^{+}$ = 399.2), which overshadows signals from the product to a large extent (Figure 38). It should be noted that ionization of different compounds varies, and that some molecules are easily ionized and will be dominant in an ESI spectrum. Also, fluorosilane (**112**) might be hydrolyzed in the MS-analysis.

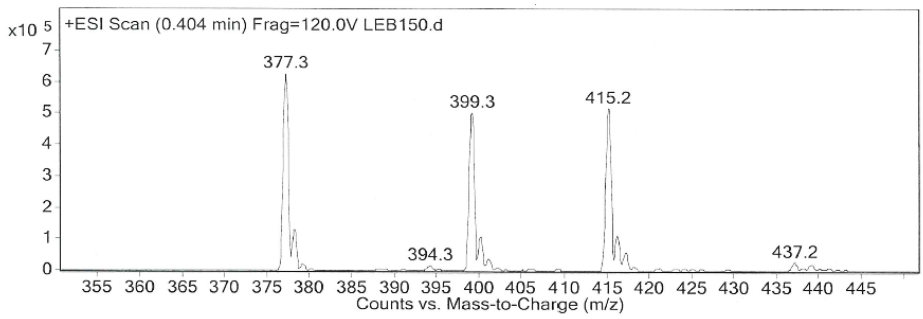

Figure 38. LRMS of crude product after SPE-cartridge filtration; Kryptofix:[M+H]$^{+}$ = 377.3, [M+Na]$^{+}$ = 399.2, [M+K]$^{+}$ = 415.2; **112** (Si-F): [M+H]$^{+}$ = 401.2, [M+K]$^{+}$ = 439.2; **113** (Si-OH): [M+H]$^{+}$ = 399.2, [M+K]$^{+}$ = 437.2

These fluorination attempts confirmed what we hoped, that the Si-O bond is broken in these reactions. Still, we did not have enough data to conclude whether the Si-F or the Si-OH compounds were produced in these reactions. Unfortunately, our 500 MHz NMR-instrument quenched at a very inconvenient time for this project, leaving us without ^{29}Si NMR and ^{19}F NMR when these reactions were performed. For further tests of the fluorination we decided that these starting materials were too complex for method development, and looked into using simpler molecules to test the FOSi-method. We therefore turned to analogues that could be analyzed by GC-MS, as most of the previously prepared analogues were not ionizable using ESI-MS.

Fluorination of ether-linked analogue

Fluorination of ether analogue **80** (for synthesis, see section 3.4), was carried out using KF and K[2.2.2] as shown in Scheme 85. We observed full conversion of starting material (by TLC-analysis) after 2 h and achieved an isolated yield of 46% after filtering through an SPE-cartridge.

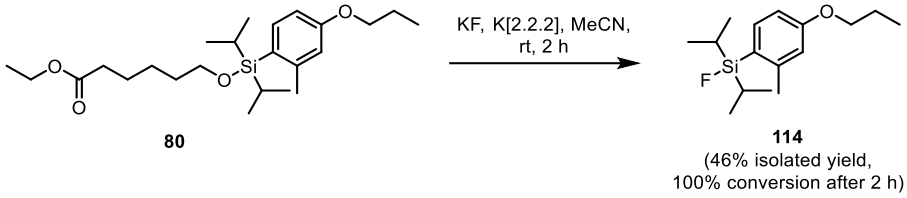

80 **114** (46% isolated yield, 100% conversion after 2 h)

Scheme 85. Successful fluorination of mono-methyl ether-analogue **80**.

The ^{1}H NMR-spectrum shown in Figure 39 confirms there is only one diisopropyl-containing moiety present (the two 6*H*-doublets around 1.05-0.90 ppm).

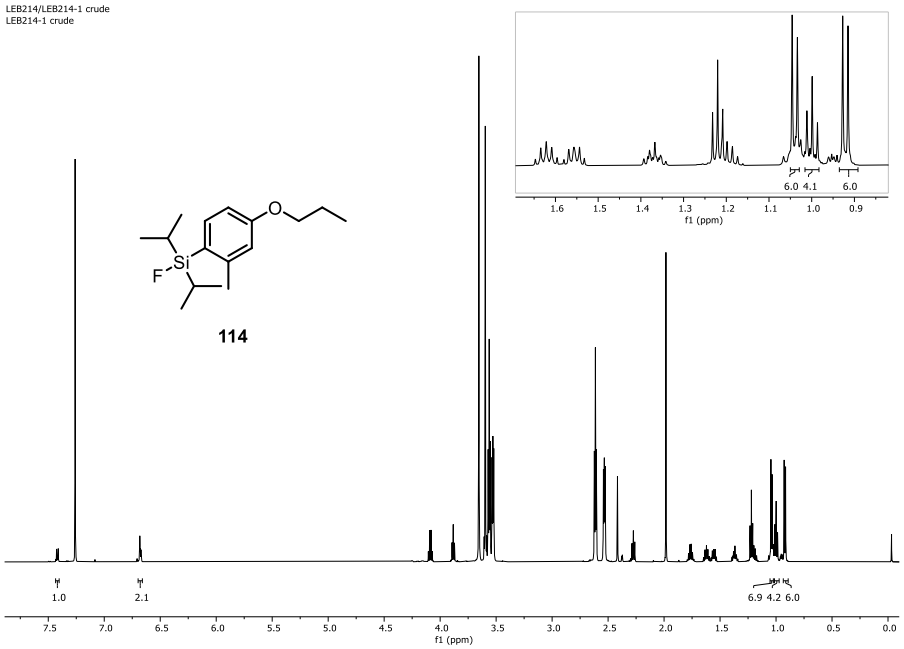

Figure 39. ^{1}H NMR-spectrum of compound **114**.

GC-MS analysis of **114**, shown in Figure 40, revealed four major peaks. The peak detected at Rt = 10.221 corresponded to the mass of the fluorinated compound **114** (exact mass = 282.1815, Figure 41), which confirms that the desired product was formed. The peak detected at Rt = 12.666 corresponds to the mass of the hydrolyzed fluorosilane (Si-OH, **115**). From the ^{1}H NMR analysis, which was performed directly after synthesis, clearly only one compound with a diisopropylsilyl-group is present. Hydrolysis of the fluorosilane could have happened during the GC-MS analysis (not anhydrous solvent, 300 ºC), or a minor amount was present in the crude product.

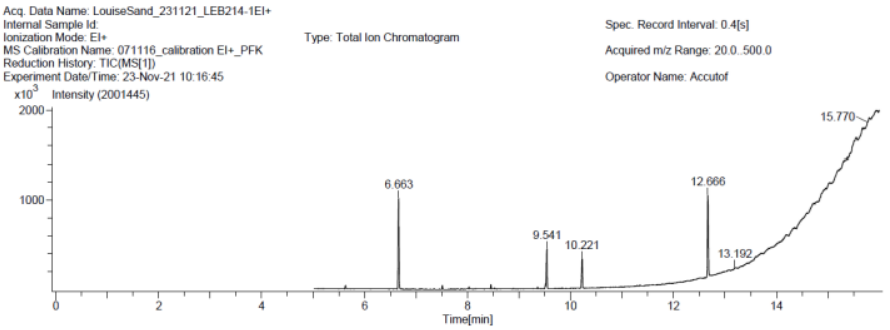

Figure 40. GC-MS analysis of fluorination of compound **80**.

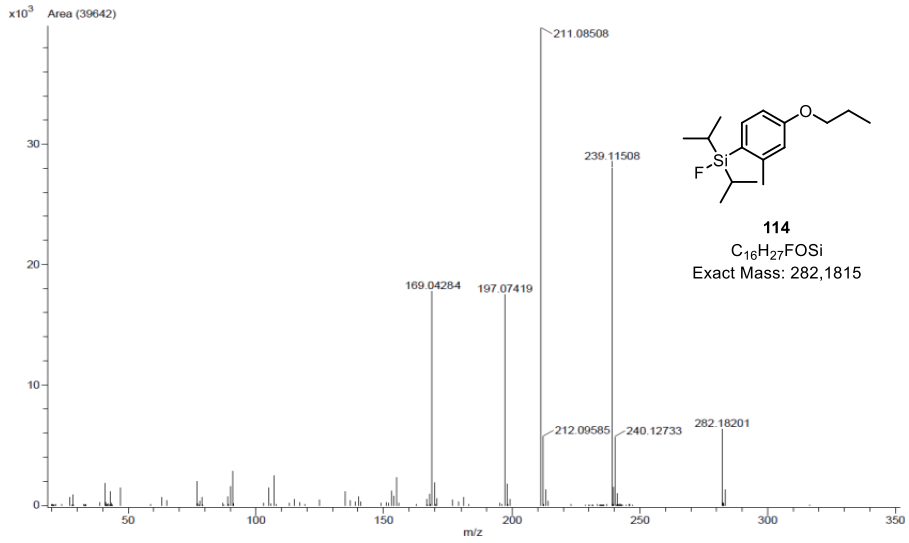

Figure 41. GC-MS spectrum at R_t = 10.221 confirming the mass of fluorosilane **114**.

Fluorination of azide analogues

In an attempt to simplify the fluorination-testing, two of the already prepared azide-analogues were subjected to fluorination conditions shown in Scheme 86.

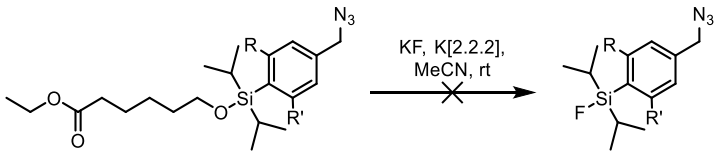

64: R = Me, R' = H
68: R = R' = Me

116: R = Me, R' = H
117: R = R' = Me

Scheme 86. Unsuccessful fluorinations of azide-analogues **64** and **68**.

This resulted in complex reaction mixtures, as four spots were evident upon TLC-analysis after 1 h stirring at rt. In addition, there was several different diisopropyl groups present in the crude product according to ^{1}H NMR analyses (Figure 42).

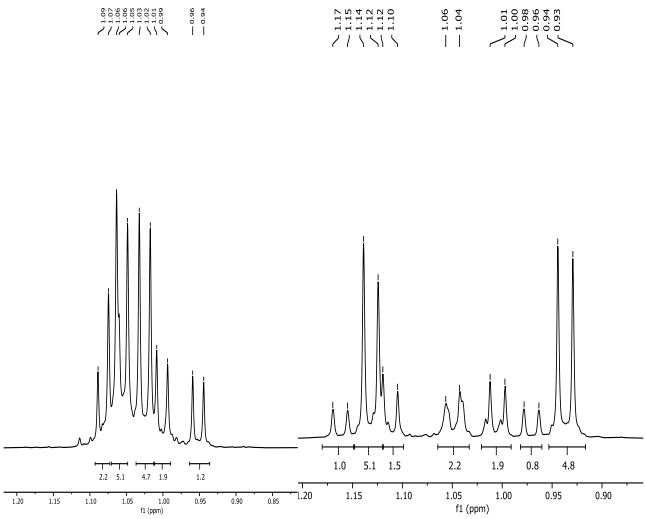

Figure 42. ^{1}H NMR spectra of the two fluorinations of the azide-analogues. Left: starting from mono-methyl analogue **64**, right: starting from di-methyl analogue **68**.

To avoid using the more expensive ethyl 6-hydroxyhexanoate alcohol (**29**), a cheaper alternative was tried, using methanol instead, to keep exploring fluorination on simplified analogue (Scheme 87). The results of the silyl-ether formations were varying, and the yields were surprisingly lower than for the longer alcohol chain. The most apparent explanation might be the dryness of the MeOH used.

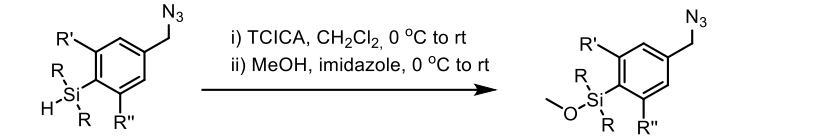

42: R = *i*Pr, R' = R'' = H
63: R = *i*Pr, R' = Me, R'' = H
67: R = *i*Pr, R' = R'' = Me
25: R = *t*Bu, R' = R'' = H

118: R = *i*Pr, R' = R'' = H, 5%
119: R = *i*Pr, R' = Me, R'' = H, 7%
120: R = *i*Pr, R' = R'' = Me, 62%
54: R = *t*Bu, R' = R'' = H, n.r.

Scheme 87. Synthesis of precursor methoxy-silyl ethers **118**-**120** and **54**.

Since the fluorinations were unsuccessful with the azide present, one of the methoxy-silyl ether analogues was transformed into a simple triazole (Scheme 88).

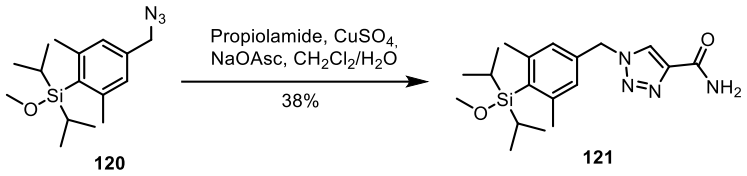

Scheme 88. Synthesis of compound **121**.

The fluorination reaction was then performed as shown in Scheme 89, using KF and K[2.2.2] in MeCN as described previously.

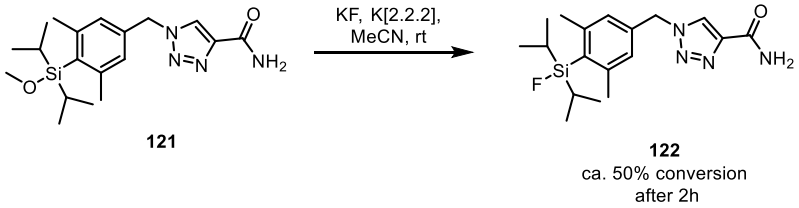

Scheme 89. Fluorination of compound **122** at room temperature leading to 50% conversion of starting material within 2 h.

Only 50% conversion of starting material was observed after 2 h and it appeared from the ^{1}H NMR spectrum (Figure 43) that there was only one product forming. We did not perform MS-analyses of this compound and could therefore not confirm if it was indeed fluorinated **122** that had been formed.

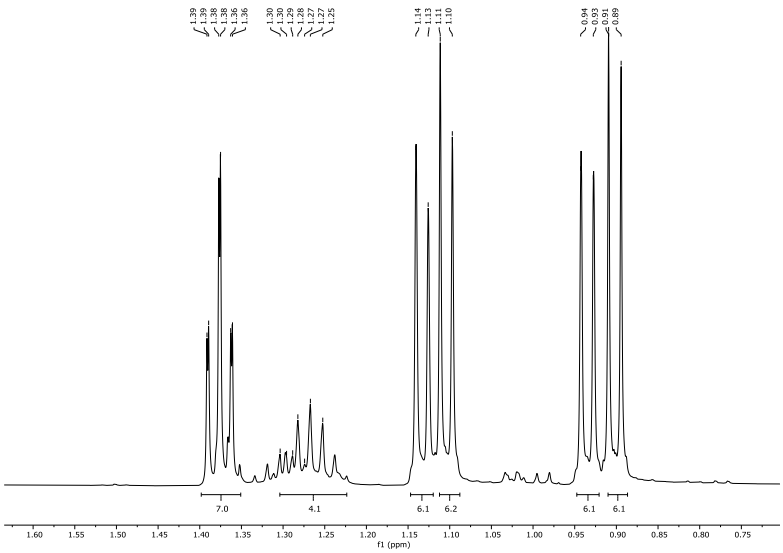

Figure 43. ^{1}H NMR-spectrum after fluorination of compound **122**.

Fluorination of aldehyde analogues

Aldehyde analogues **50**, **62** and **70** had also been prepared previously, and direct fluorination of these analogues were attempted (Scheme 90). Unfortunately, fluorinations were unsuccessful, and an unidentifiable mixture of compounds were present according to ^{1}H NMR analysis, and in addition, the aldehyde signal was missing.

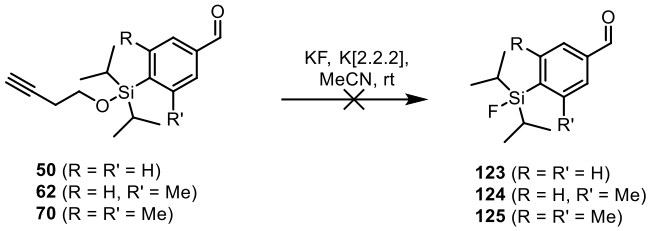

Scheme 90. Reaction pathway for the test-fluorination of aldehyde-analogues.

Fluorination of benzene analogues

Fluorination of precursors without a handle on the benzene ring was performed on diisopropyl substituted analogues **94**, **95** and **96**, and also for the di-*tert*-butyl-substituted analogue **98**. We envisioned that these experiments would give us insights into the reactivity of the silyl ethers without being complicated by interference from the handle. Also, these molecules could be analyzed by GC-MS.

Room temperature reactions

The first series of reactions were performed at room temperature, as shown in Scheme 91.

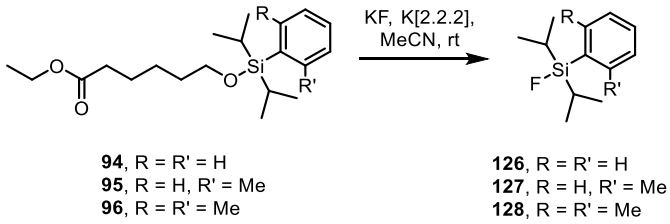

Scheme 91. Fluorination reactions of the three benzene-analogues **94**, **95** and **96**.

The fluorinated compounds have been confirmed (by GC-MS analyses), however, there are two or more diisopropyl-containing compounds in the mixtures (Figure 44) indicating that there is more than one reaction taking place. Further characterization of

the compounds in the product mixture, and further exploration of reaction conditions ought to be performed.

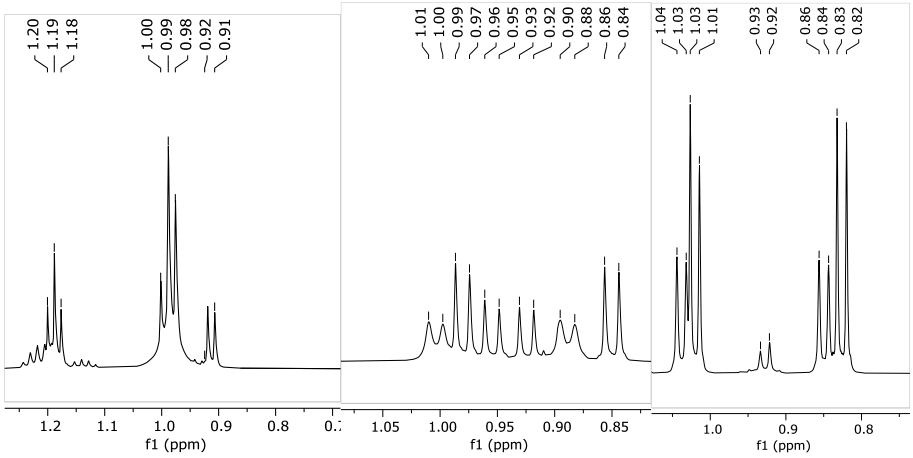

Figure 44. ^{1}H NMR of crudes after fluorination of benzene analogues. Left: non-methyl analogue, middle: mono-methyl analogue, right: di-methyl analogue.

We also attempted fluorination of di-*tert*-butyl analogue **98** under the same conditions (Scheme 92), yet no reaction was observed after 2.5 h, and further stirring did not provide any conversion of the starting material.

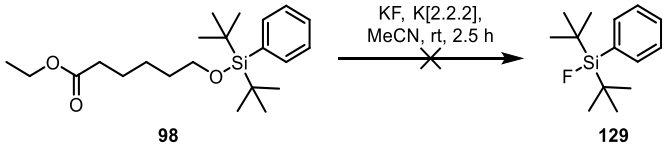

98 **129**

Scheme 92. Unsuccessful fluorination reaction of di-tert-butyl analogue **98**.

Elevated temperature reactions

Raising the temperature to 70 ºC in fluorinations of the same precursors (**94**, **95**, **96** and **98**) were attempted, though this only resulted in multiple spots in the TLC-analysis, and what appeared to be decomposition of the starting material into different substances and/or no further reaction (Scheme 93 and Scheme 94).

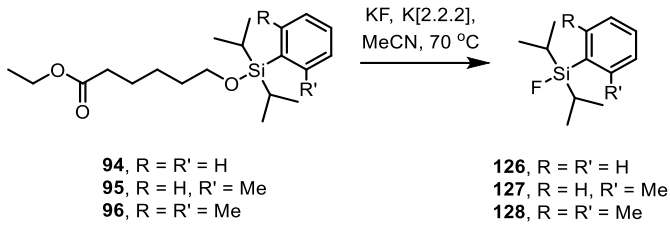

94, R = R' = H
95, R = H, R' = Me
96, R = R' = Me

126, R = R' = H
127, R = H, R' = Me
128, R = R' = Me

Scheme 93. Fluorinations of compounds **94-96** at 70 ºC.

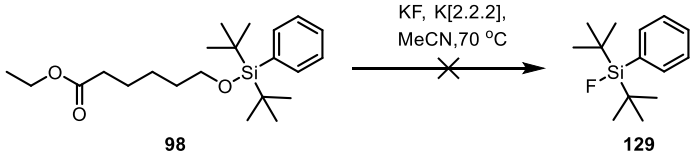

98 **129**

Scheme 94. Unsuccessful fluorination of compound **98**.

No work-up was performed for these reactions, the solvents were simply evaporated directly, and the residue submitted to NMR analyses, also confirming different compounds in the product mixtures (Figure 45).

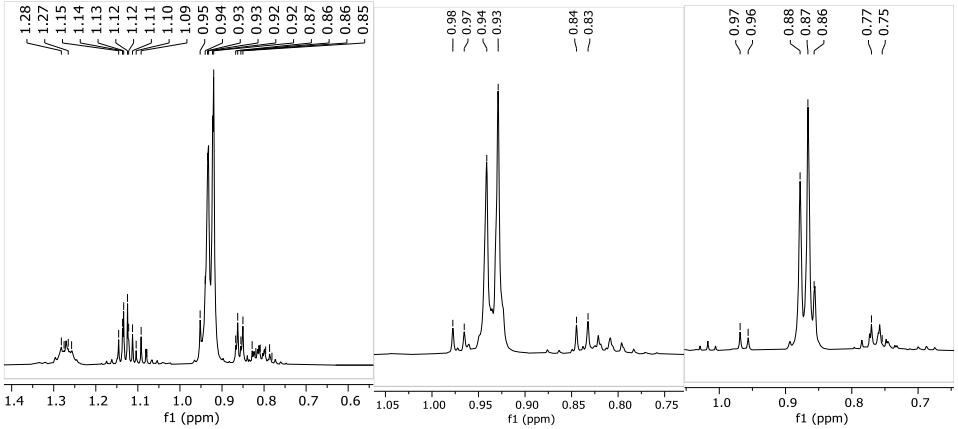

Figure 45. ^{1}H NMR after fluorination of benzene analogues at 70 ºC.
Left: non-methyl analogue, middle: mono-methyl analogue, right: di-methyl analogue.

As these reactions did not go to completion, one source of error might be that the Kryptofix[2.2.2] has decomposed or been exposed to moisture. One possible strategy for further work could be to try a different source of fluoride (e.g., TBAF), also tweaking the conditions by adding acid or base should be attempted for these types of compounds.

Fluorination of solid-phase FOSi-precursor

After the successful fluorination of compound **80**, the next step towards developing the FOSi-method was attachment of the molecule to a polymer resin and observation of fluorination on-resin. Compound **80** was hydrolyzed by sodium hydroxide in a mixed solvent system, as described by Theodorou *et al.*[206] in quantitative yield (Scheme 95).

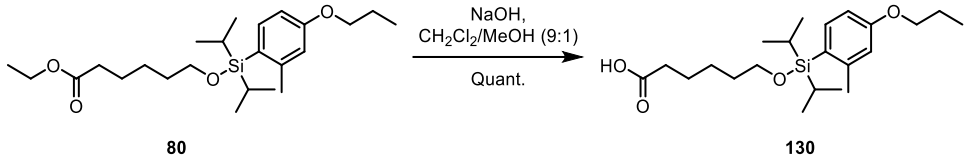

Scheme 95. Hydrolysis of ester **80** by the procedure of Theodorou *et al.*[206]

The carboxylic acid was then attached to a ChemMatrix resin functionalized with a Rink Amide linker, as used in traditional peptide synthesis. Standard coupling conditions were applied (Scheme 96) to attach **130**.

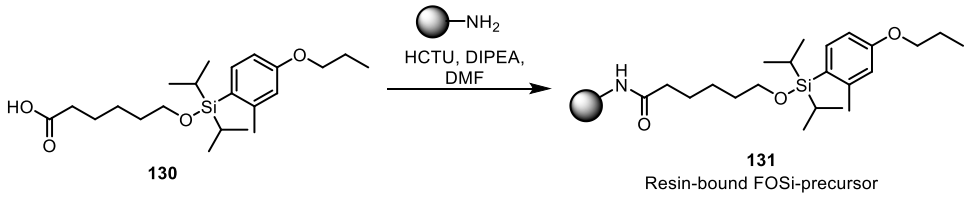

Scheme 96. Coupling of **130** to polymer support (Rink Amide resin).

Fluorination on solid phase was then attempted, by applying the same conditions as for the previous off-resin testing, as shown in Scheme 97.

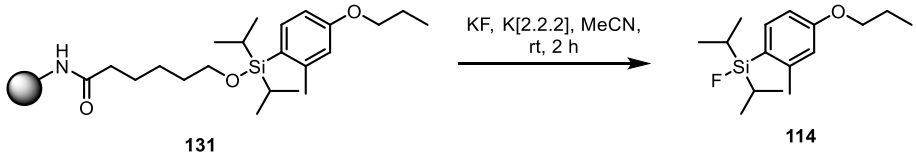

Scheme 97. First fluorination attempt of resin-bound precursor **131**.

No purification was performed, other than filtering off the solvent and evaporating the filtrate *in vacuo*. There were, as suspected, signals from Kryptofix[2.2.2] and some other minor contaminations that has not been identified, however, there is mainly one signal corresponding to the diisopropyl-silyl moiety around 1.10-0.90 ppm (Figure 46).

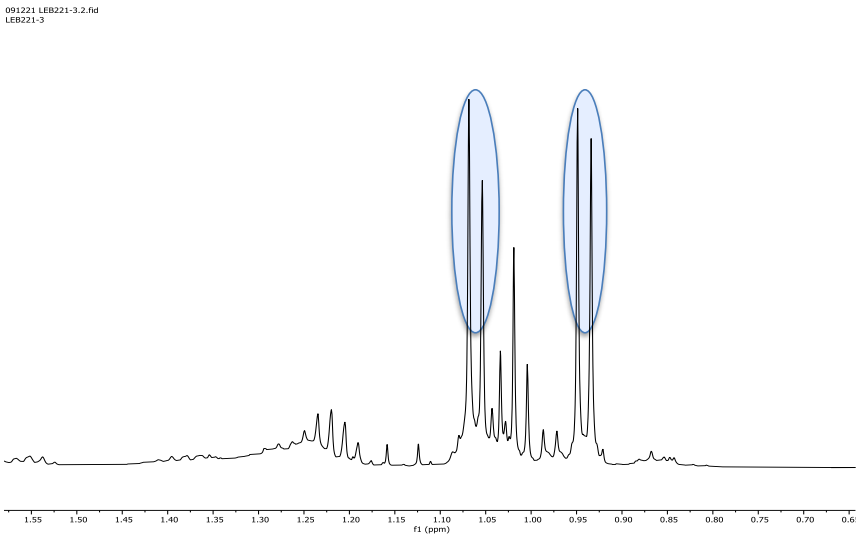

Figure 46. ^{1}H NMR of crude product after solid-phase fluorination showing only one diisopropyl-containing moiety.

The presence of fluorosilane **114** (exact mass = 282.1815, Figure 47) was confirmed by GC-MS analysis (Rt = 12.045 min in Figure 48), thus the FOSi approach had worked. The peak detected at Rt = 12.654 corresponds to the mass of the hydrolyzed fluorosilane (Si-OH, **115**). From the ^{1}H NMR analysis, which was performed directly after synthesis, we know there is mainly one compound bearing a diisopropyl-substitution, and it is possible that the fluorosilane is hydrolyzed during the GC-MS analysis (not anhydrous solvent, 300 ºC)

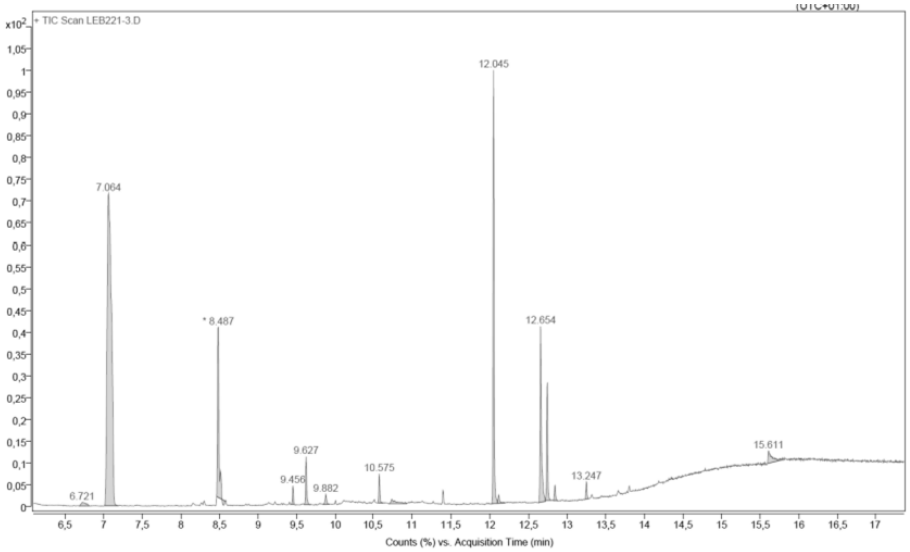

Figure 47. GC-MS spectrum after fluorination on solid-phase.

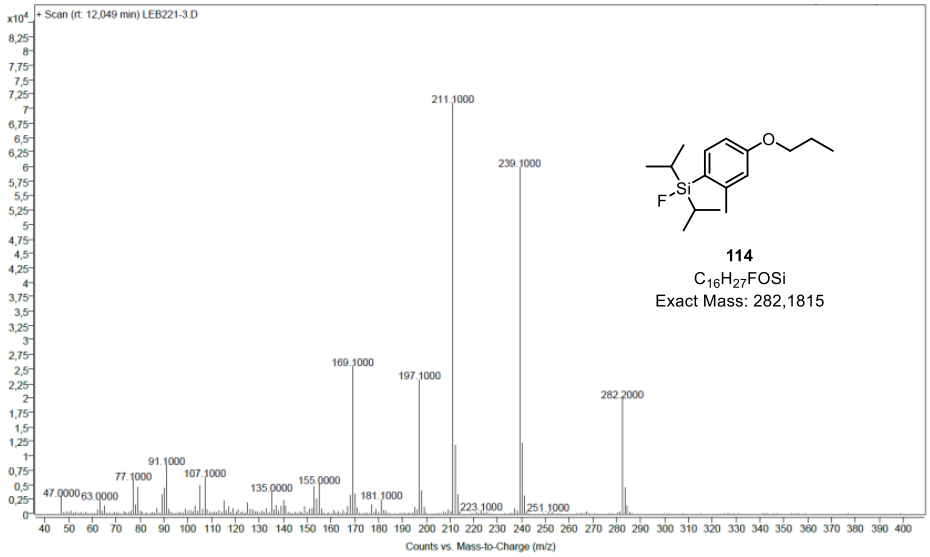

Figure 48. GC-MS analysis at Rt = 12.045, confirming that fluorosilane **114** has been cleaved from the resin.

We also conducted a ^{29}Si NMR study, where we attempted fluorination of solid-phase precursor **131** by KF and K[2.2.2] in CD_3CN, performing analyses every 10. min. Unfortunately, the crude product analyses were too dilute to provide signals in the spectra and we were left with inconclusive results, and shortly after, our 500 MHz NMR instrument quenched.

3.6 Radiolabeling of resin-bound precursor

^{18}F-Fluorinations of solid-phase FOSi-precursor

The resin-bound precursor **131**, that was fluorinated under cold conditions, was subjected to hot fluorination at the PET-center at Haukeland University Hospital (Scheme 98), supervised by Dr. Ole Heine Kvernenes, with the aim of producing [^{18}F]**114**.

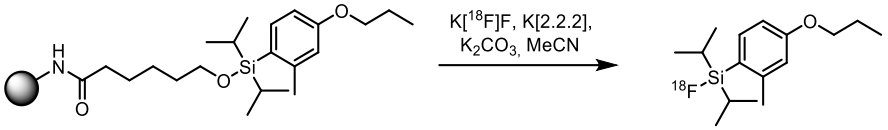

Scheme 98. Cleavage of the FOSi-precursor from the resin by [^{18}F]F$^-$.

In the first experiment the resin was stirred at rt with the fluoride source present, and radio-TLC was conducted with 30 min intervals. The solvent was azeotropically dried three times. After stirring for 30 min a new peak (R_f = 0.48) was present in the radio-TLC, but the ^{18}F$^-$ peak was still dominant. It should be noted that we did not filter the mixture through alumina to remove free ^{18}F$^-$. After 60 min stirring at rt the intensity of the product peak had increased (Figure 49).

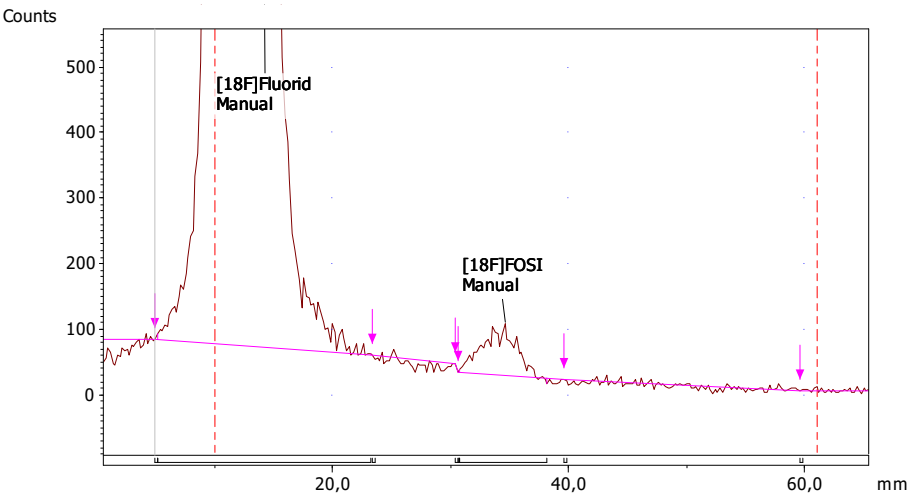

Figure 49. Radio-TLC of first ^{18}F-fluorination. Stirring at rt for 60 min.

In the next experiment the reaction mixture was heated at 50 ºC for 30 min, then radio-TLC was performed. The solvent was azeotropically dried four times. After 30 min stirring with heating, we observed one dominant peak (R_f = 0.51) and a second, smaller peak of higher R_f-value in the TLC-analysis (Figure 49). The mixture was not filtered through an alumina cartridge to remove excess $^{18}F^-$.

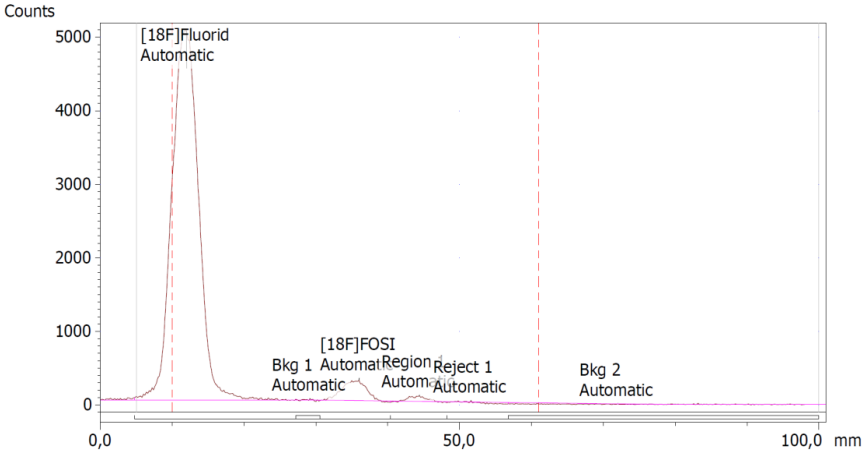

Figure 49. Radio-TLC of second experiment after 30 min stirring at 50 ºC.

The same reaction mixture was heated further to 70 ºC and stirred for 30 additional minutes before a new TLC-analysis was performed. At this time, three peaks could be observed in the chromatogram (Figure 50).

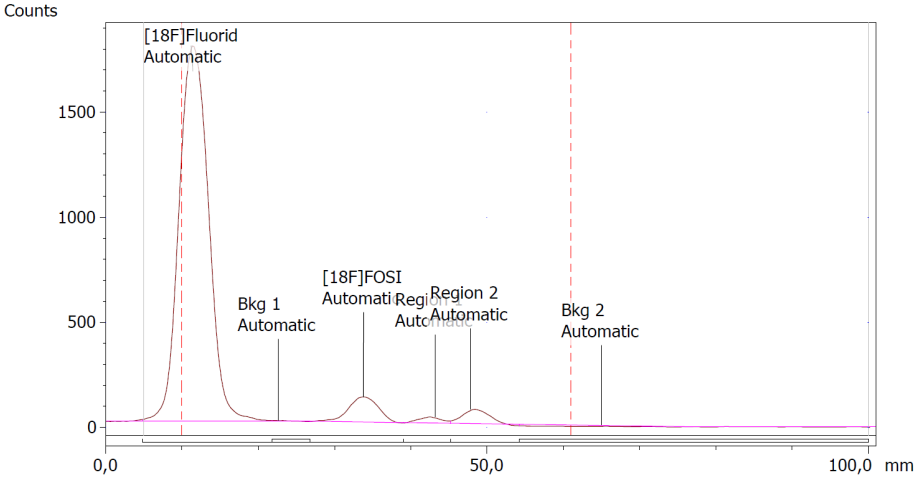

Figure 50. Radio-TLC of second experiment after stirring at 50 ºC for 30 min and then at 70 ºC for 30 min.

The reaction mixture was filtered through an alumina cartridge to remove some of the excess $^{18}F^-$, however, as can be seen in Figure 51, there was still some free $^{18}F^-$ present, but filtering the mixture resulted in a better resolution of the three radiolabeled peaks.

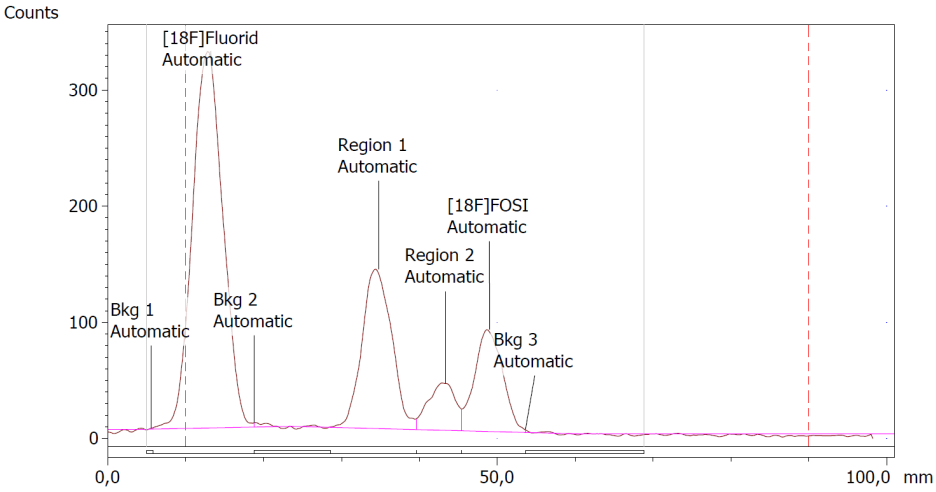

Figure 51. Radio-TLC of second experiment after stirring at 50 ºC for 30 min and then at 70 ºC for 30 min and filtering the mixture through an alumina cartridge.

From the first experiment at room temperature, we were optimistic that the cleavage to give **[^{18}F]114** was successful as we only saw one new peak arising in the radio-TLC, and the R_f-value corresponded to that of cold fluorosilane **114**. Unfortunately, we did not have access to instruments that would allow for a qualitative analysis of the radiolabeled product.

The second experiment, with heating, revealed a different reaction pattern, as there were multiple peaks arising in the radio-TLC chromatogram. Looking at the cold experiments with the benzene-analogues, presented in Section 3.5, we also observed multiple components in the TLC- and NMR-analyses when the reaction mixture was heated. It thus seems that elevating the temperature is not a suitable alternative for this strategy, although this needs to be explored further.

A third experiment was performed, using a fresh batch of solid-supported FOSi-precursor **131**, and the solvent was azeotropically dried four times. The reaction mixture was heated at 50 ºC for 30 min, and in this case only one product peak

($R_f = 0.87$) was arising in the radio-TLC chromatogram (Figure 52). This peak had a higher R_f-value than previous experiments, however, this analysis was performed on a different TLC-plate with a different eluent system.

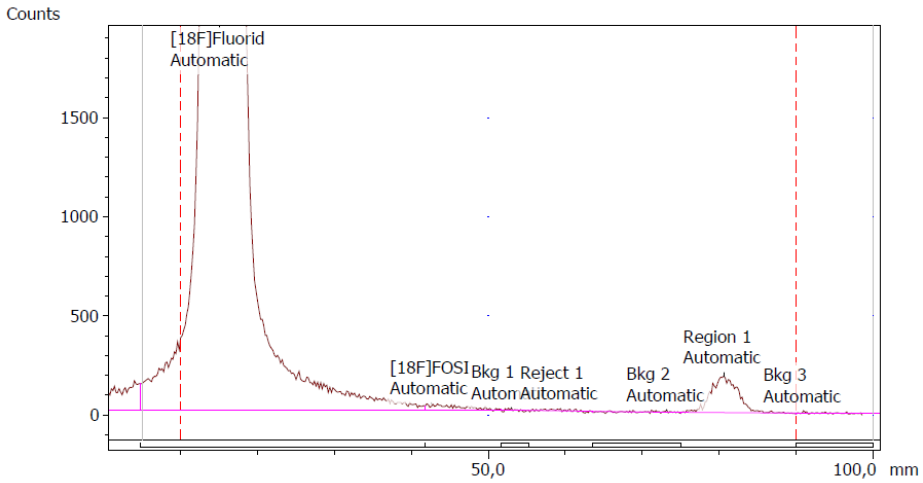

Figure 52. Radio-TLC of third experiment after stirring at 50 ºC for 30 min.

Continuous stirring at 50 ºC (60 min total) still revealed only one, single product peak ($R_f = 0.88$), as observed in the radio-TLC chromatogram after 30 min (Figure 53).

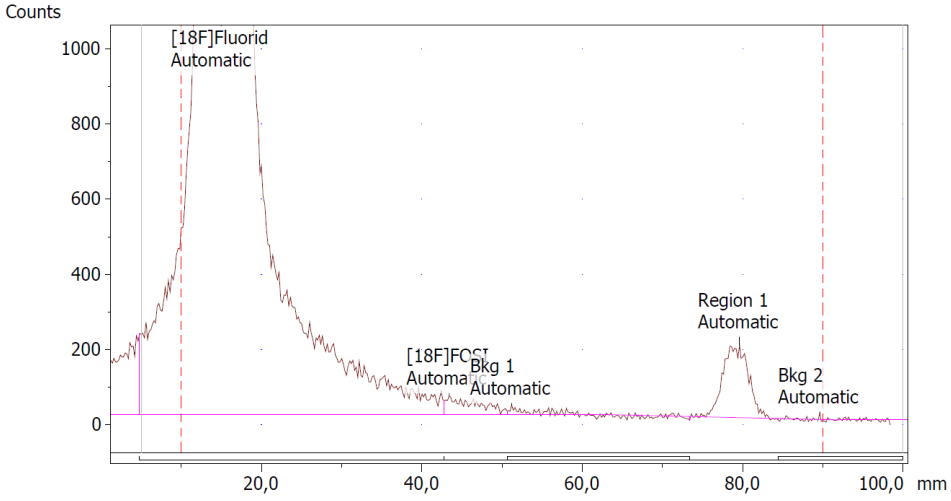

Figure 53. Radio-TLC of third experiment after stirring at 50 ºC for 60 min.

These initial results are promising, but not conclusive, as we have not been able to characterize the product peak. Nevertheless, observing only one product peak in the first and third experiment holds promise that this method could yield tracers of high SAs, given that optimized reaction conditions can be identified, thus further studies of reaction conditions and automation are imminent. It is important to note that for this strategy it is not crucial that the conversion rate is as fast as for other direct fluorination methods, because in the FOSi-method, all that is labeled and cleaved off from the resin is ready-to-use and what remains unreacted is attached to the resin and can in principle be used again in another experiment.

4. Conclusions and future work

Positron emission tomography (PET) offers a non-invasive and quantitative imaging modality for investigating biological processes, and is, together with SPECT, the most sensitive imaging modality used to diagnose and monitor diseases. To achieve the desired selectivity and sensitivity, the field depends on access to radiotracers and methods for their synthesis.

In order to facilitate PET imaging of immune responses by our collaborators, three precursors for Granzyme B (GzmB)-targeted imaging were prepared in this work. NOTA-GzmB was already an established tracer for cancer treatment response, which we have successfully re-synthesized and characterized. In addition to this, two new tracers were synthesized, bearing different chelating groups; NODAGA-GzmB and DOTA-GzmB (prepared by Dr. Markus Baumann).

The concept of immobilizing aryl silyl ethers onto a solid support and then cleaving the silicon-oxygen bond by fluorine to release fluorosilanes has been explored, and selective cleavage at room temperature confirmed by ^{1}H-NMR and GC-MS analyses. In addition, ^{18}F-fluorination of a solid-supported test compounds has been performed with promising, yet not conclusive results. Our preliminary experiments indicate that the FOSi-method is not amenable to elevated reaction temperatures, as we observed formation of multiple fluorine-containing compounds when experiments were performed at 70 ºC, both under cold and hot conditions.

Further, suitable methods to prepare a wide range of aryl silyl ethers have been identified, and the products of these efforts can be used further in systematic studies to develop the concept further and test the scope. A number of the synthesized silyl ethers have been fluorinated to produce fluorosilanes, and these experiments have revealed large variation in reactivity. The rate and outcome of fluorination reactions were clearly highly dependent on the substitution pattern on the silicon atom, presence and nature of substituents in *para*-position to the silyl group and also on the presence or absence of methyl groups on the aromatic ring *ortho* to the silyl group.

While this work provides the initial proof-of-concept for the FOSi-method, there are still many aspects that need to be explored further. Multiple variables can be altered in the hot fluorinations, as we have only begun to touch the surface of what is possible in these experiments. The amount of solvent used can influence the rate of the reaction, and it is also necessary to establish how tolerant the method is to the presence of water. The time and temperature has also been shown to play a crucial role in the rate and the formation of side-products. Other than that, different solvents should be tested, as well as addition of acidic additives (most commonly AcOH).

The FOSi-method currently involves breaking of Si-O bonds, however, it would also be interesting to investigate other types of linkers that could work on a solid support. The possibility of breaking other silicon-heteroatom bonds is an appealing path to follow.

The field of radiolabeling, and especially fluorination of organosilicons is in rapid development, with SiFA-analogues in clinical trials, and new directions for labeling precursors such as HetSiFA[117] and SiFA-radiohybrid ligands (theranostics)[118]. In addition to this, the principle of immobilizing tracers on a solid support and cleaving off a radiotracer is only at the beginning, with the publication in 2022 by Steffann *et al.*[126] marking a potential new era for solid-supported radiolabeling.

5. Experimental

5.1 General

All reactants, reagents and solvents were obtained from Sigma-Aldrich and were used as received unless otherwise is stated. Solid-phase syntheses were performed using a H-Asp(OtBu)-H NovaSyn® TG Resin provided by Merck Millipore using 10 or 30 mL reactor vials (Biotage). 2-*S*-(4-Isothiocyanatobenzyl)-1,4,7-triazacyclononane-1,4,7-triacetic acid (*p*-SCN-Bn-NOTA), 2-*S*-(4-Isothiocyanatobenzyl)-1,4,7,10-tetraaza-cyclododecane tetraacetic acid (*p*-SCN-Bn-DOTA) and 2-[1,4,7-Triazacyclononan-1-yl-4,7-bis(tBu-ester)]-1,5-pentanedioic acid (NODAGA tris-tBu ester) was purchased from Macrocyclics. All moisture-sensitive reactions were carried out under argon atmosphere using overnight oven-dried equipment (130 ºC) that was cooled down under vacuum and purged with argon prior to use.

Dry THF, hexane and CH_2Cl_2 were obtained from an anhydrous solvent delivery system (SPS-800 system from M. Braun GmbH, Garching, Germany) and stored under argon in a Schlenk flask.

Peptide syntheses were carried out on a Biotage Initiator+ Alstra microwave peptide synthesizer.

Thin layer chromatography (TLC) analyses were performed on aluminium sheets coated with Merck TLC silica gel (60 F_{254}) and visualization was achieved by using ultraviolet light (254 nm).

Flash column chromatography was performed either manually using silica gel from Merck (Silica gel 60, 0.040–0.063 mm) or on a PuriFlash XS 420 system (Interchim, Montlucon Cedex, France) using pre-packed columns as specified for each compound.

Preparative high-performance liquid chromatography (HPLC) was performed on a Thermo 321 multisolvent pump with an UltiMate 3000 variable wavelength detector using an XBridge™ Prep C18 OBS (19 x 250 mm, 5 μm) column from Waters using mixtures of acetonitrile and MilliQ water (both containing 0.1% TFA) as eluent.

Analytical HPLC was performed on a 1290 Infinity II Flexible pump with a 1260 Infinity II DAD WR detector using a ZORBAX RRHD Eclipse plus 300-SB C18 (50 x 2.1 mm, 300 Å, 1.8 µm) column with mixtures of acetonitrile and MilliQ water (both containing 0.1% TFA) as eluent.

Low resolution mass spectra (LRMS) were obtained on an Agilent 6420A triple quadrupole (QqQ configuration) mass analyzer by direct infusion using electron-spray ionization (ESI) in positive or negative mode with an ionization potential varying from 70-135 V. High-resolution mass spectra (HRMS) were recorded with an AccuTOF™ mass spectrometer operated with an orthogonal electrospray ionization (ESI) source, an orthogonal accelerated time of flight (TOF), single stage reflectron mass analyzer and a dual micro channel plate (MCP) detector.

NMR spectra were recorded using either a Bruker BioSpin AV500, AV600 or a Bruker BioSpin Ascend spectrometer operating at 850 MHz with an inverse-detected triple resonance (TCI) cryoprobe for ^{1}H NMR and 2D NMR spectra of the final compounds. ^{1}H and ^{13}C chemical shifts (δ) are reported in ppm with reference to the solvent residual peak ($CDCl_3$: δ_H 7.26 and δ_C 77.16; $(CD_3)_2SO$: δ_H 2.50 and δ_C 39.98). All coupling constants are given in Hz.

5.2 Experimental procedures

β-Ala-Gly-Gly-Ile-Glu-Phe-Asp-H (AβGGIEFD-H)

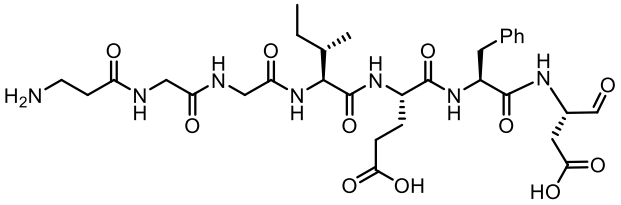

GzB peptide (A_βGGIEFD-H)

Peptide synthesis: A preloaded peptide aldehyde resin (H-Asp(O*t*-Bu))-H NovaSyn TG Resin (356 mg, loading: 0.20 mmol/g) was loaded into a reactor vial (30 mL) for automated SPPS and allowed to swell in DMF at 70 ºC for 20 min. Each of the amino

acids (3 eq.) were coupled to the resin using HCTU (2.8 eq.) and DIPEA (6 eq.) at 70 ºC for 5 min. All couplings were repeated twice. Fmoc-deprotection was facilitated using 20% piperidine in DMF at rt for 10 min. Pre-cleavage wash was performed using CH_2Cl_2. Before cleaving the peptide from the resin, the crude product was dried under high vacuum for at least 30 min.

Test-cleavage: A small amount of resin (approx. 10 mg) was subjected to treatment with TFA (2 x 10 min), washing with CH_2Cl_2 (5 x 15 mL) then cleaving the peptide from resin with AcOH/H_2O/CH_2Cl_2/MeOH (10:5:63:21, 3 x 5 mL for 30 min). The combined filtrates were concentrated under reduced pressure analyzed by MS.

LRMS (ESI+): (*m/z*) $[M+H]^+$ calcd for $C_{31}H_{45}N_7O_{11}^+$: 692.3, found: 692.2, (*m/z*) $[M+H_2O+H]^+$ calcd for $C_{31}H_{48}N_7O_{12}^+$= 710.3, found: 710.2, (*m/z*) $[M+Na+H]^+$ calcd for $C_{31}H_{46}N_7NaO_{11}^+$= 715.3, found: 715.3, (*m/z*) $[M+2H]^{2+}/2$ calcd = 347.1, found: 347.1.

NOTA-GzmB

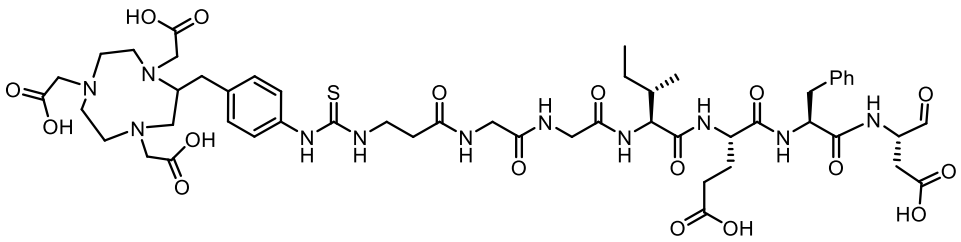

NOTA-GzmB

Resin bound AβGGIEFD-H (89 mg resin, 0.0139 mmol) was swelled in freshly degassed DMSO (1 mL) for 1 h. *p*-SCN-Bn-NOTA (8.6 mg, 0.0154 mmol, 1.1 eq.) was dissolved in freshly degassed DMSO (1 mL) and DIPEA (8 µL, 0.042 mmol, 3 eq.) were added to the swelled resin and the reaction vessel was shaken at rt under argon and protected from light overnight. The reaction vessel was drained, the resin was washed with CH_2Cl_2 (5 x 5 mL) and dried under vacuum. For cleavage the dried resin was treated with TFA (2 x 5 mL, 10 min), washed with CH_2Cl_2 (5 x 5 mL), and treated with AcOH/H_2O/CH_2Cl_2/MeOH (10:5:63:21, 3 x 5 mL, 30 min). The fractions

were concentrated under reduced pressure to give the crude product (7.0 mg). This material was purified by semi-preparative HPLC to give the title compound as a colorless fluffy solid (3.3 mg, 21%). HRMS (ESI+): (*m/z*) $[M+H]^+$ calcd for $C_{51}H_{72}N_{11}O_{17}S^+$: 1142.4823, found:1142.4820, (*m/z*) $[M+2H]^{2+}/2$ calcd = 571.7401, found: 571.7610; HPLC Purity: 97.6% (UV 206 nm).

DOTA-GzmB

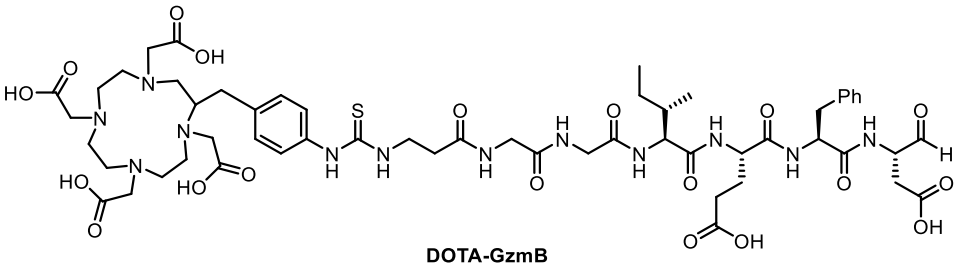

This material was prepared by Dr. Markus Baumann following a similar procedure as described for NOTA-GzmB.

LRMS (ESI+): (*m/z*) $[M+H]^+$ calcd for $C_{55}H_{79}N_{12}O_{19}S^+$: 1243.5, found:1243.4, (*m/z*) $[M+2H]^{2+}/2$ calcd = 622.3, found: 622.3; HPLC Purity: 91.0%.

NODAGA-GzmB

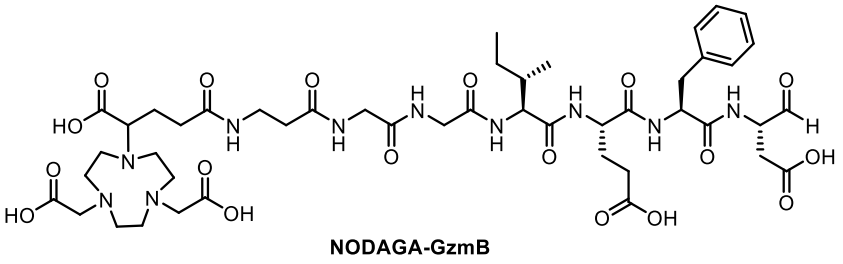

Resin bound AβGGIEFD-H (73.9 mg resin, 0.0116 mmol) was swelled in dry DMF (1 mL). In a separate vial, NODAGA-tris(*t*-Bu) ester (19 mg, 0.0349 mmol, 3 eq.) and HCTU (13.5 mg, 0.0326 mmol, 2.8 eq.) were dissolved in dry DMF (1 mL) and DIPEA (13 µL, 0.070 mmol, 6 eq.) was added and the mixture was stirred for 30 min at rt

before it was added to the resin and shaken at rt under argon overnight. The vessel was drained, and the resin was washed with DMF (5 x 5 mL), CH_2Cl_2 (5 x 5 mL) and dried under high vacuum.

Cleavage from resin:

The dried resin was treated with TFA (3 h), washed with CH_2Cl_2 and treated with AcOH/H_2O/CH_2Cl_2/MeOH (10:5:63:21, 3 x 5 mL, 30 min). The fractions were concentrated under reduced pressure to give the crude mixture (8.8 mg). The crude mixture from synthesis of NODAGA-GzmB was purified by semi-preparative HPLC to give the title compounds as a colorless fluffy solid (1.5 mg, 22%). LRMS (ESI+): (*m/z*) $[M+H]^+$ calcd for $C_{46}H_{69}N_{10}O_{18}^+$: 1049.4, found: 1049.4, (*m/z*) $[M+2H]^{2+}/2$ calcd = 525.2, found: 525.2; HPLC Purity: 95.7% (UV = 209 nm).

4-(Di-*tert*-butylsilyl)benzaldehyde (5)

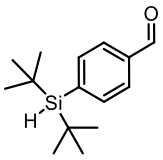

5

Method starting from acetal protected aldehyde: To a stirring solution of 4-bromobenzadehyde diethyl acetal (0.25 mL, 1.23 mmol) in dry THF (3 mL) cooled to −78 ºC, *n*-BuLi (2.5 M in hexanes, 0.35 mL, 0.75 mmol) was added dropwise over 5 min and the mixture was stirred for 30 min before another aliquot of *n*-BuLi (2.5 M in hexanes, 0.35 mL, 0.75 mmol) was added dropwise. After another 30 min of stirring at −78 ºC, di-*tert*-butylchlorosilane (0.85 mL, 4.20 mmol) was added dropwise and stirring continued for 2 h. The mixture was allowed to warm to rt and stirred overnight. The reaction mixture was poured into a solution of $NaHCO_3$ (0.3 M, 10 mL) and the two layers were separated. The aqueous layer was extracted with CH_2Cl_2 (10 mL), and the organic layers were combined, washed with saturated NaCl (20 mL), and dried over $MgSO_4$. The solvent was removed *in vacuo* and the residue was purified by flash chromatography (silica gel, hexane/EtOAc 40:1) to yield silane **5** (187 mg, 62%) as a colorless oil.

R_f = 0.66 (hexane/EtOAc, 9:1); ^{1}H NMR (500 MHz, $CDCl_3$): δ = 10.03 (s, 1H), 7.83 (d, 2H, *J* = 7.5), 7.76 (d, 2H, *J* = 7.5), 3.92 (s, 1H), 1.06 (s, 18H); ^{13}C NMR (125 MHz, $CDCl_3$): δ = 192.7, 144.6, 136.7, 136.4, 128.5, 28.8, 19.2. The analytical data were in accordance with those reported previously.[114]

Method oxidizing silane **22**: 4-(di-*tert*-butylsilyl)-benzyl alcohol (**22**) (340 mg, 1.36 mmol) was dissolved in dry CH_2Cl_2 (5 mL) and added to a suspension of activated MnO_2 (1.06 g, 13.6 mmol) in dry CH_2Cl_2 (10 mL) under argon atmosphere. The suspension was stirred at rt overnight. The black residue was filtered through a pad of Celite and washed thoroughly with CH_2Cl_2. The filtrate was concentrated in vacuo to give **5** (338 mg, quant.) as a colorless oil which required no further purification before performing the next step.

(4-(1,3-Dioxolan-2-yl)phenyl)di-*tert*-butylsilane (10)

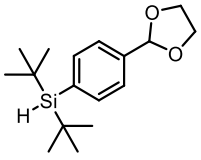

10

A stirring solution of 2-(4-bromophenyl)-1,3-dioxolane (250 mg, 1.09 mmol) in dry THF (5 mL) was cooled to −78 ºC and *n*-BuLi (2.2 M in hexanes, 0.6 mL, 1.31 mmol) was added dropwise over 5 min and the mixture was stirred for 1 h. Di-*tert*-butylchlorosilane (0.26 mL, 1.31 mmol) was added and stirring continued for 2 h at −78 ºC before the mixture was allowed to warm to rt and stirred overnight. Saturated aqueous $NaHCO_3$ (3 mL) was added to quench the reaction and the two layers were separated. The aqueous layer was extracted with CH_2Cl_2 (3 x 5 mL), and the organic layers were combined, washed with water (10 mL), and dried over $MgSO_4$. The solvents were removed *in vacuo* and the residue was purified by flash chromatography (silica gel deactivated by 3% TEA, hexane/EtOAc 30:1) to yield **10** (130 mg, 41%) as a colorless oil.

^{1}H NMR (500 MHz, $CDCl_3$): δ = 7.60 (d, *J* = 8.0, 2H), 7.45 (d, *J* = 8.0, 2H), 5.80 (s, 1H), 4.16-4.05 (m, 4H), 3.88 (s, 1H), 1.04 (s, 18H); ^{13}C NMR (125 MHz, $CDCl_3$): δ = 138.4, 137.0, 136.0, 125.6, 104.0, 65.5, 29.0, 19.1.

(4-(1,3-Dioxolan-2-yl)phenyl)di-*tert*-butylchlorosilane (11)

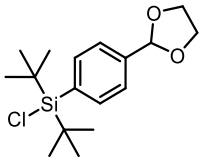

11

A stirring solution of 2-(4-bromophenyl)-1,3-dioxolane (229 mg, 1.00 mmol) in dry THF (3 mL) was cooled to −78 ºC and *n*-BuLi (2.5 M in hexanes, 0.45 mL, 1.2 mmol) was added dropwise over 5 min and the mixture was stirred for 1 h. The resulting suspension was added dropwise via syringe over a period of 20 min to a cooled (−78 ºC) and stirring solution of di-*tert*-butyldichlorosilane (0.53 mL, 2.50 mmol) in dry THF (2 mL). The resulting mixture was stirred for 1 h at −78 ºC and then allowed to warm to rt and stirring continued over night. The solvents were removed *in vacuo*, and the residue was suspended in hexane/ethyl acetate (approx. 9:1) and the precipitate was filtered off. The solvents were removed *in vacuo* and the resulting liquid containing a mixture of **11** and *n*-butylated side-product **12** (6:4, 391 mg) was used in the next reaction without further purification. NMR analysis shows some chlorosilane-impurities (too high integral at 1.18 ppm).

^{1}H NMR (500 MHz, $CDCl_3$): δ = 7.49 (d, *J* = 8.2, 2H), 7.41 – 7.36 (m, 2H), 5.83 (s, 1H), 4.15 – 4.02 (m, 4H), 1.18 (s, 18H); ^{13}C NMR (126 MHz, $CDCl_3$): δ = 138.1, 135.3, 129.3, 128.5, 126.6, 103.9, 65.4, 27.0, 24.8.

Di-*tert*-butylchloro(4-(diethoxymethyl)phenyl)silane (13)[191]

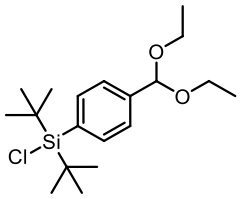

13

A solution of 4-bromobenzadehyde diethyl acetal (0.35 mL, 1.65 mmol) in dry THF (2 mL) was added slowly (over 20 min) to a suspension of magnesium lumps (45 mg, 1.72 mmol, activated by addition of an iodine crystal) in dry THF (3 mL). The mixture was stirred for 2 h, then heated to reflux for 2 h and then left to stir at rt overnight. The resulting mixture was slowly added (over 20 min) to a solution of 4-bromobenzadehyde diethyl acetal (0.50 mL, 2.37 mmol) in THF (3 mL) via syringe. The resulting mixture was heated at reflux for 4 h. After cooling to rt, the solvent was removed *in vacuo* and the yellow, oily residue was redissolved in hexane. The solution was filtered and washed three times with hexane. The combined hexane solutions were concentrated *in vacuo*. The crude product containing **13** (671 mg) has not been purified. The NMR analyses show that the crude product contains minor impurities (aliphatic and aromatic area).

^{1}H NMR (500 MHz, $CDCl_3$): δ = 7.48 (d, *J* = 8.4, 2H), 7.35 (d, *J* = 8.4, 2H), 5.51 (s, 1H), 3.63 – 3.51 (m, 6H), 1.27 – 1.25 (m, 4H) 1.16 (s, 18H); ^{13}C NMR (126 MHz, $CDCl_3$): δ = 139.2, 128.3, 126.8, 116.1, 101.7, 61.2, 58.7, 27.0, 24.8, 18.5, 15.3.

((4-(Di-*tert*-butylsilyl)phenyl)ethynyl)trimethylsilane (14)

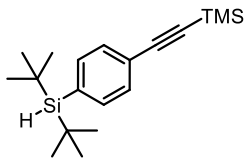

14

A stirring solution of ((4-bromophenyl)ethynyl)trimethylsilane (208 mg, 0.82 mmol) in dry THF (3 mL) was cooled to –78 ºC and *n*-BuLi (2.5 M in hexanes, 0.45 mL,

0.99 mmol) was added dropwise over 5 min and the mixture was stirred for 1 h. Di-*tert*-butylchlorosilane (0.50 mL, 2.47 mmol) was added dropwise and stirring continued for 2 h. The mixture was allowed to warm to rt and stirred overnight. The solvent was removed *in vacuo* and the residue was resuspended in hexane, filtered and the filtrate was reduced to a colorless oil *in vacuo*. The crude product containing **14** (320 mg) was used further without purification.

^{1}H NMR (500 MHz, $CDCl_3$): δ = 7.50 – 7.42 (m, 2H), 7.34 – 7.29 (m, 2H), 4.23 (s, 1H), 1.09 (s, 17H), 0.26 – 0.24 (m, 9H).

Di-*tert*-butylchloro(4-((trimethylsilyl)ethynyl)phenyl)silane (15)

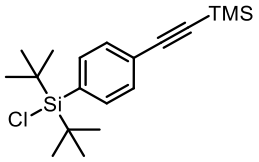

15

Method using *n*-BuLi: A stirring solution of ((4-bromophenyl)ethynyl)trimethylsilane (270 mg, 1.06 mmol) in dry THF (4 mL) was cooled to −78 ºC and *n*-BuLi (2.5 M in hexanes, 0.53 mL, 1.20 mmol) was added dropwise over 5 min and the mixture was stirred for 1 h. The resulting suspension was added dropwise via syringe over a period of 20 min to a cooled and stirring solution (−78 ºC) of di-*tert*-butyldichlorosilane (0.53 mL, 2.50 mmol) in dry THF (2 mL). The resulting mixture was stirred for 1 h at −78 ºC and then allowed to warm to rt and stirring continued over night. The solvents were removed *in vacuo*, and the residue was suspended in hexane, filtered and the filtrate was reduced to a colorless oil *in vacuo*. The crude product containing **15** (346 mg) was used further without purification. NMR analysis shows some chlorosilane-impurities (too high integral at 1.17 ppm).

^{1}H NMR (500 MHz, $CDCl_3$): δ = 7.52 – 7.43 (m, 2H), 7.31 – 7.26 (m, 2H), 1.17 (s, 18H), 0.26 (s, 9H); ^{13}C NMR (126 MHz, $CDCl_3$): δ = 133.2, 132.1, 131.2, 128.6, 128.3, 123.3, 105.3, 94.2, 27.0, 24.9, 0.1.

Grignard reaction: A solution of ((4-bromophenyl)ethynyl)trimethylsilane (0.35 mL, 1.65 mmol) in dry THF (2 mL) was added slowly (over 20 min) to a suspension of magnesium lumps (45 mg, 1.72 mmol) in dry THF (3 mL) that had been activated by addition of a crystal of iodine. The mixture was stirred for 2 h and subsequently refluxed for 2 h. The solution was stirred at rt overnight and the excess magnesium was removed. The resulting Grignard-reagent was added slowly (over 20 min) to a solution of di-*tert*-butyldichlorosilane (0.50 mL, 2.37 mmol) in THF (3 mL). The mixture was heated at reflux for 4 h and stirred further at rt overnight. The solvent was removed *in vacuo* to give a yellow, oily crude product. The crude product containing **15** (644 mg) was not purified.

1-Bromo-4-ethynylbenzene (17)

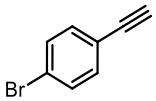

17

To a stirring solution of ((4-bromophenyl)ethynyl)trimethylsilane (519 mg, 2.1 mmol) in dry MeOH (10 mL) was added anhydrous K_2CO_3 (903 mg, 6.0 mmol). The solution was stirred at rt overnight and then poured into water (20 mL). The aqueous layer was extracted with CH_2Cl_2 (3 x 15 mL), and the combined organic layers were washed with sat. aq. NaCl (2 x 20 mL). Combined organic layers were dried over $MgSO_4$ and the solvent was removed *in vacuo*. No further purification was necessary to afford **17** (318 mg, 86%) as off-white crystals in high purity.

R_f = 0.36 (hexane); ^{1}H NMR (500 MHz, $CDCl_3$): δ = 7.46 (d, *J* = 8.8, 2H), 7.35 (d, *J* = 8.5, 2H), 3.12 (s, 1H); ^{13}C NMR (125 MHz, CDCl3): δ = 133.7, 131.8, 123.3, 121.2, 82.7, 78.5. The analytical data were in accordance with those reported.[209]

Di-*tert*-butyl(4-ethynylphenyl)silane (18)[210]

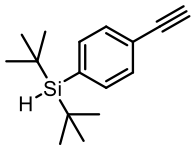

18

To a stirring solution of 4-(di-*tert*-butylsilyl)benzaldehyde (**5**) (115 mg, 0.46 mmol) in dry MeOH (4 mL) under argon atmosphere, anhydrous K_2CO_3 (141 mg, 1.1 mmol) was added. Bestmann-Ohira reagent (**20**) (1.52 g, 0.79 mmol) was dissolved in dry MeOH (1 mL) and added dropwise to the suspension over 5 min, upon which the mixture turned yellow. The reaction was monitored by TLC to full conversion of starting material (3.5 h). The reaction mixture was separated between Et_2O (10 mL) and 5% aq. $NaHCO_3$ (10 mL). The aqueous layer was extracted with Et_2O (10 mL x 3). The combined organic layers were dried over $MgSO_4$, and the solvents were evaporated *in vacuo* to give the crude mixture (228 mg) as a light-yellow oil. The crude mixture was purified by flash chromatography (hexane/EtOAc, 9:1) to give **18** (84 mg, 75%) as a colorless oil.

R_f = 0.70 (hexane/EtOAc, 9:1); ^{1}H NMR (500 MHz, $CDCl_3$): δ = 7.54 (d, *J* = 8.2, 2H), 7.45 (d, *J* = 8.2, 2H), 3.86 (s, 1H), 3.10 (s, 1H), 1.04 (s, 18H); ^{13}C NMR (125 MHz, $CDCl_3$): δ = 137.1, 135.8, 131.1, 122.7, 83.9, 77.9, 29.0, 19.2.

Bestmann-Ohira reagent (20)

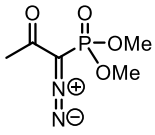

20

Sodium hydride (60% in mineral oil, 110 mg, 4.6 mmol) was suspended in a mixture of dry toluene (16 mL) and dry THF (3 mL) under argon and cooled to 0 ºC in an ice bath. A solution of dimethyl 2-oxopropylphosphonate (0.68 mL, 4.8 mmol) in dry toluene (4 mL) was added in small portions over 5 min. The mixture was then stirred at rt for 1 h before 4-acetamidobenzenesulfonyl azide (1.153 g, 4.8 mmol) dissolved in

dry THF (3 mL) was added dropwise to the suspension, upon which it turned yellow. The reaction mixture was stirred at rt overnight. The mixture was filtered through a short pad of Celite, and the Celite was washed thoroughly with Et_2O. The filtrate was concentrated *in vacuo* to give the crude product as a yellow liquid. Purification by flash chromatography (100% EtOAc) gave **20** (582 mg, 66%) as a yellow oil.

R_f = 0.28 (EtOAc); ^{1}H NMR (500 MHz, $CDCl_3$): δ = 3.77 (s, 3H), 3.75 (s, 3H), 2.28 (3H, s); ^{13}C NMR (125 MHz, $CDCl_3$): δ = 189.8 (d, *J* = 13.0), 53.5 (d, *J* = 5.6), 27.1. The analytical data was in accordance with those reported.[193] The signal for C1 is not visible in the ^{13}C spectrum.

4-(Di-*tert*-butylsilyl)phenyl)methanol (22)

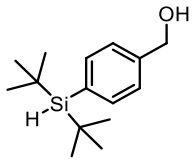

22

Method in one step: A stirring solution of 4-bromobenzyl alcohol (1.022 g, 5.46 mmol) in dry THF (20 mL) was cooled to −78 ºC and n-BuLi (2.5 M in hexanes, 5.3 mL, 13.38 mmol) was added dropwise over 10 min and the mixture was stirred for 1 h. Di-*tert*-butylchlorosilane (1.3 mL, 6.42 mmol) was added dropwise and stirring continued for 1 h at −78 ºC before the mixture was allowed to warm to rt and stirred overnight. The reaction was quenched with saturated NaHCO3 (50 mL), and the organic layer was separated. The aqueous phase was extracted with EtOAc (3 x 60 mL), and the combined organic layers were washed with water (70 mL), saturated NaCl (70 mL) and dried over $MgSO_4$. The solvents were removed in vacuo and the residue was purified by flash chromatography (hexane/EtOAc, 4:1) to give **22** (0.480 g, 37%) as white crystals.

^{1}H NMR (500 MHz, $CDCl_3$): δ = 7.58 (d, 2H, *J* = 8.0), 7.34 (d, 2H, *J* = 8.0), 4.71 (d, *J* = 8.2, 2H), 3.86 (s, 1H), 1.65 (t, *J* = 6.0, 1H), 1.04 (s, 18H); ^{13}C NMR (125 MHz, $CDCl_3$): δ = 141.6, 136.2, 135.0, 126.2, 65.5, 29.1, 19.2.

Method in two steps:[194] To a stirring suspension of sodium hydride (60% dispersion in mineral oil, 121 mg, 2.94 mmol) in THF (10 mL) was added a solution of 4-bromobenzylalcohol (491 mg, 2.62 mmol) in THF (1 mL). The mixture was heated to 45 °C for 3 h and then cooled to −78 ºC, and *n*-BuLi (2.2 M in hexanes, 1.4 mL, 2.94 mmol) was added dropwise to the suspension, after which stirring was continued for 30 min at −78 ºC. Di-*tert*-butylchlorosilane (0.60 mL, 2.94 mmol) was added, and the mixture was stirred for 30 min before it was allowed to warm to rt and stirred overnight. The pH of the reaction mixture was adjusted to 5 by addition of 0.1 M aq. $KHSO_4$, layers were separated, and the aqueous layer was extracted with CH_2Cl_2 (3 x 20 mL). The combined organic layers were washed with water (10 mL), saturated NaCl (10 mL), then dried over Na_2SO_4, filtered, and concentrated *in vacuo* to obtain the crude product as a light yellow oil (897 mg). Purification by flash chromatography (silica gel, hexane/EtOAc 4:1) provided **22** (128 mg, 20%) as a colorless oil.

(4-(Azidomethyl)phenyl)di-*tert*-butylsilane (25)

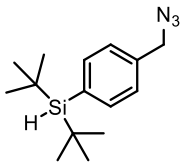

25

To a stirring solution of 4-(di-*tert*-butylsilyl)-benzyl alcohol (**22**) (101 mg, 0.40 mmol) in dry DMF (2 mL), DBU (0.12 mL, 0.80 mmol) and DPPA (0.18 mL, 0.80 mmol) were added. The reaction mixture was stirred at rt overnight, and then extracted with pentane (5 x 10 mL). The organic layers were combined and the solvent was evaporated *in vacuo* to give **25** (88 mg, 80%) as a colourless oil.

^{1}H NMR (500 MHz, $CDCl_3$): δ = 7.60 (d, *J* = 8.0, 2H), 7.27 (d, *J* = 8.0, 2H), 4.36 (s, 2H), 3.88 (s, 1H), 1.05 (s, 18H); ^{13}C NMR (125 MHz, $CDCl_3$): δ = 136.4, 136.2, 135.9, 127.3, 55.0, 29.0, 19.2. The analytical data were in accordance with those reported.[112]

2-(4-Bromophenethoxy)tetrahydro-2*H*-pyran (31)[107]

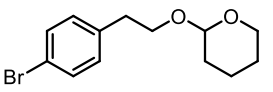

31

To a solution of 2-(4-bromophenyl)ethan-1-ol (0.70 mL, 4.97 mmol) in CH_2Cl_2 (20 mL), DHP (3.2 mL, 34.8 mmol) and pyridinium *para*-toluenesulfonate (22 mg, 0.08 mmol) were added. After stirring at rt overnight the mixture was washed with saturated $NaHCO_3$ (20 mL), saturated NaCl (20 mL) and dried over $MgSO_4$. The solvent was removed *in vacuo* to give **31** (1.704 g) as a colorless liquid, which was used in the next step without further purification.

^{1}H NMR (500 MHz, $CDCl_3$): δ = 7.39 (d, *J* = 8.3, 2H), 7.11 (d, *J* = 8.3, 2H), 4.59 – 4.54 (m, 1H), 3.94 – 3.89 (m, 1H), 3.73 (ddd, *J* = 11.2, 8.6, 3.2, 1H), 3.58 (dt, *J* = 9.7, 6.9, 1H), 3.47 – 3.43 (m, *z*1H), 2.85 (t, *J* = 7.0, 2H), 1.83 – 1.75 (m, 1H), 1.71 – 1.65 (m, 1H), 1.58 – 1.46 (m, 5H); ^{13}C NMR (126 MHz, $CDCl_3$): δ = 138.4, 131.4, 130.9, 120.1, 98.8, 67.9, 62.3, 35.9, 30.7, 25.5, 19.6. The analytical data were in accordance with those reported.[211]

2-(4-(Diisopropylsilyl)phenyl)ethan-1-ol (33)[105]

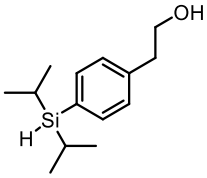

33

Step 1: A stirring solution of bromide **31** (1.010 g, 2.92 mmol) in dry THF (15 mL) was cooled to −78 ºC and *n*-BuLi (1.6 M in hexanes, 12.7 mL, 4.30 mmol) was added dropwise over 5 min and the mixture was stirred for 1 h at −78 ºC. Diisopropylchlorosilane (0.72 mL, 4.21 mmol) was added, and the mixture was allowed to warm to rt and stirred overnight. The reaction was quenched by addition of saturated $NaHCO_3$ (15 mL) and extracted with EtOAc (2 x 15 mL). The combined organic layers were washed with saturated NaCl (2 x 20 mL) and dried over $MgSO_4$.

The solvents were removed *in vacuo* and the colorless, oily residue containing THP-ether **32** (1.324 g) which was used in the next step without further purification.

Step 2: *Para*-toluenesulfonic acid (491 mg, 2.85 mmol) was added to THP-ether **32** (913 mg, 2.85 mmol) in EtOH (30 mL) and stirred at rt for 2 h. The reaction mixture was then poured into saturated $NaHCO_3$ (15 mL) and extracted with CH_2Cl_2 (3 x 50 mL). The combined organic extracts were washed with saturated NaCl (2 x 100 mL) and dried over $MgSO_4$. Evaporation of the solvent *in vacuo* gave the crude product (1.408 g) which was purified by flash chromatography (hexane/EtOAc 4:1) to give alcohol **33** (315 mg, 47% over two steps, containing 35% of *n*-butyl side-product **38**) as a colorless oil.

R_f = 0.20 (hexane/EtOAc, 4:1); ^{1}H NMR (500 MHz, $CDCl_3$): δ = 7.47 (d, *J* = 8.0, 2H), 7.22 (d, *J* = 7.9, 2H), 3.94 (s, 1H), 3.88 (s, 2H), 2.87 (s, 2H), 1.52 (bs, 1H), 1.25 – 1.19 (m, 2H), 1.07 (d, *J* = 7.3, 6H), 1.00 (d, *J* = 7.3, 6H); ^{13}C NMR (126 MHz, $CDCl_3$): δ = 139.5, 135.9, 132.0, 128.5, 63.7, 39.4, 18.8, 18.6, 10.9. The analytical data were in accordance with those previously reported.[105]

2-(2-(4-Bromophenoxy)ethoxy)tetrahydro-2*H*-pyran (35)

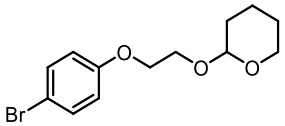

35

4-Bromophenol (998.7 mg, 5.78 mmol) was dissolved in $(CH_3)_2SO$ (15 mL) and KOH (1.483 g, 26.0 mmol) was added. After 5 min of stirring, 2-(2-bromopropoxy)-tetrahydro-2*H*-pyran (1.3 mL, 8.67 mmol) was added. The reaction mixture was stirred at rt overnight and then partitioned between water (100 mL) and CH_2Cl_2 (100 mL). The aqueous layer was extracted with CH_2Cl_2 (2 x 50 mL) and the combined organic layers were washed with saturated NaCl (3 x 100 mL), dried over $MgSO_4$.The solvents were removed *in vacuo* and the residue was purified by flash chromatography (silica gel deactivated by 3% TEA, hexane/EtOAc 4:1. Removal of the solvent under reduced pressure gave **35** as a colorless oil (1.105 g, 65%).

R_f = 0.33 (hexane/EtOAc, 4:1); ^{1}H NMR (500 MHz, $CDCl_3$): δ 7.36 (d, *J* = 9.0, 2H), 6.81 (d, *J* = 9.0, 2H), 4.71 – 4.67 (m, 1H), 4.13 – 4.10 (m, 2H), 4.06 – 4.02 (m, 1H), 3.89 (td, *J* = 8.1, 4.1, 1H), 3.82 – 3.77 (m, 1H), 3.54 – 3.50 (m, 1H), 1.87 – 1.79 (m, 1H), 1.77 – 1.70 (m, 1H), 1.65 – 1.50 (m, 4H); ^{13}C NMR (126 MHz, $CDCl_3$): δ = 158.2, 132.3, 116.7, 113.1, 99.2, 67.8, 65.9, 62.3, 30.6, 25.5, 19.5; HRMS (ESI+): *m/z* $[M+Na]^+$ calcd for $C_{13}H_{17}BrNaO_3^+$: 323.0253/325.0233, found 323.0253/325.0233, *m/z* $[2M+Na]^+$ calcd for $C_{26}H_{34}Br_2NaO_6^+$: 625.0594, found 625.0588.

2-(4-(Diisopropylsilyl)phenoxy)ethan-1-ol (37)

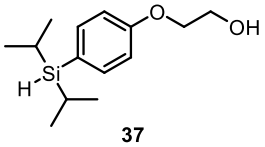

37

Step 1: A stirring solution of bromide **35** (530 mg, 1.76 mmol) in dry THF (5 mL) was cooled to −78 ºC and *n*-BuLi (2.0 M in hexanes, 1.8 mL, 3.51 mmol) was added dropwise over 5 min and the mixture was stirred for 1 h. Diisopropylchlorosilane (0.36 mL, 2.11 mmol) was added, and the mixture was allowed to warm to rt and stirred overnight. The reaction was quenched with saturated $NaHCO_3$ (20 mL) and extracted with EtOAc (2 x 20 mL). The combined organic layers were washed with saturated NaCl (2 x 20 mL) and dried over $MgSO_4$. The solvents were removed *in vacuo* and the residue containing THP-ether **36** (592 mg) was judged to be pure enough to continue to the next step without further purification.

Step 2: To a solution of THP-ether **36** (592 mg, 1.76 mmol) in MeOH (20 mL) was added PPTS (53 mg, 0.21 mmol) and the mixture was stirred at rt overnight. The resulting mixture was then poured into water (50 mL) and extracted with CH_2Cl_2 (2 x 50 mL). The combined organic layers were washed with saturated NaCl (2 x 100 mL) and dried over $MgSO_4$. The solvent was removed *in vacuo* to leave an oily/solid residue (412 mg) which was purified by flash chromatography (hexane/EtOAc 4:1) to give compound **37** (241 mg, 55%) as a colorless oil.

R_f = 0.17 (hexane/EtOAc, 4:1); ^{1}H NMR (500 MHz, $CDCl_3$): δ = 7.44 (d, *J* = 8.6, 2H), 6.92 (d, *J* = 8.6, 2H), 4.11 – 4.08 (m, 2H), 3.98 – 3.95 (m, 2H), 3.92 (d, *J* = 3.1, 1H),

2.13 (s, 1H), 1.24 – 1.16 (m, 2H), 1.06 (d, J = 7.3, 6H), 0.98 (d, J = 7.3, 6H); ^{13}C NMR (126 MHz, $CDCl_3$): δ = 159.7, 137.1, 125.6, 114.2, 69.0, 61.6, 18.8, 18.6, 10.9.

(4-(Diisopropylsilyl)phenyl)methanol (41)

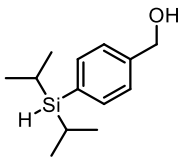

41

A stirring solution of 4-bromobenzylalcohol (1.472 g, 7.87 mmol) in dry THF (60 mL) was cooled to −78 ºC and *n*-BuLi (2.5 M in hexanes, 6.8 mL, 16.8.0 mmol) was added dropwise over 10 min and the mixture was stirred for 1 h. Diisopropylchlorosilane (1.64 mL, 9.62 mmol) was added dropwise and stirring continued for 1 h at −78 ºC before the mixture was allowed to warm to rt and stirred overnight. The reaction was quenched by addition of saturated $NaHCO_3$ (70 mL), and the resulting layers were separated. The aqueous layer was extracted with EtOAc (3 x 50 mL), and the combined organic layers were washed with water (70 mL), saturated NaCl (70 mL) and dried over $MgSO_4$. The solvents were removed *in vacuo* and the residue was purified by flash chromatography (hexane/EtOAc, 4:1) to give **41** (1.424 g, 81%) as a colorless oil.

R_f = 0.30 (hexane/EtOAc, 4:1); ^{1}H NMR (500 MHz, $CDCl_3$): δ = 7.51 (d, J = 8.0, 2H), 7.35 (d, J = 8.0, 2H), 4.69 (s, 2H), 3.95 (t, J = 3.2, 1H), 1.81 (bs, 1H), 1.27-1.19 (m, 2H), 1.06 (d, J = 7.3, 6H), 0.99 (d, J = 7.4, 6H); ^{13}C NMR (125 MHz, $CDCl_3$): δ = 141.7, 136.8, 133.5, 126.2, 65.3, 18.7, 18.5, 10.7. The analytical data were in accordance with those previously reported.[198]

(4-(Azidomethyl)phenyl)diisopropyl silane (42)

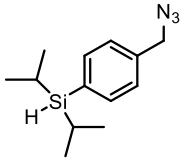

42

Method A: To a stirring solution of benzyl alcohol **41** (476 mg, 2.14 mmol) in dry DMF (5 mL), DBU (0.64 mL, 4.29 mmol) and DPPA (0.96 mL, 4.28) were added and stirring

continued at rt overnight. Water (10 mL) was added and the resulting mixture was extracted with pentane (3 x 20 mL). The combined organic layers were washed with water (30 mL), 5% citric acid (30 mL) and saturated NaCl (30 mL) and dried over $MgSO_4$. The solvent was evaporated *in vacuo* to give the crude product as a yellow oil, which was purified by flash chromatography (hexane/EtOAc, 4:1) to give **42** (366 mg, 77%) as a colorless oil.

R_f = 0.72 (hexane/EtOAc, 4:1); ^{1}H NMR (500 MHz, $CDCl_3$): δ = 7.54 (d, *J* = 8.0, 2H), 7.31 (d, *J* = 8.0, 2H), 4.36 (s, 2H), 3.96 (t, *J* = 3.2, 1H), 1.28 – 1.20 (m, 2H), 1.08 (d, *J* = 7.4, 6H), 1.00 (d, *J* = 7.4, 6H); ^{13}C NMR (126 MHz, $CDCl_3$): δ = 136.4, 136.1, 134.6, 127.5, 55.0, 18.8, 18.6, 10.8. The analytical data were in accordance with those reported.[113]

Method B: To a stirring solution of benzyl alcohol **41** (442 mg, 2.0 mmol) in dry DMF (10 mL), DBU (0.6 mL, 4.0 mmol) and DPPA (0.9 mL, 4.0 mmol) were added and stirring continued at rt overnight. The reaction mixture was extracted with pentane (5 x 20 mL), the organic layers were combined, and the solvent was evaporated *in vacuo* to give **42** (272 mg, 55%) as a colorless oil which required no further purification before performing the next step.

4-(Diisopropylsilyl)benzaldehyde (43)

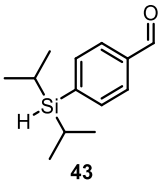

43

Method using manganese(IV)dioxide:[110, 195] (4-(Diisopropylsilyl)phenyl)methanol (**41**) (216 mg, 0.97 mmol) was dissolved in dry CH_2Cl_2 (4 mL) and added to a suspension of activated MnO_2 (843 mg, 9.7 mmol) in dry CH_2Cl_2 (10 mL) under argon atmosphere. The suspension was stirred at rt overnight. The black residue was filtered through a pad of Celite and the Celite was washed thoroughly with CH_2Cl_2. The filtrate was concentrated *in vacuo* to give **43** (195 mg, 91%) as a colorless oil which was used in the next step without further purification.

R_f = 0.59 (hexane/EtOAc, 9:1); ^{1}H NMR (500 MHz, $CDCl_3$): δ = 10.03 (s, 1H), 7.84 (d, *J* = 8.0, 2H), 7.69 (d, *J* = 8.0, 2H), 3.99 (t, *J* = 3.3, 1H), 1.30 – 1.22 (m, 2H), 1.07 (d, *J* = 7.4, 6H), 0.99 (d, *J* = 7.4, 6H); ^{13}C NMR (125 MHz, $CDCl_3$): δ = 192.8, 143.4, 136.9, 136.1, 128.6, 18.7, 18.5, 10.7. The analytical data were in accordance with those reported.[110, 195]

Method using Dess-Martin oxidation:[212] Dess-Martin periodinane (DMP) (443 mg, 1.05 mmol) was added to a solution of (4-(diisopropylsilyl)phenyl)methanol (**41**) (155 mg, 0.69 mmol) in dry CH_2Cl_2 (5 mL) at 0 °C. The reaction mixture was stirred at rt overnight and then Et_2O (3 mL) was added. The organic layer was washed with 1.5 M NaOH (10 mL), and the aqueous layer was extracted with CH_2Cl_2 (3 x 10 mL), and the combined organic layers were washed with saturated NaCl (2 x 35 mL), dried over $MgSO_4$ and the solvent was removed *in vacuo* to give the aldehyde **43** (140 mg, 92%) as a colorless oil which required no further purification.

Note: These results could not be reproduced.

Ethyl 6-(((4-(azidomethyl)phenyl)diisopropylsilyl)oxy)hexanoate (45)

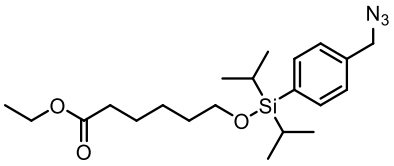

45

Azide **42** (272.0 mg, 1.11 mmol) was dissolved in dry CH_2Cl_2 (18 mL) under argon atmosphere. Trichloroisocyanuric acid (89.0 mg, 0.37 mmol) was added at 0 ºC, and the mixture was stirred for 2 h at rt. The mixture was cooled to 0 ºC before imidazole (340 mg, 4.99 mmol) and ethyl 6-hydroxyhexanoate (0.22 µL, 1.33 mmol) were added. The mixture was allowed to warm to rt and stirring was continued overnight. The resulting suspension was separated between $CHCl_3$ (50 mL) and saturated NaCl (50 mL), and the organic layer was dried over Na_2SO_4. The solvents were removed *in vacuo* and the resulting oil was purified by flash chromatography (hexane/EtOAc, 9:1) to give **45** (326 mg, 72%) as a colorless oil.

R_f = 0.35 (hexane/EtOAc, 9:1); ^{1}H NMR (500 MHz, $CDCl_3$): δ = 7.56 (d, *J* = 8.0, 2H), 7.31 (d, *J* = 8.0, 2H), 4.36 (s, 2H), 4.13 (q, *J* = 7.1, 2H), 3.75 (t, *J* = 6.5, 2H), 2.32 (t, *J* = 7.6, 2H), 1.70-1.61 (m, 4H), 1.47-1.40 (m, 2H), 1.28-1.23 (m, 5H), 1.05 (d, *J* = 7.4, 6H), 0.99 (d, *J* = 7.4, 6H); ^{13}C NMR (125 MHz, $CDCl_3$): δ = 173.9, 136.4, 135.2, 135.1, 127.4, 63.8, 60.3, 55.0, 34.5, 32.7, 25.6, 25.0, 17.5, 17.4, 14.4, 12.2; HRMS (ESI+): *m/z* $[M+Na]^+$ calcd for $C_{21}H_{35}N_3NaO_3Si^+$: 428.2340; found: 428.2340.

(4-(1,3-Dioxolan-2-yl)phenyl)di-*tert*-butylsilane (10)

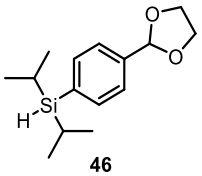

46

A stirring solution of 2-(4-bromophenyl)-1,3-dioxolane (250 mg, 1.09 mmol) in dry THF (2.5 mL) was cooled to −78 ºC and *n*-BuLi (2.2 M in hexanes, 1.1 mL, 2.18 mmol) was added dropwise over 5 min and the mixture was stirred for 30 min. Diisopropylchlorosilane (0.21 mL, 1.20 mmol) was added and stirring continued for 2 h at −78 ºC before the mixture was allowed to warm to rt and stirred overnight. Saturated aqueous $NaHCO_3$ (3 mL) was added to quench the reaction and the two layers were separated. The aqueous layer was extracted with EtOAc (3 x 15 mL), and the organic layers were combined, washed with saturated NaCl (10 mL), and dried over $MgSO_4$. The solvents were removed *in vacuo* and the residue was purified by flash chromatography (silica gel deactivated by 3% TEA, hexane/EtOAc 9:1. Removal of the solvent under reduced pressure gave a colorless oil (101 mg) of a mixture of **46** and the *n*-butylated side-product **47.** The ratio between **46** and **47** was approx. 7:3. The calculated yield for **46** was 25%.

^{1}H NMR (500 MHz, $CDCl_3$) δ 7.54 (d, *J* = 8.1, 2H), 7.46 (d, *J* = 8.1, 2H), 5.81 (s, 1H), 4.17 – 4.12 (m, 2H), 4.06 – 4.03 (m, 2H), 3.95 (t, *J* = 3.2, 1H), 1.25 – 1.19 (m, 2H), 1.06 (d, *J* = 7.4, 6H), 0.98 (d, *J* = 7.3, 6H); ^{13}C NMR (126 MHz, $CDCl_3$): δ = 138.7, 135.7, 125.8, 103.9, 65.4, 18.7, 18.5, 10.8.

(4-Ethynylphenyl)diisopropyl(methoxy)silane (49)

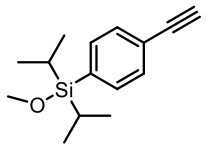

49

Silane **41** (303 mg, 1.35 mmol) was dissolved in anhydrous THF (20 mL) and activated MnO_2 (587 mg, 6.75 mmol) was added. The suspension was stirred at rt for 4 h. Anhydrous MeOH (18 mL) was added and anhydrous K_2CO_3 (373 mg, 2.70 mmol) was added. Bestmann-Ohira's reagent **20** (311 mg, 1.62 mmol) was dissolved in anhydrous MeOH (2 mL) and added drop-wise to the suspension over 5 minutes. The mixture was stirred at rt overnight and then filtered through a pad of Celite and washed thoroughly with CH_2Cl_2. The organic solvents were removed *in vacuo* and the residue was dissolved in CH_2Cl_2 (30 mL) and washed with 5% $NaHCO_3$ (30 mL), saturated NaCl (30 mL) dried over $MgSO_4$. The solvent was evaporated *in vacuo* to give the crude product containing **49** (119 mg, 36%) as a yellow oil.

R_f = 0.69 (hexane/EtOAc, 9:1); ^{1}H NMR (500 MHz, $CDCl_3$): δ = 7.52 – 7.47 (m, 4H), 3.61 (s, 3H), 3.11 (s, 1H), 1.32 – 1.27 (m, 2H), 1.06 (d, *J* = 7.4, 7H), 1.00 (d, *J* = 7.5, 6H); ^{13}C NMR (125 MHz, $CDCl_3$): δ = 135.7, 134.6, 131.3, 123.0, 83.9, 77.9, 52.2, 17.5, 17.3, 12.0; HRMS (GC-EI+): *m/z* M^+ calcd for $C_{15}H_{22}OSi^+$: 246.1434, found: 246.1444; fragmentation *m/z* 246 (M^+), 203 (M – isopropyl), 175 (M – isopropyl – 28), 145.

4-((But-3-yn-1-yloxy)diisopropylsilyl)benzaldehyde (50)

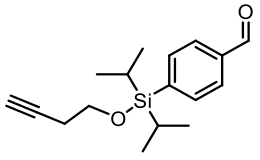

50

Silane **43** (165 mg, 0.75 mmol) was dissolved in dry CH_2Cl_2 (15 mL) under argon atmosphere. Trichloroisocyanuric acid (59 mg, 0.25 mmol) was added at 0 ºC, and the mixture was stirred at rt for 2 h. The mixture was cooled to 0 ºC before imidazole (230 mg, 3.4 mmol) and 3-butyn-1-ol (69 µL, 0.90 mmol) were added after which the

mixture was allowed to warm to rt and stirred overnight. The resulting suspension was separated between $CHCl_3$ (80 mL) and saturated NaCl (80 mL), and the organic layer was collected and dried over Na_2SO_4. The solvents were removed *in vacuo* to give an oil (257 mg), which was purified by flash chromatography (hexane/EtOAc, 9:1) to give **50** as a colorless oil (124 mg, 58%).

R_f = 0.35 (hexane/EtOAc, 9:1); ^{1}H NMR (500 MHz, $CDCl_3$): δ = 10.04 (s, 1H), 7.86 (d, *J* = 8.2, 2H), 7.75 (d, *J* = 8.2, 2H), 3.92 (t, *J* = 7.0, 2H), 2.53 (dt, *J* = 7.0, 2.6, 2H), 2.00 (t, *J* = 2.6, 1H), 1.35 – 1.29 (m, 2H), 1.07 (d, *J* = 7.4, 6H), 1.01 (d, *J* = 7.4, 6H); ^{13}C NMR (125 MHz, $CDCl_3$): δ = 192.8, 143.2, 137.0, 135.2, 128.6, 81.4, 69.8, 62.5, 23.0, 17.4, 17.3, 12.1; HRMS (GC-EI+): *m/z* M^+ calcd for $C_{17}H_{24}O_2Si^+$: 288.1546, found [M-43] = 245.0990; fragmentation *m/z* 288 (M^+), 245 (M – isopropyl), 215 (M – isopropyl – 30), 173.

(4-(Azidomethyl)phenyl)di-*tert*-butylchlorosilane (51)

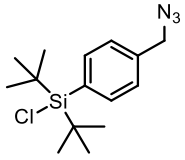

51

To a stirring solution of **25** (172.8 mg, 0.63 mmol) in anhydrous CH_2Cl_2 (6 mL) under argon at 0 ºC, was added trichloroisocyanuric acid (48.1 mg, 0.21 mmol) carefully. The reaction mixture was stirred for 2 h. The resulting suspension was separated between $CHCl_3$ (30 mL) and saturated NaCl (30 mL), and the organic phase was collected and dried over Na2SO4. The solvents were removed in vacuo and the crude oil (829 mg) was purified by flash chromatography (hexane/EtOAc, 9:1) to give **51** as a colorless oil (107.9 mg, 56%).

R_f = 0.47 (hexane/EtOAc, 9:1); ^{1}H NMR (500 MHz, $CDCl_3$): δ = 7.78 (d, 2H, *J* = 8.2), 7.34 (d, 2H, *J* = 8.2), 4.38 (s, 2H), 1.11 (s, 18H); ^{13}C NMR (125 MHz, $CDCl_3$): δ = 137.0, 135.5, 133.2, 127.3, 54.8, 28.1, 22.2.

Ethyl 6-(((4-(azidomethyl)phenyl)di-*tert*-butylsilyl)oxy)hexanoate (53)

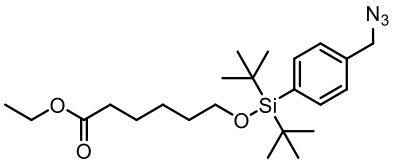

53

Azide **25** (116.5 mg, 0.43 mmol) was dissolved in dry CH_2Cl_2 (1.5 mL) under argon atmosphere. Trichloroisocyanuric acid (33.0 mg, 0.14 mmol) was added at 0 ºC, and the mixture was stirred for 2 h at rt. The mixture was cooled to 0 ºC before imidazole (132 mg, 1.94 mmol), ethyl 6-hydroxyhexanoate (0.7 mL, 4.3 mmol) and anhydrous DMF (1 mL) were added. The mixture was stirred at 40 ºC overnight. The resulting suspension was separated between $CHCl_3$ (50 mL) and saturated NaCl (50 mL), and the organic phase was collected and dried over Na_2SO_4. The solvents were removed in vacuo and the crude oil (153 mg) was purified by flash chromatography (hexane/EtOAc, 9:1) to give **53** as a colorless oil (23.3 mg, 13%).

R_f = 0.40 (hexane/EtOAc, 9:1); ^{1}H NMR (500 MHz, CDCl3): δ = 7.62 (d, *J* = 8.1, 2H), 7.30 (d, *J* = 8.1, 2H), 4.36 (s, 2H), 4.14 (q, *J* = 7.1, 2H), 3.91 (t, *J* = 6.4, 2H), 2.34 (t, *J* = 7.5, 2H), 1.75 – 1.66 (m, 4H), 1.52 – 1.46 (m, 2H), 1.26 (t, *J* = 7.1, 3H), 1.04 (s, 18H); ^{13}C NMR (125 MHz, $CDCl_3$): δ = 173.9, 136.1, 135.6, 135.0, 127.1, 64.4, 60.4, 55.0, 34.6, 32.8, 28.5, 28.1, 25.6, 25.0, 21.1, 14.4; HRMS (ESI+): *m/z* $[M+Na]^+$ calcd for $C_{23}H_{39}N_3NaO_3Si^+$: 456.2653; found: 456.2653.

(4-Bromo-3-methylphenyl)methanol (59)

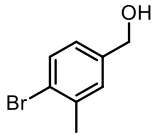

59

Finely powdered sodium borohydride (2.0671 g, 54.4 mmol) was suspended in a solution of methyl 4-bromo-3-methylbenzoate (2.012 g, 8.74 mmol) in THF (20 mL). The resulting mixture was stirred for 15 min at 65 °C. Methanol (8 mL) was then added dropwise for 30 min and effervescence was observed. Stirring at 65 °C was maintained until TLC analysis indicated that the starting material had been consumed. The mixture

was cooled to rt and quenched by addition of saturated NH_4Cl (40 mL) and the resulting layers were separated. The aqueous layer was extracted with EtOAc (2 × 25 mL), and the combined organic layers were dried over $MgSO_4$ and concentrated *in vacuo*. The crude material was purified using a Biotage Sfär silica gel cartridge (20 µm, 25 g) using hexane/EtOAc (4:1) as eluent and 40 mL/min flow rate. The peak that eluted at approx. 3-9 min was collected. Removal of the solvent under reduced pressure gave **59** (1.659 g, 95%) as a light-orange oil.

R_f = 0.15 (hexane/EtOAc, 4:1); ^{1}H NMR (500 MHz, $CDCl_3$): δ 7.50 (d, *J* = 8.2, 1H), 7.24 (d, *J* = 2.5, 1H), 7.04 (dd, *J* = 8.1, 2.6, 1H), 4.52 (s, 2H), 2.40 (s, 3H), 1.71 (s, 1H); ^{13}C NMR (125 MHz, $CDCl_3$): δ = 140.2, 138.1, 132.5, 129.5, 126.0, 124.0, 64.7, 23.1. The spectral data matched those previously reported[213]

((4-(Diisopropylsilyl)-3-methylphenyl)methanol (60)

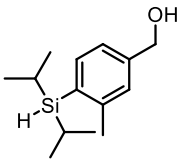

60

A stirring solution of (4-bromo-3-methylphenyl)methanol (1.113 g, 4.97 mmol) in dry THF (37 mL) was cooled to −78 ºC and *n*-BuLi (2.5 M in hexanes, 4.2 mL, 10.45 mmol) was added dropwise over 10 min and the mixture was stirred for 1 h. Diisopropylchlorosilane (1.0 mL, 5.96 mmol) was added dropwise and stirring continued for 1 h at −78 ºC before the mixture was allowed to warm to rt and stirred overnight. The reaction was quenched by addition of saturated $NaHCO_3$ (40 mL) and the two layers were separated. The aqueous layer was extracted with EtOAc (3 x 30 mL), and the combined organic layers were washed with water (50 mL), saturated NaCl (50 mL) and dried over $MgSO_4$. The solvents were removed *in vacuo* and the crude product was purified using a Biotage Sfär silica gel cartridge (20 µm, 25 g) using hexane/EtOAc (4:1) as eluent and 20 mL/min flow rate. The peak that eluted at approx. 2-4.5 min was collected. Removal of the solvent under reduced pressure gave **60** (715 mg, 55%) as a colorless oil. The material contains residual EtOAc.

R_f = 0.33 (hexane/EtOAc, 4:1); ^{1}H NMR (500 MHz, $CDCl_3$): δ = 7.43 (d, *J* = 7.5, 1H), 7.18 (s, 1H), 7.15 (d, *J* = 7.5, 1H), 4.66 (s, 2H), 4.08 (t, *J* = 3.7, 1H), 2.45 (s, 3H), 1.69 (bs, 1H), 1.31 – 1.22 (m, 2H), 1.09 (d, *J* = 7.3, 6H), 0.96 (d, *J* = 7.4, 6H); ^{13}C NMR (125 MHz, $CDCl_3$): δ = 144.7, 141.9, 136.6, 133.1, 128.4, 123.4, 65.5, 23.4, 19.2, 19.0, 11.3; HRMS (GC-EI+): *m/z* M^+ calcd for $C_{14}H_{24}OSi^+$: 236.1591; found: 236.1600; fragmentation *m/z* 236 (M^+), 193 (M – $CH_2CH_2CH_3$), 165 (M – $CH_2CH_2CH_3$– CH_2=CH_2), 151 (M – $CH_2CH_2CH_3$ – CH_2CHCH_3)

4-(Diisopropylsilyl)-3-methylbenzaldehyde (61)

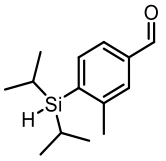

61

Benzylic alcohol **60** (600 mg, 2.54 mmol) was added to a suspension of activated MnO_2 (2.250 g, 25.2 mmol) in dry CH_2Cl_2 (40 mL) under argon atmosphere. The suspension was stirred at rt overnight and the resulting black suspension was filtered through a pad of Celite and the Celite was washed thoroughly with CH_2Cl_2. The filtrate was concentrated *in vacuo* to give **61** (536 mg, 90%) as a colorless oil which was used in the next step without further purification.

R_f = 0.70 (hexane/EtOAc, 4:1); ^{1}H NMR (500 MHz, $CDCl_3$): δ = 9.99 (s, 1H), 7.67 – 7.58 (m, 3H), 4.12 (t, *J* = 3.8, 1H), 2.53 (s, 3H), 1.34 – 1.27 (m, 2H), 1.10 (d, *J* = 7.4, 6H), 0.97 (d, *J* = 7.4, 6H); ^{13}C NMR (126 MHz, $CDCl_3$): δ = 193.0, 145.2, 142.8, 137.0, 136.7, 130.2, 125.9, 23.4, 19.1, 19.0, 11.2; HRMS (GC-EI+): *m/z* M^+ calcd for $C_{14}H_{22}OSi^+$: 234.1434, found: $[M\text{-}43]^+$ = 191.0788; fragmentation *m/z* 234 (M^+), 191 (M – $CH_2CH_2CH_3$), 163 (M – $CH_2CH_2CH_3$ – CH_2=CH_2), 149 (M – $CH_2CH_2CH_3$ – CH_2CHCH_3)

4-((But-3-yn-1-yloxy)diisopropylsilyl)-3-methylbenzaldehyde (62)

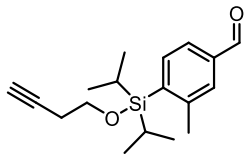

62

Silane **61** (506 mg, 2.15 mmol) was dissolved in dry CH_2Cl_2 (6 mL) under argon atmosphere and cooled to 0 ºC before trichloroisocyanuric acid (166 mg, 0.71 mmol) was added. The cooling bath was removed, and the mixture was stirred at rt for 3 h before it was cooled to 0 ºC and imidazole (658 mg, 9.68 mmol) and 3-butyn-1-ol (0.25 mL, 3.20 mmol) were added. The mixture was allowed to warm to rt and stirred overnight. The resulting suspension was separated between $CHCl_3$ (80 mL) and saturated NaCl (80 mL), and the organic layer was dried over $MgSO_4$. The solvents were removed *in vacuo* and the crude product was purified using a Biotage Sfär silica gel cartridge (20 µm, 10 g) using hexane/EtOAc (19:1 → 4:1) as eluent and 20 mL/min flow rate. The peak that eluted at approx. 1-3 min was collected. Removal of the solvent under reduced pressure gave **62** (453 mg, 70%) as a colorless oil.

R_f = 0.47 (hexane/EtOAc, 9:1); ^{1}H NMR (500 MHz, $CDCl_3$): δ = 10.03 (s, 1H), 7.74 (d, *J* = 8.0, 1H), 7.70 – 7.65 (m, 2H), 3.98 (t, *J* = 7.0, 2H), 2.56 – 2.53 (m, 5H), 2.02 (t, *J* = 2.7, 1H), 1.41 (p, *J* = 7.4, 2H), 1.12 (d, *J* = 7.4, 6H), 1.04 (d, *J* = 7.4, 6H); ^{13}C NMR (126 MHz, $CDCl_3$): δ = 193.0, 145.1, 142.4, 137.0, 136.4, 130.8, 125.7, 81.4, 69.8, 62.6, 23.2, 23.0, 17.8, 17.7, 13.2; HRMS (GC-EI+): *m/z* M^+ calcd for $C_{18}H_{26}O_2Si^{\bullet+}$: 302.1697, found: $[M-43]^+$ = 259.1150; fragmentation *m/z* 302 (M^+), 259 (M – $CH_2CH_2CH_3$), 229 (M – $CH_2CH_2CH_3$ – 30), 201 (M – $CH_2CH_2CH_3$ – 30 – CH_2=CH_2), 187 (M – $CH_2CH_2CH_3$ – 30 – $CH_2CH_2CH_3$).

(4-(Azidomethyl)-2-methylphenyl)diisopropyl silane (63)

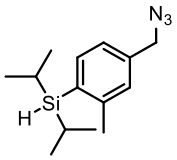

63

To a stirring solution of benzyl alcohol **60** (700 mg, 3.29 mmol) in dry DMF (6 mL), DBU (1.0 mL, 6.59 mmol) and DPPA (1.5 mL, 6.59 mmol) were added and stirring continued at rt overnight. The reaction mixture was extracted with pentane (5 x 10 mL), and the solvent was evaporated *in vacuo* to give a light-yellow oil. The crude product was purified using a Biotage Sfär silica gel cartridge (20 µm, 25 g) using hexanes/EtOAc (19:1) as eluent and 40 mL/min flow rate. The peak that eluted at approx. 1.5-2.5 min was collected. Removal of the solvent under reduced pressure gave **63** (641 mg, 83%) as a colorless oil.

R_f = 0.67 (hexane/EtOAc, 4:1); ^{1}H NMR (600 MHz, $CDCl_3$): δ = 7.46 (d, *J* = 7.5, 1H), 7.15 – 7.10 (m, 2H), 4.32 (s, 2H), 4.11 (t, *J* = 3.7, 1H), 2.47 (s, 3H), 1.31 – 1.24 (m, 2H), 1.09 (d, *J* = 7.4, 6H), 0.97 (d, *J* = 7.4, 6H); ^{13}C NMR (151 MHz, $CDCl_3$): δ = 144.9, 136.7, 136.4, 133.9, 129.4, 124.5, 54.9, 23.4, 19.2, 19.0, 11.3; HRMS (GC-EI+): *m/z* M^+ calcd for $C_{14}H_{23}N_3Si^+$: 261.1611, found: $[M-43]^+$ = 218.1112; fragmentation *m/z* 261 (M^+), 218 (M – $CH_2CH_2CH_3$), 190 (M – $CH_2CH_2CH_3$ – CH_2=CH_2), 162, 148.

Ethyl 6-(((4-(azidomethyl)-2-methylphenyl)diisopropylsilyl)oxy)hexanoate (64)

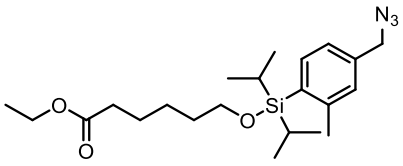

64

Silane **63** (541 mg, 2.07 mmol) was dissolved in dry CH_2Cl_2 (6 mL) under argon atmosphere. Trichloroisocyanuric acid (165 mg, 0.69 mmol) was added at 0 ºC, and the mixture was stirred for 2 h at rt. The mixture was cooled to 0 ºC before imidazole (650 mg, 9.55 mmol) and ethyl 6-hydroxyhexanoate (0.50 mL, 3.07 mmol) were added. The mixture was warmed to rt and stirred overnight. The resulting suspension

was separated between $CHCl_3$ (70 mL) and saturated NaCl (70 mL), and the organic layer was dried over Na_2SO_4. The solvents were removed *in vacuo* and the crude material was purified using a Biotage Sfär silica gel cartridge (20 µm, 10 g) using hexane/EtOAc (19:1) as eluent and 20 mL/min flow rate. The peak that eluted at approx. 1.5-3 min was collected. Removal of the solvent under reduced pressure gave title compound **64** (612 mg, 71%) as a colorless oil.

R_f = 0.48 (hexane/EtOAc, 9:1); ^{1}H NMR (500 MHz, $CDCl_3$): δ = 7.50 (d, *J* = 8.0, 1H), 7.12 – 7.10 (m, 2H), 4.31 (s, 2H), 4.13 (q, *J* = 7.2, 2H), 3.77 (t, *J* = 6.5, 2H), 2.47 (s, 3H), 2.32 (t, *J* = 7.6, 2H), 1.70 – 1.61 (m, 4H), 1.48 – 1.40 (m, 2H), 1.33 (p, *J* = 7.5, 2H), 1.25 (t, *J* = 7.2, 3H), 1.07 (d, *J* = 7.4, 6H), 1.00 (d, *J* = 7.4, 6H); ^{13}C NMR (126 MHz, $CDCl_3$): δ = 173.9, 144.9, 136.4, 136.3, 134.2, 129.9, 124.3, 63.8, 60.3, 54.9, 34.5, 32.6, 25.6, 25.0, 23.2, 17.9, 17.8, 14.4, 13.2; ^{29}Si NMR (99 MHz, $CDCl_3$): δ = 7.43; HRMS (ESI+): (*m/z*) $[M+Na]^+$ calcd for $C_{22}H_{37}NaN_3O_3Si^+$: 442.2496; found: 442.2500.

(4-(Diisopropylsilyl)-3,5-dimethylphenyl)methanol (66)

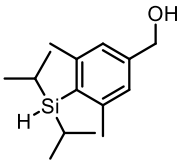

66

A stirring solution of (4-bromo-3,5-dimethylphenyl)methanol (534 mg, 2.48 mmol) in dry THF (18 mL) was cooled to −78 ºC and *n*-BuLi (2.5 M in hexanes, 2.5 mL, 6.21 mmol) was added dropwise over 2 min and the mixture was stirred for 2 h. Diisopropylchlorosilane (0.51 mL, 2.98 mmol) was added dropwise and stirring continued for 1 h at −78 ºC before the mixture was allowed to warm to rt and stirred overnight. The reaction was quenched by addition of saturated $NaHCO_3$ (30 mL) and the two layers were separated. The aqueous layer was extracted with EtOAc (3 x 30 mL), and the combined organic layers were washed with water (60 mL), saturated NaCl (60 mL) and dried over $MgSO_4$. The solvents were removed *in vacuo* and the crude product was purified using a Biotage Sfär silica gel cartridge (20 µm, 25 g) using

hexane/EtOAc (1:4) as eluent and 40 mL/min flow rate. The peak that eluted at approx. 3-6 min was collected. Removal of the solvent under reduced pressure gave **66** (260 mg, 42%) as a colorless oil.

R_f = 0.39 (hexane/EtOAc, 4:1); ^{1}H NMR (500 MHz, $CDCl_3$): δ = 6.99 (s, 2H), 4.61 (s, 2H), 4.17 (t, *J* = 4.9, 1H), 2.45 (s, 6H), 1.66 (bs, 1H), 1.36 – 1.28 (m, 2H), 1.15 (d, *J* = 7.1, 6H), 0.92 (d, *J* = 7.3, 6H); ^{13}C NMR (126 MHz, $CDCl_3$): δ = 145.0, 141.5, 133.0, 126.1, 65.4, 24.7, 20.4, 19.9, 12.6; HRMS (GC-EI+): *m/z* M^+ calcd for $C_{15}H_{26}OSi^+$: 250.1703, found: 250.1758; fragmentation *m/z* 250 (M^+), 207 (M – $CH_2CH_2CH_3$), 165 (M – $CH_2CH_2CH_3$ – CH_2CHCH_3)

(4-(Azidomethyl)-2,5-dimethylphenyl)diisopropyl silane (67)

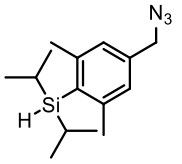

67

To a stirring solution of benzyl alcohol **65** (117 mg, 0.47 mmol) in dry DMF (2 mL), DBU (0.14 mL, 0.93 mmol) and DPPA (0.21 mL, 0.93 mmol) were added and stirring continued at rt overnight. Water (10 mL) was added, and the resulting mixture was extracted with Et_2O (3 x 15 mL). The combined organic layers were washed with water (20 mL), saturated aqueous NH_4Cl (20 mL), saturated NaCl (20 mL), and dried over $MgSO_4$. Evaporation *in vacuo* gave the crude product as a light yellow oil, which was purified using a Biotage Sfär silica gel cartridge (20 µm, 10 g) using hexane/EtOAc (19:1) as eluent and 20 mL/min flow rate. The peak that eluted at approx. 0.5-1.5 min was collected. Removal of the solvent under reduced pressure gave **67** (104 mg, 82%) as a colorless oil.

R_f = 0.77 (hexane/EtOAc, 4:1); ^{1}H NMR (500 MHz, $CDCl_3$): δ = 6.93 (s, 2H), 4.26 (s, 2H), 4.16 (t, *J* = 4.9, 1H), 2.46 (s, 6H), 1.36 – 1.28 (m, 2H), 1.15 (d, *J* = 7.4, 6H), 0.91 (d, *J* = 7.4, 6H); ^{13}C NMR (126 MHz, $CDCl_3$); δ = 145.2, 136.1, 133.9, 127.2, 54.8, 24.7, 20.4, 19.9, 12.6; HRMS (GC-EI+): *m/z* M^+ calcd for $C_{15}H_{25}N_3Si^+$: 275.1768, found: $[M-43]^+$ = 232.1277; fragmentation *m/z* 275 (M^+), 232 (M – $CH_2CH_2CH_3$), 204

(M – $CH_2CH_2CH_3$ – CH_2=CH_2), 162 (M – $CH_2CH_2CH_3$ – CH_2=CH_2 – CH_2CHCH_3, 147.

Ethyl 6-(((4-(azidomethyl)-2,6-dimethylphenyl)diisopropylsilyl)oxy)-hexanoate (68)

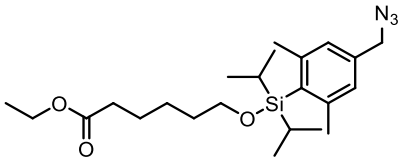

68

Silane **67** (96.6 mg, 0.37 mmol) was dissolved in dry CH_2Cl_2 (3 mL) under argon atmosphere. Trichloroisocyanuric acid (27.0 mg, 0.12 mmol) was added at 0 ºC, and the mixture was stirred for 2 h at rt. The mixture was cooled to 0 ºC before imidazole (140 mg, 2.06 mmol) and ethyl 6-hydroxyhexanoate (0.1 mL, 0.61 mmol) were added and the resulting mixture was allowed to warm to rt and stirring continued overnight. The resulting suspension was separated between $CHCl_3$ (30 mL) and saturated NaCl (30 mL), and the organic layer was dried over $MgSO_4$. The solvents were removed *in vacuo* and the crude product was purified using a Biotage Sfär silica gel cartridge (20 µm, 10 g) using hexane/EtOAc (19:1) as eluent and 20 mL/min flow rate. The peak that eluted at approx. 2.5-4 min was collected. Removal of the solvent under reduced pressure gave **68** (98.7 mg, 62%) as a colorless oil.

R_f = 0.47 (hexane/EtOAc, 9:1); ^{1}H NMR (500 MHz, $CDCl_3$): δ = 6.90 (s, 2H), 4.26 (s, 2H), 4.13 (q, *J* = 7.1, 2H), 3.82 (t, *J* = 6.5, 2H), 2.48 (s, 6H), 2.32 (t, *J* = 7.6, 2H), 1.70 – 1.61 (m, 4H), 1.46 – 1.41 (m, 2H), 1.40 – 1.34 (m, 2H), 1.25 (t, *J* = 7.2, 3H), 1.11 (d, *J* = 7.3, 6H), 1.01 (d, *J* = 7.6, 6H); ^{13}C NMR (126 MHz, $CDCl_3$): δ = 173.9, 145.6, 135.8, 134.2, 127.9, 63.7, 60.3, 54.7, 34.5, 32.5, 25.7, 25.0, 24.6, 18.4, 18.3 15.3, 14.4; HRMS (ESI+): (*m/z*) $[M+Na]^+$ calcd for $C_{23}H_{39}NaN_3O_3Si^+$: 456.2653; found: 456.2653.

4-(Diisopropylsilyl)-3,5-dimethylbenzaldehyde (69)

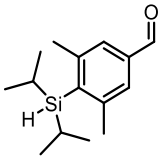

69

Benzylic alcohol **65** (299 mg, 1.12 mmol) was added to a suspension of activated MnO_2 (1.108 g, 12.7 mmol) in dry CH_2Cl_2 (20 mL) under argon atmosphere. The suspension was stirred at rt overnight and the resulting black suspension was filtered through a pad of Celite and the Celite was washed thoroughly with CH_2Cl_2. The filtrate was concentrated *in vacuo* to give **69** (249 mg, 84%) as a colorless oil which was used in the next step without further purification.

R_f = 0.70 (hexane/EtOAc, 4:1); ^{1}H NMR (500 MHz, $CDCl_3$): δ = 9.94 (s, 1H), 7.46 (s, 2H), 4.20 (t, *J* = 5.0, 1H), 2.53 (s, 6H), 1.40 – 1.31 (m, 2H), 1.17 (d, *J* = 7.3, 6H), 0.91 (d, *J* = 7.4, 6H); ^{13}C NMR (126 MHz, $CDCl_3$): δ = 193.1, 145.5, 142.8, 136.7, 128.2, 24.7, 20.3, 19.8, 12.5; HRMS (GC-EI+): *m/z* M^+ calcd for $C_{15}H_{24}OSi^+$: 248.1596, found: $[M-43]^+$ = 205.0855; fragmentation *m/z* 248 (M^+), 205 (M – $CH_2CH_2CH_3$), 163 (M – $CH_2CH_2CH_3$ – CH_2CHCH_3).

4-((But-3-yn-1-yloxy)diisopropylsilyl)-3,5-dimethylbenzaldehyde (70)

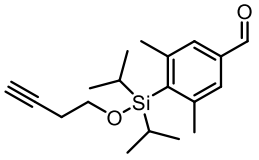

70

Silane **69** (240 mg, 0.97 mmol) was dissolved in dry CH_2Cl_2 (3 mL) under argon atmosphere. Trichloroisocyanuric acid (75 mg, 0.32 mmol) was added at 0 ºC, and the mixture was stirred at rt for 3 h. The mixture was cooled to 0 ºC before imidazole (297 mg, 4.37 mmol) and 3-butyn-1-ol (0.11 mL, 1.46 mmol) were added. The mixture was warmed to rt and stirred overnight. The resulting suspension was separated between $CHCl_3$ (40 mL) and saturated NaCl (40 mL), and the organic layer was collected and dried over $MgSO_4$. The solvents were removed *in vacuo*. The crude

material was purified using a Biotage Sfär silica gel cartridge (20 µm, 10 g) using hexane/EtOAc (19:1 → 4:1) as eluent and 20 mL/min flow rate. The peak that eluted at approx. 1-3 min was collected. Removal of the solvent under reduced pressure gave **70** (207 mg, 68%) as a colorless oil.

R_f = 0.44 (hexane/EtOAc, 9:1); ^{1}H NMR (500 MHz, $CDCl_3$): δ = 9.94 (s, 1H), 7.43 (s, 2H), 4.00 (t, *J* = 7.2, 2H), 2.56 (s, 6H), 2.53 (td, *J* = 7.2, 3.6, 2H), 1.99 (t, *J* = 2.7, 1H), 1.42 (p, *J* = 7.5, 2H), 1.15 (d, *J* = 7.4, 6H), 1.02 (d, *J* = 7.5, 6H); ^{13}C NMR (126 MHz, $CDCl_3$): δ = 193.1, 145.8, 142.5, 136.4, 129.0, 81.4, 69.8, 62.6, 24.6, 22.8, 18.3, 18.2, 15.2; HRMS (GC-EI+): *m/z* M^+ calcd for $C_{19}H_{28}O_2Si^{\bullet+}$: 316.1853, found: $[M-43]^+$ = 273.1309; fragmentation *m/z* 316 (M^+), 273 (M – $CH_2CH_2CH_3$), 243 (M – $CH_2CH_2CH_3$ – 30), 201 (M – $CH_2CH_2CH_3$ – 30 – CH_2CHCH_3)

1-Bromo-2-methyl-4-propoxybenzene (73)

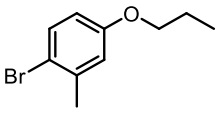

73

A suspension of 4-bromo-3-methylphenol (1.016 g, 5.43 mmol), 1-iodopropane (0.56 mL, 5.70 mmol) and K_2CO_3 (1.868 g, 13.58 mmol) in DMF (25 mL) was stirred at rt overnight after which TLC analysis revealed full conversion of the starting material. The resulting mixture was partitioned between Et_2O (200 mL), and water (125 mL) and the organic layer was washed with water (125 mL x 2) and saturated NaCl (125 mL), dried over $MgSO_4$ and evaporated *in vacuo*. The crude material was purified using a Biotage Sfär silica gel cartridge (20 µm, 25 g) using hexane/EtOAc (4:1) as eluent and 40 mL/min flow rate. The peak that eluted at approx. 1-2 min was collected. Removal of the solvent under reduced pressure **73** (1.146 g, 93%) as a viscous, colorless oil.

^{1}H NMR (600 MHz, $CDCl_3$): δ = 7.38 (d, *J* = 8.7, 1H), 6.79 (d, *J* = 3.8, 1H), 6.61 (dd, *J* = 8.7, 3.0, 1H), 3.88 (t, *J* = 6.6, 2H), 2.36 (s, 3H), 1.79 (h, *J* = 7.4, 2H), 1.03 (t, *J* = 7.4, 3H); ^{13}C NMR (150 MHz, $CDCl_3$): δ = 158.5, 138.9, 132.9, 117.3, 115.3, 113.6, 69.8,

23.3, 22.7, 10.6. The spectral data were in accordance with those previously reported.[214]

1-Bromo-2,6-dimethyl-4-propoxybenzene (74)

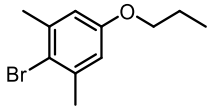

74

A suspension of 4-bromo-3,5-dimethylphenol (0.971 g, 4.83 mmol), 1-iodopropane (0.50 mL, 5.07 mmol) and K_2CO_3 (1.669 g, 12.07 mmol) in DMF (25 mL) was stirred at rt overnight, after which TLC analysis revealed full conversion of the starting material. The resulting mixture was partitioned between Et_2O (200 mL) and water (125 mL). The organic layer was washed with water (125 mL x 2) and saturated NaCl (125 mL), dried over $MgSO_4$ and evaporated *in vacuo*. The crude material was purified using a Biotage Sfär silica gel cartridge (20 µm, 25 g) using hexane/EtOAc (4:1) as eluent and 40 mL/min flow rate. The peak that eluted at approx. 1-2 min was collected. Removal of the solvent under reduced pressure gave title compound **74** (1.082 g, 93%) as a viscous, colorless oil.

^{1}H NMR (600 MHz, $CDCl_3$): δ = 6.65 (s, 2H), 3.87 (t, *J* = 6.6, 2H), 2.38 (s, 6H), 1.79 (app h, *J* = 7.4, 2H), 1.03 (t, *J* = 7.4, 3H); ^{13}C NMR (150 MHz, $CDCl_3$): δ = 157.8, 139.1, 118.1, 114.6, 69.7, 24.2, 22.7, 10.6. The spectral data were in accordance with those previously reported[215].

Diisopropyl(2-methyl-4-propoxyphenyl)silane (75)

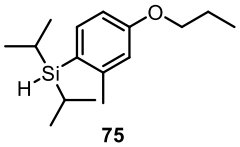

75

A stirring solution of bromide **73** (1.002 g, 4.40 mmol) in dry THF (33 mL) was cooled to −78 ºC and *n*-BuLi (2.5 M in hexanes, 2.0 mL, 4.83 mmol) was added dropwise and the mixture was stirred for 1 h at −78 ºC. Diisopropylchlorosilane (0.85 mL, 4.83 mmol) was added, and the mixture was stirred for 30 min at −78 ºC and then

allowed to warm to rt and stirred overnight. The reaction was quenched with saturated $NaHCO_3$ (30 mL) and extracted with EtOAc (2 x 30 mL). The combined organic layers were washed with saturated NaCl (2 x 100 mL), dried over $MgSO_4$, and the solvents were removed *in vacuo*. The crude material was purified using a Biotage Sfär silica gel cartridge (20 µm, 25 g) using hexane/EtOAc (19:1) as eluent and 40 mL/min flow rate. The peak that eluted at approx. 1-2 min was collected. Removal of the solvent under reduced pressure gave title compound **75** (1.123 g, 97%) as a viscous, colorless oil. The material contains an unidentified aliphatic impurity.

^{1}H NMR (600 MHz, $CDCl_3$): δ = 7.33 (d, *J* = 8.1, 1H), 6.75 (d, *J* = 2.6, 1H), 6.71 (dd, *J* = 8.1, 2.6, 1H), 4.04 (t, *J* = 3.6, 1H), 3.92 (t, *J* = 6.6, 2H), 2.41 (s, 3H), 1.80 (h, *J* = 7.4, 2H), 1.28 – 1.20 (m, 2H), 1.08 (d, *J* = 7.4, 6H), 1.06 – 1.00 (m, 3H), 0.96 (d, *J* = 7.4, 6H); ^{13}C NMR (150 MHz, $CDCl_3$): δ = 160.2, 146.0, 137.6, 124.2, 116.3, 110.8, 69.2, 23.6, 22.8, 19.2, 19.1, 11.4, 10.7; HRMS (GC-EI+): M^+ calcd for $C_{16}H_{28}OSi^+$: 264.1903; found: 264.1903; fragmentation *m/z* 264 (M^+), 221 (M – $CH_2CH_2CH_3$), 179 (M – $CH_2CH_2CH_3$ – CH_2CHCH_3)

(2,6-Dimethyl-4-propoxyphenyl)diisopropyl silane (76)

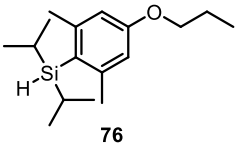

76

A stirring solution of bromide **74** (963 mg, 3.97 mmol) in dry THF (30 mL) was cooled to −78 ºC and *n*-BuLi (2.5 M in hexanes, 1.8 mL, 4.38 mmol) was added dropwise and the mixture was stirred for 1 h at −78 ºC. Diisopropylchlorosilane (0.75 mL, 4.38 mmol) was added, and the mixture was stirred for 30 min at −78 ºC and then allowed to warm to rt and stirred overnight. The reaction was quenched by addition of saturated $NaHCO_3$ (30 mL) and the resulting mixture was extracted with EtOAc (2 x 30 mL). The combined organic layers were washed with saturated NaCl (2 x 100 mL) and dried over $MgSO_4$. The solvents were removed *in vacuo* and the crude material was purified using a Biotage Sfär silica gel cartridge (20 µm, 25 g) using hexane/EtOAc (1:19) as eluent and 40 mL/min flow rate. The peak that eluted at

approx. 1-2 min was collected. Removal of the solvent under reduced pressure gave title compound **76** (1.05 g, 95%) as a viscous, colorless oil. The material contains aliphatic impurities.

^{1}H NMR (600 MHz, $CDCl_3$): δ = 6.56 (s, 2H), 4.12 (t, *J* = 4.8, 1H), 3.90 (t, *J* = 6.5, 2H), 2.41 (s, 6H), 1.79 (app h, *J* = 6.9, 2H), 1.32 – 1.25 (m, 3H), 1.14 (d, *J* = 7.2, 6H), 1.03 (t, *J* = 7.4, 3H), 0.92 (d, *J* = 7.4, 6H); ^{13}C NMR (150 MHz, $CDCl_3$): δ = 159.7, 146.3, 124.3, 113.7, 69.0, 25.0, 22.8, 20.4, 19.9, 12.7, 10.7; HRMS (GC-EI+): M^+ calcd for $C_{17}H_{30}OSi^+$: 278.2060; found: 278.2061; fragmentation *m/z* 278 (M^+), 235 (M – $CH_2CH_2CH_3$), 193 (M – $CH_2CH_2CH_3$ – CH_2CHCH_3)

1-Bromo-4-propoxybenzene (77)

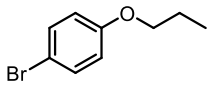

77

A suspension of 4-bromo-3-methylphenol (1.751 g, 10.12 mmol), 1-iodopropane (1.10 mL, 11.13 mmol), and K_2CO_3 (3.530 g, 25.30 mmol) in DMF (25 mL) were stirred at rt overnight, until full conversion of the starting material as confirmed by TLC analysis. The mixture was quenched with water (40 mL) and extracted with Et_2O (2 x 30 mL). The combined organic extracts were washed with water (2 x 60 mL) and saturated NaCl (60 mL), dried over $MgSO_4$ and evaporated *in vacuo* to give **77** (2.114 g, 97%) as a viscous, colorless oil. The material contains residual Et_2O.

R_f = 0.08 (hexane/EtOAc, 9:1); ^{1}H NMR (500 MHz, $CDCl_3$): δ = 7.36 (d, *J* = 9.1, 2H), 6.77 (d, *J* = 9.1, 2H), 3.88 (t, *J* = 6.5, 2H), 1.85 – 1.74 (m, 2H), 1.03 (t, *J* = 7.5, 3H); ^{13}C NMR (126 MHz, $CDCl_3$): δ = 158.4, 132.3, 116.5, 112.7, 69.9, 22.6, 10.6. The spectral data were in accordance with those previously reported.[216]

Ethyl 6-((diisopropyl(2-methyl-4-propoxyphenyl)silyl)oxy)hexanoate (80)

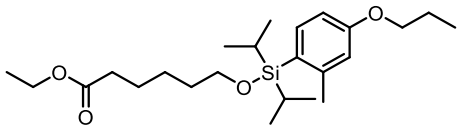

80

Silane **75** (799 mg, 3.03 mmol) was dissolved in dry CH_2Cl_2 (9 mL) under argon atmosphere, cooled to 0 ºC in an ice bath. Trichloroisocyanuric acid (233 mg, 1.00 mmol) was added, the ice bath was removed, and the mixture was stirred for 2 h at rt. The mixture was cooled to 0 ºC before imidazole (919 mg, 13.5 mmol) and ethyl 6-hydroxyhexanoate (0.6 mL, 3.64 mmol) were added. The mixture was warmed to rt and stirred overnight. The resulting suspension was separated between $CHCl_3$ (200 mL) and saturated NaCl (200 mL), and the organic layer was collected and dried over Na_2SO_4. The solvents were removed *in vacuo* and the crude product was purified using a Biotage Sfär silica gel cartridge (20 µm, 10 g) using hexane/EtOAc (1:19) as eluent and 20 mL/min flow rate. The peak that eluted at approx. 7-9 min was collected. Removal of the solvent under reduced pressure gave title compound **80** (271.6 mg, 22%) as a colorless oil.

R_f = 0.39 (hexane/EtOAc, 9:1); ^{1}H NMR (600 MHz, $CDCl_3$): δ = 7.38 (d, *J* = 8.2, 1H), 6.74 – 6.69 (m, 2H), 4.12 (q, *J* = 7.1, 2H), 3.92 (t, *J* = 6.5, 2H), 3.74 (t, *J* = 6.6, 2H), 2.43 (s, 3H), 2.31 (t, *J* = 7.6, 2H), 1.80 (app h, *J* = 7.4, 2H), 1.70 – 1.59 (m, 4H), 1.46 – 1.39 (m, 2H), 1.33 – 1.27 (m, 2H), 1.25 (t, *J* = 7.1, 3H), 1.06 (d, *J* = 7.4, 6H), 1.03 (t, *J* = 7.4, 3H), 1.00 (d, *J* = 7.5, 6H); ^{13}C NMR (150 MHz, $CDCl_3$): δ = 174.0, 160.1, 146.2, 137.3, 124.5, 116.7, 110.5, 69.1, 63.7, 60.3, 34.6, 32.7, 25.7, 25.0, 23.4, 22.8, 18.0, 17.9, 14.4, 13.3, 10.7; HRMS (ESI+): (*m/z*) $[M+Na]^+$ calcd for $C_{24}H_{42}NaO_4Si^+$: 445.2745; found: 445.2744.

2-(2-(4-Bromo-3-methylphenoxy)ethoxy)tetrahydro-2*H*-pyran (82)

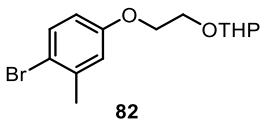

82

4-Bromo-3-methylphenol (1.011 g, 5.41 mmol) was dissolved in $(CH_3)_2SO$ (13 mL) and KOH (1.363 g, 24.3 mmol) was added. After 5 min stirring, 2-(2-bromopropoxy)-tetrahydro-2*H*-pyran (1.22 mL, 8.10 mmol) was added. The reaction mixture was stirred at rt overnight and then partitioned between water (100 mL) and CH_2Cl_2 (100 mL). The aqueous layer was extracted with CH_2Cl_2 (2 x 100 mL). The combined organic layers were washed with saturated NaCl (3 x 100 mL), dried over $MgSO_4$, and the solvent was evaporated *in vacuo*. The crude material was purified using a Biotage Sfär silica gel cartridge (20 µm, 25 g) using hexane/EtOAc (95:9 → 75:25) as eluent and 40 mL/min flow rate. The peak that eluted at approx. 4-8 min was collected. Removal of the solvent under reduced pressure gave **82** (1.453 g, 86%) as a colorless oil.

^{1}H NMR (500 MHz, $CDCl_3$): δ = 7.38 (d, *J* = 8.8, 1H), 6.83 (d, *J* = 3.8, 1H), 6.67 – 6.60 (m, 1H), 4.71 – 4.68 (m, 1H), 4.14 – 4.08 (m, 2H), 4.05 – 3.99 (m, 1H), 3.89 (ddd, *J* = 11.4, 8.3, 3.3, 1H), 3.80 (ddd, *J* = 11.2, 6.3, 4.1, 1H), 3.55 – 3.50 (m, 1H), 2.35 (s, 3H), 1.86 – 1.79 (m, 1H), 1.77 – 1.71 (m, 1H), 1.64 – 1.51 (m, 4H); ^{13}C NMR (126 MHz, $CDCl_3$) δ = 158.2, 138.9, 132.9, 117.5, 115.7, 113.8, 99.1, 67.7, 65.9, 62.3, 30.6, 25.5, 23.2, 19.5; HRMS (ESI+): (*m/z*) $[M+Na]^+$ calcd for $C_{14}H_{19}BrNaO_3^+$: 337.0410/339.0489, found: 337.0411/339.0398, (*m/z*) $[2M+Na]^+$ calcd for $C_{28}H_{38}Br_2NaO_6^+$: 653.0907, found 653.0845.

2-(2-(4-Bromo-3,5-dimethylphenoxy)ethoxy)tetrahydro-2*H*-pyran (83)

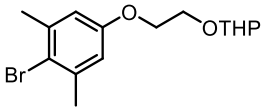

83

4-Bromo-3,5-dimethylphenol (0.998 g, 4.96 mmol) was dissolved in $(CH_3)_2SO$ (13 mL) and KOH (1.322 g, 23.5 mmol) was added. After 5 min of stirring, 2-(2-bromopropoxy)-tetrahydro-2*H*-pyran (1.13 mL, 7.5 mmol) was added. The reaction mixture was stirred at rt overnight and then partitioned between water (100 mL) and CH_2Cl_2 (100 mL). The aqueous layer was extracted with CH_2Cl_2 (2 x 100 mL). The combined organic layers were washed with saturated NaCl (3 x 100 mL), dried over $MgSO_4$, and the solvent was evaporated *in vacuo*. The crude material was purified using a Biotage Sfär silica gel cartridge (20 µm, 25 g) using hexane/EtOAc (95:5 → 75:25) as eluent and 40 mL/min flow rate. The peak that eluted at approx. 4.5-10.5 min was collected. Removal of the solvent under reduced pressure gave **83** (1.114 g, 69%) as a colorless oil.

R_f = 0.43 (hexane/EtOAc, 4:1); ^{1}H NMR (500 MHz, $CDCl_3$): δ = 6.68 (s, 2H), 4.71 – 4.69 (m, 1H), 4.15 – 4.07 (m, 2H), 4.05 – 4.00 (m, 1H), 3.92 – 3.86 (m, 1H), 3.82 – 3.76 (m, 1H), 3.56 – 3.50 (m, 1H), 2.37 (s, 6H), 1.88 – 1.79 (m, 1H), 1.77 – 1.70 (m, 1H), 1.65 – 1.48 (m, 4H); ^{13}C NMR (126 MHz, $CDCl_3$): δ = 157.5, 139.2, 118.5, 114.8, 99.1, 67.7, 66.0, 62.3, 30.6, 25.5, 24.2, 19.5; HRMS (ESI+): (*m/z*) $[M+Na]^+$ calcd for $C_{15}H_{21}BrNaO_3^+$: 351.0566/353.0566, found: 351.0568/353.0568, (*m/z*) $[2M+Na]^+$ calcd for $C_{30}H_{42}Br_2NaO_6^+$: 681.1220, found 681.1106.

Diisopropyl (2-methyl-4-(2-((tetrahydro-2*H*-pyran-2-yl)oxy)ethoxy)phenyl)silane (84)

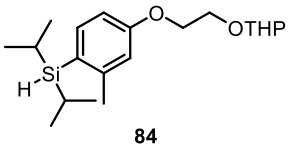

84

A stirring solution of bromide **82** (1.187 g, 3.78 mmol) in dry THF (30 mL) was cooled to –78 ºC and *n*-BuLi (2.5 M in hexanes, 1.66 mL, 4.16 mmol) was added dropwise

and the mixture was stirred for 1 h at −78 ºC. Diisopropylchlorosilane (0.85 mL, 4.16 mmol) was added, and the mixture was stirred for 30 min at −78 ºC and then allowed to warm to rt and stirred overnight. The reaction was quenched by addition of saturated $NaHCO_3$ (30 mL) and extracted with EtOAc (2 x 50 mL). The combined organic layers were washed with saturated NaCl (2 x 100 mL) and dried over $MgSO_4$. The solvents were removed *in vacuo* and the residue containing **84** (1.431 g) was used in the next step without further purification.

^{1}H NMR (500 MHz, $CDCl_3$): δ = 7.32 (d, *J* = 8.0, 1H), 6.77 (d, *J* = 2.7, 1H), 6.73 (dd, *J* = 8.1, 2.6, 1H), 4.74 – 4.69 (m, 1H), 4.18 – 4.12 (m, 2H) 4.06 – 4.03 (m, 2H), 3.93 – 3.86 (m, 1H), 3.84 (s, 1H), 3.54-3.51 (m, 1H), 2.41 (s, 3H), 1.88 – 1.78 (m, 1H), 1.77 – 1.69 (m, 1H), 1.67 – 1.46 (m, 6H), 1.26-1.19 (m, 2H), 1.07 (d, *J* = 7.4, 6H), 1.02 (t, *J* = 7.0, 3H), 0.95 (d, *J* = 7.4, 6H); ^{13}C NMR (126 MHz, CDCl3) δ = 159.9, 146.0, 137.6, 124.6, 116.4, 111.0, 99.0, 67.1, 66.0, 62.3, 30.6, 25.6, 23.6, 19.5, 19.2, 19.0, 17.4, 17.3, 13.4, 11.4.

(2,6-Dimethyl-4-(2-((tetrahydro-2H-pyran-2-yl)oxy)ethoxy)phenyl)-diisopropylsilane (85)

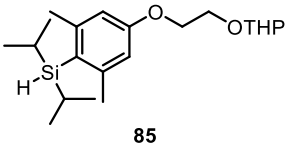

85

A stirring solution of bromide **83** (664 mg, 2.02 mmol) in dry THF (20 mL) was cooled to −78 ºC and *n*-BuLi (2.5 M in hexanes, 0.9 mL, 2.23 mmol) was added dropwise and the mixture was stirred for 1 h at −78 ºC. Diisopropylchlorosilane (0.38 mL, 2.23 mmol) was added, and the mixture was stirred for 30 min at −78 ºC and then allowed to warm to rt and stirred overnight. The reaction was quenched with saturated $NaHCO_3$ (20 mL) and extracted with EtOAc (2 x 30 mL). The combined organic layers were washed with saturated NaCl (2 x 50 mL) and dried over $MgSO_4$. The solvents were removed *in vacuo* to give a colorless oily crude product containing **85** (771 mg). The crude product was used in the next step without further purification.

^{1}H NMR (500 MHz, $CDCl_3$): δ =6.58 (s, 2H), 4.74 – 4.67 (m, 1H), 4.14 (s, 3H), 4.01 (s, 2H), 3.94 (s, 1H), 3.83 – 3.78 (m, 1H), 3.53 – 3.51 (m, 1H), 2.41 (s, 6H), 1.80 (s, 1H), 1.69 (s, 1H), 1.66 – 1.57 (m, 2H), 1.55 (s, 2H), 1.25 (s, 3H), 1.13 (d, *J* = 7.2, 6H), 1.02 (t, *J* = 6.9, 6H), 0.91 (d, *J* = 7.4, 7H); ^{13}C NMR (126 MHz, $CDCl_3$) δ = 159.4, 146.3, 124.7, 113.9, 112.6, 99.0, 66.9, 66.0, 62.3, 30.6, 25.6, 24.9, 20.4, 19.9, 19.4, 17.4, 17.3, 13.4, 12.7.

2-(4-(Diisopropylsilyl)-3-methylphenoxy)ethan-1-ol (86)

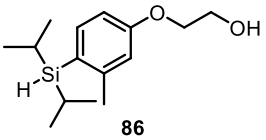

86

To a solution of THP ether **84** (1.325 g, 3.77 mmol) in EtOH (50 mL) was added *p*-TSA (657.2 mg, 3.81 mmol) and the mixture was stirred for 2 h at rt. The reaction mixture was poured into saturated $NaHCO_3$ (50 mL), and the resulting mixture was extracted with CH_2Cl_2 (3 x 50 mL). The combined organic layers were washed with saturated NaCl (100 mL) and dried over $MgSO_4$, filtered and solvent evaporated *in vacuo*. The crude material was purified using a Biotage Sfär silica gel cartridge (20 µm, 25 g) using hexane/EtOAc (90:10 → 70:30) as eluent and 40 mL/min flow rate. The peak that eluted at approx. 5-10 min was collected. Removal of the solvent under reduced pressure gave **86** (630 mg, 63% over two steps) as a viscous colorless oil.

^{1}H NMR (500 MHz, $CDCl_3$): δ = 7.34 (d, *J* = 8.2, 1H), 6.77 (d, *J* = 2.5, 1H), 6.72 (dd, *J* = 8.1, 2.5, 1H), 4.10 – 4.07 (m, 2H), 4.04 (t, *J* = 3.6, 1H), 3.95 (td, *J* = 6.1, 3.9, 2H), 2.42 (s, 3H), 2.04 (t, *J* = 6.3, 1H), 1.08 (d, *J* = 7.4, 6H), 0.96 (d, *J* = 7.4, 6H); ^{13}C NMR (126 MHz, $CDCl_3$): δ = 159.6, 146.2, 137.7, 125.2, 116.3, 110.9, 68.9, 61.7, 23.6, 19.2, 19.0, 11.4; HRMS (GC-EI+): *m/z* M^+ calcd for $C_{15}H_{26}O_2Si^+$: 266.1697, found: 266.1698; fragmentation *m/z* 266 (M^+), 223 (M – $CH_2CH_2CH_3$), 181 (M – $CH_2CH_2CH_3$ – CH_2CHCH_3)

2-(4-(Diisopropylsilyl)-3,5-dimethylphenoxy)ethan-1-ol (87)

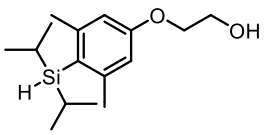

87

The crude product of THP ether **85** was dissolved in MeOH (30 mL) and pyridinium *p*-toluenesulfonate (PPTS, 10 mol%, 0.20 mmol, 51 mg) was added. The resulting mixture was stirred overnight at rt after which full conversion was confirmed by TLC. The reaction mixture was poured into saturated aqueous $NaHCO_3$ (30 mL) and extracted with CH_2Cl_2 (2 x 40 mL). The combined organic layers were washed with water (80 mL) and saturated NaCl (80 mL), dried over $MgSO_4$ and evaporated *in vacuo*. The crude material was purified using a Biotage Sfär silica gel cartridge (20 µm, 25 g) using hexane/EtOAc (95:5 → 75:25) as eluent and 40 mL/min flow rate. The peak that eluted at approx. 4.5-10.5 min was collected. Removal of the solvent under reduced pressure gave **87** (361 mg, 64% over two steps) as a colorless oil.

^{1}H NMR (500 MHz, $CDCl_3$): δ = 6.58 (s, 2H), 4.12 (t, *J* = 4.8, 1H), 4.07 (t, *J* = 4.9, 2H), 3.94 (t, *J* = 4.6, 2H), 2.42 (s, 6H), 2.07 (bs, 1H), 1.33 – 1.26 (m, 2H), 1.14 (d, *J* = 7.1, 6H), 0.92 (d, *J* = 7.4, 6H); ^{13}C NMR (126 MHz, $CDCl_3$): δ = 159.1, 146.5, 125.3, 113.8, 68.7, 61.7, 25.0, 20.4, 19.9, 12.7; HRMS (GC-EI+): *m/z* M^+ calcd for $C_{16}H_{28}O_2Si^+$: 280.1853, found: 280.1853; fragmentation *m/z* 280 (M^+), 237 (M – $CH_2CH_2CH_3$), 195 (M – $CH_2CH_2CH_3$ – CH_2CHCH_3)

Diisopropyl(phenyl)silane (91)

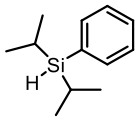

91

A stirring solution of bromobenzene (1.10 mL, 10.51 mmol) in dry THF (50 mL) was cooled to −78 ºC and *n*-BuLi (2.5 M in hexanes, 4.6 mL, 11.57 mmol) was added dropwise and the mixture was stirred for 1 h at −78 ºC. Diisopropylchlorosilane (2.15 mL, 12.61 mmol) was added, and the mixture was stirred for 1 h at −78 ºC and

then allowed to warm to rt and stirred overnight. The reaction was quenched by addition of saturated $NaHCO_3$ (70 mL) and extracted with EtOAc (2 x 50 mL). The combined organic layers were washed with saturated NaCl (70 mL), H_2O (70 mL) and dried over $MgSO_4$. The solvents were removed *in vacuo* and the crude material was purified using a Biotage Sfär silica gel cartridge (20 µm, 50 g) using hexane/EtOAc (19:1) as eluent and 60 mL/min flow rate. The peak that eluted at approx. 1-3 min was collected. Removal of the solvent under reduced pressure gave **91** (2.170 g, quantitative) as a colorless oil. The material contains residual EtOAc.

^{1}H NMR (500 MHz, $CDCl_3$): δ = 7.53 (dd, *J* = 7.7, 1.7, 2H), 7.41 – 7.33 (m, 3H), 3.94 (t, *J* = 3.2, 1H), 1.27 – 1.20 (m, 2H), 1.09 (d, *J* = 7.3, 6H), 1.01 (d, *J* = 7.4, 6H); ^{13}C NMR (126 MHz, $CDCl_3$): δ = 135.6, 134.3, 129.2, 127.8, 18.8, 18.6, 10.8. The analytical data were in accordance with those previously reported.[217]

Diisopropyl(o-tolyl)silane (92)

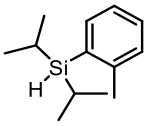

92

A stirring solution of 2-bromotoluene (1.20 mL, 10.15 mmol) in dry THF (50 mL) was cooled to −78 ºC and *n*-BuLi (2.5 M in hexanes, 4.5 mL, 11.17 mmol) was added dropwise and the mixture was stirred for 1 h at −78 ºC. Diisopropylchlorosilane (2.08 mL, 12.18 mmol) was added, and the mixture was stirred for 1 h at −78 ºC and then allowed to warm to rt and stirred overnight. The reaction was quenched with saturated $NaHCO_3$ (70 mL) and extracted with EtOAc (2 x 50 mL). The combined organic layers were washed with saturated NaCl (70 mL), H_2O (70 mL) and dried over $MgSO_4$. The solvents were removed *in vacuo* and the crude product was purified using a Biotage Sfär silica gel cartridge (20 µm, 50 g) using hexane/EtOAc (19:1) as eluent and 60 mL/min flow rate. The peak that eluted at approx. 1-1.5 min was collected. Removal of the solvent under reduced pressure gave **92** (2.128 g, 91%) as a colorless oil.

^{1}H NMR (500 MHz, $CDCl_3$): δ = 7.43 (dd, *J* = 7.3, 1.7, 1H), 7.29 – 7.25 (m, 1H), 7.19 – 7.13 (m, 2H), 4.09 (t, *J* = 3.6, 1H), 2.45 (s, 3H), 1.31-1.24 (m, 2H), 1.10 (d, *J* = 7.4, 6H), 0.98 (d, *J* = 7.3, 6H); ^{13}C NMR (126 MHz, $CDCl_3$): δ = 144.2, 136.2, 133.6, 129.7, 129.3, 124.8, 23.5, 19.2, 19.1, 11.3; HRMS (GC-EI+): *m/z* M^+ calcd for $C_{13}H_{22}Si^{\bullet+}$: 206.1485, found: 206.1489; fragmentation *m/z* 206 (M^+), 163 (M – $CH_2CH_2CH_3$), 135 (M – $CH_2CH_2CH_3$ – CH_2=CH_2), 121 (M – $CH_2CH_2CH_3$ – CH_2CHCH_3)

(2,6-Dimethylphenyl)diisopropyl silane (93)

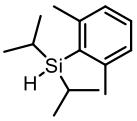

93

A stirring solution of 2-bromo-*m*-xylene (1.40 mL, 10.57 mmol) in dry THF (50 mL) was cooled to −78 ºC and *n*-BuLi (2.5 M in hexanes, 4.7 mL, 11.63 mmol) was added dropwise and the mixture was stirred for 2 h at −78 ºC. Diisopropylchlorosilane (2.17 mL, 12.68 mmol) was added, and the mixture was stirred for 1 h at −78 ºC and then allowed to warm to rt and stirred overnight. The reaction was quenched with saturated $NaHCO_3$ (70 mL) and extracted with EtOAc (2 x 50 mL). The combined organic layers were washed with saturated NaCl (70 mL), H_2O (70 mL) and dried over $MgSO_4$. The solvents were removed *in vacuo*. The crude material was purified using a Biotage Sfär silica gel cartridge (20 µm, 50 g) using hexane/EtOAc (19:1) as eluent and 60 mL/min flow rate. The peak that eluted at approx. 1-2 min was collected. Removal of the solvent under reduced pressure gave **93** (2.212 g, 84%) as a colorless oil.

^{1}H NMR (500 MHz, $CDCl_3$): δ = 7.14 (t, *J* = 7.6, 1H), 6.98 (d, *J* = 7.6, 2H), 4.18 (t, *J* = 4.9, 1H), 2.45 (s, 6H), 1.36-1.29 (m, 2H), 1.16 (d, *J* = 7.3, 6H), 0.93 (d, *J* = 7.4, 6H); ^{13}C NMR (126 MHz, $CDCl_3$): δ = 144.5, 133.6, 129.1, 127.5, 24.8, 20.4, 19.9, 12.6; HRMS (GC-EI+): *m/z* M^+ calcd for $C_{14}H_{24}Si^{\bullet+}$: 220.1642, found: 220.1642; fragmentation *m/z* 220 (M^+), 177 (M – $CH_2CH_2CH_3$), 149 (M – $CH_2CH_2CH_3$ – CH_2=CH_2), 135.

Ethyl 6-((diisopropyl(phenyl)silyl)oxy)hexanoate (94)

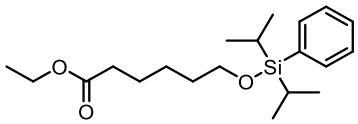

94

Silane **91** (983 mg, 5.11 mmol) was dissolved in dry CH_2Cl_2 (15 mL) under argon atmosphere. Trichloroisocyanuric acid (401.6 mg, 1.69 mmol) was added at 0 ºC, and the mixture was stirred for 2 h at rt. The mixture was cooled to 0 ºC before imidazole (1.565 g, 23.00 mmol) and ethyl 6-hydroxyhexanoate (1.0 mL, 6.13 mmol) were added. The mixture was warmed to rt and stirred overnight. The resulting suspension was separated between $CHCl_3$ (150 mL) and saturated NaCl (150 mL), and the organic layer was collected and dried over $MgSO_4$. The solvents were removed *in vacuo.* The crude material was purified using a Biotage Sfär silica gel cartridge (20 µm, 25 g) using hexane/EtOAc (19:1) as eluent and 40 mL/min flow rate. The peak that eluted at approx. 2-4 min was collected. Removal of the solvent under reduced pressure gave **94** (1.067 g, 60%) as a colorless oil.

R_f = 0.50 (hexane/EtOAc, 9:1); ^{1}H NMR (500 MHz, $CDCl_3$): δ = 7.54 (dd, *J* = 7.5, 2.0, 2H), 7.40 – 7.33 (m, 3H), 4.13 (q, *J* = 7.1, 2H), 3.76 (d, *J* = 6.6, 2H), 2.32 (t, *J* = 7.6, 2H), 1.70 – 1.60 (m, 4H), 1.47 – 1.40 (m, 2H), 1.30 – 1.22 (m, 5H), 1.06 (d, *J* = 7.4, 6H), 1.00 (d, *J* = 7.4, 6H); ^{13}C NMR (126 MHz, $CDCl_3$): δ = 173.9, 134.8, 134.7, 129.3, 127.7, 63.8, 60.3, 34.6, 32.7, 25.6, 25.0, 17.6, 17.5, 14.4, 12.2; HRMS (ESI+): (*m/z*) $[M+Na]^+$ calcd for $C_{20}H_{34}NaO_3Si^+$: 373.2169, found: 373.2179.

Ethyl 6-((diisopropyl(o-tolyl)silyl)oxy)hexanoate (95)

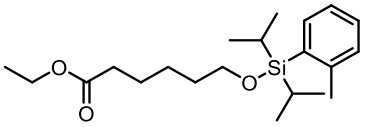

95

Silane **92** (973 mg, 4.72 mmol) was dissolved in dry CH_2Cl_2 (15 mL) under argon atmosphere. Trichloroisocyanuric acid (366.2 mg, 1.56 mmol) was added at 0 ºC, and the mixture was stirred for 2 h at rt. The mixture was cooled to 0 ºC before imidazole (1445 mg, 21.24 mmol) and ethyl 6-hydroxyhexanoate (0.92 mL, 5.66 mmol) were

added. The mixture was warmed to rt and stirred overnight. The resulting suspension was separated between $CHCl_3$ (150 mL) and saturated NaCl (150 mL), and the organic layer was collected and dried over $MgSO_4$. The solvents were removed *in vacuo.* The crude material was purified using a Biotage Sfär silica gel cartridge (20 µm, 25 g) using hexane/EtOAc (19:1) as eluent and 40 mL/min flow rate. The peak that eluted at approx. 2-4 min was collected. Removal of the solvent under reduced pressure gave **95** (975 mg, 63%) as a colorless oil.

R_f = 0.52 (hexane/EtOAc, 9:1); ^{1}H NMR (500 MHz, $CDCl_3$): δ = 7.48 (dd, *J* = 7.8, 1.7, 1H), 7.29 – 7.24 (m, 1H), 7.17-7.14 (m, 2H), 4.12 (q, *J* = 7.1, 2H), 3.77 (t, *J* = 6.5, 2H), 2.46 (s, 3H), 2.32 (t, *J* = 7.4, 2H), 1.70-1.62 (m, 4H), 1.47 – 1.40 (m, 2H), 1.33 (p, *J* = 7.5, 2H), 1.25 (t, *J* = 7.1, 3H), 1.07 (d, *J* = 7.4, 6H), 1.01 (d, *J* = 7.6, 6H); ^{13}C NMR (126 MHz, $CDCl_3$): δ = 173.9, 144.2, 135.8, 133.9, 130.3, 129.3, 124.6, 63.6, 60.3, 34.5, 32.7, 25.7, 25.0, 23.3, 18.0, 17.8, 14.4, 13.2; HRMS (ESI+): (*m/z*) $[M+Na]^+$ calcd for $C_{21}H_{36}NaO_3Si^+$: 387.2326, found: 387.2337.

Ethyl 6-(((2,6-dimethylphenyl)diisopropylsilyl)oxy)hexanoate (96)

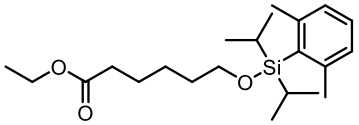

96

Silane **93** (995 mg, 4.52 mmol) was dissolved in dry CH_2Cl_2 (15 mL) under argon atmosphere. Trichloroisocyanuric acid (345.0 mg, 1.49 mmol) was added at 0 ºC, and the mixture was stirred for 2 h at rt. The mixture was cooled to 0 ºC before imidazole (1384 mg, 20.34 mmol) and ethyl 6-hydroxyhexanoate (0.9 mL, 5.52 mmol) were added. The mixture was warmed to rt and stirred overnight. The resulting suspension was separated between $CHCl_3$ (150 mL) and saturated NaCl (150 mL), and the organic layer was collected and dried over $MgSO_4$. The solvents were removed *in vacuo.* The crude material was purified using a Biotage Sfär silica gel cartridge (20 µm, 25 g) using hexane/EtOAc (19:1) as eluent and 40 mL/min flow rate. The peak that eluted at approx. 2-4 min was collected. Removal of the solvent under reduced pressure gave **96** (964 mg, 66%) as a colorless oil.

R_f = 0.54 (hexane/EtOAc, 9:1); ^{1}H NMR (500 MHz, $CDCl_3$): δ = 7.48 (dd, *J* = 7.8, 1.7, 1H), 7.29 – 7.24 (m, 1H), 7.17-7.14 (m, 2H), 4.12 (q, *J* = 7.1, 2H), 3.77 (t, *J* = 6.5, 2H), 2.46 (s, 3H), 2.32 (d, *J* = 7.4, 2H), 1.70-1.62 (m, 4H), 1.47 – 1.40 (m, 2H), 1.33 (p, *J* = 7.5, 2H), 1.25 (t, *J* = 7.1, 3H), 1.07 (d, *J* = 7.4, 6H), 1.01 (d, *J* = 7.6, 6H); ^{13}C NMR (126 MHz, $CDCl_3$): δ = 173.9, 144.8, 133.9, 128.8, 128.3, 63.6, 60.3, 34.5, 32.5, 25.7, 25.1, 24.6, 18.5, 18.3, 15.3, 14.4; HRMS (ESI+): (*m/z*) $[M+Na]^+$ calcd for $C_{22}H_{38}NaO_3Si^+$: 401.2482, found: 401.2492.

Di-*tert*-butyl(phenyl)silane (97)

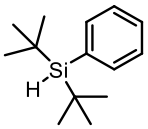

97

A stirring solution of bromobenzene (1.10 mL, 10.51 mmol) in dry THF (50 mL) was cooled to −78 ºC and *n*-BuLi (2.5 M in hexanes, 4.6 mL, 11.57 mmol) was added dropwise and the mixture was stirred for 1 h at −78 ºC. Di-*tert*-butylchlorosilane (2.55 mL, 12.61 mmol) was added and the mixture was stirred for 1 h at −78 ºC and then allowed to warm to rt and stirred overnight. The reaction was quenched with saturated $NaHCO_3$ (70 mL) and extracted with EtOAc (2 x 50 mL). The combined organic layers were washed with saturated NaCl (70 mL), H_2O (70 mL) and dried over $MgSO_4$. The solvents were removed *in vacuo* and the residue was purified by flash column chromatography (100% hexane) to yield **97** (2.015 g, 87%) as a colorless oil.

^{1}H NMR (500 MHz, $CDCl_3$): δ = 7.59 – 7.56 (m, 2H), 7.39 – 7.32 (m, 3H), 3.87 (s, 1H), 1.06 (s, 18H); ^{13}C NMR (126 MHz, $CDCl_3$): δ = 135.9, 135.7, 129.0, 127.6, 29.1, 19.2. The analytical data were in accordance with those previously reported.[218]

Ethyl 6-((di-*tert*-butyl(phenyl)silyl)oxy)hexanoate (98)

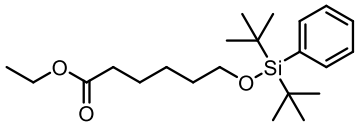

98

Silane **97** (357 mg, 1.63 mmol) was dissolved in dry CH_2Cl_2 (4 mL) under argon atmosphere. Trichloroisocyanuric acid (142 mg, 0.54 mmol) was added at 0 ºC, and the mixture was stirred for 2 h at rt. The mixture was cooled to 0 ºC before imidazole (522 mg, 3.26 mmol) and ethyl 6-hydroxyhexanoate (0.53 mL, 3.26 mmol) were added. The mixture was warmed to rt and stirred overnight. Anhydrous DMF (3 mL) was added, and the reaction mixture was stirred for a week. The resulting suspension was separated between $CHCl_3$ (30 mL) and saturated NaCl (30 mL), and the organic layer was collected and dried over $MgSO_4$. The solvents were removed *in vacuo* and the crude oil was purified by flash chromatography twice (hexane/EtOAc, 19:1) to give **98** (178 mg, 30%) as a colorless oil.

R_f = 0.56 (hexane/EtOAc, 9:1); ^{1}H NMR (500 MHz, $CDCl_3$): δ = 7.65-7.59 (m, 2H), 7.36 – 7.34 (m, 3H), 4.14 (q, *J* = 7.2, 2H), 3.91 (t, *J* = 6.4, 2H), 2.35 (t, *J* = 7.6 , 2H), 1.74 – 1.67 (m, 4H), 1.51-1.48 (m, 2H), 1.26 (t, *J* = 7.1, 3H), 1.05 (s, 18H); ^{13}C NMR (126 MHz, $CDCl_3$): δ = 174.0, 135.7, 135.1, 134.5, 128.9, 127.4, 64.4, 60.4, 34.6, 32.8, 28.6, 28.1, 25.7, 21.1, 14.4; HRMS (ESI-TOF+): (m/z) $[M+Na]^+$ calcd for $C_{22}H_{38}O_3NaSi^+$: 379.2663; found: 379.2664.

6-(((4-(Azidomethyl)phenyl)diisopropylsilyl)oxy)hexanoic acid (99)

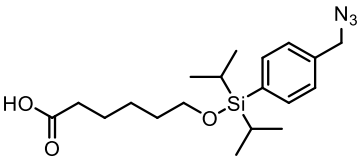

99

To a stirring solution of ester **45** (104 mg, 0.25 mmol) in a 9:1 mixture of CH_2Cl_2/CH_3OH (8 mL), NaOH (42 mg, 1.1 mmol) was added, and the mixture was stirred until complete conversion of starting material as monitored by TLC (48 h). The solvents were removed *in vacuo* and the residue diluted with water (20 mL) and the

aqueous solution was extracted with Et_2O (20 mL) to remove any unreacted ester. The aqueous layer was then cooled in an ice/water bath and acidified to pH 3 by addition of 10% citric acid and then extracted with Et_2O (3 x 30 mL). The combined organic layers were dried over Na_2SO_4 and evaporated *in vacuo* to give **99** (90 mg, 97%) as a colorless oil. The material contains residual Et_2O but was taken to the next step without any further purification.

R_f = 0 (hexane/EtOAc, 9:1); ^{1}H NMR (500 MHz, $CDCl_3$): δ = 7.56 (d, *J* = 8.0, 2H), 7.31 (d, *J* = 8.0, 2H), 4.36 (s, 2H), 3.76 (t, *J* = 6.5, 2H), 2.38 (t, *J* = 7.5, 2H), 1.72-1.61 (m, 4H), 1.46-1.41 (m, 2H), 1.29-1.24 (m, 2H), 1.05 (d, *J* = 7.4, 6H), 0.99 (d, *J* = 7.4, 6H); ^{13}C NMR (125 MHz, $CDCl_3$): δ = 179.4, 136.4, 136.2, 136.1, 127.4, 63.7, 55.0, 34.1, 32.7, 25.5, 24.7, 17.6, 17.4, 12.2; HRMS (ESI-): *m/z* $[M-H]^-$ calcd for $C_{19}H_{30}N_3O_3Si^-$: 376.2062; found: 376.2054.

_N_-(2-Amino-2-oxoethyl)-6-(((4-(azidomethyl)phenyl)diisopropylsilyl)oxy)-hexanamide (101)

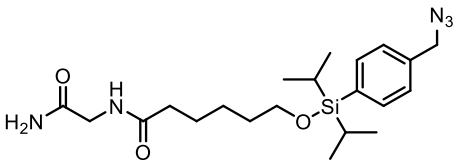

101

DIPEA (0.15 mL, 0.88 mmol), azide **99** (133 mg, 0.352 mmol) and HCTU (170 mg, 0.41 mmol) were added to a solution of glycinamide hydrochloride salt **62** (65 mg, 0.59 mmol) in DMF (4 mL). The reaction mixture was stirred at rt over night, after which the DMF was evaporated *in vacuo*. The residue was diluted with EtOAc (10 mL), washed with saturated $NaHCO_3$ (15 mL), saturated aqueous NaCl (15 mL) and dried over anhydrous $MgSO_4$. The solvent was evaporated *in vacuo* to give title compound **101** (91 mg, 84%) as a colorless liquid. The material contains residual EtOAc.

^{1}H NMR (500 MHz, $CDCl_3$): δ = 7.55 (d, *J* = 8.0, 2H), 7.31 (d, *J* = 7.9, 2H), 6.26 (bs, 1H), 6.09 (bs, 1H), 5.43 (bs, 1H), 4.36 (s, 2H), 3.95 (d, *J* = 5.1, 2H), 3.75 (t, *J* = 6.5, 2H), 2.27 (t, *J* = 7.6, 2H), 1.72 – 1.66 (m, 2H), 1.64 – 1.60 (m, 2H), 1.50 – 1.41 (m,

2H), 1.29 – 1.23 (m, 2H), 1.04 (d, *J* = 7.4, 6H), 0.99 (d, *J* = 7.5, 6H); ^{13}C NMR (126 MHz, $CDCl_3$): δ = 173.8, 171.1, 136.5, 135.2, 135.1, 127.4, 63.8, 55.0, 43.0, 36.5, 32.7, 25.7, 25.6, 17.6, 17.4, 12.2.

1-(4-(((6-((2-Amino-2-oxoethyl)amino)-6-oxohexyl)oxy)diisopropylsilyl)benzyl)-1*H*-1,2,3-triazole-4-carboxamide (103)

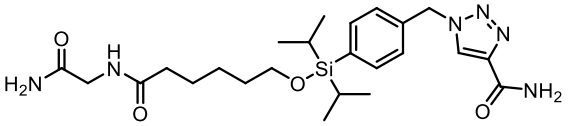

103

To a solution of propiolamide (15 mg, 0.20 mmol) and azide **101** (88.5 mg, 0.20 mmol) in a mixture of H_2O and CH_2Cl_2 (1:1, 8 mL) were added $CuSO_4 \cdot 5H_2O$ (5.4 mg, 9.3 µmol), Na_2CO_3 (44 mg, 0.41 mmol) and ascorbic acid (71.5 mg, 0.41 mmol). The mixture was stirred at rt until TLC showed full conversion of the starting material after which the mixture was filtered, and the precipitate washed with H_2O (10 mL). The filtrate was extracted with EtOAc (3 x 10 mL), and the organic layers were combined with the precipitate. These combined layers were washed with 5% $NaHCO_3$ (25 mL), H_2O (25 mL) and saturated NaCl (25 mL), dried over $MgSO_4$, filtered and the solvent was removed *in vacuo*. The crude product was purified by flash chromatography (EtOAc/MeOH, 95:5 → 9:1) to yield FOSi-precursor **103** (33 mg, 36%) as a colorless solid. The material contains residual EtOAc.

R_f = 0.12 (EtOAc/MeOH, 9:1); ^{1}H NMR (500 MHz, $CDCl_3$): δ = 8.11 (s, 1H), 7.55 (d, *J* = 8.1, 2H), 7.28 (d, *J* = 8.1, 2H), 7.17 (bs, 1H), 6.57 (bs, 1H), 6.48 (bs, 1H), 6.06 (bs, 1H), 5.88 (bs, 1H), 5.55 (s, 2H), 3.95 (d, *J* = 5.1, 2H), 3.71 (t, *J* = 6.4, 2H), 2.24 (t, *J* = 7.6, 2H), 1.67 – 1.56 (m, 4H), 1.42 – 1.36 (m, 2H), 1.28 – 1.22 (m, 2H), 1.03 (d, *J* = 7.4, 6H), 0.97 (d, *J* = 7.5, 6H); ^{13}C NMR (126 MHz, $CDCl_3$): δ = 173.8, 171.3, 162.3, 143.1, 136.4, 135.6, 134.6, 127.5, 126.2, 63.7, 54.7, 42.9, 36.4, 32.6, 25.7, 25.5, 17.5, 17.4, 12.1.

2-(Aminooxy)-*N*-benzylacetamide (108)

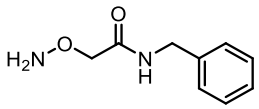

108

(Boc-aminooxy)acetic acid (243 mg, 1.27 mmol), benzylamine (0.15 mL, 1.38 mmol), HCTU (571 mg, 1.38 mmol) and DIPEA (0.57 mL, 3.28 mmol) were dissolved in dry DMF (18 mL) under argon atmosphere and stirred at rt overnight. DMF was removed *in vacuo* and the residue diluted with EtOAc (30 mL). The organic layer was washed with saturated $NaHCO_3$ (2 x 30 mL), saturated NaCl (30 mL) and dried over $MgSO_4$ before the solvent was evaporated *in vacuo* to give the crude product (593 mg) as a brownish oil with some crystals, which was directly deprotected in the next step without further purification.

The crude product was dissolved in 4 M HCl in dioxane (15 mL) and stirred at rt for 3 h after which time the product had precipitated. EtOAc (15 mL) was added and the organic layer was washed with saturated $NaHCO_3$ (2 x 25 mL), keeping the aqueous layer basic during the extraction, and then washed with saturated NaCl (25 mL), dried over Na_2SO_4 and evaporated *in vacuo* to give a clear oil (384 mg) which was purified by flash chromatography (95:5, EtOAc/MeOH) to give **108** (147 mg, 67%) as a colorless solid.

R_f = 0.23 (95:5, EtOAc/MeOH); ^{1}H NMR (500 MHz, $(CD_3)_2SO$): δ = 8.32 (t, *J* = 5.4, 1H), 7.33 – 7.22 (m, 5H), 6.38 (s, 2H), 4.33 (d, *J* = 6.2, 2H), 4.01 (s, 2H); ^{13}C NMR (126 MHz, $(CD_3)_2SO$): δ = 169.9, 139.5, 128.2, 127.1, 126.7, 74.4, 41.6; HRMS (ESI+): *m/z* $[M+Na]^+$ calcd for $C_9H_{12}N_2NaO_2^+$: 203.0791; found: 203.0791.

(*E*)-*N*-Benzyl-2-(((4-((but-3-yn-1-yloxy)diisopropylsilyl)benzylidene)amino)oxy) acetamide (109)

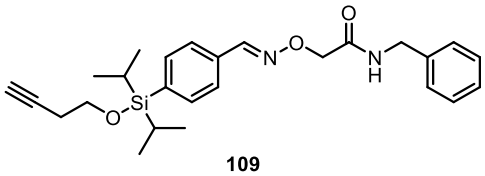

109

Aldehyde **43** (150 mg, 0.52 mmol), aminooxy-modified **108** (137 mg, 0.76 mmol) and pyridine (0.1 mL, 1.15 mmol) were dissolved in dry CH_2Cl_2 (6 mL) and stirred under argon atmosphere overnight. The resulting mixture was washed with 5% citric acid (3 x 10 mL), saturated NaCl (2 x 25 mL) and dried over Na_2SO_4. The solvent was removed *in vacuo* to give the crude product (300 mg) as a pale white oil which was purified by flash chromatography (100% EtOAc) to give the **109** (149 mg, 64%) as a colorless, sticky oil which solidified upon standing.

R_f = 0.59 (EtOAc); ^{1}H NMR (500 MHz, $CDCl_3$): δ = 8.16 (s, 1H), 7.59 (d, *J* = 8.2, 2H), 7.56 (d, *J* = 8.2, 2H), 7.31 – 7.24 (m, 5H), 6.54 (bs, 1H), 4.72 (s, 2H), 4.55 (d, *J* = 5.9, 2H), 3.90 (t, *J* = 7.1, 2H), 2.52 (dt, *J* = 7.1, 2.7, 2H), 1.99 (t, *J* = 2.7, 1H), 1.32 – 1.27 (m, 2H), 1.07 (d, *J* = 7.4, 6H), 1.01 (d, *J* = 7.5, 6H); ^{13}C NMR (126 MHz, $CDCl_3$): δ = 169.7, 151.2, 138.1, 137.9, 135.1, 132.0, 128.8, 127.7, 127.6, 126.5, 81.5, 73.5, 69.7, 62.5, 43.0, 23.0, 17.4, 17.3, 12.1; HRMS (ESI+): *m/z* $[M+Na]^+$ calcd for $C_{26}H_{34}N_2NaO_3Si^+$: 473.2231; found: 473.2229.

(*E*)-*N*-Benzyl-2-(((4-(diisopropyl(2-(1-phenyl-1*H*-1,2,3-triazol-4-yl)ethoxy)silyl)-benzylidene)amino)oxy)acetamide (111)

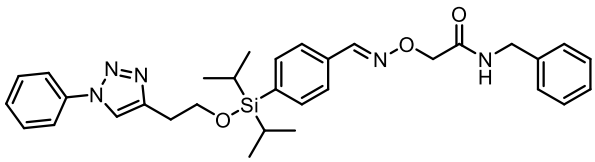

111

To a solution of alkyne **109** (105 mg, 0.23 mmol) and azidobenzene (0.5 M in Me-THF, 0.51 mL, 0.26 mmol) in *tert*-butanol (3 mL), a solution of $CuSO_4 \cdot 5H_2O$ (6.7 mg, 0.05 mmol) in water (1.5 mL) and sodium ascorbate (10.6 mg, 0.15 mmol) in water (1.5 mL) were added. The mixture was stirred at rt until TLC showed full conversion

of the starting material after which the mixture was diluted with H_2O (10 mL) and extracted with CH_2Cl_2 (3 x 15 mL). The combined organic layers were washed with saturated $NaHCO_3$ (30 mL), saturated NaCl (30 mL), dried over $MgSO_4$, filtered and the solvent was removed *in vacuo*. The crude product was purified by flash column chromatography (hexane/EtOAc, 4:1 → 0:100) to yield FOSi-precursor **111** (52 mg, 39%) as a colorless, sticky oil.

R_f = 0.64 (EtOAc); ^{1}H NMR (500 MHz, $CDCl_3$): δ = 8.14 (s, 1H), 7.85 (s, 1H), 7.70 – 7.67 (m, 2H), 7.56 – 7.47 (m, 6H), 7.44 – 7.40 (m, 1H), 7.28 – 7.21 (m, 5H), 6.54 (app t, 1H), 4.71 (s, 2H), 4.54 (d, *J* = 5.9, 2H), 4.11 (t, *J* = 6.5, 2H), 3.13 (t, *J* = 6.5, 2H), 1.34 – 1.28 (m, 2H), 1.05 (d, *J* = 7.4, 6H), 1.00 (d, *J* = 7.5, 6H); ^{13}C NMR (126 MHz, $CDCl_3$): δ = 169.6, 151.2, 146.0, 138.1, 138.0, 137.4, 135.0, 132.0, 129.9, 128.8, 128.7, 127.7, 127.6, 126.5, 120.6, 120.3, 73.5, 63.2, 43.0, 29.7, 17.5, 17.4, 12.1; HRMS (ESI+): *m/z* $[M+Na]^+$ calcd for $C_{32}H_{39}N_5NaO_3Si^+$: 592.2714; found: 592.2714.

(4-(Azidomethyl)phenyl)diisopropyl(methoxy)silane (118)

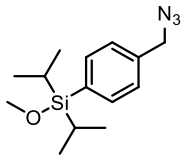

118

Silane **42** (91.9 mg, 0.37 mmol) was dissolved in dry CH_2Cl_2 (3 mL) under argon atmosphere and cooled to 0 ºC in an ice bath before trichloroisocyanuric acid (30.2 mg, 0.13 mmol) was added. The cooling bath was removed, and the mixture was stirred for 2 h at rt. The mixture was cooled to 0 ºC before imidazole (114 mg, 1.67 mmol) and anhydrous MeOH (0.15 mL, 3.7 mmol) were added, and the resulting mixture was allowed to warm to rt and stirred overnight. The resulting suspension was separated between $CHCl_3$ (15 mL) and saturated NaCl (15 mL), and the organic layer was dried over $MgSO_4$. The solvents were removed *in vacuo* and the crude product was purified using a Biotage Sfär silica gel cartridge (20 µm, 10 g) using hexane/EtOAc (19:1) as eluent and 20 mL/min flow rate. The peak that eluted at approx. 1.1-1.9 min was collected. Removal of the solvent under reduced pressure gave **118** (5.0 mg, 5%) as a colorless oil.

^{1}H NMR (500 MHz, $CDCl_3$) δ 7.57 (d, *J* = 8.0, 2H), 7.33 (d, *J* = 8.0, 2H), 4.36 (s, 2H), 3.62 (s, 3H), 1.32 – 1.28 (m, 2H), 1.07 (d, *J* = 7.4, 6H), 1.02 (d, *J* = 7.6, 6H); ^{13}C NMR (126 MHz, $CDCl_3$): δ = 136.6, 135.3, 127.5, 55.0, 52.2, 17.6, 17.4, 12.1 (aromatic signal missing due to low concentration of sample).

(4-(Azidomethyl)-2-methylphenyl)diisopropyl(methoxy)silane (119)

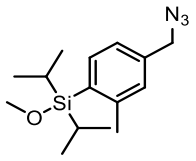

119

Silane **63** (214 mg, 0.82 mmol) was dissolved in dry CH_2Cl_2 (3 mL) under argon atmosphere and cooled to 0 ºC in an ice bath before trichloroisocyanuric acid (64.0 mg, 0.27 mmol) was added. The cooling bath was removed, and the mixture was stirred for 2 h at rt. The mixture was cooled to 0 ºC before imidazole (251 mg, 3.7 mmol) and anhydrous MeOH (0.33 mL, 8.2 mmol) were added and the resulting mixture was allowed to warm to rt and stirred overnight. The resulting suspension was separated between $CHCl_3$ (15 mL) and saturated NaCl (15 mL), and the organic layer was dried over $MgSO_4$. The solvents were removed *in vacuo* and the crude product was purified using a Biotage Sfär silica gel cartridge (20 µm, 10 g) using hexane/EtOAc (19:1) as eluent and 20 mL/min flow rate. The peak that eluted at approx. 1.2-1.8 min was collected. Removal of the solvent under reduced pressure gave **119** (59 mg, 25%) as a colorless oil.

R_f = 0.60 (hexane/EtOAc, 9:1); ^{1}H NMR (500 MHz, $CDCl_3$): δ = 7.50 (d, *J* = 8.0, 1H), 7.13 – 7.12 (m, 2H), 4.32 (s, 2H), 3.62 (s, 3H), 2.49 (s, 3H), 1.34 (app h, *J* = 7.5, 2H), 1.09 (d, *J* = 7.4, 6H), 1.03 (d, *J* = 7.4, 6H); ^{13}C NMR (126 MHz, $CDCl_3$): δ = 145.0, 136.5, 136.4, 133.7, 130.0, 124.3, 54.9, 52.1, 23.0, 17.9, 17.7, 13.2; HRMS (GC-EI+): *m/z* M^+ calcd for $C_{15}H_{25}N_3OSi^+$: 291.1717, found: $[M-43]^+$ = 248.1213; fragmentation *m/z* 291 (M^+), 248 (M – $CH_2CH_2CH_3$), 220 (M – $CH_2CH_2CH_3$ – CH_2=CH_2), 192 (M – $CH_2CH_2CH_3$ – CH_2=CH_2 – 28), 162.

(4-(Azidomethyl)-2,6-dimethylphenyl)diisopropyl(methoxy)silane (120)

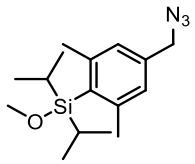

120

Silane **67** (265 mg, 0.96 mmol) was dissolved in dry CH_2Cl_2 (3 mL) under argon atmosphere and cooled to 0 ºC in an ice bath before trichloroisocyanuric acid (80 mg, 0.32 mmol) was added. The cooling bath was removed, and the mixture was stirred for 2 h at rt. The mixture was cooled to 0 ºC before imidazole (294 mg, 4.32 mmol) and anhydrous MeOH (0.4 mL, 9.6 mmol) were added. The cooling bath was removed, and the mixture was allowed to warm to rt and stirring continued overnight. The resulting suspension was separated between $CHCl_3$ (15 mL) and saturated NaCl (15 mL), and the organic layer was collected and dried over $MgSO_4$. The solvents were removed *in vacuo* and the crude product was purified using a Biotage Sfär silica gel cartridge (20 µm, 10 g) using hexane/EtOAc (19:1) as eluent and 20 mL/min flow rate. The peak that eluted at approx. 1.2-2 min was collected. Removal of the solvent under reduced pressure gave **120** (194 mg, 66%) as a colorless oil.

R_f = 0.63 (hexane/EtOAc, 9:1); ^{1}H NMR (500 MHz, $CDCl_3$): δ = 6.92 (s, 2H), 4.27 (s, 2H), 3.63 (s, 3H), 2.50 (s, 6H), 1.37 (app h, *J* = 7.4, 2H), 1.14 (d, *J* = 7.4, 6H), 1.03 (d, *J* = 7.6, 6H); ^{13}C NMR (126 MHz, $CDCl_3$): δ = 145.7, 135.9, 133.7, 128.0, 54.7, 52.0, 24.2, 18.4, 18.1, 15.3; HRMS (GC-EI+): *m/z* M^+ calcd for $C_{16}H_{27}N_3OSi^+$: 305.1918, found: $[M\text{-}43]^+$ = 262.1317; fragmentation *m/z* 305 (M^+), 262 (M – $CH_2CH_2CH_3$), 234 (M – $CH_2CH_2CH_3$ – CH_2=CH_2), 206 (M – $CH_2CH_2CH_3$ – CH_2=CH_2 – 28), 176.

Ethyl 1-(4-(diisopropyl(methoxy)silyl)-3,5-dimethylbenzyl)-1H-1,2,3-triazole-4-carboxylate (121)[219]

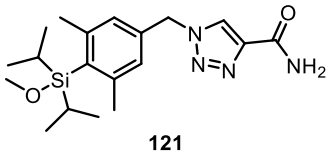

121

Azide **120** (80 mg, 0.26 mmol), ethyl propiolate (30 µL, 0.26 mmol), $CuSO_4 \cdot 5H_2O$ (3.3 mg, 0.013 mmol) and sodium ascorbate (10.6 mg, 0.15 mmol) were suspended in a mixture of H_2O/CH_2Cl_2 (1:3, 2 mL). The mixture was stirred at rt until TLC showed full conversion of the starting material after which the mixture was diluted with H_2O (10 mL) and extracted with CH_2Cl_2 (2 x 15 mL). The combined organic layers were washed with saturated $NaHCO_3$ (30 mL), saturated NaCl (30 mL), dried over $MgSO_4$, filtered and the solvent was removed *in vacuo*. The crude product was purified by flash column chromatography (hexane/EtOAc, 1:1) to give **121** (39 mg, 38%) as a colorless solid.

^{1}H NMR (500 MHz, $CDCl_3$): δ = 8.01 (s, 1H), 6.85 (s, 2H), 5.46 (s, 2H), 4.41 (q, *J* = 7.2, 2H), 3.61 (s, 3H), 2.45 (s, 6H), 1.40 (t, *J* = 7.1, 3H), 1.40 – 1.30 (m, 2H), 1.12 (d, *J* = 7.4, 6H), 1.01 (d, *J* = 7.6, 6H); ^{13}C NMR (126 MHz, $CDCl_3$): δ = 161.0, 146.3, 140.7, 135.1, 134.0, 127.9, 127.6, 61.5, 54.3, 52.0, 24.2, 18.4, 18.1, 15.3, 14.4.

6-((Diisopropyl(2-methyl-4-propoxyphenyl)silyl)oxy)hexanoic acid (130)

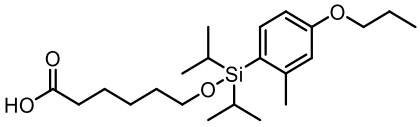

130

To a stirring solution of ester **80** (295 mg, 0.71 mmol) in CH_2Cl_2/MeOH (9:1, 20 mL), NaOH (134 mg, 3.35 mmol) was added, and the mixture was stirred until complete conversion of starting material as monitored by TLC (overnight). Saturated NH_4Cl (20 mL) was added, and the resulting mixture was stirred while HCl (3 M) was added until pH 3. The two layers were separated, and the aqueous layer was extracted with CH_2Cl_2 (2 x 25 mL). The combined organic layers were dried over $MgSO_4$ and evaporated *in vacuo* to **130** (276 mg, quantitative) as a viscous, colorless oil. The material was used in the next step without any further purification.

R_f = 0.00 (hexane/EtOAc, 9:1); ^{1}H NMR (500 MHz, $CDCl_3$): δ = 10.88 (bs, 1H), 7.38 (d, *J* = 8.2, 1H), 6.74 – 6.68 (m, 2H), 3.92 (t, *J* = 6.6, 2H), 3.74 (t, *J* = 6.5, 2H), 2.43 (s, 3H), 2.37 (t, *J* = 7.5, 2H), 1.80 (app h, *J* = 7.4, 2H), 1.71 – 1.61 (m, 4H), 1.49 – 1.44 (m, 2H), 1.30 (p, *J* = 7.4, 2H), 1.06 (d, *J* = 7.4, 6H), 1.03 (t, *J* = 7.4, 3H), 1.00 (d, *J* = 7.4, 6H); ^{13}C NMR (125 MHz, $CDCl_3$): δ = 179.3, 160.1, 146.2, 137.3, 124.5, 116.7, 110.5, 69.1, 63.6, 34.1, 32.6, 25.6, 24.7, 23.4, 22.8, 18.0, 17.9, 13.3, 10.7; HRMS (ESI-): (*m/z*) [M-H]$^-$ calcd for $C_{22}H_{37}O_4Si^-$: 393.2467; found: 393.2455, (*m/z*) [2M-H]$^-$ calcd for $C_{44}H_{75}O_8Si_2^-$: 787.5006; found: 788.5040.

Diisopropyl(4-propoxyphenyl)silane (132)

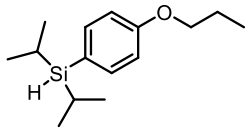

132

A stirring solution of 1-bromo-4-propoxybenzene (**77**) (294 mg, 1.37 mmol) in dry THF (10 mL) was cooled to −78 ºC and *n*-BuLi (2.5 M in hexanes, 0.60 mL, 1.51 mmol) was added dropwise and the mixture was stirred for 1 h at −78 ºC. Diisopropylchlorosilane (0.26 mL, 1.51 mmol) was added, and the mixture was stirred for 30 min at −78 ºC and then allowed to warm to rt and stirring continued overnight. The reaction was quenched by addition of saturated $NaHCO_3$ (10 mL), and the resulting mixture was extracted with EtOAc (2 x 10 mL). The combined organic layers were washed with saturated NaCl (2 x 20 mL) and dried over $MgSO_4$. The solvents were removed *in vacuo* and the crude product was purified using a Biotage Sfär silica gel cartridge (20 µm, 25 g) using hexane/EtOAc (19:1) as eluent and 40 mL/min flow rate. The peak that eluted at approx. 7-9 min was collected. Removal of the solvent under reduced pressure gave **132** (315 mg, 92%) as a colorless oil. The material contains aliphatic impurities (unreacted chlorosilane).

^{1}H NMR (500 MHz, $CDCl_3$): δ = 7.43 (d, *J* = 8.7, 2H), 6.90 (d, *J* = 8.7, 2H), 3.96 – 3.90 (m, 3H), 1.82 (h, *J* = 7.4, 2H), 1.24 – 1.15 (m, 2H), 1.08 – 1.05 (m, 6H), 1.03 (d, *J* = 7.3, 4H), 0.99 (d, *J* = 7.3, 6H); ^{13}C NMR ^{13}C NMR (126 MHz, $CDCl_3$): δ = 160.2, 137.0, 124.7, 114.1, 69.3, 22.8, 18.8, 18.6, 11.0.

Di-*tert*-butyl(4-propoxyphenyl)silane (133)

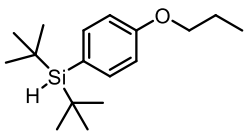

133

A stirring solution of 1-bromo-4-propoxybenzene (**77**) (310 mg, 1.44 mmol) in dry THF (10 mL) was cooled to −78 ºC and *n*-BuLi (2.5 M in hexanes, 0.61 mL, 1.53 mmol) was added dropwise and the mixture was stirred for 1 h at −78 ºC. Di-*tert*-butylchlorosilane (0.31 mL, 1.53 mmol) was added and the mixture was stirred for 1 h at −78 ºC and then allowed to warm to rt and stirring continued overnight. The reaction was quenched by addition of saturated $NaHCO_3$ (20 mL) and extracted with EtOAc (2 x 20 mL). The combined organic layers were washed with saturated NaCl (40 mL), H_2O (70 mL) and dried over $MgSO_4$. The solvents were removed *in vacuo.* The crude material was attempted purified using a Biotage Sfär silica gel cartridge (20 µm, 10 g) using hexane/EtOAc (19:1) as eluent and 20 mL/min flow rate. The peak that eluted at approx. 7-9 min was collected. Removal of the solvent under reduced pressure gave 286 mg of a mixture of **133** and the *n*-butylated side-product **79** (Ratio **139**/**79** ≈ 6:4). The calculated yield for **133** was 43%.

^{1}H NMR (500 MHz, $CDCl_3$): δ = 7.48 (d, *J* = 8.7, 2H), 6.89 (d, *J* = 8.7, 2H), 3.94 (t, *J* = 6.5, 2H), 3.84 (bs, 1H), 1.86 – 1.77 (m, 3H), 1.04 (s, 18H), 1.04 (t, *J* = 3.7, 2H); ^{13}C NMR (126 MHz, $CDCl_3$): δ = 160.1, 137.3, 126.1, 113.9, 69.2, 29.1, 22.8, 19.2, 10.7.

6-(((4-(Azidomethyl)-2-methylphenyl)diisopropylsilyl)oxy)hexanoic acid (134)

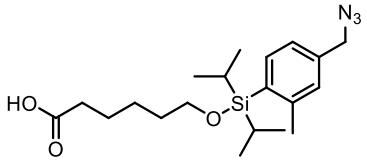

134

To a stirring solution of **126** (255.8 mg, 0.61 mmol) in CH_2Cl_2/MeOH (9:1, 20 mL) NaOH (105 mg, 2.44 mmol) was added, and the mixture was stirred until complete conversion of starting material as monitored by TLC (24 h). The reaction mixture was diluted with saturated NH_4Cl (40 mL), acidified to pH 3 using 3M HCl and the two layers were separated. The aqueous layer was extracted with CH_2Cl_2 (2 x 25 mL) and the combined organic layers were dried over Na_2SO_4 and solvent removed *in vacuo* to give **136** (224 mg, 94%) as a colorless oil.

R_f = 0.0 (hexane/EtOAc, 9:1); ^{1}H NMR (500 MHz, $CDCl_3$): δ = 7.50 (d, *J* = 8.0, 1H), 7.11-7.10 (m, 2H), 4.31 (s, 2H), 3.78 (t, *J* = 6.5, 2H), 2.48 (s, 3H), 2.38 (t, *J* = 7.6, 2H), 1.72 – 1.61 (m, 4H), 1.50 – 1.43 (m, 2H), 1.32 (h, *J* = 7.4, 2H), 1.07 (d, *J* = 7.4, 6H), 1.00 (d, *J* = 7.6, 6H); ^{13}C NMR (126 MHz, $CDCl_3$): δ = 179.3, 145.0, 136.4, 136.3, 134.2, 129.9, 124.3, 63.7, 54.9, 34.0, 32.6, 25.6, 24.7, 23.2, 17.9, 17.8, 13.2; HRMS (ESI+): (*m/z*) $[M-H]^-$ calcd for $C_{20}H_{32}N_3O_3Si^-$: 390.2218, found: 390.2216, (*m/z*) $[2M-H]^-$ calcd for $C_{40}H_{65}N_6O_6Si_2^-$: 781.4510; found: 781.4423.

Coupling of FOSi-precursor to resin

Rink amide ChemMatrix (162.9 mg, 0.076 mmol) was swelled in DMF at rt for 1 h. The solvent was drained off and carboxylic acid **130** (90 mg, 0.228 mmol, 3 eq.) and HCTU (88 mg, 0.213 mmol, 2.8 eq.) dissolved in DMF (5 mL) were added followed by addition of DIPEA (80 µL, 0.456 mmol, 6 eq.). The resin vial was shaken at rt for 24-48 h. The resin was washed with DMF (5 x 10 mL) and CH_2Cl_2 (5 x 10 mL) and then dried under vacuum overnight.

General fluorination protocols

Method 1: The desired silyl ether (1 eq.) was dissolved in dry THF (50 mL/mmol) and cooled to 0 °C. TBAF (1M in THF, 2.0 eq.) was added, and the solution was warmed to rt and stirred until completion (followed by TLC-analysis). The crude mixture was concentrated *in vacuo* and analyzed by ^{1}H NMR immediately. The crude product was diluted with EtOAc, washed with $NaHCO_3$, saturated NaCl and the organic layer was dried over $MgSO_4$, and solvent was evaporated *in vacuo*.

Method 2: KF (1.1 eq) and Kryptofix (K[2.2.2], 1.1 eq.) were added in dry MeCN and stirred for 10 min. Desired silyl ether (1 eq.) was added and the reaction was followed by TLC until full conversion of starting material. Alternative: The crude mixture was filtered through an alumina SPE-cartridge. The solvent was evaporated, and NMR analyses of the crude mixture were performed.

Fluorodiisopropyl(2-methyl-4-propoxyphenyl)silane (114)

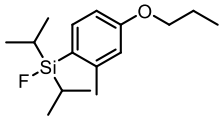

114

Synthesized as described in general fluorination method 2. ^{1}H NMR (600 MHz, $CDCl_3$): δ = 7.43 (d, *J* = 8.7, 1H), 6.72 (d, *J* = 7.0, 2H), 3.92 (t, *J* = 6.5, 2H), 2.44 (s, 3H), 1.83 – 1.76 (m, 2H), 1.27 – 1.23 (m, 2H), 1.07 (d, *J* = 7.4, 6H), 1.02 (t, *J* = 7.4, 3H), 0.95 (d, *J* = 7.5, 6H); ^{13}C NMR (151 MHz, $CDCl_3$): δ = 160.3, 145.6, 136.8, 125.1, 116.7, 110.6, 69.2, 23.6, 22.8, 17.7, 17.5, 13.7, 10.7; HRMS (GC-EI+): *m/z* M^+ calcd for $C_{16}H_{27}FOSi$ = 282.1815, found: 282.1820; fragmentation *m/z* 282 (M^+), 239 (M – $CH_2CH_2CH_3$), 211 (M – $CH_2CH_2CH_3$ – CH_2=CH_2), 197, 169. The material contains some aliphatic impurities, probably remains of the cleaved aliphatic chain.

Solid-phase fluorination

Resin-bound **131** (25 mg, 0.012 mmol, 1 eq.) was loaded into a 10 mL peptide synthesis vessel and suspended in MeCN (2.5 mL). KF (0.8 mg, 0.014 mmol, 1.2 eq.) and K[2.2.2] (5.3 mg, 0.014 mmol, 1.2 eq.) were added and the vial was shaken for 2 h.

The solvent was filtered off and evaporated *in vacuo*, and ^{1}H NMR was obtained immediately.

Compound **114**: ^{1}H NMR (500 MHz, $CDCl_3$): δ = 7.41 (d, *J* = 9.0, 1H), 6.68 – 6.66 (m, 2H), 3.88 (t, *J* = 6.6, 2H), 2.41 (s, 3H), 1.78 – 1.73 (m, 2H), 1.21 – 1.16 (m, 2H), 1.06 (d, *J* = 7.4, 6H), 1.02 (t, *J* = 7.4, 3H), 0.94 (d, *J* = 7.4, 6H); LRMS (GC-EI+): *m/z* M^+ calcd for $C_{16}H_{27}FOSi$ = 282.2, found: 282.2; fragmentation *m/z* 282 (M^+), 239 (M – $CH_2CH_2CH_3$), 211 (M – $CH_2CH_2CH_3$ – CH_2=CH_2), 197, 169. The material contains some aliphatic impurities and remaining K[2.2.2].

Solid-phase ^{18}F-fluorination

First run: ^{18}F was retrieved from a QMA-cartridge by flushing with a K[2.2.2]/K_2CO_3 mixture (0.4 mL) in MeCN–H_2O (80:20). The solvent was azeotropically dried (3 x 1 mL dry MeCN) and then dry MeCN was added to the reaction mixture (1.0 mL). The resin (28.4 mg) was then added to the vial and stirred with a magnet bar for 30 min before analysis by Radio-TLC (hexane/EtOAc, 1:1) (reference to appendix). The reaction mixture was stirred further at rt for 30 min and another radio-TLC analysis (hexane/EtOAc, 1:1) was performed. The mixture was then heated to 50 ºC for 30 min and one final radio-TLC analysis (hexane/EtOAc, 1:1) was performed (reference to appendix). Initial activity: 1.634 GBq.

Second run: ^{18}F was retrieved from a QMA-cartridge by flushing with a K[2.2.2]/K_2CO_3 mixture (0.4 mL) in MeCN–H_2O (80:20). The solvent was azeotropically dried (4 x 1 mL dry MeCN) and then dry MeCN was added to the reaction mixture (0.5 mL). The resin (32.4 mg) was then added to the vial. The resin was stirred with a magnet bar at 50 ºC for 30 min and then analyzed by Radio-TLC (hexane/EtOAc, 1:1). The reaction mixture was then heated to 70 ºC and stirred for 30 min before analysis by radio-TLC (hexane/EtOAc, 1:1). Initial activity: 1.354 GBq.

Third run: ^{18}F was retrieved from a QMA-cartridge by flushing with a K[2.2.2]/K_2CO_3 mixture (0.4 mL) in MeCN–H_2O (80:20). The solvent was azeotropically dried (4 x 1 mL dry MeCN) and then dry MeCN was added to the reaction mixture (0.5 mL). The

resin (42.6 mg) was then added to the vial. The resin was stirred with a magnet bar at 50 ºC for 30 min and then analyzed by Radio-TLC (hexane/EtOAc, 1:1). The reaction mixture was stirred further for 30 min at 50 ºC before analysis by radio-TLC (hexane/EtOAc, 1:1). Initial activity: 3.05 GBq.

References

1. Wang, Z. J.; Chang, T.-T. A.; Slauter, R., A Comprehensive Guide to Toxicology in Preclinical Drug Development. *Academic Press*. **2013**; 759-775.
2. Fowler, J. S., Wolf, A. P. Synthesis of carbon-11, fluorine-18, and nitrogen-13 labeled radiotracers for biomedical applications. *United States.* **1981**
3. Lieser, K. H., Nuclear and radiochemistry - fundamentals and applications. *Wiley-VCH.* **2001**; p 462.
4. Lewis, J. S., Windhorst, Albert D., Zeglis, Brian M., Radiopharmaceutical Chemistry. *Springer Cham*. **2019**; p 651.
5. Beyer, T.; Townsend, D. W.; Brun, T.; Kinahan, P. E.; Charron, M.; Roddy, R.; Jerin, J.; Young, J.; Byars, L.; Nutt, R., A combined PET/CT scanner for clinical oncology. *J Nucl Med* **2000,** *41*, 1369-1379.
6. Townsend, D. W., Dual-modality imaging: combining anatomy and function. *J. Nucl. Med.* **2008,** *49*, 938-955.
7. Ljungberg, M.; Pretorius, P. H., SPECT/CT: an update on technological developments and clinical applications. *Brit. J. Radiology* **2018,** *91*, 20160402.
8. Mariani, G.; Bruselli, L.; Kuwert, T.; Kim, E. E.; Flotats, A.; Israel, O.; Dondi, M.; Watanabe, N., A review on the clinical uses of SPECT/CT. *European J. Nucl. Med. Mol. Imaging* **2010,** *37*, 1959-1985.
9. Judenhofer, M. S.; Wehrl, H. F.; Newport, D. F.; Catana, C.; Siegel, S. B.; Becker, M.; Thielscher, A.; Kneilling, M.; Lichy, M. P.; Eichner, M.; Klingel, K.; Reischl, G.; Widmaier, S.; Röcken, M.; Nutt, R. E.; Machulla, H. J.; Uludag, K.; Cherry, S. R.; Claussen, C. D.; Pichler, B. J., Simultaneous PET-MRI: a new approach for functional and morphological imaging. *Nat. Med.* **2008,** *14*, 459-465.
10. Pichler, B. J.; Kolb, A.; Nägele, T.; Schlemmer, H. P., PET/MRI: paving the way for the next generation of clinical multimodality imaging applications. *J. Nucl. Med.* **2010,** *51*, 333-336.
11. Vandenberghe, S.; Marsden, P. K., PET-MRI: a review of challenges and solutions in the development of integrated multimodality imaging. *Phys. Med. Biol.* **2015,** *60*, R115.
12. Keresztes, A.; Borics, A.; Tömböly, C., Therapeutic and diagnostic radiopharmaceuticals. *Int. J. Pharm.* **2015**.
13. Pimlott, S. L.; Sutherland, A., Molecular tracers for the PET and SPECT imaging of disease. *Chem. Soc. Rev.* **2011,** *40*, 149-162.
14. Olberg, D. E.; Cuthbertson, A.; Solbakken, M.; Arukwe, J. M.; Qu, H.; Kristian, A.; Bruheim, S.; Hjelstuen, O. K., Radiosynthesis and Biodistribution of a Prosthetic Group ([18F]FENMA) Conjugated to Cyclic RGD Peptides. *Bioconjugate Chem.* **2010,** *21*, 2297-2304.
15. McQuade, P.; Rowland, D. J.; Lewis, J. S.; Welch, M. J., Positron-emitting isotopes produced on biomedical cyclotrons. *Curr. Med. Chem.* **2005,** *12*, 807-18.
16. Olberg, D. E. Novel [18F] fluorinated prosthetic groups for the labelling of peptides for positron emission tomography (PET). *University of Tromsø*. **2009**.

17. Kawada, K.; Iwamoto, M.; Sakai, Y., Mechanisms underlying [18F]fluorodeoxyglucose accumulation in colorectal cancer. *World J. Radiol.* **2016,** *8*, 880-886.
18. Khalil, M. M., Basic Sciences of Nuclear Medicine. 1st ed.; *Spinger-Verlag Berlin Heidelberg*. **2011**; p 423.
19. Richter, S.; Wuest, F., [18F]-Labeled Peptides: The Future Is Bright. *Molecules* **2014,** *19*, 20536-20556.
20. Fani, M.; André, J. P.; Maecke, H. R., 68Ga-PET: a powerful generator-based alternative to cyclotron-based PET radiopharmaceuticals. *Contrast Media Mol. Imaging* **2008,** *3*, 53-63.
21. Jacobson, O.; Kiesewetter, D. O.; Chen, X., Fluorine-18 radiochemistry, labeling strategies and synthetic routes. *Bioconjugate Chem.* **2015,** *26*, 1-18.
22. Volker, J. F.; Hodge, H. C.; Wilson, H. J.; Van Voorhis, S. N., The adsorption of fluorides by enamel, dentin, bone, and hydroxyapatite as shown by the radioactive isotope. *J. Bio. Chem.* **1940,** *134*, 543-548.
23. https://dailymed.nlm.nih.gov/dailymed/drugInfo.cfm?setid=262503e7-de09-4b42-9963-ec00cbc7c35c. *DailyMed.* 12.10. 19. Retrieved 22.01.23
24. Jerabek, P. A.; Patrick, T. B.; Kilbourn, M. R.; Dischino, D. D.; Welch, M. J., Synthesis and biodistribution of 18F-labeled fluoronitroimidazoles: Potential in vivo markers of hypoxic tissue. *Int. J. Rad. Applic. Instrument. Part A. Appl. Rad. and Isotopes* **1986,** *37*, 599-605.
25. Chapman, J. D., The detection and measurement of hypoxic cells in solid tumors. *Cancer* **1984,** *54*, 2441-9.
26. Rajendran, J. G.; Mankoff, D. A.; O'Sullivan, F.; Peterson, L. M.; Schwartz, D. L.; Conrad, E. U.; Spence, A. M.; Muzi, M.; Farwell, D. G.; Krohn, K. A., Hypoxia and Glucose Metabolism in Malignant Tumors: Evaluation by [18F]Fluoromisonidazole and [18F]Fluorodeoxyglucose Positron Emission Tomography Imaging. *Clin. Cancer Res.* **2004,** *10*, 2245-2252.
27. Fleming, I. N.; Manavaki, R.; Blower, P. J.; West, C.; Williams, K. J.; Harris, A. L.; Domarkas, J.; Lord, S.; Baldry, C.; Gilbert, F. J., Imaging tumour hypoxia with positron emission tomography. *Br. J. Cancer* **2015,** *112*, 238-250.
28. Volkert, W. A.; Hoffman, T. J., Therapeutic Radiopharmaceuticals. *Chem. Rev.* **1999,** *99*, 2269-2292.
29. Herrero Álvarez, N.; Bauer, D.; Hernández-Gil, J.; Lewis, J. S., Recent Advances in Radiometals for Combined Imaging and Therapy in Cancer. *Chem. Med. Chem.* **2021,** *16*, 2909-2941.
30. Dammes, N.; Peer, D., Monoclonal antibody-based molecular imaging strategies and theranostic opportunities. *Theranostics* **2020,** *10*, 938-955.
31. Portnow, L. H.; Vaillancourt, D. E.; Okun, M. S., The history of cerebral PET scanning: from physiology to cutting-edge technology. *Neurology* **2013,** *80*, 952-956.
32. Vāvere, A. L.; Scott, P. J. H., Clinical Applications of Small-molecule PET Radiotracers: Current Progress and Future Outlook. *Semin. Nucl. Med.* **2017,** *47*, 429-453.
33. Wagner, M.; Seitz, U.; Buck, A.; Neumaier, B.; Schultheiss, S.; Bangerter, M.; Bommer, M.; Leithäuser, F.; Wawra, E.; Munzert, G.; Reske, S. N., 3'-

[18F]fluoro-3'-deoxythymidine ([18F]-FLT) as positron emission tomography tracer for imaging proliferation in a murine B-Cell lymphoma model and in the human disease. *Cancer Res.* **2003,** *63*, 2681-2687.

34. Köhler, C., Hall, H., Ögren, S.-O., Gawell, L. Specific in vitro and in vivo binding of 3H-raclopride a potent substituted benzamide drug with high affinity for dopamine D-2 receptors in the rat brain. *Biochem. Pharm.* **1985** *34*(13), 2251-2259.
35. Whitwam, J. G., Amrein, R. Pharmacology of flumazenil. *Acta Anaesthesiol. Scand.* **1995**, *39*(108), 3-14.
36. Cipollaro, C.; Mansi, L., Anatoliy Granov, Leonid Tiutin, Thomas Schwarz (eds): Positron Emission Tomography. *Springer*. **2014**.
37. Schliebs, R.; Arendt, T., The cholinergic system in aging and neuronal degeneration. *Behavioural Brain Research* **2011,** *221*, 555-563.
38. Ohtani, T.; Kurihara, H.; Ishiuchi, S.; Saito, N.; Oriuchi, N.; Inoue, T.; Sasaki, T., Brain tumour imaging with carbon-11 choline: comparison with FDG PET and gadolinium-enhanced MR imaging. *Eur. J. Med. Chem.* **2001,** *28*, 1664-1670.
39. Hara, T.; Kosaka, N.; Kishi, H., PET imaging of prostate cancer using carbon-11-choline. *J. Nucl. Med.* **1998,** *39*, 990-995.
40. Lipinski, C. A.; Lombardo, F.; Dominy, B. W.; Feeney, P. J., Experimental and computational approaches to estimate solubility and permeability in drug discovery and development settings. *Adv. Drug Delivery Rev.* **1997,** *23*, 3-25.
41. Manna, S.; Di Natale, C.; Florio, D.; Marasco, D., Peptides as Therapeutic Agents for Inflammatory-Related Diseases. *Int. J. Mol. Sci.* **2018,** *19*, 2714.
42. Kolenc Peitl, P.; Tamma, M.; Kroselj, M.; Braun, F.; Waser, B.; Reubi, J. C.; Sollner Dolenc, M.; Maecke, H. R.; Mansi, R., Stereochemistry of Amino Acid Spacers Determines the Pharmacokinetics of 111In–DOTA–Minigastrin Analogues for Targeting the CCK2/Gastrin Receptor. *Bioconj. Chem.* **2015,** *26*, 1113-1119.
43. Antunes, P.; Ginj, M.; Walter, M. A.; Chen, J.; Reubi, J.-C.; Maecke, H. R., Influence of Different Spacers on the Biological Profile of a DOTA−Somatostatin Analogue. *Bioconj. Chem.* **2007,** *18*, 84-92.
44. Kapp, T. G.; Rechenmacher, F.; Neubauer, S.; Maltsev, O. V.; Cavalcanti-Adam, E. A.; Zarka, R.; Reuning, U.; Notni, J.; Wester, H.-J.; Mas-Moruno, C.; Spatz, J.; Geiger, B.; Kessler, H., A Comprehensive Evaluation of the Activity and Selectivity Profile of Ligands for RGD-binding Integrins. *Sci. Rep.* **2017,** *7*, 39805.
45. Liese, S.; Netz, R. R., Influence of length and flexibility of spacers on the binding affinity of divalent ligands. *Beilstein J. Org. Chem.* **2015,** *11*, 804-816.
46. Brandt, M.; Cardinale, J.; Aulsebrook, M. L.; Gasser, G.; Mindt, T. L., An Overview of PET Radiochemistry, Part 2: Radiometals. *J. Nucl. Med.* **2018,** *59*, 1500-1506.
47. Evans, B. J.; King, A. T.; Katsifis, A.; Matesic, L.; Jamie, J. F., Methods to Enhance the Metabolic Stability of Peptide-Based PET Radiopharmaceuticals. *Molecules* **2020,** *25*, 2314.

48. Fani, M.; Maecke, H. R.; Okarvi, S. M., Radiolabeled Peptides: Valuable Tools for the Detection and Treatment of Cancer. *Theranostics* **2012,** *2*, 481-501.
49. Schottelius, M.; Wester, H.-J., Molecular imaging targeting peptide receptors. *Methods* **2009,** *48*, 161-177.
50. Lee, S.; Xie, J.; Chen, X., Peptide-Based Probes for Targeted Molecular Imaging. *Biochem.* **2010,** *49*, 1364-1376.
51. Mankoff, D. A.; Link Jm Fau - Linden, H. M.; Linden Hm Fau - Sundararajan, L.; Sundararajan L Fau - Krohn, K. A.; Krohn, K. A., Tumor receptor imaging. *J. Nucl. Med.* **2008,** *49*, 149S–163S.
52. Reubi, J. C., Peptide Receptors as Molecular Targets for Cancer Diagnosis and Therapy. *Endocr. Rev.* **2003,** *24*, 389-427.
53. Merrifield, R. B., Solid Phase Peptide Synthesis. I. The Synthesis of a Tetrapeptide. *J. Am. Chem. Soc.* **1963,** *85*, 2149-2154.
54. Reubi, J. C.; Landolt, A. M., High Density of Somatostatin Receptors in Pituitary Tumors from Acromegalic Patients. *J. Clin. Endocrin. Met.* **1984,** *59*, 1148-1151.
55. Krenning, E. P.; Breeman, W. A. P.; Kooij, P. P. M.; Lameris, J. S.; Bakker, W. H.; Koper, J. W.; Ausema, L.; Reubi, J. C.; Lamberts, S. W. J., Localization of endocrine-related tumours with radioiodinated analogues of somatostatin. *The Lancet* **1989,** *333*, 242-244.
56. deGruyter, J. N.; Malins, L. R.; Baran, P. S., Residue-Specific Peptide Modification: A Chemist's Guide. *Biochem.* **2017,** *56*, 3863-3873.
57. Veronese, F. M., Peptide and protein PEGylation: a review of problems and solutions. *Biomaterials* **2001,** *22*, 405-417.
58. Kumarasinghe, I. R.; Hruby, V. J., Modification of Peptides to Limit Metabolism. In *Pept. Chem. Drug Des.* **2015**, 247-270.
59. Wallace, R. J., Acetylation of peptides inhibits their degradation by rumen micro-organisms. *Br. J. Nutr.* **1992,** *68*, 365-372.
60. Arnesen, T., Towards a Functional Understanding of Protein N-Terminal Acetylation. *PLoS Biol.* **2011,** *9*, e1001074.
61. Kim, K.-H.; Seong, B. L., Peptide amidation: Production of peptide hormonesin vivo andin vitro. *Biotechnol. Bioprocess Eng.* **2001,** *6*, 244-251.
62. Myung, J.; Kim, K. B.; Crews, C. M., The ubiquitin-proteasome pathway and proteasome inhibitors. *Med. Res. Rev.* **2001,** *21*, 245-273.
63. Wilk, S.; Orlowski, M., Evidence that pituitary cation-sensitive neutral endopeptidase is a multicatalytic protease complex. *J. Neurochem.* **1983,** *40*, 842-849.
64. Jackson, I. M.; Scott, P. J. H.; Thompson, S., Clinical Applications of Radiolabeled Peptides for PET. *Semin. Nucl. Med.* **2017,** *47*, 493-523.
65. Tsechelidis, I.; Vrachimis, A., PSMA PET in Imaging Prostate Cancer. *Front. Oncol.* **2022,** *12*.
66. Haubner, R.; Weber, W. A.; Beer, A. J.; Vabuliene, E.; Reim, D.; Sarbia, M.; Becker, K.-F.; Goebel, M.; Hein, R.; Wester, H.-J.; Kessler, H.; Schwaiger, M., Noninvasive Visualization of the Activated αvβ3 Integrin in Cancer Patients by Positron Emission Tomography and [18F]Galacto-RGD. *PLOS Medicine* **2005,** *2*, e70.

67. Demmer, O.; Gourni, E.; Schumacher, U.; Kessler, H.; Wester, H. J., PET imaging of CXCR4 receptors in cancer by a new optimized ligand. *Chem. Med. Chem.* **2011,** *6*, 1789-1791.
68. Herrmann, K.; Schottelius, M.; Lapa, C.; Osl, T.; Poschenrieder, A.; Hänscheid, H.; Lückerath, K.; Schreder, M.; Bluemel, C.; Knott, M.; Keller, U.; Schirbel, A.; Samnick, S.; Lassmann, M.; Kropf, S.; Buck, A. K.; Einsele, H.; Wester, H. J.; Knop, S., First-in-Human Experience of CXCR4-Directed Endoradiotherapy with 177Lu- and 90Y-Labeled Pentixather in Advanced-Stage Multiple Myeloma with Extensive Intra- and Extramedullary Disease. *J. Nucl. Med.* **2016,** *57*, 248-251.
69. Kircher, M.; Herhaus, P.; Schottelius, M.; Buck, A. K.; Werner, R. A.; Wester, H.-J.; Keller, U.; Lapa, C., CXCR4-directed theranostics in oncology and inflammation. *Ann. Nucl. Med.* **2018,** *32*, 503-511.
70. Maurer, S.; Herhaus, P.; Lippenmeyer, R.; Hänscheid, H.; Kircher, M.; Schirbel, A.; Maurer, H. C.; Buck, A. K.; Wester, H.-J.; Einsele, H.; Grigoleit, G.-U.; Keller, U.; Lapa, C., Side effects of CXC-chemokine receptor 4 – directed Endoradiotherapy with Pentixather prior to Hematopoietic Stem Cell Transplantation. *J. Nucl. Med.* **2019**, *60*, 1399-1405.
71. Larimer, B. M.; Wehrenberg-Klee, E.; Dubois, F.; Mehta, A.; Kalomeris, T.; Flaherty, K.; Boland, G.; Mahmood, U., Granzyme B PET Imaging as a Predictive Biomarker of Immunotherapy Response. *Cancer Res.* **2017,** *77*, 2318-2327.
72. Decazes, P.; Bohn, P., Immunotherapy by Immune Checkpoint Inhibitors and Nuclear Medicine Imaging: Current and Future Applications. *Cancers* **2020,** *12*.
73. Larimer, B. M.; Bloch, E.; Nesti, S.; Austin, E. E.; Wehrenberg-Klee, E.; Boland, G.; Mahmood, U., The Effectiveness of Checkpoint Inhibitor Combinations and Administration Timing Can Be Measured by Granzyme B PET Imaging. *Clin. Cancer Res.* **2019,** *25*, 1196-1205.
74. LaSalle, T.; Austin, E. E.; Rigney, G.; Wehrenberg-Klee, E.; Nesti, S.; Larimer, B.; Mahmood, U., Granzyme B PET imaging of immune-mediated tumor killing as a tool for understanding immunotherapy response. *J. Immunother. Cancer* **2020,** *8*, 1-10.
75. Capaccione, K. M.; Doubrovin, M.; Bhatt, N.; Mintz, A.; Molotkov, A., Granzyme B PET Imaging of the Innate Immune Response. *Molecules* **2020,** *25*.
76. Patrick, G. L., An introduction to medicinal chemistry. 5th ed.; *Oxfird University Press.* **2013**.
77. Chowdhury, D.; Lieberman, J., Death by a Thousand Cuts: Granzyme Pathways of Programmed Cell Death. *Annu. Rev. Immunol.* **2008,** *26*, 389-420.
78. Rotonda, J.; Garcia-Calvo, M.; Bull, H. G.; Geissler, W. M.; McKeever, B. M.; Willoughby, C. A.; Thornberry, N. A.; Becker, J. W., The three-dimensional structure of human granzyme B compared to caspase-3, key mediators of cell death with cleavage specificity for aspartic acid in P1. *Chem. Biol.* **2001,** *8*, 357-68.
79. Willoughby, C. A.; Bull, H. G.; Garcia-Calvo, M.; Jiang, J.; Chapman, K. T.; Thornberry, N. A., Discovery of potent, selective human granzyme B inhibitors

that inhibit CTL mediated apoptosis. *Bioorg. Med. Chem. Lett.* **2002,** *12*, 2197-200.
80. Garousi, J.; Orlova, A.; Frejd, F. Y.; Tolmachev, V., Imaging using radiolabelled targeted proteins: radioimmunodetection and beyond. *EJNMMI Radiopharm. Chem.* **2020,** *5*, 16.
81. Köhler, G.; Milstein, C., Continuous cultures of fused cells secreting antibody of predefined specificity. *Nature* **1975,** *256*, 495-497.
82. Vallabhajosula, S., Molecular Imaging - Radiopharmaceuticals for PET and SPECT. *Springer-Verlag Berlin Heidelberg*. **2009**; p 372.
83. Chun, J.-H.; Morse, C. L.; Chin, F. T.; Pike, V. W., No-carrier-added [18F]fluoroarenes from the radiofluorination of diaryl sulfoxides. *Chem. Commun.* **2013,** *49*, 2151-2153.
84. Hamacher, K.; Coenen, H. H.; Stöcklin, G., Efficient stereospecific synthesis of no-carrier-added 2-[18F]-fluoro-2-deoxy-D-glucose using aminopolyether supported nucleophilic substitution. *J. Nucl. Med.* **1986,** *27*, 235-238.
85. Kręcisz, P.; Czarnecka, K.; Królicki, L.; Mikiciuk-Olasik, E.; Szymański, P., Radiolabeled Peptides and Antibodies in Medicine. *Bioconjugate Chem.* **2021,** *32*, 25-42.
86. McBride, W. J.; Sharkey, R. M.; Karacay, H.; Souza, C. A.; Rossi, E. A.; Laverman, P.; Chang, C.-H.; Boerman, O. C.; Goldenberg, D. M., A Novel Method of [18F] Radiolabeling for PET. *J. Nucl. Med.* **2009,** *50*, 991.
87. McBride, W. J.; Sharkey, R. M.; Goldenberg, D. M., Radiofluorination using aluminum-fluoride (Al18F). *EJNMMI Res.* **2013,** *3*, 36.
88. Cleeren, F.; Lecina, J.; Billaud, E. M. F.; Ahamed, M.; Verbruggen, A.; Bormans, G. M., New Chelators for Low Temperature Al18F-Labeling of Biomolecules. *Bioconjugate Chem.* **2016,** *27*, 790-798.
89. Green, M.; Lowe, J.; Kadirvel, M.; McMahon, A.; Westwood, N.; Chua, S.; Brown, G., Radiosynthesis of no-carrier-added meta-[(124)I]iodobenzylguanidine for PET imaging of metastatic neuroblastoma. *J. Radioanal. Nucl. Chem.* **2017,** *311*, 727-732.
90. Schirrmacher, R.; Bradmoeller, G.; Schirrmacher, E.; Thews, O.; Tillmanns, J.; Siessmeier, T.; Bucholz, H. G.; Bartenstein, P.; Waengler, B.; Niemeyer, C. M.; Jurkschat, K., [18F]-labeling of peptides by means of an organosilicon-based fluoride acceptor. *Angew. Chem. Int. Ed.* **2006,** *45*, 6047-6050.
91. Schirrmacher, R.; Bradtmöller, G.; Schirrmacher, E.; Thews, O.; Tillmanns, J.; Siessmeier, T.; Buchholz, H. G.; Bartenstein, P.; Wängler, B.; Niemeyer, C. M.; Jurkschat, K., 18F-Labeling of Peptides by means of an Organosilicon-Based Fluoride Acceptor. *Angew. Chem., Int. Ed.* **2006,** *45*, 6047-6050.
92. Schirrmacher, E., Wängler, B., Cypryk, M., Bradtmöller, G., Schäfer, M., Eisenhut, M., Jurkschat, K., Schirrmacher, R., Synthesis of p-(Di-tert-butyl[18F]fluorosilyl)benzaldehyde ([18F]SiFA-A) with High Specific Activity by Isotopic Exchange: A Convenient Labeling Synthon for the 18F-Labeling of N-amino-oxy Derivatized Peptides. *Bioconjugate Chem.* **2007,** *18*, 2085-2089.
93. Iovkova, L.; Wängler, B.; Schirrmacher, E.; Schirrmacher, R.; Quandt, G.; Boening, G.; Schürmann, M.; Jurkschat, K., para-Functionalized Aryl-di-tert-

butylfluorosilanes as Potential Labeling Synthons for 18F Radiopharmaceuticals. *Chem.– Eur. J.* **2009,** *15*, 2140-2147.

94. Wängler, C.; Waser, B.; Alke, A.; Iovkova, L.; Buchholz, H.-G.; Niedermoser, S.; Jurkschat, K.; Fottner, C.; Bartenstein, P.; Schirrmacher, R.; Reubi, J.-C.; Wester, H.-J.; Wängler, B., One-Step [18F]-Labeling of Carbohydrate-Conjugated Octreotate-Derivatives Containing a Silicon-Fluoride-Acceptor (SiFA): In Vitro and in Vivo Evaluation as Tumor Imaging Agents for Positron Emission Tomography (PET). *Bioconj. Chem.* **2010,** *21*, 2289-2296.
95. Iovkova, L.; Könning, D.; Wängler, B.; Schirrmacher, R.; Schoof, S.; Arndt, H. D.; Jurkschat, K., SiFA-Modified Phenylalanine: A Key Compound for the Efficient Synthesis of 18F-Labelled Peptides. *Eur. J. Inorg. Chem.* **2011,** *2011*, 2238-2246.
96. Wängler, C.; Niedermoser, S.; Chin, J.; Orchowski, K.; Schirrmacher, E.; Jurkschat, K.; Iovkova-Berends, L.; Kostikov, A. P.; Schirrmacher, R.; Wängler, B., One-step [18F]-labeling of peptides for positron emission tomography imaging using the SiFA methodology. *Nat. Protoc.* **2012,** *7*, 1946.
97. Zheng, Q.; Xu, H.; Wang, H.; Du, W.-G. H.; Wang, N.; Xiong, H.; Gu, Y.; Noodleman, L.; Sharpless, K. B.; Yang, G.; Wu, P., Sulfur [18F]Fluoride Exchange Click Chemistry Enabled Ultrafast Late-Stage Radiosynthesis. *J. Am. Chem. Soc.* **2021**.
98. Gens, T. A.; Wethongton, J. A.; Brosi, A. R., The Exchange of 18F between Metallic Fluorides and Silicon Tetrafluoride. *J. Phys. Chem.* **1958,** *62*, 1593-1593.
99. Winfield, J. M., Preparation and use of 18-fluorine labelled inorganic compounds. *J. Fluorine Chem.* **1980,** *16*, 1-17.
100. Rosenthal, M. S.; Bosch, A. L.; Nickles, R. J.; Gatley, S. J., Synthesis and some characteristics of no-carrier added [18F]fluorotrimethylsilane. *Int. J. Appl. Radiat. Isot.* **1985,** *36*, 318-319.
101. Pilcher, A. S.; Ammon, H. L.; DeShong, P., Utilization of tetrabutylammonium triphenylsilyldifluoride as a fluoride source for nucleophilic fluorination. *J. Am. Chem. Soc.* **1995,** *117*, 5166-5167.
102. Ting, R.; Adam, M. J.; Ruth, T. J.; Perrin, D. M., Arylfluoroborates and alkylfluorosilicates as potential PET imaging agents: high-yielding aqueous biomolecular 18F-labeling. *J. Am. Chem. Soc.* **2005,** *127*, 13094-13095.
103. Choudhry, U.; Martin, K. E.; Biagini, S.; Blower, P. J., A49 Alkoxysilane groups for instant labelling of biomolecules with 18F. *Nucl. Med. Commun.* **2006,** *27*, 293.
104. Bernard-Gauthier, V.; Bailey, J. J.; Liu, Z.; Wängler, B.; Wängler, C.; Jurkschat, K.; Perrin, D. M.; Schirrmacher, R., From Unorthodox to Established: The Current Status of [18F]-Trifluoroborate- and 18F-SiFA-Based Radiopharmaceuticals in PET Nuclear Imaging. *Bioconjugate Chem.* **2016,** *27*, 267-279.
105. Mu, L.; Höhne, A.; Schubiger, P. A.; Ametamey, S. M.; Graham, K.; Cyr, J. E.; Dinkelborg, L.; Stellfeld, T.; Srinivasan, A.; Voigtmann, U.; Klar, U., Silicon-Based Building Blocks for One-Step [18F]-Radiolabeling of Peptides for PET Imaging. *Angew. Chem., Int. Ed.* **2008,** *47*, 4922-4925.

106. Höhne, A.; Mu, L.; Honer, M.; Schubiger, P. A.; Ametamey, S. M.; Graham, K.; Stellfeld, T.; Borkowski, S.; Berndorff, D.; Klar, U.; Voigtmann, U.; Cyr, J. E.; Friebe, M.; Dinkelborg, L.; Srinivasan, A., Synthesis, [18F]-Labeling, and in Vitro and in Vivo Studies of Bombesin Peptides Modified with Silicon-Based Building Blocks. *Bioconjugate Chem.* **2008,** *19*, 1871-1879.
107. Höhne, A.; Yu, L.; Mu, L.; Reiher, M.; Voigtmann, U.; Klar, U.; Graham, K.; Schubiger, P. A.; Ametamey, S. M., Organofluorosilanes as Model Compounds for [18F]Labeled Silicon-Based PET Tracers and their Hydrolytic Stability: Experimental Data and Theoretical Calculations (PET=Positron Emission Tomography). *Chem. – Eur. J.* **2009,** *15*, 3736-3743.
108. Bernard-Gauthier, V.; Wängler, C.; Schirrmacher, E.; Kostikov, A.; Jurkschat, K.; Wängler, B.; Schirrmacher, R., [18F]-labeled silicon-based fluoride acceptors: potential opportunities for novel positron emitting radiopharmaceuticals. *BioMed Res. Int.* **2014,** *2014*, 454503-454503.
109. Al-huniti, M. H.; Lu, S.; Pike, V. W.; Lepore, S. D., Enhanced nucleophilic fluorination and radiofluorination of organosilanes appended with potassium-chelating leaving groups. *J. Fluorine Chem.* **2014,** *158*, 48-52.
110. Jana, S.; Al-huniti, M. H.; Yang, B. Y.; Lu, S.; Pike, V. W.; Lepore, S. D., Crown Ether Nucleophilic Catalysts (CENCs): Agents for Enhanced Silicon Radiofluorination. *J. Org. Chem.* **2017,** *82*, 2329-2335.
111. Tietze, L. F.; Schmuck, K., SiFA Azide: A New Building Block for PET Imaging Using Click Chemistry. *Synlett* **2011,** *2011*, 1697-1700.
112. James, D.; Escudier, J.-M.; Amigues, E.; Schulz, J.; Vitry, C.; Bordenave, T.; Szlosek-Pinaud, M.; Fouquet, E., A 'click chemistry' approach to the efficient synthesis of modified nucleosides and oligonucleotides for PET imaging. *Tetrahedron Lett.* **2010,** *51*, 1230-1232.
113. Gonzalez, C.; Sanchez, A.; Collins, J.; Lisova, K.; Lee, J. T.; Michael van Dam, R.; Alejandro Barbieri, M.; Ramachandran, C.; Wnuk, S. F., The 4-N-acyl and 4-N-alkyl gemcitabine analogues with silicon-fluoride-acceptor: Application to 18F-Radiolabeling. *Eur. J. Med. Chem.* **2018,** *148*, 314-324.
114. Rugeri, B.; Audi, H.; Jewula, P.; Koudih, R.; Malacea-Kabbara, R.; Vimont, D.; Schulz, J.; Fernandez, P.; Jugé, S., Designing Silylated l-Amino Acids using a Wittig Strategy: Synthesis of Peptide Derivatives and 18F-Labelling. *Eur. J. Org. Chem.* **2017,** *2017*, 5399-5409.
115. Scroggie, K. R.; Alcock, L. J.; Matos, M. J.; Bernardes, G. J. L.; Perkins, M. V.; Chalker, J. M., A silicon-labelled amino acid suitable for late-stage fluorination and unexpected oxidative cleavage reactions in the preparation of a key intermediate in the Strecker synthesis. *Pept. Sci.* **2018,** *110*, e24069.
116. Otaru, S.; Niemikoski, H.; Sarparanta, M.; Airaksinen, A. J., Metabolism of a Bioorthogonal PET Tracer Candidate [19F/18F]SiFA-Tetrazine in Mouse Liver Microsomes: Biotransformation Pathways and Defluorination Investigated by UHPLC-HRMS. *Mol. Pharmaceutics* **2020,** *17*, 3106-3115.
117. Narayanam, M. K.; Toutov, A. A.; Murphy, J. M., Rapid One-Step [18F]-Labeling of Peptides via Heteroaromatic Silicon-Fluoride Acceptors. *Org. Lett.* **2020,** *22*, 804-808.

118. Wurzer, A.; Di Carlo, D.; Schmidt, A.; Beck, R.; Eiber, M.; Schwaiger, M.; Wester, H.-J., Radiohybrid Ligands: A Novel Tracer Concept Exemplified by 18F- or 68Ga-Labeled rhPSMA Inhibitors. *J. Nucl. Med.* **2020,** *61*, 735.
119. Schulz, J.; Vimont, D.; Bordenave, T.; James, D.; Escudier, J. M.; Allard, M.; Szlosek-Pinaud, M.; Fouquet, E., Silicon-Based Chemistry: An Original and Efficient One-Step Approach to [18F]-Nucleosides and [18F]-Oligonucleotides for PET Imaging. *Chem. - Eur. J.* **2011,** *17*, 3096-3100.
120. Joyard, Y.; Azzouz, R.; Bischoff, L.; Papamicaël, C.; Labar, D.; Bol, A.; Bol, V.; Vera, P.; Grégoire, V.; Levacher, V.; Bohn, P., Synthesis of new 18F-radiolabeled silicon-based nitroimidazole compounds. *Bioorg. Med. Chem.* **2013,** *21*, 3680-3688.
121. Tisseraud, M.; Schulz, J.; Vimont, D.; Berlande, M.; Fernandez, P.; Hermange, P.; Fouquet, E., Highly hindered 2-(aryl-di-tert-butylsilyl)-N-methyl-imidazoles: a new tool for the aqueous 19F- and 18F-fluorination of biomolecule-based structures. *Chem. Commun.* **2018,** *54*, 5098-5101.
122. Sutcliffe-Goulden, J. L.; O'Doherty, M. J.; Bansal, S. S., Solid phase synthesis of [18F]Labelled peptides for positron emission tomography. *Bioorg. Med. Chem. Lett.* **2000,** *10*, 1501-1503.
123. Sutcliffe-Goulden, J. L.; O'Doherty, M. J.; Marsden, P. K.; Hart, I. R.; Marshall, J. F.; Bansal, S. S., Rapid solid phase synthesis and biodistribution of [18F]-labelled linear peptides. *Eur. J. Nucl. Med. Mol. Imaging* **2002,** *29*, 754-759.
124. Marik, J.; Hausner, S. H.; Fix, L. A.; Gagnon, M. K. J.; Sutcliffe, J. L., Solid-Phase Synthesis of 2-[18F]Fluoropropionyl Peptides. *Bioconjugate Chem.* **2006,** *17*, 1017-1021.
125. Brown, L. J.; Bouvet, D. R.; Champion, S.; Gibson, A. M.; Hu, Y.; Jackson, A.; Khan, I.; Ma, N.; Millot, N.; Wadsworth, H.; Brown, R. C. D., A Solid-Phase Route to [18F]-Labeled Tracers, Exemplified by the Synthesis of [18F]2-Fluoro-2-deoxy-D-glucose. *Angew. Chem. Int. Ed.* **2007,** *46*, 941-944.
126. Steffann, M.; Tisseraud, M.; Bluet, G.; Roy, S.; Aubert, C.; Fouquet, E.; Hermange, P., Last-step [18F]-fluorination of supported 2-(aryl-di-tert-butylsilyl)-N-methyl-imidazole conjugates for applications in positron emission tomography. *Chem. Commun.* **2022,** *58*, 9140-9143.
127. Thornberry, N. A.; Rano, T. A.; Peterson, E. P.; Rasper, D. M.; Timkey, T.; Garcia-Calvo, M.; Houtzager, V. M.; Nordstrom, P. A.; Roy, S.; Vaillancourt, J. P.; Chapman, K. T.; Nicholson, D. W., A Combinatorial Approach Defines Specificities of Members of the Caspase Family and Granzyme B: Functional relationships established for key mediators of apoptosis*. *J. Bio. Chem.* **1997,** *272*, 17907-17911.
128. Cullen , S. P.; Adrain , C.; Lüthi , A. U.; Duriez , P. J.; Martin , S. J., Human and murine granzyme B exhibit divergent substrate preferences. *J. Cell Biol.* **2007,** *176*, 435-444.
129. Casciola-Rosen, L.; Garcia-Calvo, M.; Bull, H.; Becker, J.; Hines, T.; Thornberry, N.; Rosen, A., Mouse and Human Granzyme B Have Distinct Tetrapeptide Specificities and Abilities to Recruit the Bid Pathway. *J. Biol. Chem.* **2007,** *282*, 4545-52.

130. Tak, P. P.; Spaeny-Dekking, L.; Kraan, M. C.; Breedveld, F. C.; Froelich, C. J.; Hack, C. E., The levels of soluble granzyme A and B are elevated in plasma and synovial fluid of patients with rheumatoid arthritis (RA). *Clin. Exp. Immunol.* **1999,** *116*, 366-70.
131. Boivin, W. A.; Cooper, D. M.; Hiebert, P. R.; Granville, D. J., Intracellular versus extracellular granzyme B in immunity and disease: challenging the dogma. *Lab Invest.* **2009,** *89*, 1195-220.
132. Kalla, R.; Adams, A. T.; Bergemalm, D.; Vatn, S.; Kennedy, N. A.; Ricanek, P.; Lindstrom, J.; Ocklind, A.; Hjelm, F.; Ventham, N. T.; Ho, G. T.; Petren, C.; Repsilber, D.; Söderholm, J.; Pierik, M.; D'Amato, M.; Gomollón, F.; Olbjorn, C.; Jahnsen, J.; Vatn, M. H.; Halfvarson, J.; Satsangi, J., Serum proteomic profiling at diagnosis predicts clinical course, and need for intensification of treatment in inflammatory bowel disease. *J. Crohns Colitis* **2021,** *15*, 699-708.
133. Napier, T. S.; Hunter, C. L.; Song, P. N.; Larimer, B. M.; Sorace, A. G., Preclinical PET Imaging of Granzyme B Shows Promotion of Immunological Response Following Combination Paclitaxel and Immune Checkpoint Inhibition in Triple Negative Breast Cancer. *Pharmaceutics* **2022**, *14*.
134. Konishi, M.; Erdem, S. S.; Weissleder, R.; Lichtman, A. H.; McCarthy, J. R.; Libby, P., Imaging Granzyme B Activity Assesses Immune-Mediated Myocarditis. *Circ. Res.* **2015,** *117*, 502-512.
135. Janiszewski, T.; Kołt, S.; Kaiserman, D.; Snipas, S. J.; Li, S.; Kulbacka, J.; Saczko, J.; Bovenschen, N.; Salvesen, G.; Drąg, M.; Bird, P. I.; Kasperkiewicz, P., Noninvasive optical detection of granzyme B from natural killer cells with enzyme-activated fluorogenic probes. *J. Biol. Chem.* **2020,** *295*, 9567-9582.
136. Scott, J. I.; Gutkin, S.; Green, O.; Thompson, E. J.; Kitamura, T.; Shabat, D.; Vendrell, M., A Functional Chemiluminescent Probe for in Vivo Imaging of Natural Killer Cell Activity Against Tumours. *Angew. Chem. Int. Ed.* **2021,** *60*, 5699-5703.
137. Scott, J. I.; Mendive-Tapia, L.; Gordon, D.; Barth, N. D.; Thompson, E. J.; Cheng, Z.; Taggart, D.; Kitamura, T.; Bravo-Blas, A.; Roberts, E. W.; Juarez-Jimenez, J.; Michel, J.; Piet, B.; de Vries, I. J.; Verdoes, M.; Dawson, J.; Carragher, N. O.; Connor, R. A. O.; Akram, A. R.; Frame, M.; Serrels, A.; Vendrell, M., A fluorogenic probe for granzyme B enables in-biopsy evaluation and screening of response to anticancer immunotherapies. *Nature Commun.* **2022,** *13*, 2366.
138. Jullian, M.; Hernandez, A.; Maurras, A.; Puget, K.; Amblard, M.; Martinez, J.; Subra, G., N-terminus FITC labeling of peptides on solid support: the truth behind the spacer. *Tetrahedron Lett.* **2009,** *50*, 260-263.
139. Cai, Z.; Anderson, C. J., Chelators for copper radionuclides in positron emission tomography radiopharmaceuticals. *J. Labelled Comp. Radiopharm.* **2014,** *57*, 224-230.
140. Cooper, M. S.; Ma, M. T.; Sunassee, K.; Shaw, K. P.; Williams, J. D.; Paul, R. L.; Donnelly, P. S.; Blower, P. J., Comparison of [64Cu]-Complexing Bifunctional Chelators for Radioimmunoconjugation: Labeling Efficiency, Specific Activity, and in Vitro/in Vivo Stability. *Bioconjugate Chem.* **2012,** *23*, 1029-1039.

141. Fani, M.; Del Pozzo, L.; Abiraj, K.; Mansi, R.; Tamma, M. L.; Cescato, R.; Waser, B.; Weber, W. A.; Reubi, J. C.; Maecke, H. R., PET of Somatostatin Receptor–Positive Tumors Using [64Cu]- and [68Ga]-Somatostatin Antagonists: The Chelate Makes the Difference. *J. Nucl. Med.* **2011,** *52*, 1110.
142. Dearling, J. L.; Voss, S. D.; Dunning, P.; Snay, E.; Fahey, F.; Smith, S. V.; Huston, J. S.; Meares, C. F.; Treves, S. T.; Packard, A. B., Imaging cancer using PET--the effect of the bifunctional chelator on the biodistribution of a (64)Cu-labeled antibody. *Nucl. Med. Biol.* **2011,** *38*, 29-38.
143. Tsionou, M. I.; Knapp, C. E.; Foley, C. A.; Munteanu, C. R.; Cakebread, A.; Imberti, C.; Eykyn, T. R.; Young, J. D.; Paterson, B. M.; Blower, P. J.; Ma, M. T., Comparison of macrocyclic and acyclic chelators for gallium-68 radiolabelling. *RSC Adv.* **2017,** *7*, 49586-49599.
144. Ghosh, S. C.; Pinkston, K. L.; Robinson, H.; Harvey, B. R.; Wilganowski, N.; Gore, K.; Sevick-Muraca, E. M.; Azhdarinia, A., Comparison of DOTA and NODAGA as chelators for [64Cu]-labeled immunoconjugates. *Nucl. Med. Biol.* **2015,** *42*, 177-83.
145. Woo, J.-T.; Sigeizumi, S.; Yamaguchi, K.; Sugimoto, K.; Kobori, T.; Tsuji, T.; Kondo, K., Peptidyl aldehyde derivatives as potent and selective inhibitors of cathepsin L. *Bioorg. Med. Chem. Lett.* **1995,** *5*, 1501-1504.
146. Guichard, G.; Briand, J. P.; Friede, M., Synthesis of arginine aldehydes for the preparation of pseudopeptides. *Pept. Res.* **1993,** *6*, 121-4.
147. Fehrentz, J.-A.; Paris, M.; Heitz, A.; Velek, J.; Liu, C.-F.; Winternitz, F.; Martinez, J., Improved solid phase synthesis of C-terminal peptide aldehydes. *Tetrahedron Lett.* **1995,** *36*, 7871-7874.
148. McConnell, R. M.; York, J. L.; Frizzell, D.; Ezell, C., Inhibition studies of some serine and thiol proteinases by new leupeptin analogs. *J. Med. Chem.* **1993,** *36*, 1084-1089.
149. Chapman, K. T., Synthesis of a potent, reversible inhibitor of interleukin-1β converting enzyme. *Bioorg. Med. Chem. Lett.* **1992,** *2*, 613-618.
150. Murphy, A. M.; Dagnino, R., Jr.; Vallar, P. L.; Trippe, A. J.; Sherman, S. L.; Lumpkin, R. H.; Tamura, S. Y.; Webb, T. R., Automated synthesis of peptide C-terminal aldehydes. *J. Am. Chem. Soc.* **1992,** *114*, 3156-3157.
151. Pothion, C.; Paris, M.; Heitz, A.; Rocheblave, L.; Rouch, F.; Fehrentz, J.-A.; Martinez, J., Use of ozonolysis in the synthesis of C-terminal peptide aldehydes on solid support. *Tetrahedron Lett.* **1997,** *38*, 7749-7752.
152. Guillaumie, F.; Kappel, J. C.; Kelly, N. M.; Barany, G.; Jensen, K. J., Solid-phase synthesis of C-terminal peptide aldehydes from amino acetals anchored to a backbone amide linker (BAL) handle. *Tetrahedron Lett.* **2000,** *41*, 6131-6135.
153. Kappel, J. C.; Barany, G., Backbone amide linker (BAL) strategy for Nα-9-fluorenylmethoxycarbonyl (Fmoc) solid-phase synthesis of peptide aldehydes. *J. Pept. Sci.* **2005,** *11*, 525-535.
154. Huisgen, R., 1,3-Dipolar Cycloadditions. Past and Future. *Angew. Chem. Int. Ed. Eng.* **1963,** *2*, 565-598.

155. Rostovtsev, V. V.; Green, L. G.; Fokin, V. V.; Sharpless, K. B., A Stepwise Huisgen Cycloaddition Process: Copper(I)-Catalyzed Regioselective "Ligation" of Azides and Terminal Alkynes. *Angew. Chem. Int. Ed.* **2002,** *41*, 2596-2599.
156. Colvin, E. W., Silicon reagents in organic synthesis. *Academic Press.* **1988**.
157. Mirza-Aghayan, M.; Boukherroub, R.; Bolourtchian, M., Palladium-catalyzed protection of alcohols and cleavage of triethylsilyl ethers. *J. Organomet. Chem.* **2005,** *690*, 2372-2375.
158. Nishiyama, Y.; Xu, S.; Hanatani, Y.; Tsuda, S.; Umeda, R., Rhenium complex-catalyzed deoxygenation and silylation of alcohols with hydrosilane. *Tetrahedron Lett.* **2022,** *99*, 153839.
159. Chouthaiwale, P. V.; Rawat, V.; Sudalai, A., Pd-catalyzed selective hydrosilylation of aryl ketones and aldehydes. *Tetrahedron Lett.* **2012,** *53*, 148-150.
160. Purkayshtha A., B. J. B., Some aspects of palladium and rhodium catalysis for synthesis of silylethers from Si-H bond. *J. Mol. Catal. A: Chem.* **2003,** *198*, 47-55.
161. Toutov, A. A.; Betz, K. N.; Haibach, M. C.; Romine, A. M.; Grubbs, R. H., Sodium Hydroxide Catalyzed Dehydrocoupling of Alcohols with Hydrosilanes. *Org. lett.* **2016,** *18*, 5776-5779.
162. DeLucia, N. A.; Das, N.; Vannucci, A. K., Mild synthesis of silyl ethers via potassium carbonate catalyzed reactions between alcohols and hydrosilanes. *Org. Biomol. Chem.* **2018,** *16*, 3415-3418.
163. Weickgenannt, A.; Oestreich, M., Potassium tert-Butoxide-Catalyzed Dehydrogenative Si-O Coupling: Reactivity Pattern and Mechanism of an Underappreciated Alcohol Protection. *Chem. Asian J.* **2009,** *4*, 406-410.
164. Blackwell, J. M.; Foster, K. L.; Beck, V. H.; Piers, W. E., B(C6F5)3-Catalyzed Silation of Alcohols: A Mild, General Method for Synthesis of Silyl Ethers. *J. Org. Chem.* **1999,** *64*, 4887-4892.
165. Corey, E.; Venkateswarlu, A., Protection of hydroxyl groups as tert-butyldimethylsilyl derivatives. *J. Am. Chem. Soc.* **1972,** *94*, 6190-6191.
166. Ogilvie, K. K.; McGee, D. P.; Boisvert, S. M.; Hakimelahi, G. H.; Proba, Z. A., The preparation of protected arabinonucleosides. *Can. J. Chem.* **1983,** *61*, 1204-1212.
167. D'Sa, B. A.; McLeod, D.; Verkade, J. G., Nonionic Superbase-Catalyzed Silylation of Alcohols. *J. Org. Chem.* **1997,** *62*, 5057-5061.
168. Bartoszewicz, A.; Kalek, M.; Stawinski, J., Iodine-promoted silylation of alcohols with silyl chlorides. Synthetic and mechanistic studies. *Tetrahedron* **2008,** *64*, 8843-8850.
169. Porto, R. S.; Vasconcellos, M. L. A. A.; Ventura, E.; Coelho, F., Diastereoselective Epoxidation of Allylic Diols Derived from Baylis-Hillman Adducts. *Synthesis* **2005,** *2005*, 2297-2306.
170. Savela, R.; Zawartka, W.; Leino, R., Iron-Catalyzed Chlorination of Silanes. *Organometallics* **2012,** *31*, 3199-3206.
171. Naka, A.; Matsumoto, Y.; Itano, T.; Hasegawa, K.; Shimamura, T.; Ohshita, J.; Kunai, A.; Takeuchi, T.; Ishikawa, M., Nanosized starlike molecules. Synthesis

and optical properties of tris-and tetrakis [oligo (disilanylenebithienylene) dimethylsilyl] benzene. *J. Organomet. Chem.* **2009,** *694*, 346-352.
172. Pongkittiphan, V.; Theodorakis, E. A.; Chavasiri, W., Hexachloroethane: a highly efficient reagent for the synthesis of chlorosilanes from hydrosilanes. *Tetrahedron Lett.* **2009,** *50*, 5080-5082.
173. Strauss, F. J.; Cantillo, D.; Guerra, J.; Kappe, C. O., A laboratory-scale continuous flow chlorine generator for organic synthesis. *React. Chem. Eng.* **2016,** *1*, 472-476.
174. Varaprath, S.; Stutts, D. H., Utility of trichloroisocyanuric acid in the efficient chlorination of silicon hydrides. *J. Organomet. Chem.* **2007,** *692*, 1892-1897.
175. Uhlig, W., Silyl triflates–valuable synthetic materials in organosilicon chemistry. *Chem. Ber.* **1996,** *129*, 733-739.
176. Kuchar, M.; Mamat, C., Methods to Increase the Metabolic Stability of [18F]-Radiotracers. *Molecules* **2015,** *20*, 16186.
177. Ting, R.; Adam, M. J.; Ruth, T. J.; Perrin, D. M., Arylfluoroborates and Alkylfluorosilicates as Potential PET Imaging Agents: High-Yielding Aqueous Biomolecular 18F-Labeling. *J. Am. Chem. Soc.* **2005,** *127*, 13094-13095.
178. Walsh, J. C. F., L.M.; Satyamurthy, N.; Barrio, J.R.; Phelps, M.E.; Gambhir, S.S.; Toyokuni, T. , Application of silicon-fluoride chemistry for the development of amine-reactive F-18-labeling agents for biomolecules. *J. Nucl. Med.* **2000,** *41*, 249P.
179. Wängler, C.; Kostikov, A.; Zhu, J.; Chin, J.; Wängler, B.; Schirrmacher, R., Silicon-[18F]Fluorine Radiochemistry: Basics, Applications and Challenges. *Appl. Sci.* **2012,** *2*, 277-302.
180. Balentova, E.; Collet, C.; Lamandé-Langle, S.; Chrétien, F.; Thonon, D.; Aerts, J.; Lemaire, C.; Luxen, A.; Chapleur, Y., Synthesis and hydrolytic stability of novel 3-[18F]fluoroethoxybis(1-methylethyl)silyl]propanamine-based prosthetic groups. *J. Fluorine Chem.* **2011,** *132*, 250-257.
181. Niedermoser, S.; Chin, J.; Wängler, C.; Kostikov, A.; Bernard-Gauthier, V.; Vogler, N.; Soucy, J.-P.; McEwan, A. J.; Schirrmacher, R.; Wängler, B., In Vivo Evaluation of [18F]SiFAlin–Modified TATE: A Potential Challenge for [68Ga]-DOTATATE, the Clinical Gold Standard for Somatostatin Receptor Imaging with PET. *J. Nucl. Med.* **2015,** *56*, 1100-1105.
182. Ilhan, H.; Todica, A.; Lindner, S.; Boening, G.; Gosewisch, A.; Wängler, C.; Wängler, B.; Schirrmacher, R.; Bartenstein, P., First-in-human [18F]SiFAlin-TATE PET/CT for NET imaging and theranostics. *Eur. J. Nucl. Med. Mol. Imaging* **2019,** *46*, 2400-2401.
183. Ilhan, H.; Lindner, S.; Todica, A.; Cyran, C. C.; Tiling, R.; Auernhammer, C. J.; Spitzweg, C.; Boeck, S.; Unterrainer, M.; Gildehaus, F. J.; Böning, G.; Jurkschat, K.; Wängler, C.; Wängler, B.; Schirrmacher, R.; Bartenstein, P., Biodistribution and first clinical results of [18F]SiFAlin-TATE PET: a novel [18F]-labeled somatostatin analog for imaging of neuroendocrine tumors. *Eur. J. Nucl. Med. Mol. Imaging* **2020,** *47*, 870-880.
184. Wängler, C.; Beyer, L.; Bartenstein, P.; Wängler, B.; Schirrmacher, R.; Lindner, S., Favorable SSTR subtype selectivity of SiTATE: new momentum for clinical [18F]SiTATE PET. *EJNMMI Radiopharm. Chem.* **2022,** *7*.

185. Fujita, T., Iwasa, J., Hansch, C., A New Substituent Constant, π, Derived from Partition Coefficients. *J. Am. Chem. Soc.* **1964,** *86* 5175–5180.
186. Lindner, S.; Michler, C.; Leidner, S.; Rensch, C.; Wängler, C.; Schirrmacher, R.; Bartenstein, P.; Wängler, B., Synthesis and in Vitro and in Vivo Evaluation of SiFA-Tagged Bombesin and RGD Peptides as Tumor Imaging Probes for Positron Emission Tomography. *Bioconjugate Chem.* **2014,** *25*, 738-749.
187. Dialer, L. O.; Selivanova, S. V.; Müller, C. J.; Müller, A.; Stellfeld, T.; Graham, K.; Dinkelborg, L. M.; Krämer, S. D.; Schibli, R.; Reiher, M.; Ametamey, S. M., Studies toward the Development of New Silicon-Containing Building Blocks for the Direct 18F-Labeling of Peptides. *J. Med. Chem.* **2013,** *56*, 7552-7563.
188. Liu, B.; Thayumanavan, S., Substituent Effects on the pH Sensitivity of Acetals and Ketals and Their Correlation with Encapsulation Stability in Polymeric Nanogels. *J. Am. Chem. Soc.* **2017,** *139*, 2306-2317.
189. Diesen J., S., A. H., Organisk Kjemi. *Universitetsforlaget.* **2019**.
190. Bailey, W. F.; Luderer, M. R.; Jordan, K. P., Effect of Solvent on the Lithium−Bromine Exchange of Aryl Bromides: Reactions of n-Butyllithium and tert-Butyllithium with 1-Bromo-4-tert-butylbenzene at 0 °C. *J. Org. Chem.* **2006,** *71*, 2825-2828.
191. Abdelbagi, M. E. M.; Alt, H. G., Unbridged 1- and 2-substituted bis(silylindenyl) zirconium(IV) and hafnium(IV) dichloride complexes as catalyst precursors for ethylene polymerization. *Polyhedron* **2017,** *137*, 284-295.
192. Ohira, S., Methanolysis of dimethyl (1-diazo-2-oxopropyl) phosphonate: generation of dimethyl (diazomethyl) phosphonate and reaction with carbonyl compounds. *Synth. Commun.* **1989,** *19*, 561-564.
193. Pietruszka, J.; Witt, A., Synthesis of the Bestmann-Ohira Reagent. *Synthesis* **2006,** *2006*, 4266-4268.
194. Sternson, S. M.; Wong, J. C.; Grozinger, C. M.; Schreiber, S. L., Synthesis of 7200 Small Molecules Based on a Substructural Analysis of the Histone Deacetylase Inhibitors Trichostatin and Trapoxin. *Organic Lett.* **2001,** *3*, 4239-4242.
195. Chen, C. H.; Chen, W. H.; Liu, Y. H.; Lim, T. S.; Luh, T. Y., Folding of Alternating Dialkylsilylene-Spaced Donor–Acceptor Copolymers: The Oligomer Approach. *Chem. - Eur. J.* **2012,** *18*, 347-354.
196. Yu, C.; Liu, B.; Hu, L., A convenient biphasic process for the monosilylation of symmetrical 1,n-primary diols. *Tetrahedron Lett.* **2000,** *41*, 4281-4285.
197. Hansen, A. M. Studies towards a total synthesis of manzamine A. University of Glasgow2010.
198. Ohkubo, A.; Noma, Y.; Aoki, K.; Tsunoda, H.; Seio, K.; Sekine, M., Introduction of 3′-Terminal Nucleosides Having a Silyl-Type Linker into Polymer Supports without Base Protection. *J. Org. Chem.* **2009,** *74*, 2817-2823.
199. Prasad, A. B.; Kanth, J. B.; Periasamy, M., Convenient methods for the reduction of amides, nitriles, carboxylic esters, acids and hydroboration of alkenes using NaBH4/I2system. *Tetrahedron* **1992,** *48*, 4623-4628.

200. Periasamy, M.; Thirumalaikumar, M., Methods of enhancement of reactivity and selectivity of sodium borohydride for applications in organic synthesis. *J. Organomet. Chem.* **2000,** *609*, 137-151.
201. Yamakawa, T.; Masaki, M.; Nohira, H., A new reduction of some carboxylic esters with sodium borohydride and zinc chloride in the presence of a tertiary amine. *Bull. Chem. Soc. Jp.* **1991,** *64*, 2730-2734.
202. Soai, K.; Oyamada, H.; Takase, M.; Ookawa, A., Practical Procedure for the Chemoselective Reduction of Esters by Sodium Borohydride. Effect of the Slow Addition of Methanol. *Bull. Chem. Soc. Jp.* **1984,** *57*, 1948-1953.
203. Boechat, N.; da Costa, J. C. S.; de Souza Mendonça, J.; de Oliveira, P. S. M.; Vinícius Nora De Souza, M., A simple reduction of methyl aromatic esters to alcohols using sodium borohydride–methanol system. *Tetrahedron Lett.* **2004,** *45*, 6021-6022.
204. Grajewska, A.; Oestreich, M., Base-Catalyzed Dehydrogenative Si-O Coupling of Dihydrosilanes: Silylene Protection of Diols. *Synlett* **2010,** *2010*, 2482-2484.
205. Baumann, M.; Nome, L. M.; Zachariassen, Z. G.; Karlshøj, S.; Fossen, T.; Rosenkilde, M. M.; Våbenø, J.; Haug, B. E., Synthesis of a novel tripeptidomimetic scaffold and biological evaluation for CXC chemokine receptor 4 (CXCR4) antagonism. *Tetrahedron* **2017,** *73*, 3866-3877.
206. Theodorou, V.; Skobridis, K.; Tzakos, A. G.; Ragoussis, V., A simple method for the alkaline hydrolysis of esters. *Tetrahedron Lett.* **2007,** *48*, 8230-8233.
207. Harmsen, R. A. G.; Sydnes, L. K.; Törnroos, K. W.; Haug, B. E., Synthesis of trans-4-Triazolyl-Substituted 3-Hydroxypiperidines. *Synthesis* **2011,** *2011*, 749-754.
208. Gantt, R. W.; Peltier-Pain, P.; Cournoyer, W. J.; Thorson, J. S., Using simple donors to drive the equilibria of glycosyltransferase-catalyzed reactions. *Nat. Chem. Biol.* **2011,** *7*, 685-691.
209. Wu, R.; Schumm, J. S.; Pearson, D. L.; Tour, J. M., Convergent Synthetic Routes to Orthogonally Fused Conjugated Oligomers Directed toward Molecular Scale Electronic Device Applications. *J. Org. Chem.* **1996,** *61*, 6906-6921.
210. Roth, G. J.; Liepold, B.; Müller, S. G.; Bestmann, H. J., Further Improvements of the Synthesis of Alkynes from Aldehydes. *Synthesis* **2004,** *2004*, 59-62.
211. Higgs, T. C. Fluorophore and fluorescent sensor compound containing same. WO: 2010116142, *Glysure Ltd., UK.* **2010.**
212. Saitton, S.; Del Tredici, A. L.; Saxin, M.; Stenström, T.; Kihlberg, J.; Luthman, K., Synthesis and evaluation of novel pyridine based PLG tripeptidomimetics. *Org. Biomol. Chem.* **2008,** *6*, 1647-1654.
213. Dodani, S. C.; Firl, A.; Chan, J.; Nam, C. I.; Aron, A. T.; Onak, C. S.; Ramos-Torres, K. M.; Paek, J.; Webster, C. M.; Feller, M. B.; Chang, C. J., Copper is an endogenous modulator of neural circuit spontaneous activity. *Proc. Natl. Acad. Sci.* **2014,** *111*, 16280-16285.
214. Bourbeau, M. P.; Siegmund, A.; Allen, J. G.; Shu, H.; Fotsch, C.; Bartberger, M. D.; Kim, K.-W.; Komorowski, R.; Graham, M.; Busby, J.; Wang, M.; Meyer, J.; Xu, Y.; Salyers, K.; Fielden, M.; Véniant, M. M.; Gu, W., Piperazine

Oxadiazole Inhibitors of Acetyl-CoA Carboxylase. *J. Med. Chem.* **2013,** *56*, 10132-10141.

215. Sasikumar, D.; Takano, Y.; Biju, V., Photoinduced Betaine Generation for Efficient Photothermal Energy Conversion. *Chem. - Eur. J.* **2020,** *26*, 2060-2066.
216. Belloni, M.; Manickam, M.; Ashton, P. R.; Kariuki, B. M.; Preece, J. A.; Spencer, N.; Wilkie, J., The X-Ray Crystal Structures and Computational Analysis of NH…π Hydrogen Bonded Banana-Shaped Carbazole Derivatives and Thermal Analysis of Higher Mesogenic Homologues. *Mol. Cryst. Liq. Cryst. Sci. Technol., Sect. A* **2001,** *369*, 17-35.
217. Knölker, H.-J.; Foitzik, N.; Goesmann, H.; Graf, R.; Jones, P. G.; Wanzl, G., Highly Stereoselective Synthesis of Bicyclo[n.3.0]alkanes by Titanium Tetrachloride Promoted [3 + 2] Cycloaddition of Allylsilanes and 1-Acetylcycloalkenes. *Chem. - Eur. J.* **1997,** *3*, 538-551.
218. Kusukawa, T.; Ando, W., Photochemical functionalizations of C60 with phenylpolysilanes. *J. Organomet. Chem.* **1998,** *559*, 11-22.
219. Farooq, T.; Sydnes, L. K.; Törnroos, K. W.; Haug, B. E., Debenzylation of Functionalized 4- and 5-Substituted 1,2,3-Triazoles. *Synthesis* **2012,** *44*, 2070-2078.

Appendix

Table of contents

Overview of synthesized compounds (FOSi-project)

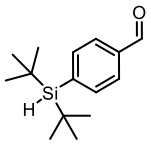

5

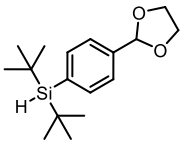

10

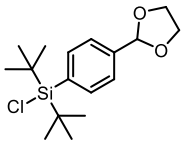

11

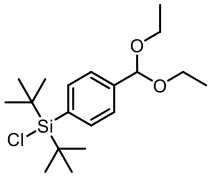

13

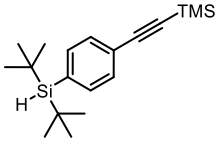

14

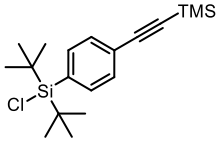

15

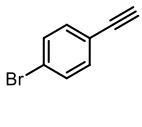

17

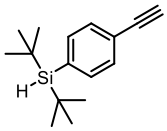

18

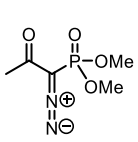

20

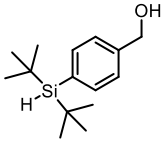

22

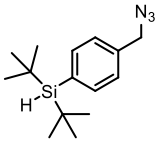

25

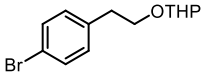

31

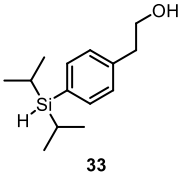

33

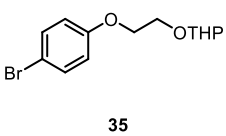

35

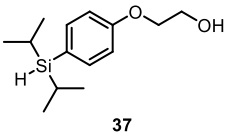

37

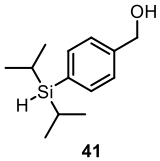

41

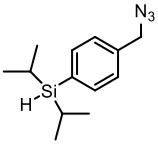

42

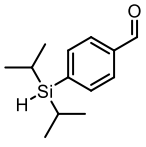

43

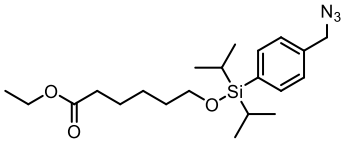

45

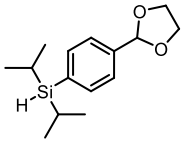

46

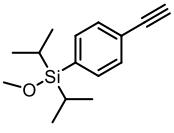

49

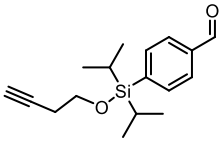

50

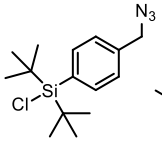

51

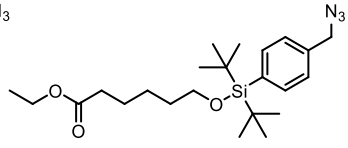

53

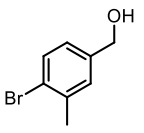

59

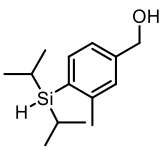

60

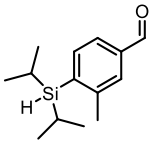

61

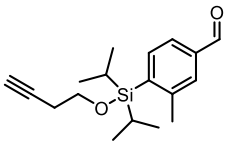

62

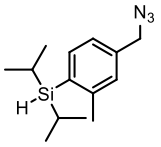

63

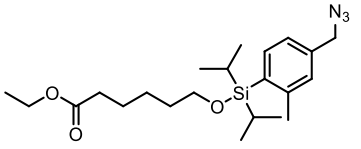

64

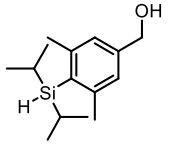

66

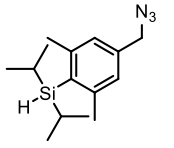

67

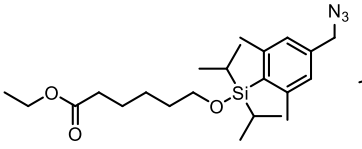

68

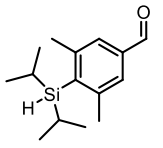

69

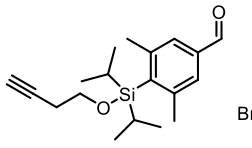

70

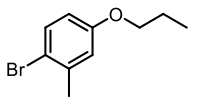

73

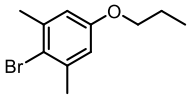

74

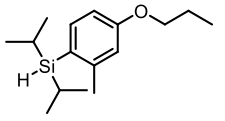

75

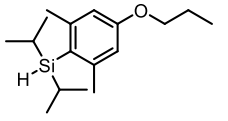

76

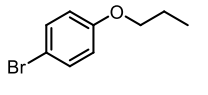

77

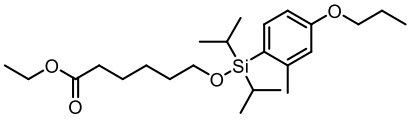

80

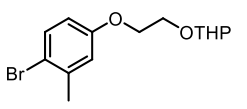

82

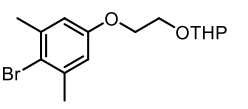

83

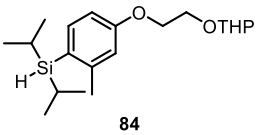

84

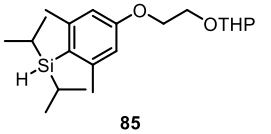

85

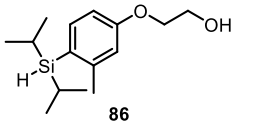

86

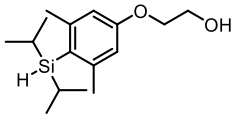

87

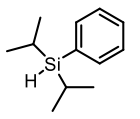

91

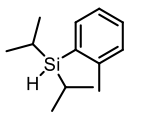

92

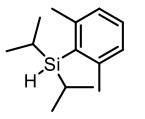

93

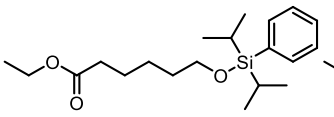

94

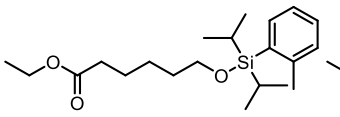

95

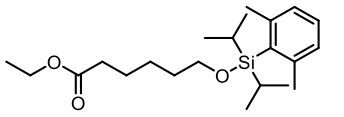

96

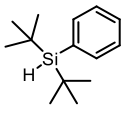

97

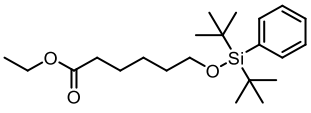

98

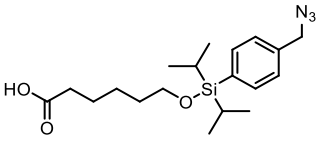

99

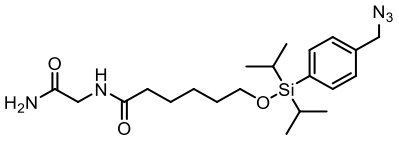

101

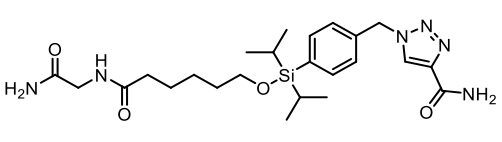

103

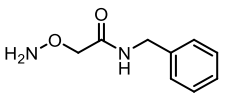

108

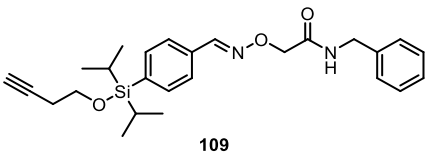

109

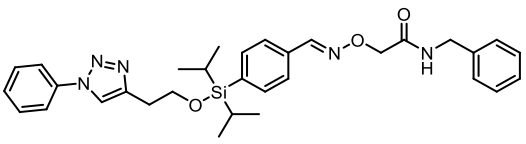

111

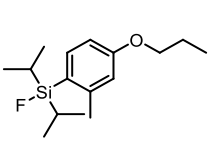

114

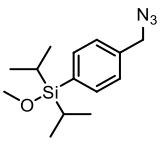

118

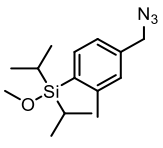

119

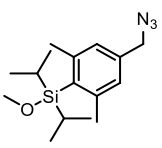

120

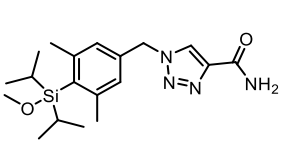

121

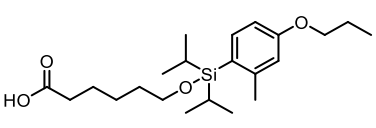

130

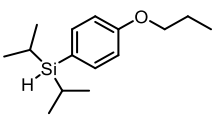

132

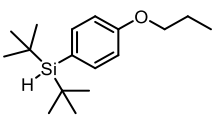

133

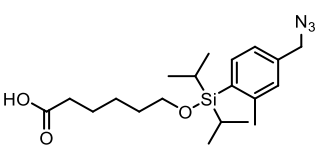

134

Spectral data

NOTA-GzmB Semi-prep HPLC

HPLC program:

Time (min)	A (%)	B (%)
0	99	1
30	80	20
33	20	80
40	99	1

Flow: 15 mL/min
Initial pressure: 81 mbar

Column**:** XBridge™ Prep C18 OBS (19 x 250 mm, 5 µm) column from Waters
Ca retention time (product): 21.0 – 22.5 min

NODAGA-GzmB Semi-prep HPLC

HPLC program:

Time (min)	A (%)	B (%)
0	99	1
5	80	20
30	50	50
33	20	80
40	99	1

Flow: 12 mL/min
Initial pressure: 97 mbar

Column: XBridge™ Prep C18 OBS (19 x 250 mm, 5 µm) column from Waters
Ca retention time (product): 11 – 12.5 min

Figure A-1. LRMS spectrum of GzmB-peptide from test cleavage

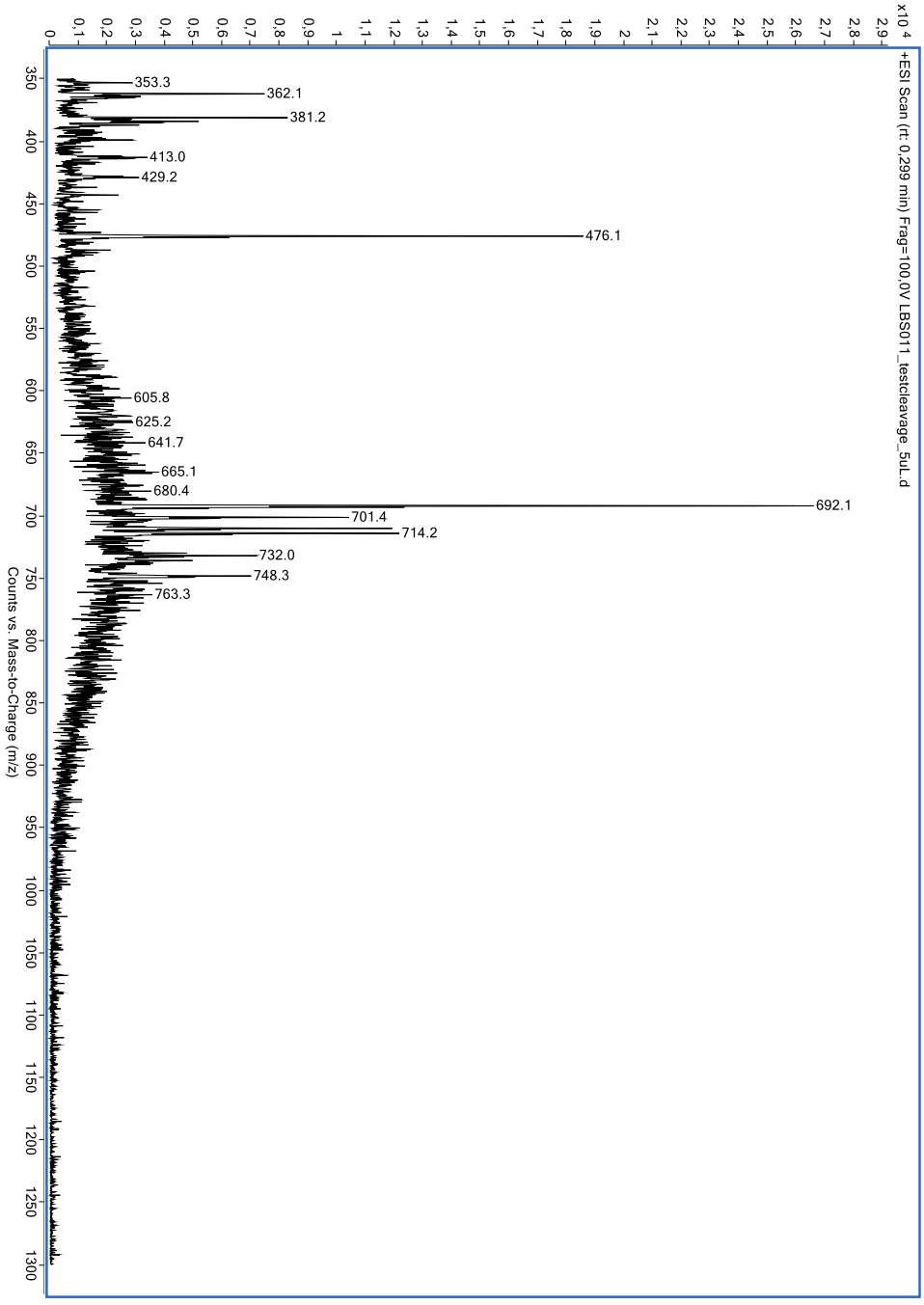

Figure A-2. HRMS spectrum of NOTA-GzmB

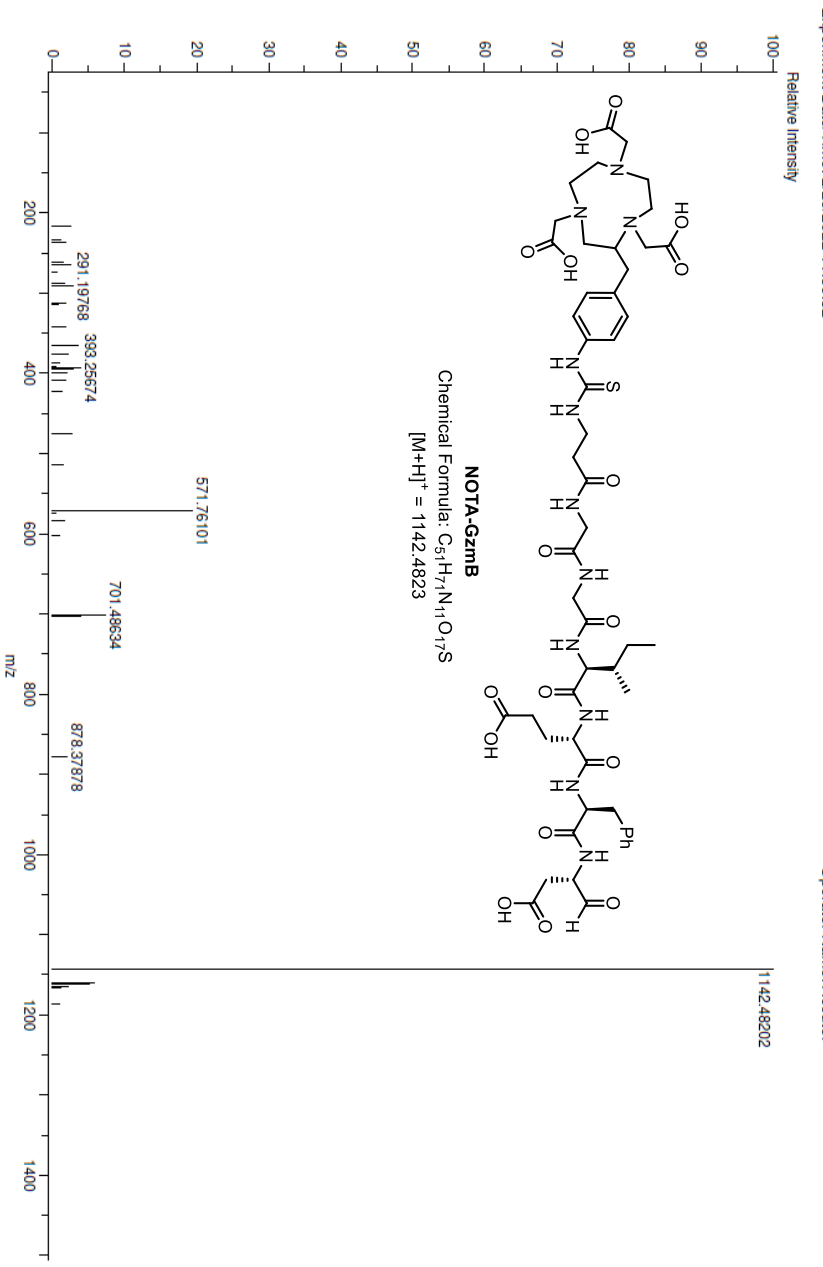

Figure A-3. Analytical HPLC of NOTA-GzmB (Run 1, Fraction 6)

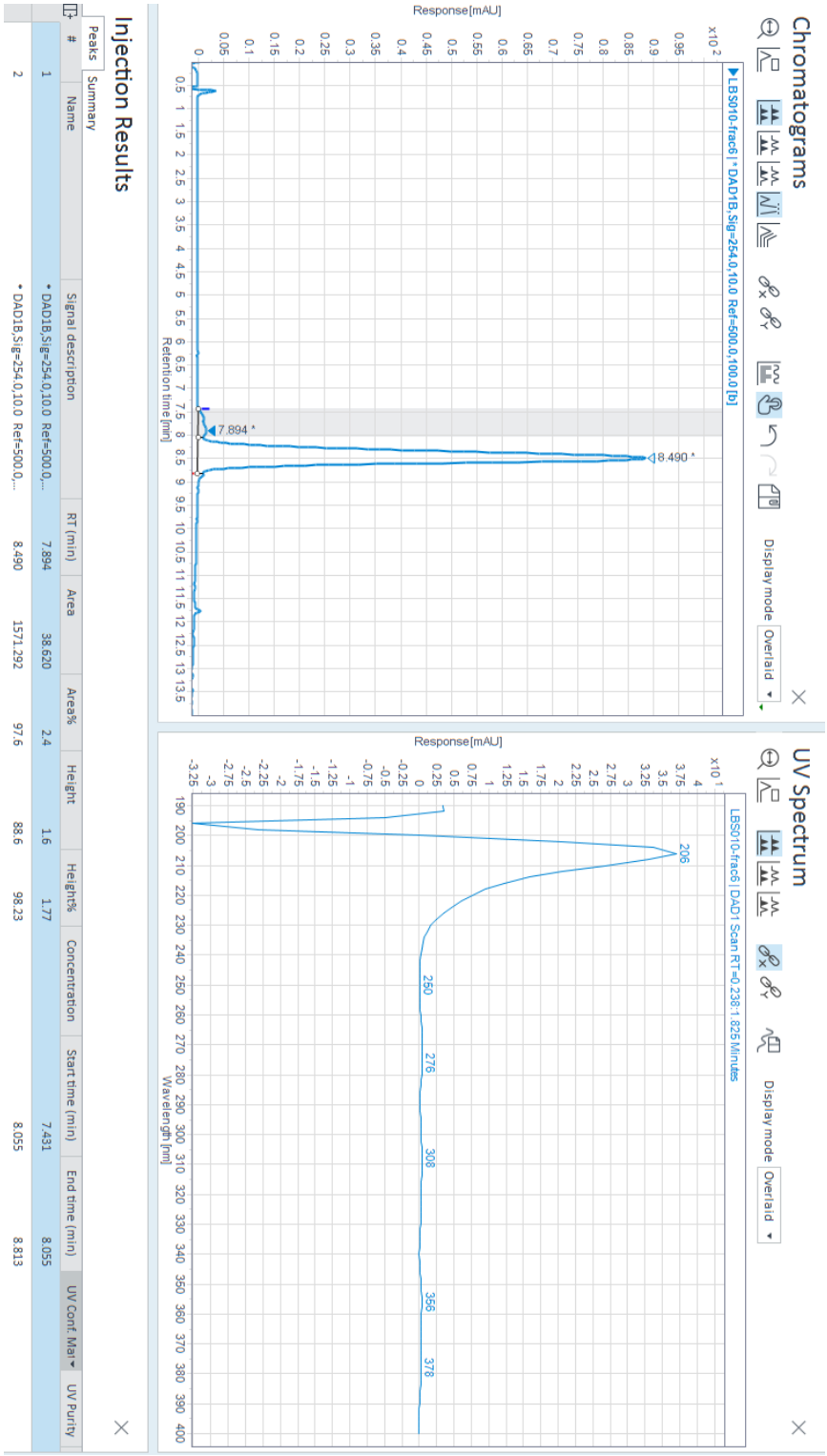

Figure A-4. LRMS spectrum of NOTA-GzmB (Run 2, Fraction 6)

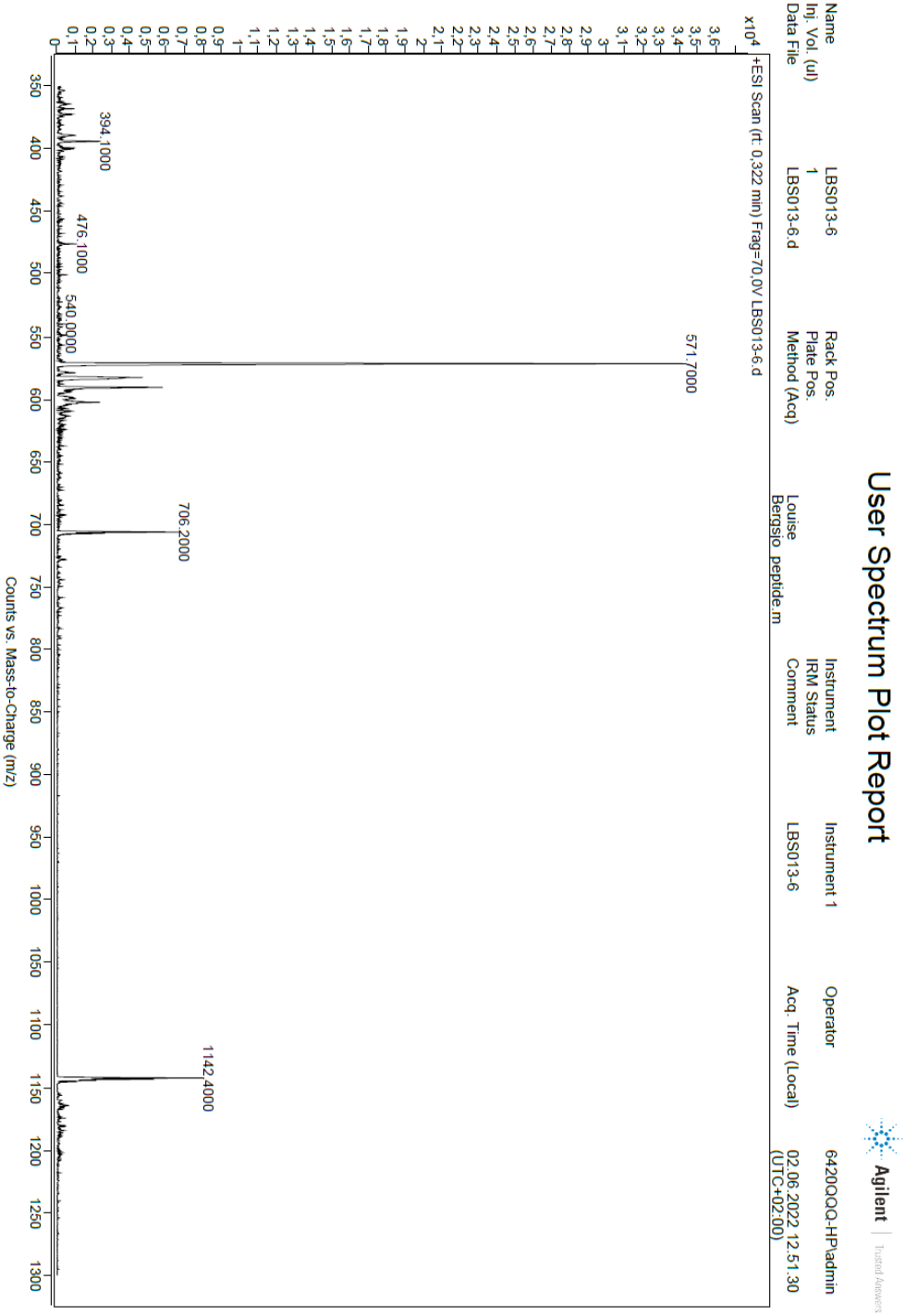

Figure A-5. Analytical HPLC of NODAGA-GzmB (Run 2, Fraction 2)

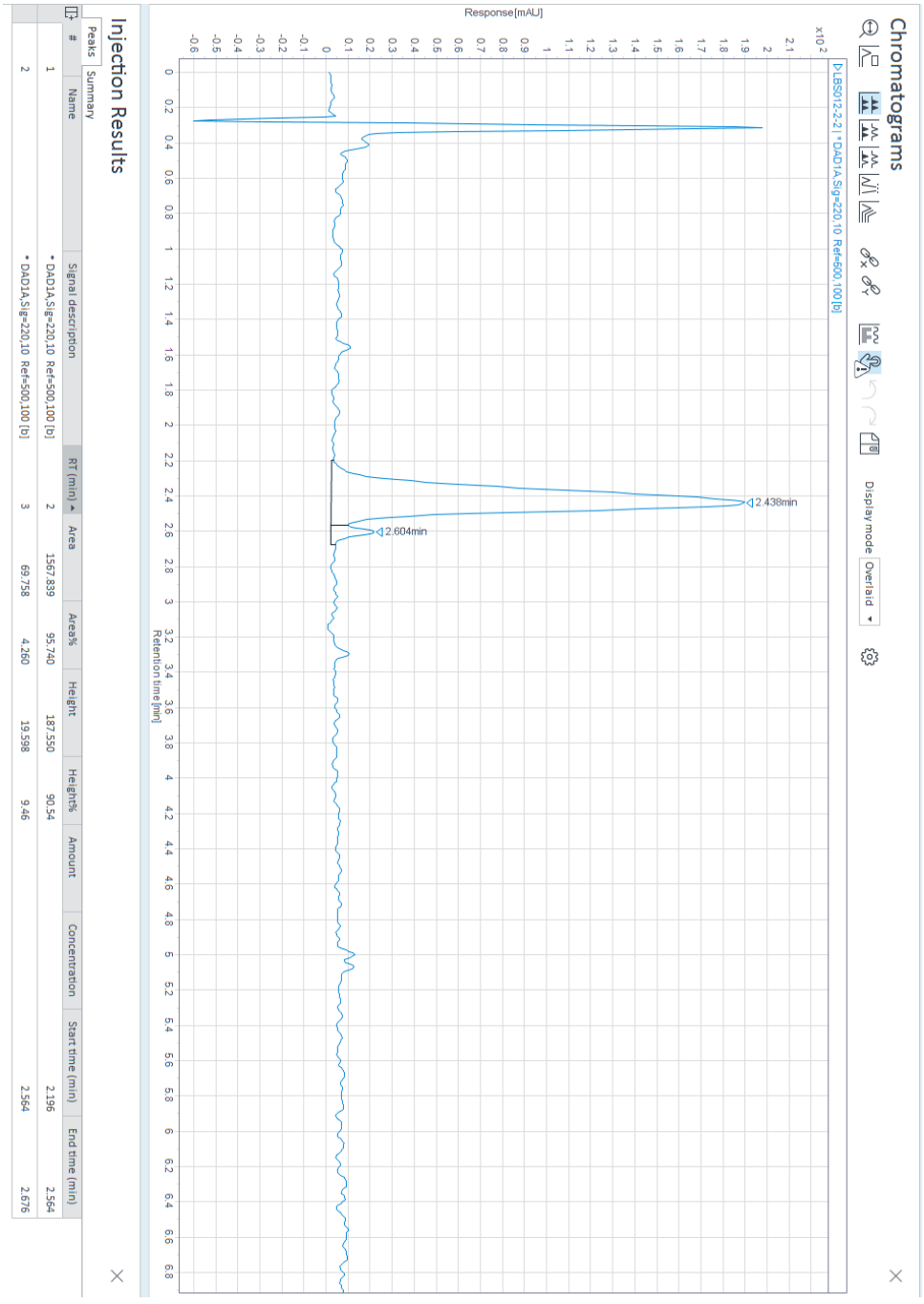

Figure A-6. LRMS spectrum of NODAGA-GzmB (Run 2, Fraction 2)

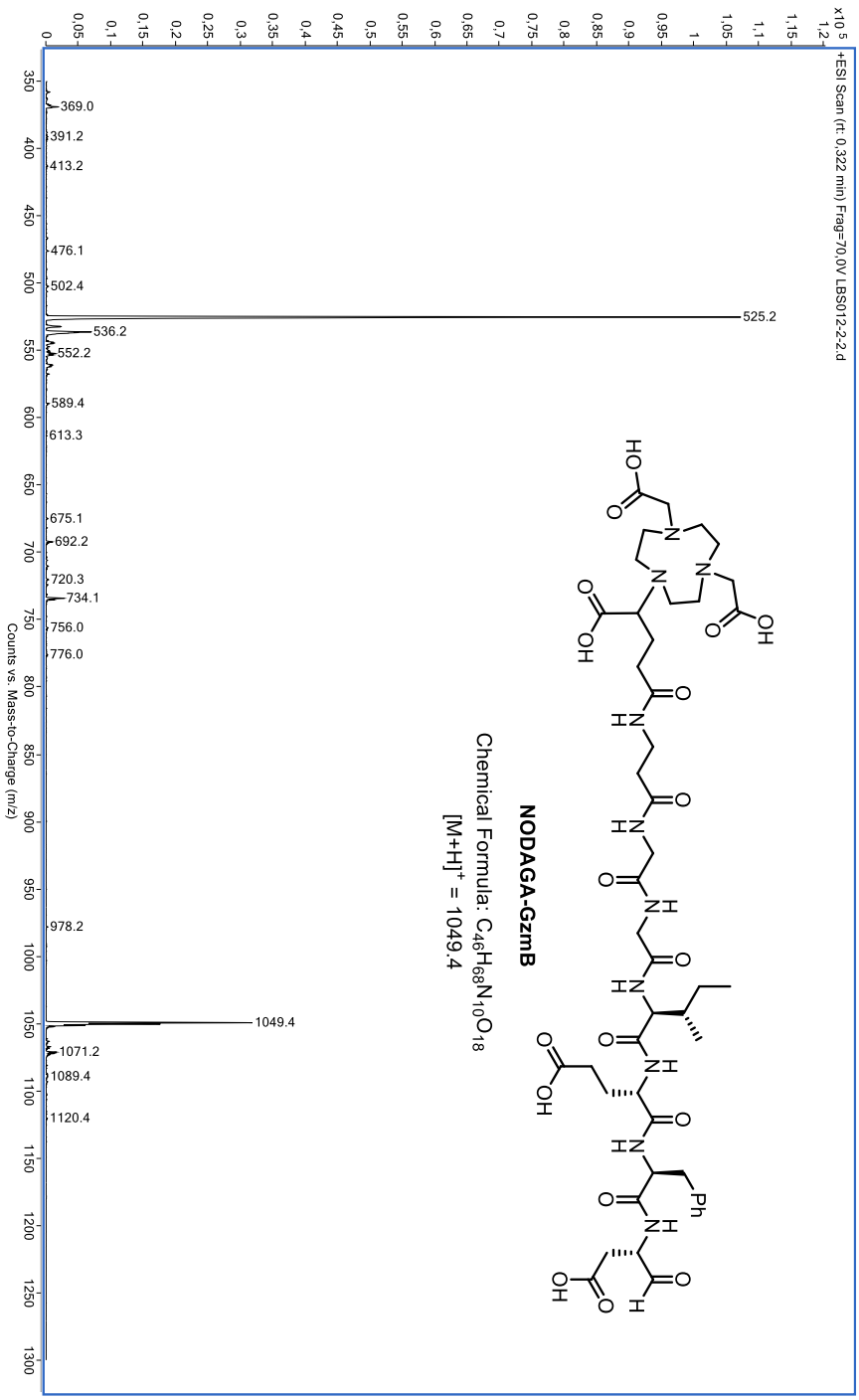

Figure A-7. Analytical HPLC of DOTA-GzmB (performed by Dr. Markus Baumann)

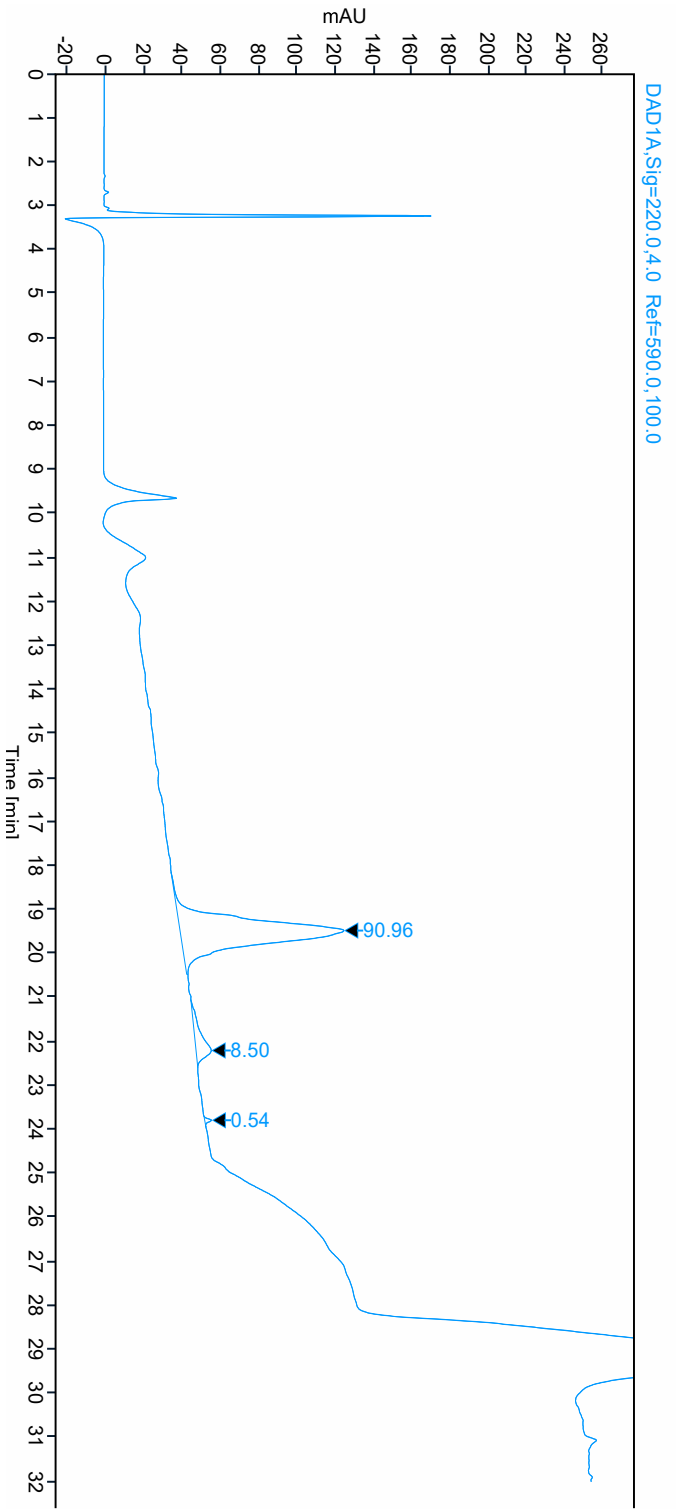

Figure A-8. LRMS Spectrum of DOTA-GzmB (performed by Dr. Markus Baumann)

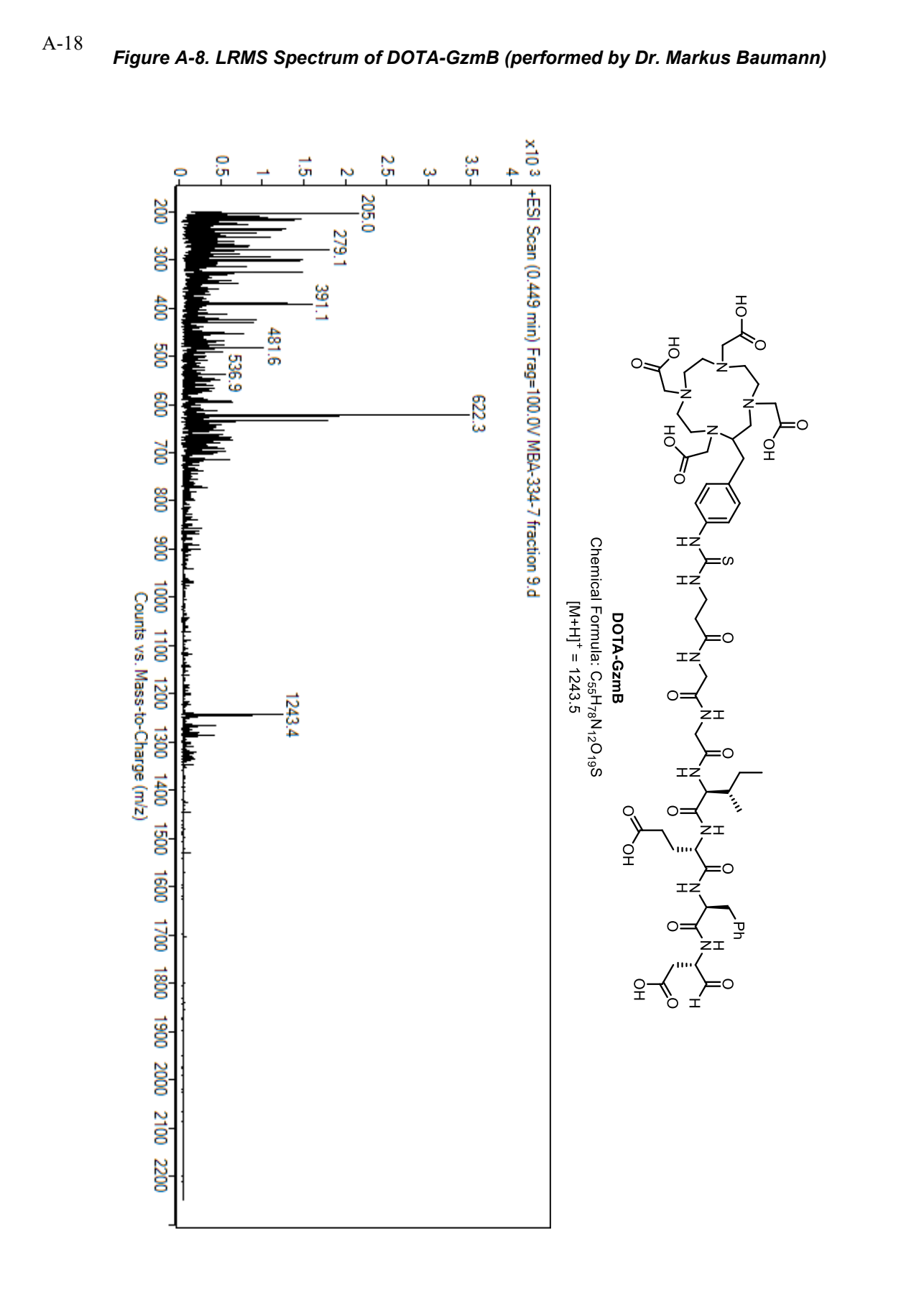

Figure A-9. ^{1}H-NMR of NODAGA-GzmB

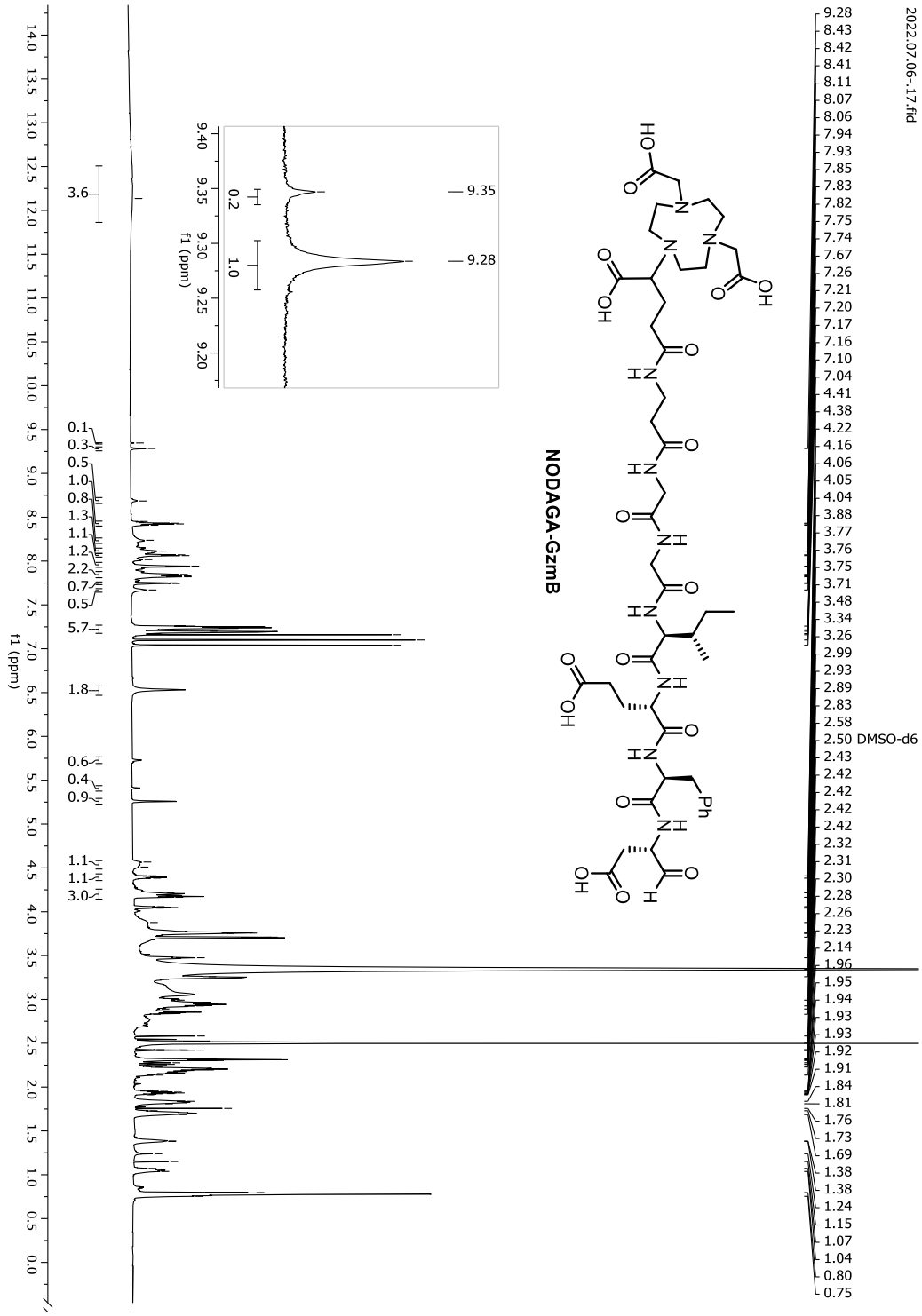

Figure A-10. ^{1}H-NMR of NOTA-GzB

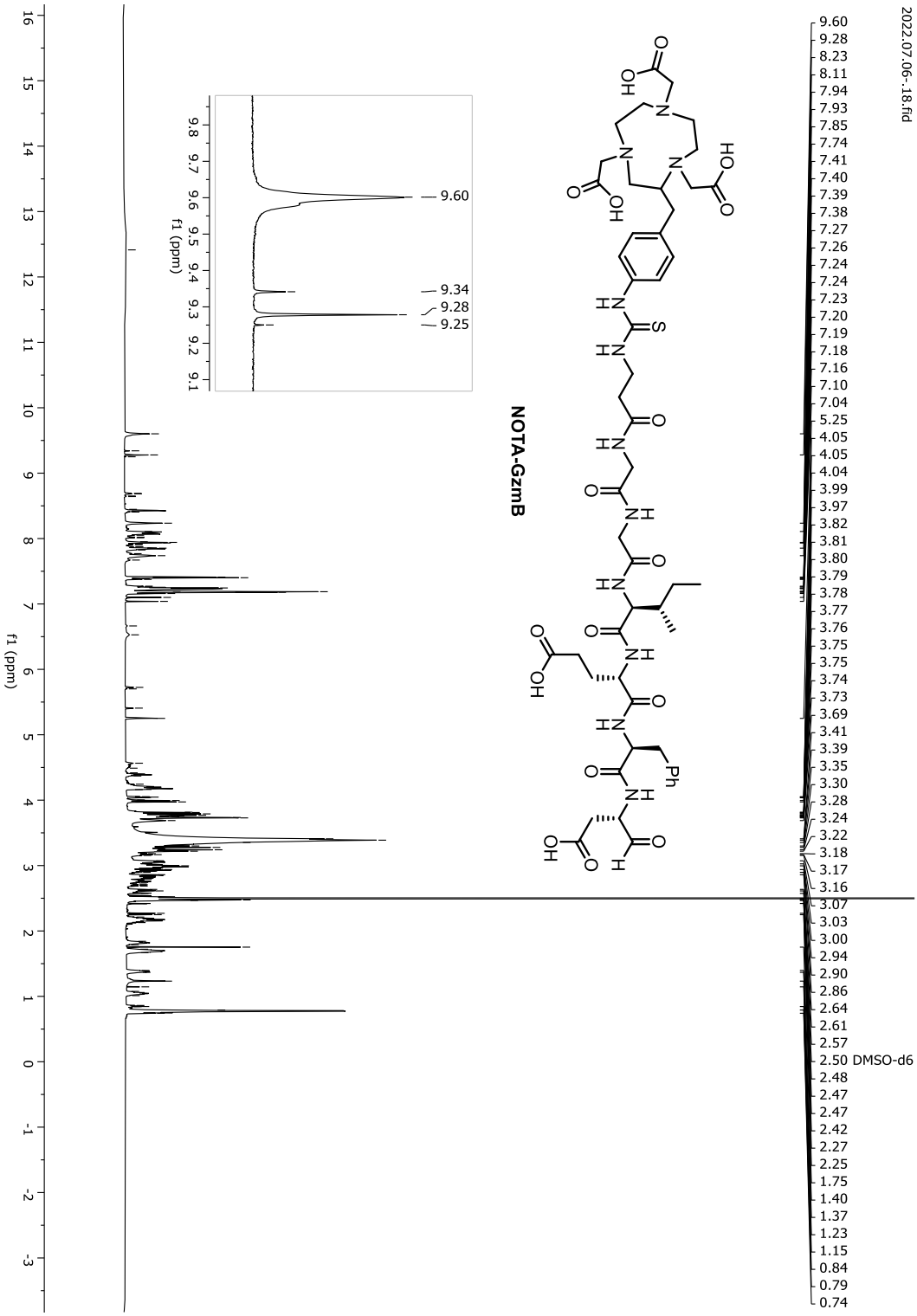

Figure A-11. ^{1}H-NMR of compound 5

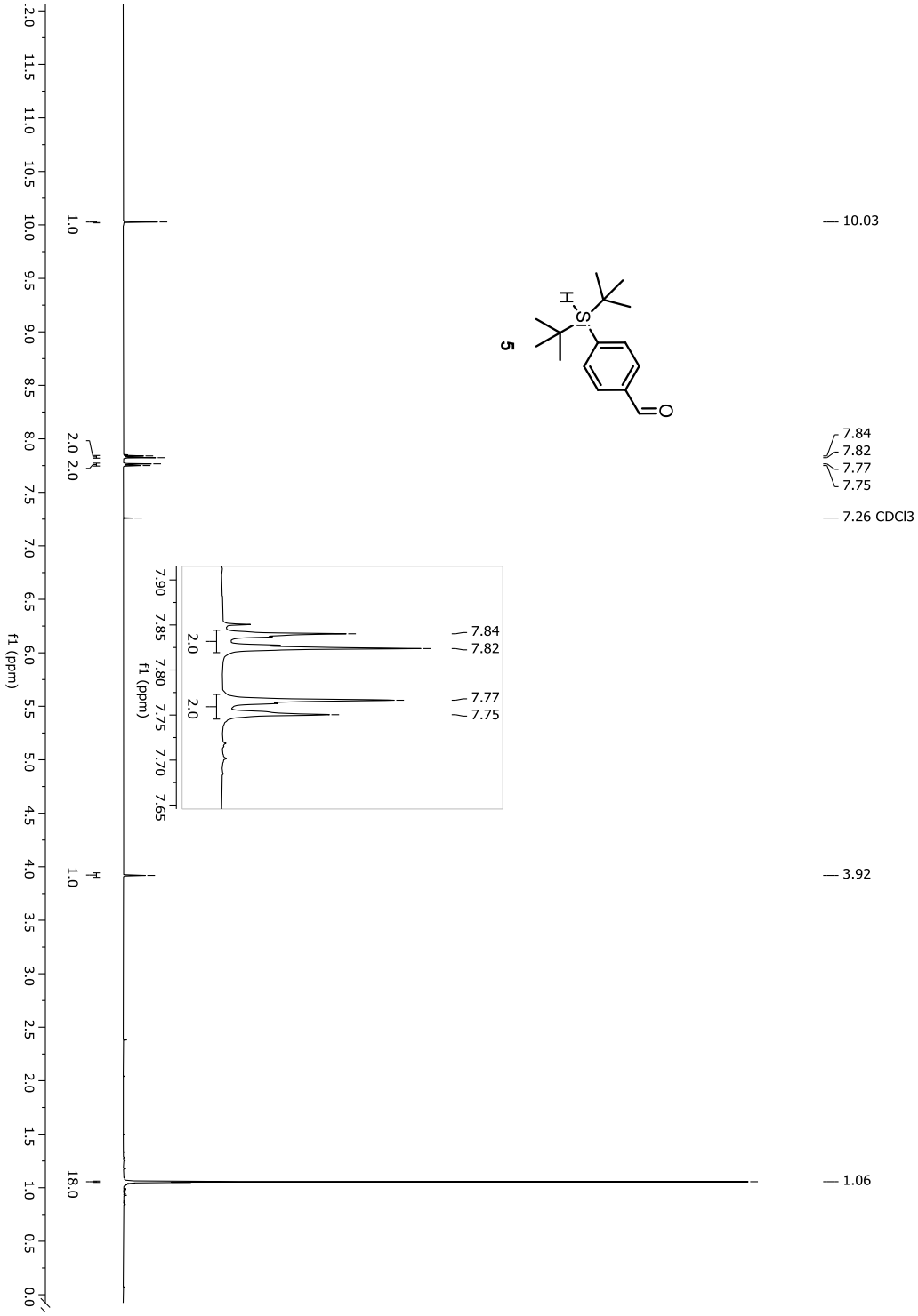

Figure A-12. ^{13}C-NMR of compound 5

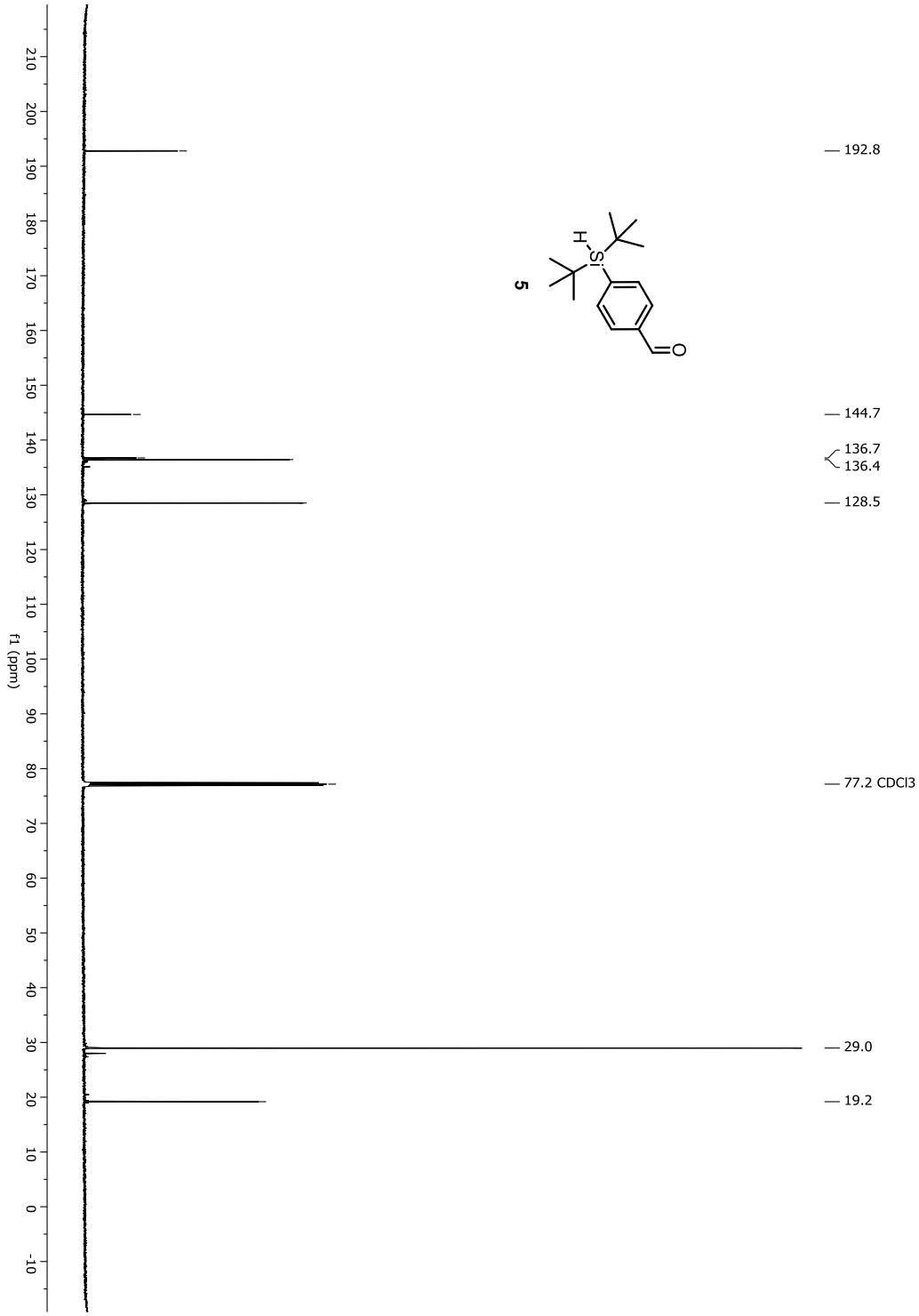

Figure A-13. ^{1}H-NMR spectrum of compound 10

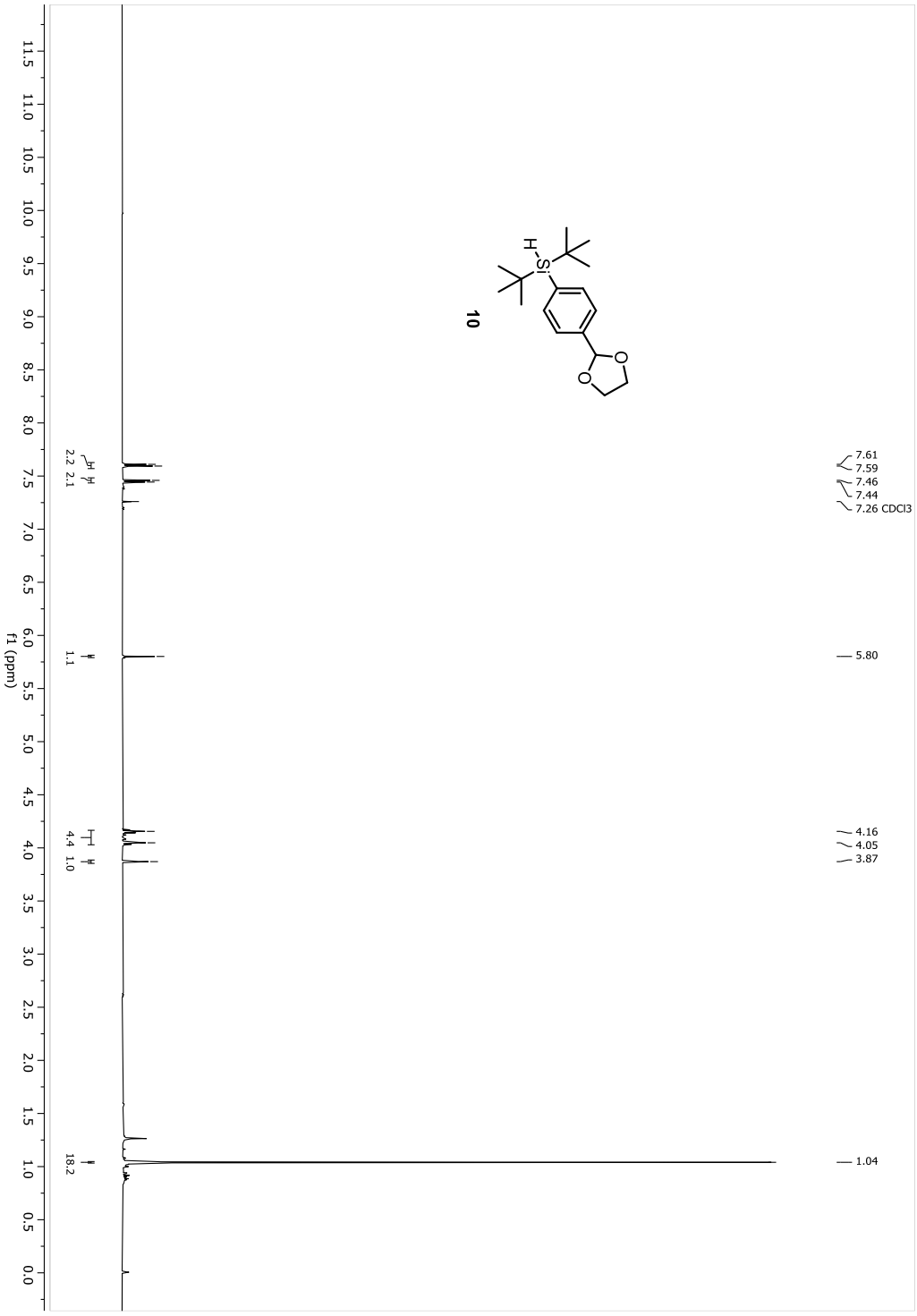

Figure A-14. ^{13}C-NMR spectrum of compound 10

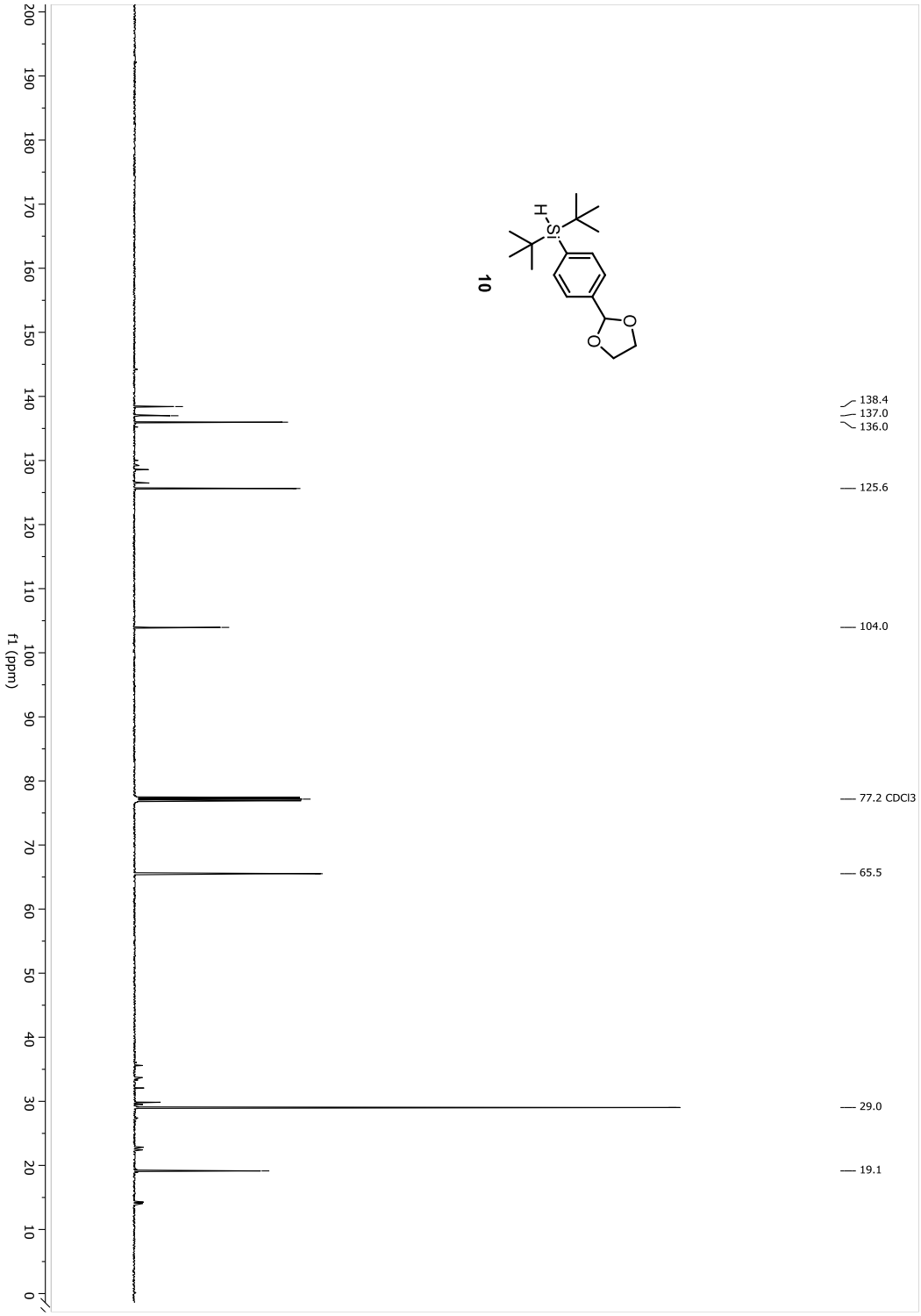

Figure A-15. ^{1}H-NMR spectrum of compound 11 (crude)

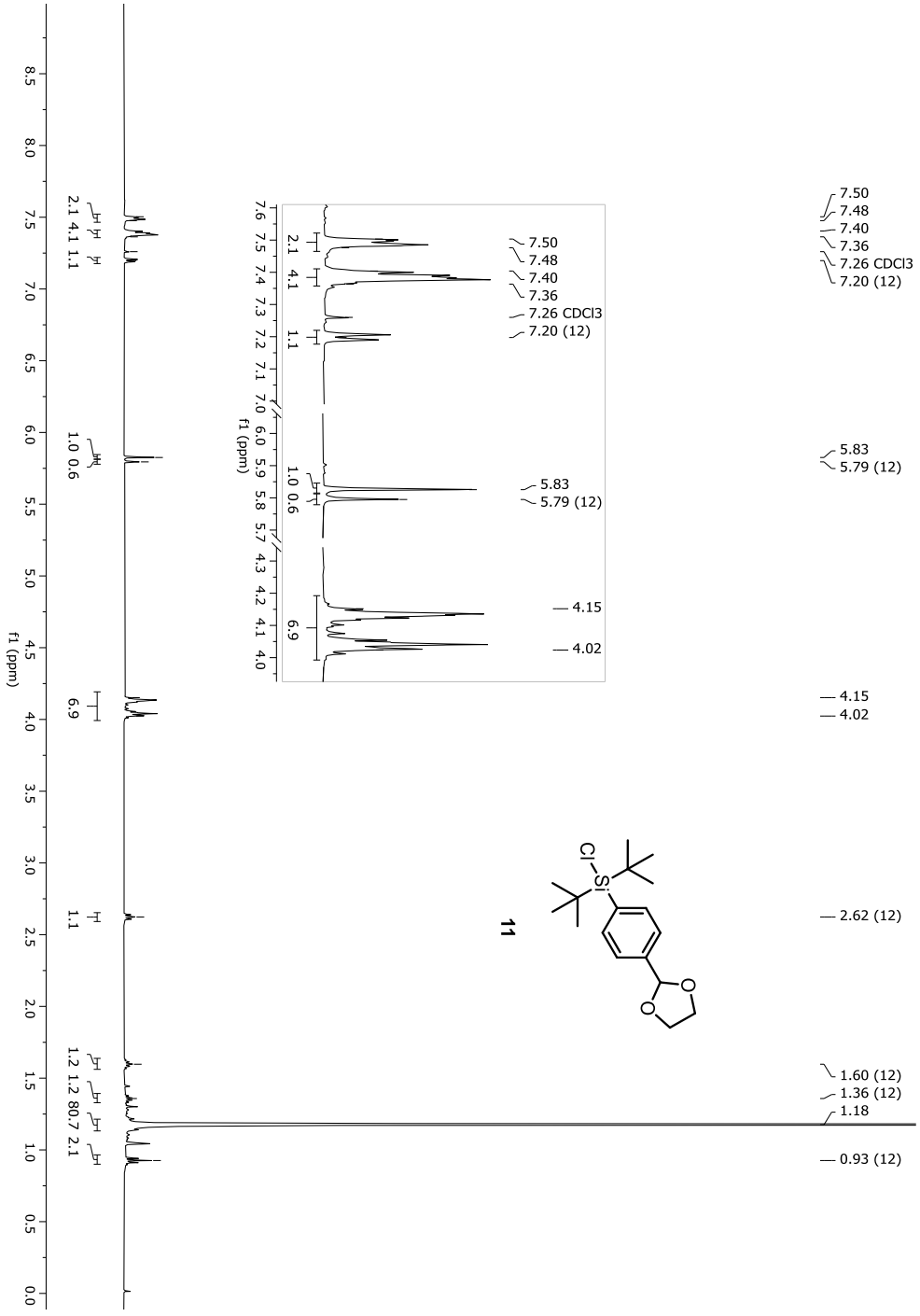

Figure A-16. ^{13}C-NMR spectrum of compound 11(crude)

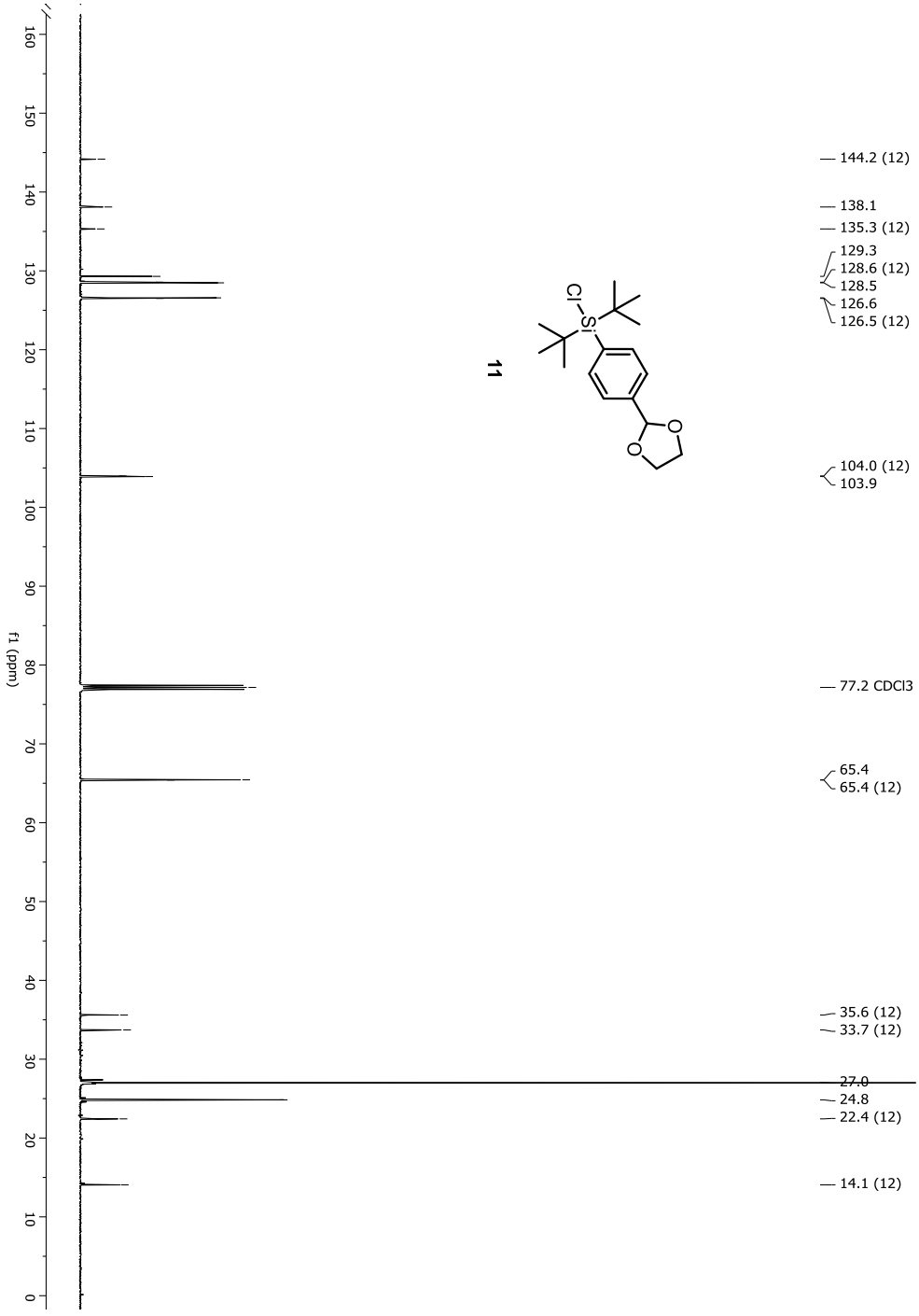

Figure A-17. ^{1}H-NMR spectrum of compound 13 (crude)

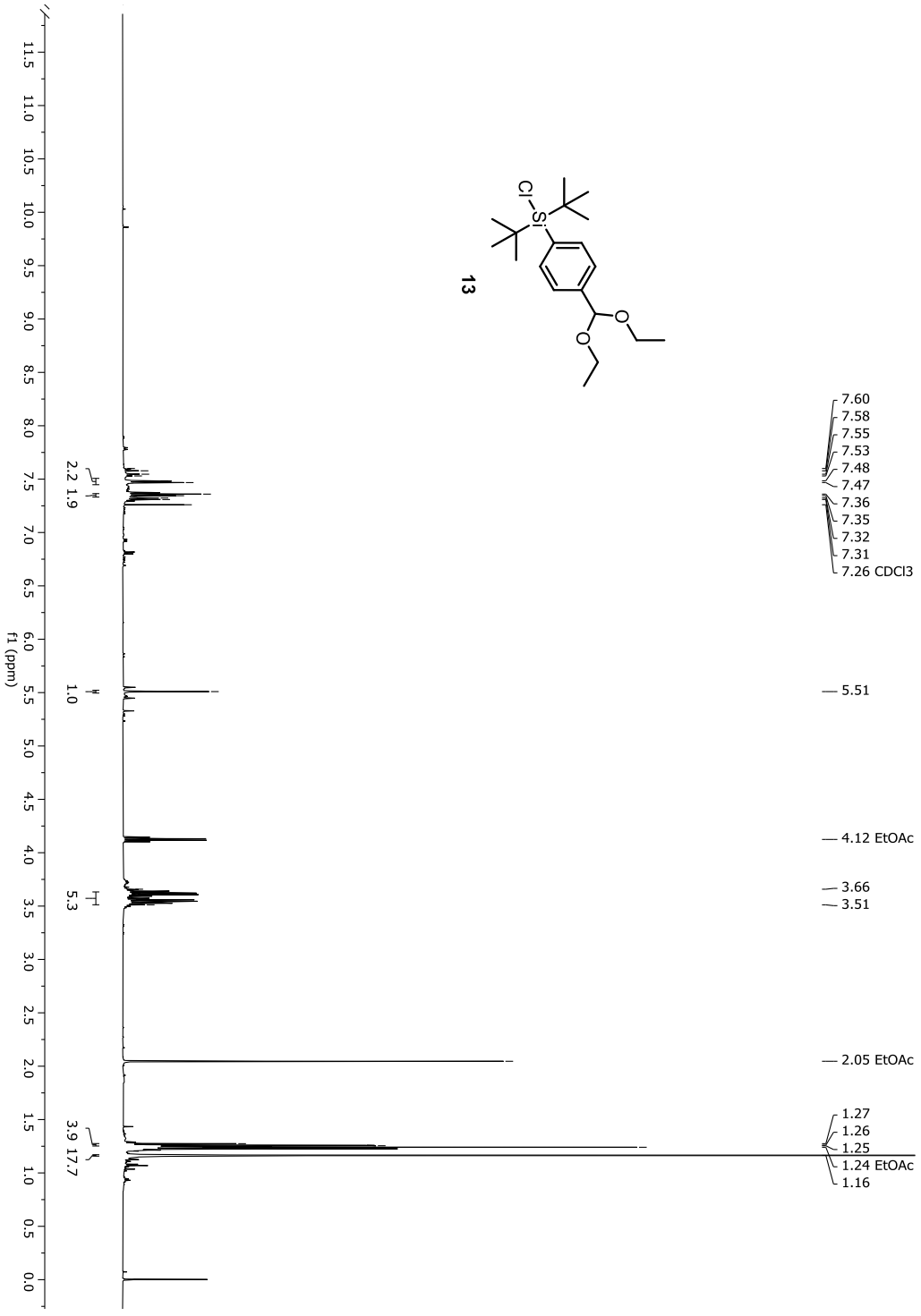

Figure A-18. ^{13}C-NMR spectrum of compound 13 (crude)

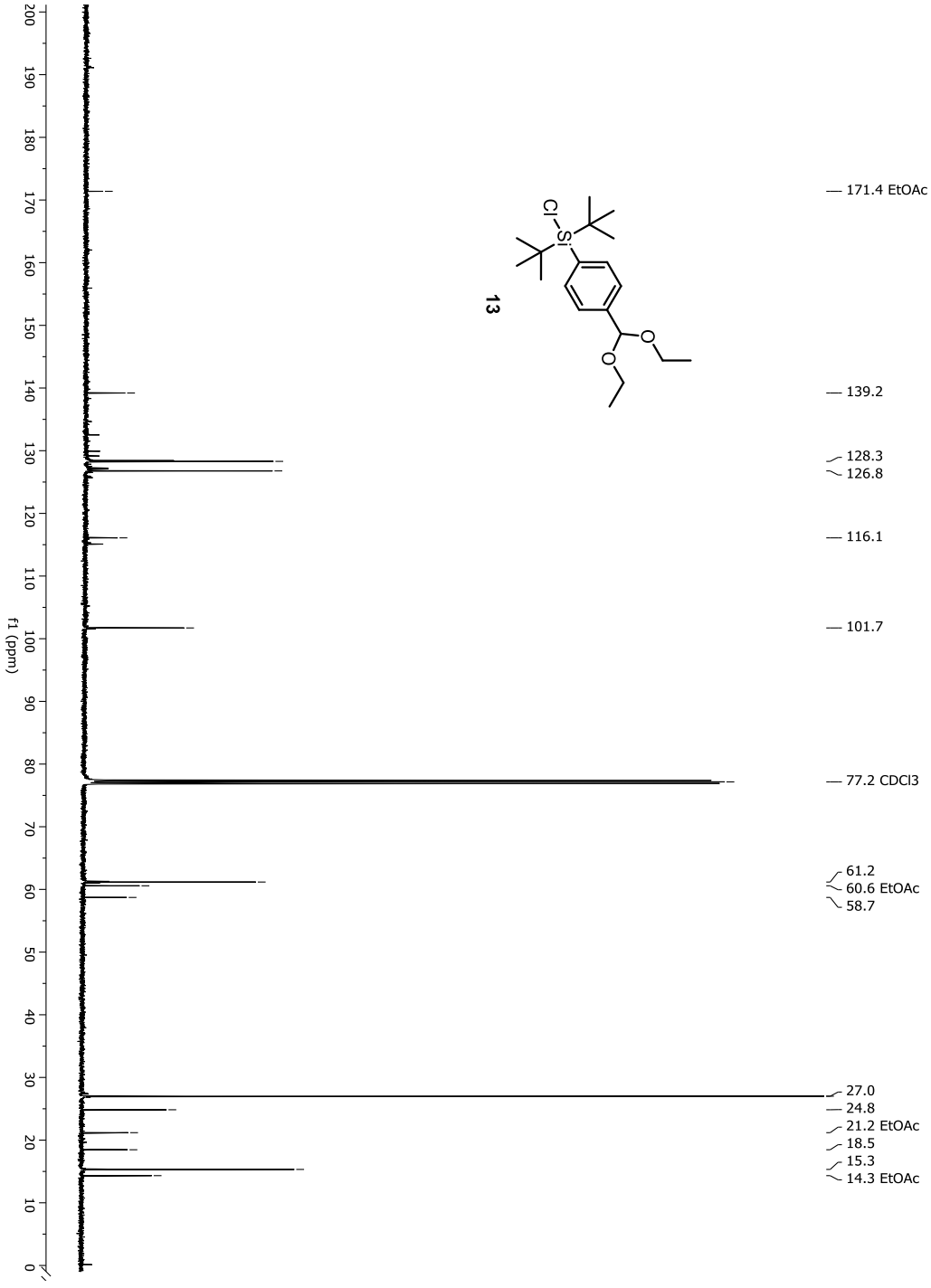

Figure A-19. ^{1}H-NMR spectrum of compound 14 (crude)

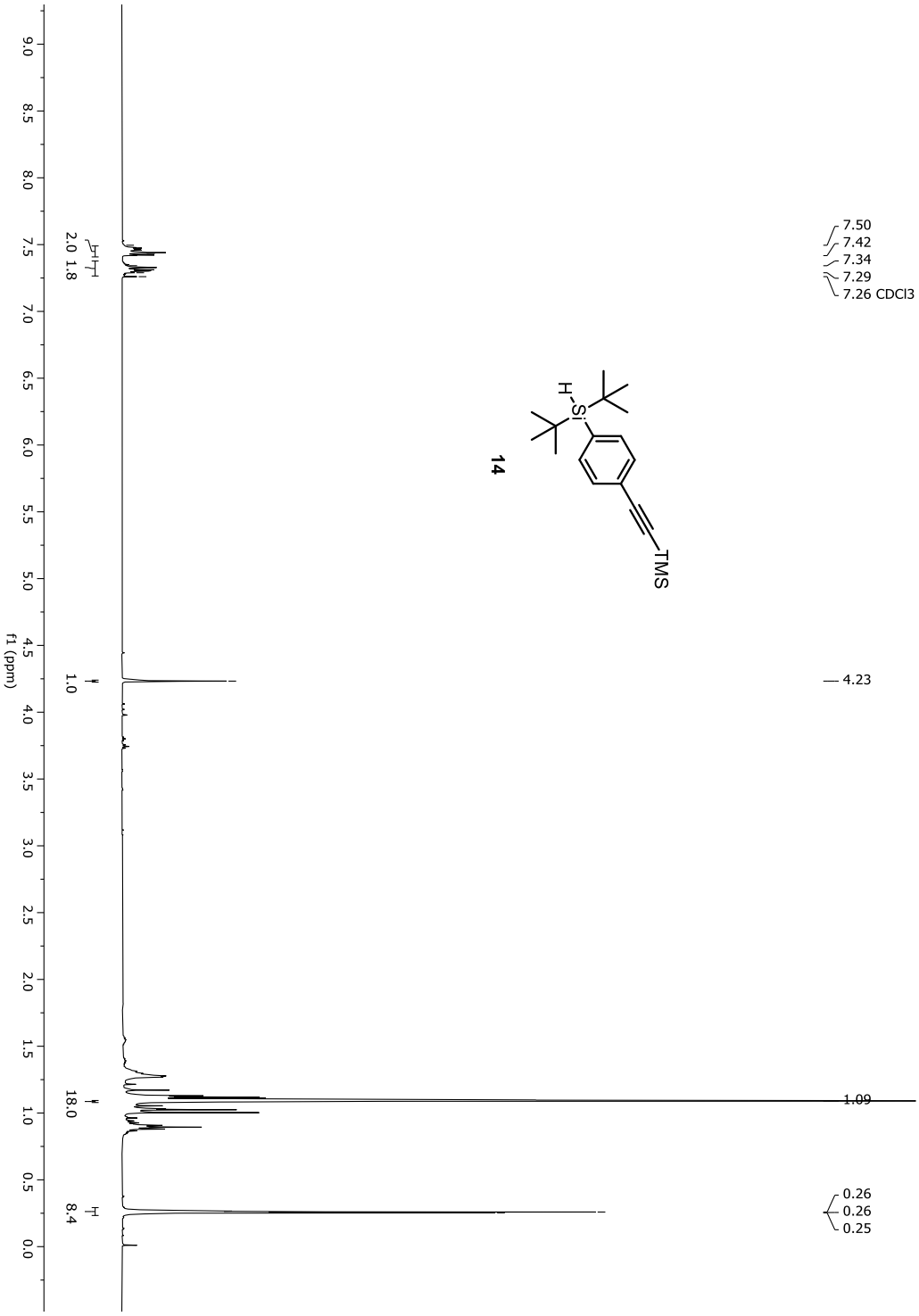

Figure A-20. ^{1}H-NMR spectrum of compound 15 (crude)

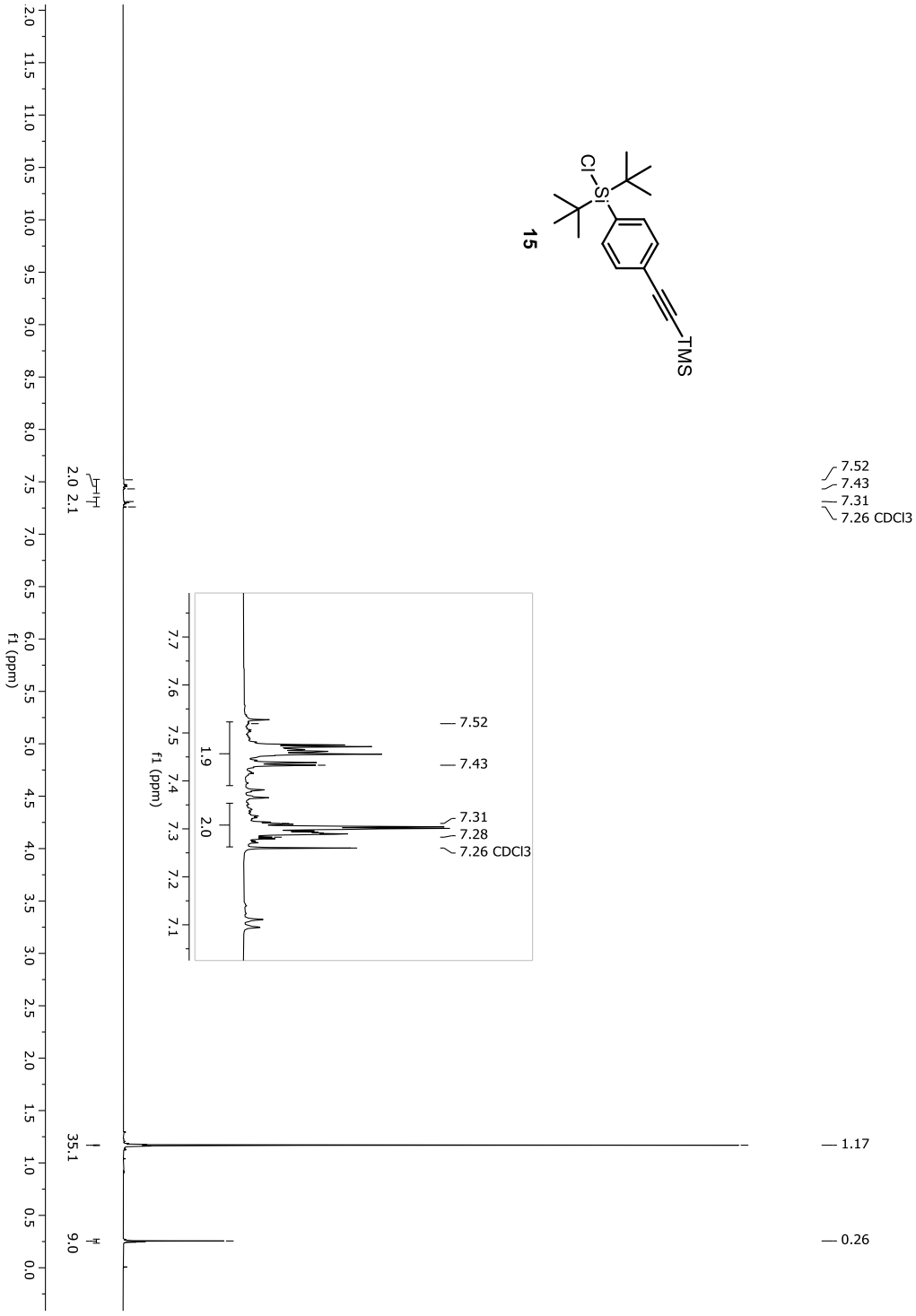

Figure A-21. ^{13}C-NMR spectrum of compound 15 (crude)

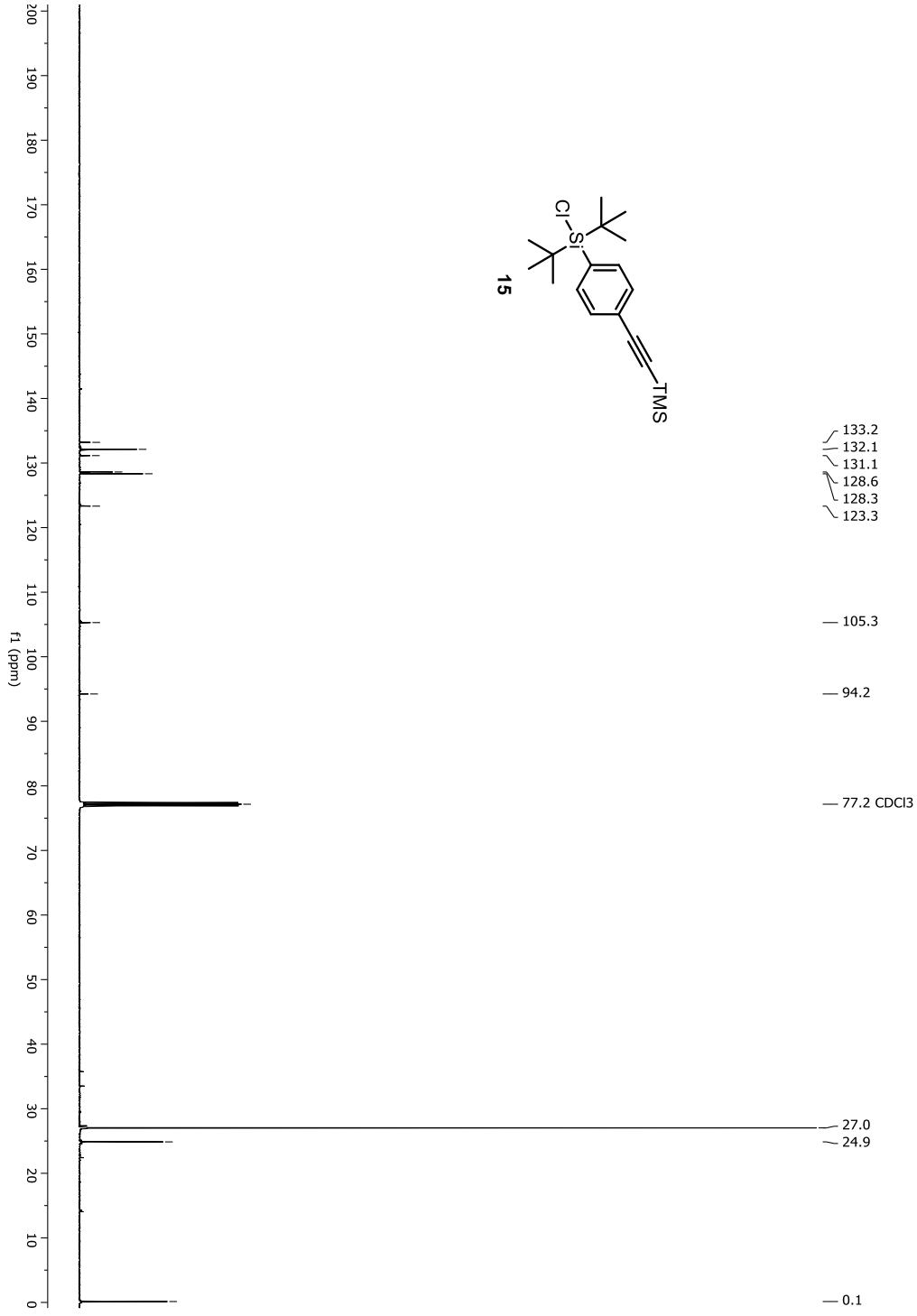

Figure A-22. ^{1}H-NMR spectrum of compound 17

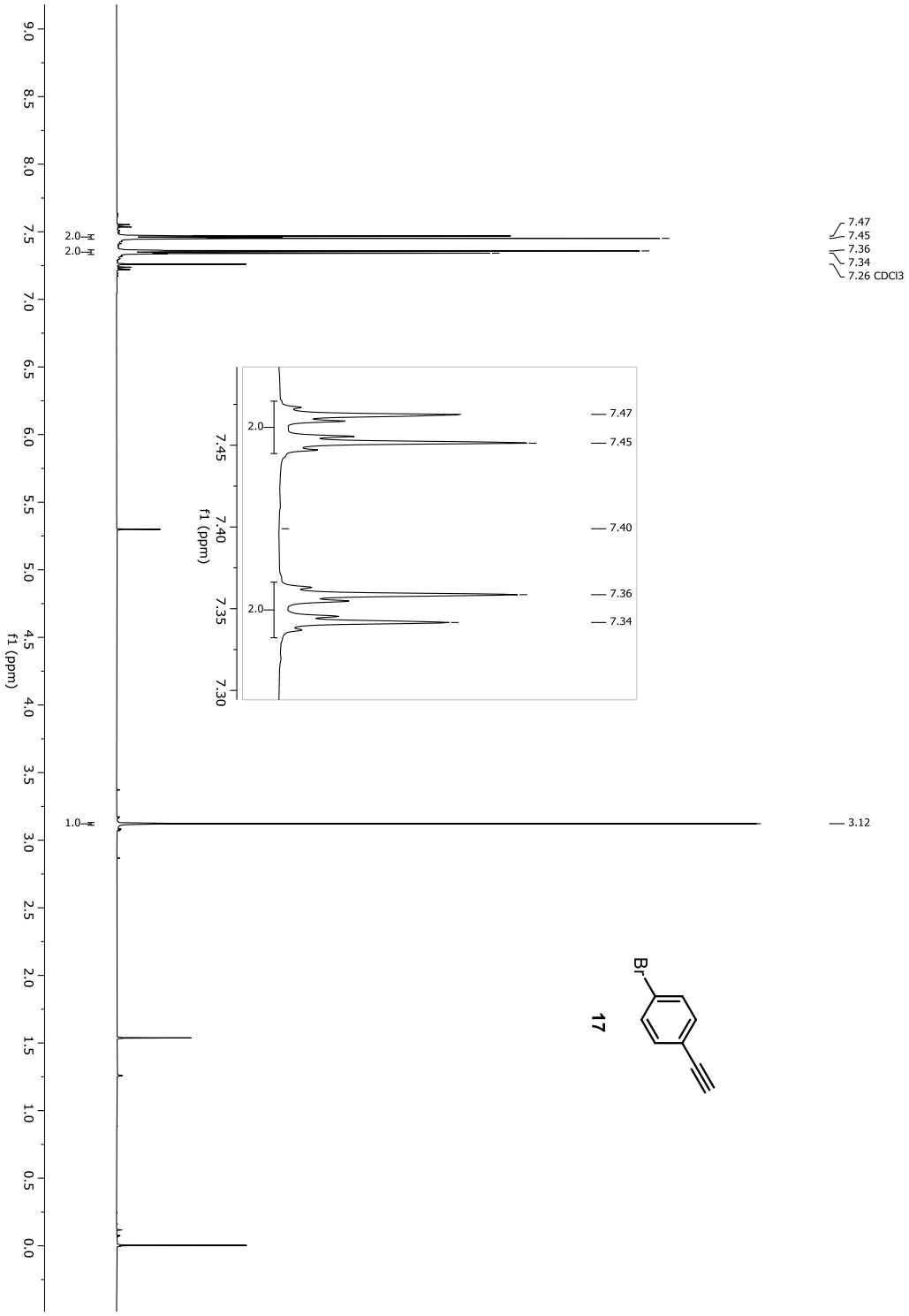

Figure A-23. ^{13}C-NMR spectrum of compound 17

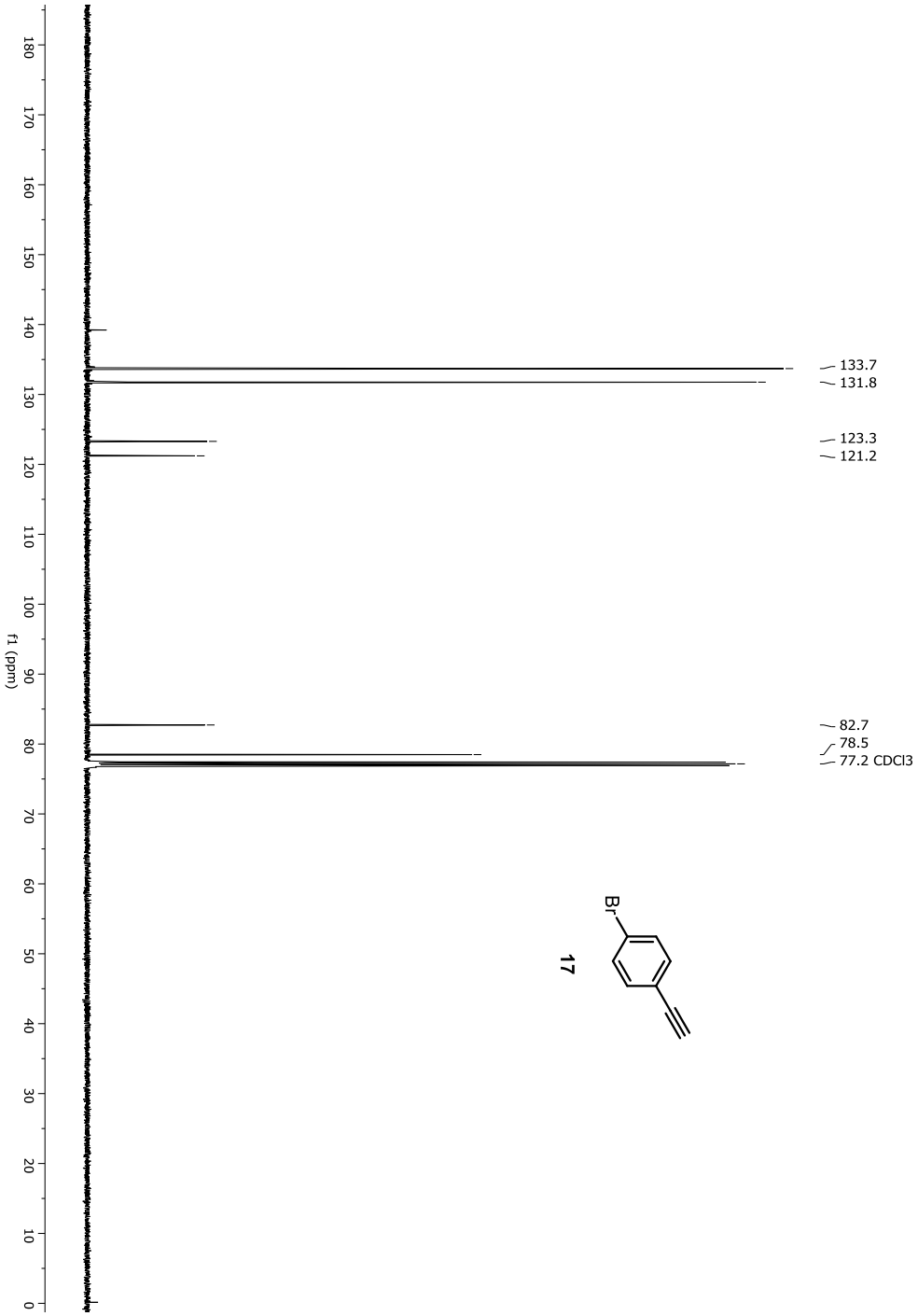

Figure A-24. ^{1}H-NMR spectrum of compound 18

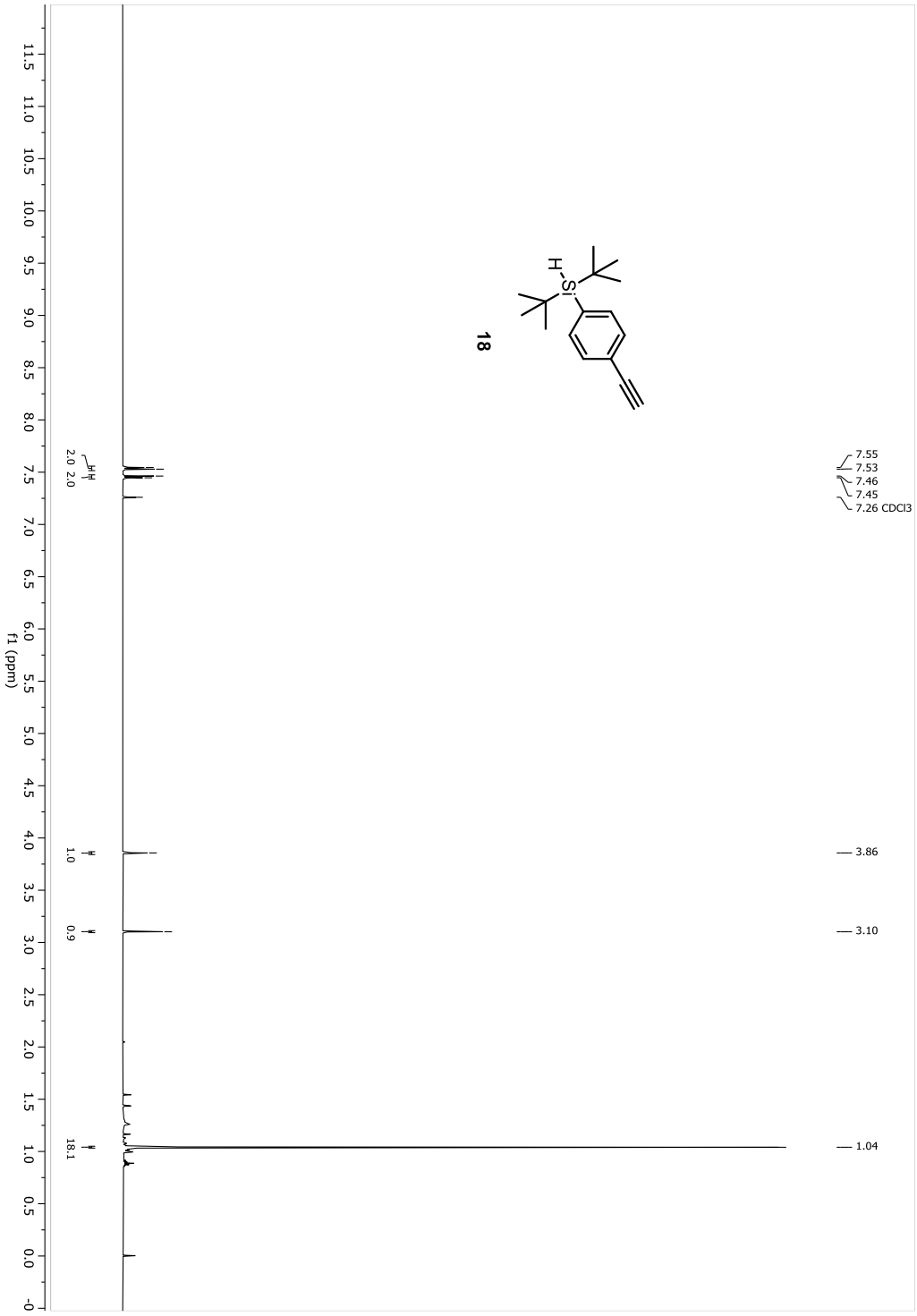

Figure A-25. ^{13}C-NMR spectrum of compound 18

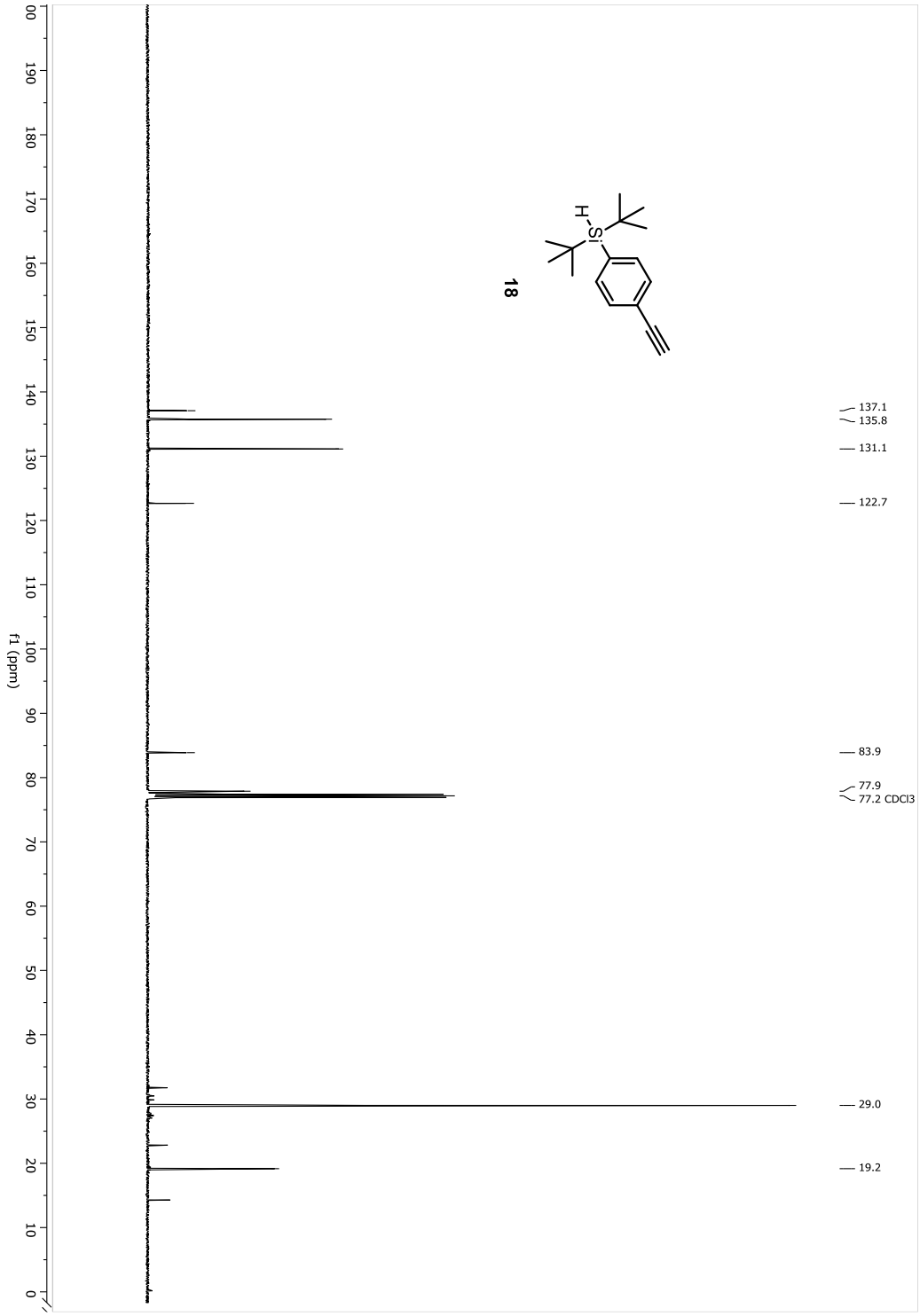

Figure A-26. ^{1}H-NMR spectrum of compound 20

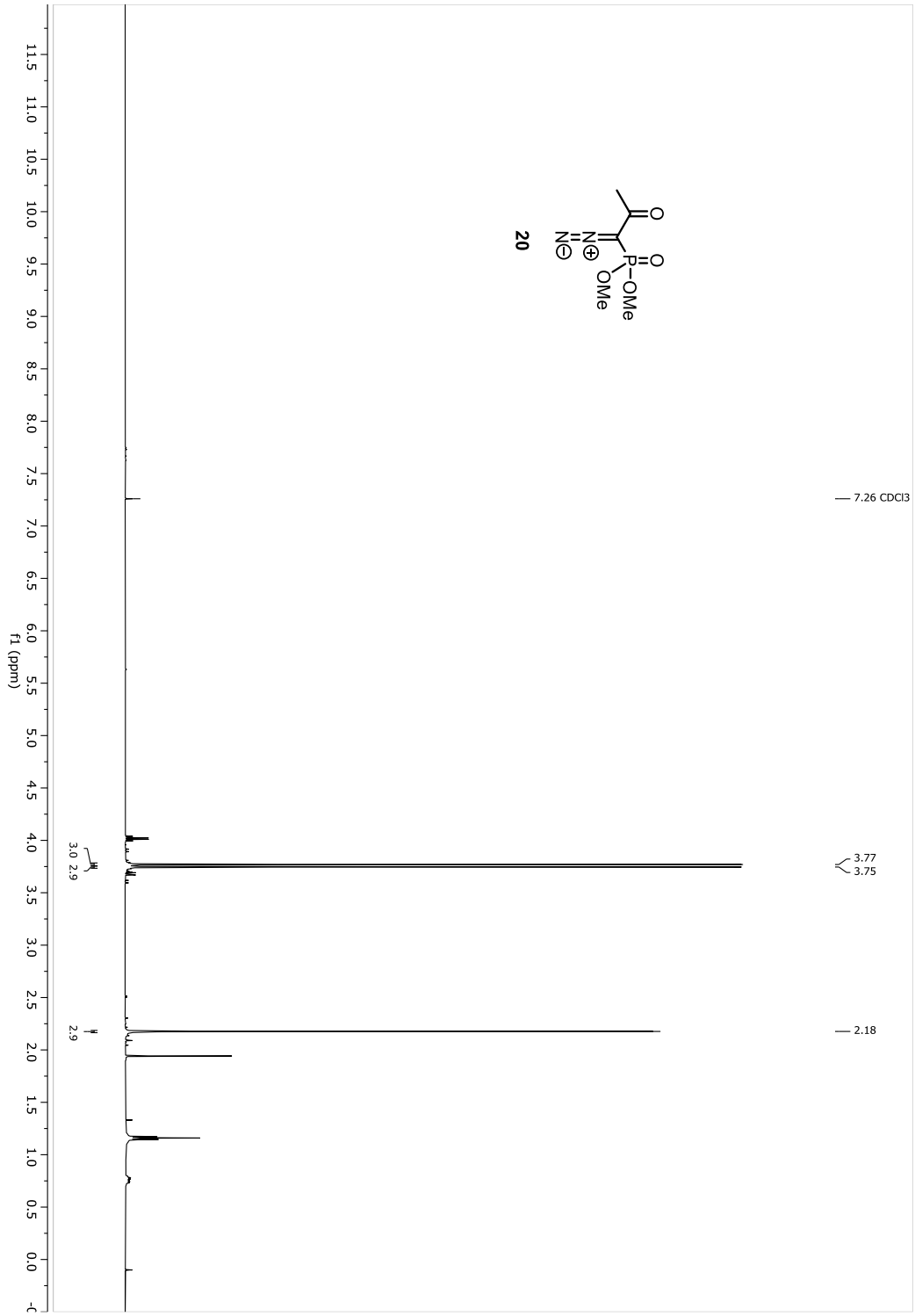

Figure A-27. ^{13}C-NMR spectrum of compound 20

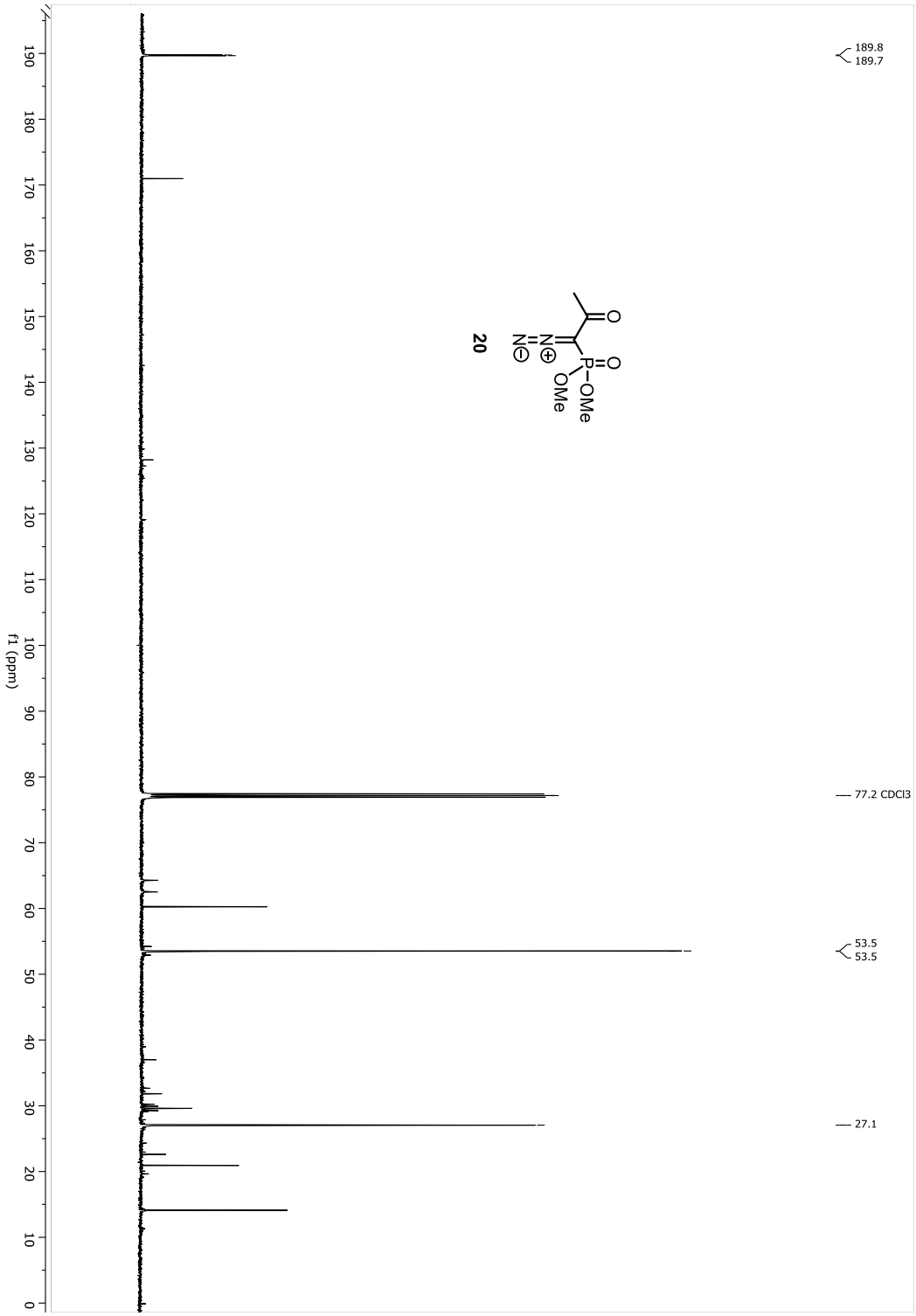

Figure A-28. ^{1}H-NMR spectrum of compound 22

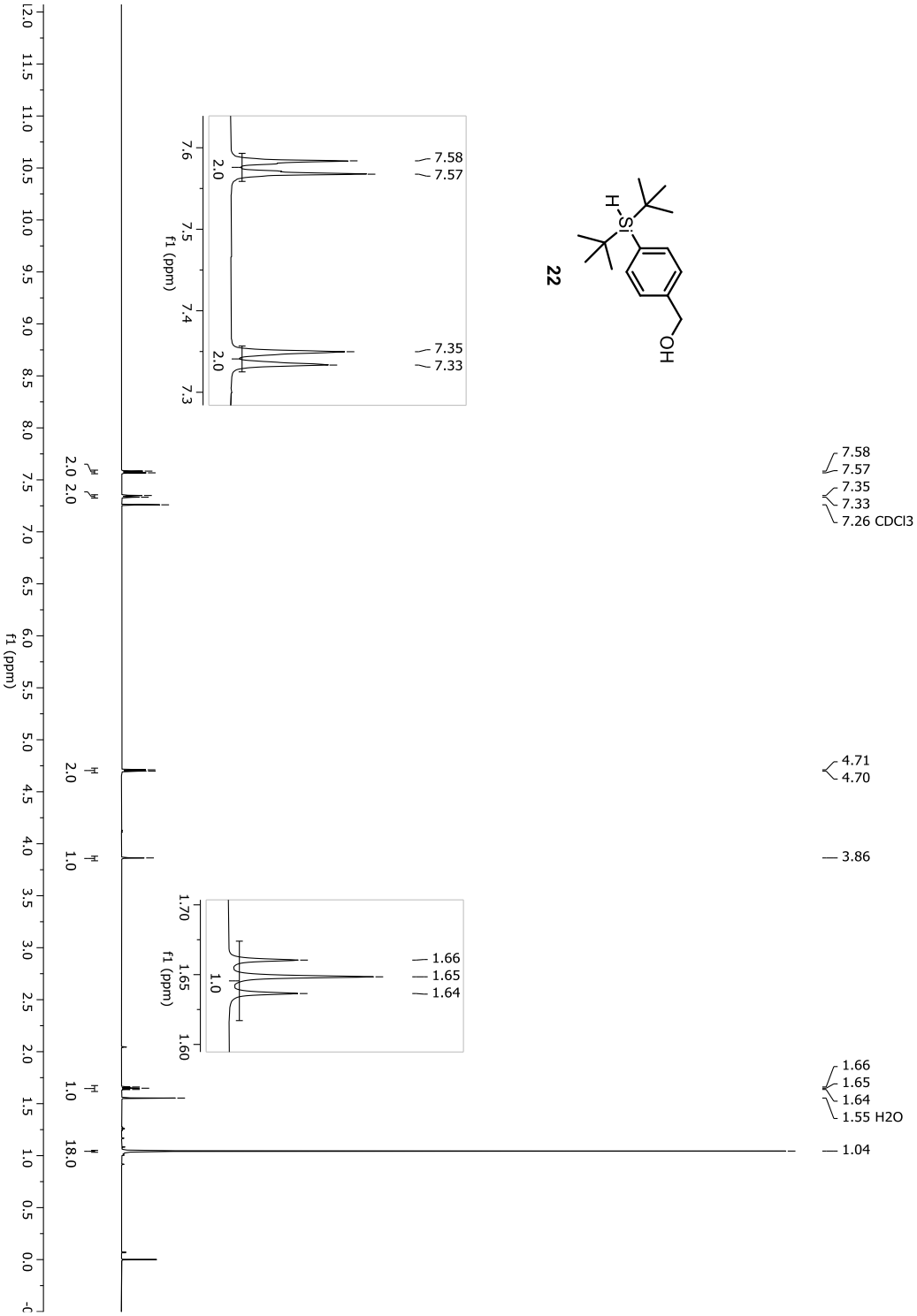

Figure A-29. ^{13}C-NMR spectrum of compound 22

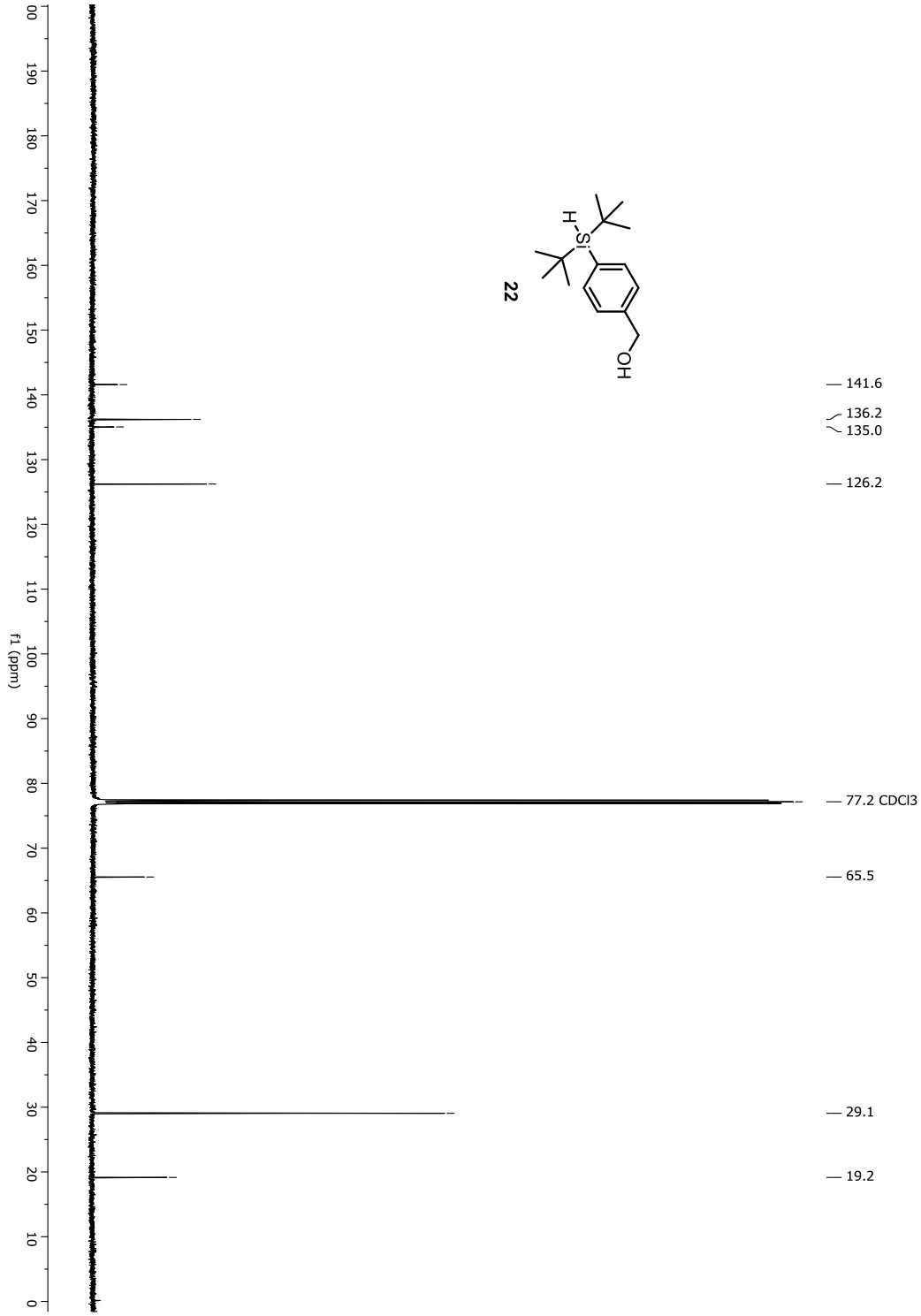

Figure A-30. ^{1}H-NMR spectrum of compound 25

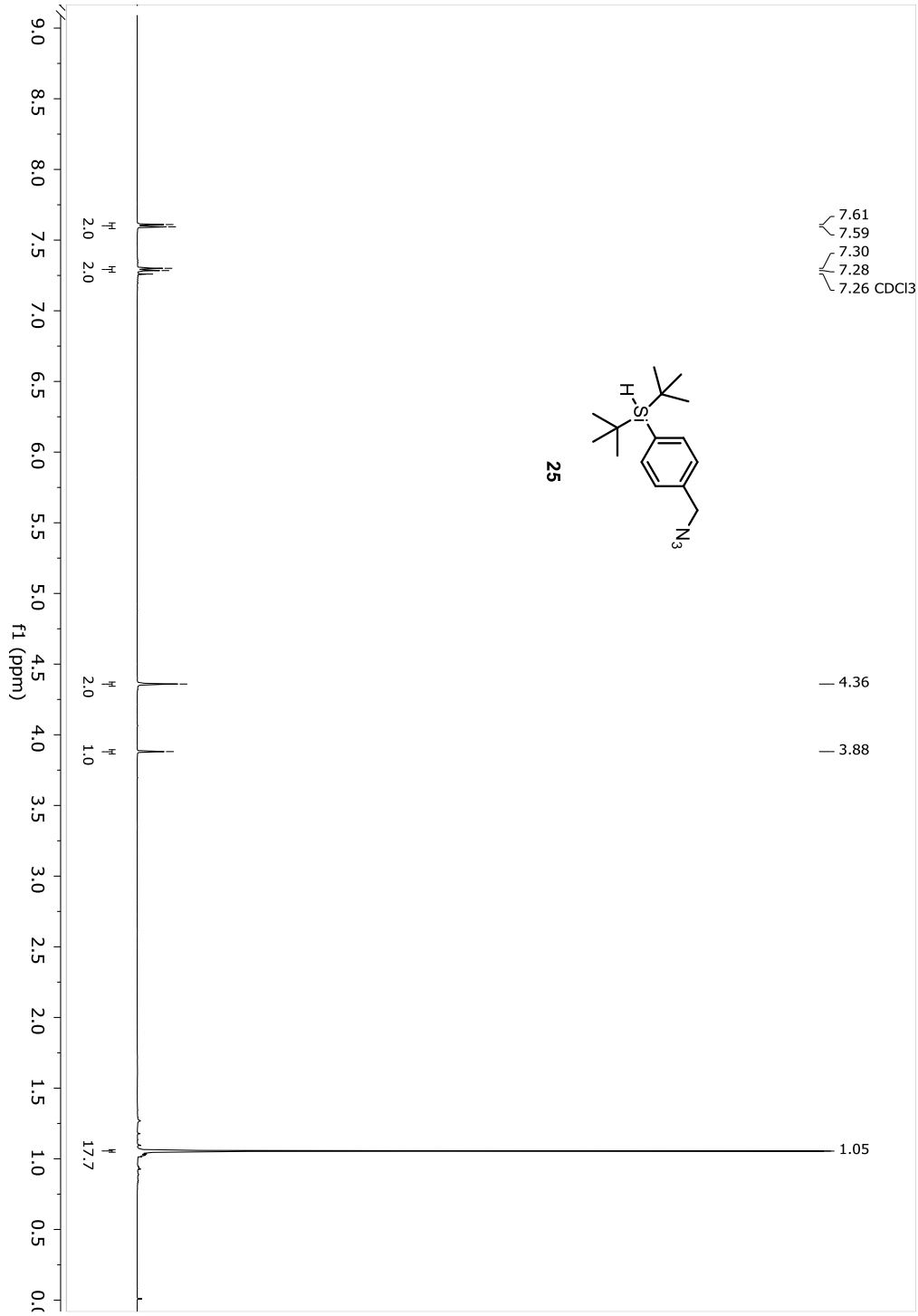

Figure A-31. ^{13}C-NMR spectrum of compound 25

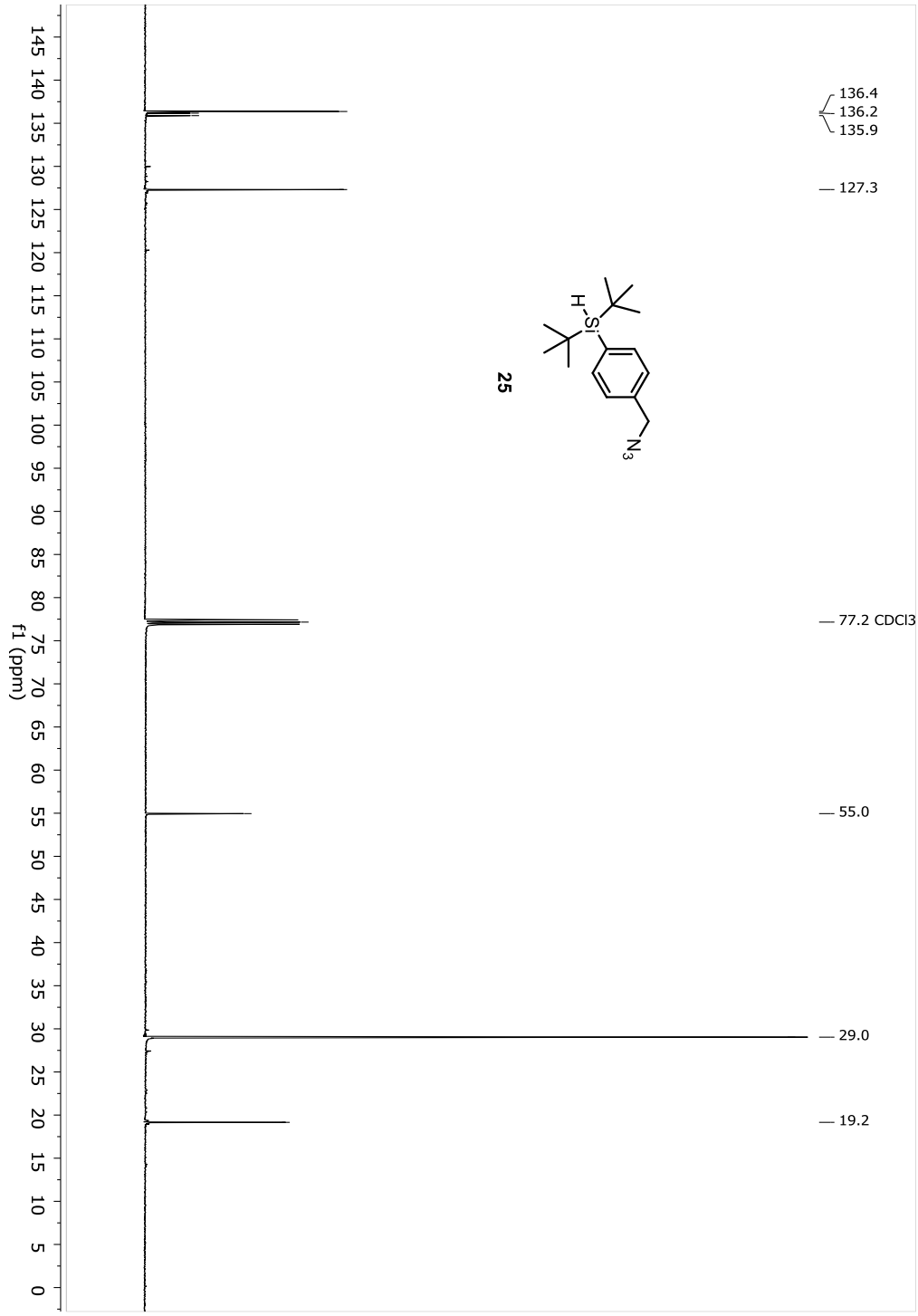

Figure A-32. ^{1}H-NMR spectrum of compound 31

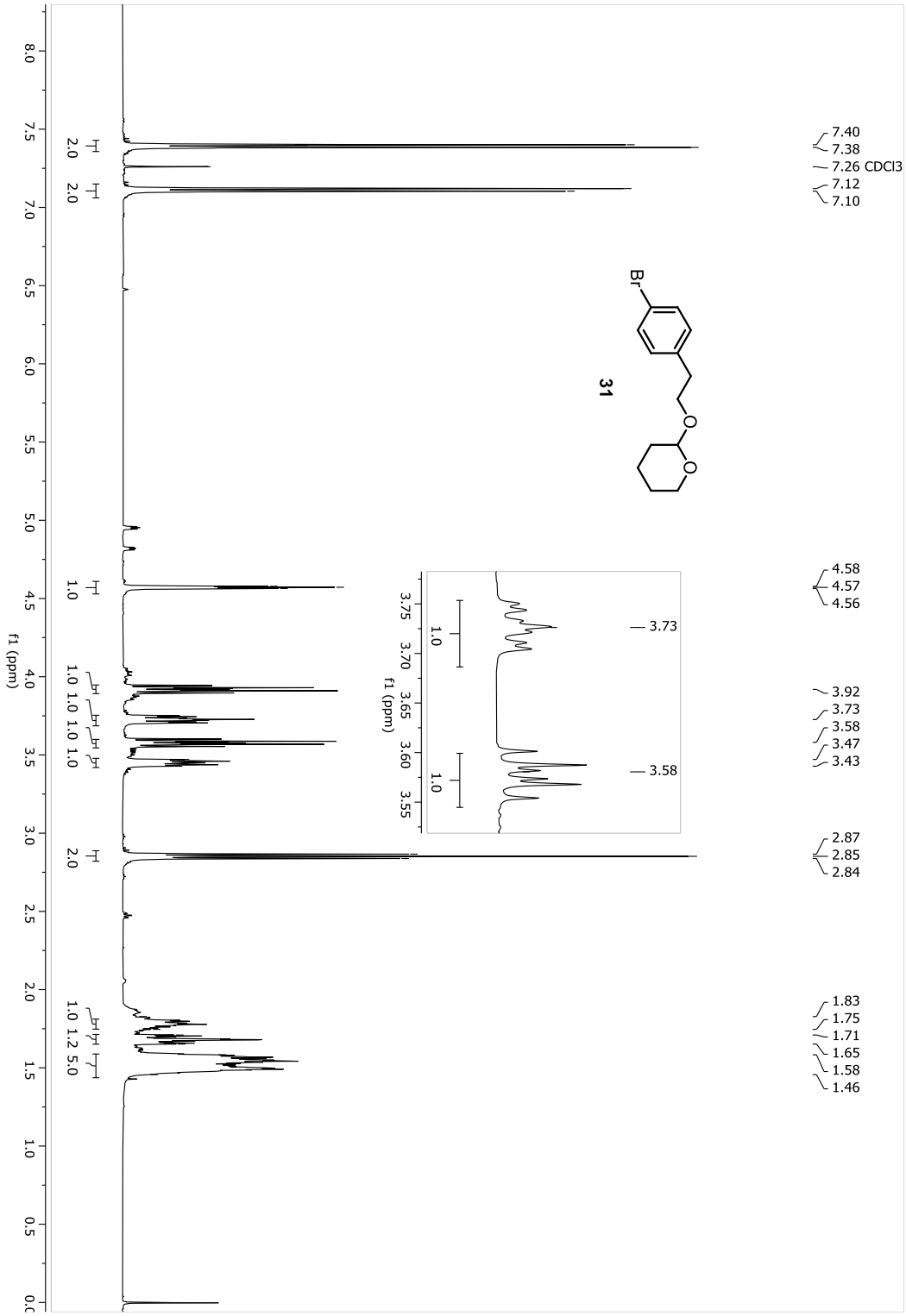

Figure A-33. ^{13}C-NMR spectrum of compound 31

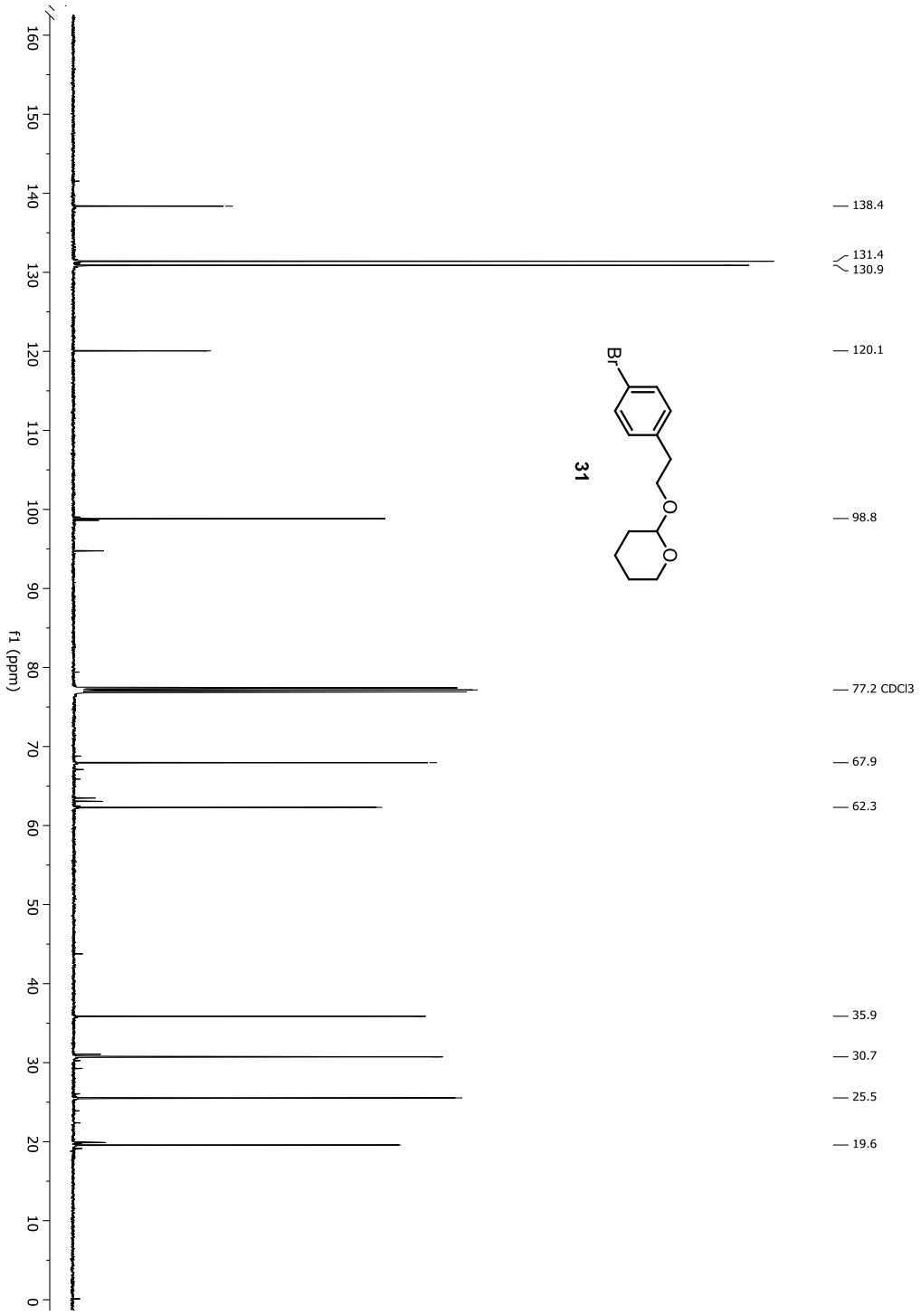

Figure A-34. ^{1}H-NMR spectrum of compound 33

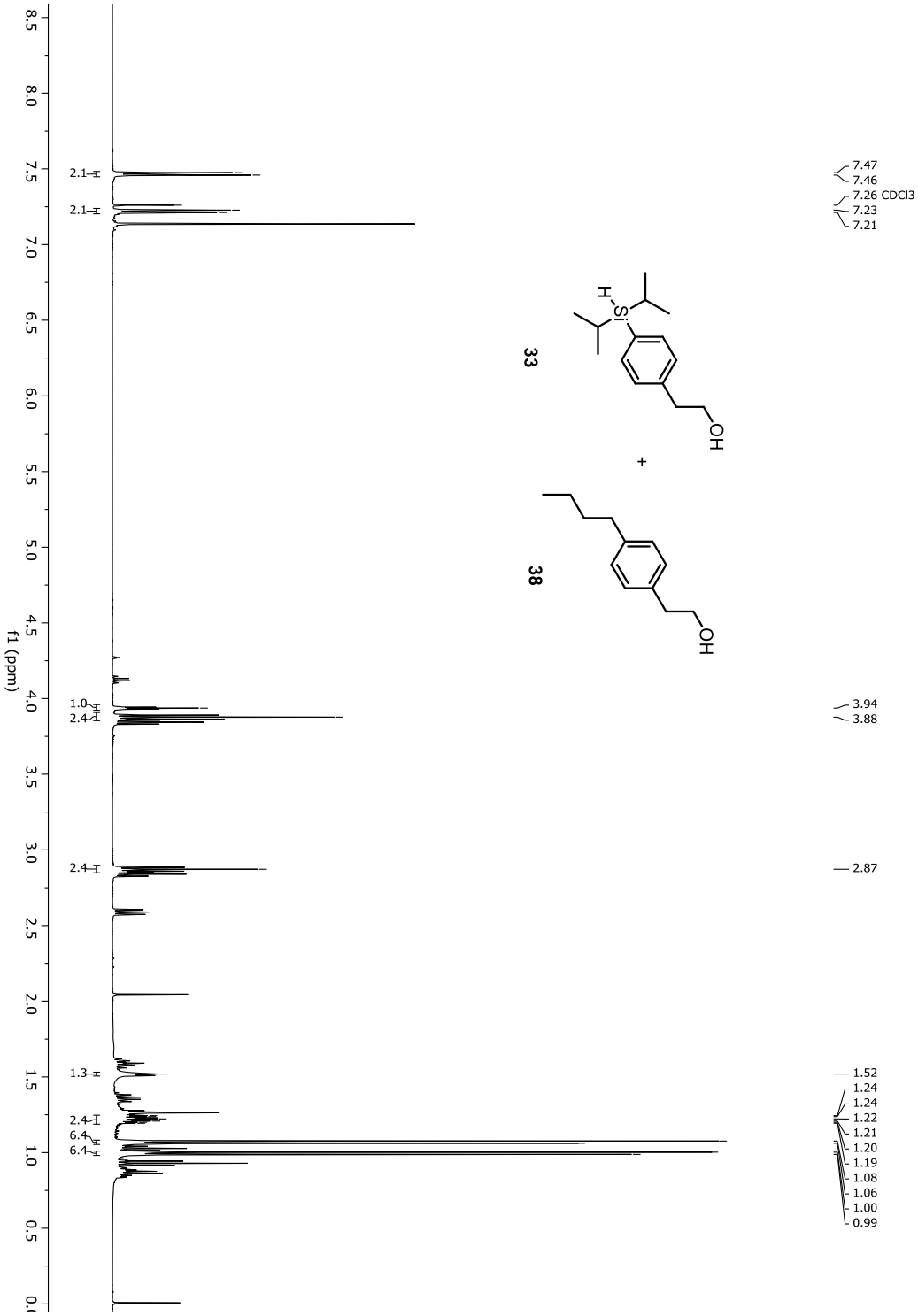

Figure A-35. ^{13}C-NMR spectrum of compound 33

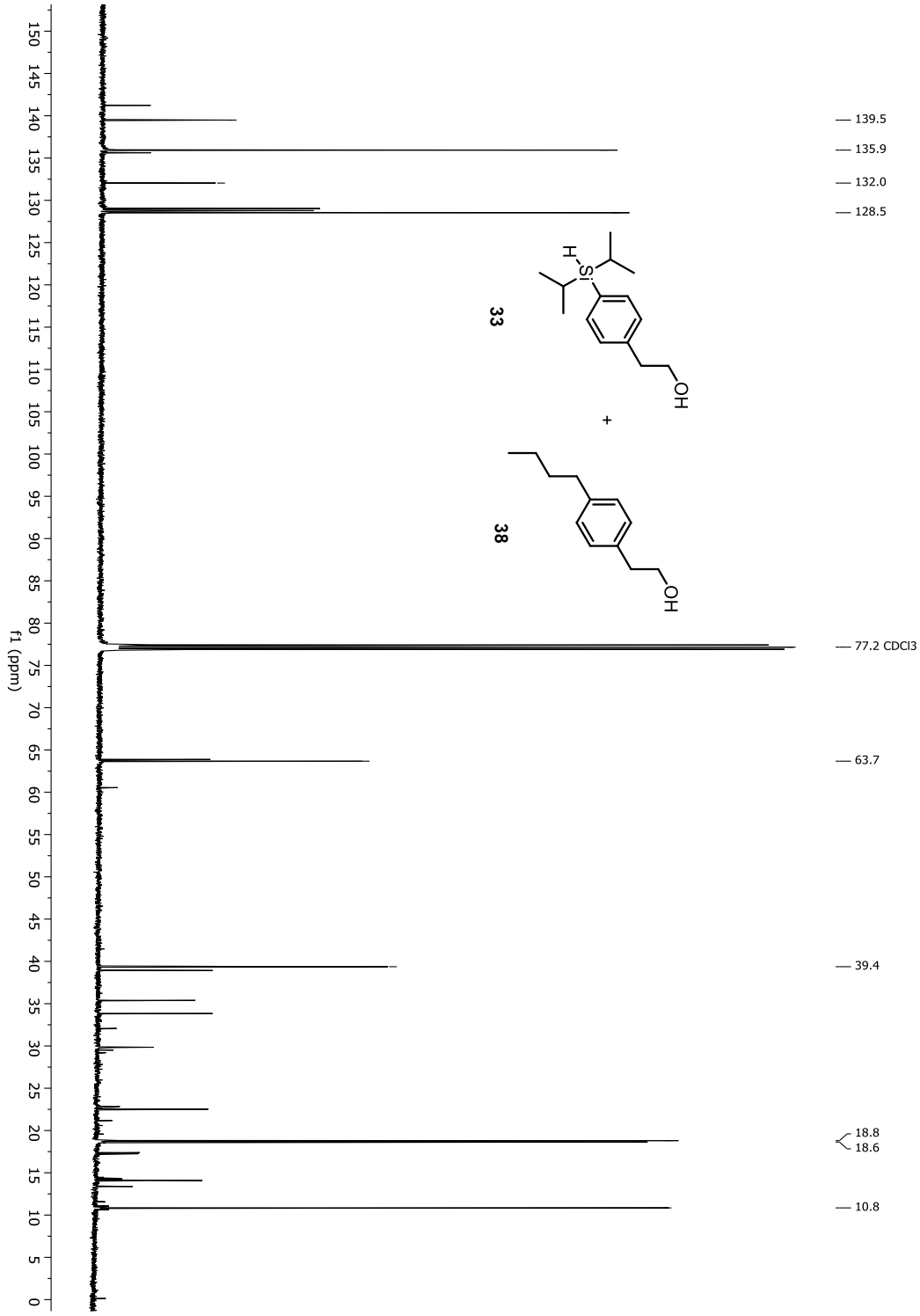

Figure A-36. ^{1}H-NMR spectrum of compound 35

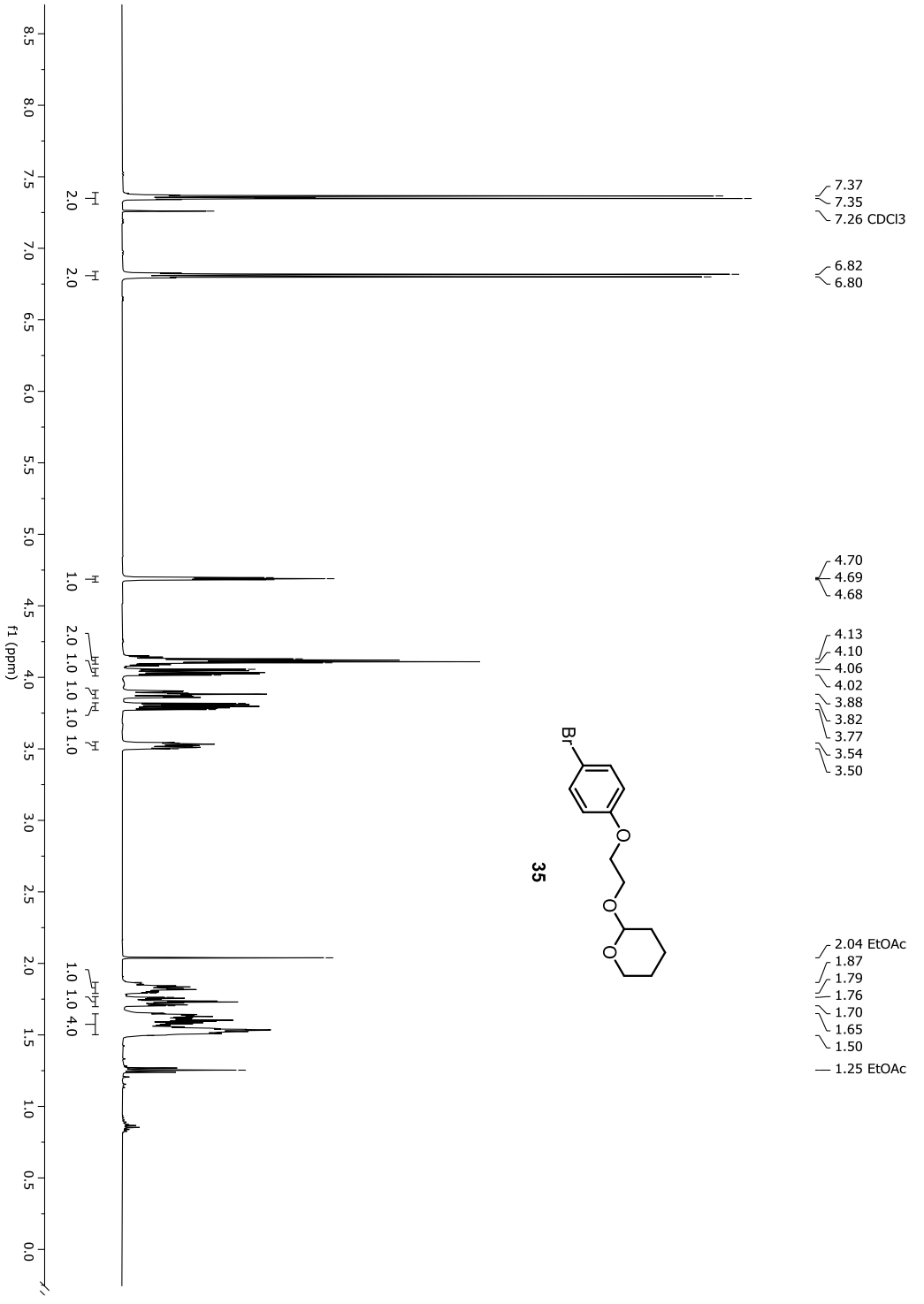

Figure A-37. ^{13}C-NMR spectrum of compound 35

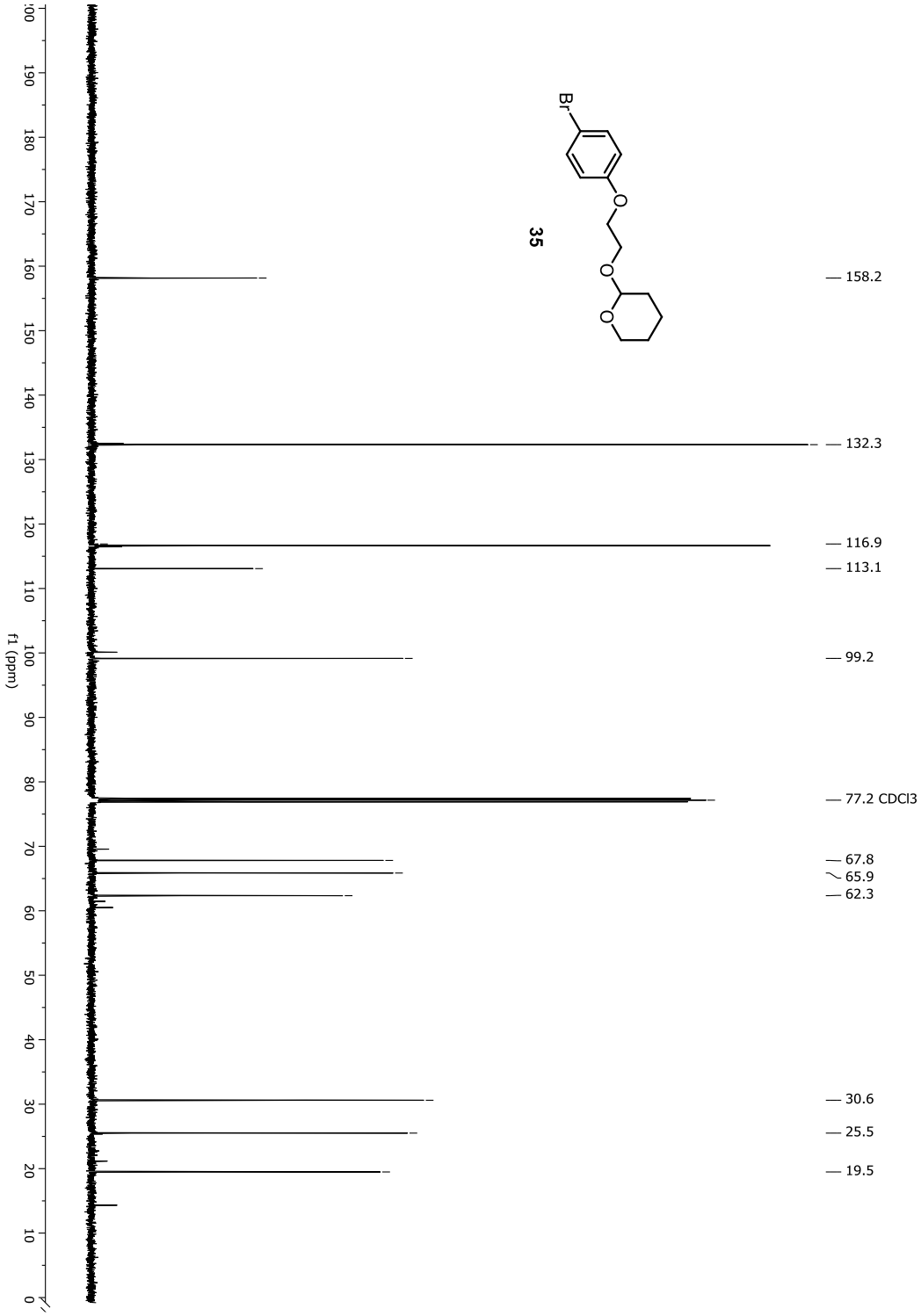

Figure A-38. HRMS spectrum of compound 35

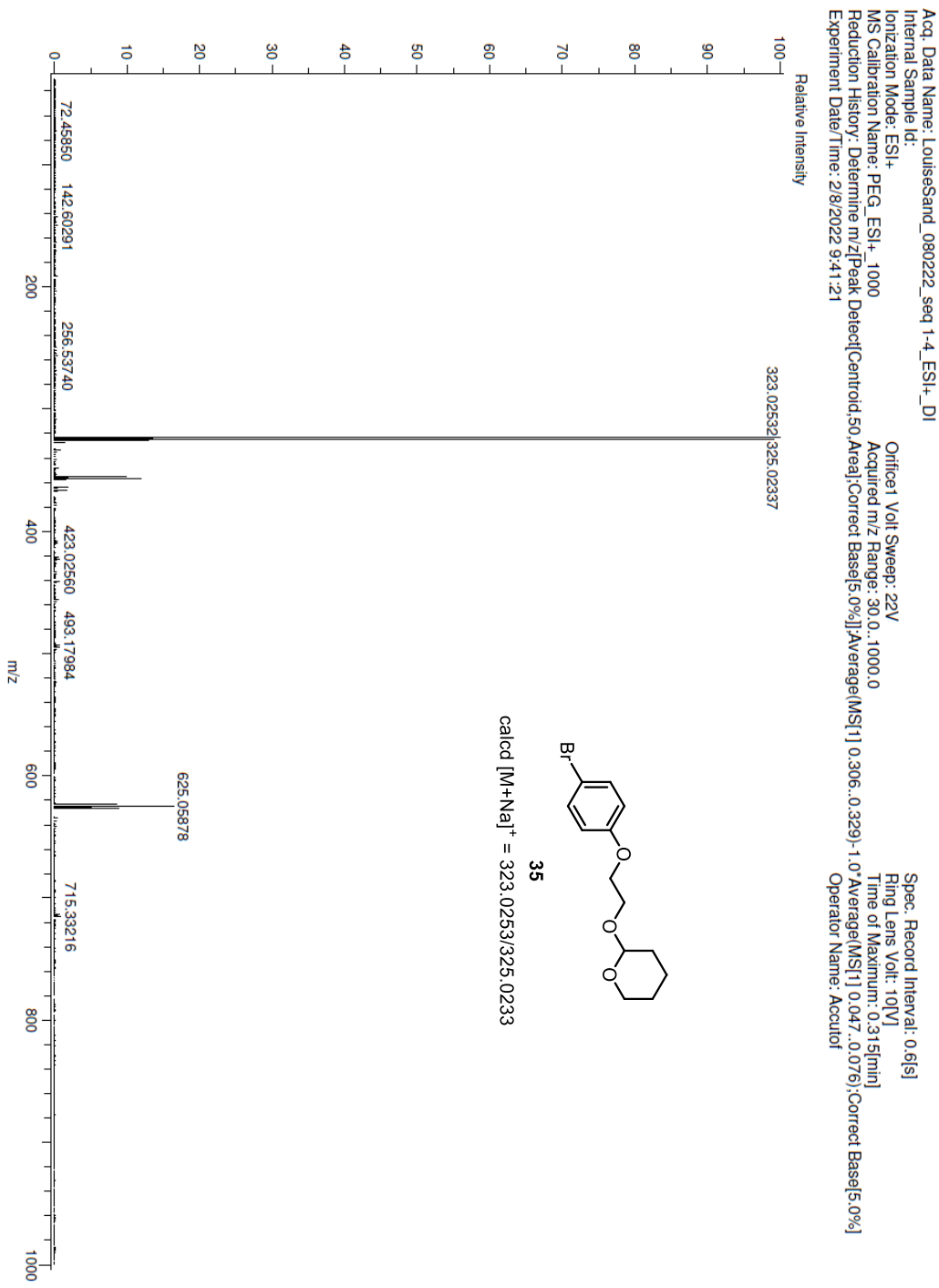

Figure A-39. ^{1}H-NMR spectrum of compound 37

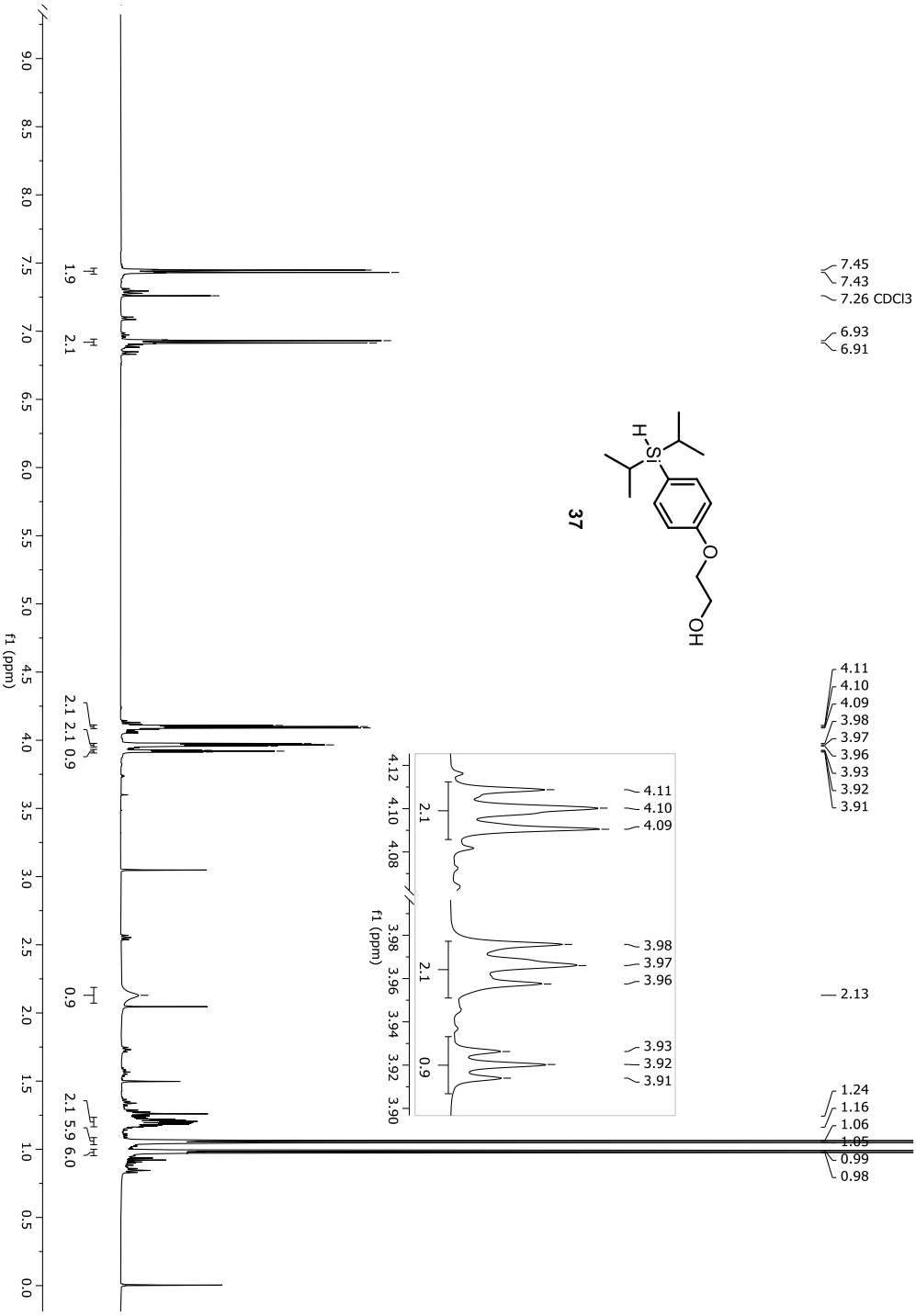

Figure A-40. ^{13}C-NMR spectrum of compound 37

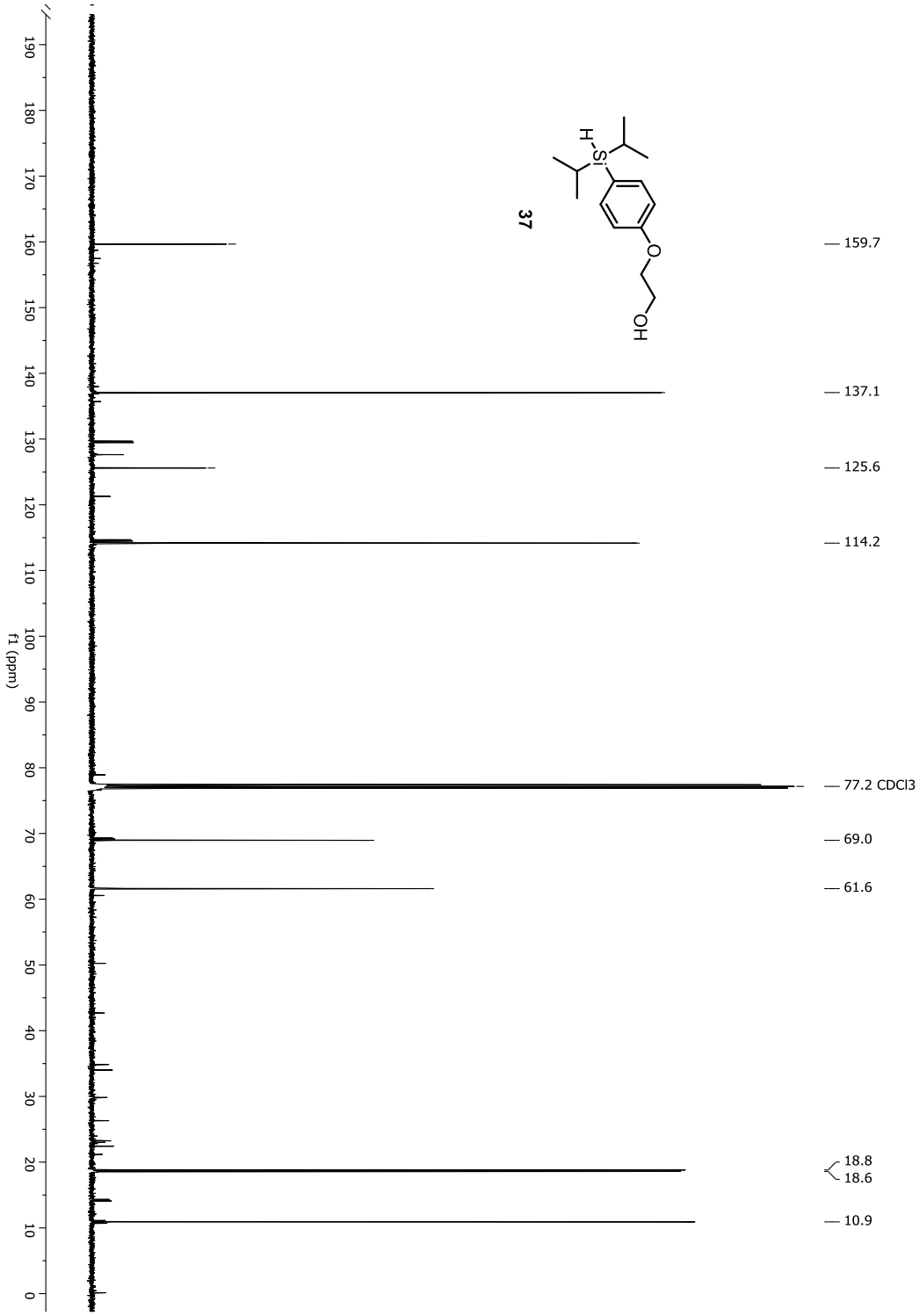

Figure A-41. ^{1}H-NMR spectrum of compound 41

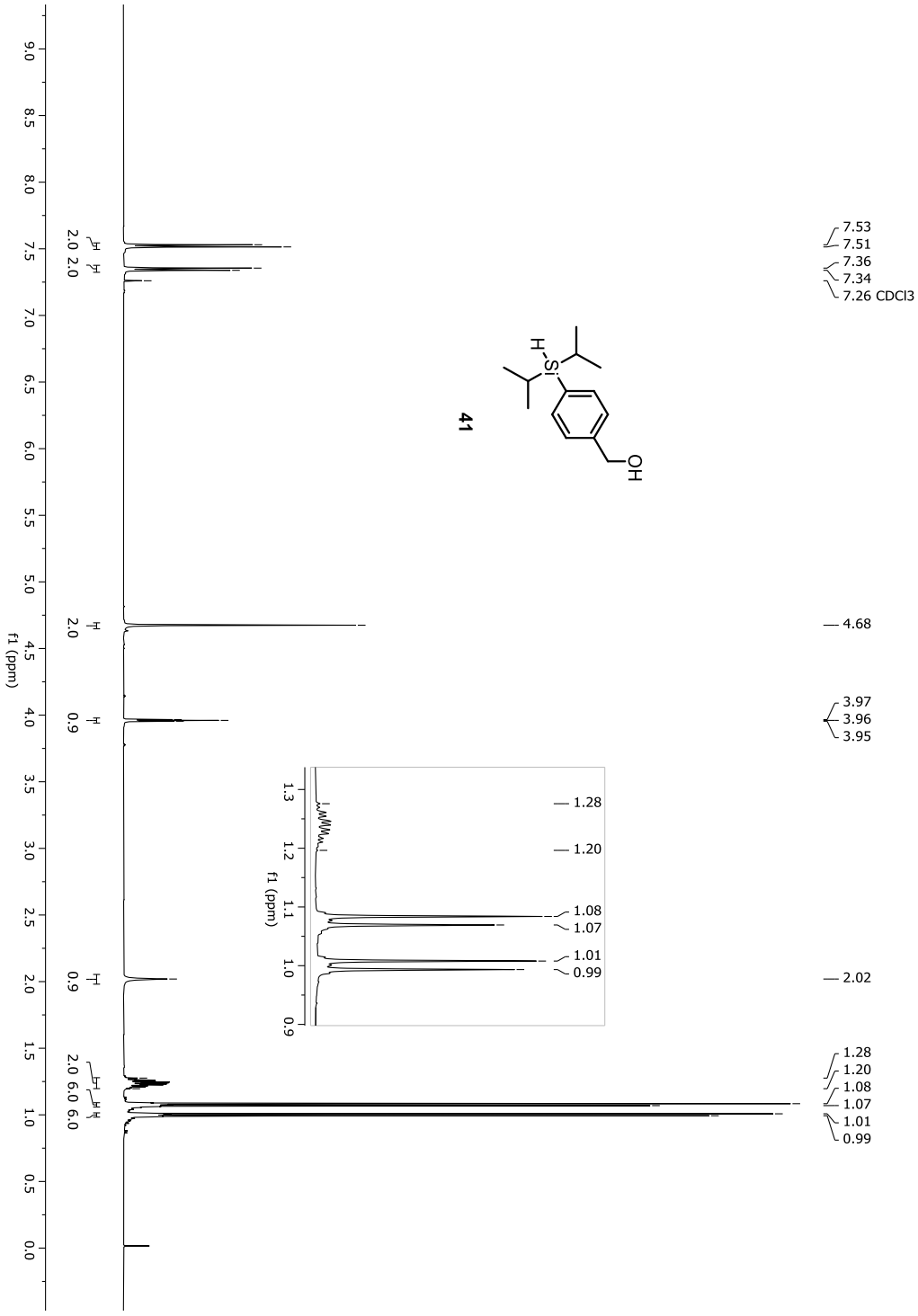

Figure A-42. ^{13}C-NMR spectrum of compound 41

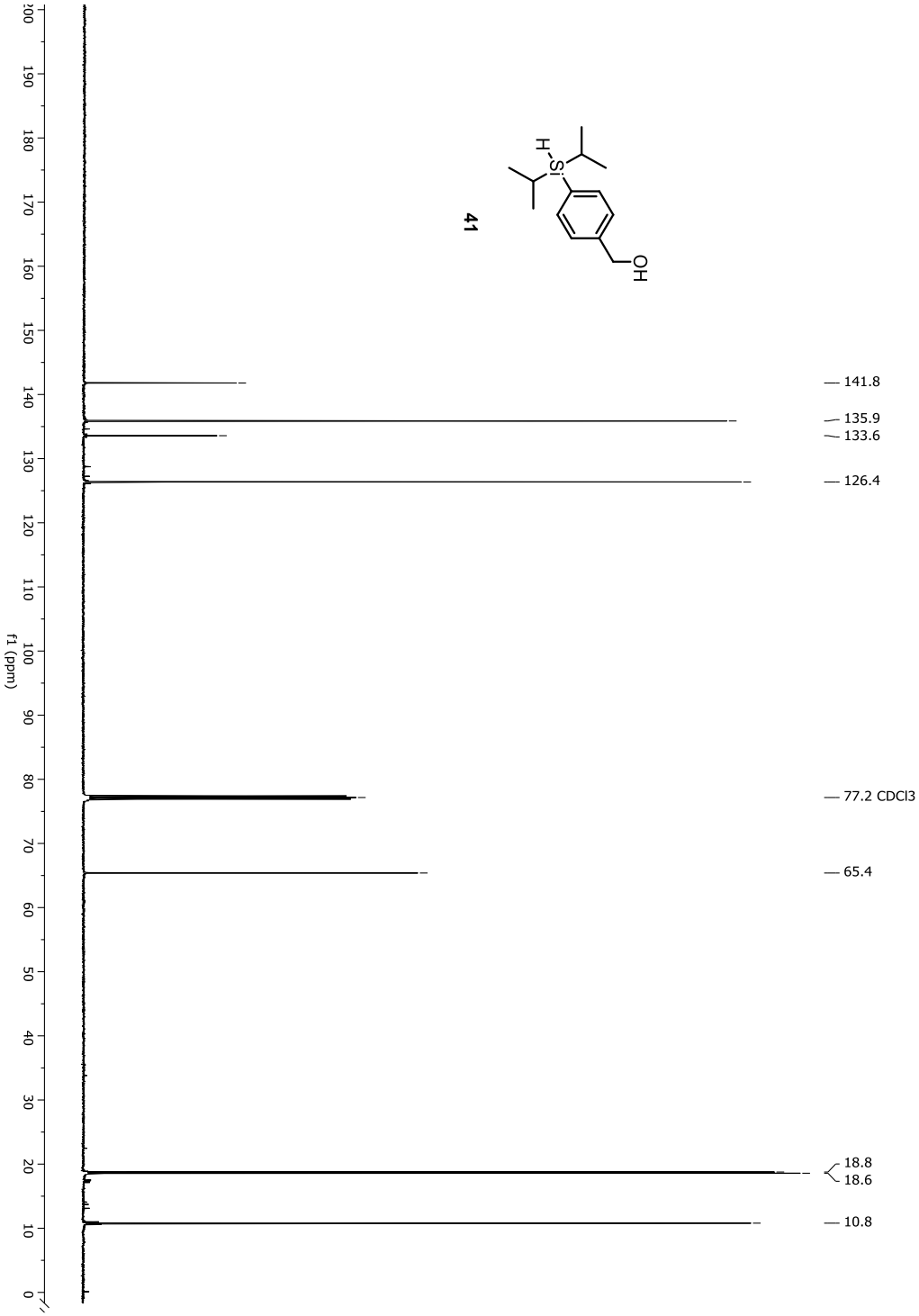

Figure A-43. ^{1}H-NMR spectrum of compound 42

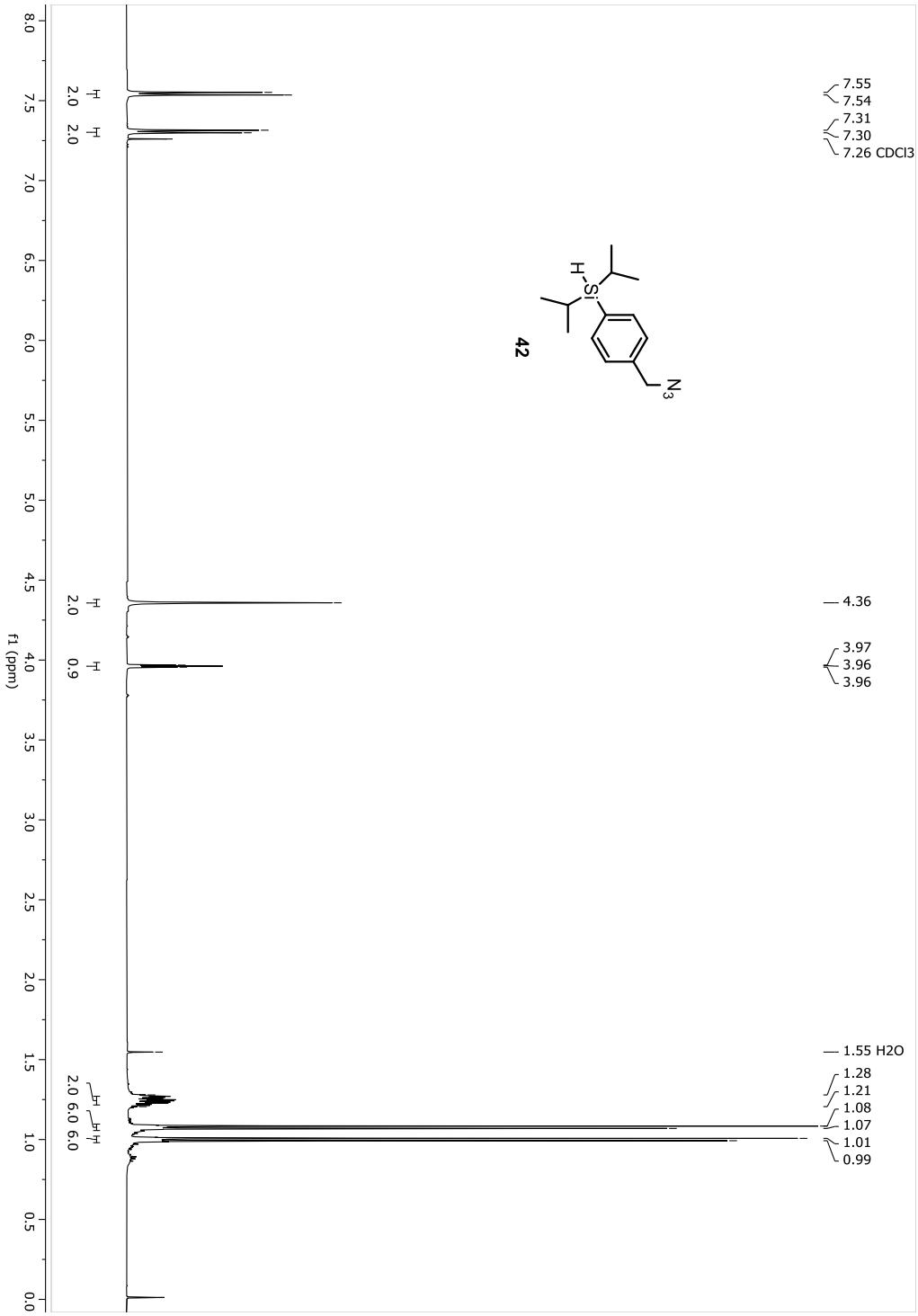

Figure A-44. ^{13}C-NMR spectrum of compound 42

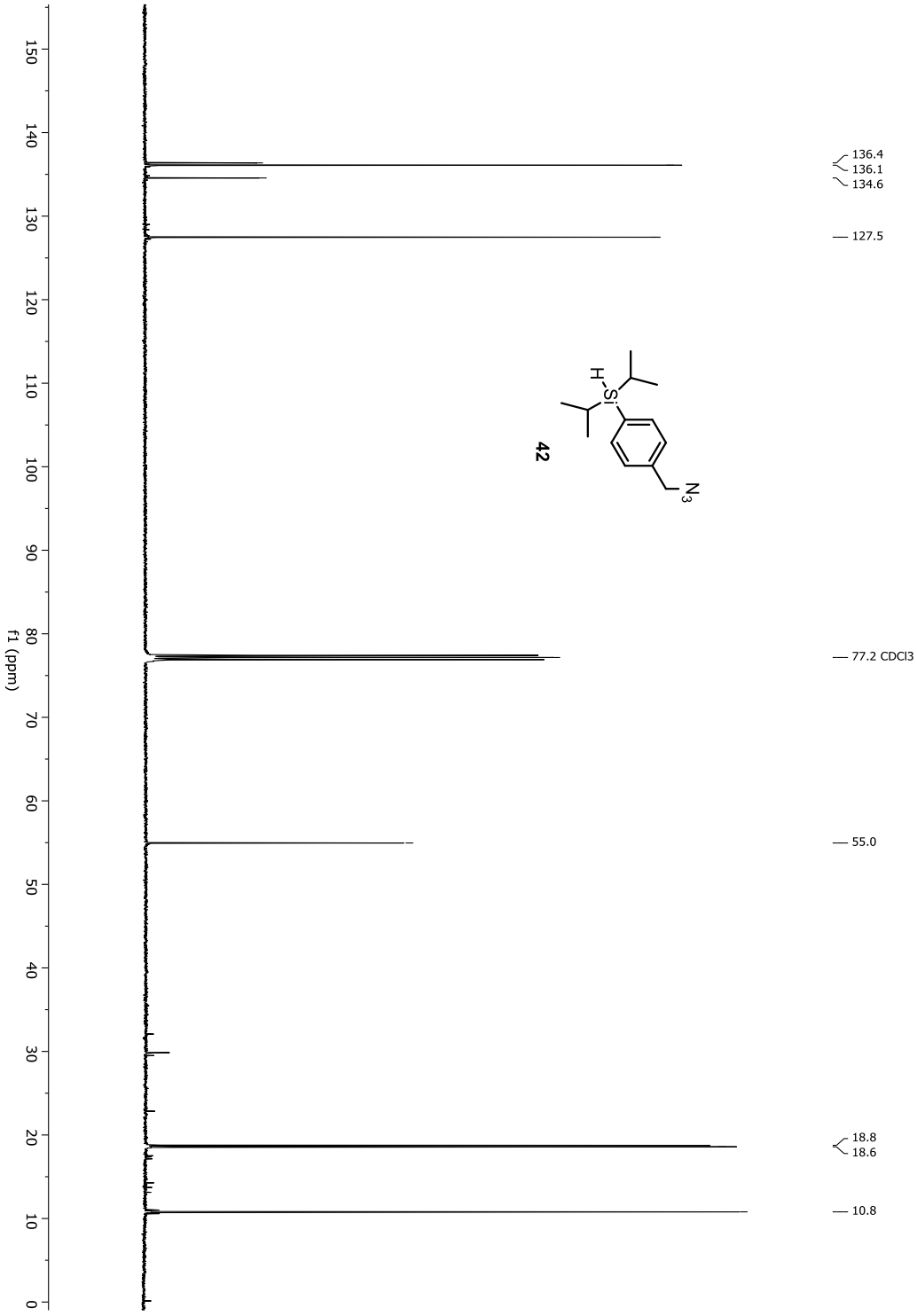

Figure A-45. ^{1}H-NMR spectrum of compound 43

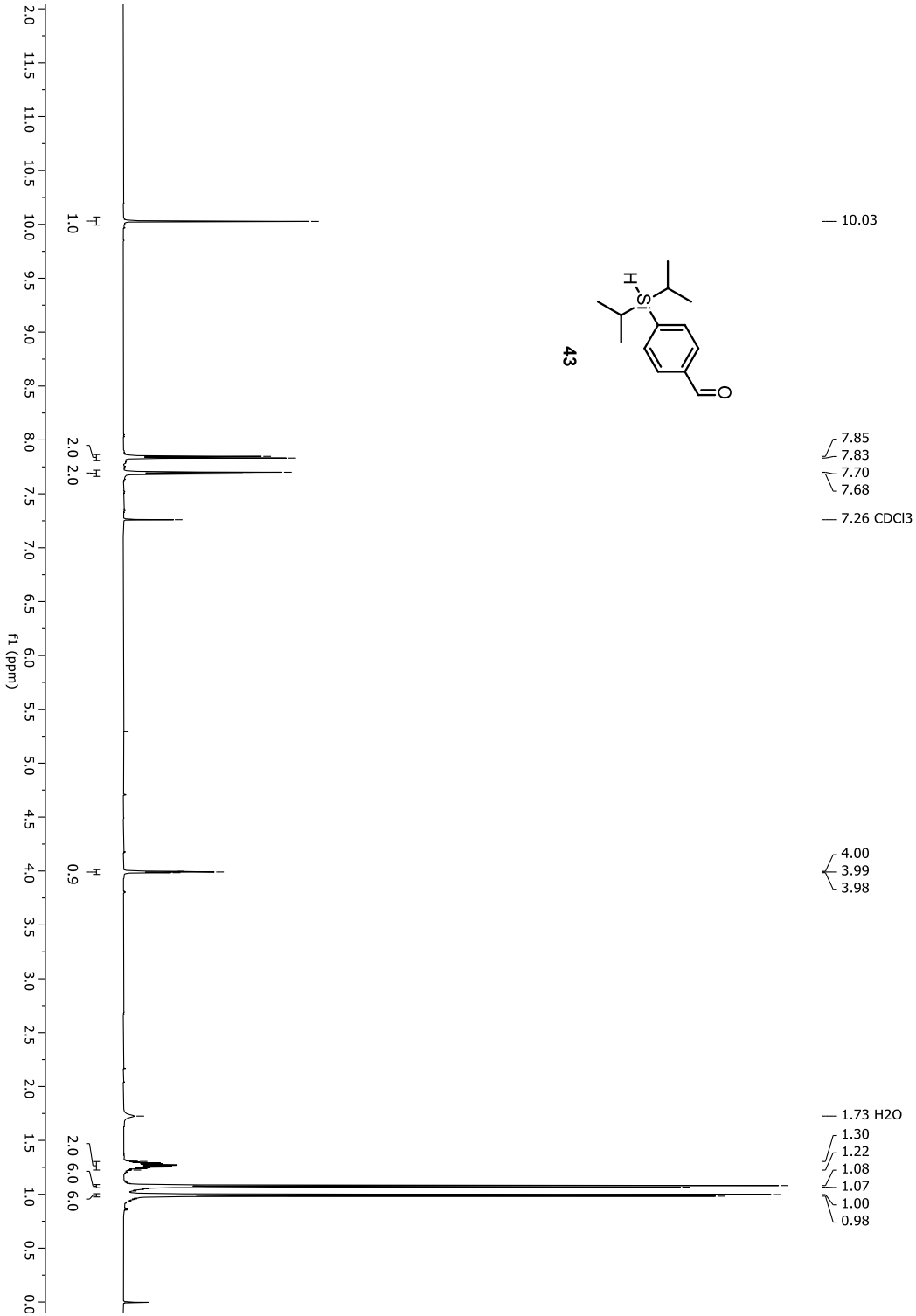

Figure A-46. ^{13}C-NMR spectrum of compound 43

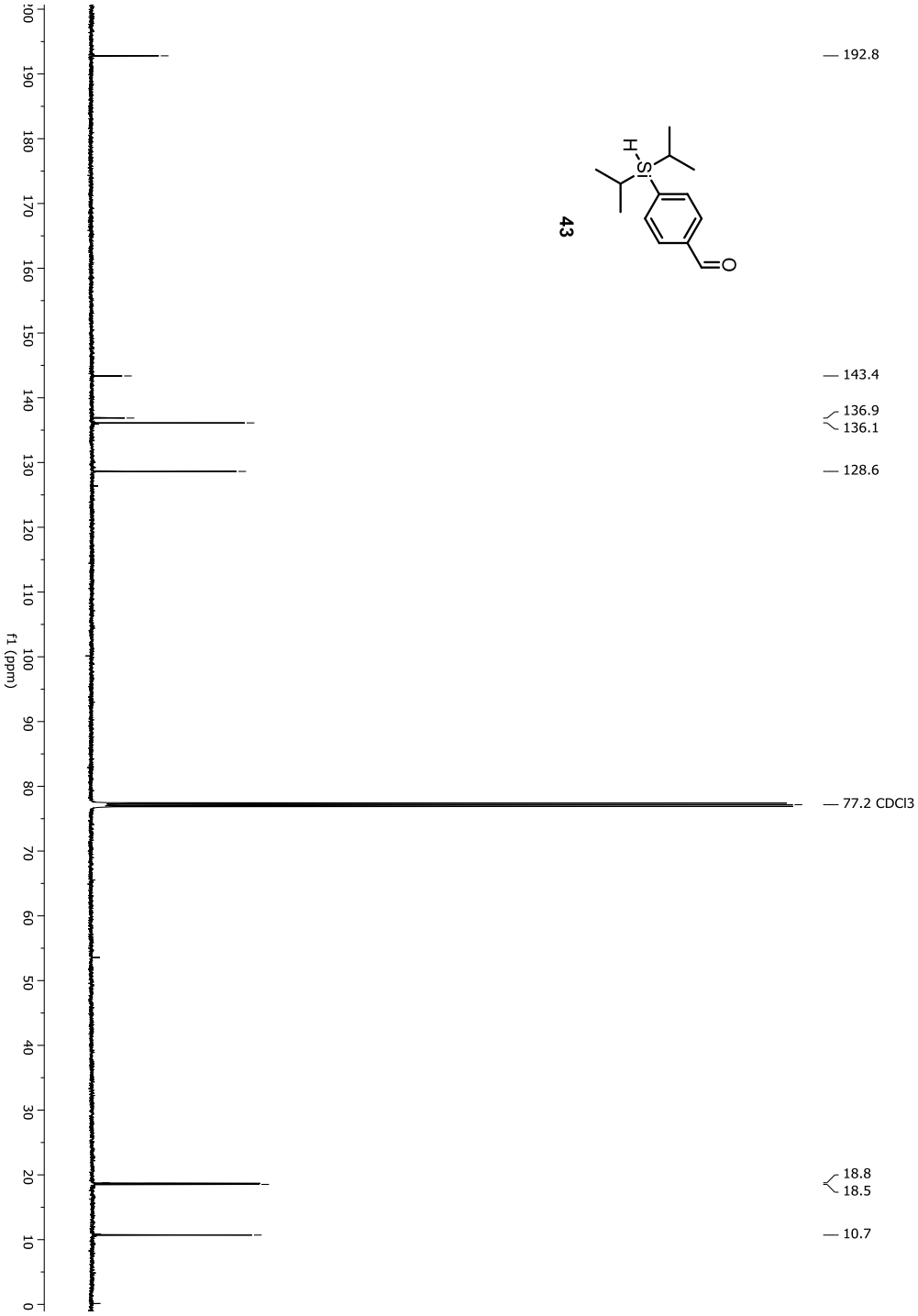

Figure A-47. ^{1}H-NMR spectrum of compound 45

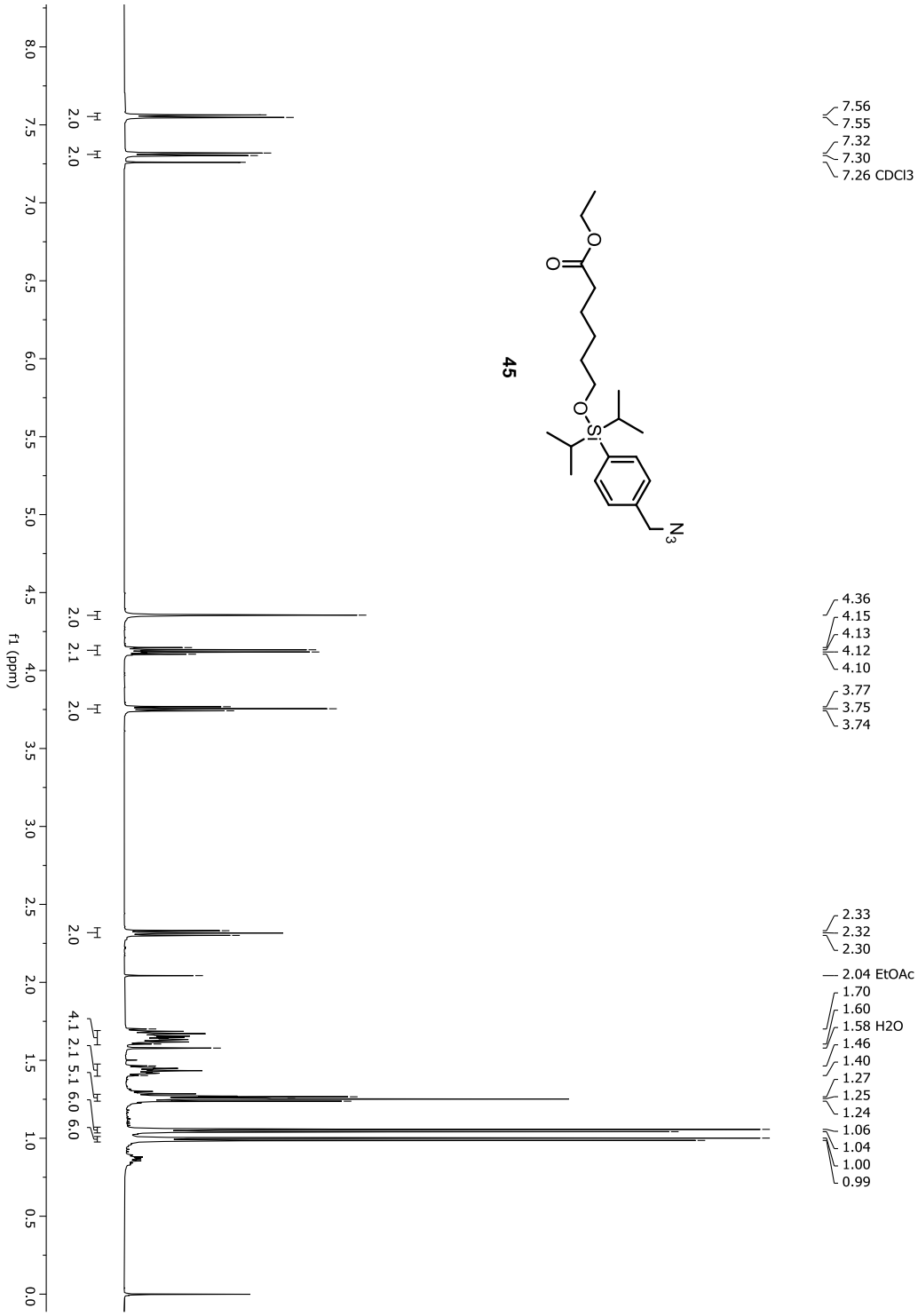

Figure A-48. ^{13}C-NMR spectrum of compound 45

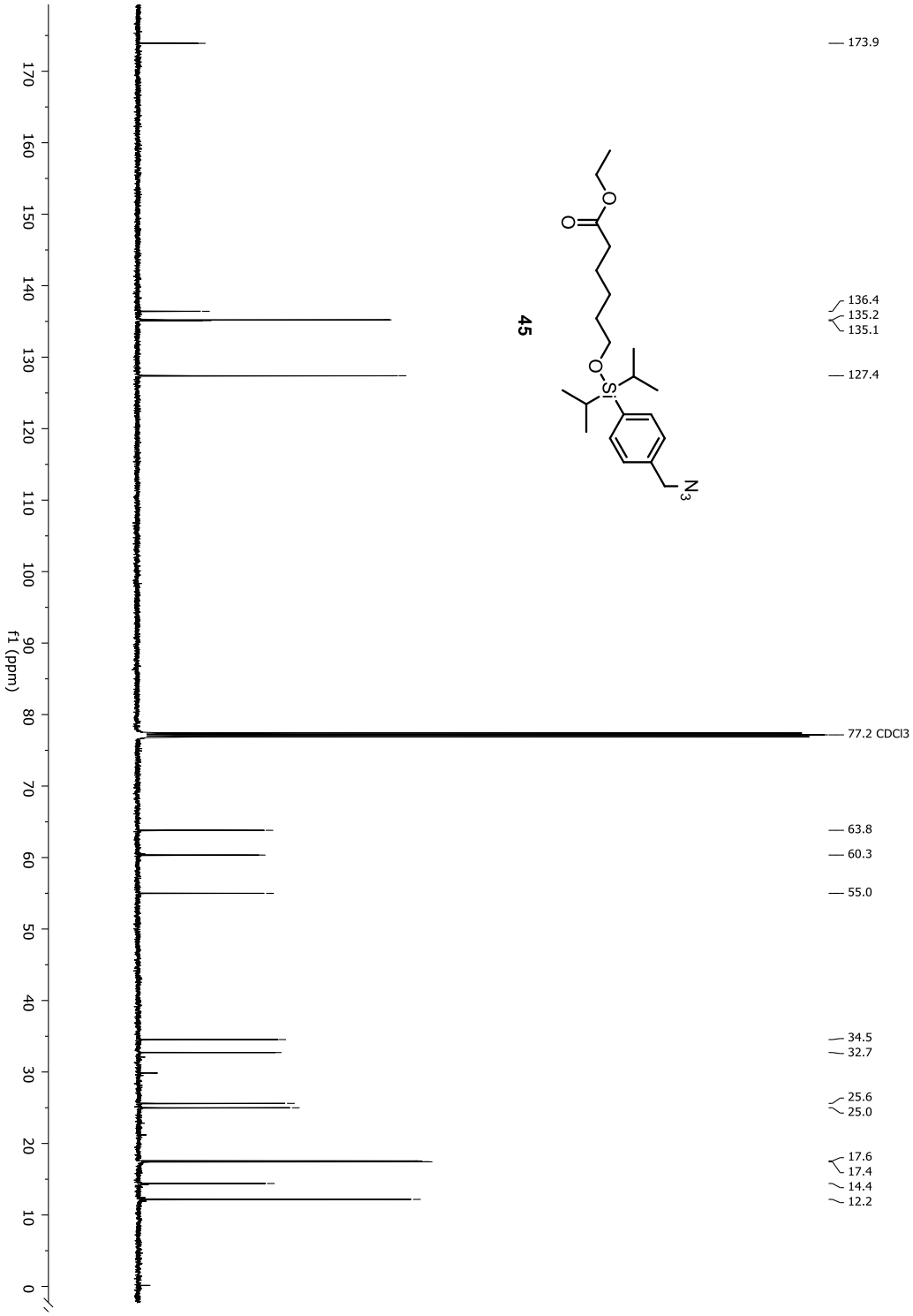

Figure A-49. HRMS spectrum of compound 59

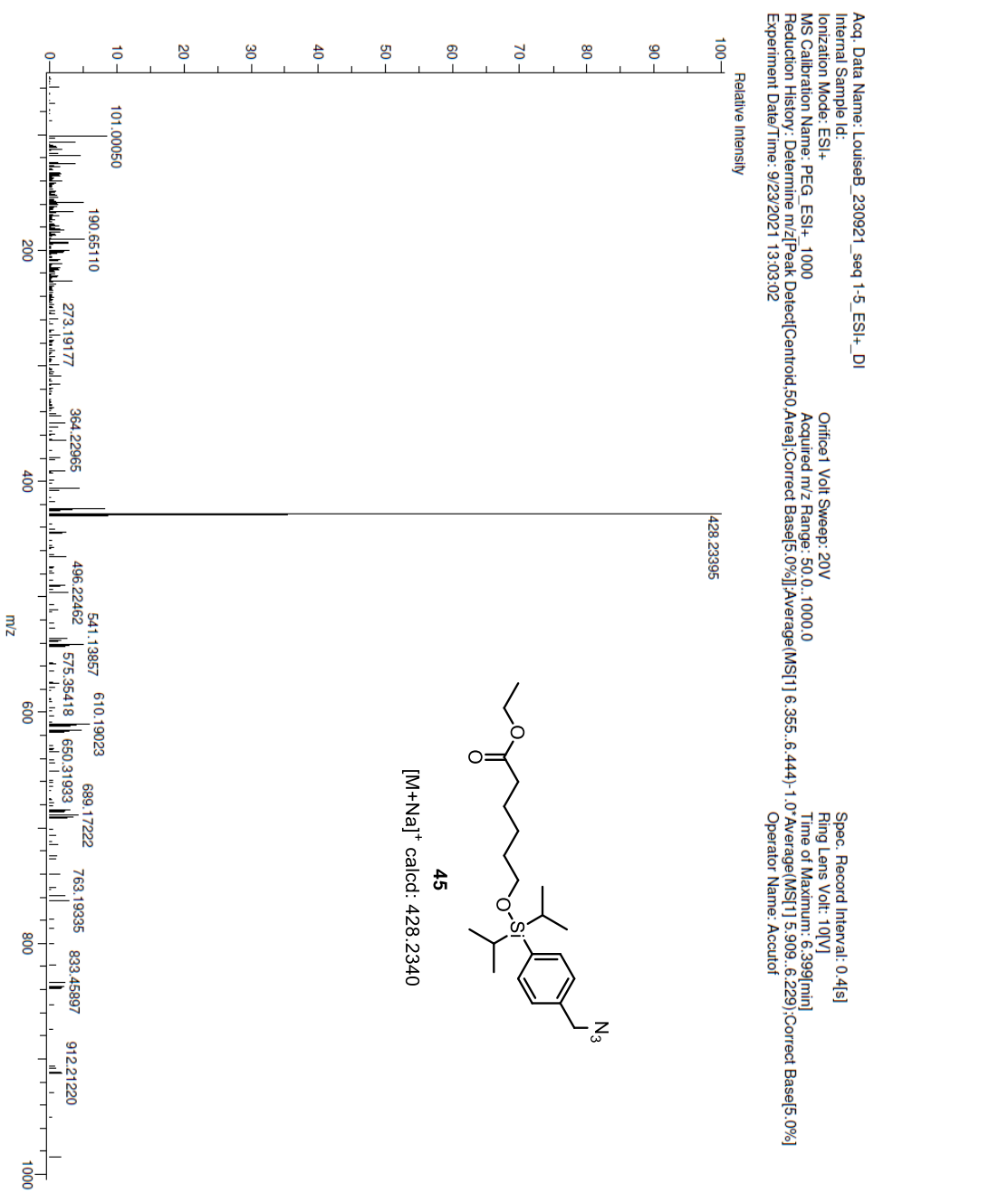

Figure A-50. ^{1}H-NMR spectrum of compound 46

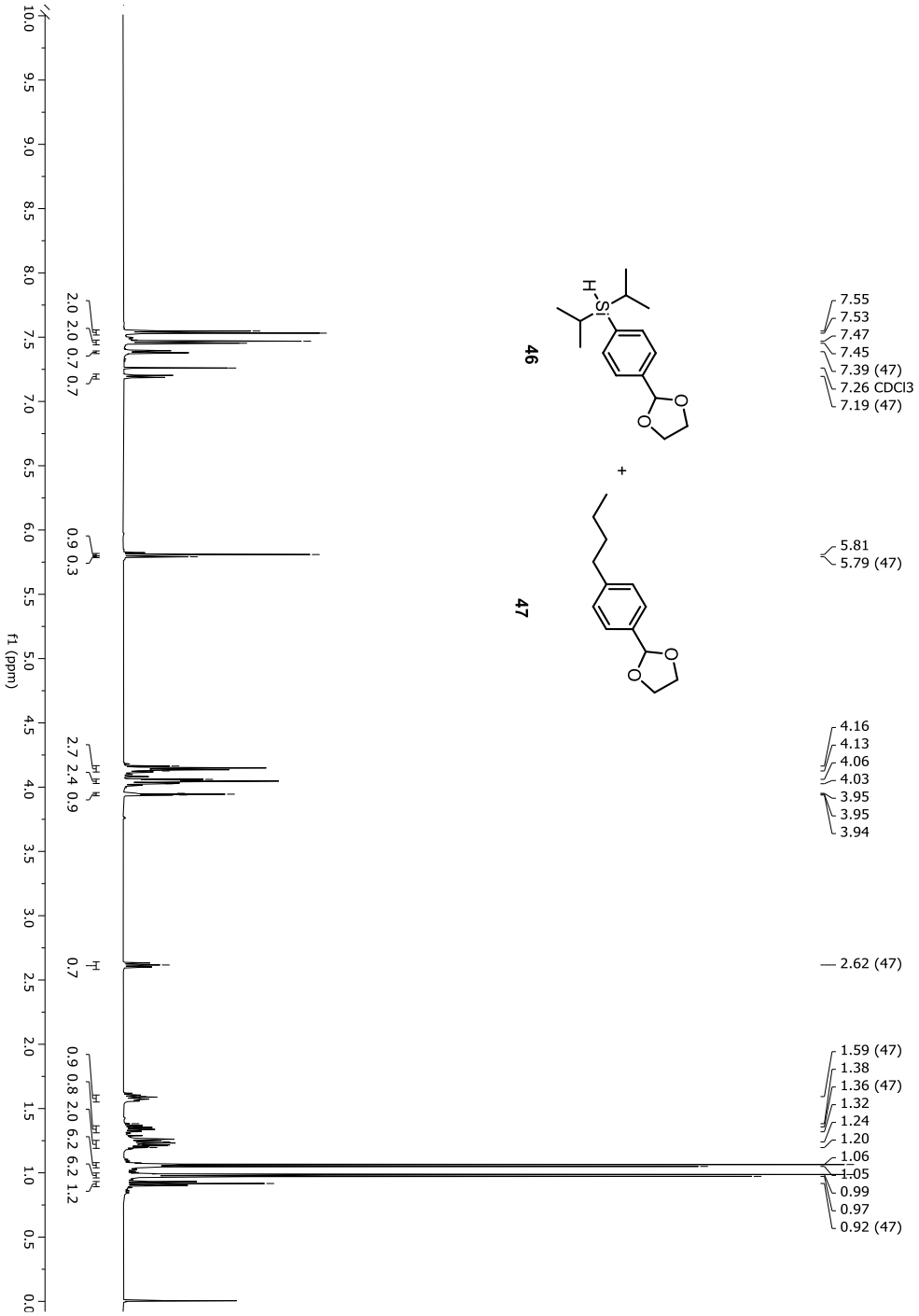

Figure A-51. ^{13}C-NMR spectrum of compound 46

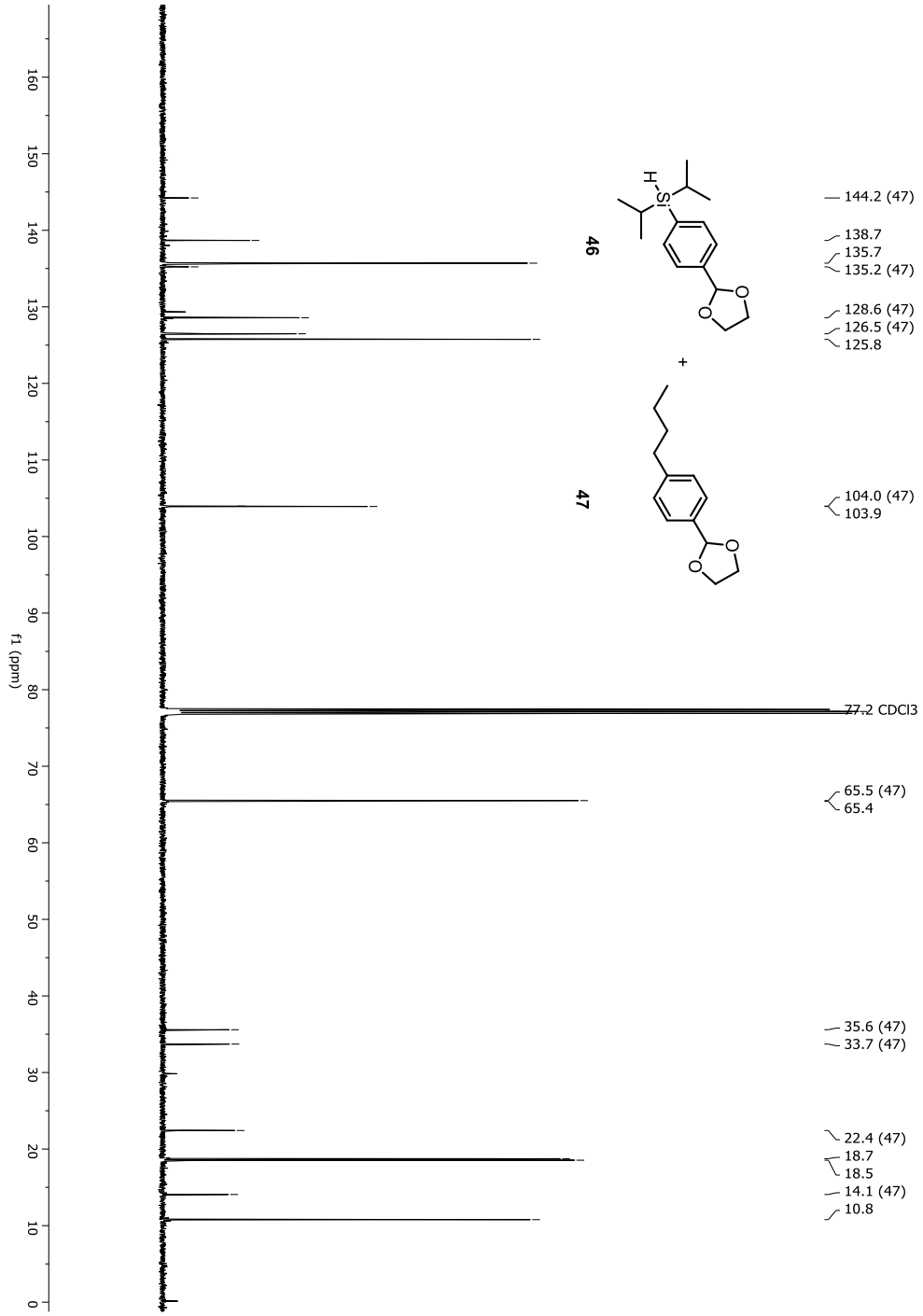

Figure A-52. ^{1}H-NMR spectrum of compound 49

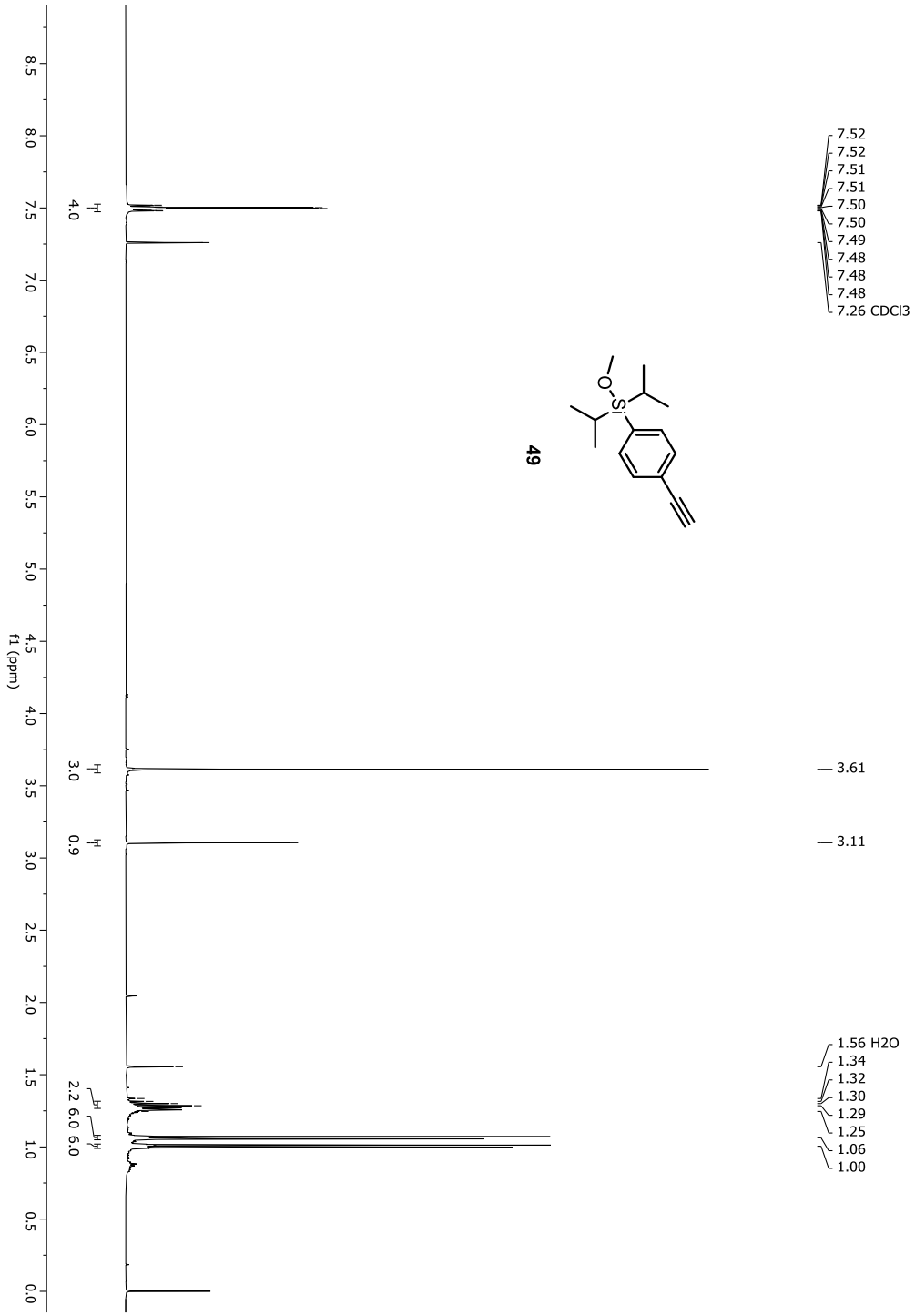

Figure A-53. ^{13}C-NMR spectrum of compound 77

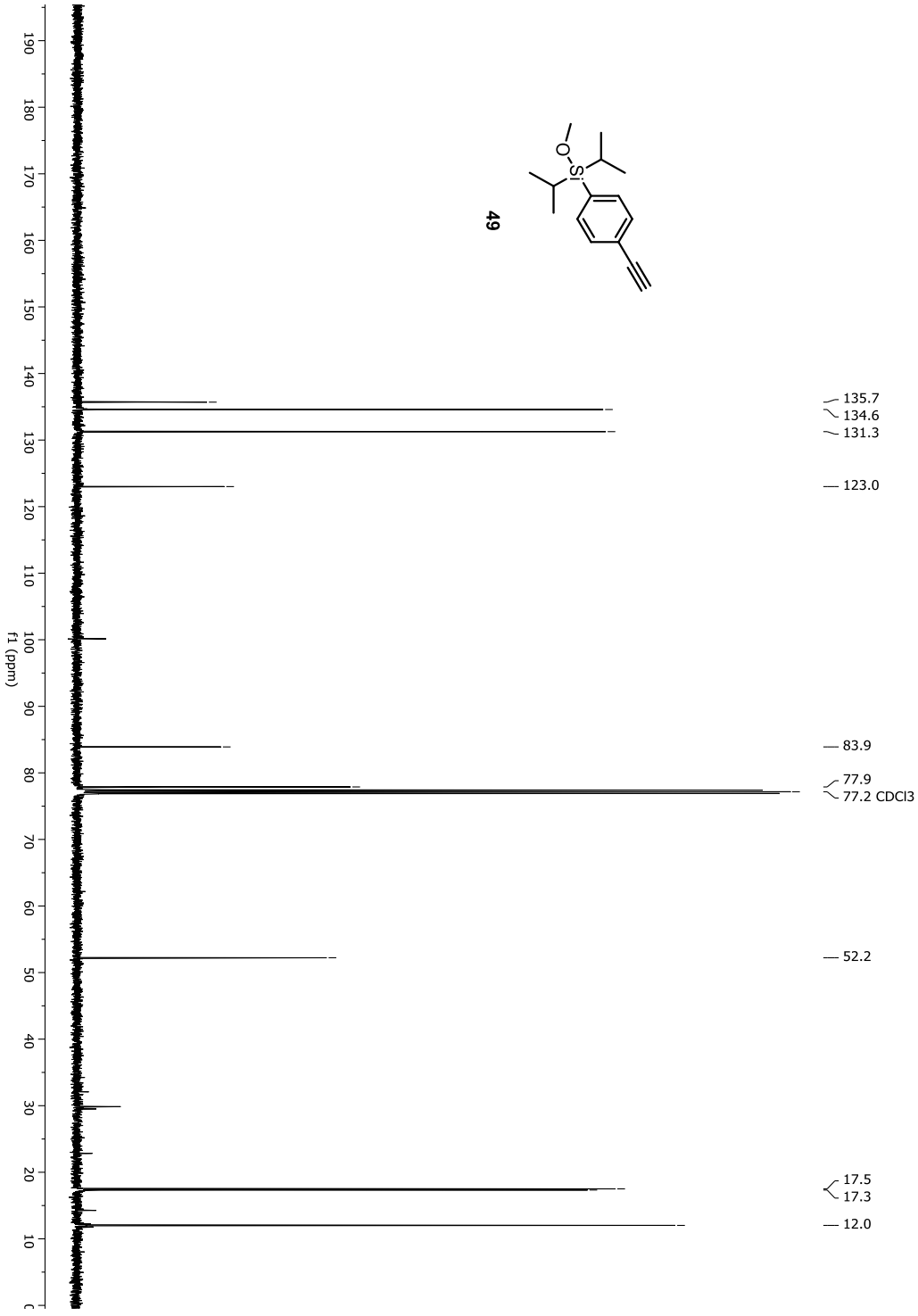

Figure A-54. HRMS spectrum of compound 77

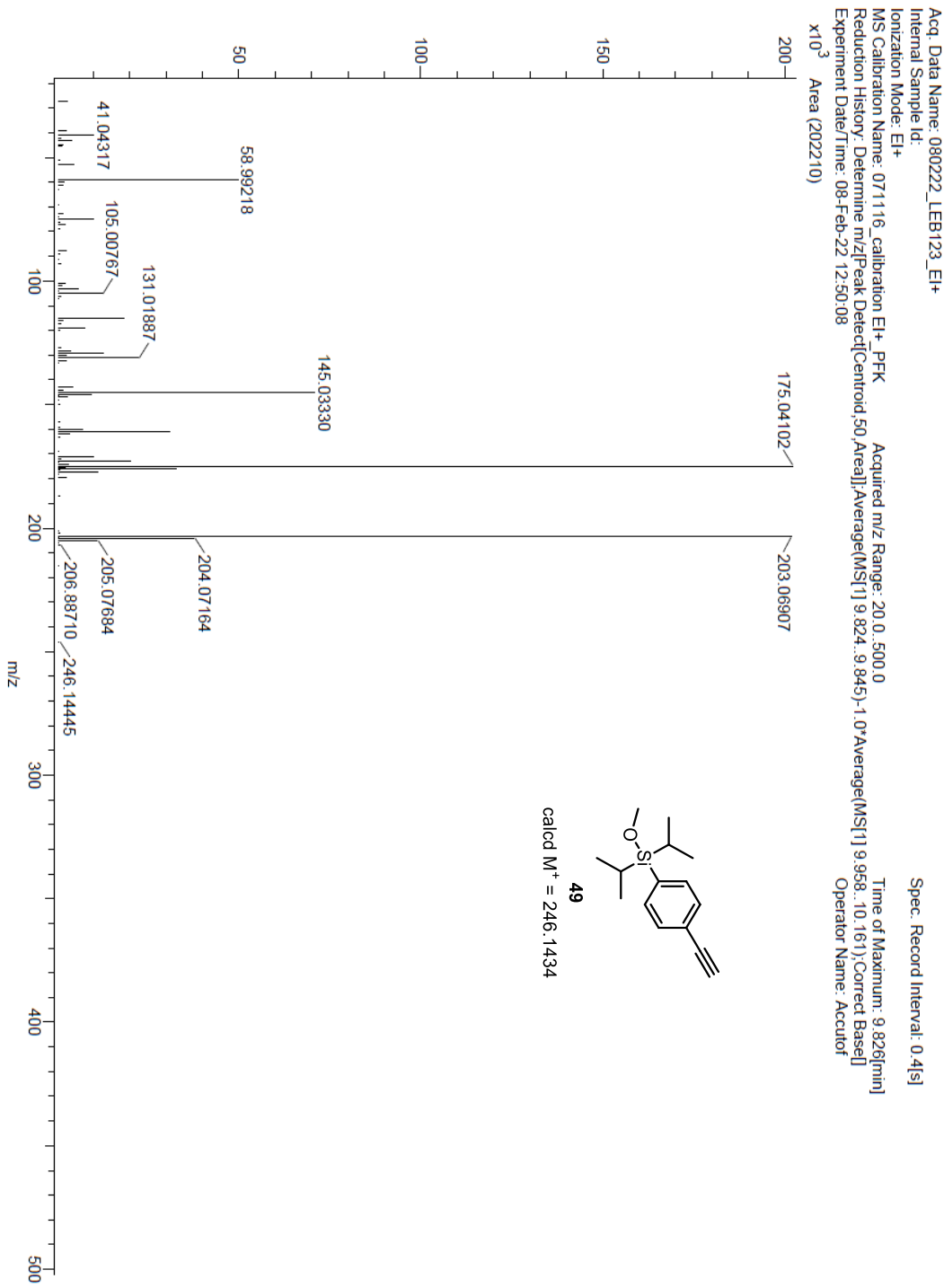

Figure A-55. ^{1}H-NMR spectrum of compound 50

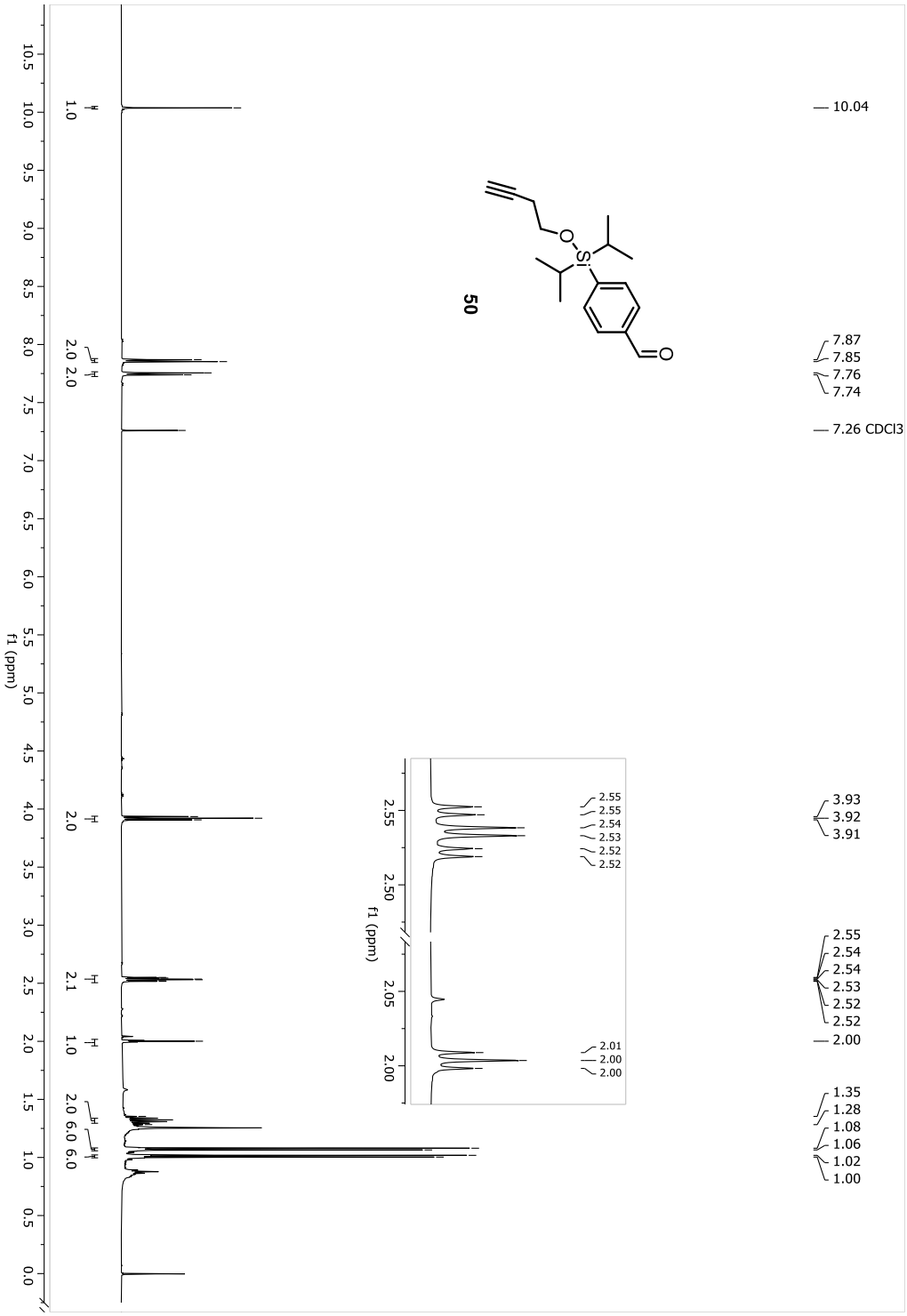

Figure A-56. ^{13}C-NMR spectrum of compound 50

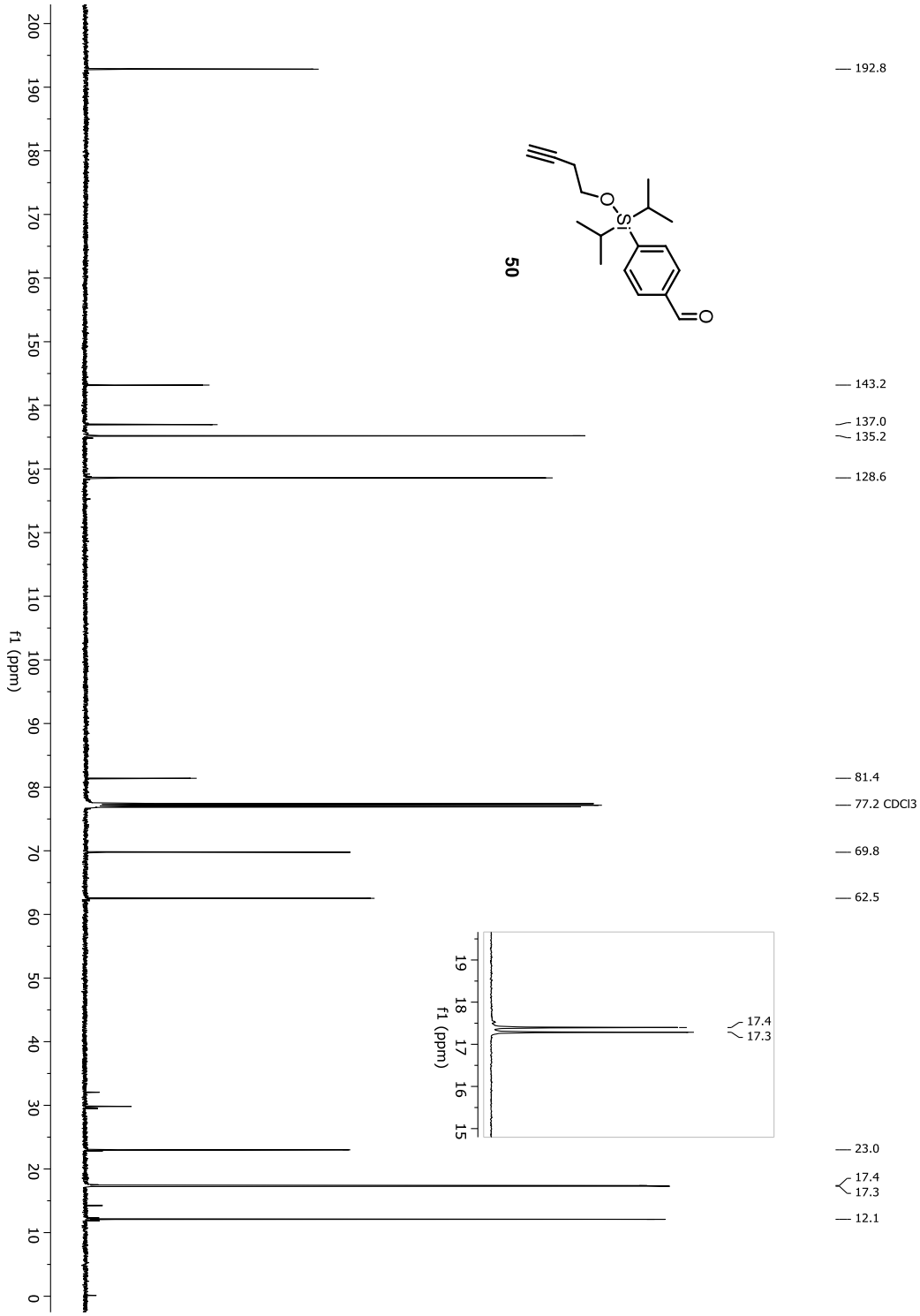

Figure A-57. HRMS spectrum of compound 54

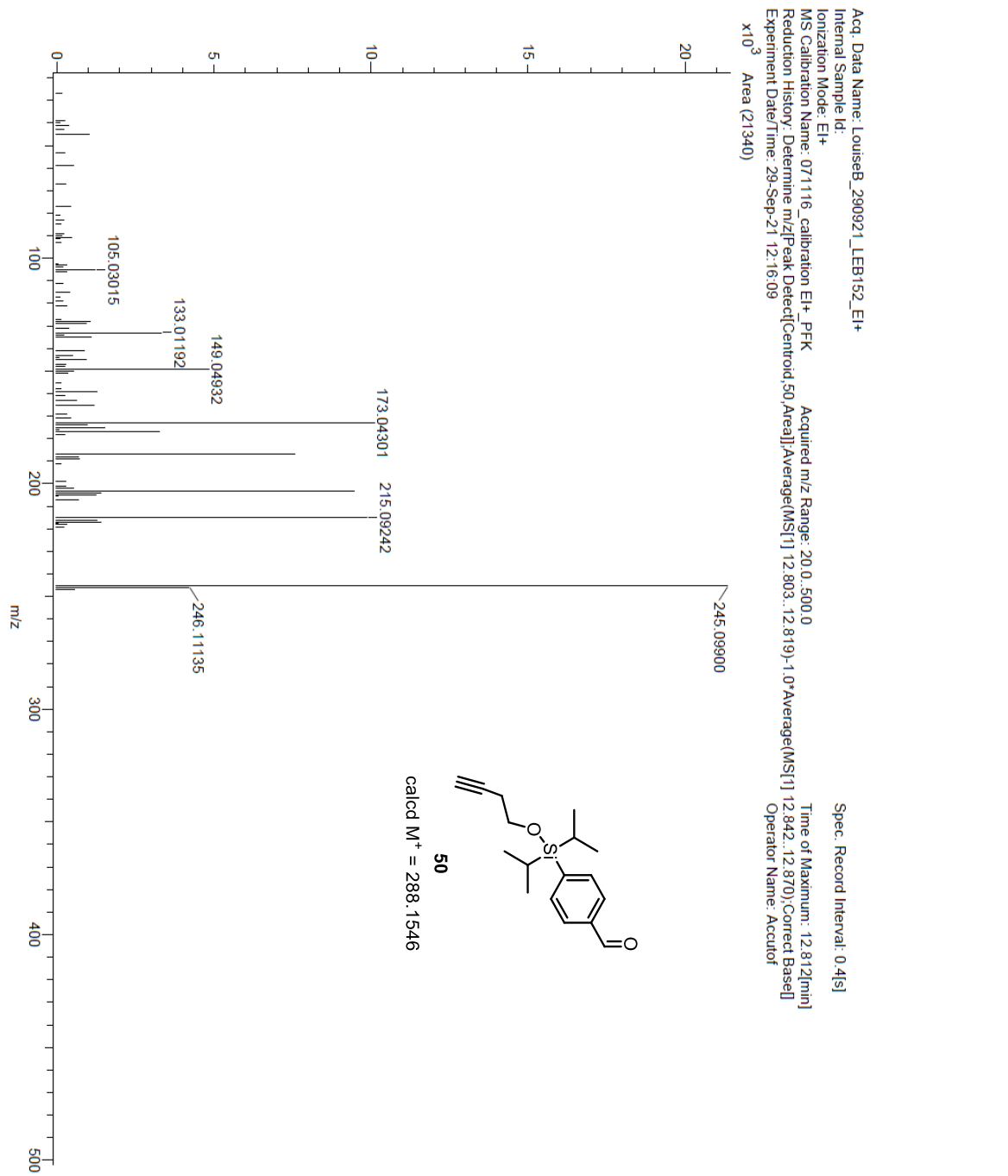

Figure A-58. ^{1}H NMR spectrum of compound 51

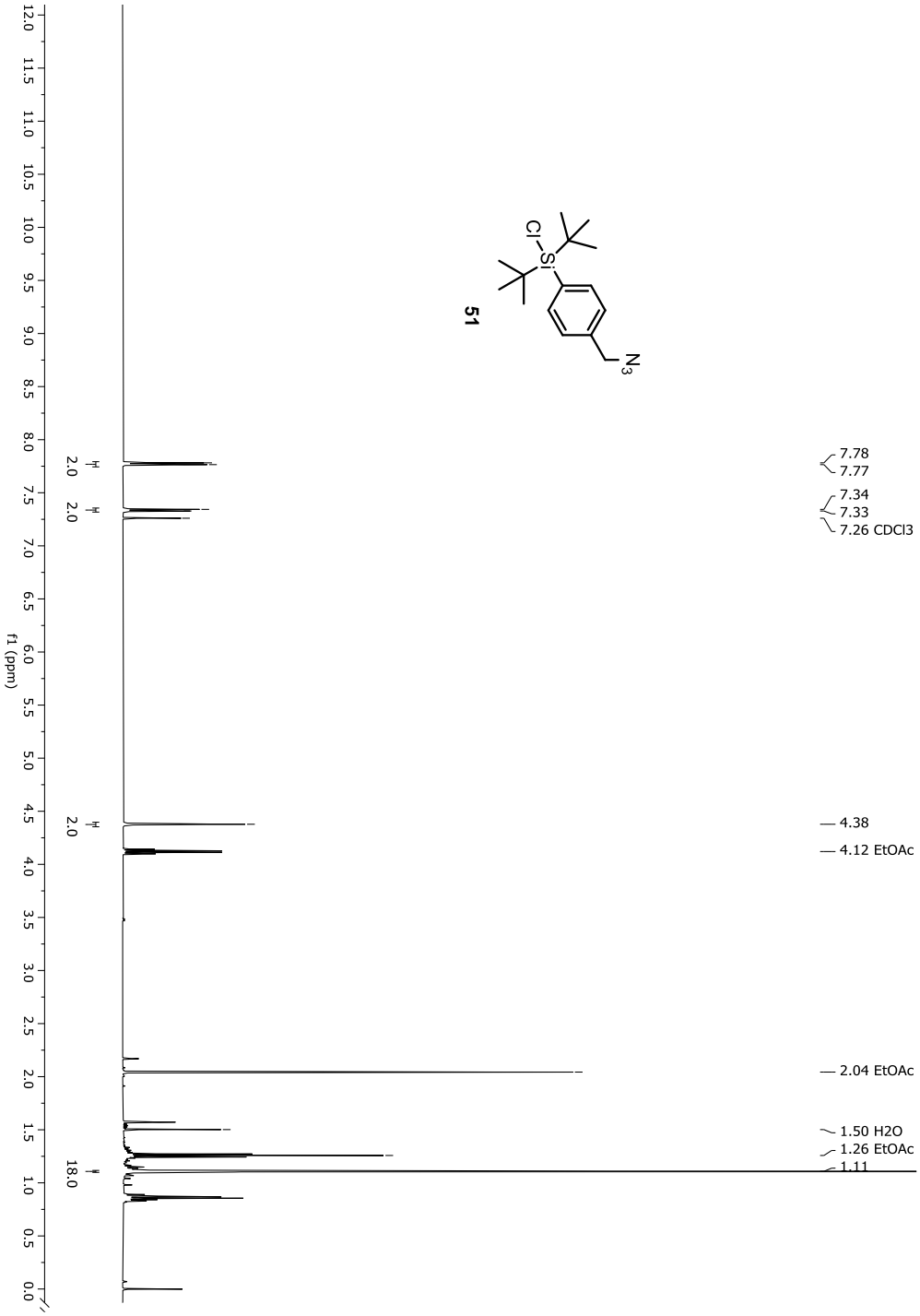

Figure A-59. ^{13}C NMR spectrum of compound 51

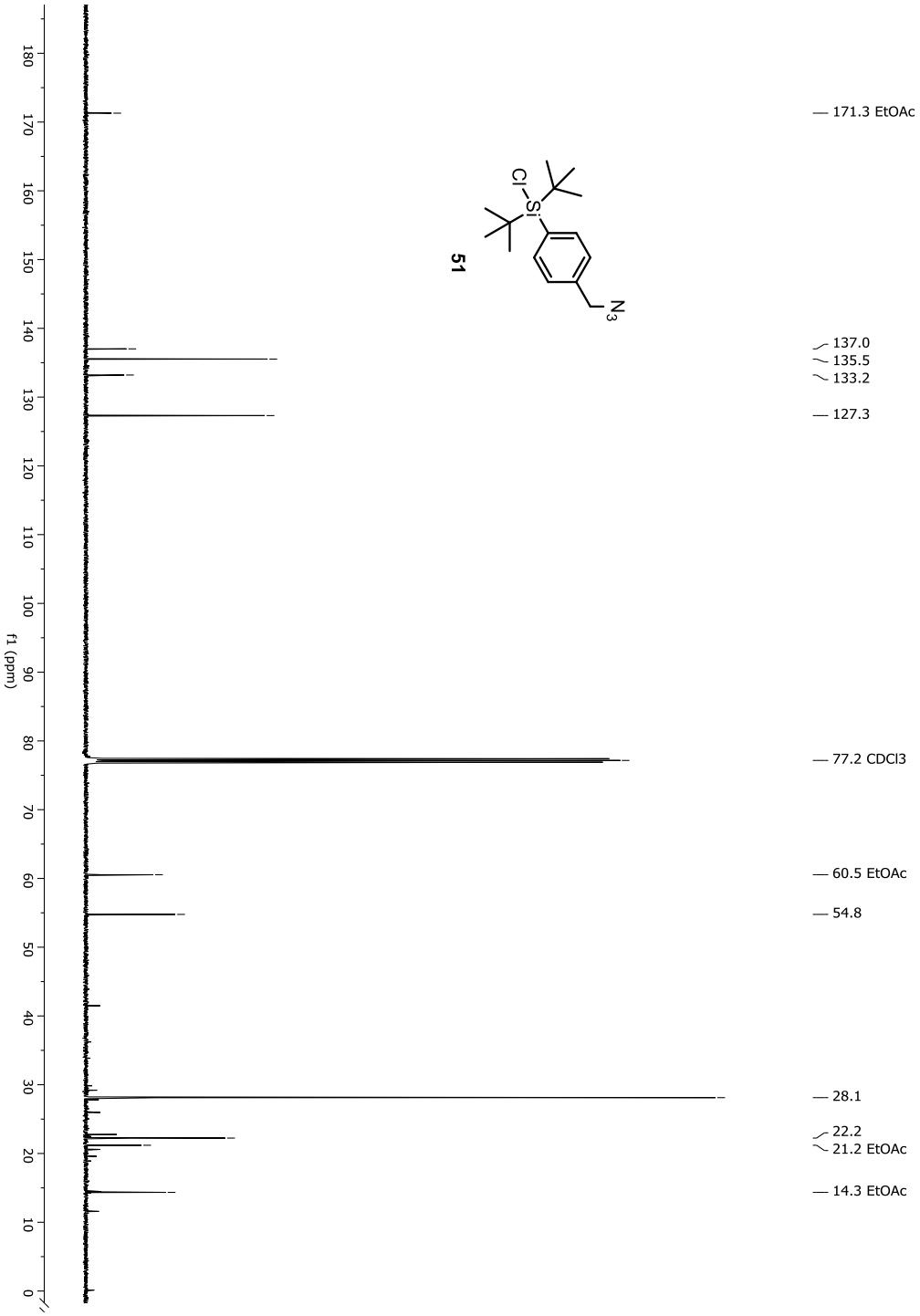

Figure A-60. ^{1}H-NMR spectrum of compound 53

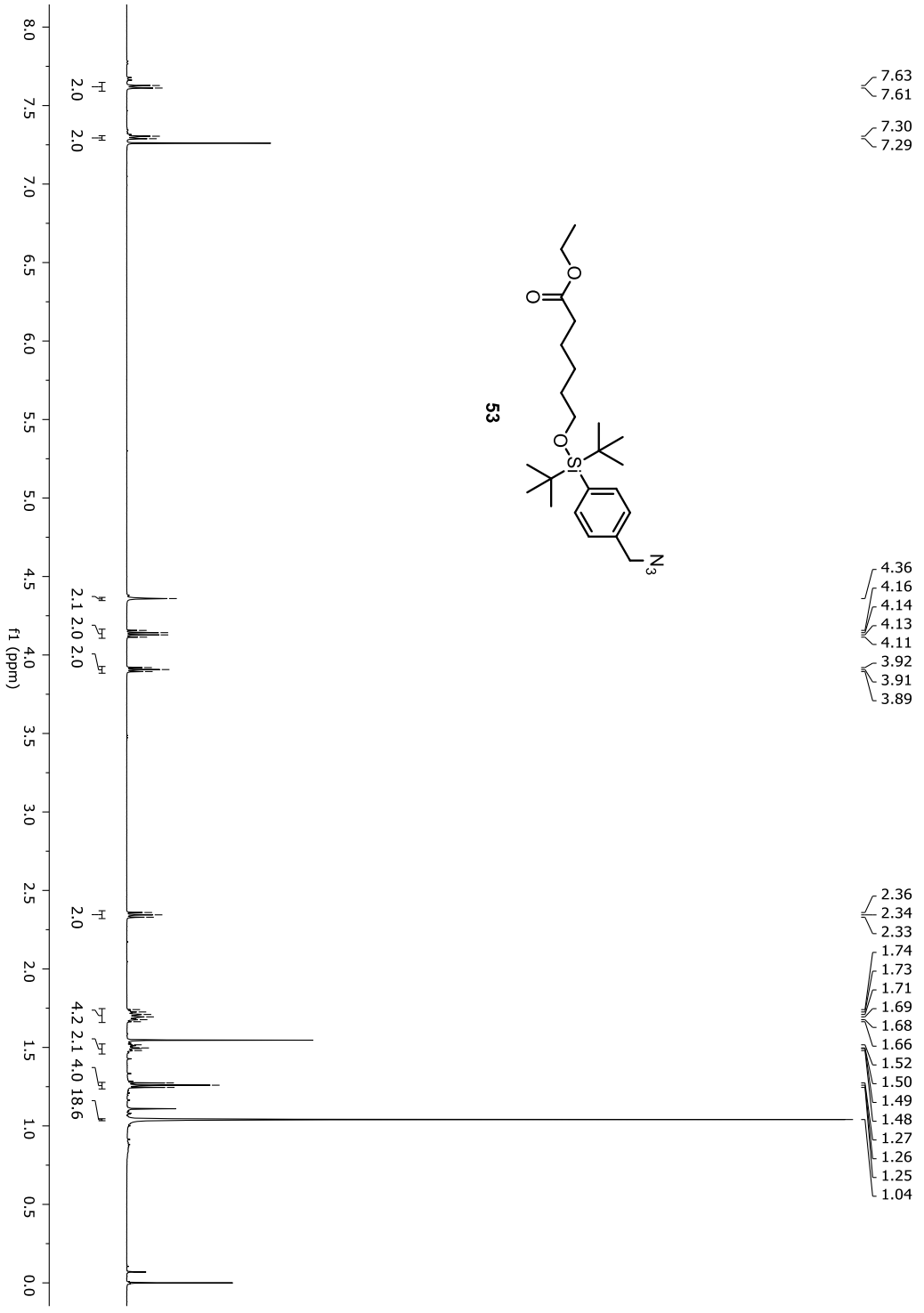

Figure A-61. ^{13}C-NMR spectrum of compound 53

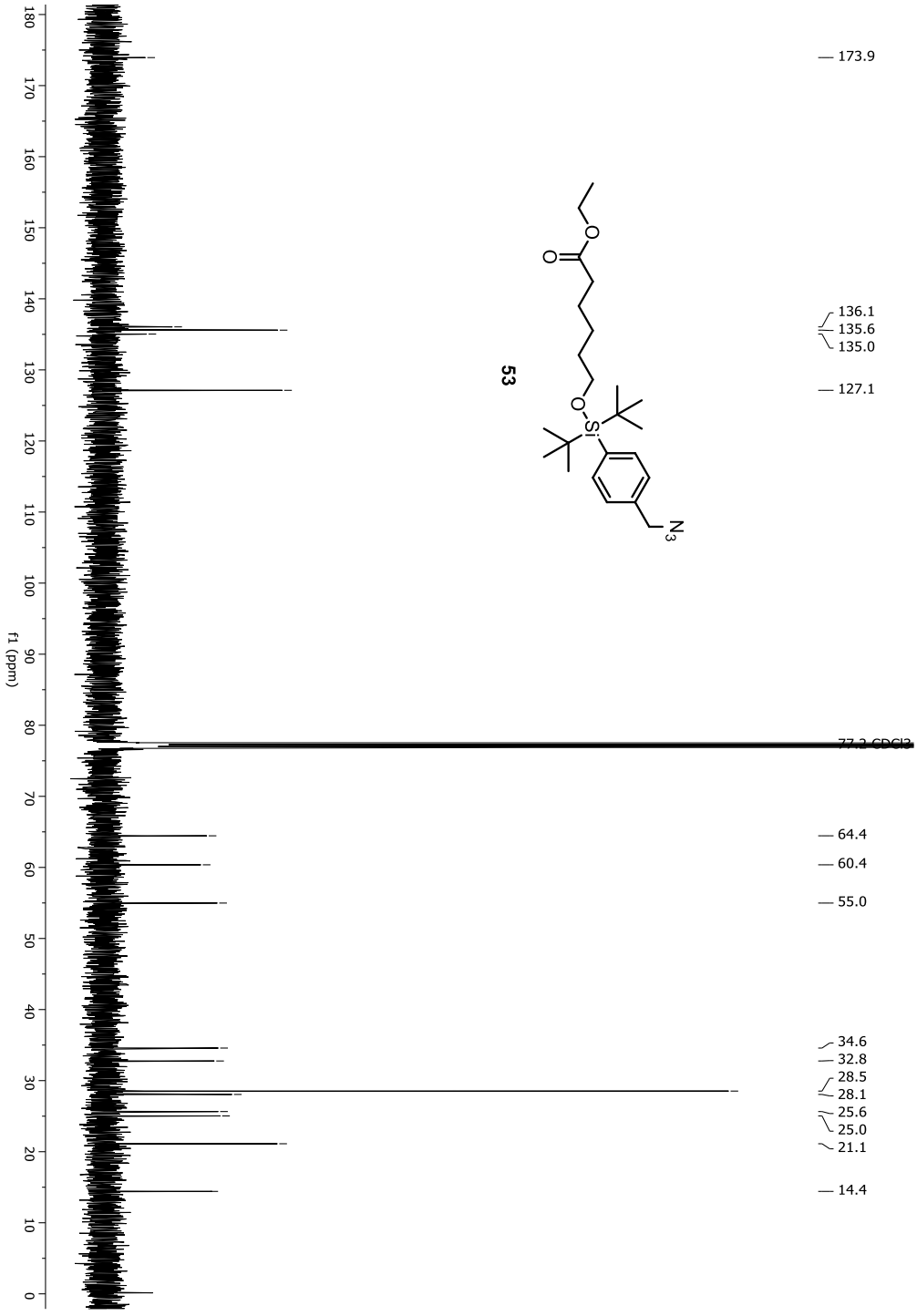

Figure A-62. HRMS spectrum of compound 85

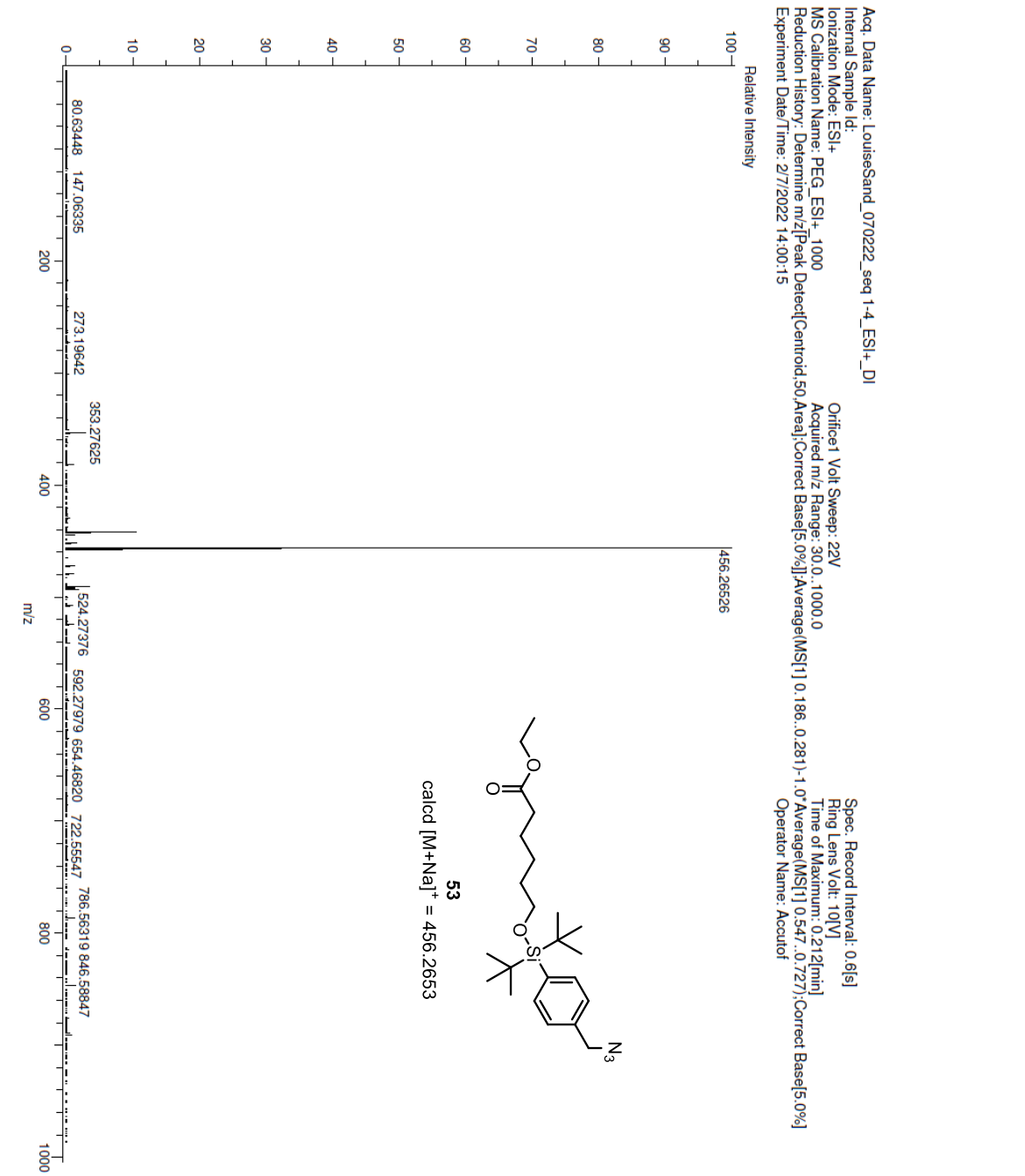

Figure A-63. ^{1}H-NMR spectrum of compound 59

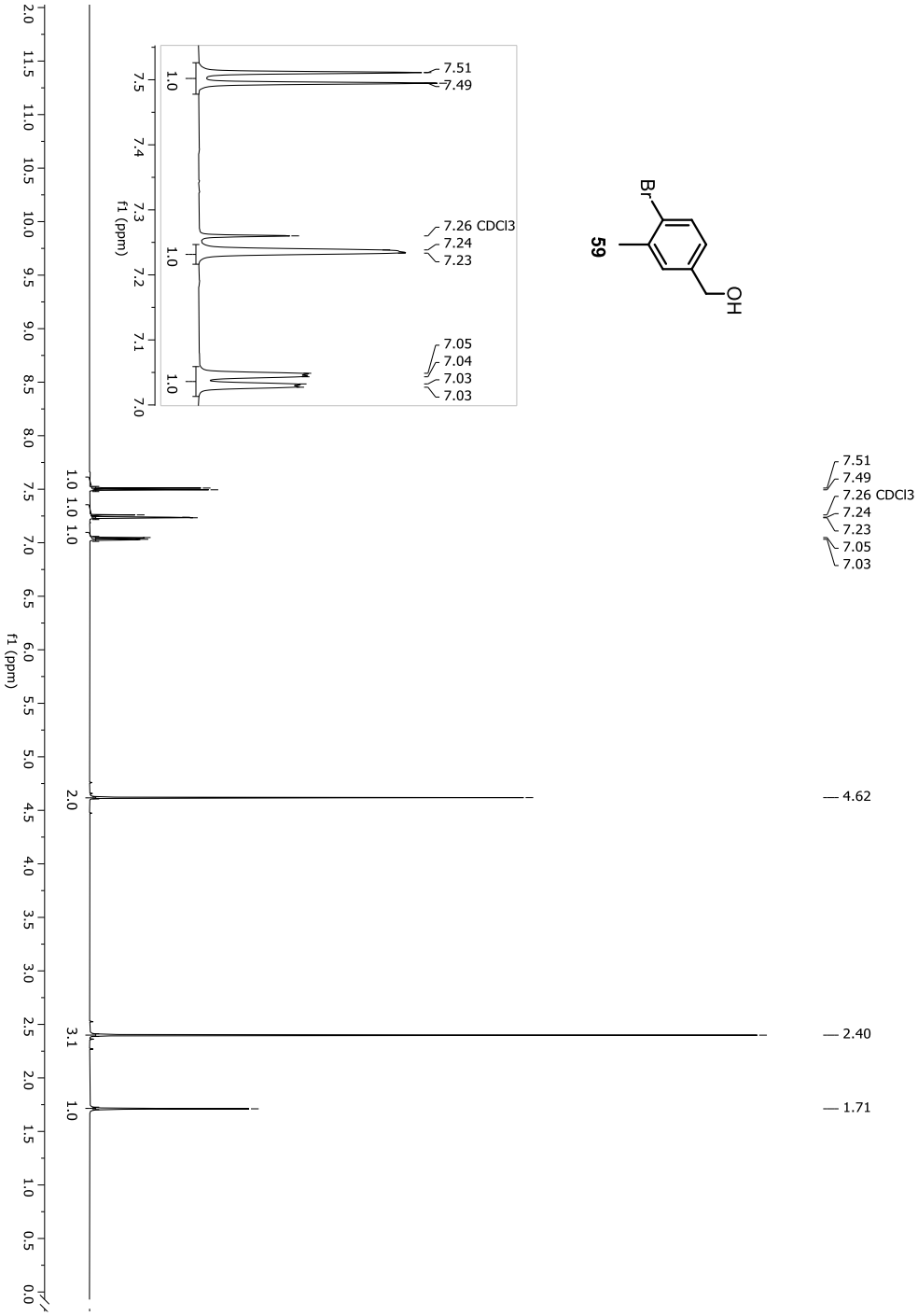

Figure A-64. ^{13}C-NMR spectrum of compound 59

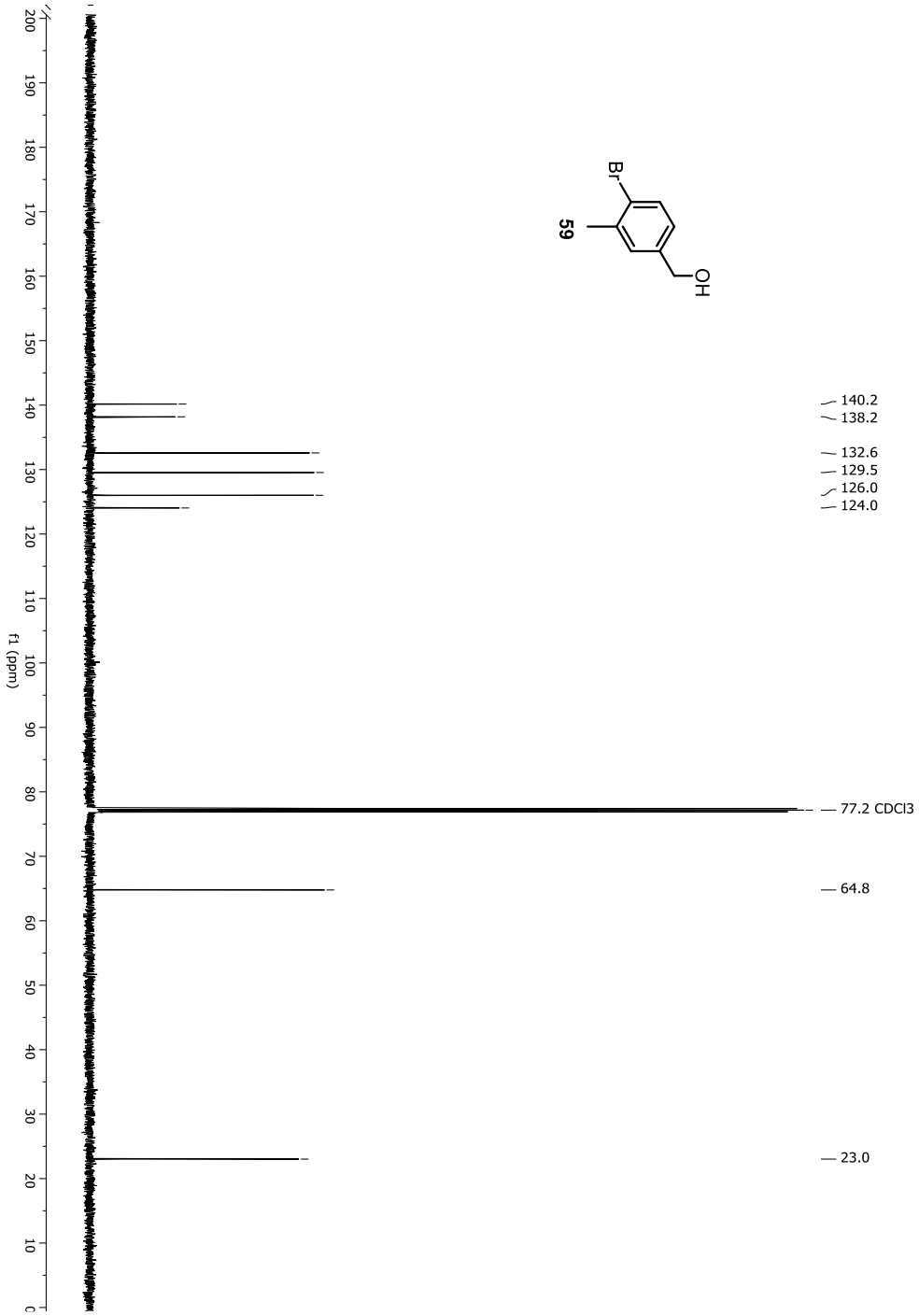

Figure A-65. ^{1}H-NMR spectrum of compound 60

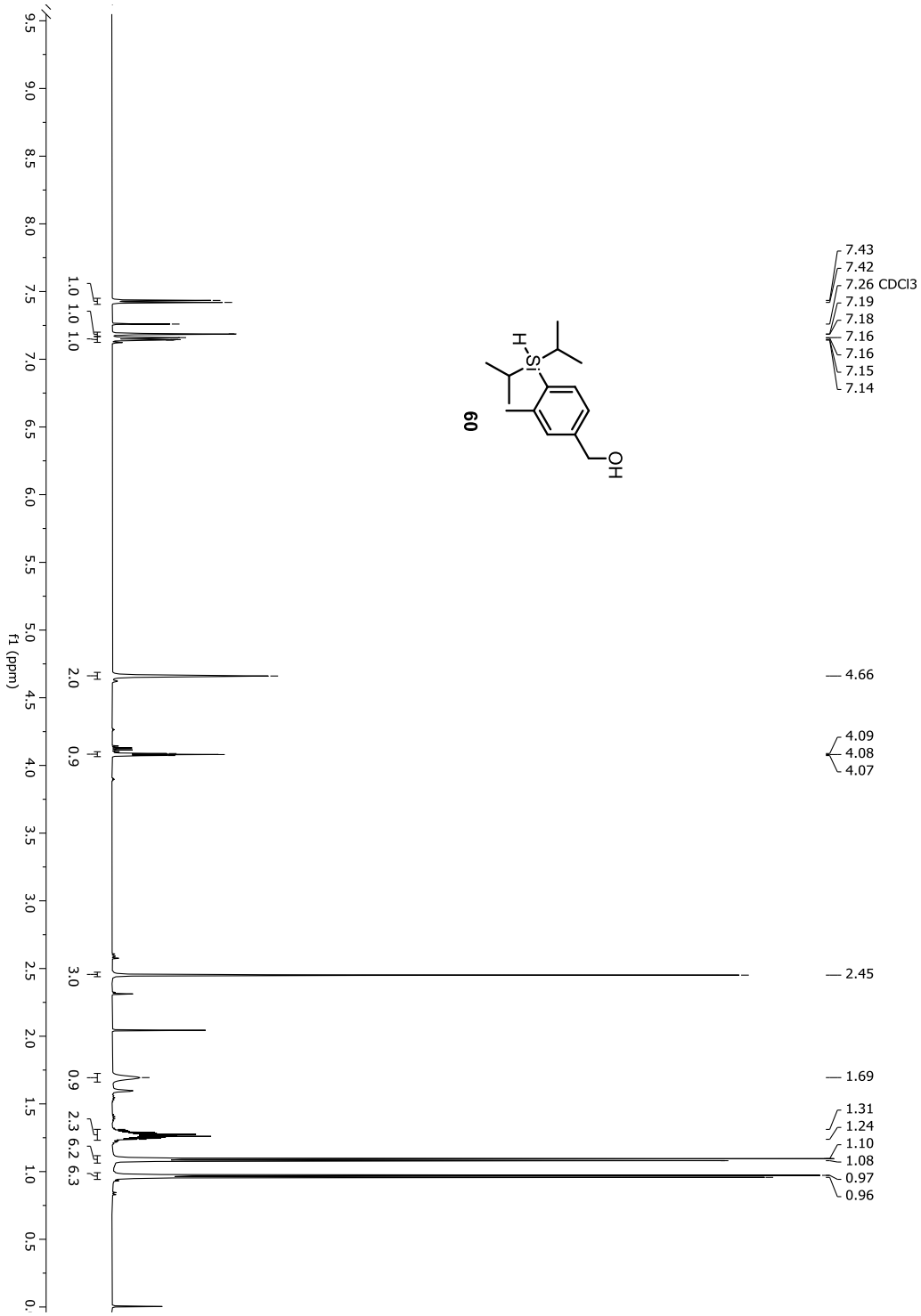

Figure A-66. ^{13}C-NMR spectrum of compound 60

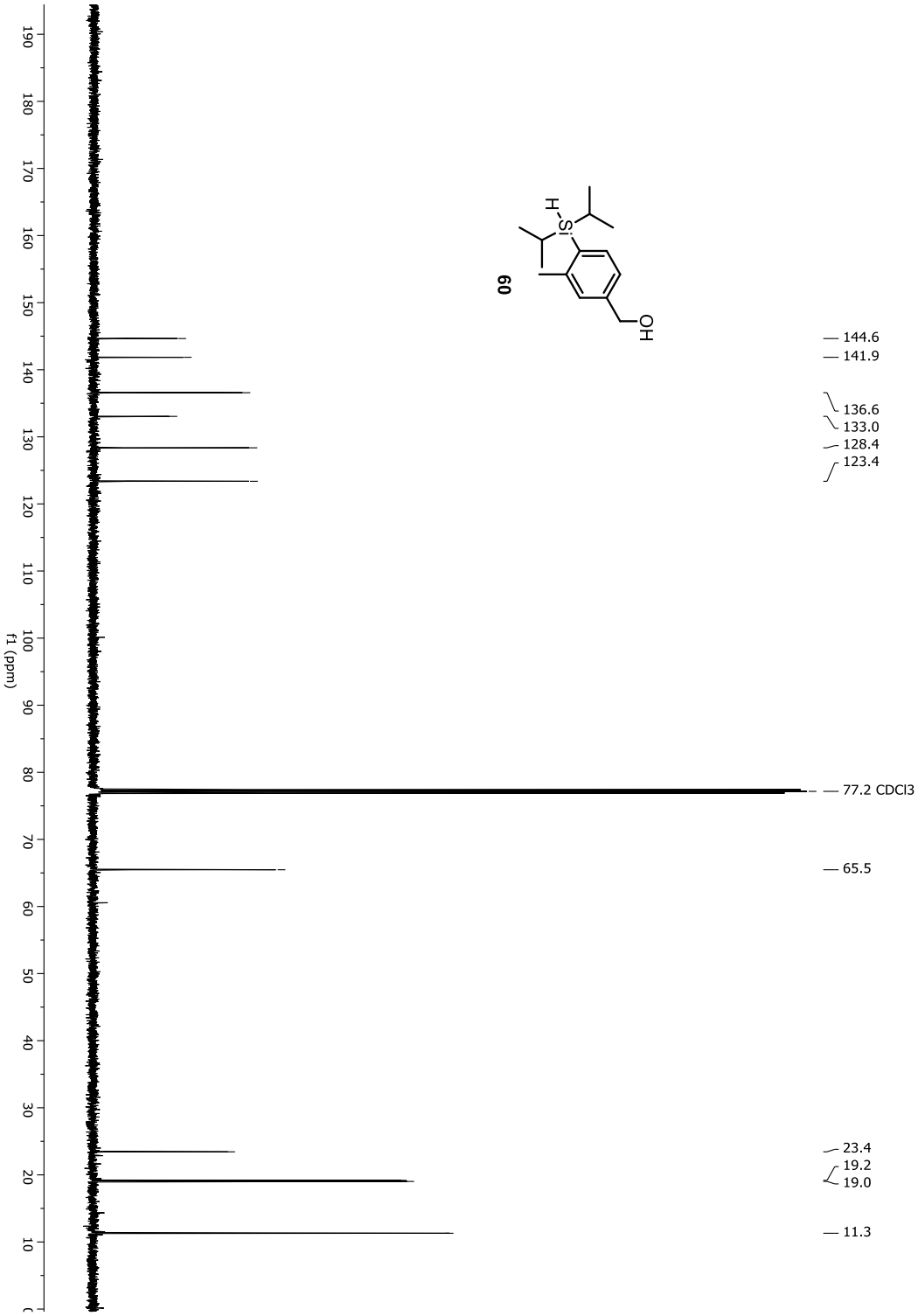

Figure A-67. HRMS spectrum of compound 60

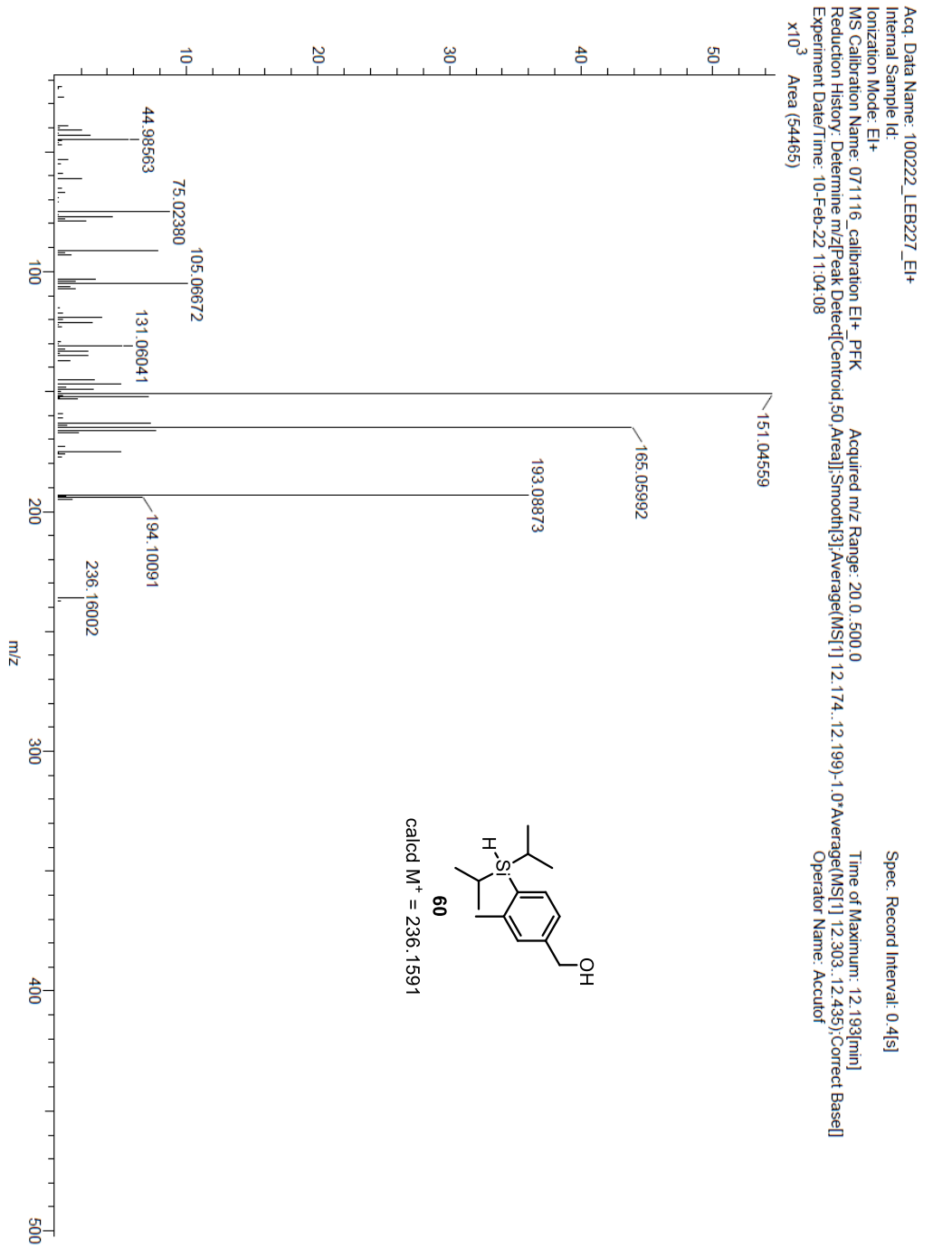

Figure A-68. ^{1}H-NMR spectrum of compound 61

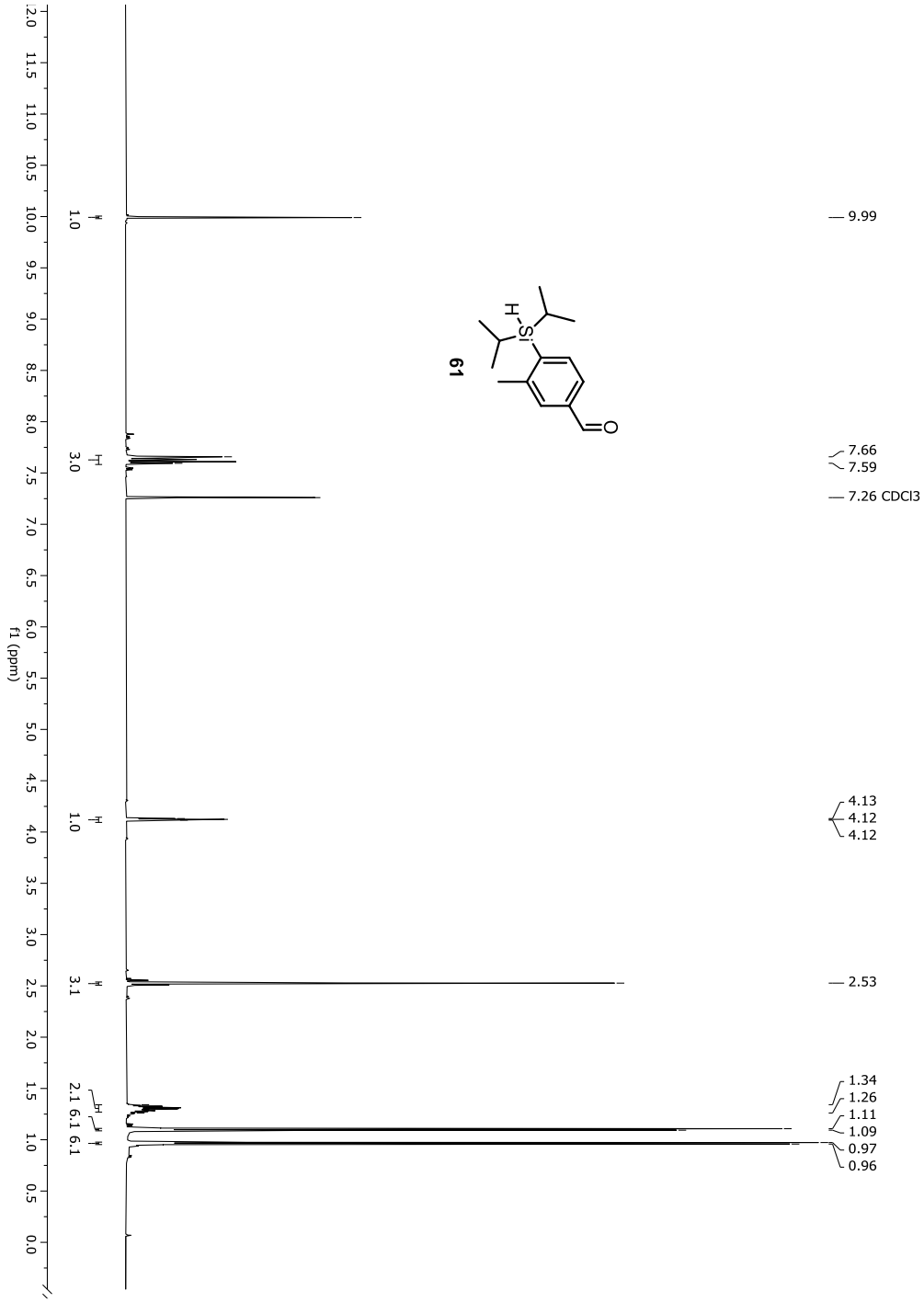

Figure A-69. ^{13}C-NMR spectrum of compound 61

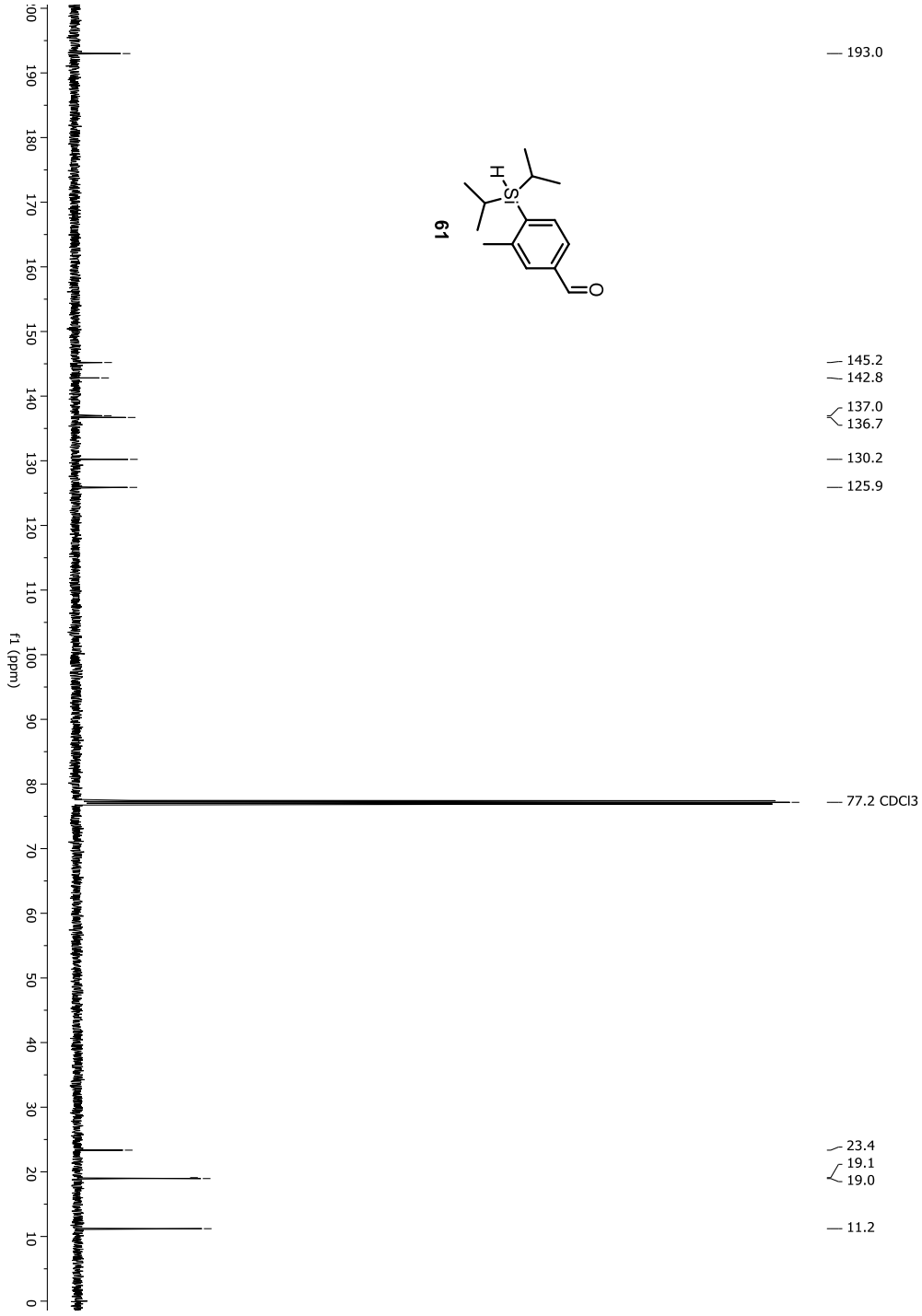

Figure A-70. HRMS spectrum of compound 61

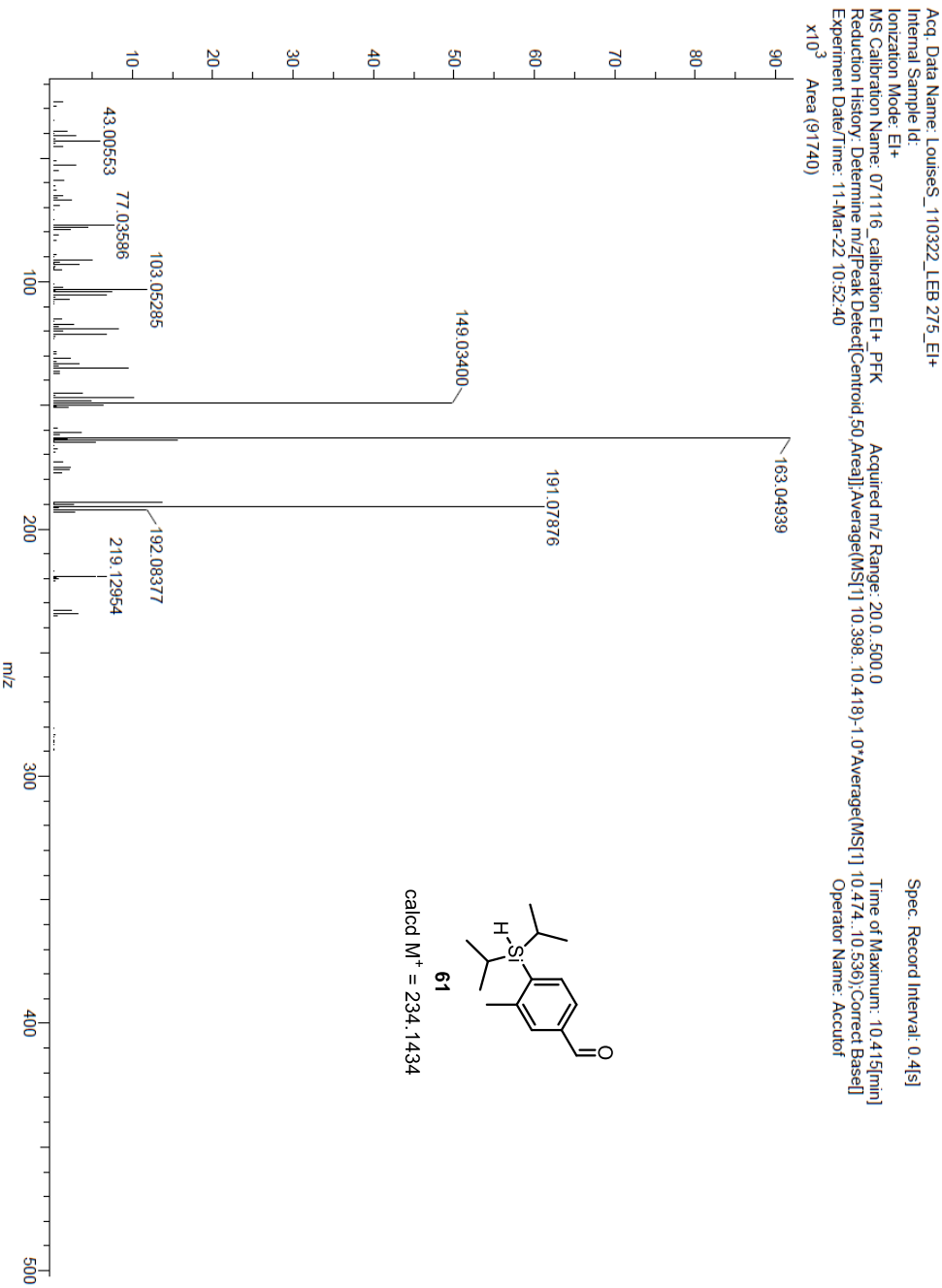

Figure A-71. ^{1}H-NMR spectrum of compound 62

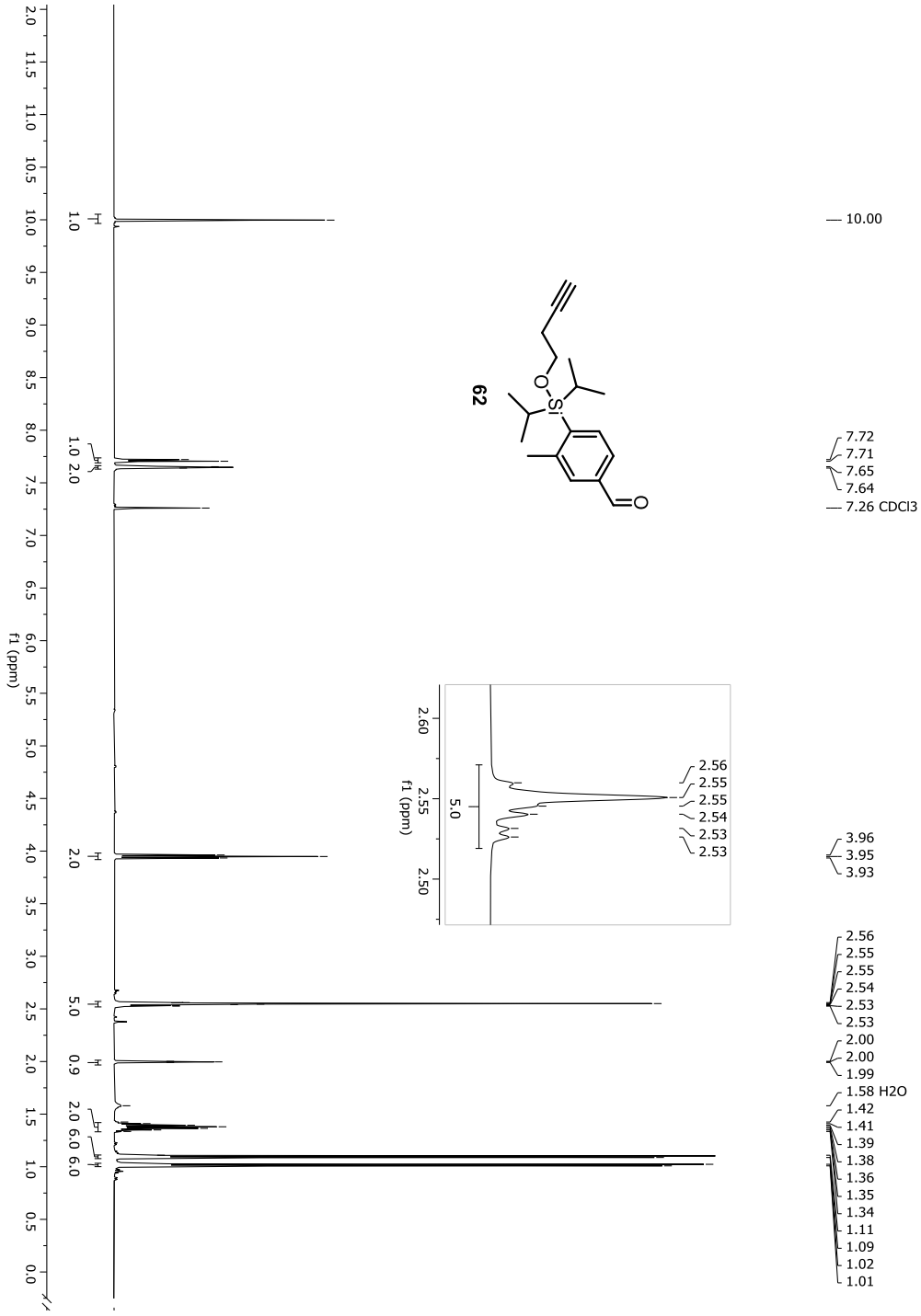

Figure A-72. ^{13}C-NMR spectrum of compound 62

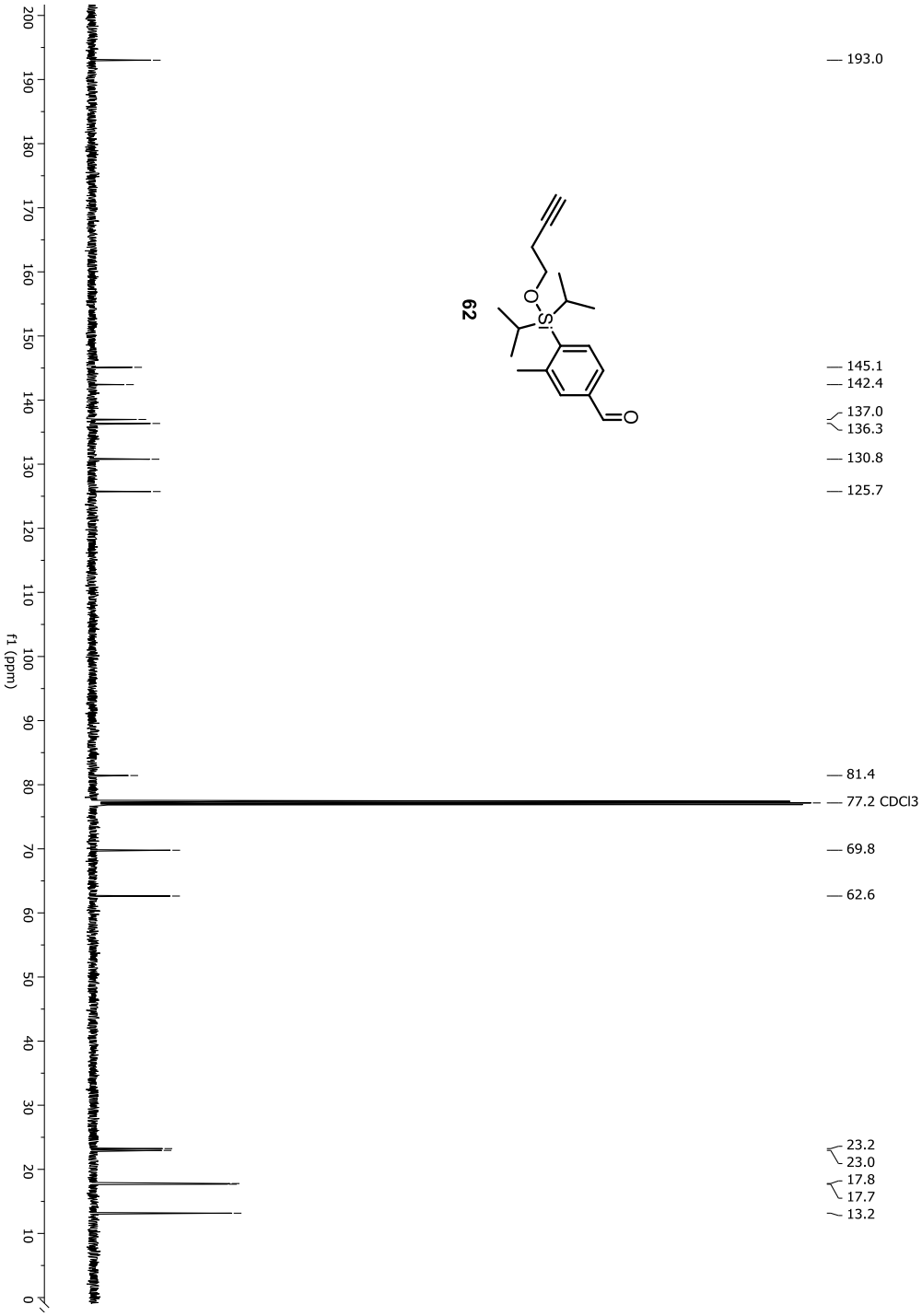

Figure A-73. HRMS spectrum of compound 62

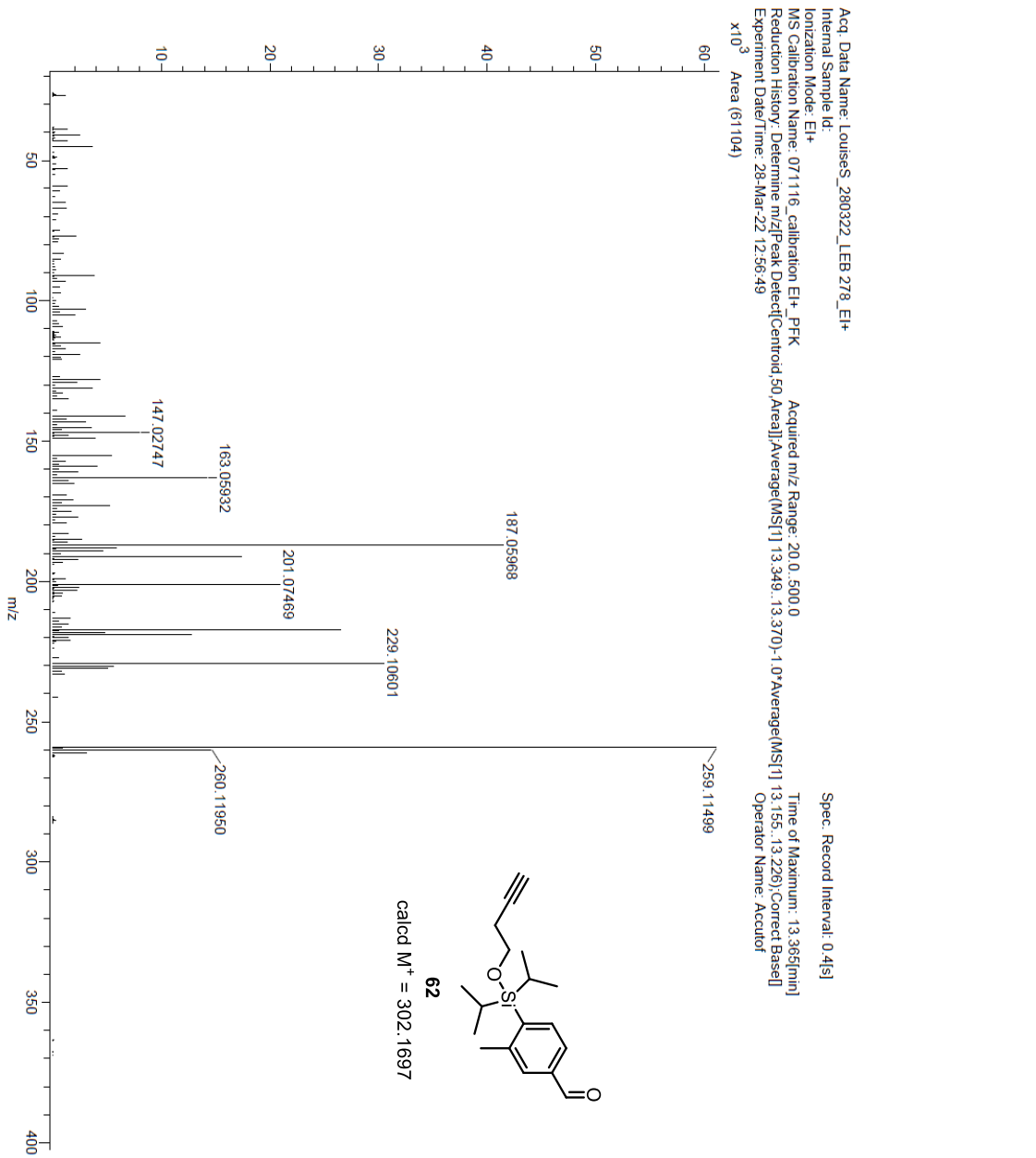

Figure A-74. ^{1}H-NMR spectrum of compound 63

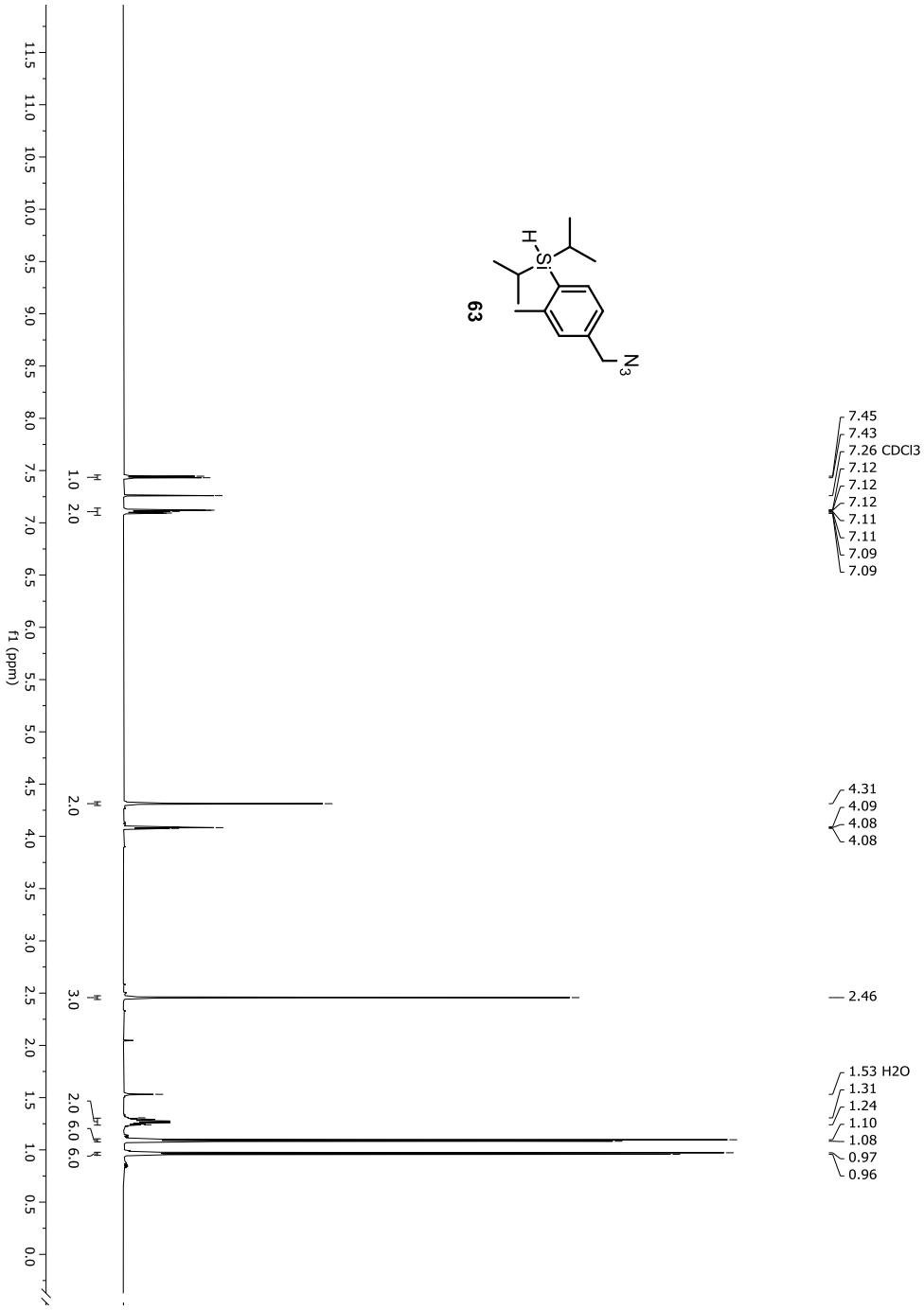

Figure A-75. ^{13}C-NMR spectrum of compound 63

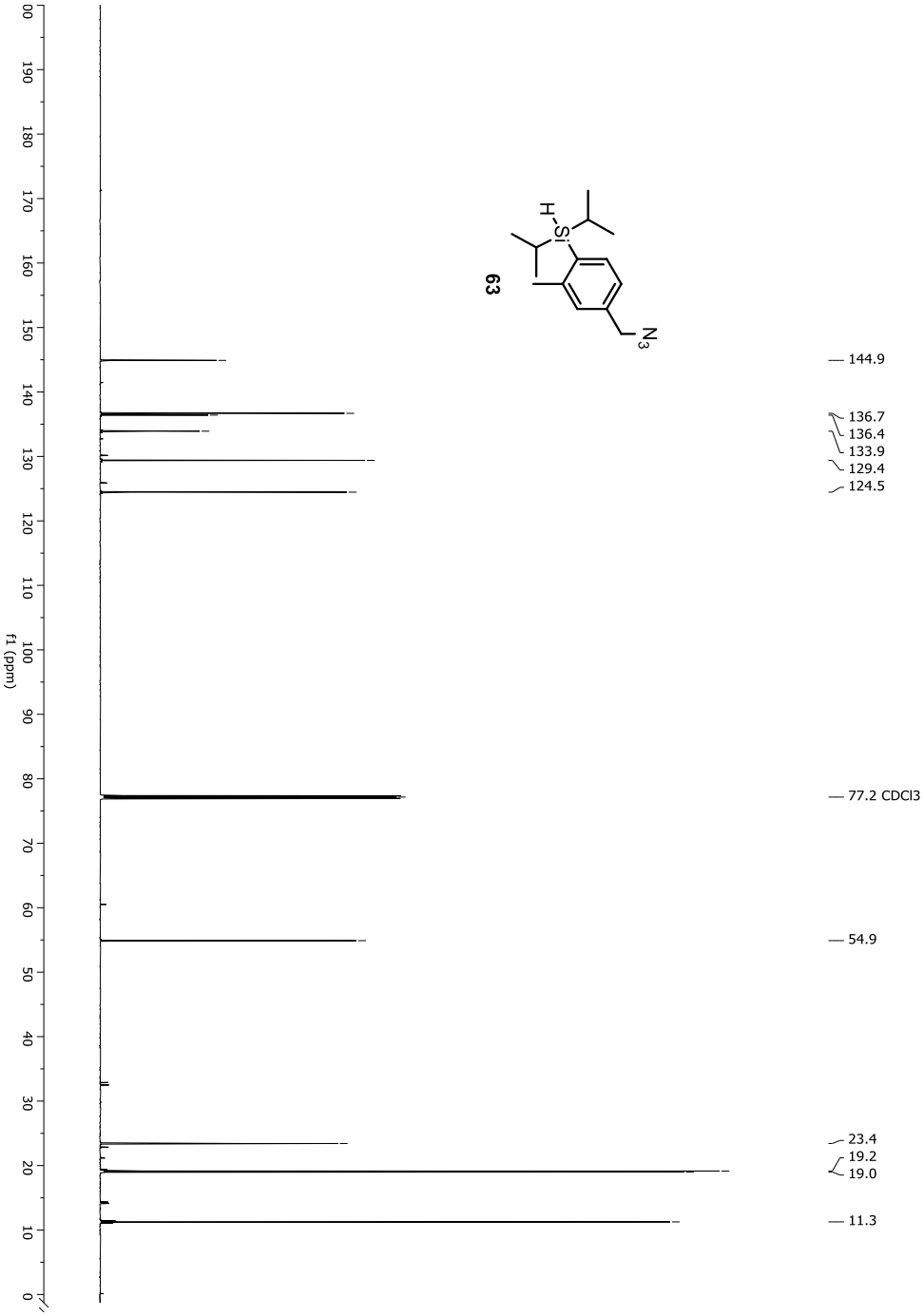

Figure A-76. HRMS spectrum of compound 63

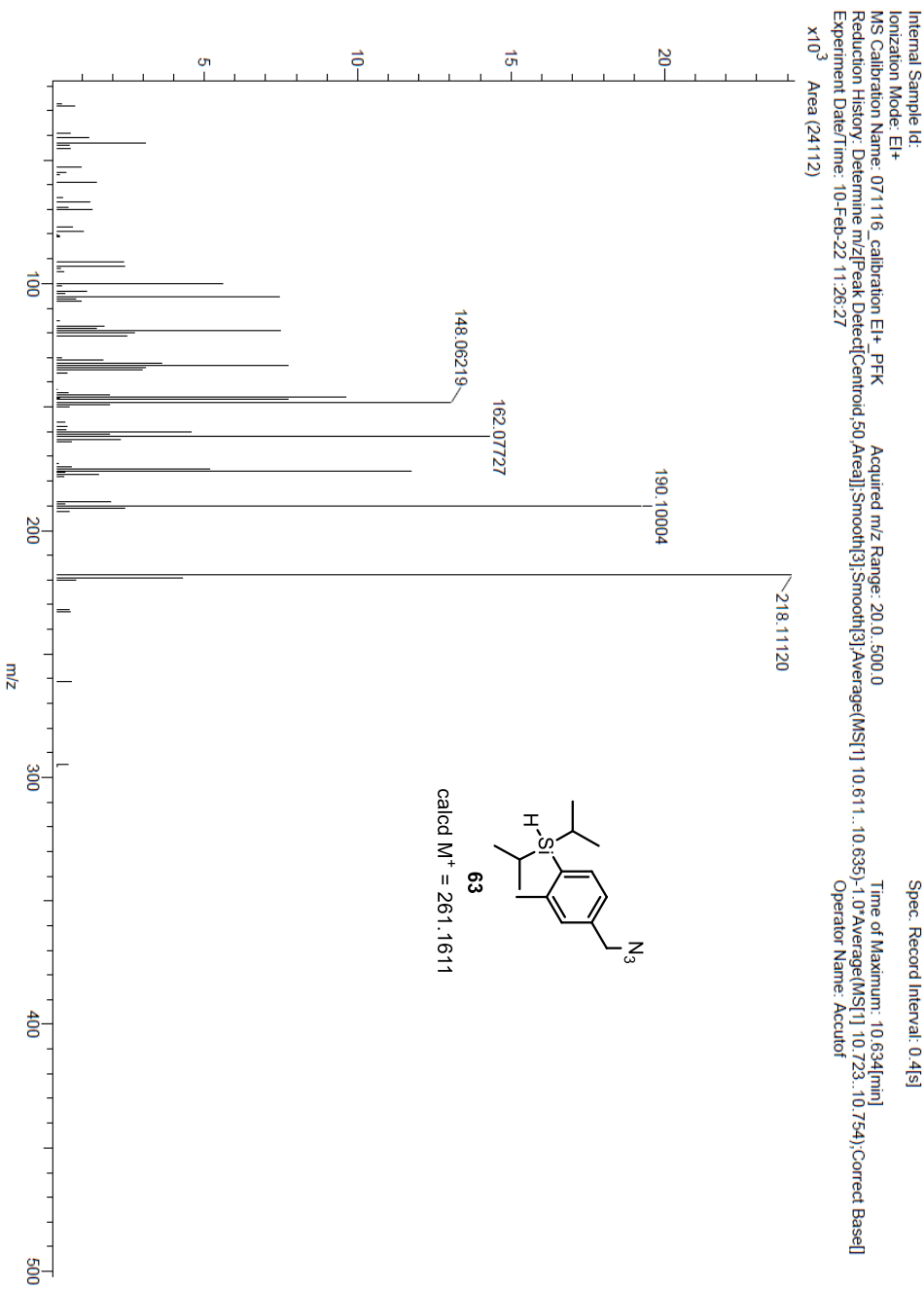

Figure A-77. ^{1}H-NMR spectrum of compound 64

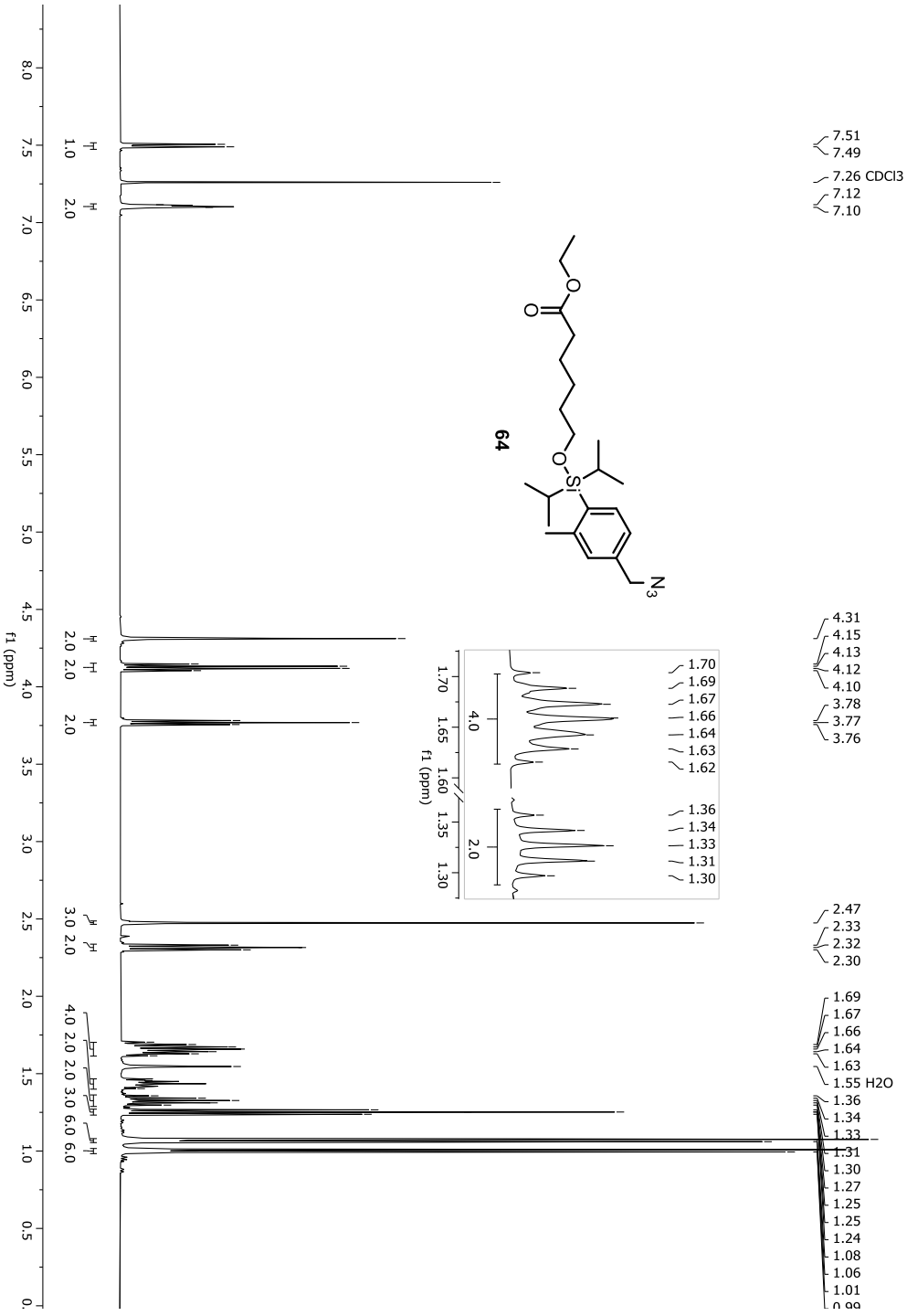

Figure A-78. ^{13}C-NMR spectrum of compound 64

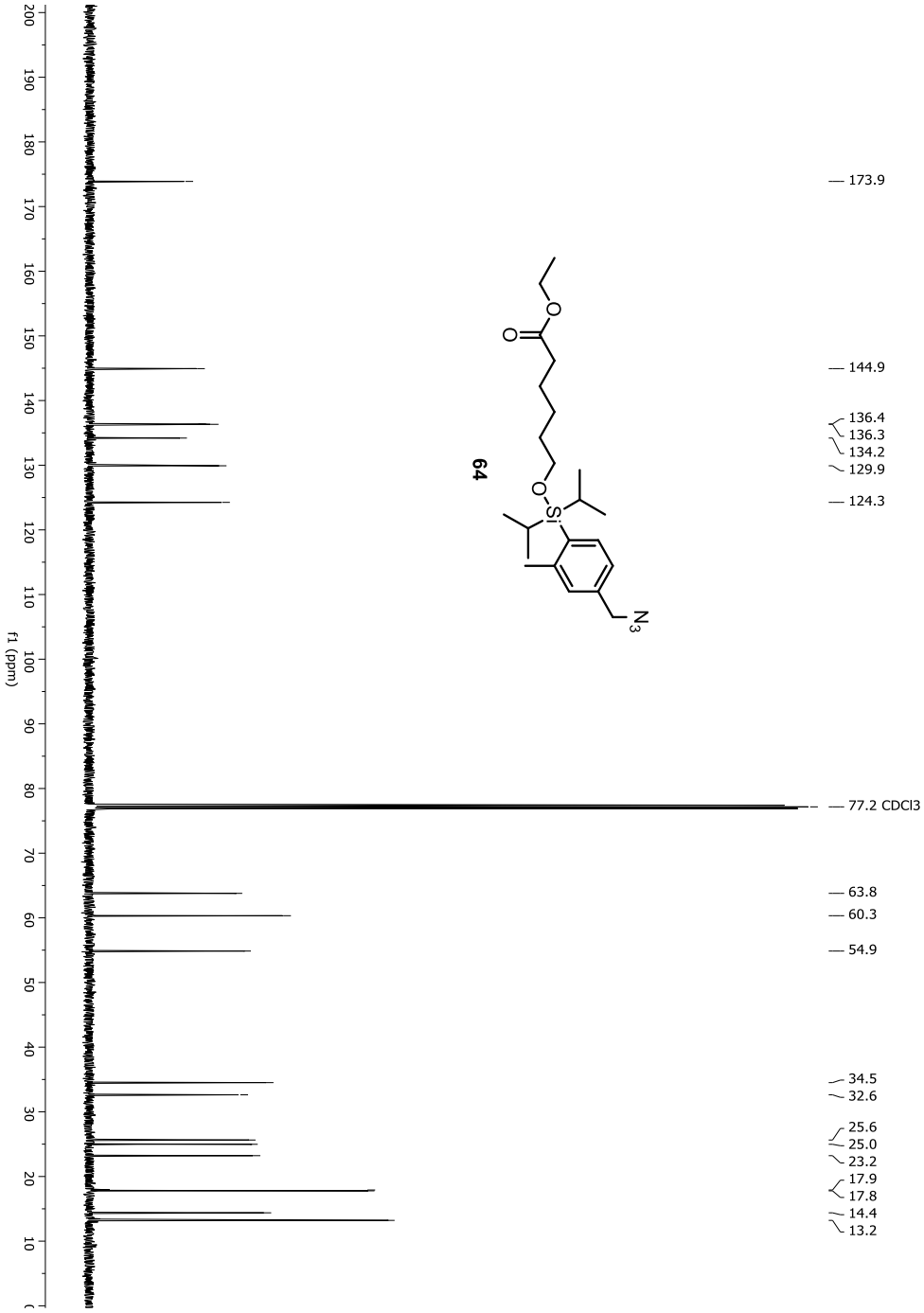

Figure A-79. ^{29}Si-NMR spectrum of compound 64

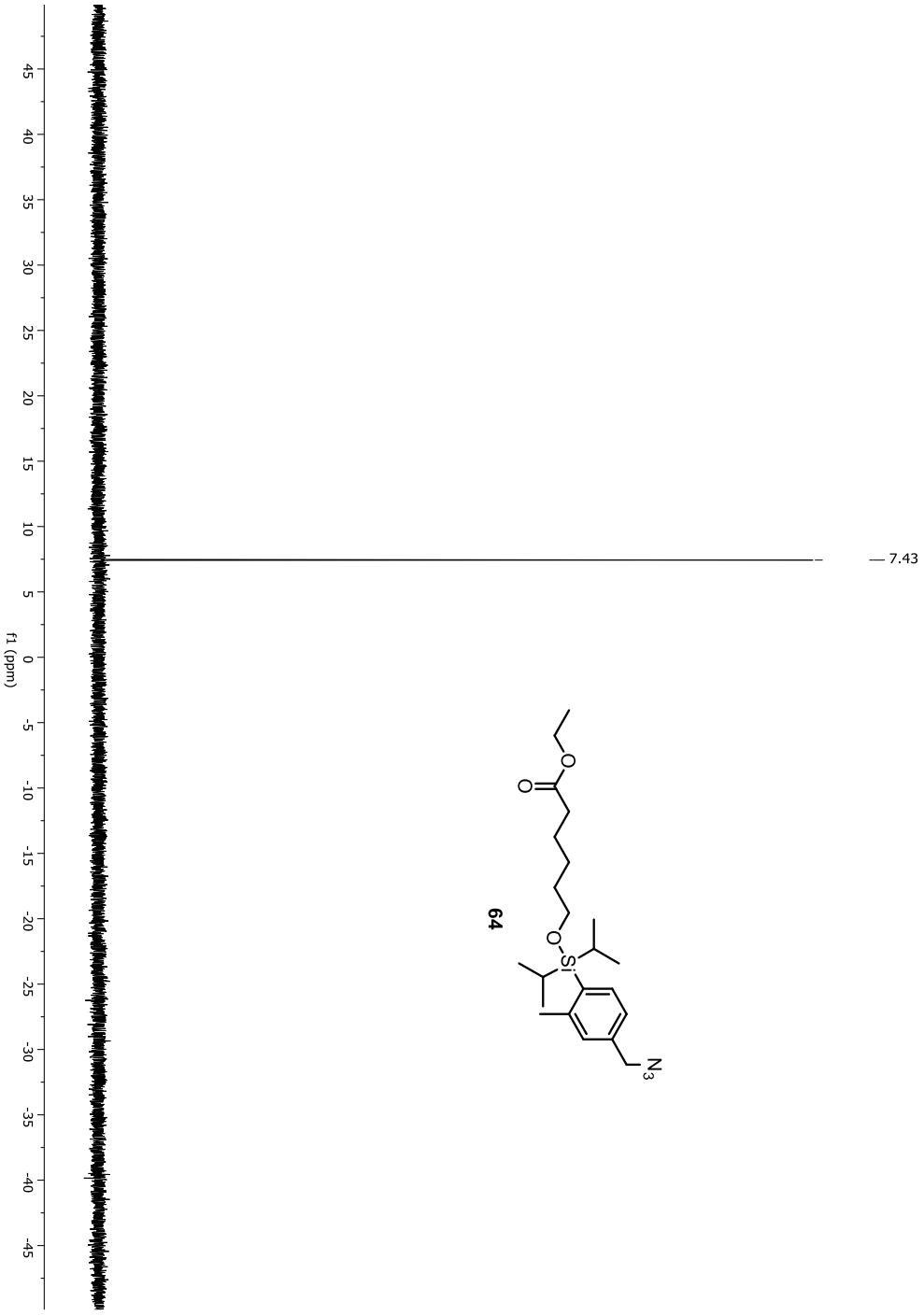

Figure A-80. HRMS spectrum of compound 64

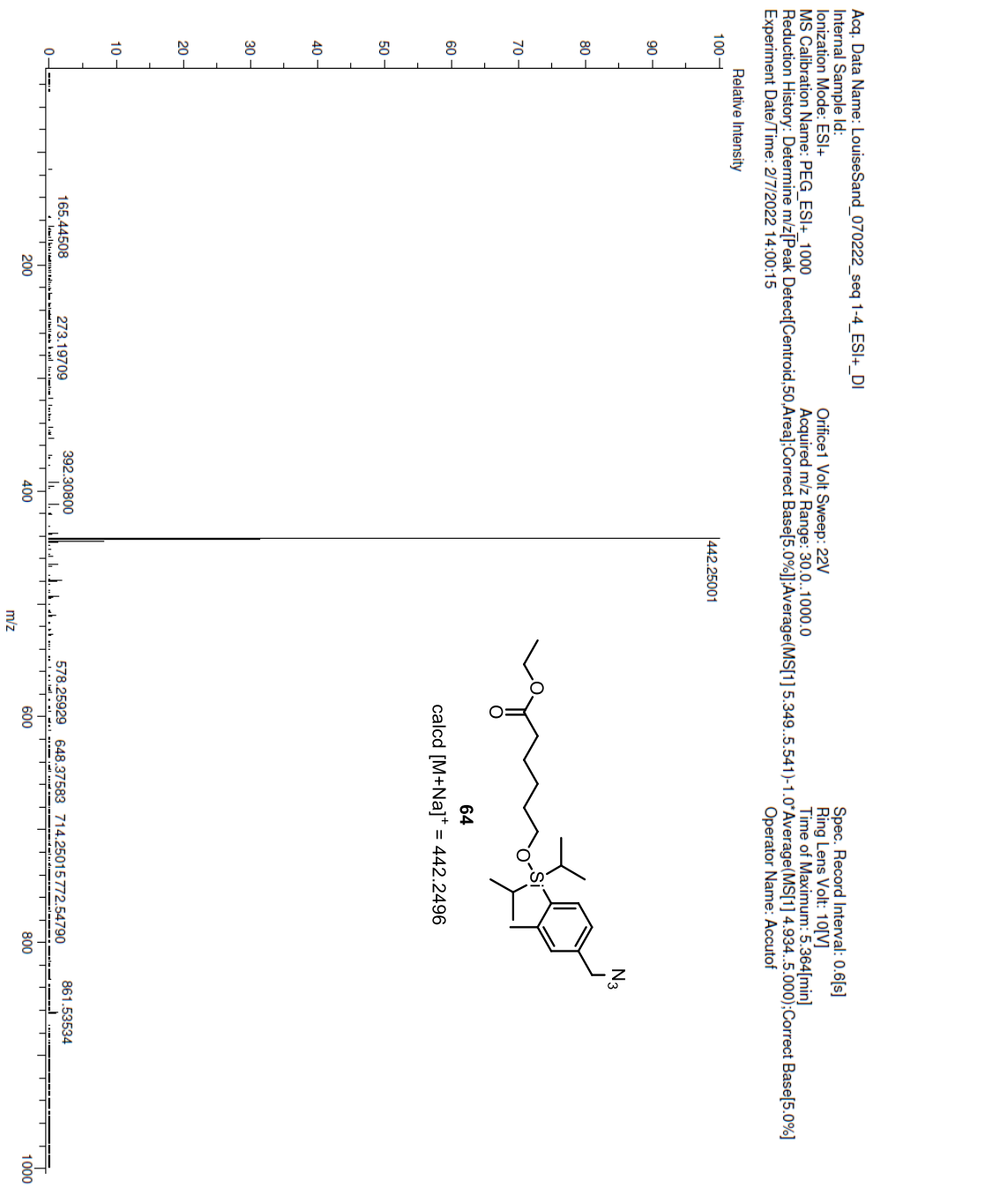

Figure A-81. ^{1}H-NMR spectrum of compound 66

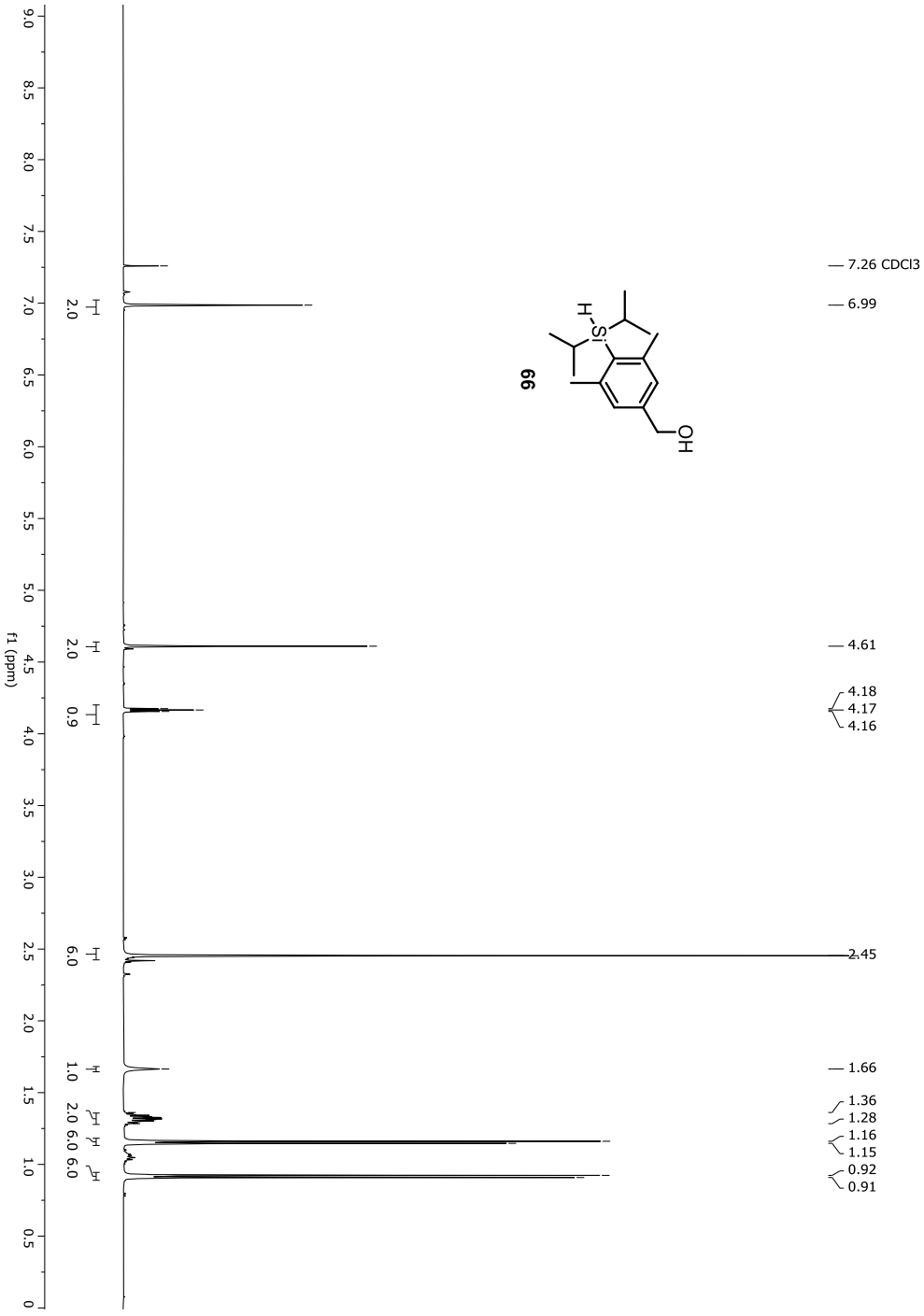

Figure A-82. ^{13}C-NMR spectrum of compound 66

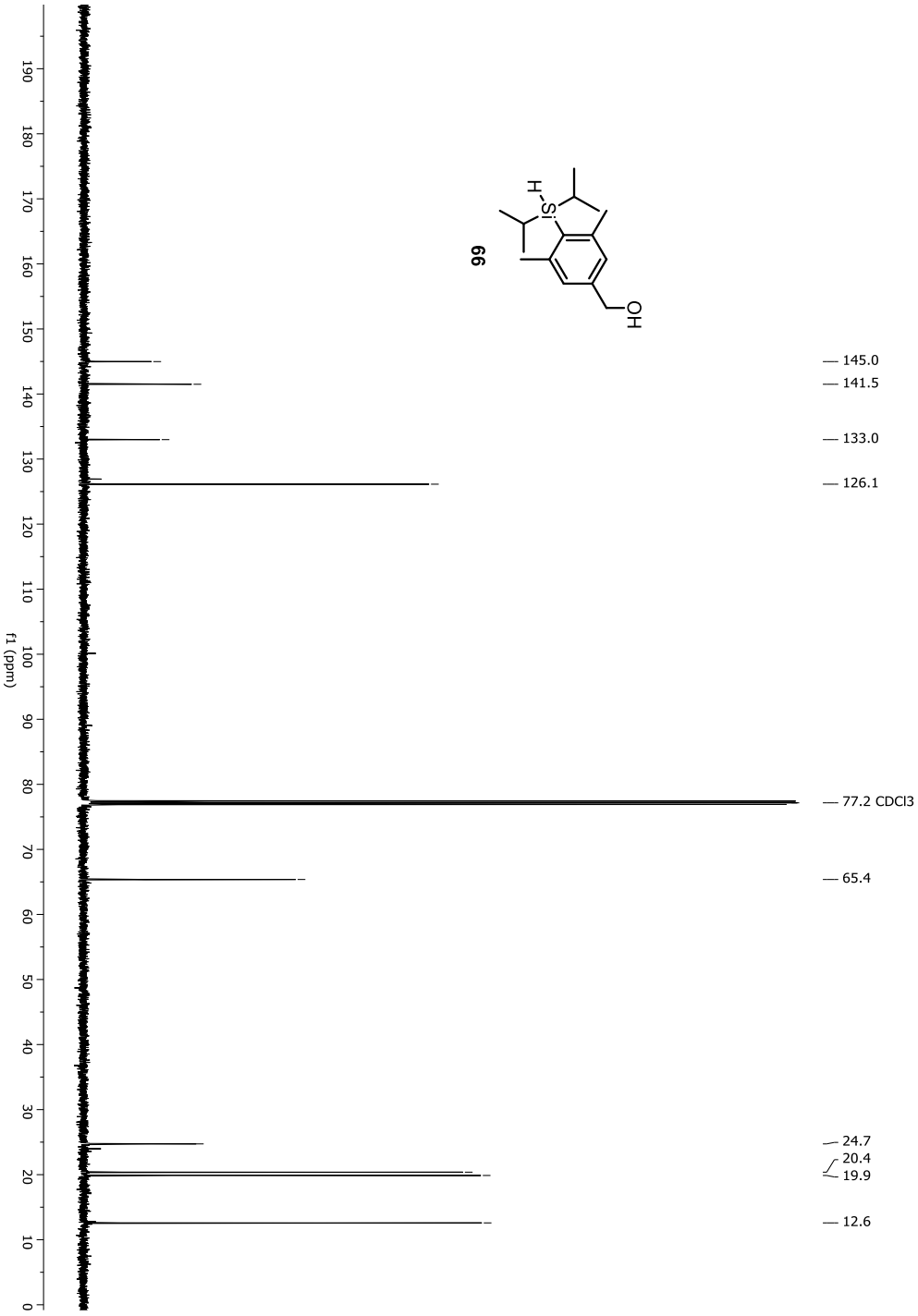

Figure A-83. HRMS spectrum of compound 66

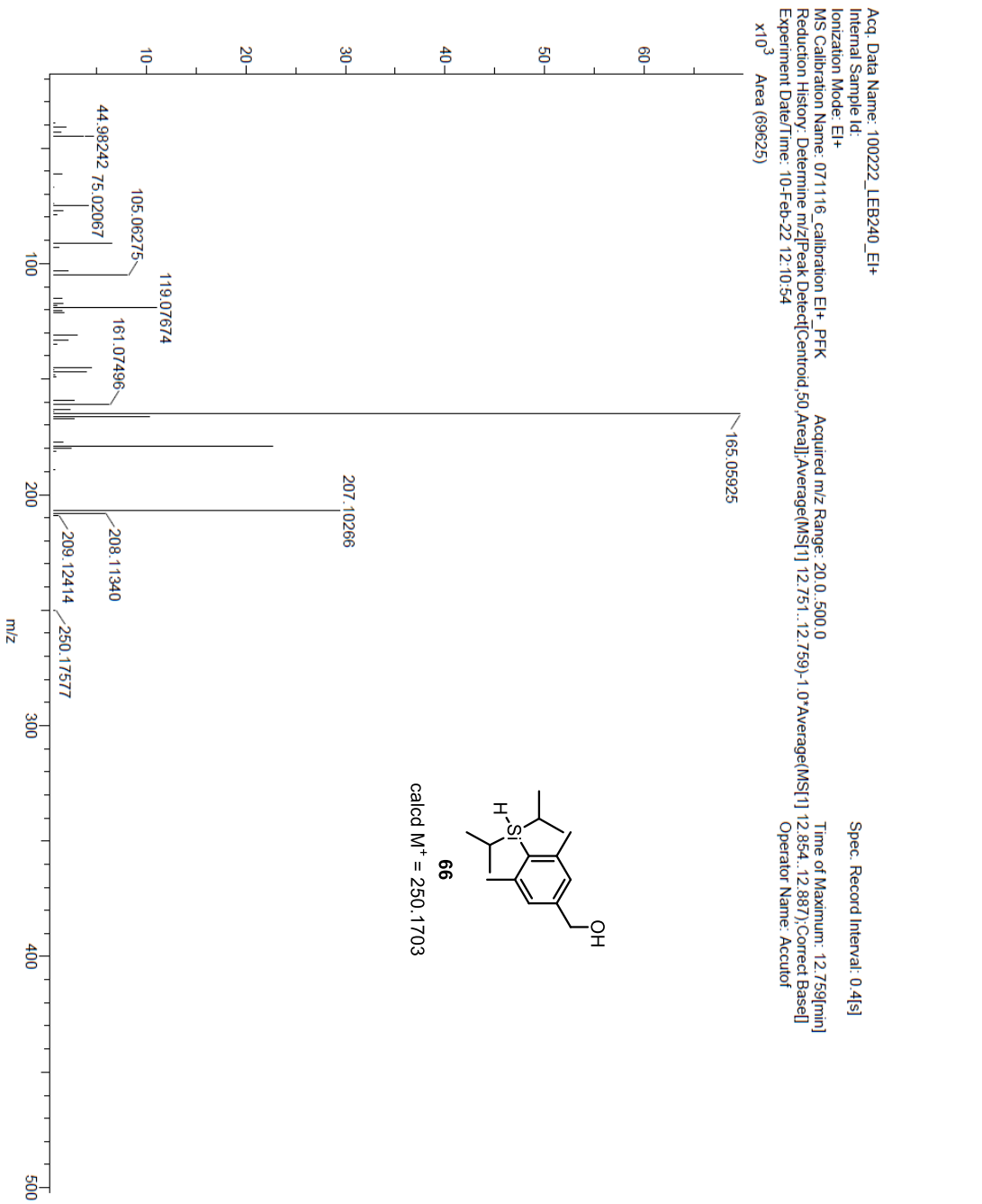

Figure A-84. ^{1}H-NMR spectrum of compound 67

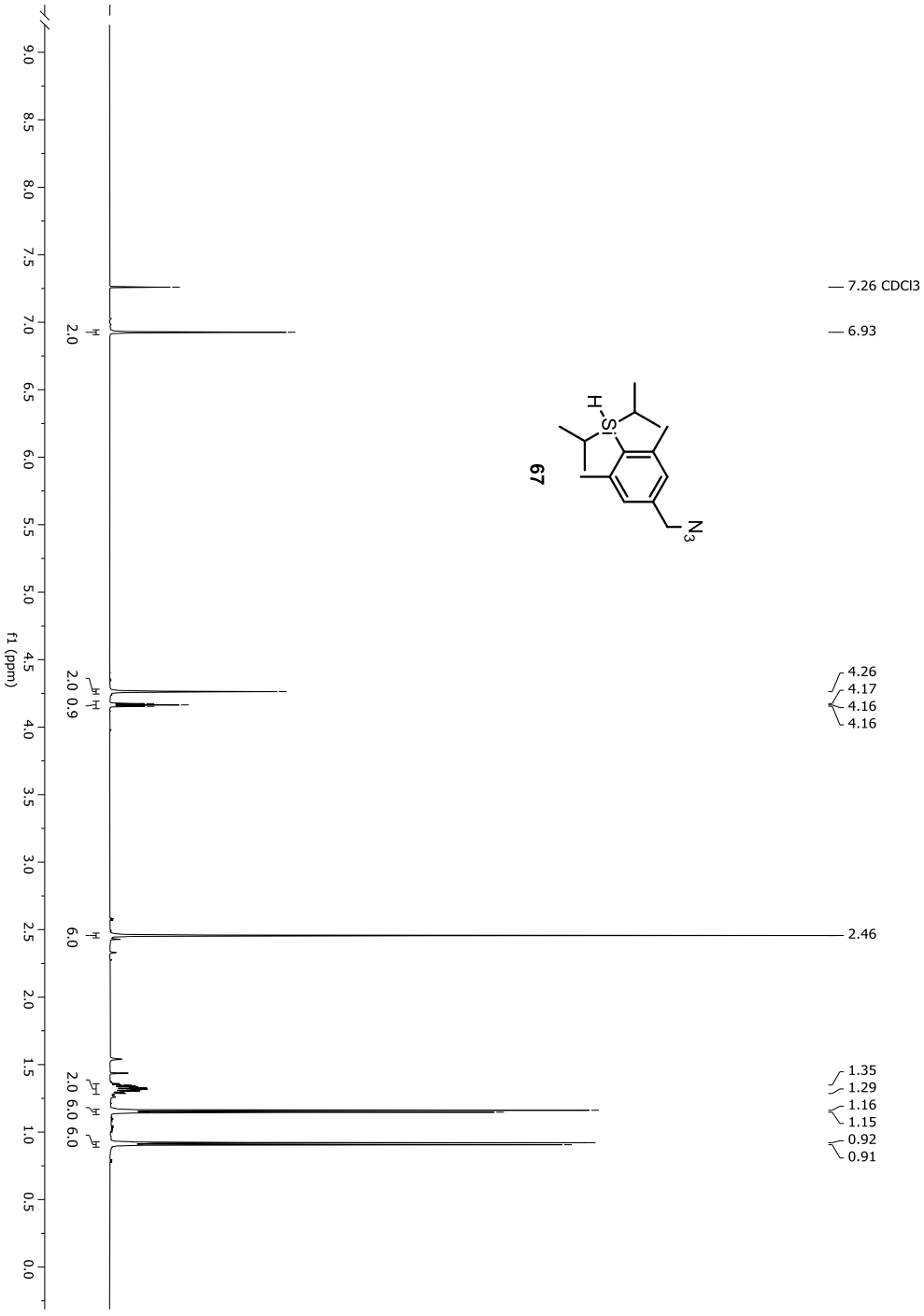

Figure A-85. ^{13}C-NMR spectrum of compound 67

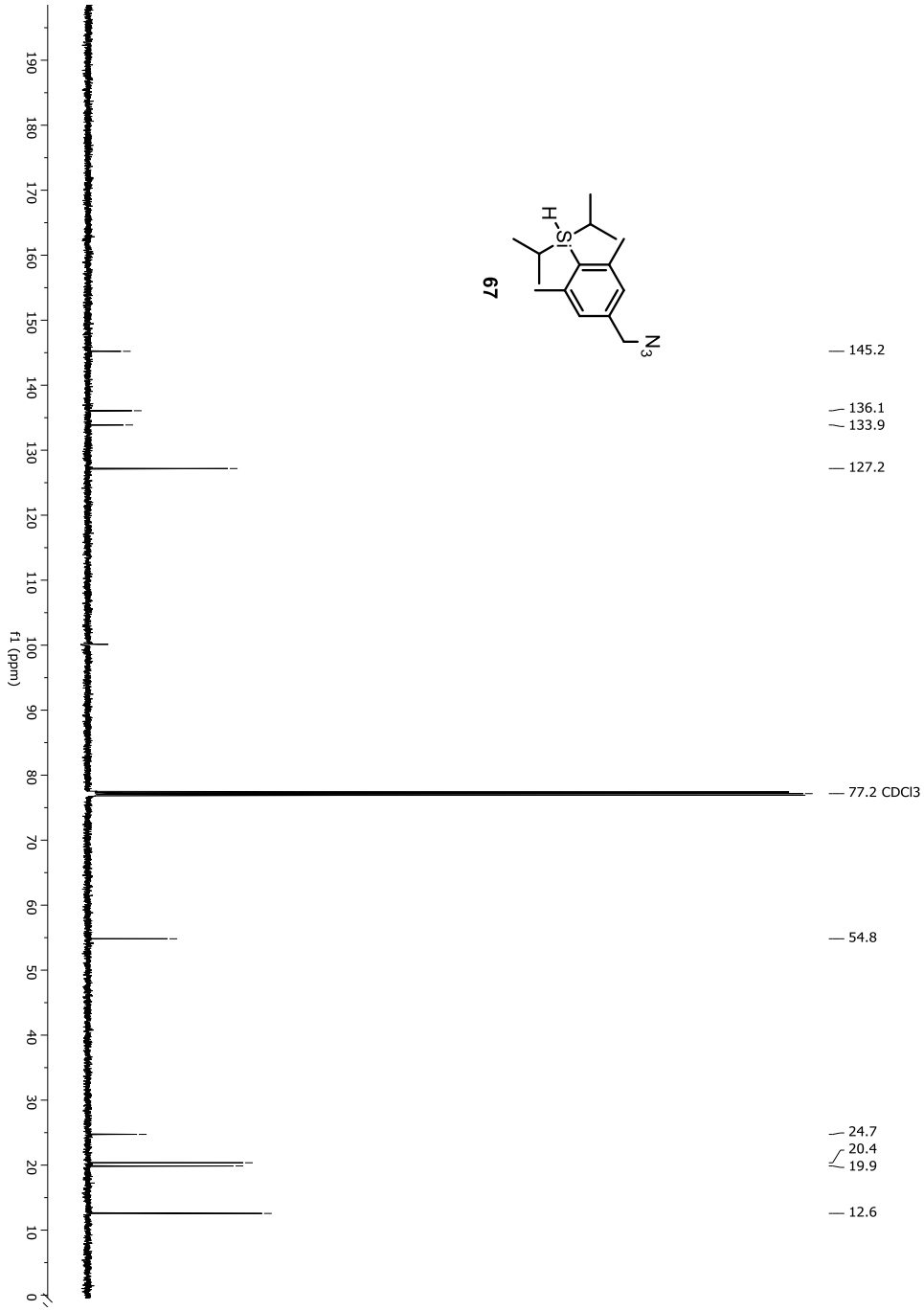

Figure A-86. HRMS spectrum of compound 67

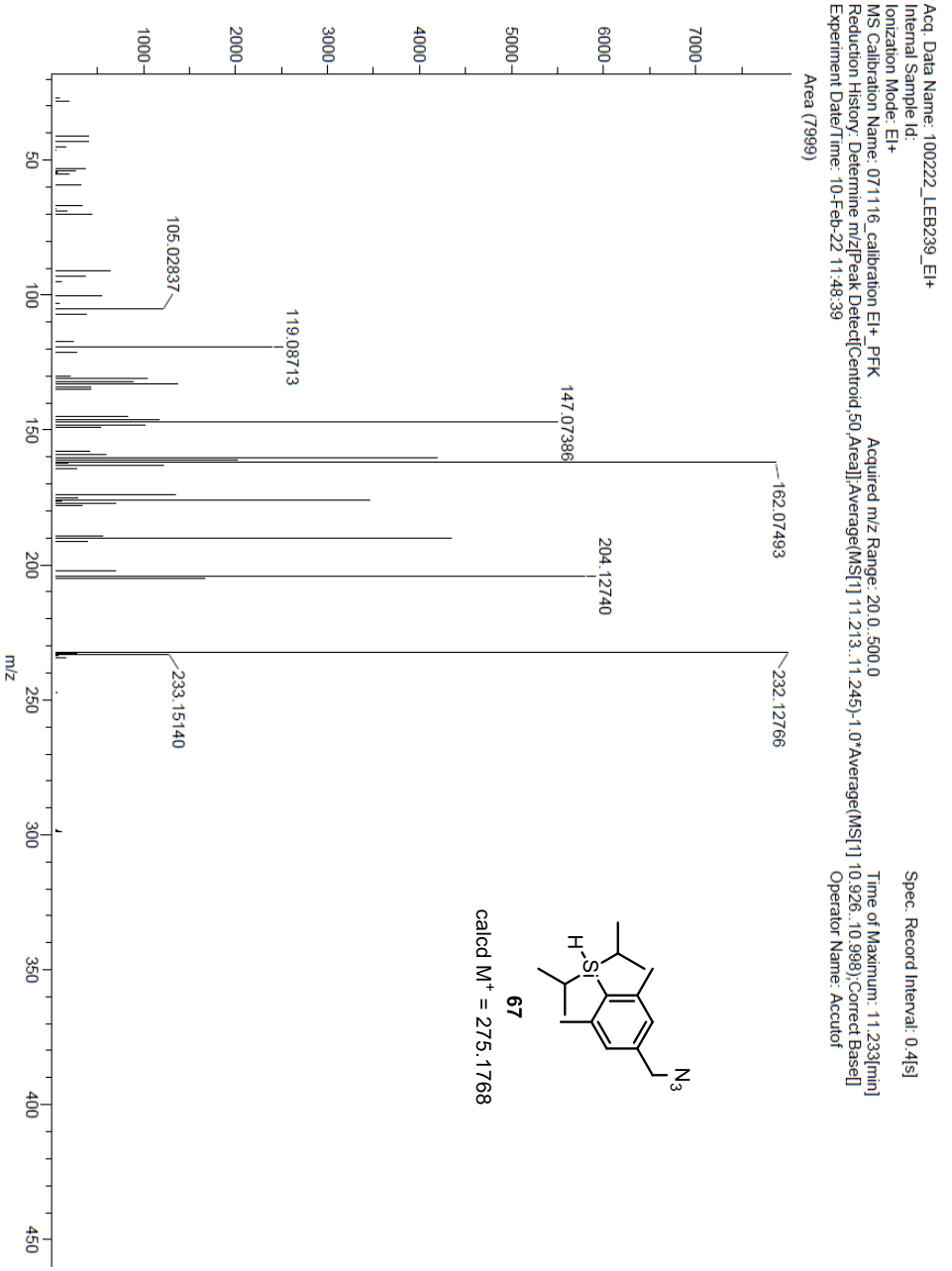

Figure A-87. ^{1}H-NMR spectrum of compound 68

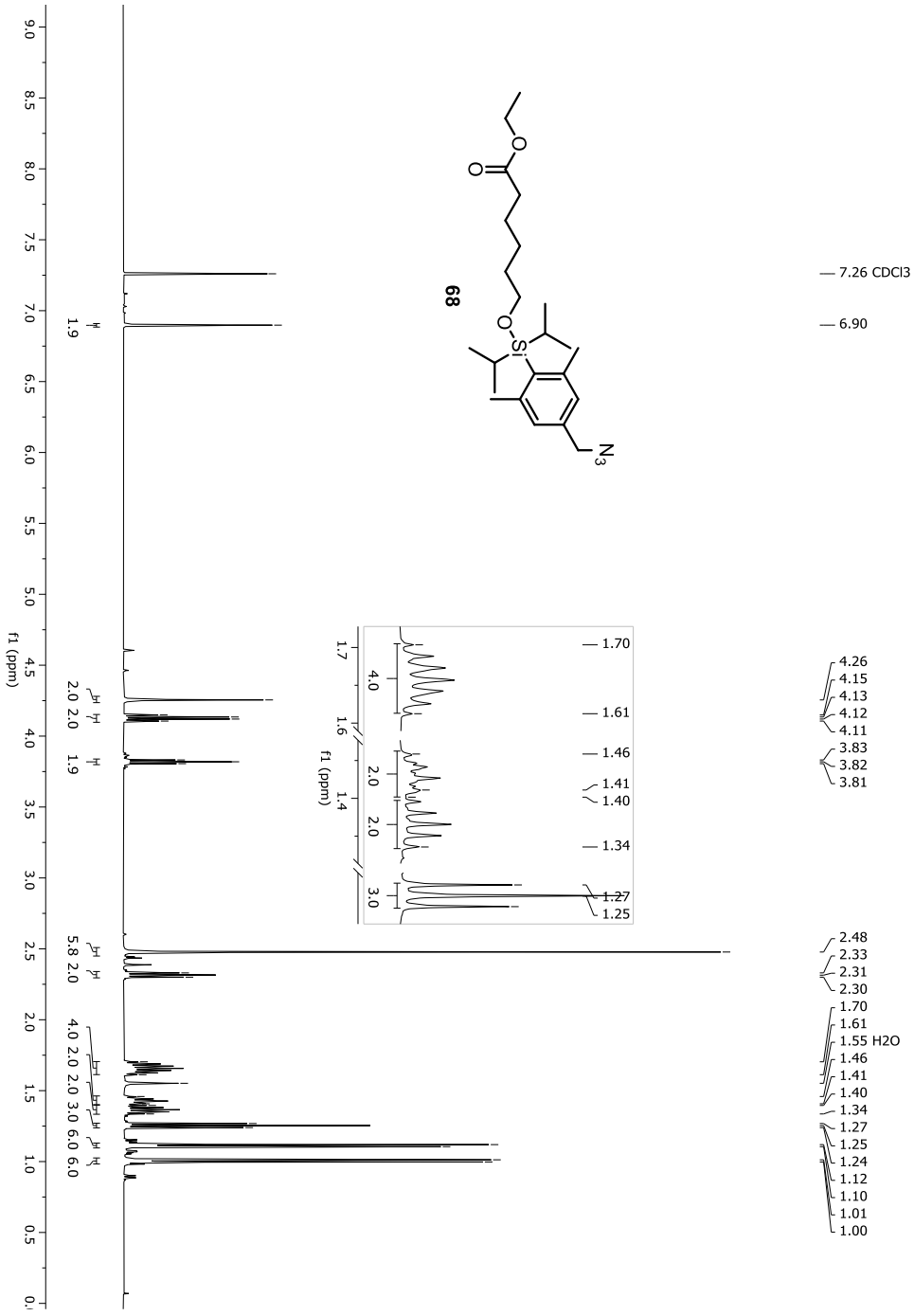

Figure A-88. ^{13}C-NMR spectrum of compound 68

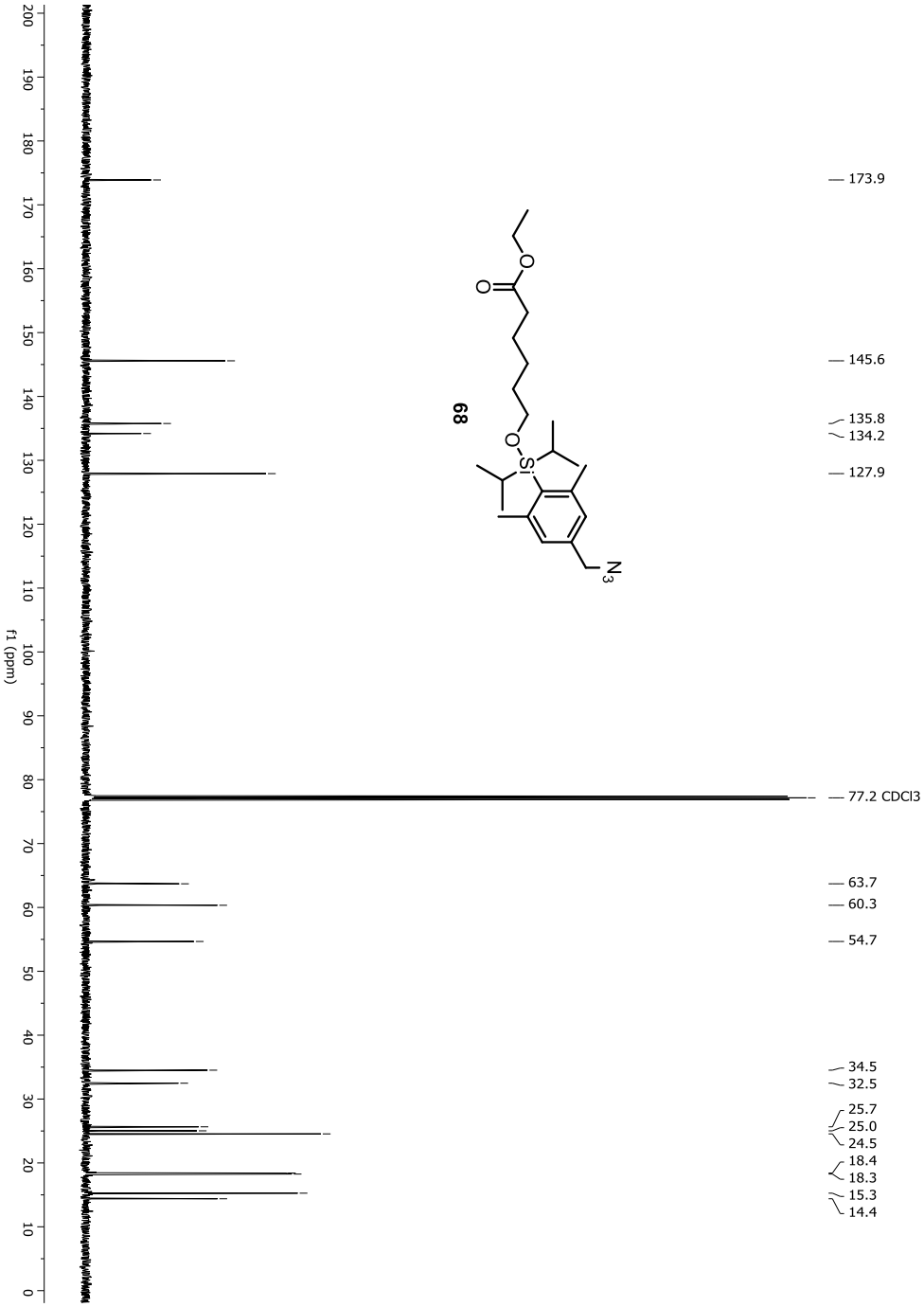

Figure A-89. HRMS spectrum of compound 68

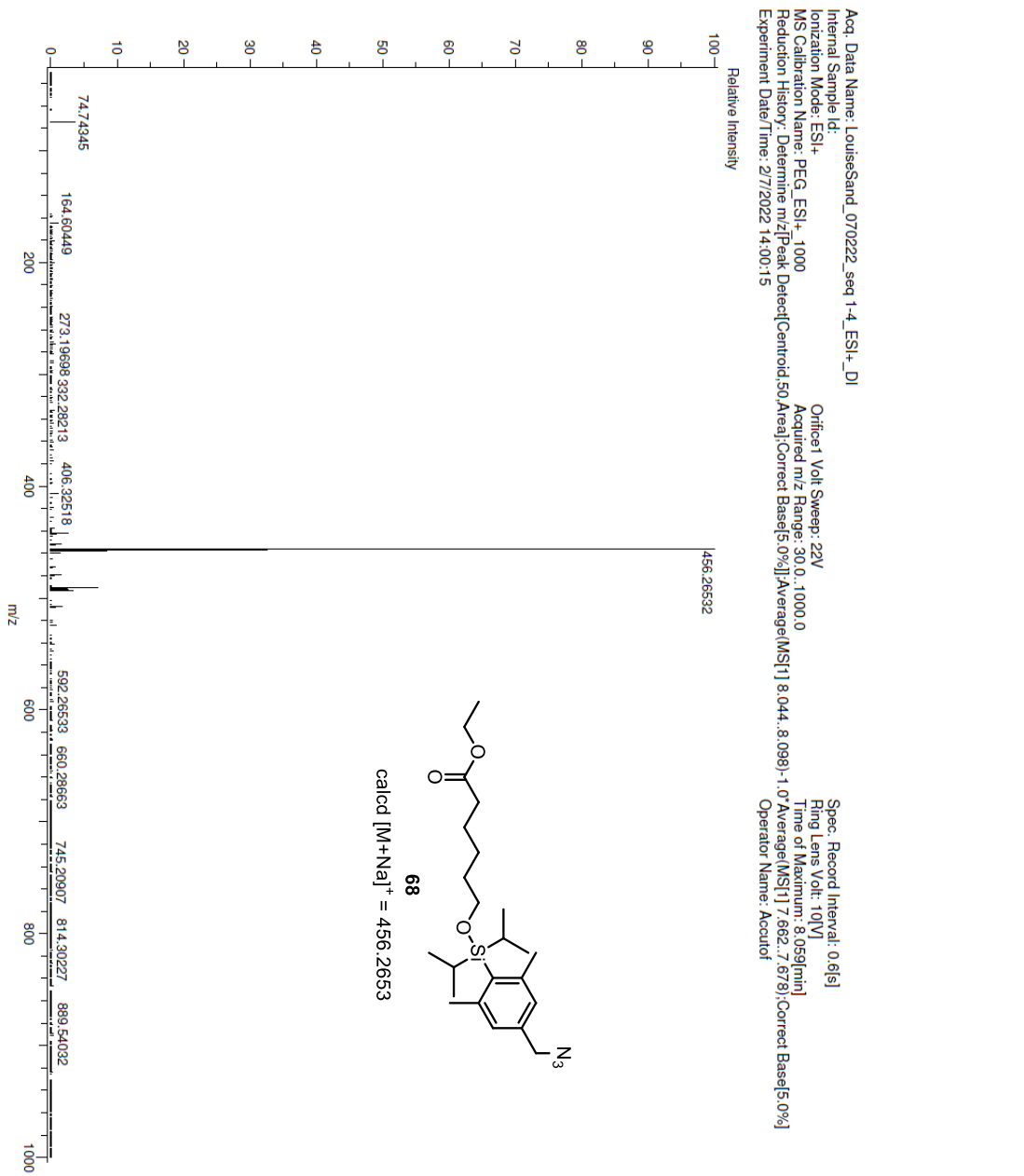

Figure A-90. ^{1}H-NMR spectrum of compound 69

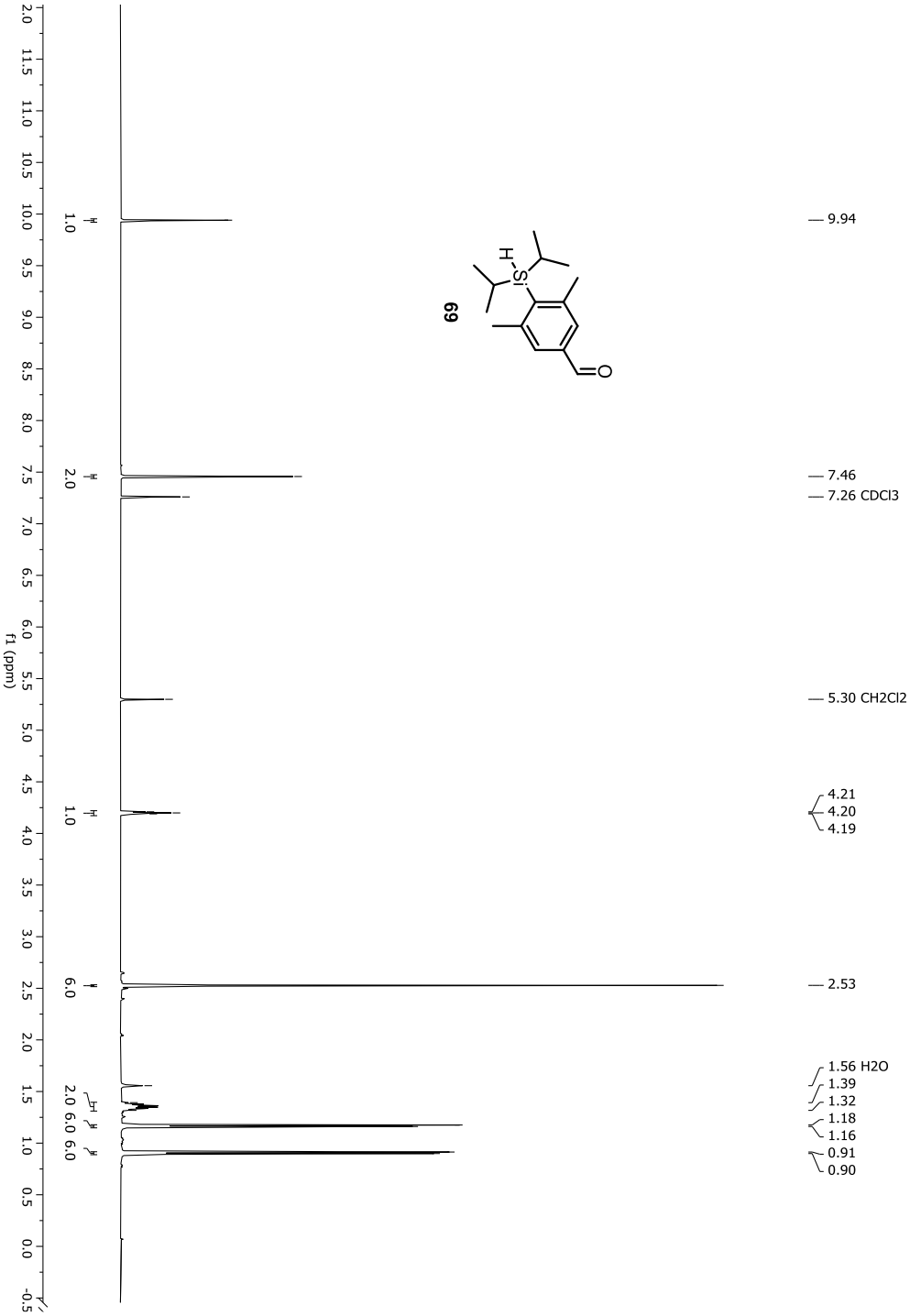

Figure A-91. ^{13}C-NMR spectrum of compound 69

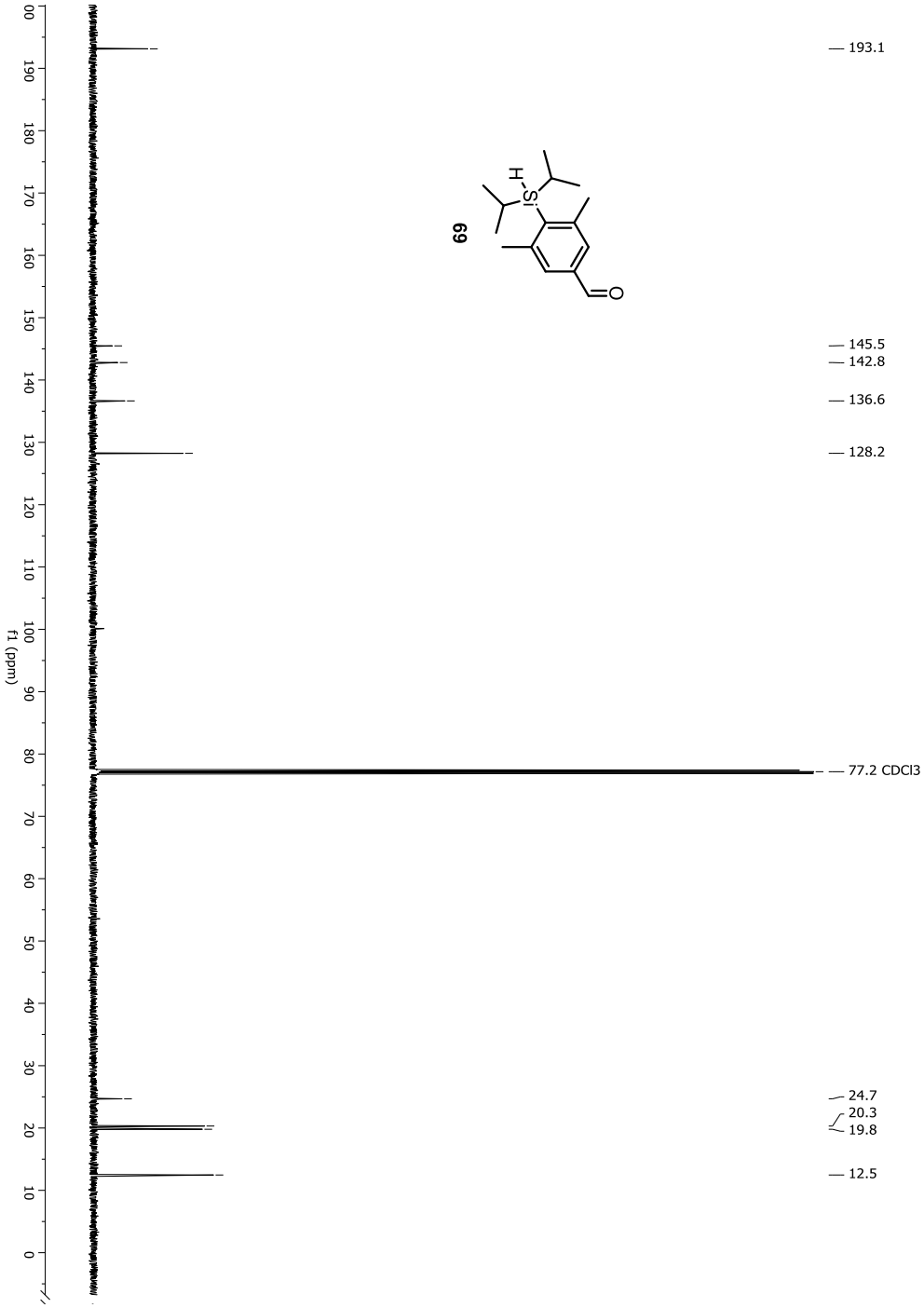

Figure A-92. HRMS spectrum of compound 69

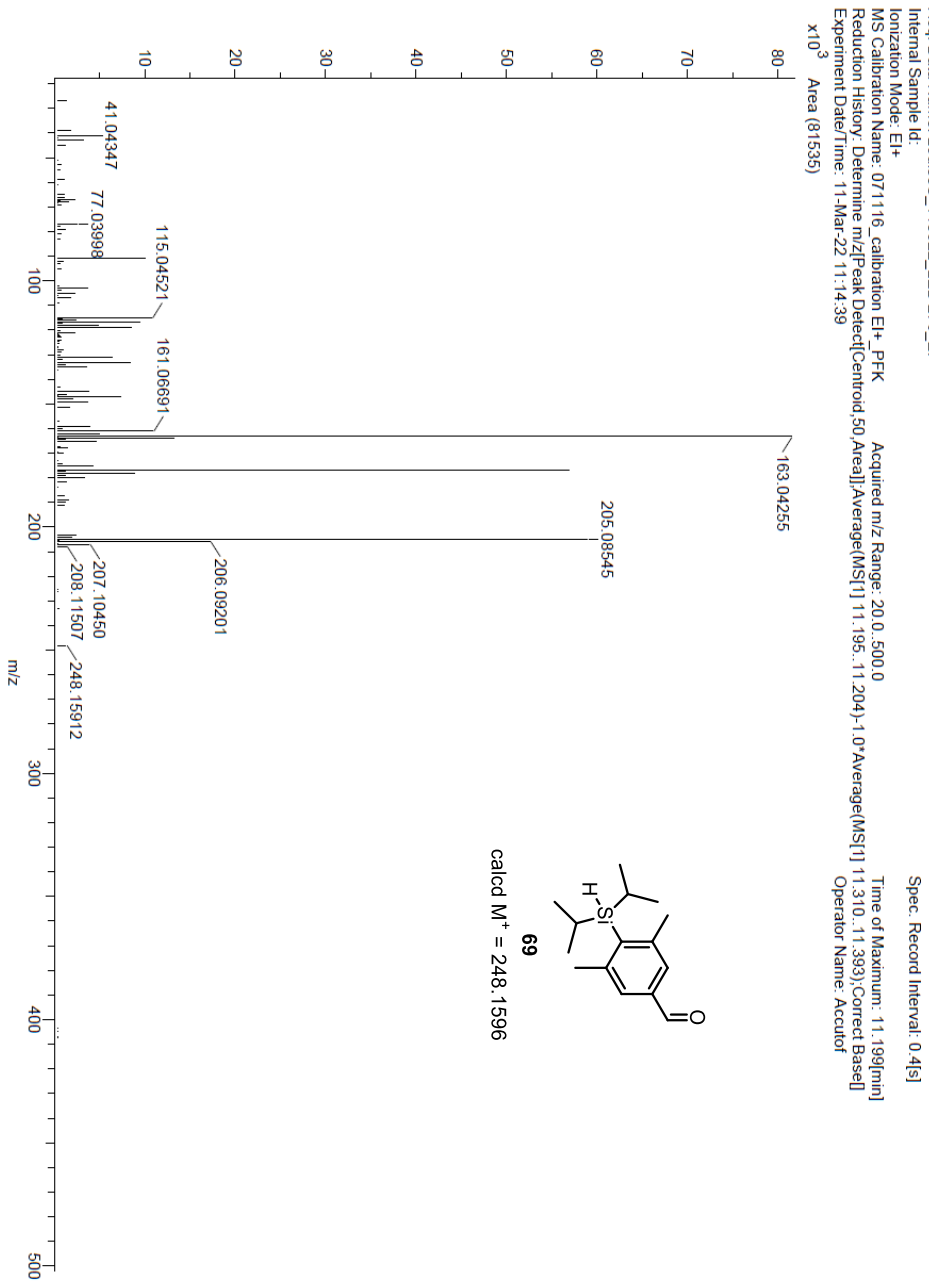

Figure A-93. ^{1}H-NMR spectrum of compound 70

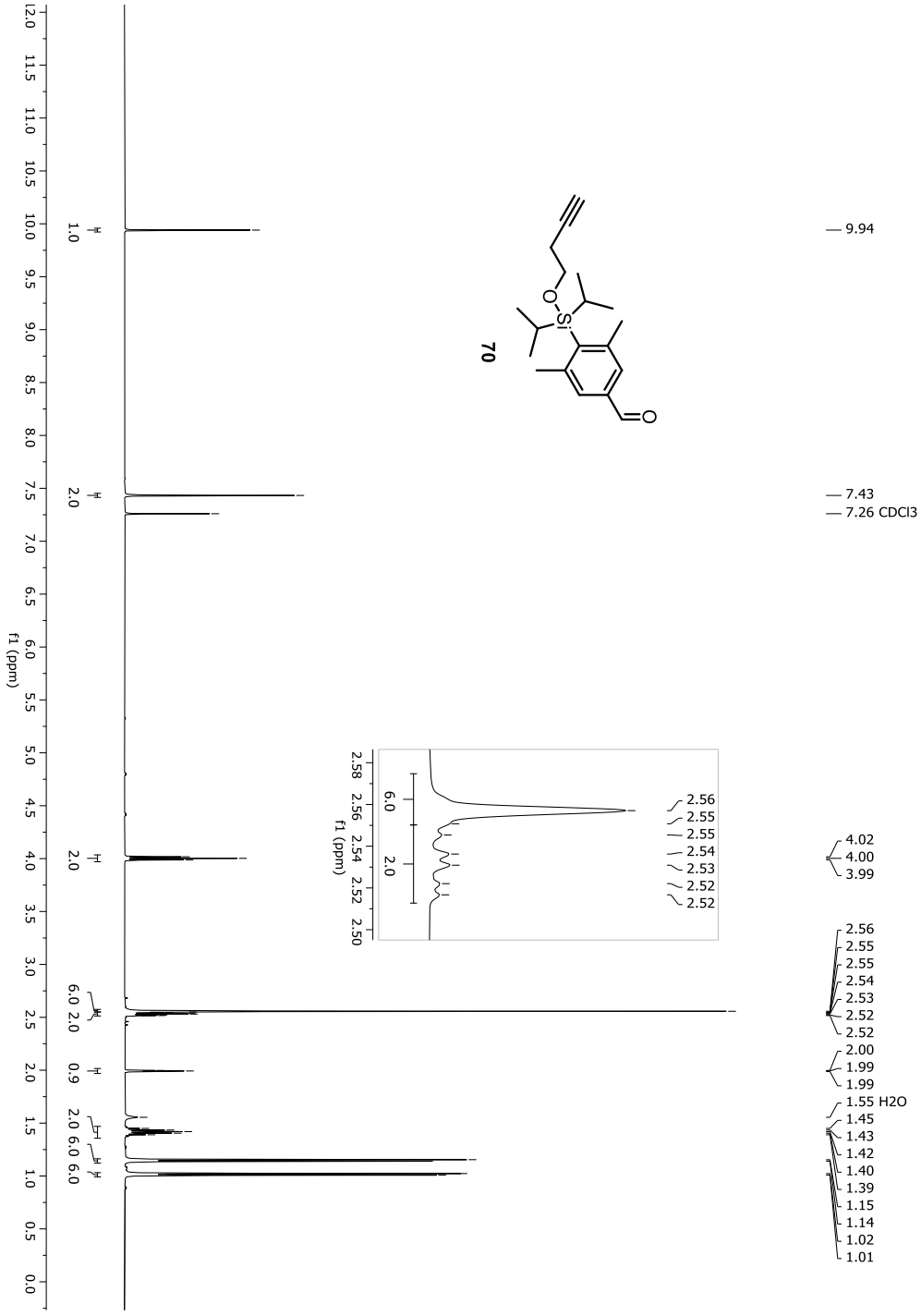

Figure A-94. ^{13}C-NMR spectrum of compound 70

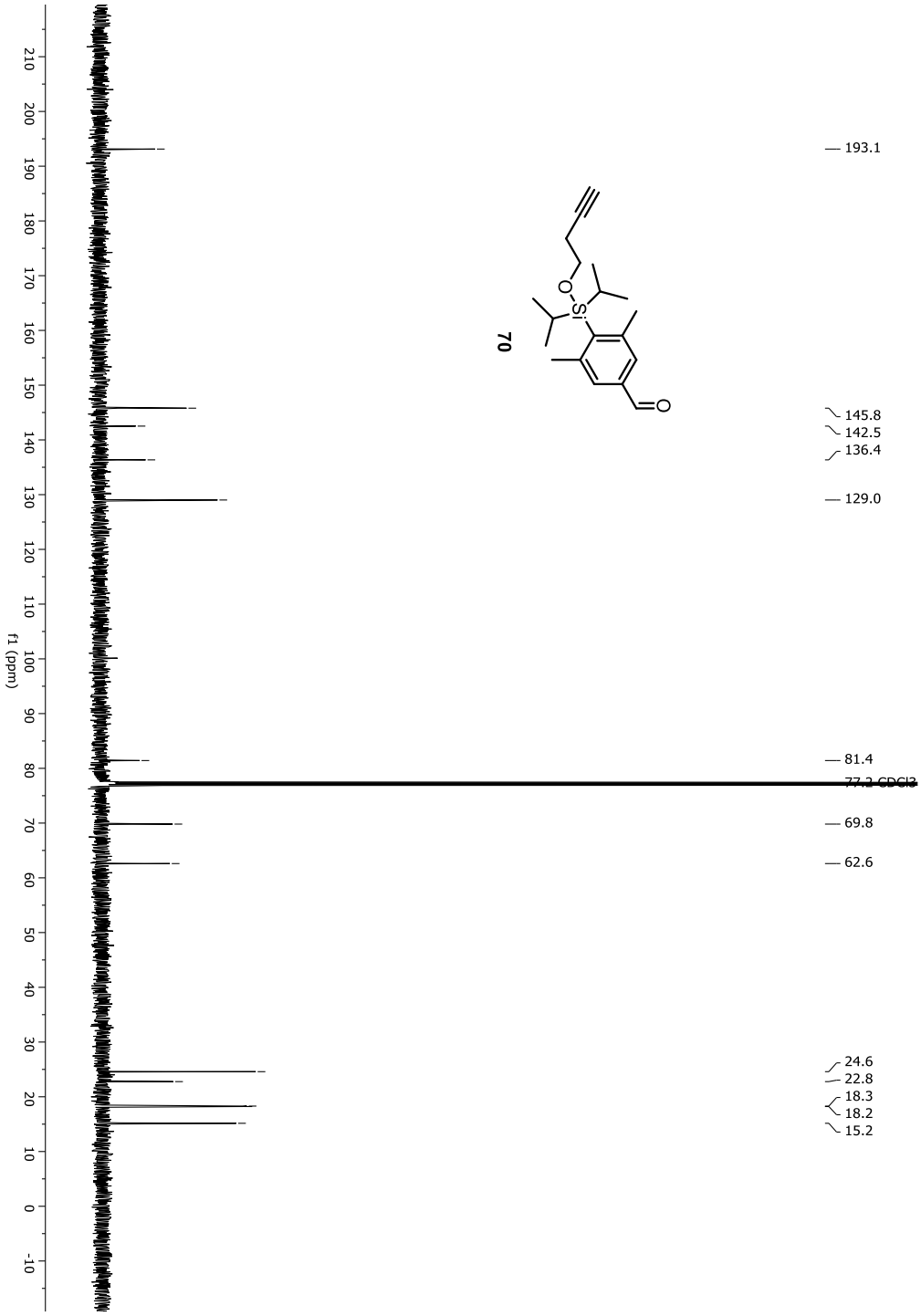

Figure A-95. HRMS spectrum of compound 70

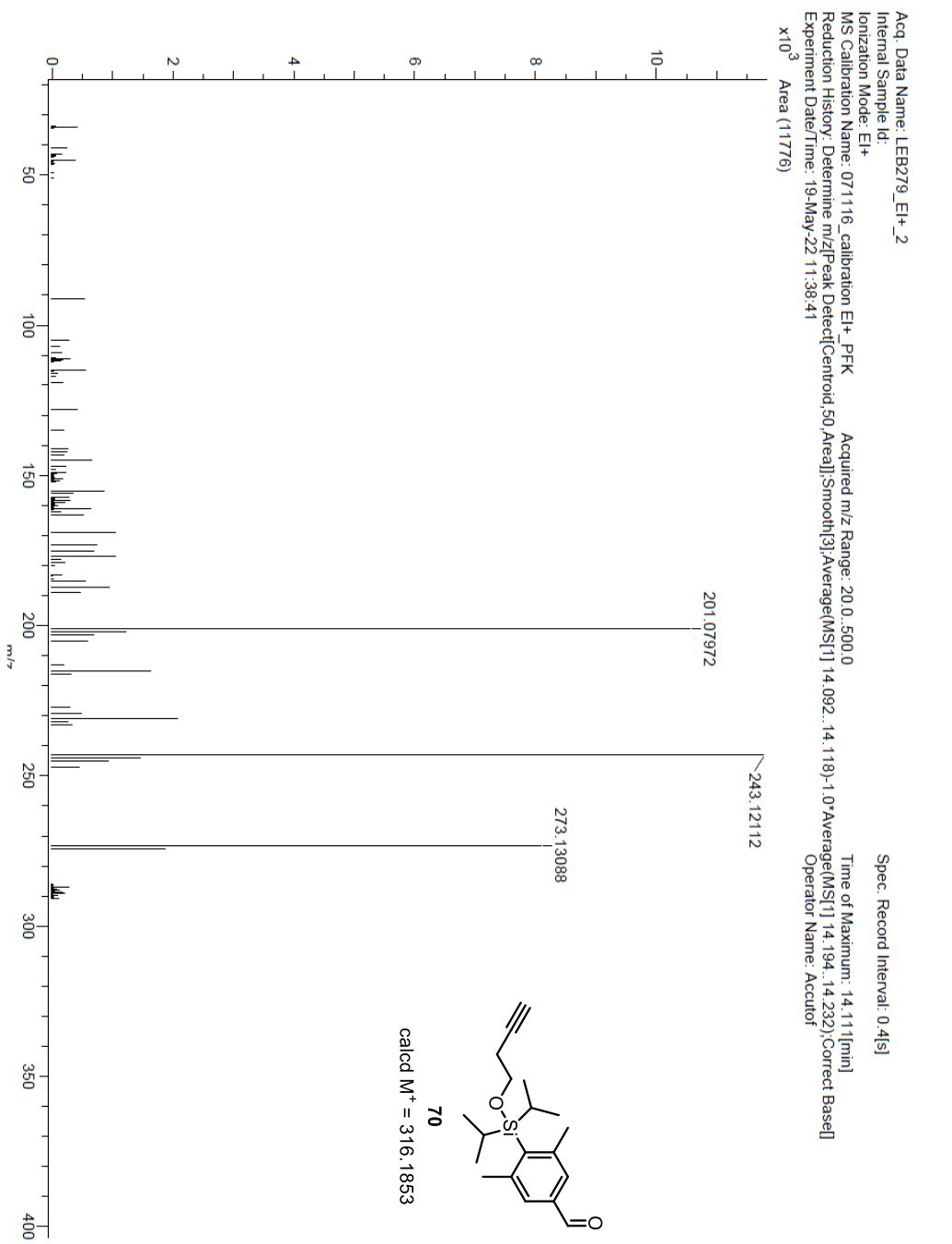

Figure A-96. ^{1}H-NMR spectrum of compound 73

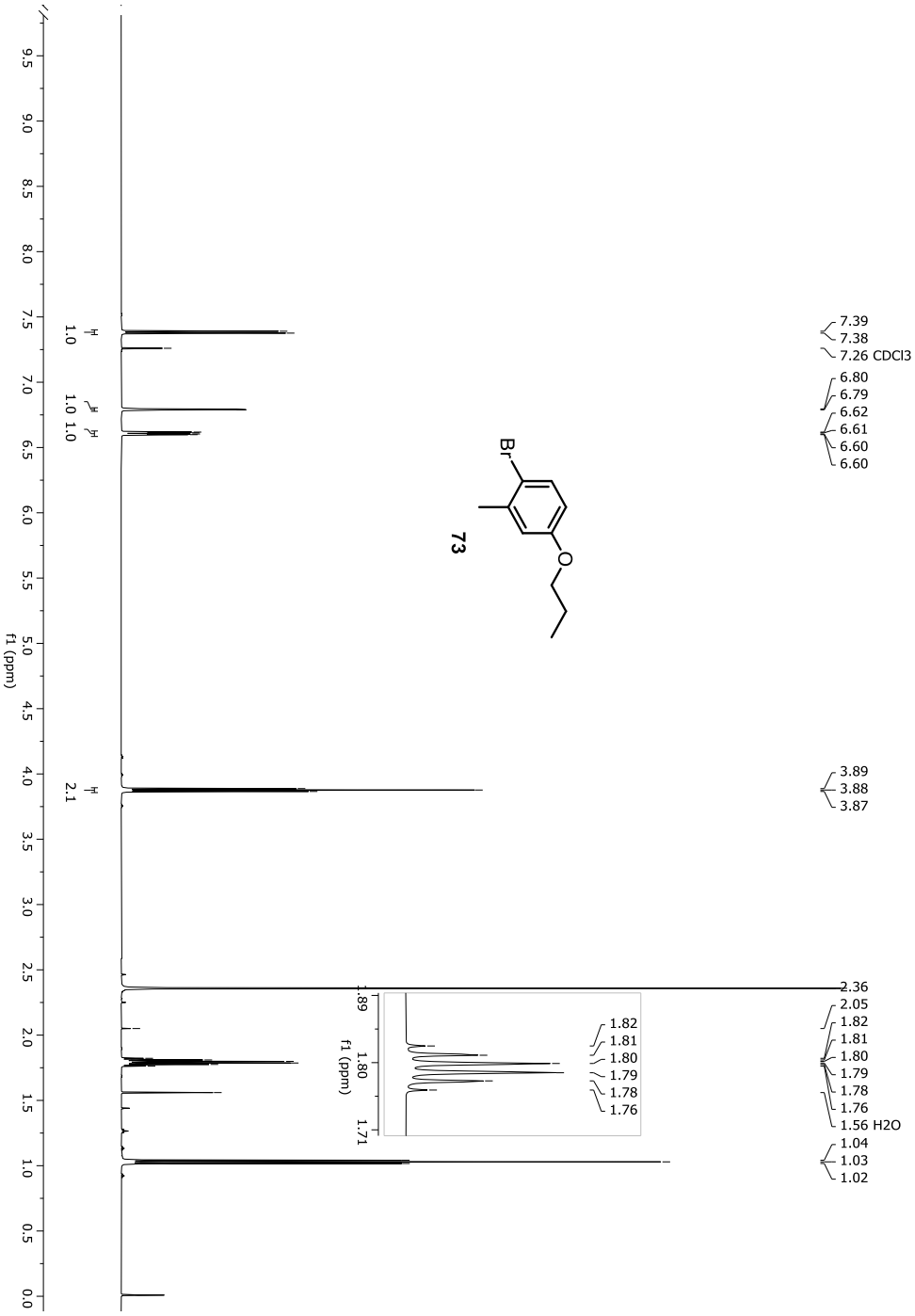

Figure A-97. ^{13}C-NMR spectrum of compound 73

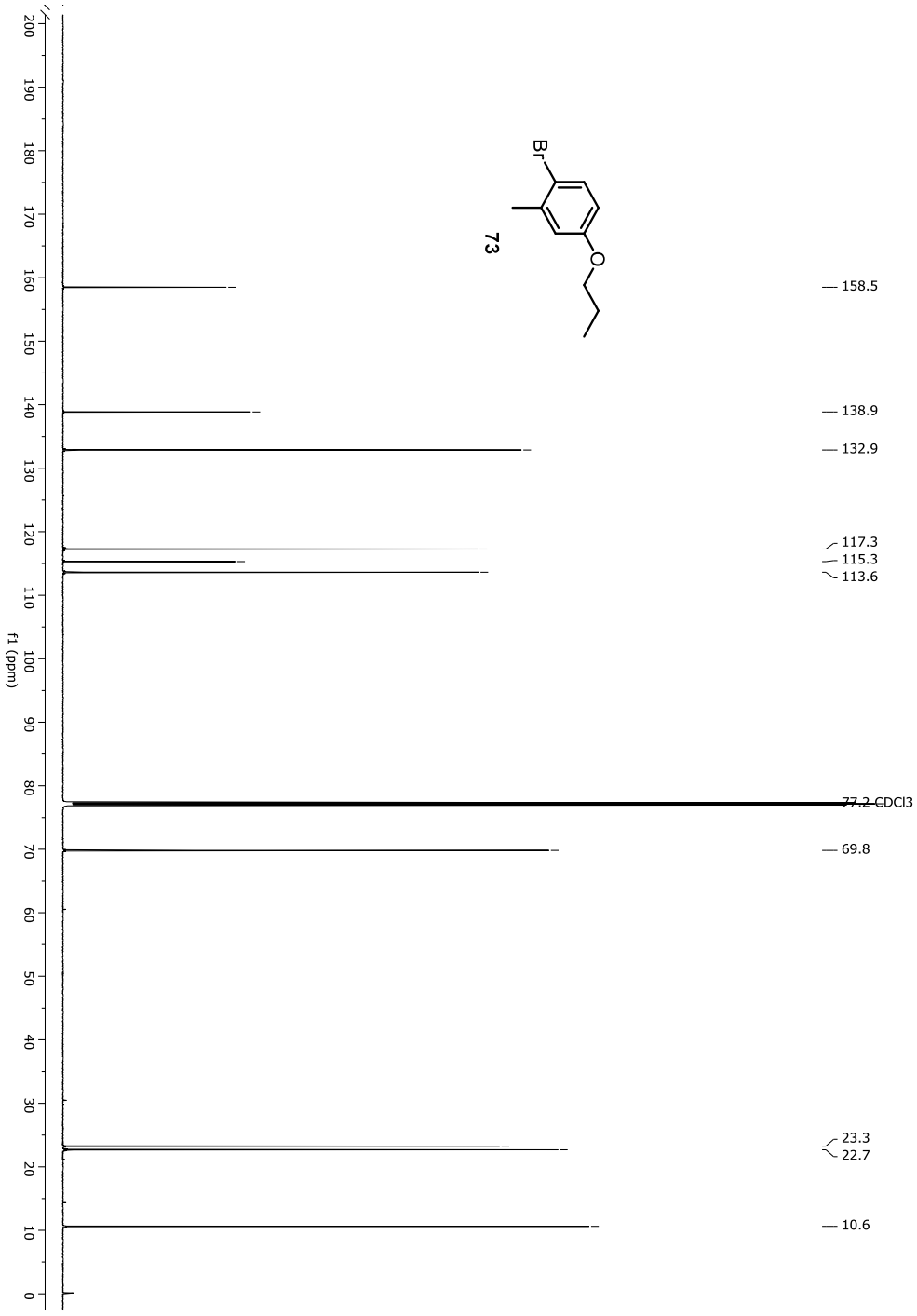

Figure A-98. ^{1}H-NMR spectrum of compound 74

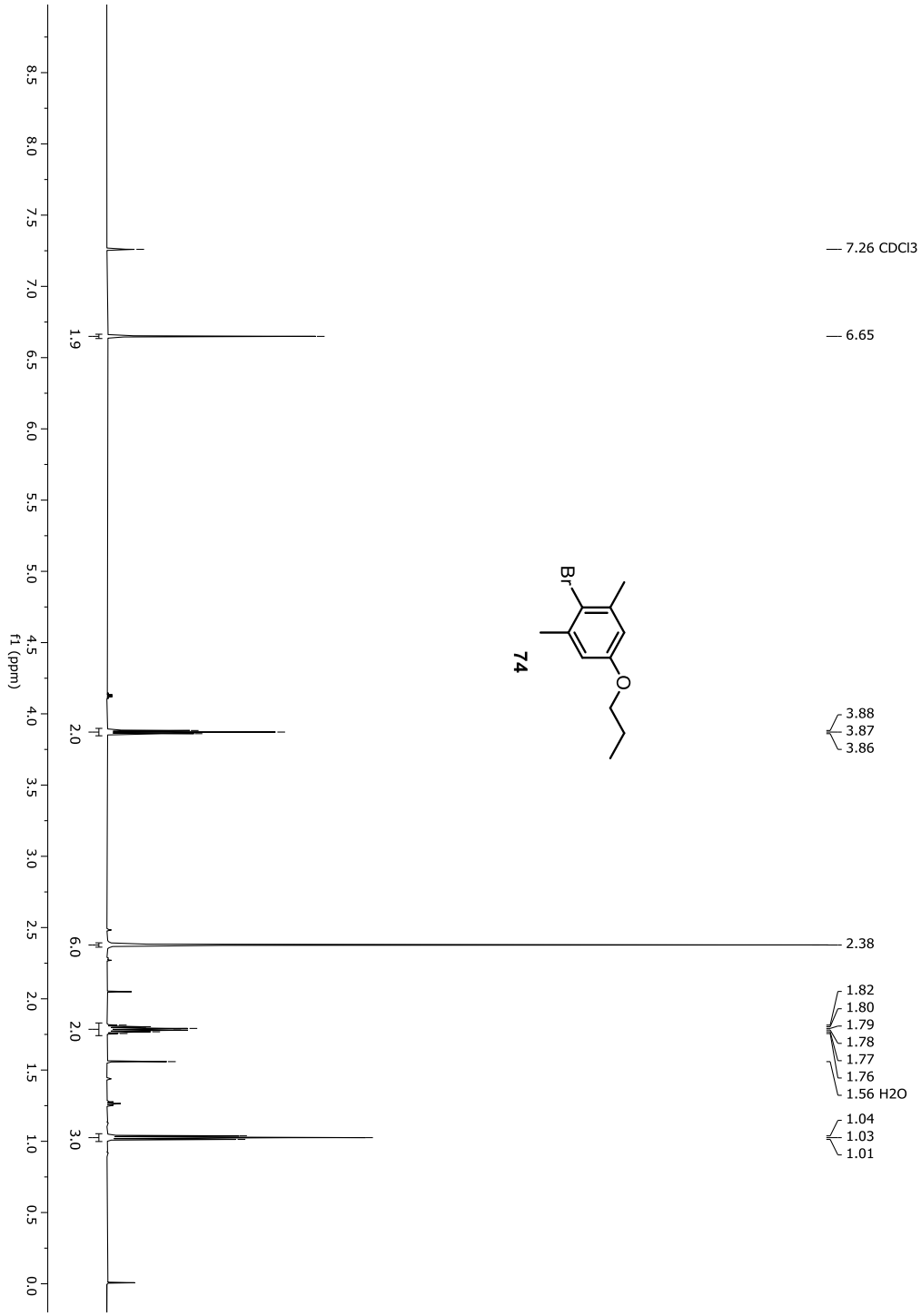

Figure A-99. ^{13}C-NMR spectrum of compound 74

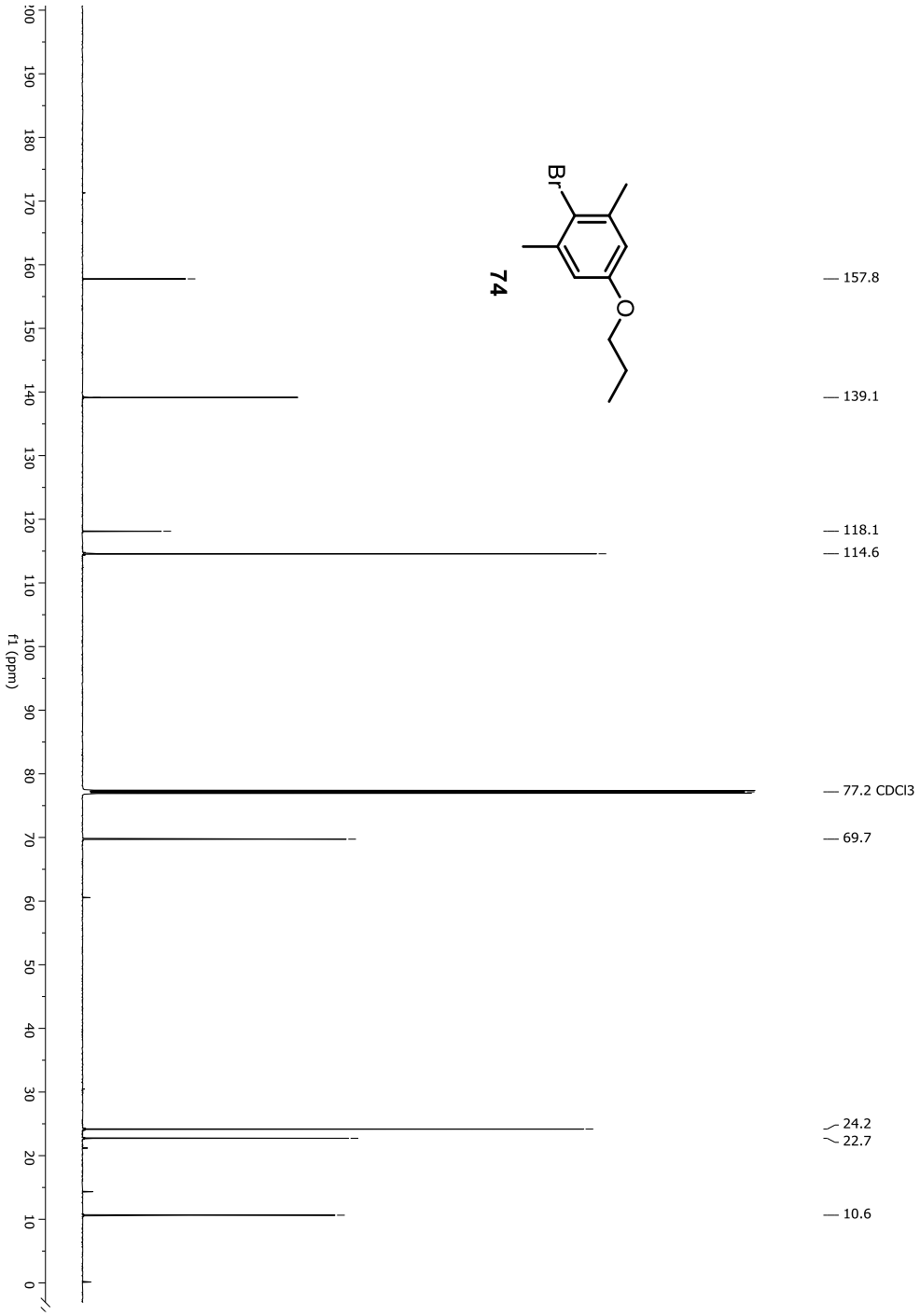

Figure A-100. ^{1}H-NMR spectrum of compound 75

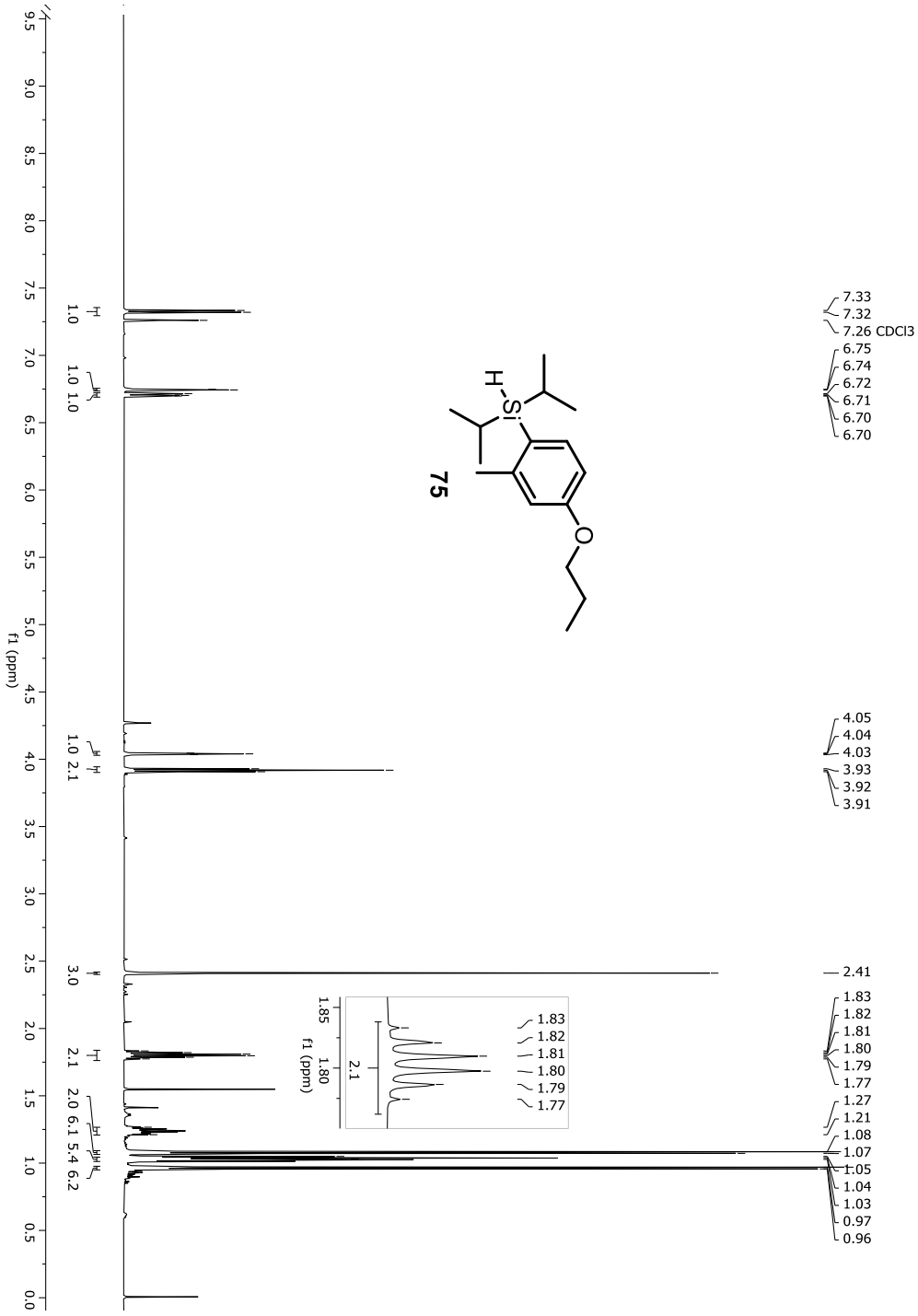

Figure A-101. ^{13}C-NMR spectrum of compound 75

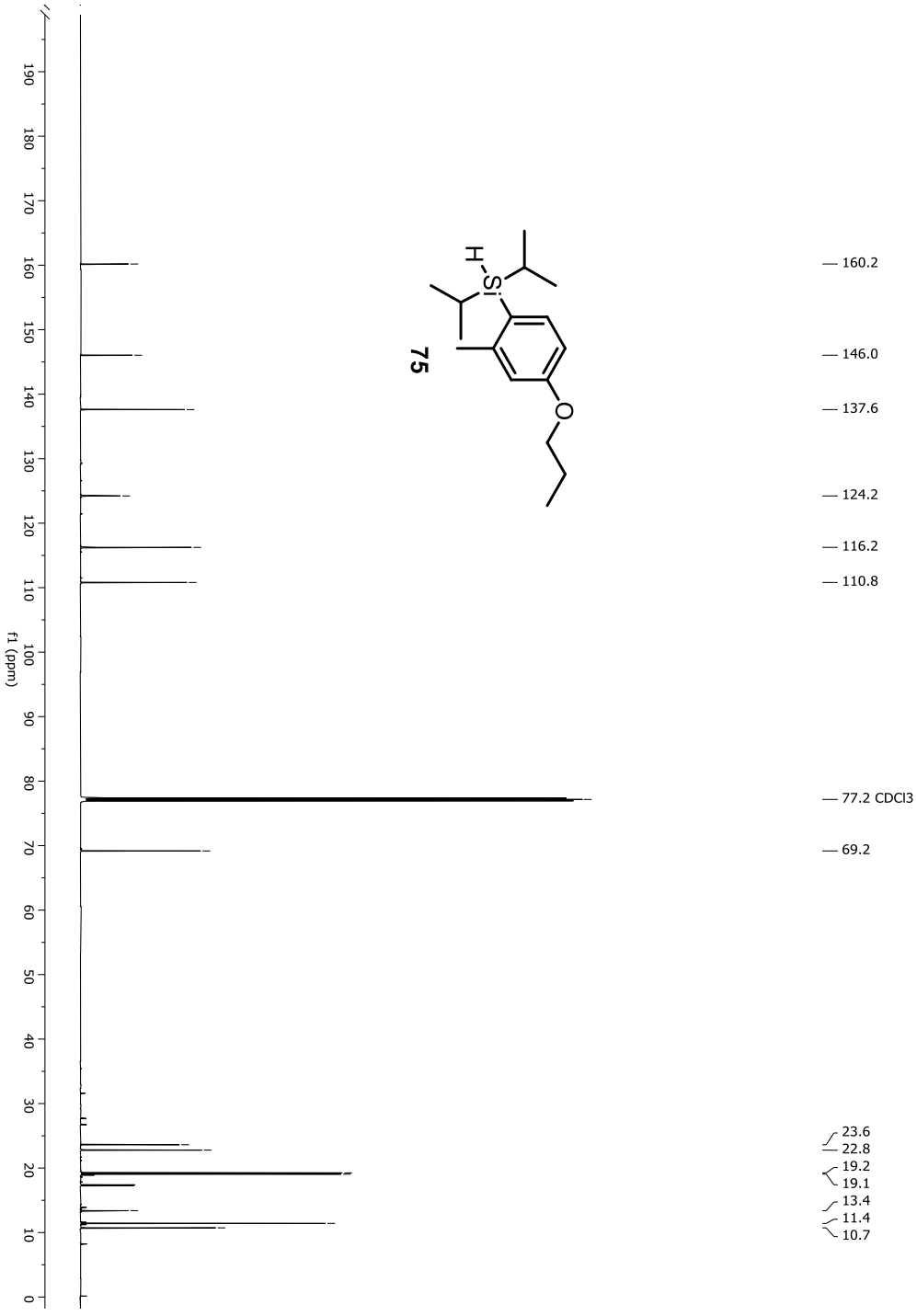

Figure A-102. HRMS spectrum of compound 75

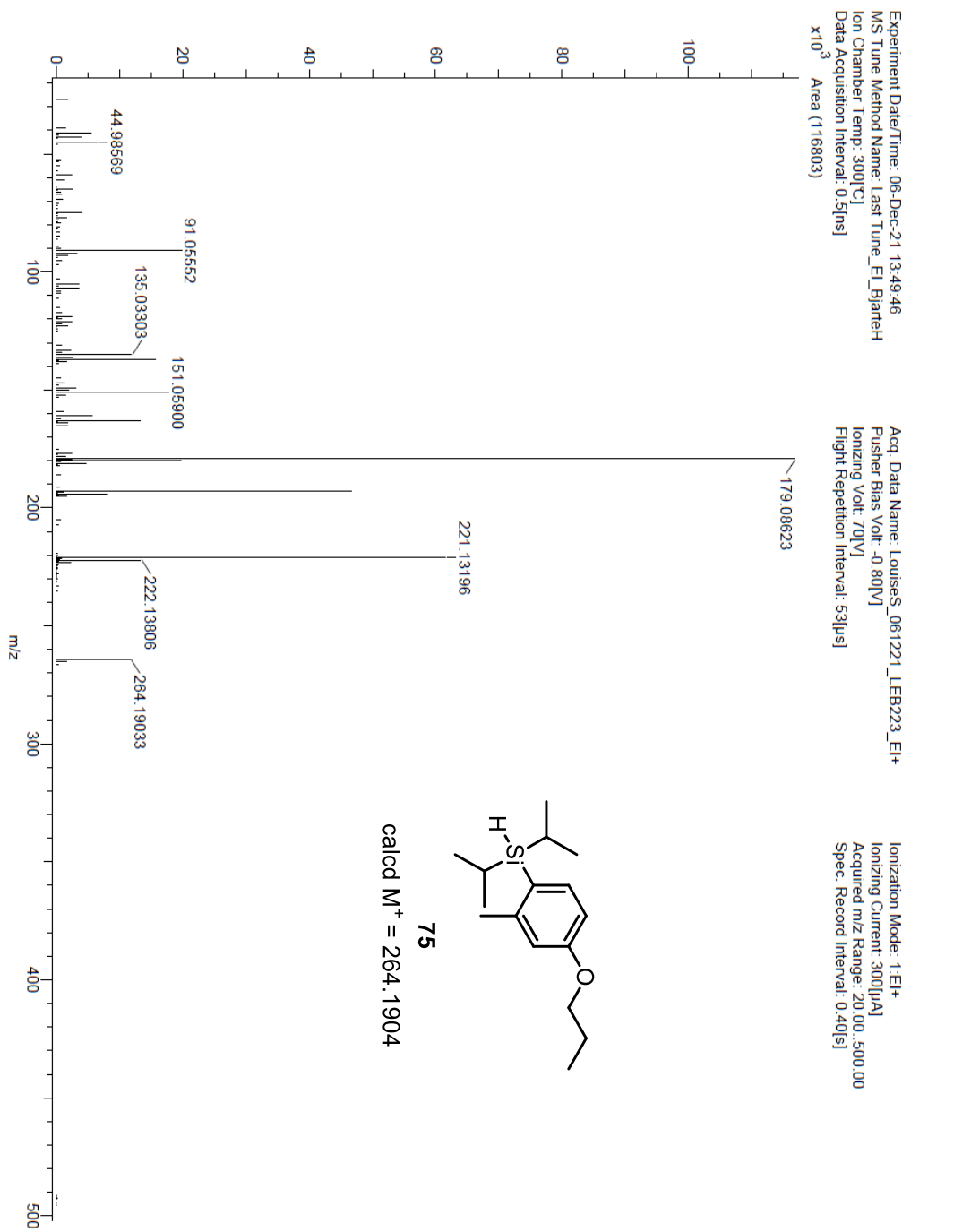

Figure A-103. ^{1}H-NMR spectrum of compound 76

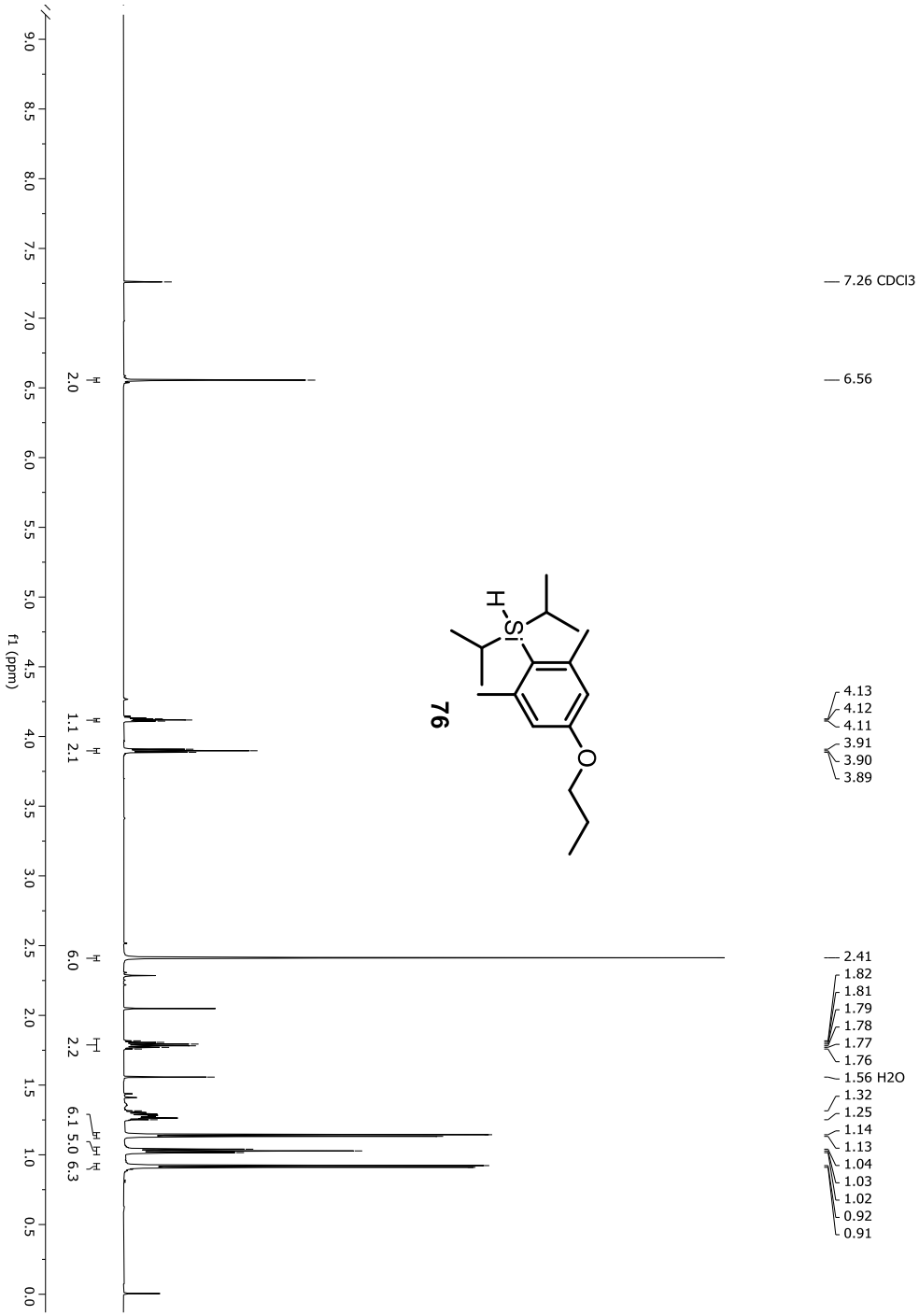

Figure A-104. ^{13}C-NMR spectrum of compound 76

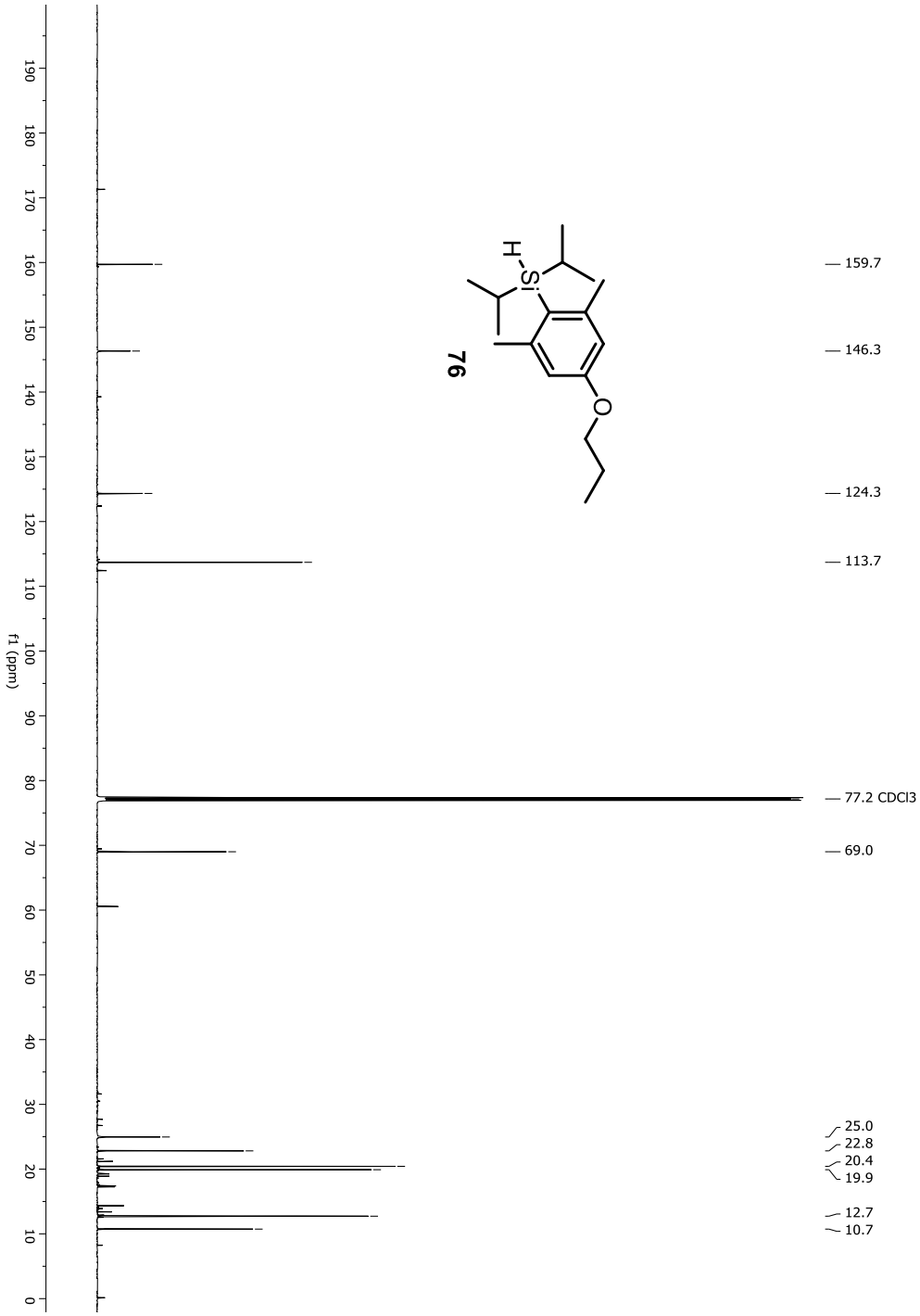

Figure A-105. HRMS spectrum of compound 115

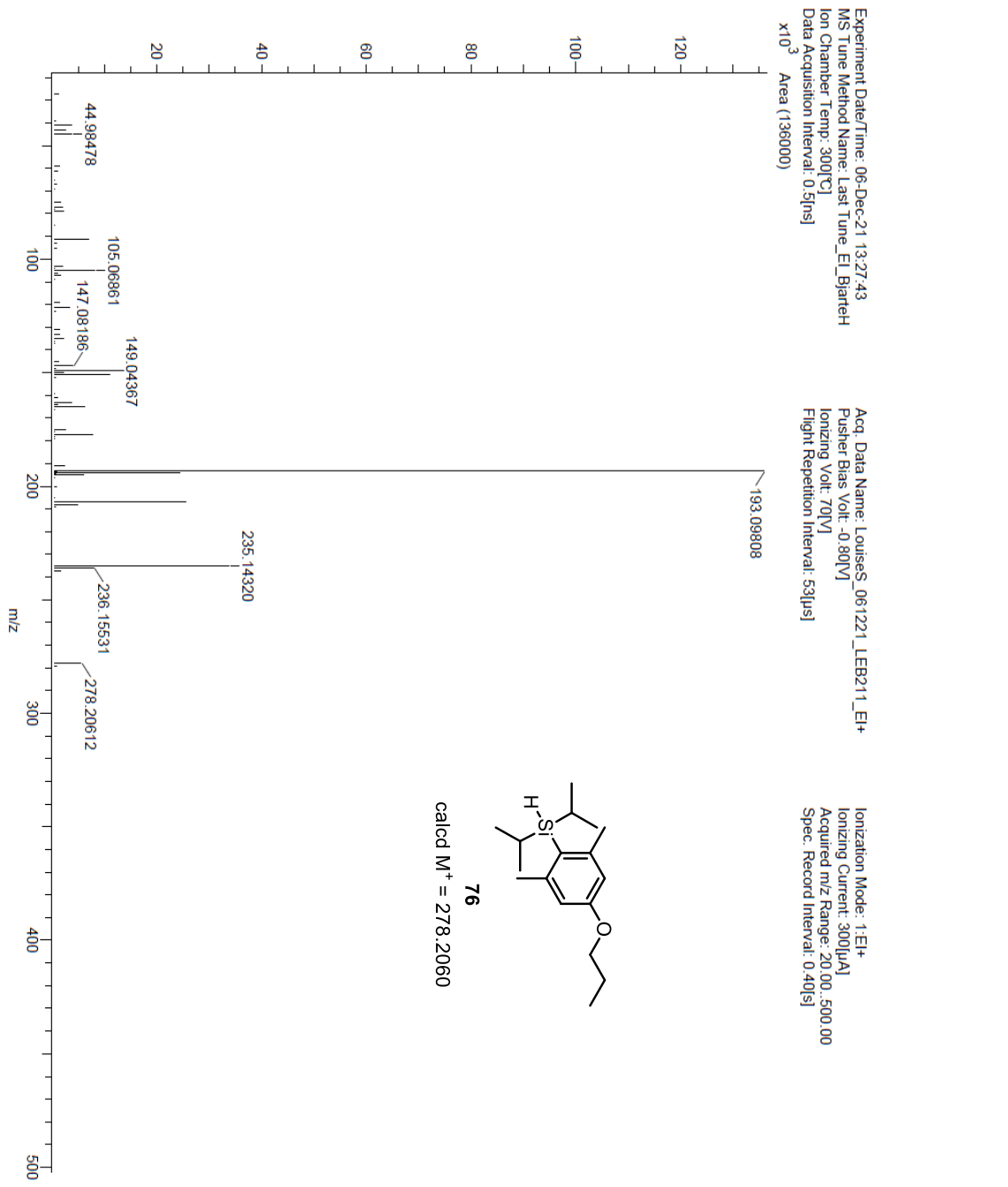

Figure A-106. ^{1}H-NMR spectrum of compound 77

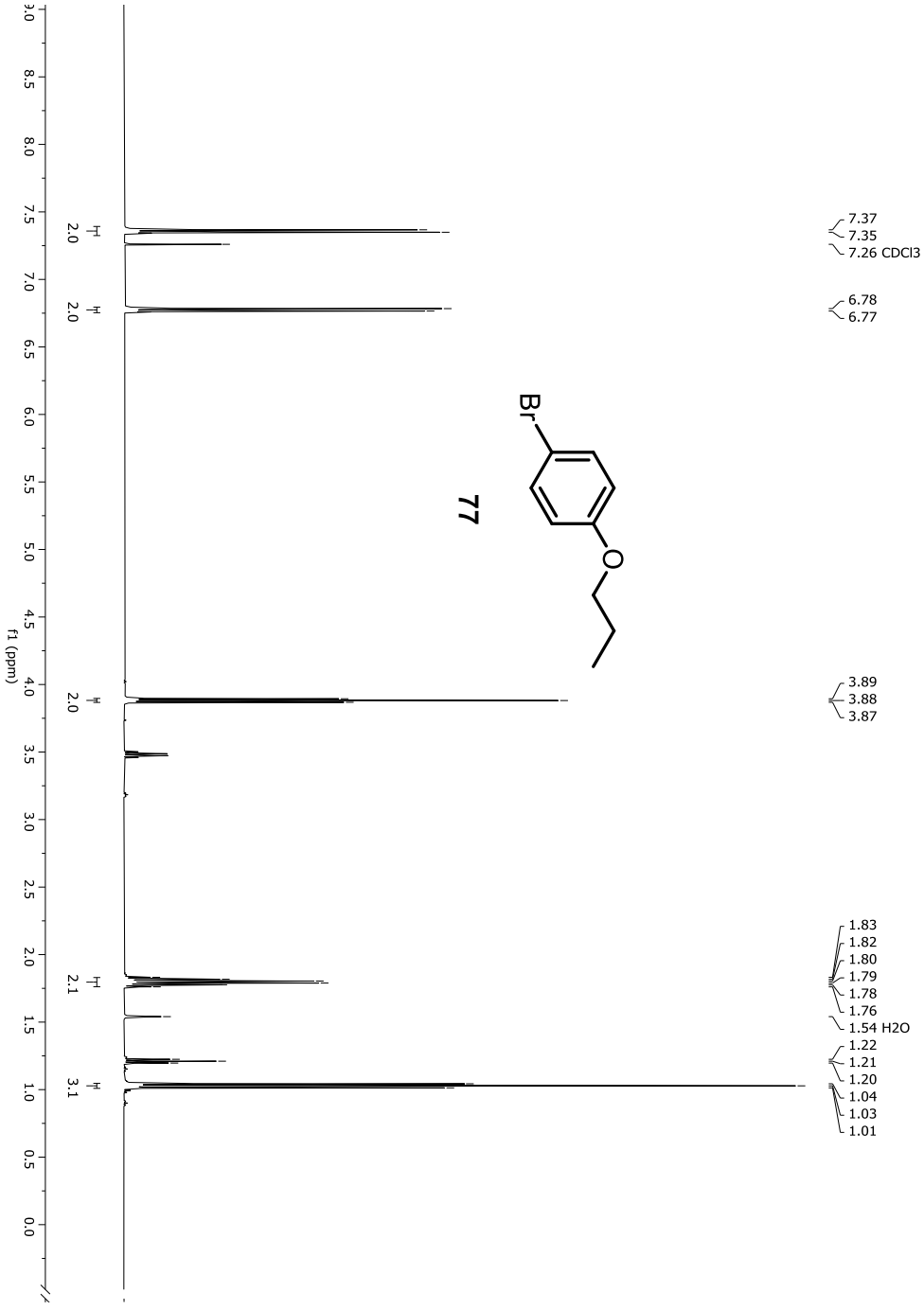

Figure A-107. ^{13}C-NMR spectrum of compound 77

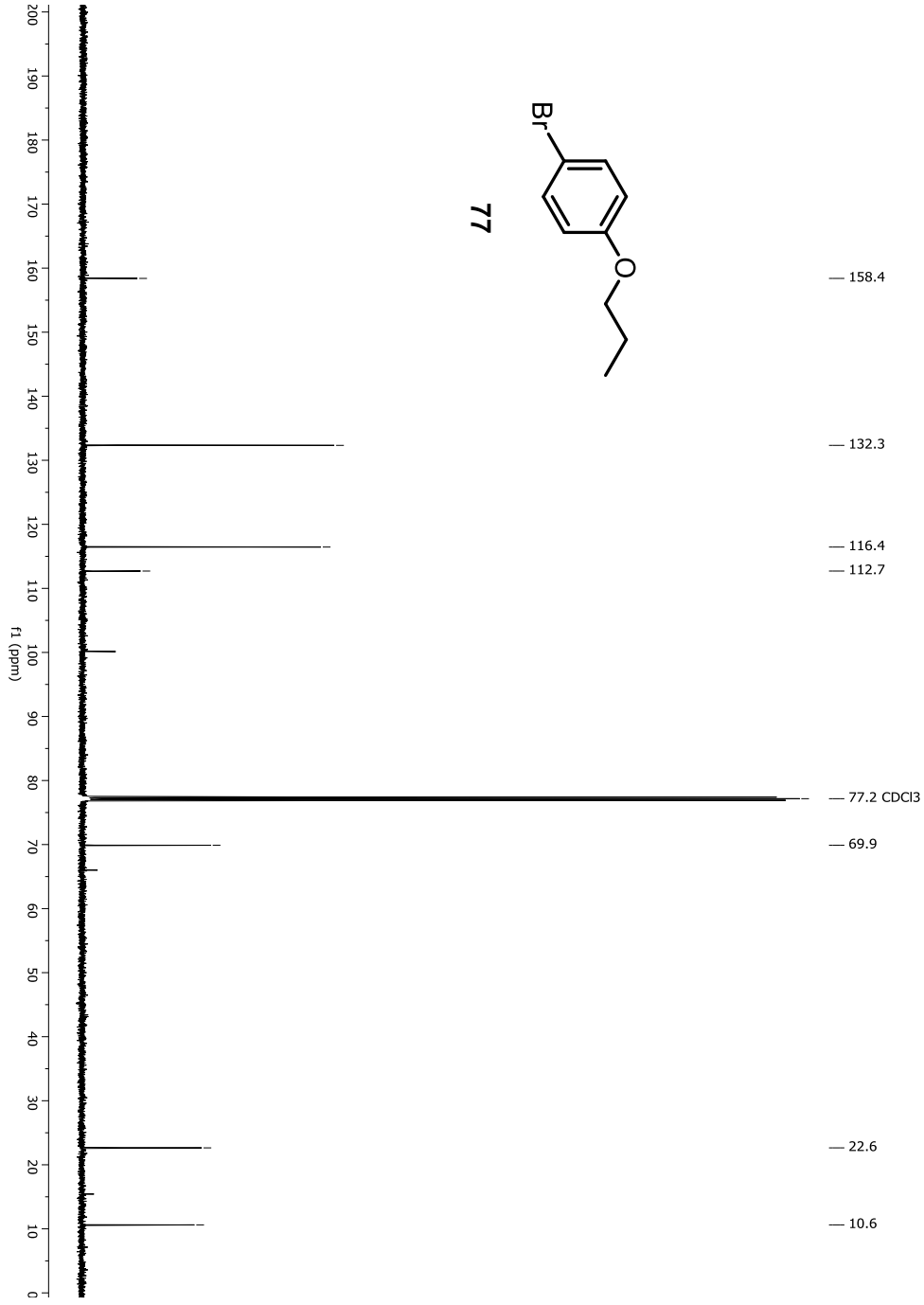

Figure A-108. ^{1}H-NMR spectrum of compound 80

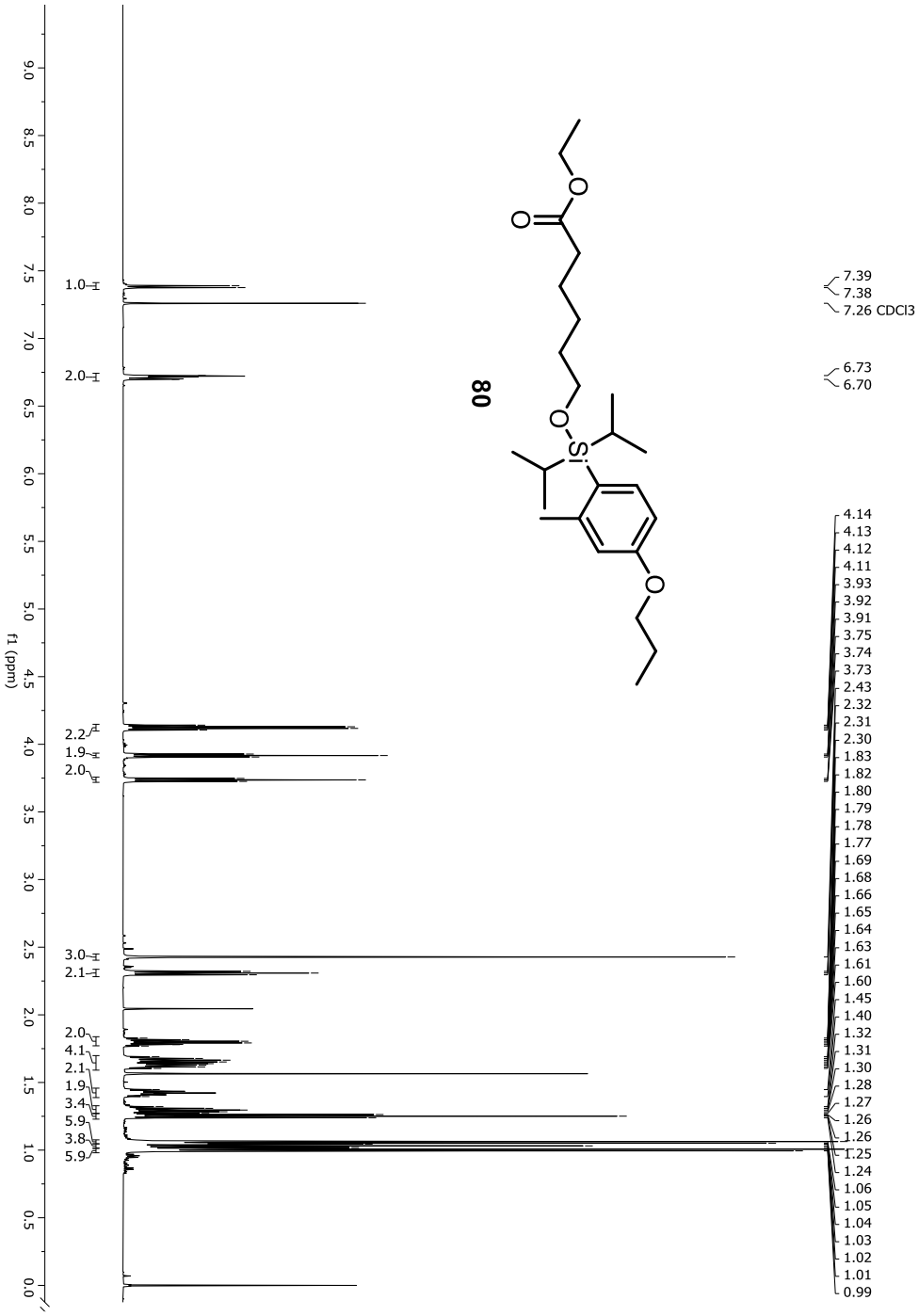

Figure A-109. ^{13}C-NMR spectrum of compound 80

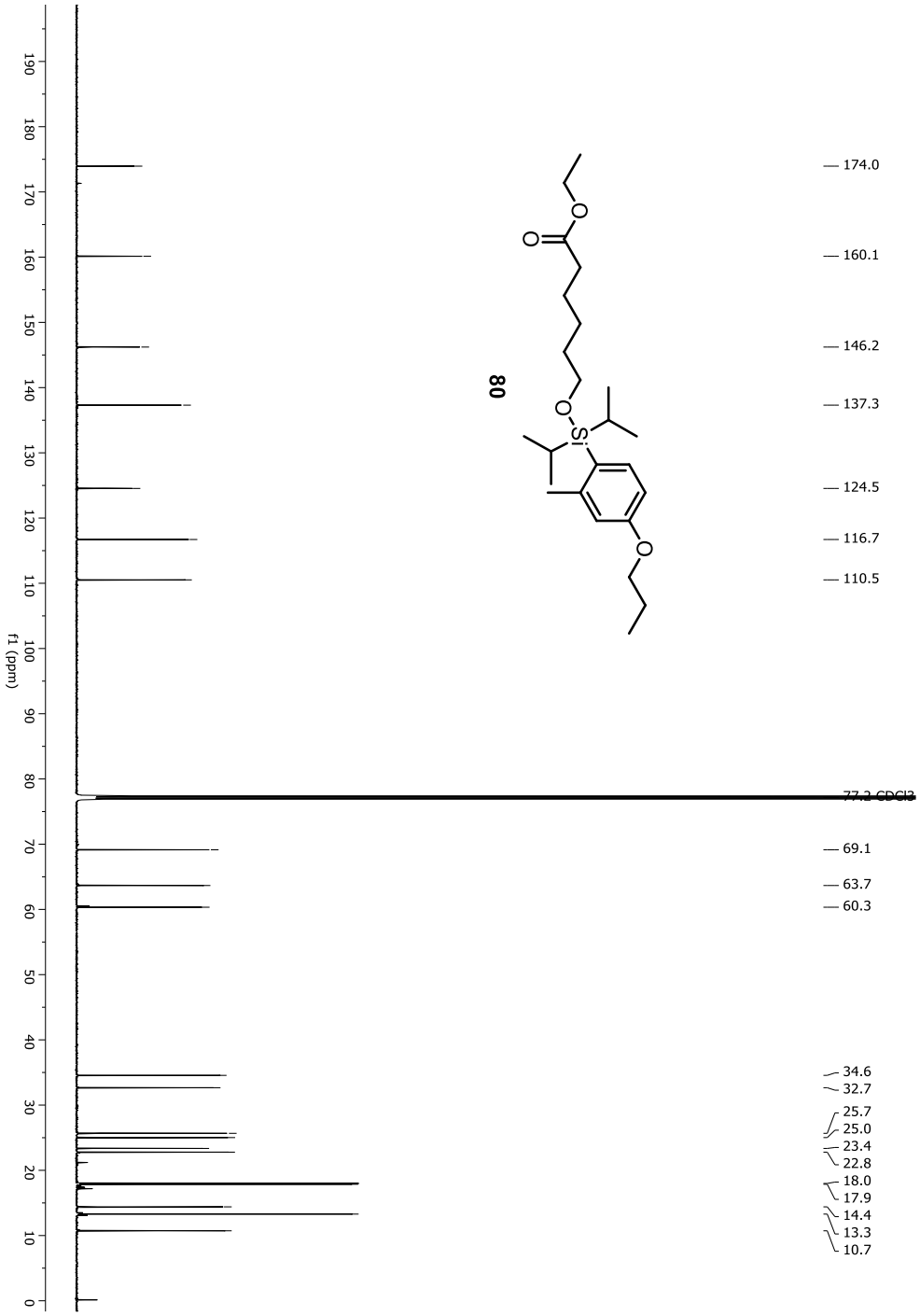

Figure A-110. HRMS spectrum of compound 80

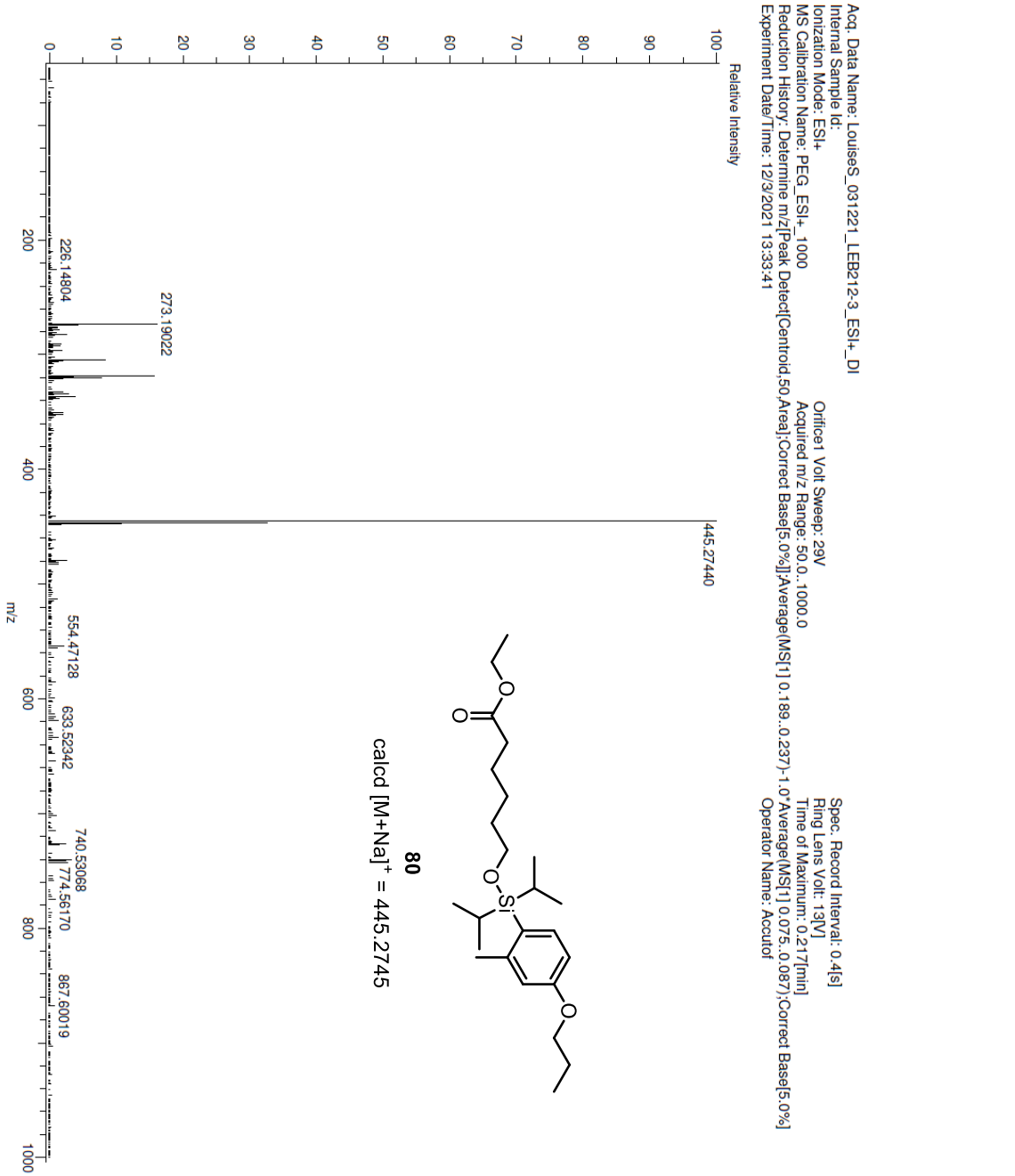

Figure A-111. ^{1}H-NMR spectrum of compound 82

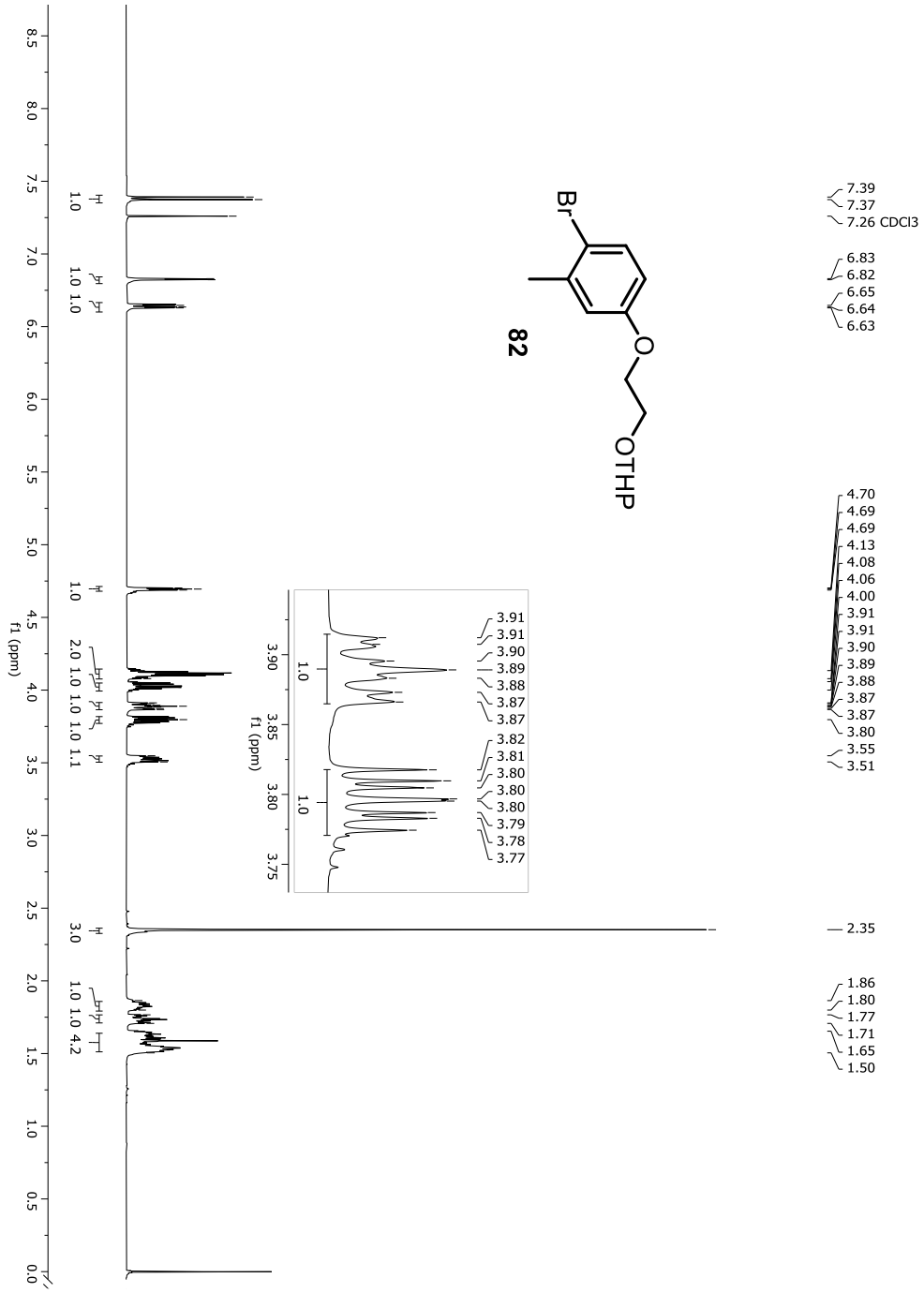

Figure A-112. ^{13}C-NMR spectrum of compound 82

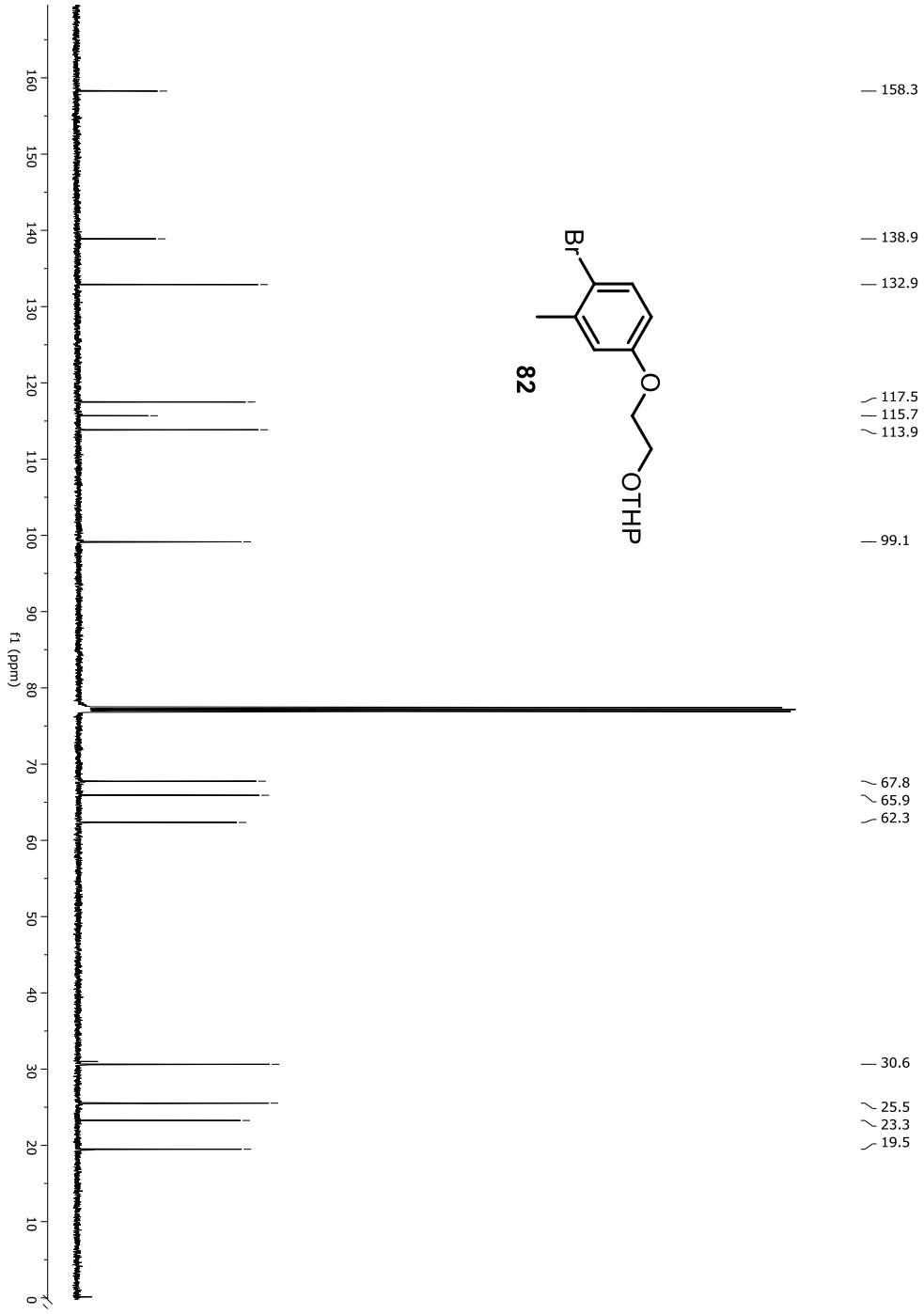

Figure A113. HRMS spectrum of compound 82

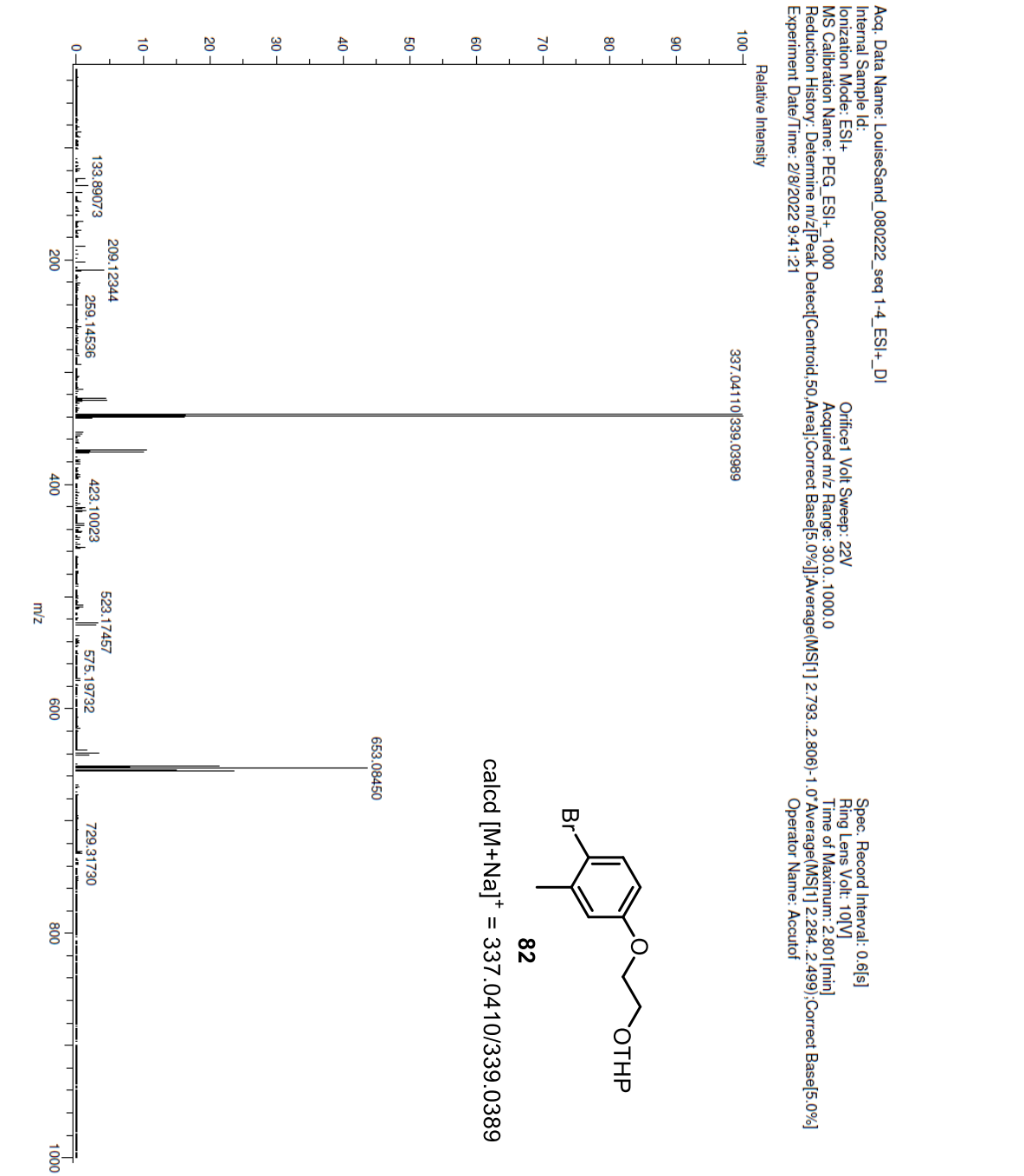

Figure A-114. ^{1}H-NMR spectrum of compound 83

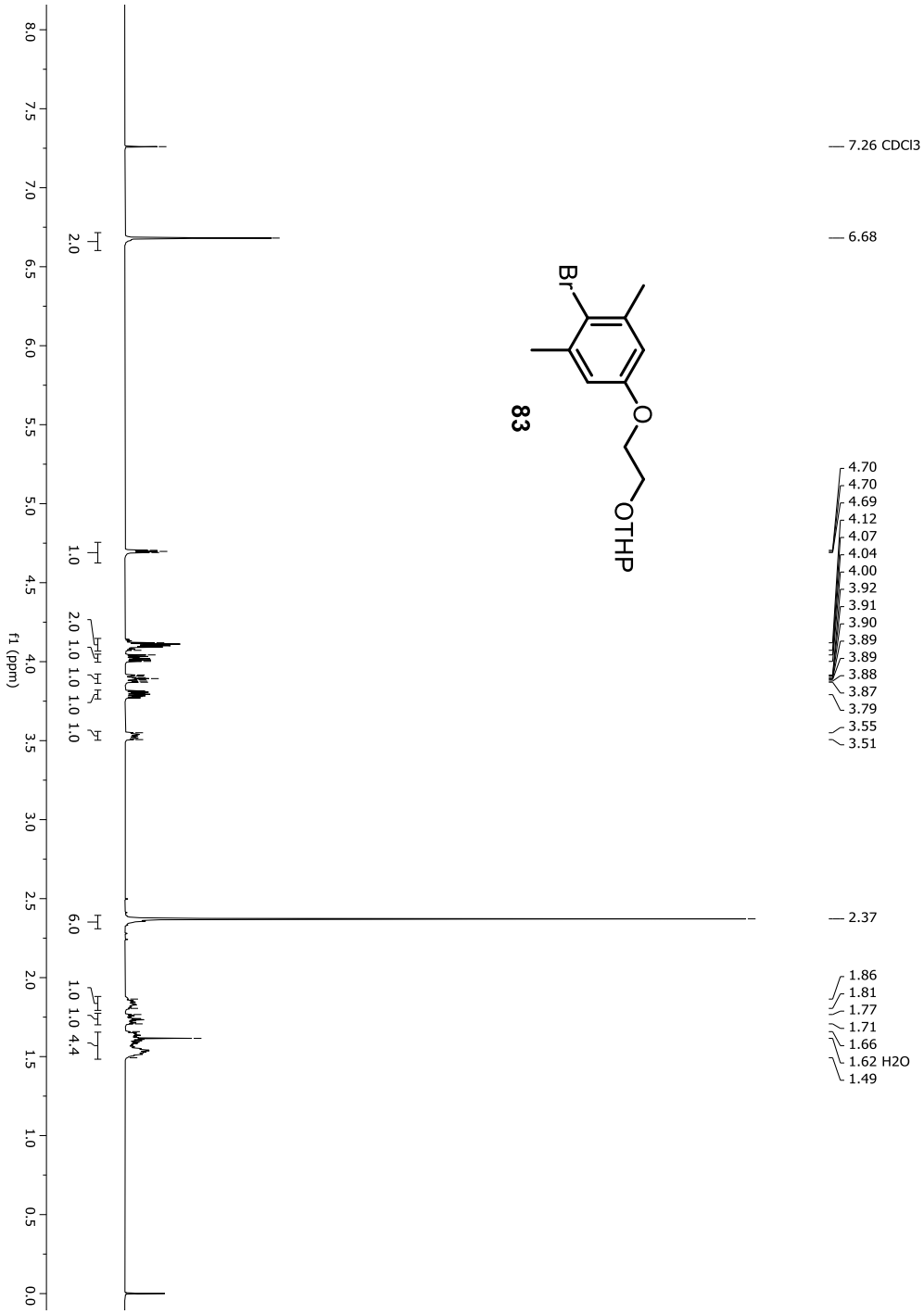

Figure A-115. ^{13}C-NMR spectrum of compound 83

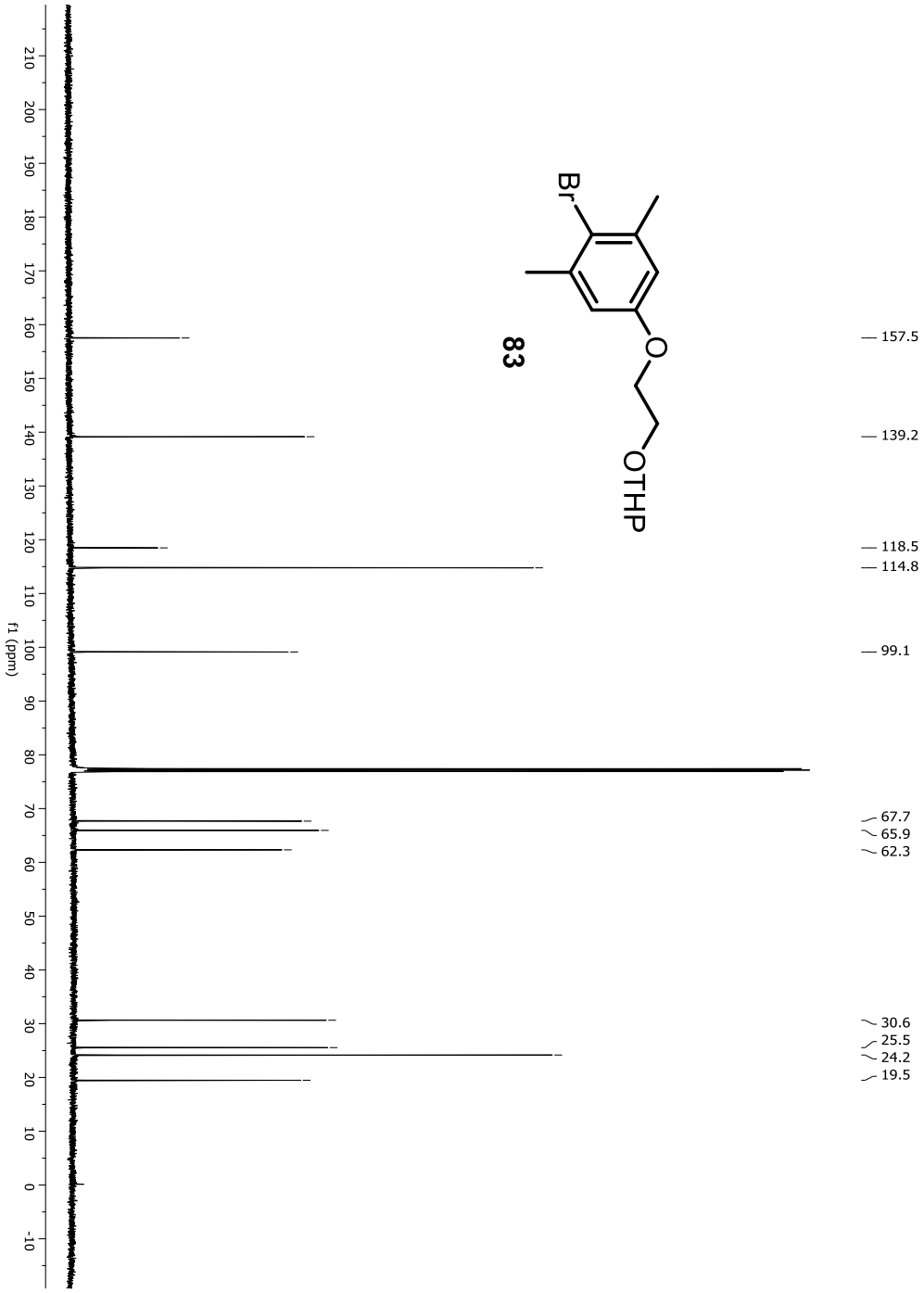

Figure A-116. HRMS spectrum of compound 83

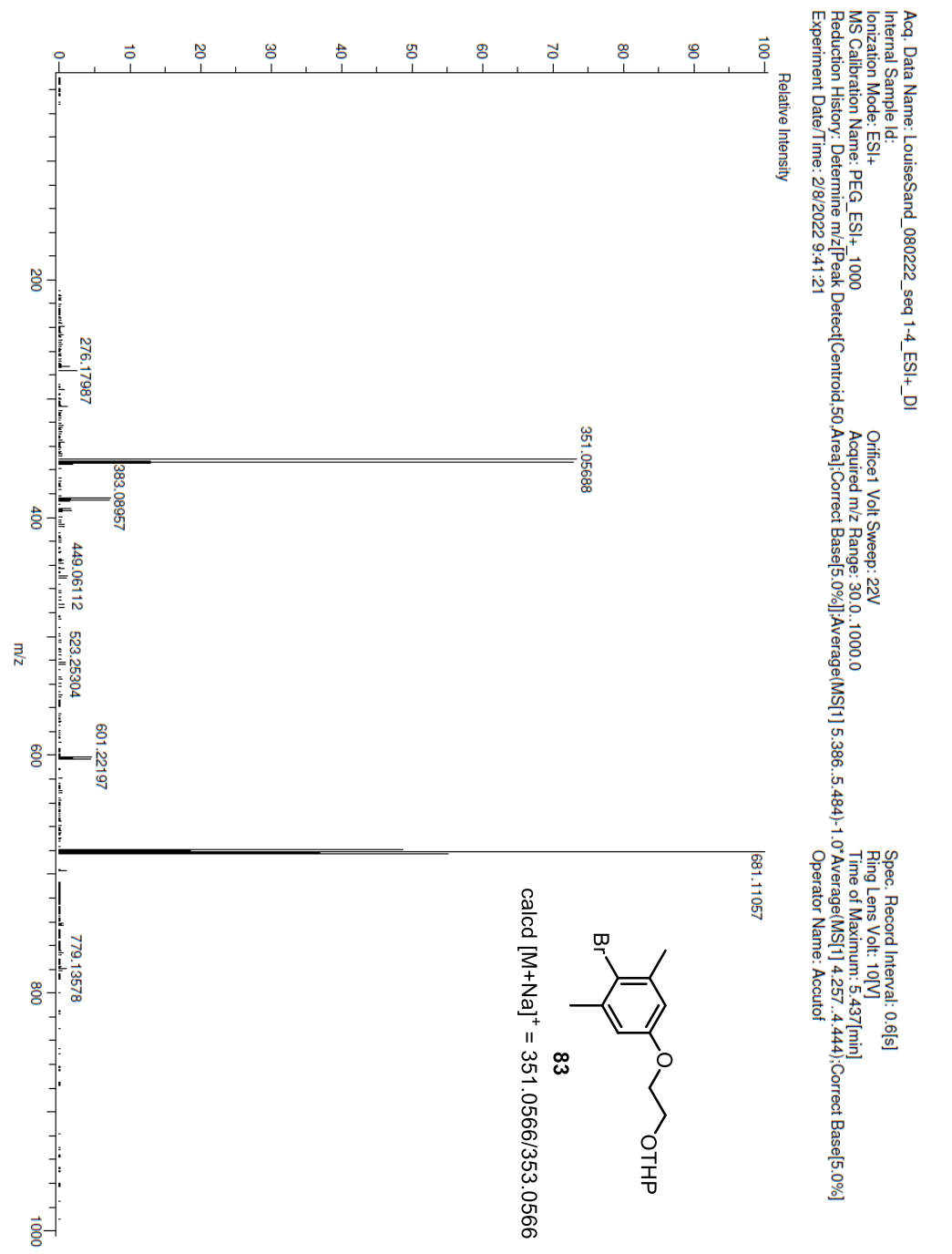

Figure A-117. ^{1}H NMR spectrum of compound 84

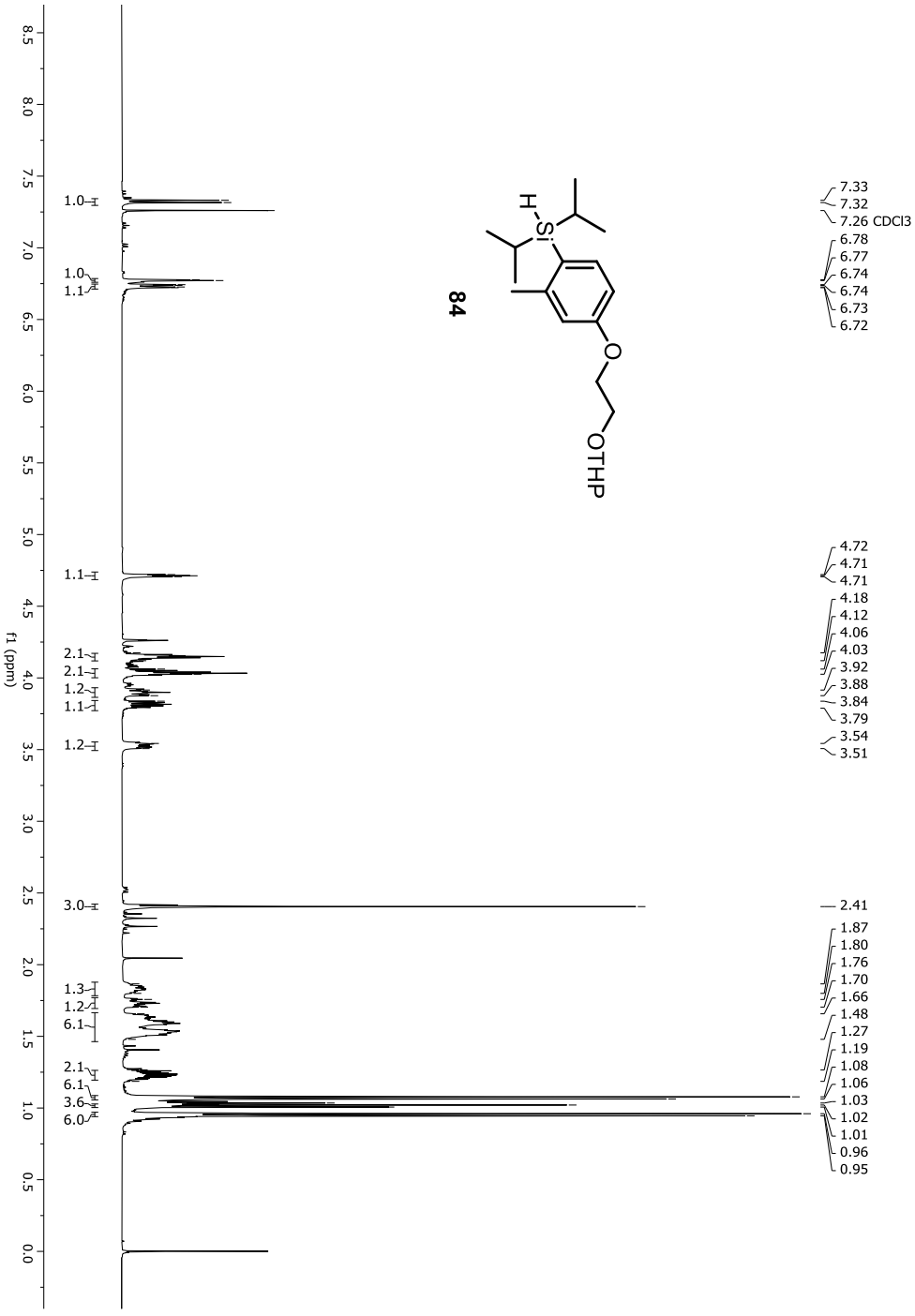

Figure A-118. ^{13}C-NMR spectrum of compound 84

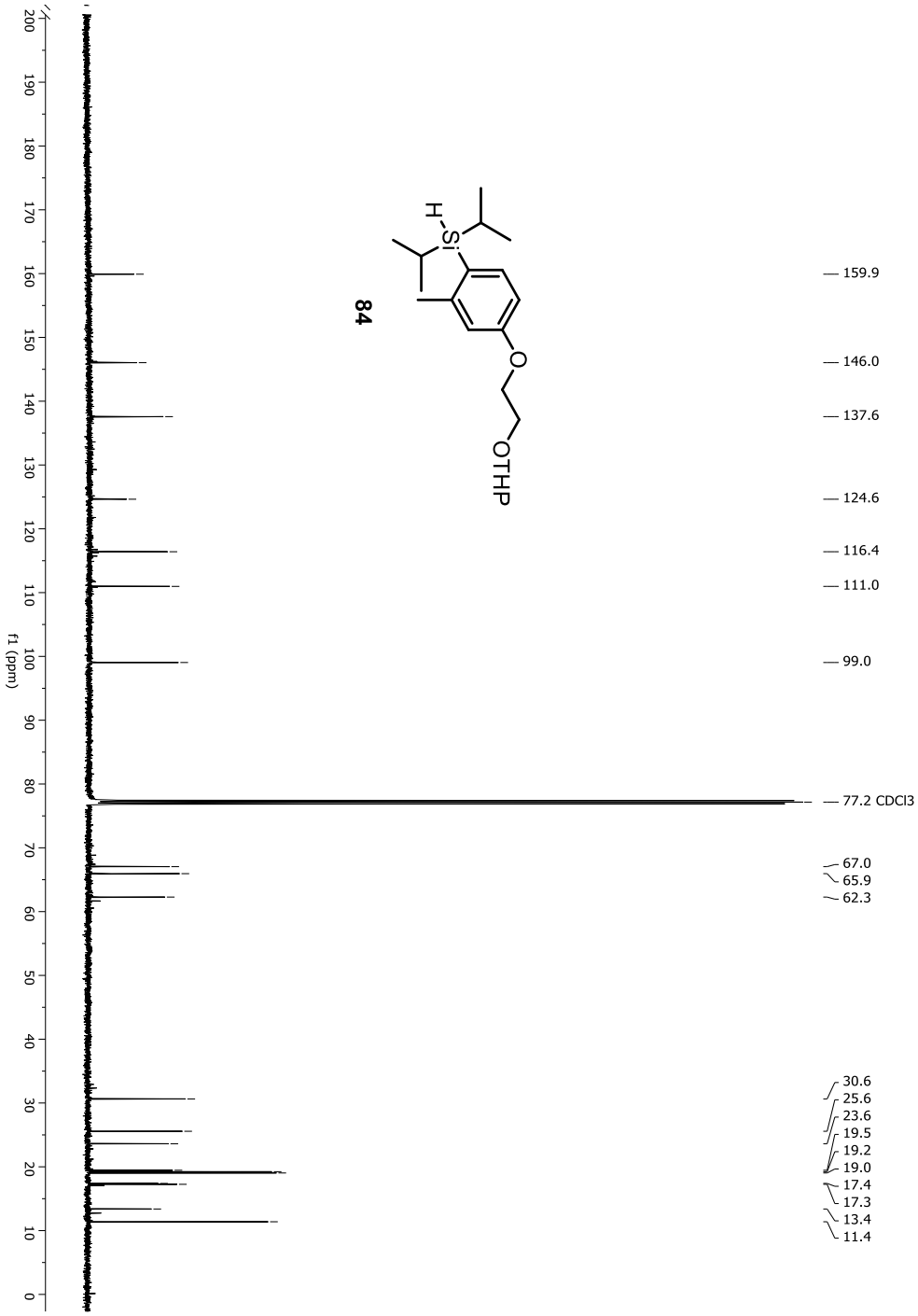

Figure A-119. ^{1}H-NMR spectrum of compound 85

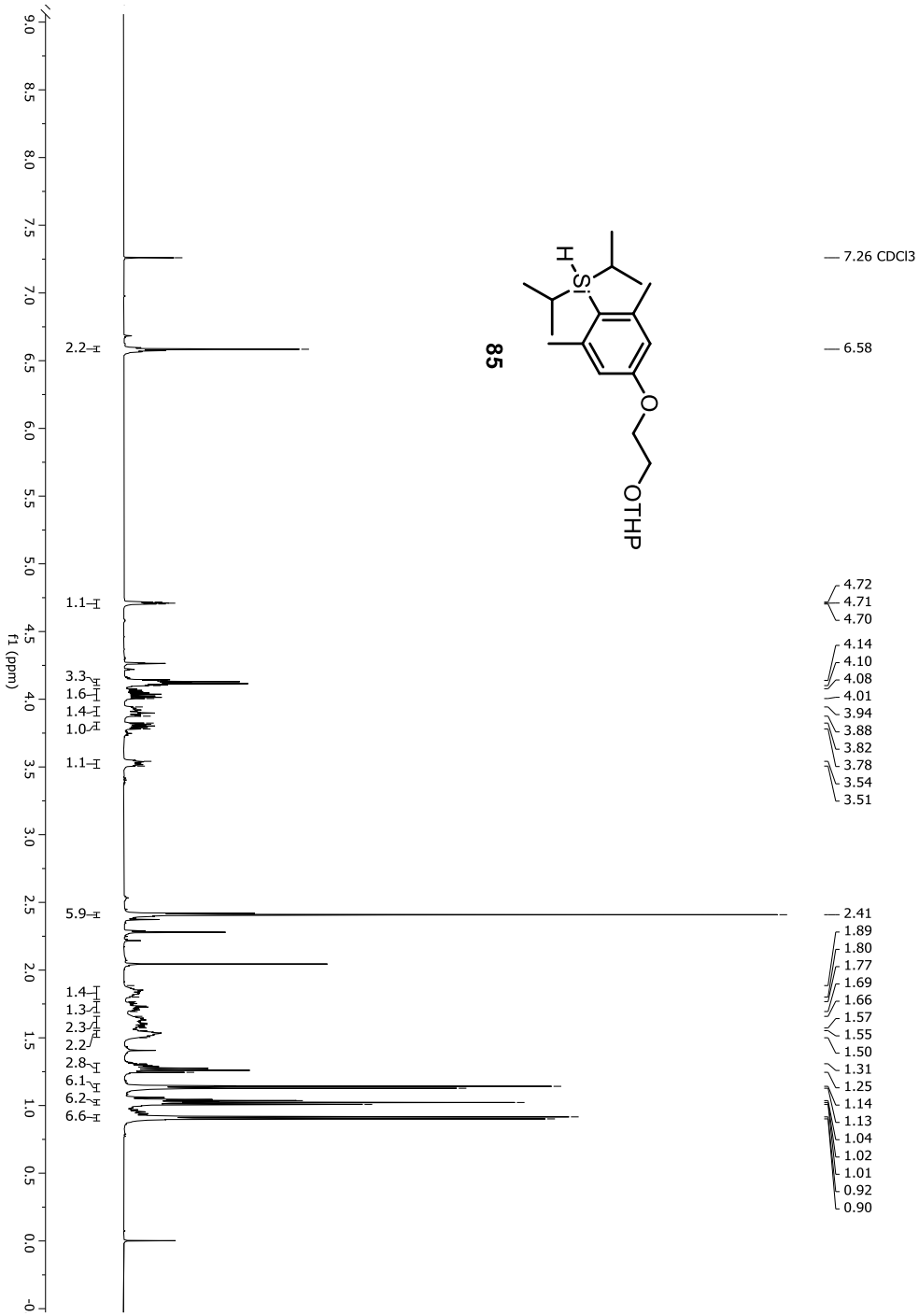

Figure A-120. ^{13}C-NMR spectrum of compound 85

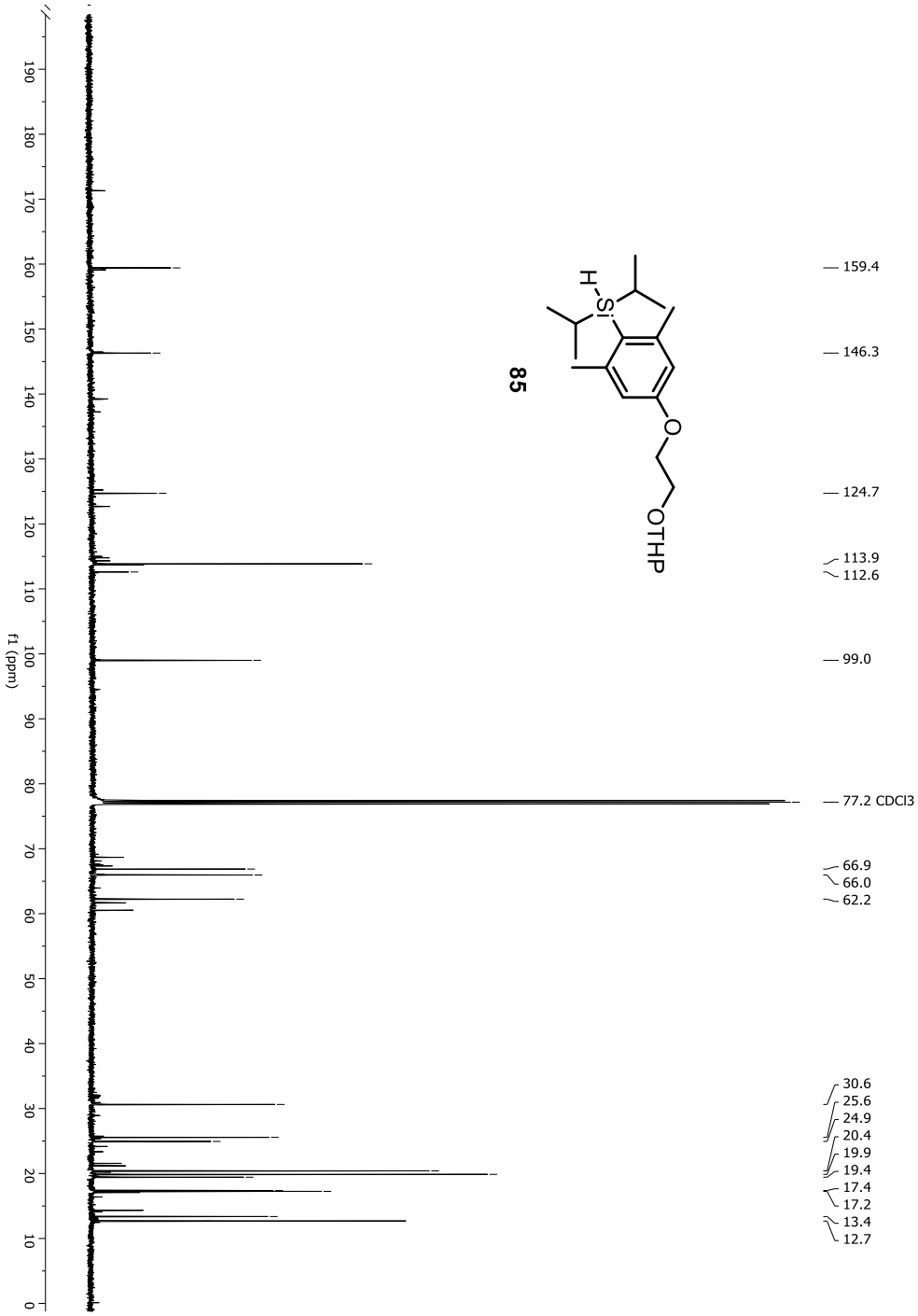

Figure A-121. ^{1}H-NMR spectrum of compound 86

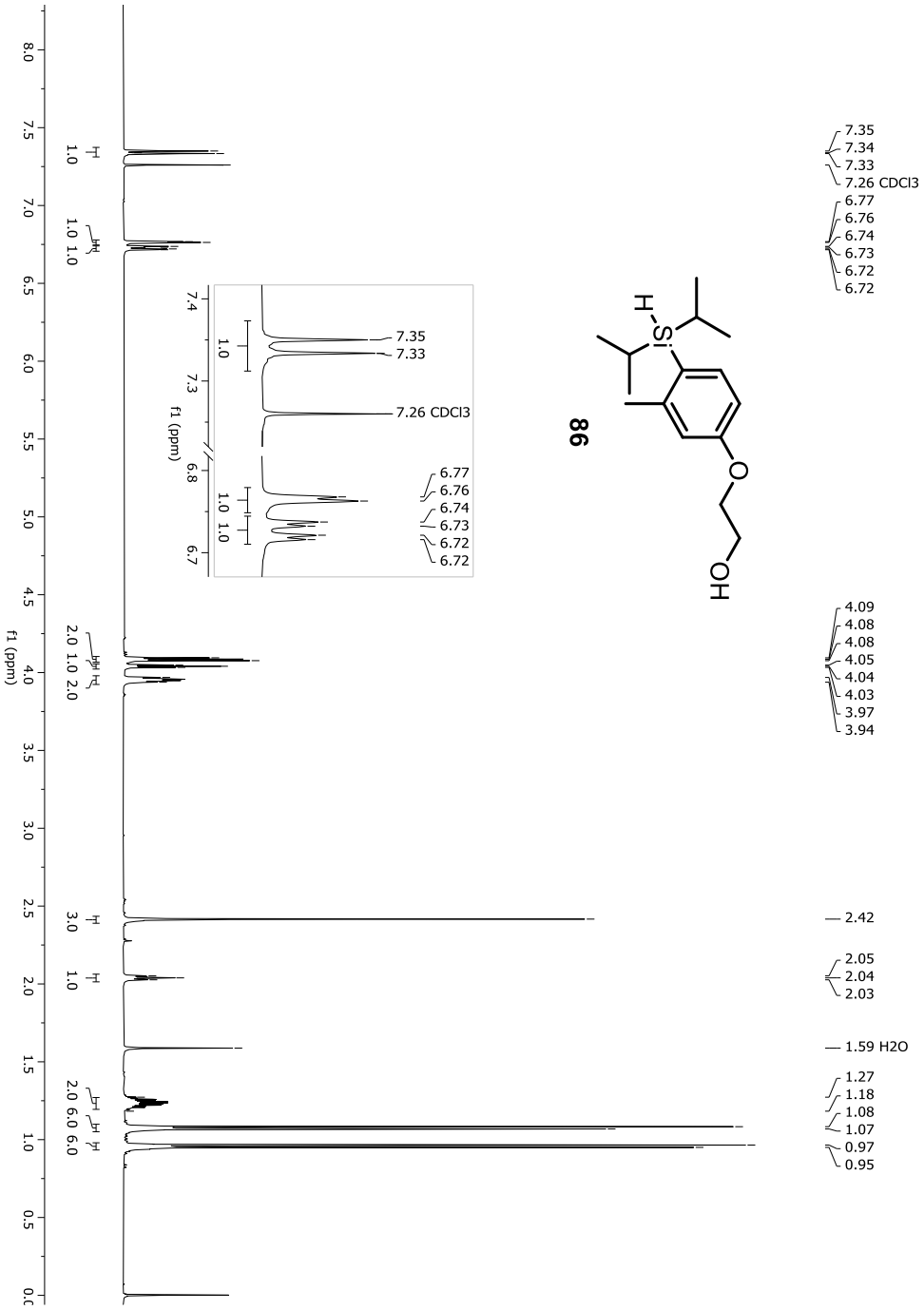

Figure A-122. ^{13}C-NMR spectrum of compound 86

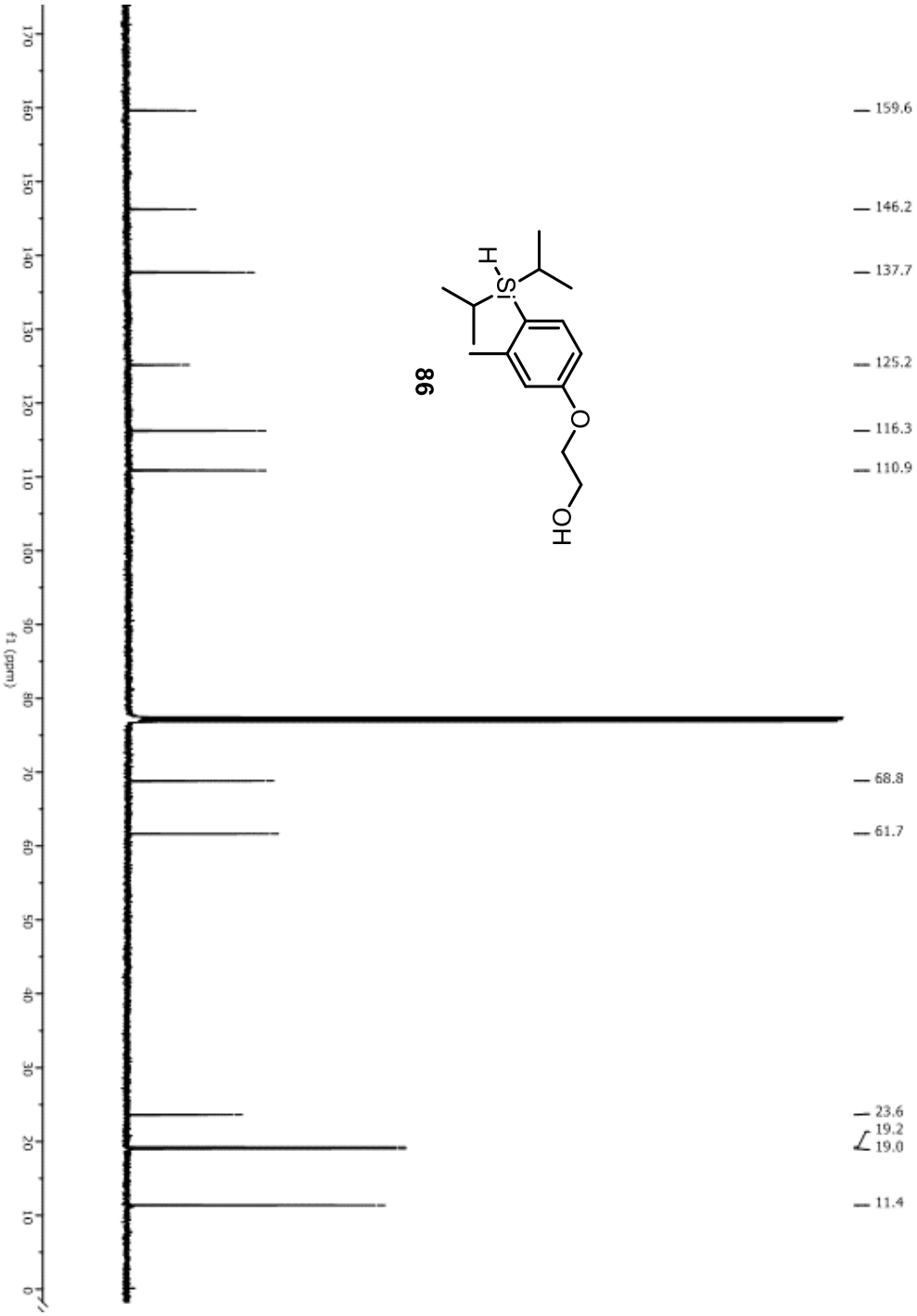

Figure A-123. HRMS spectrum of compound 86

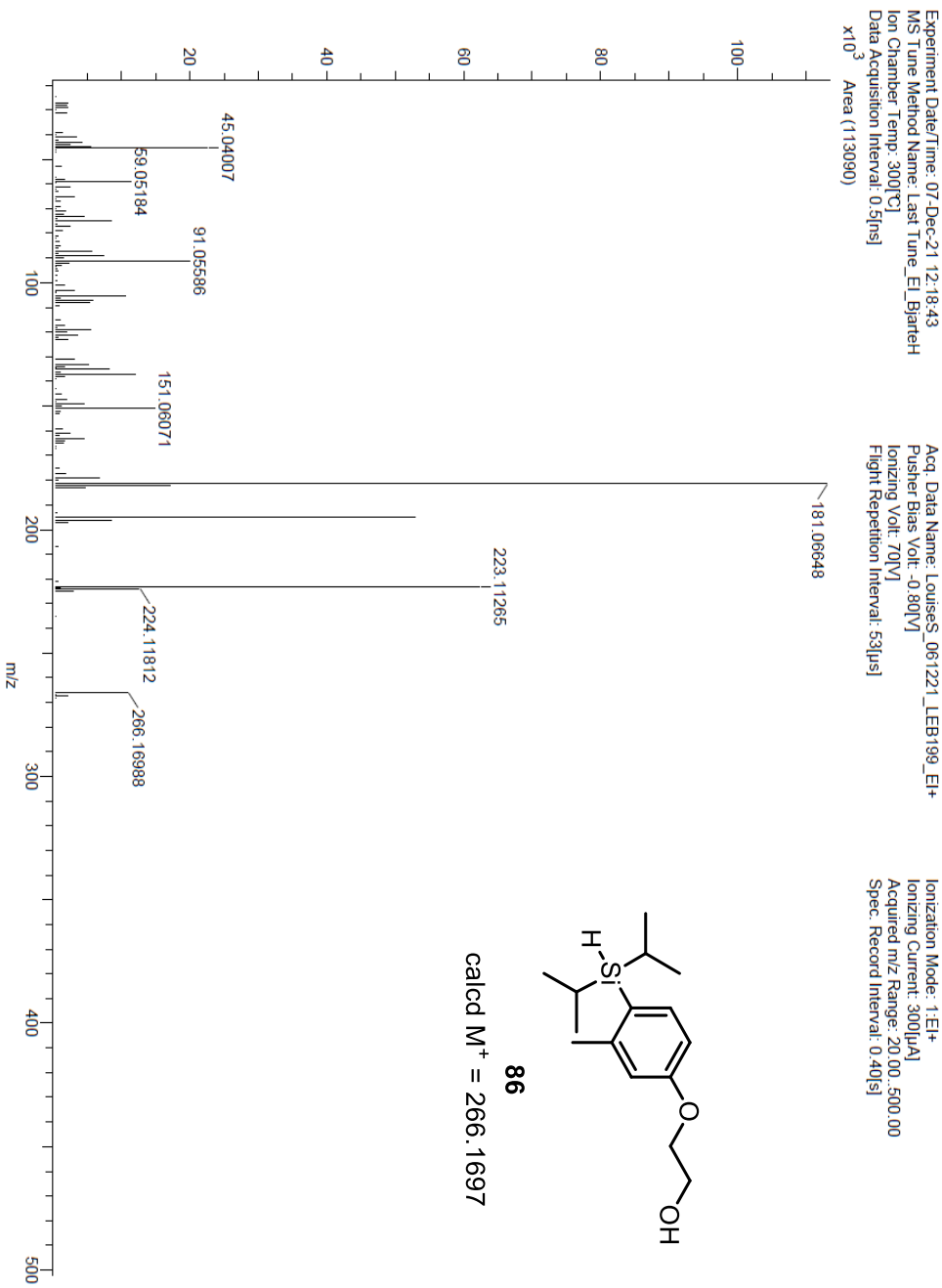

Figure A-124. ^{1}H-NMR spectrum of compound 87

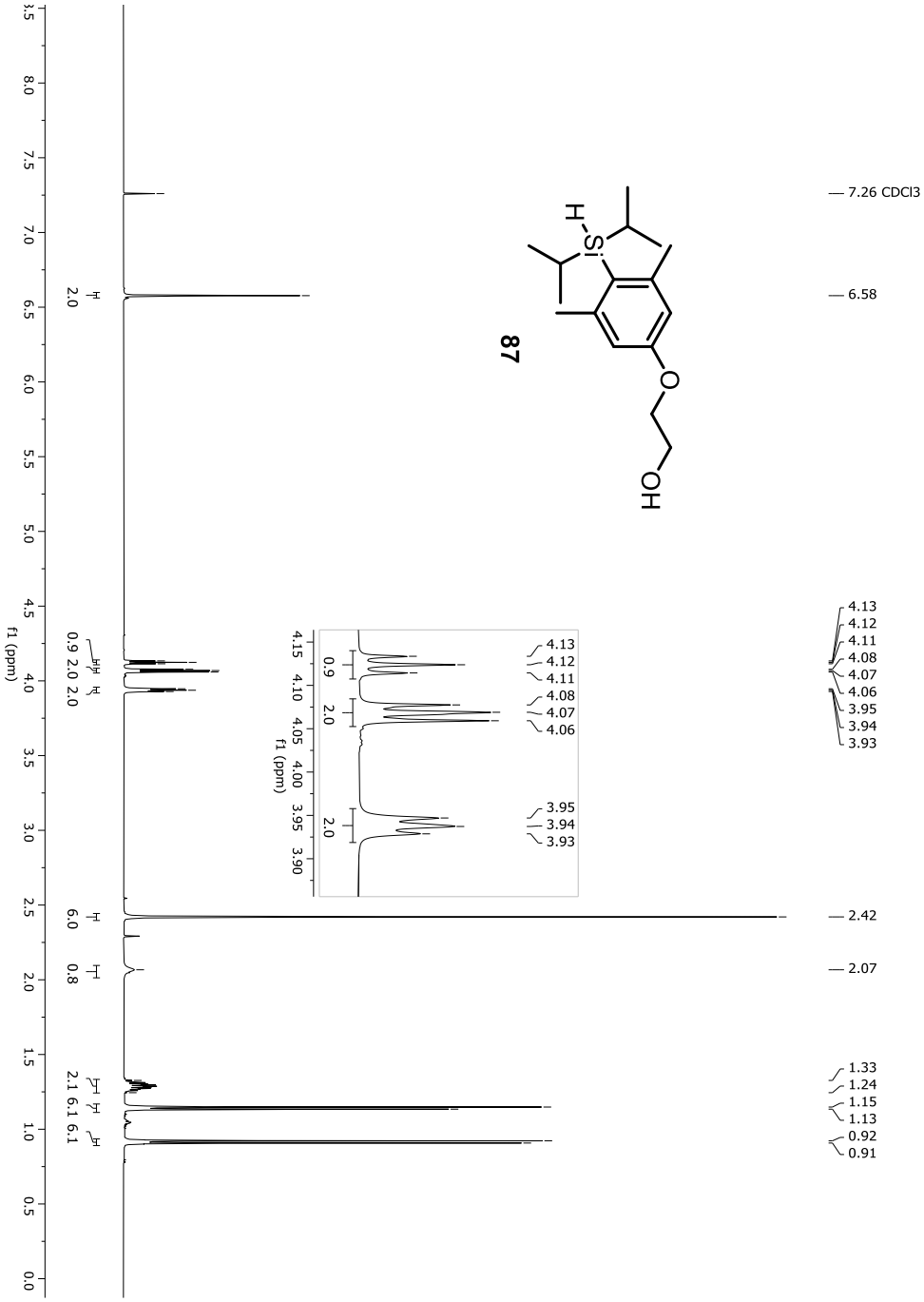

Figure A-125. ^{13}C-NMR spectrum of compound 87

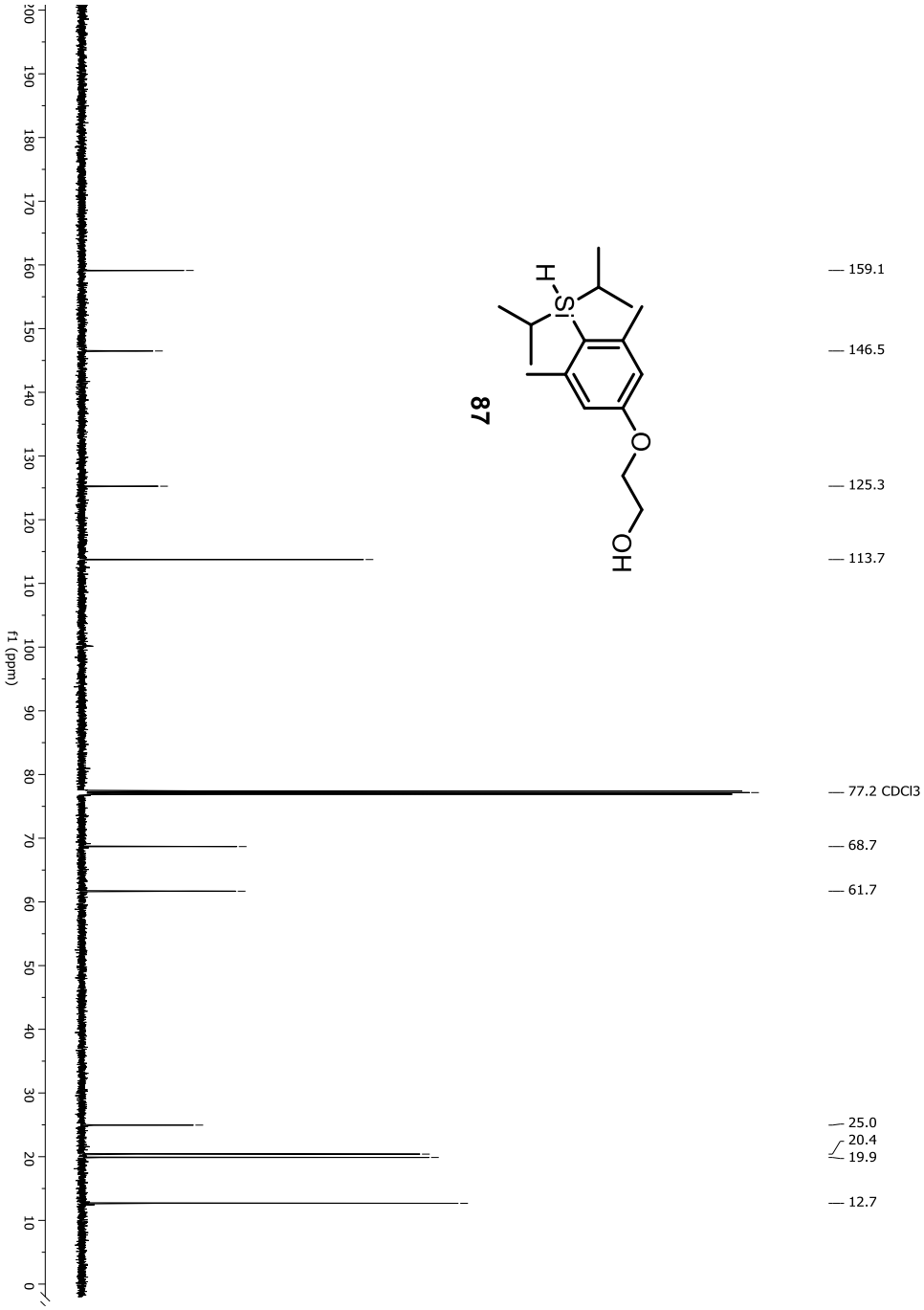

Figure A-126. HRMS spectrum of compound 87

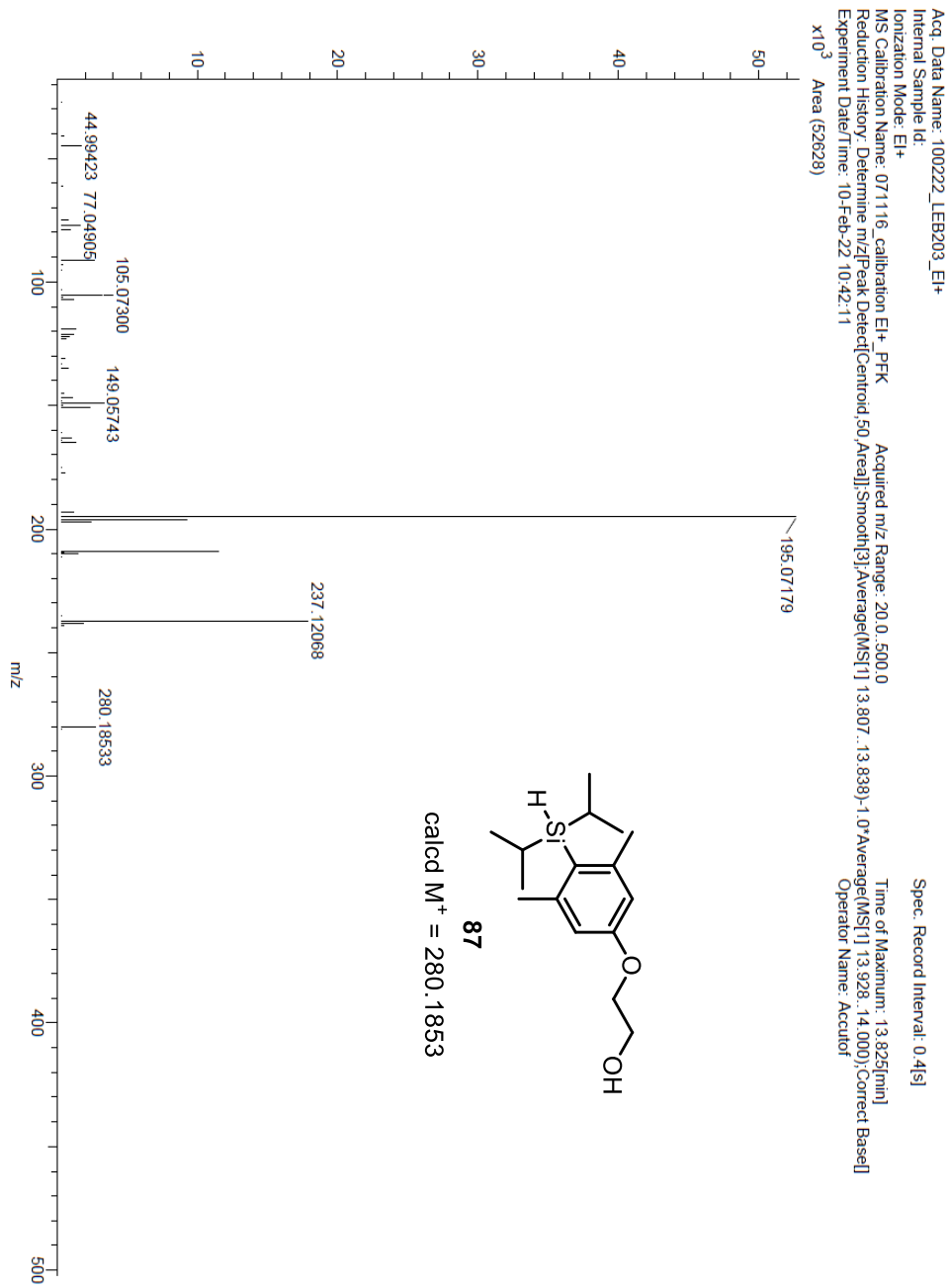

Figure A-127. ^{1}H-NMR spectrum of compound 91

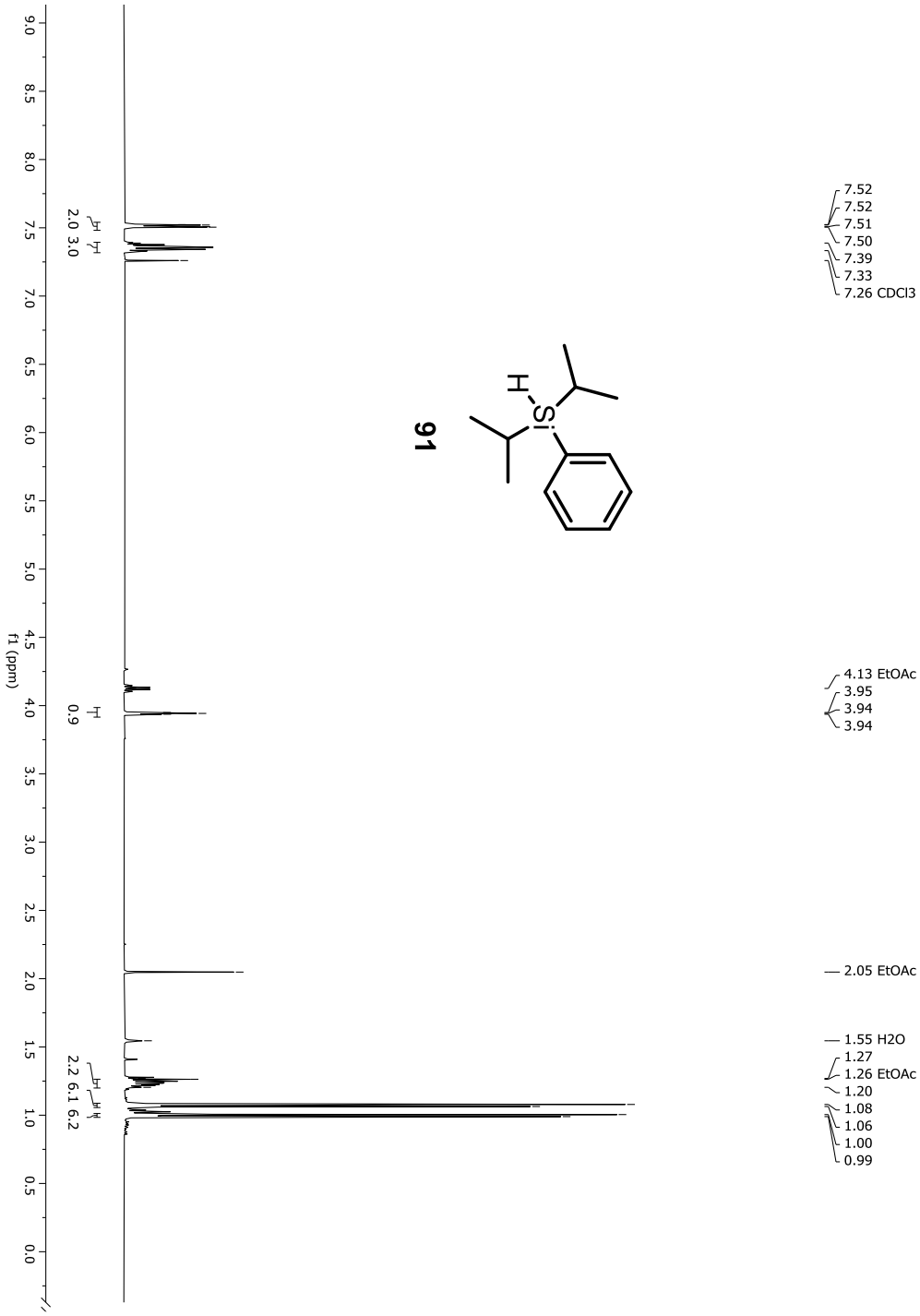

Figure A-128. ^{13}C-NMR spectrum of compound 91

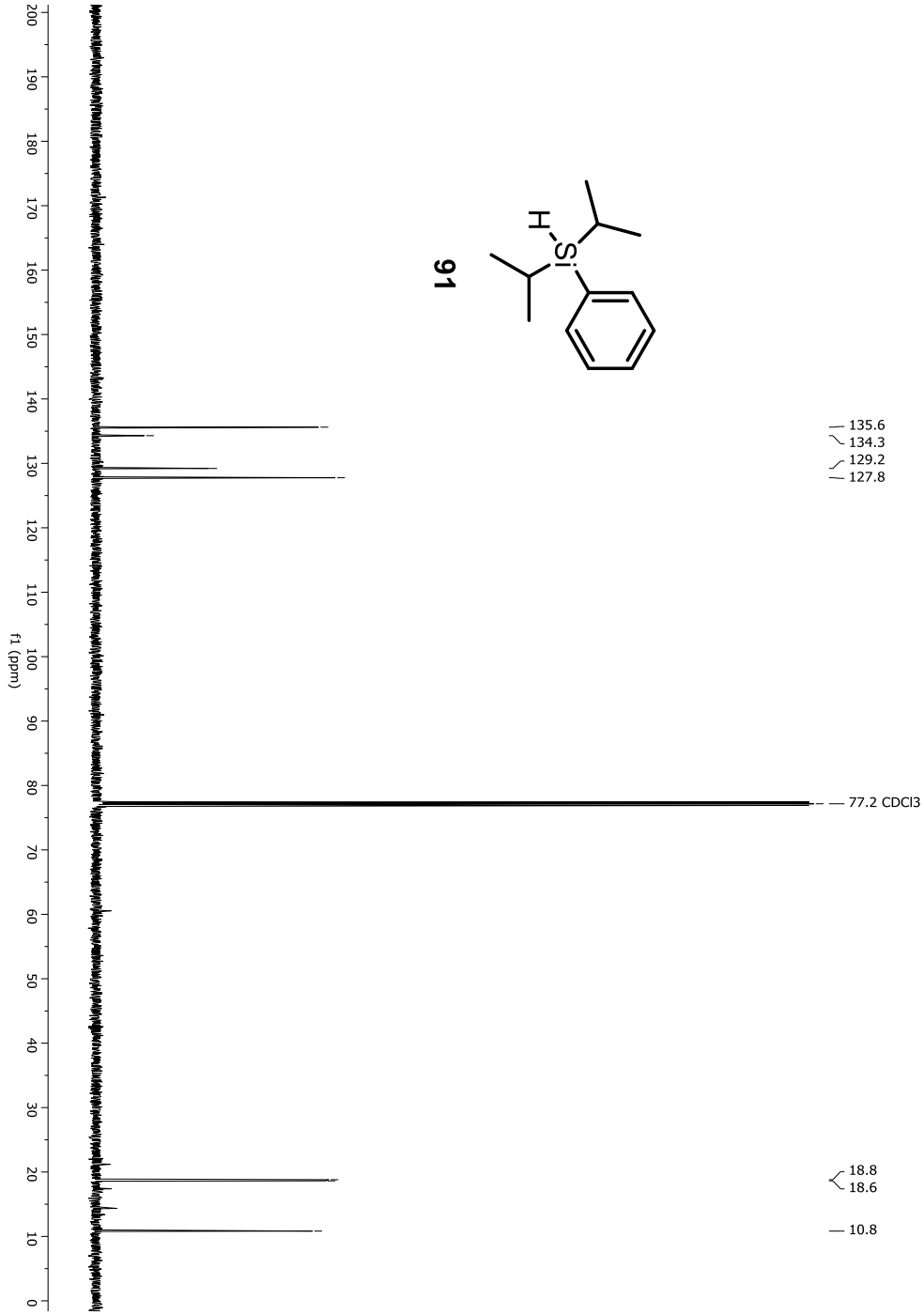

Figure A-130. ^{1}H-NMR spectrum of compound 92

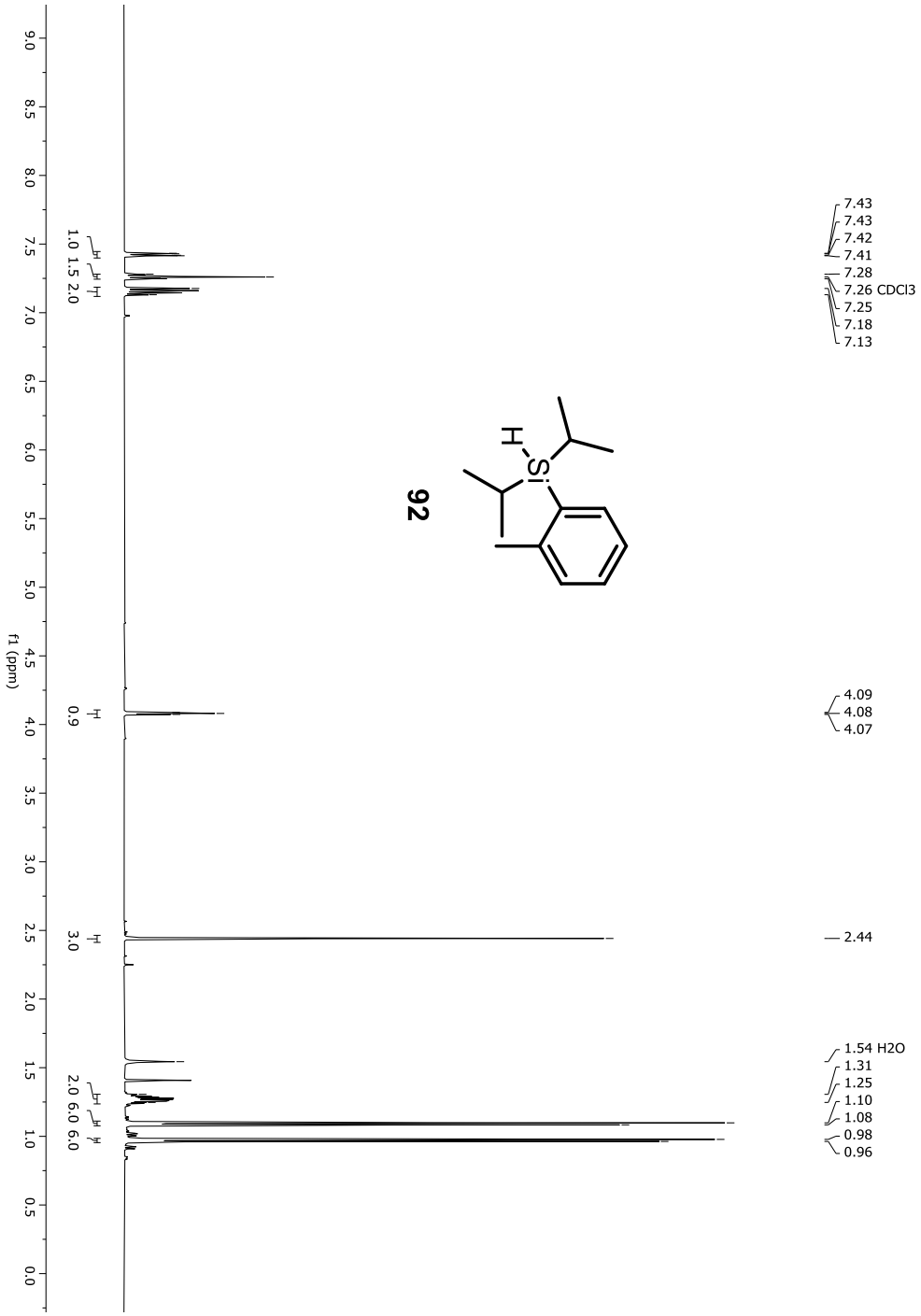

Figure A-131. ^{13}C-NMR spectrum of compound 92

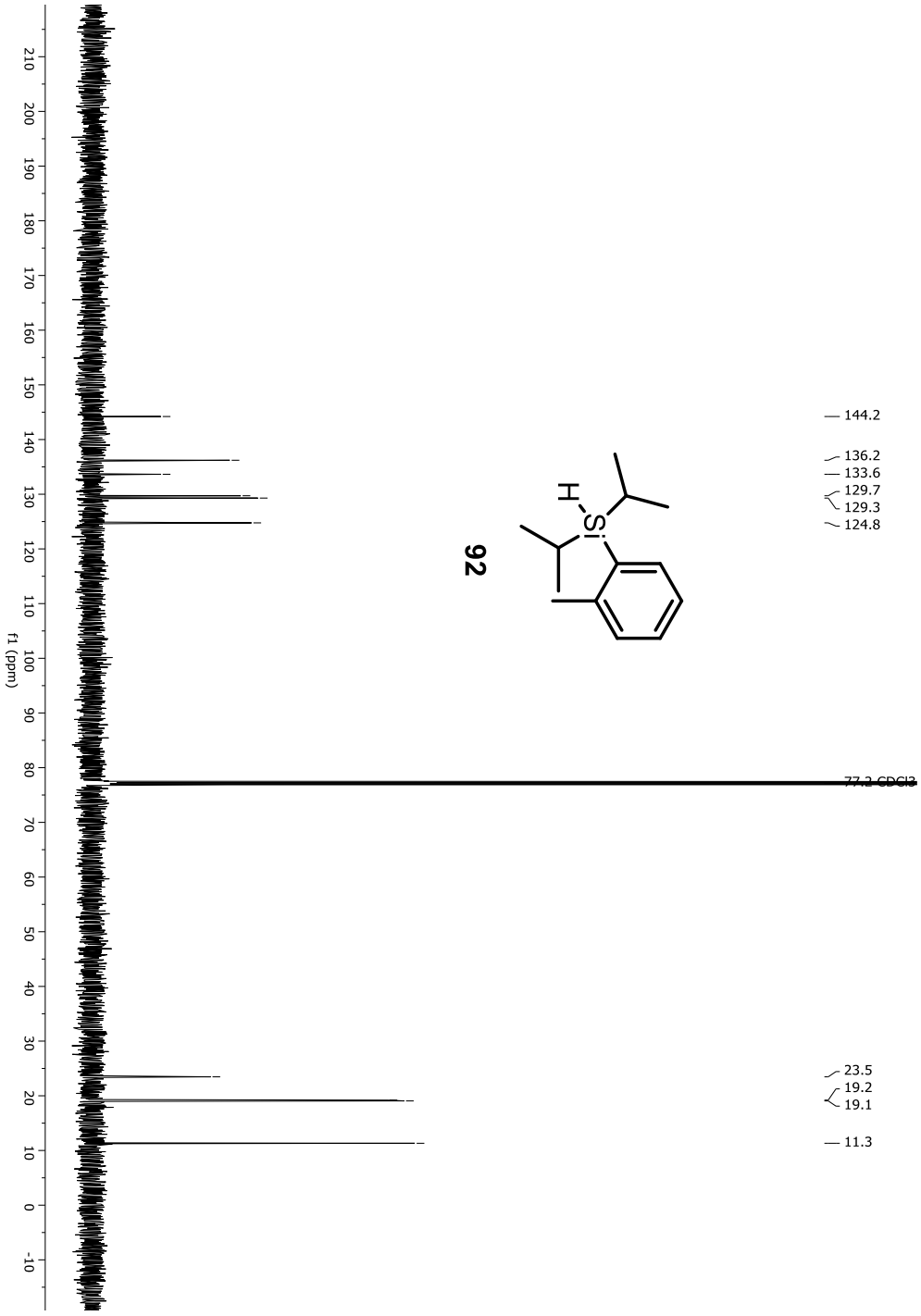

Figure A-132. HRMS spectrum of compound 92

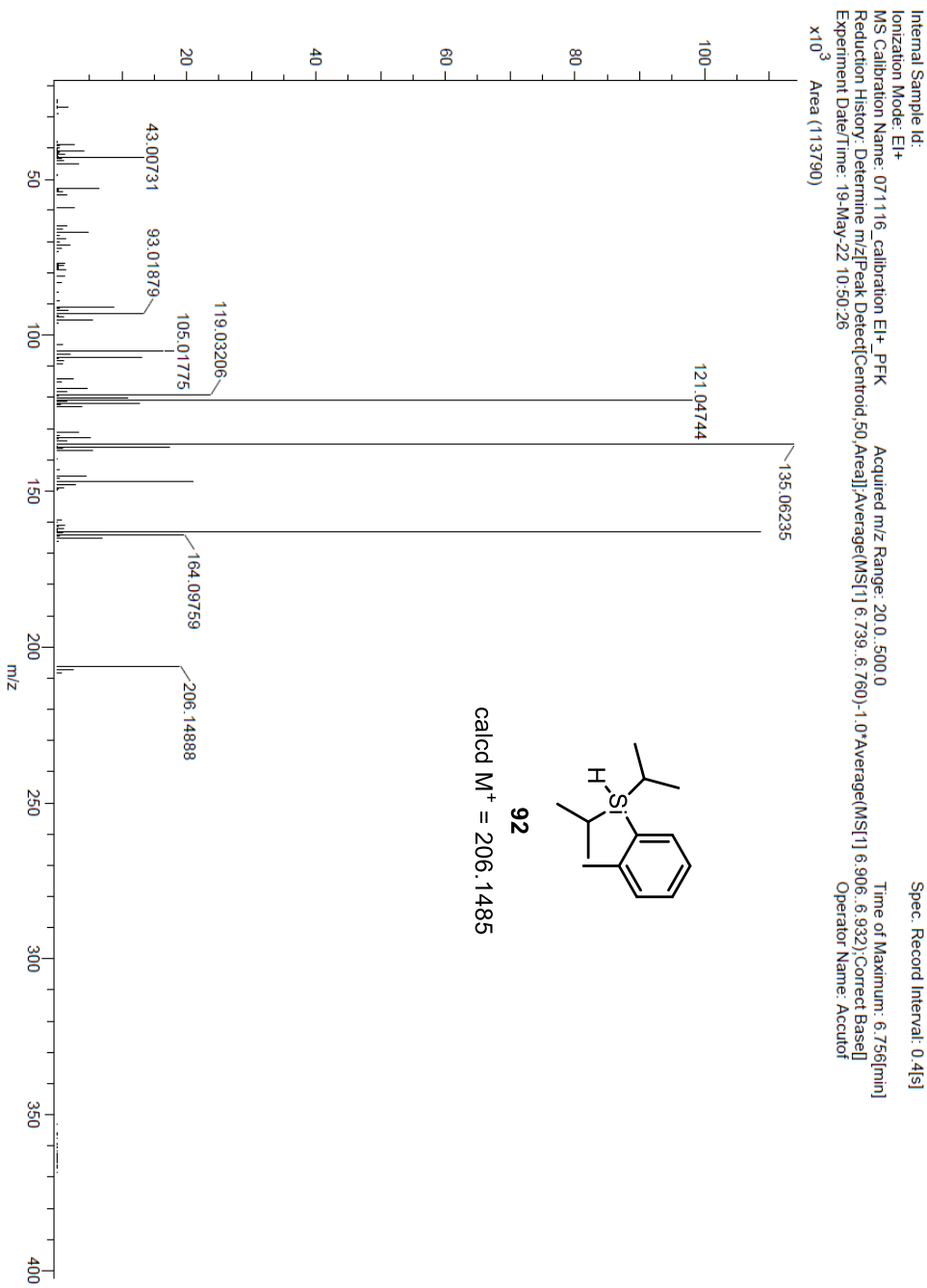

Figure A-133. ^{1}H-NMR spectrum of compound 93

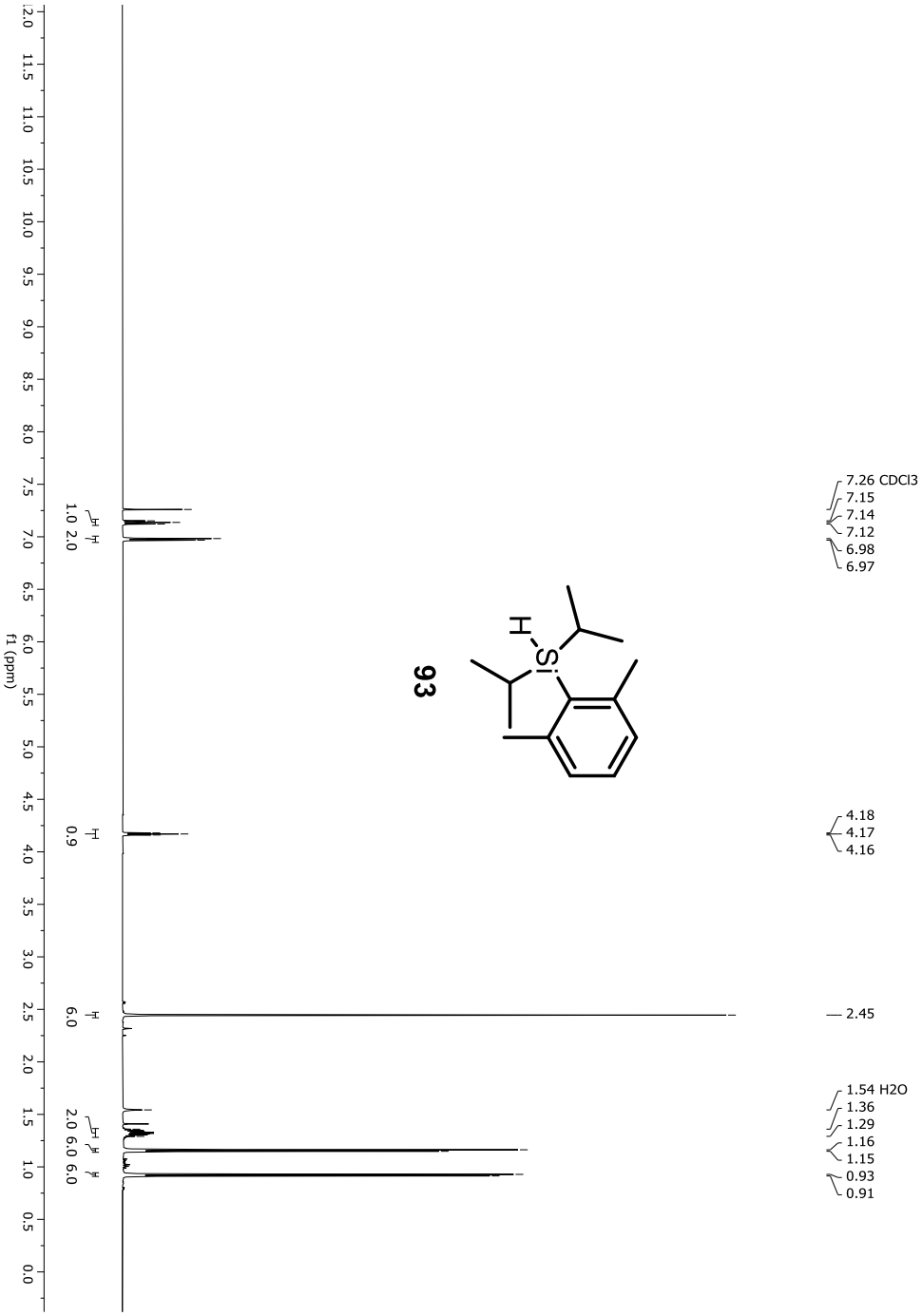

Figure A-134. ^{13}C-NMR spectrum of compound 93

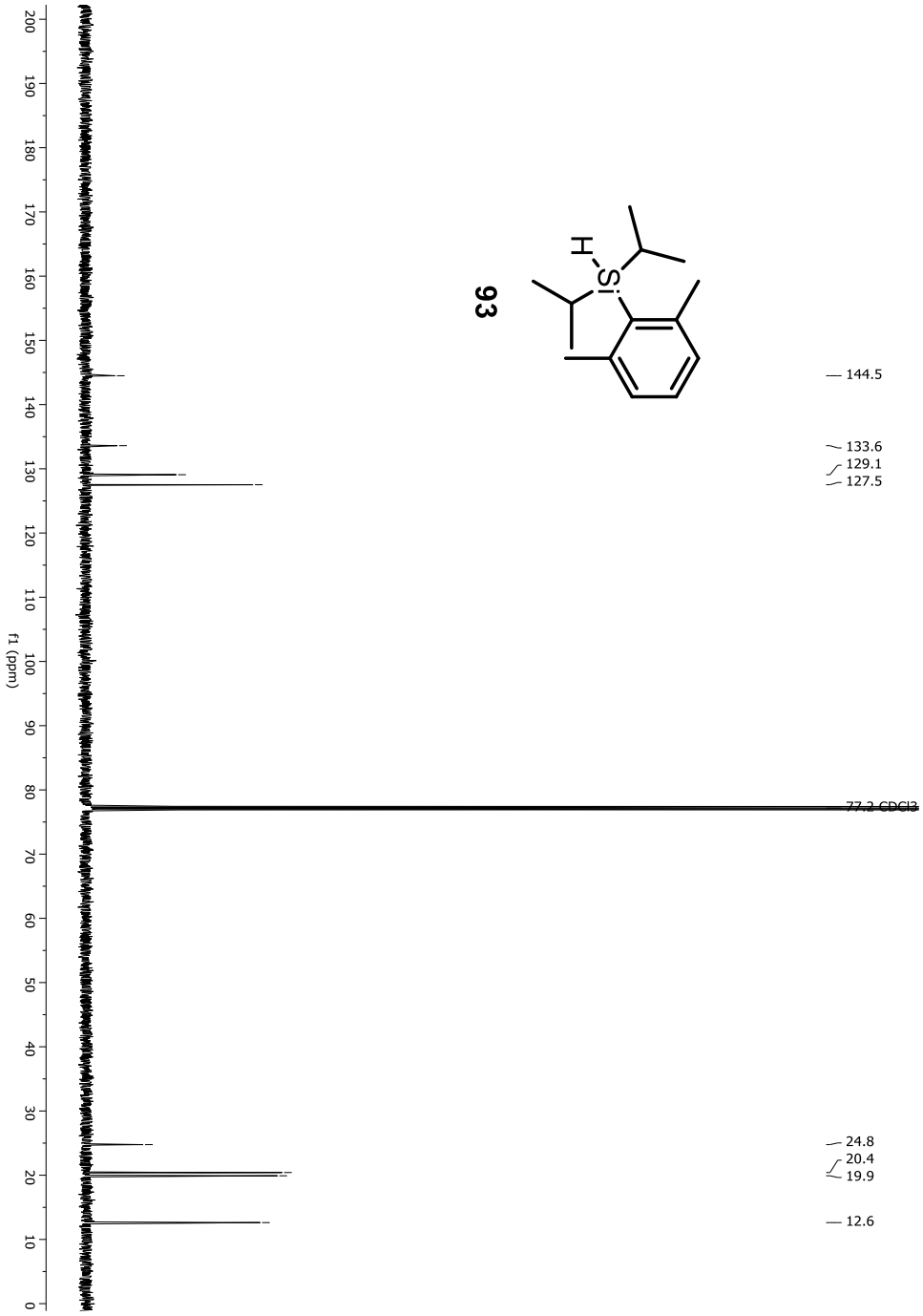

Figure A-135. HRMS spectrum of compound 93

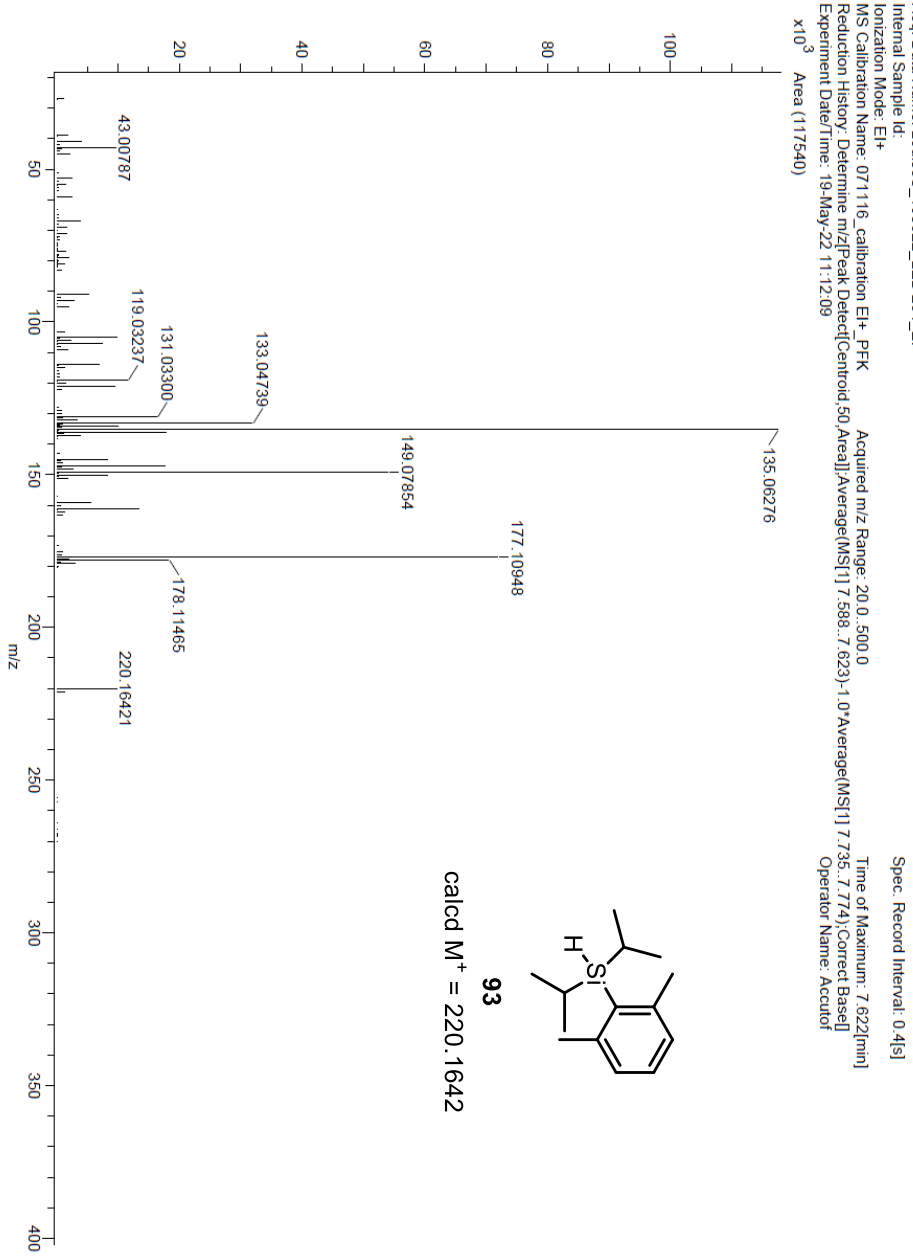

Figure A-136. ^{1}H-NMR spectrum of compound 94

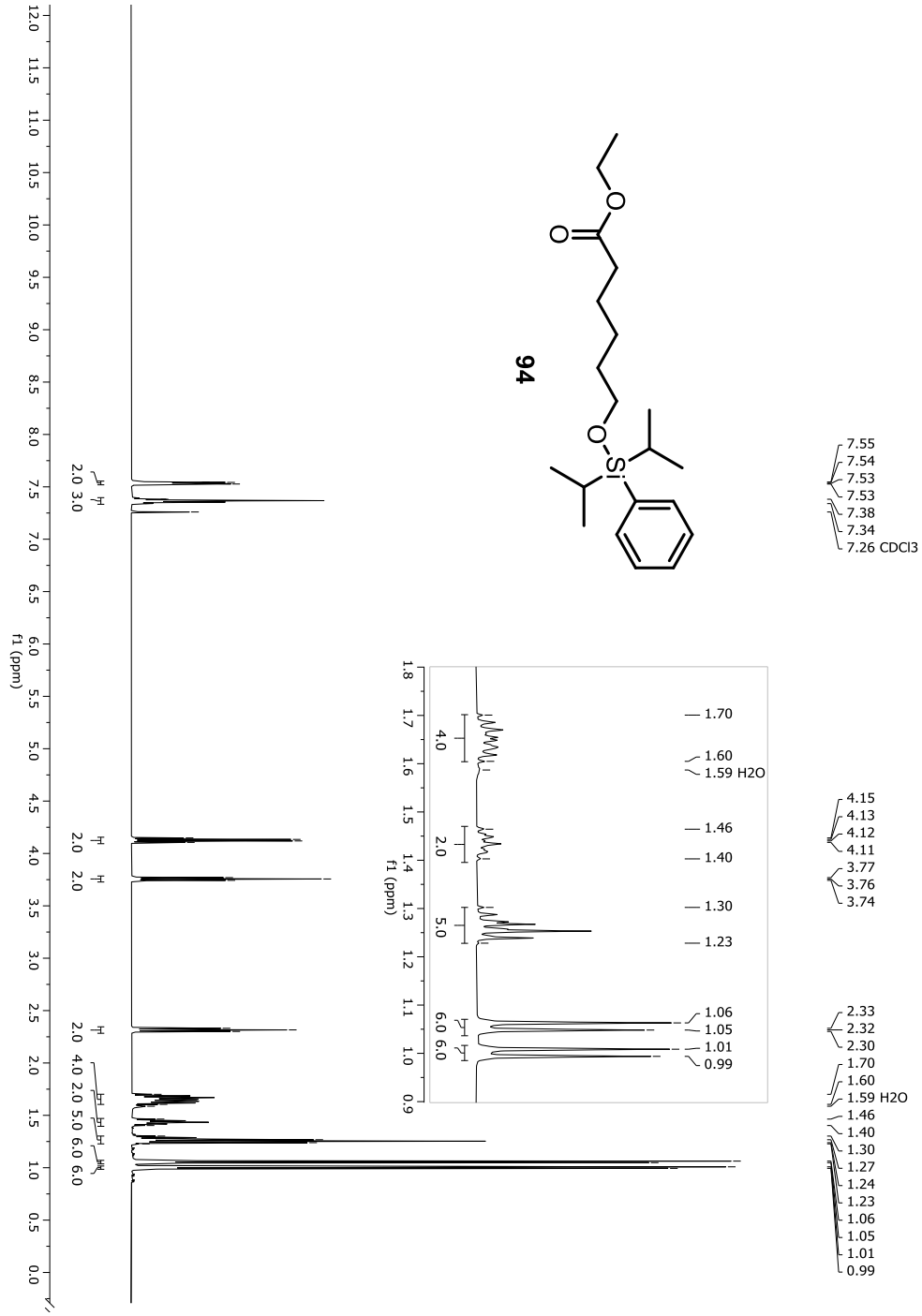

Figure A-137. ^{13}C-NMR spectrum of compound 94

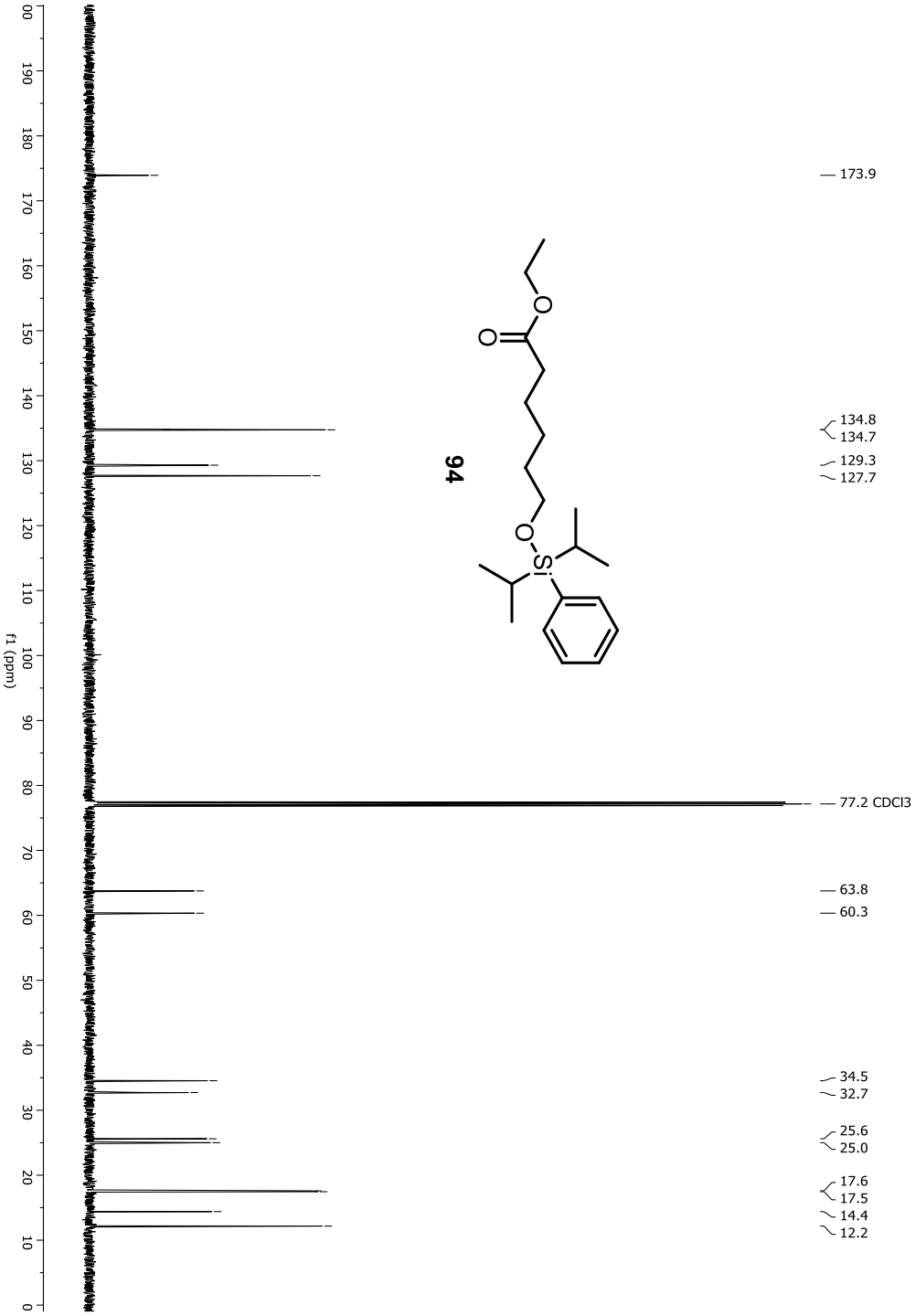

Figure A-138. HRMS spectrum of compound 94

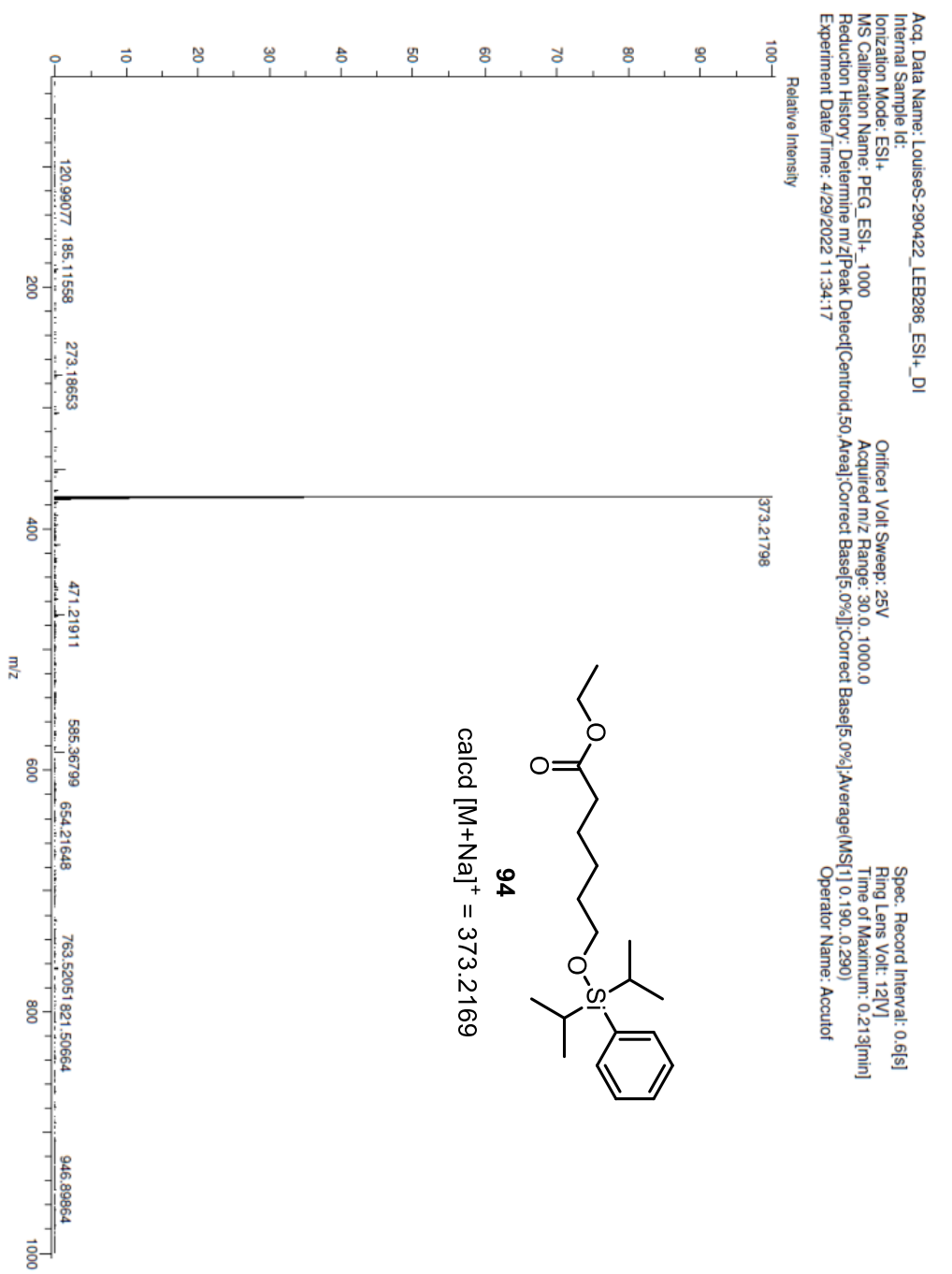

Figure A-139. ^{1}H-NMR spectrum of compound 95

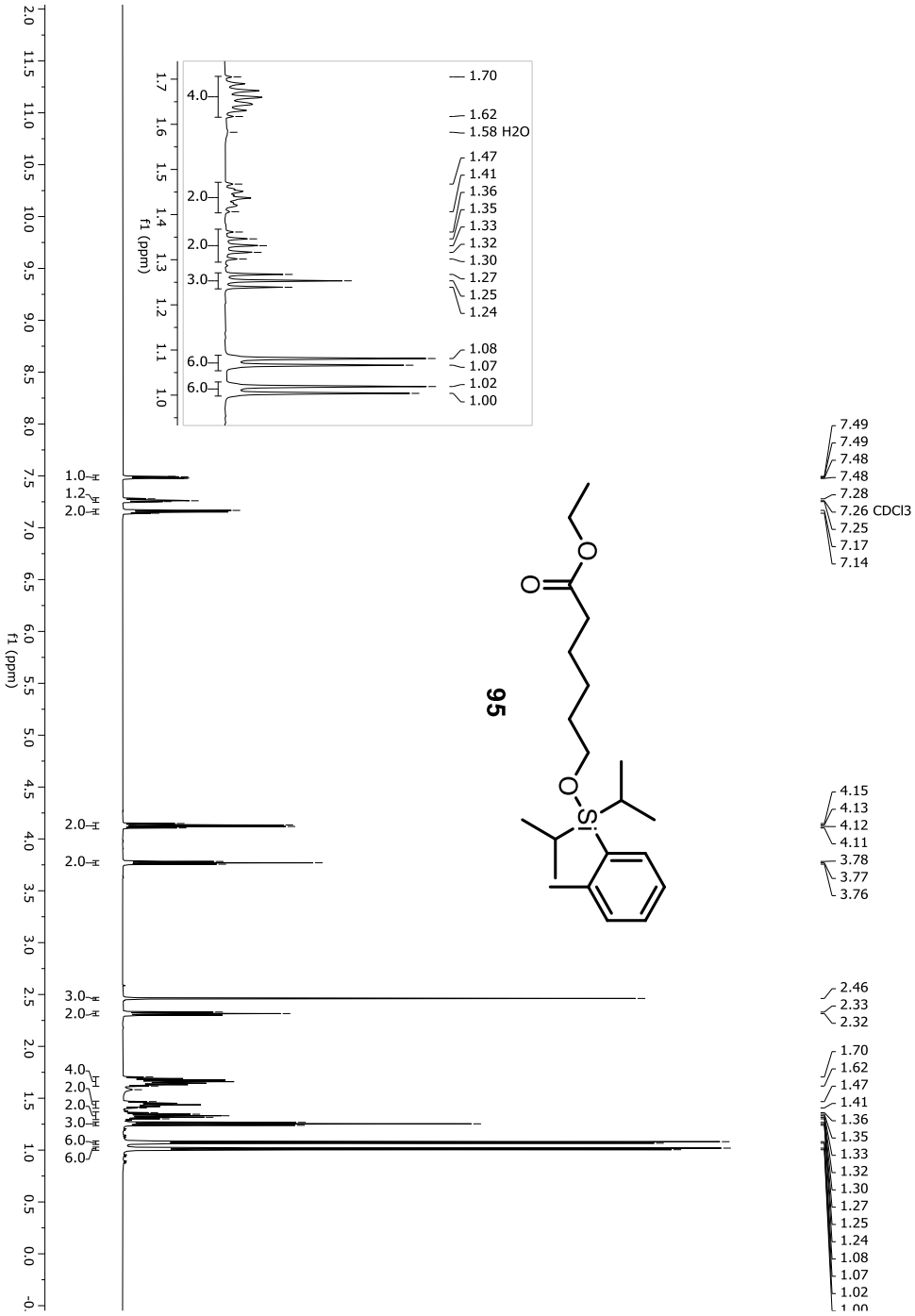

Figure A-140. ^{13}C-NMR spectrum of compound 95

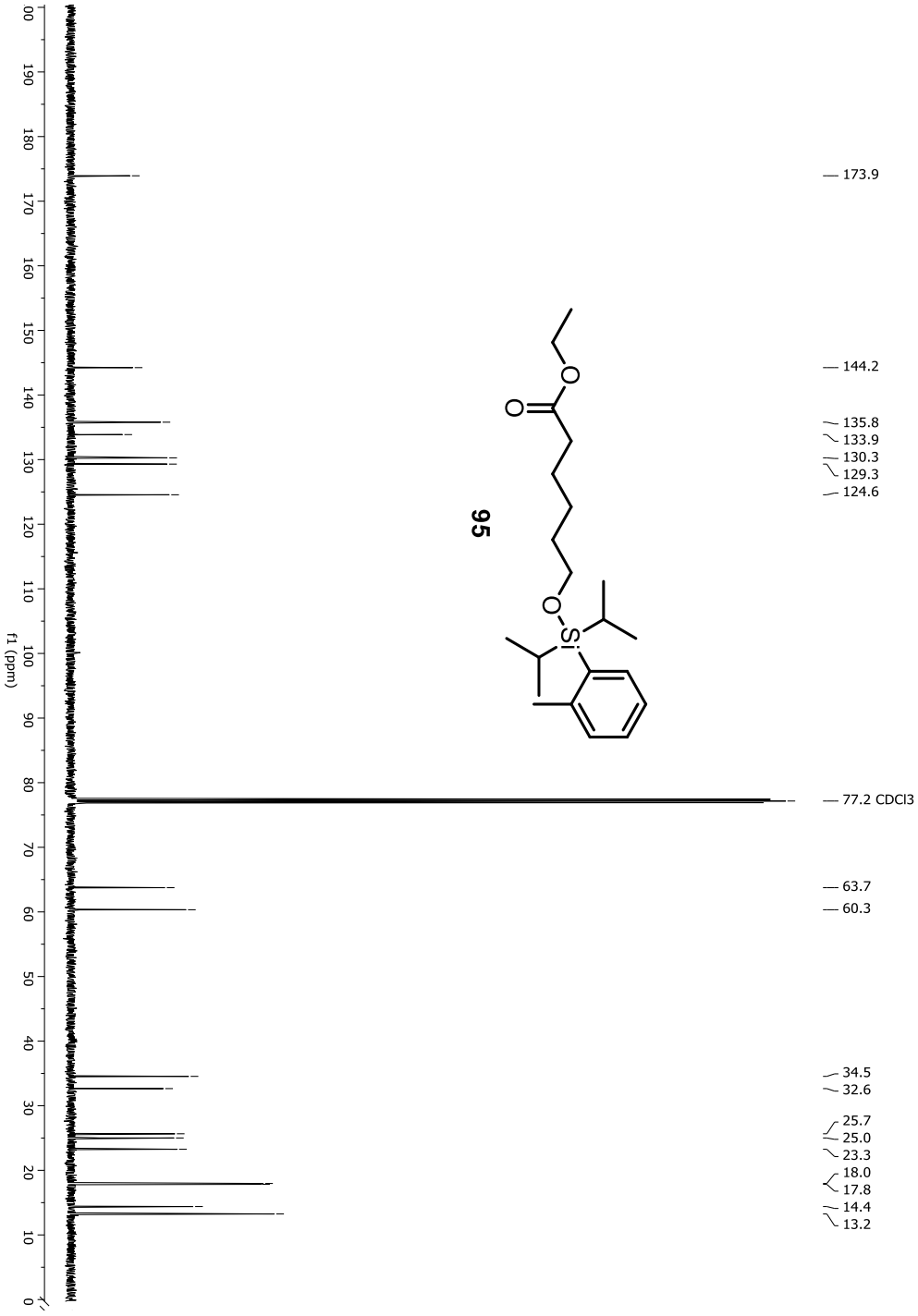

Figure A-141. HRMS spectrum of compound 95

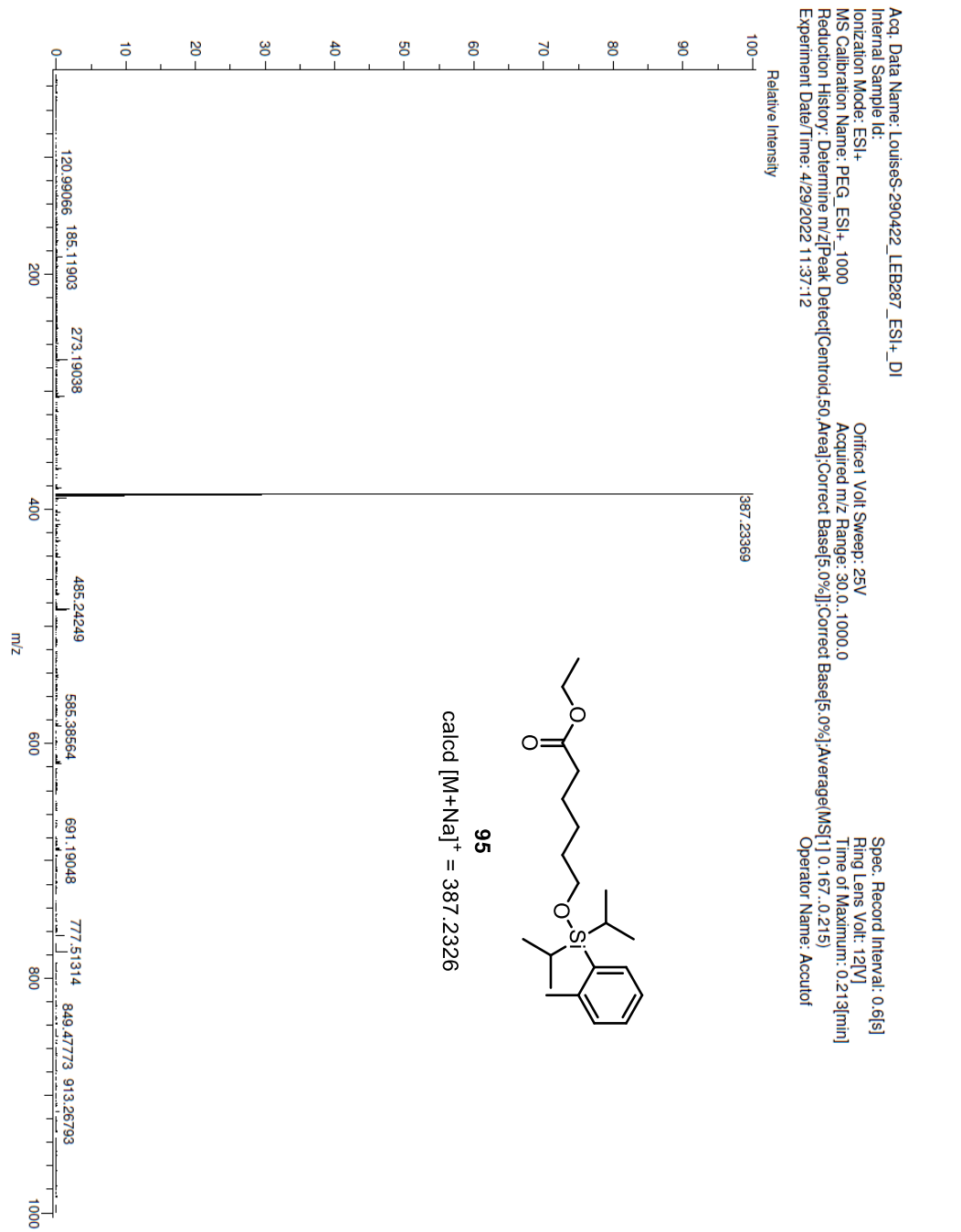

Figure A-142. ^{1}H-NMR spectrum of compound 96

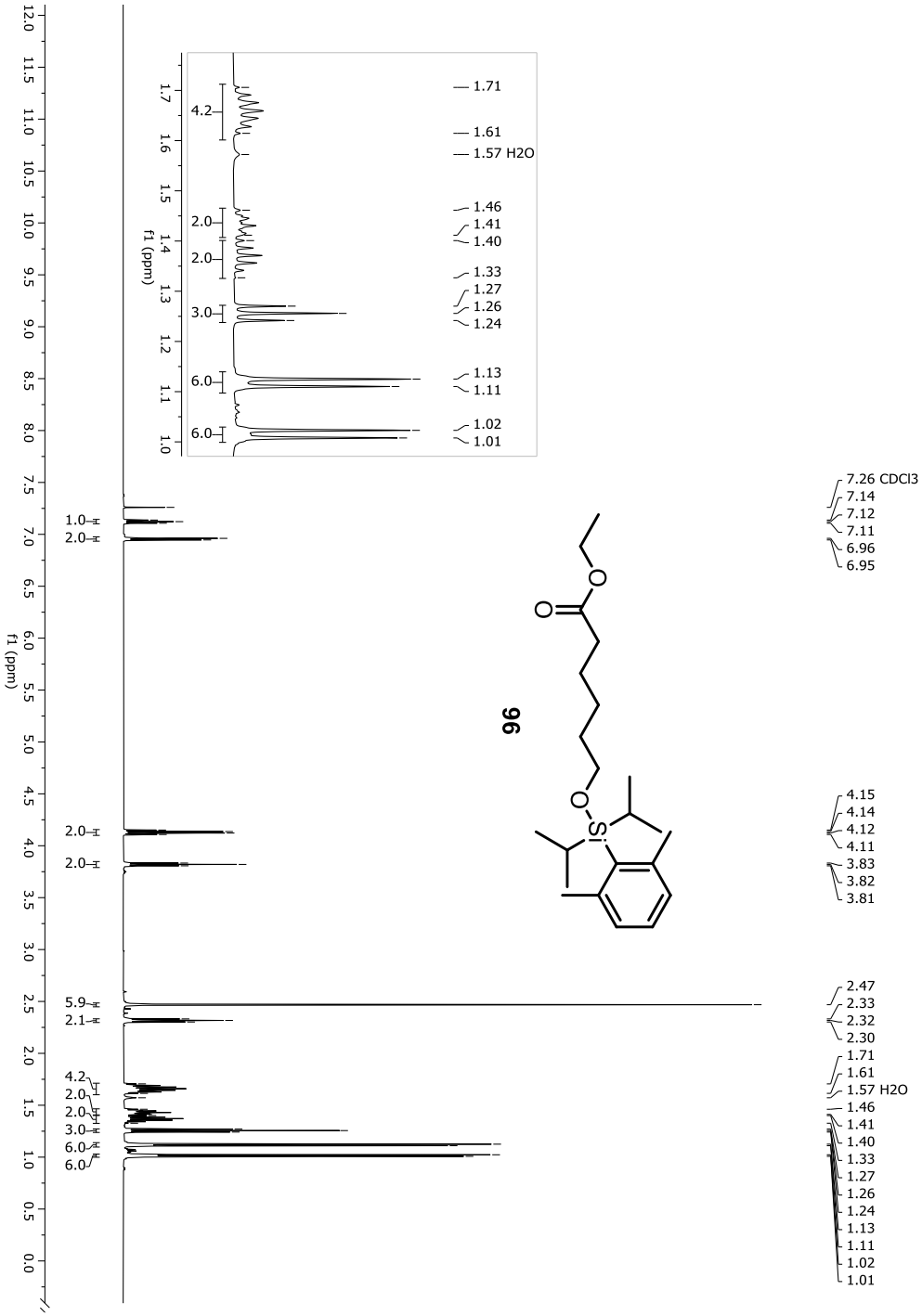

Figure A-143. ^{13}C-NMR spectrum of compound 96

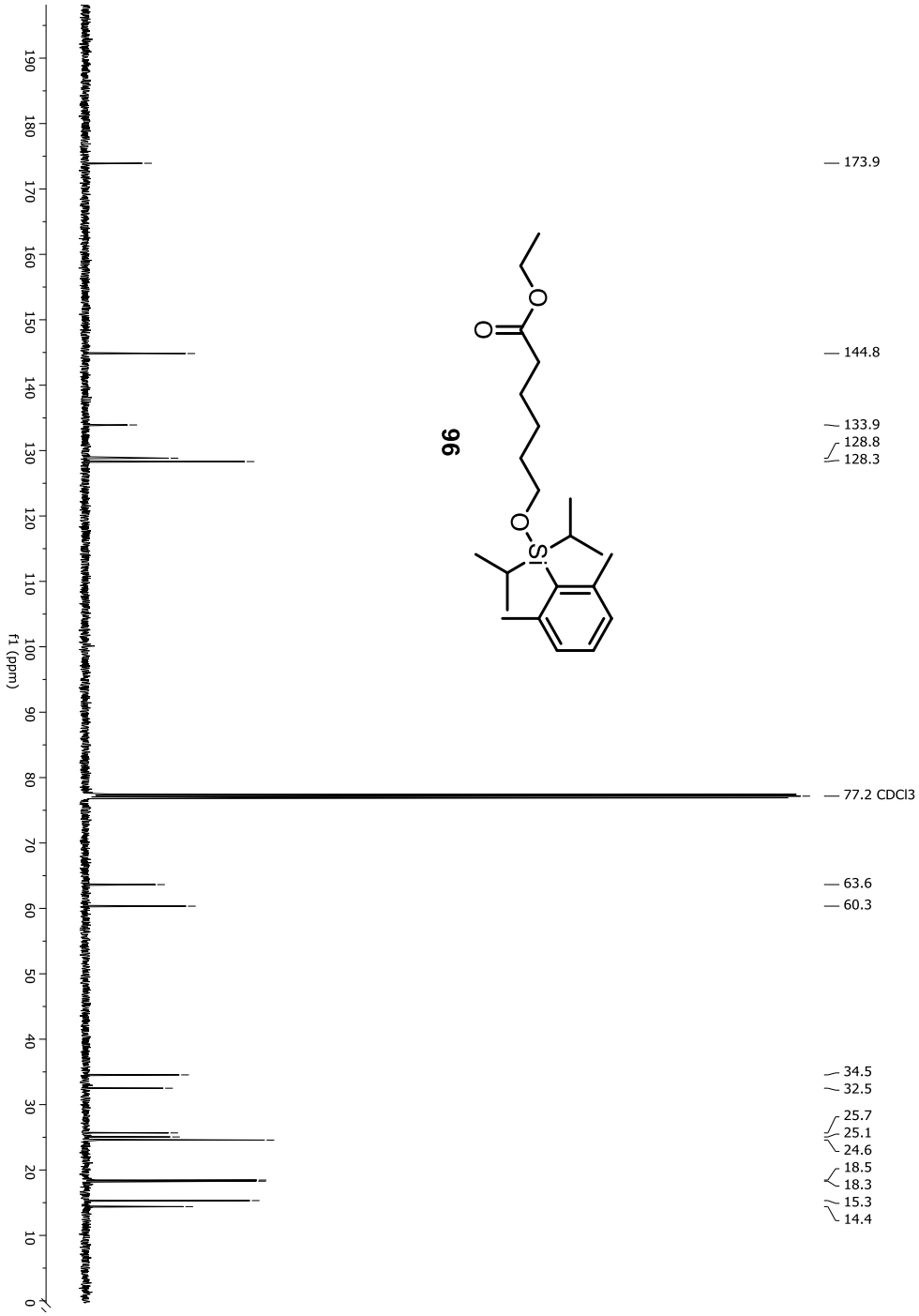

Figure A-144. HRMS spectrum of compound 96

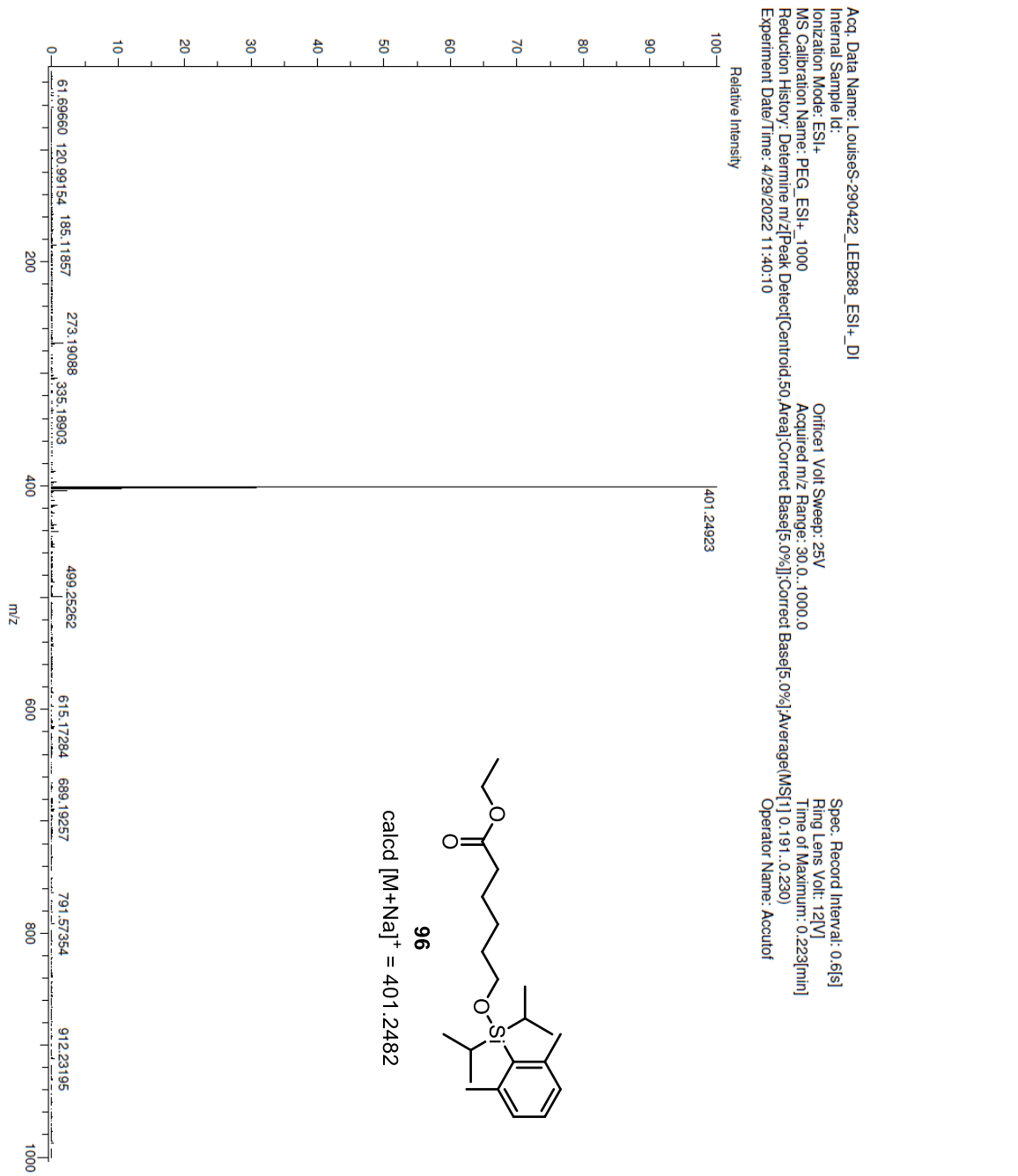

Figure A-145. ^{1}H-NMR spectrum of compound 97

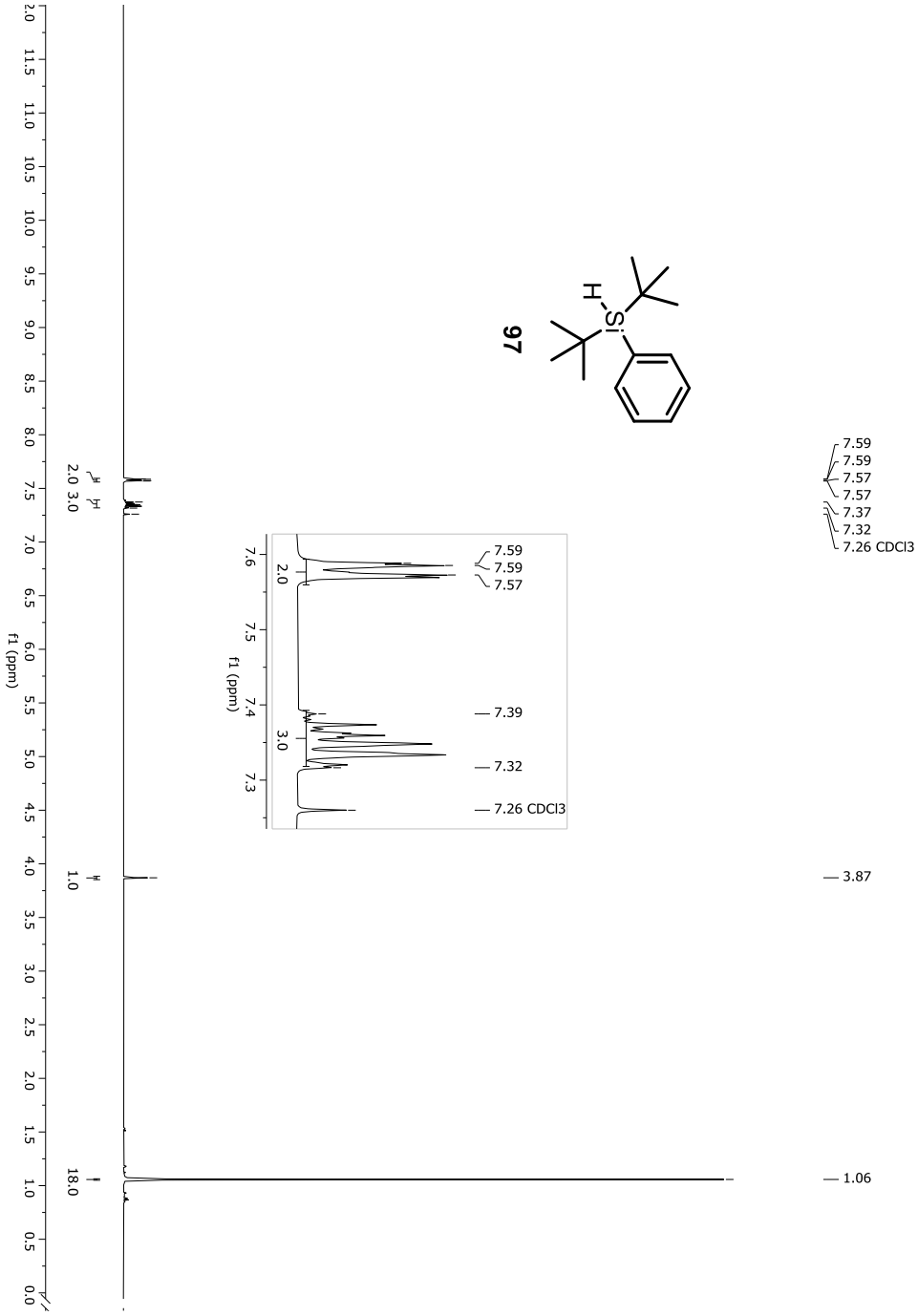

Figure A-146. ^{13}C-NMR spectrum of compound 97

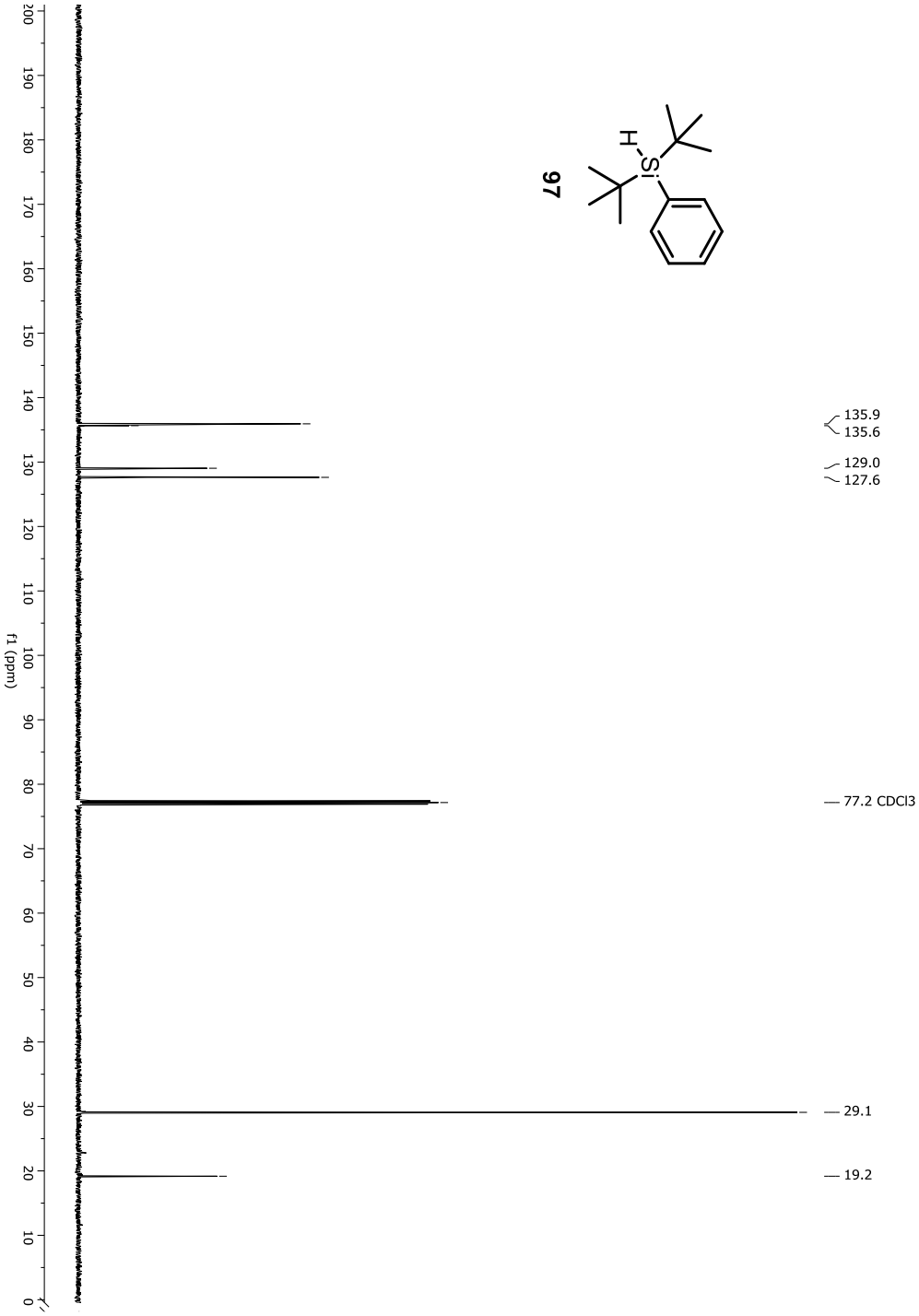

Figure A-147. ^{1}H-NMR spectrum of compound 98

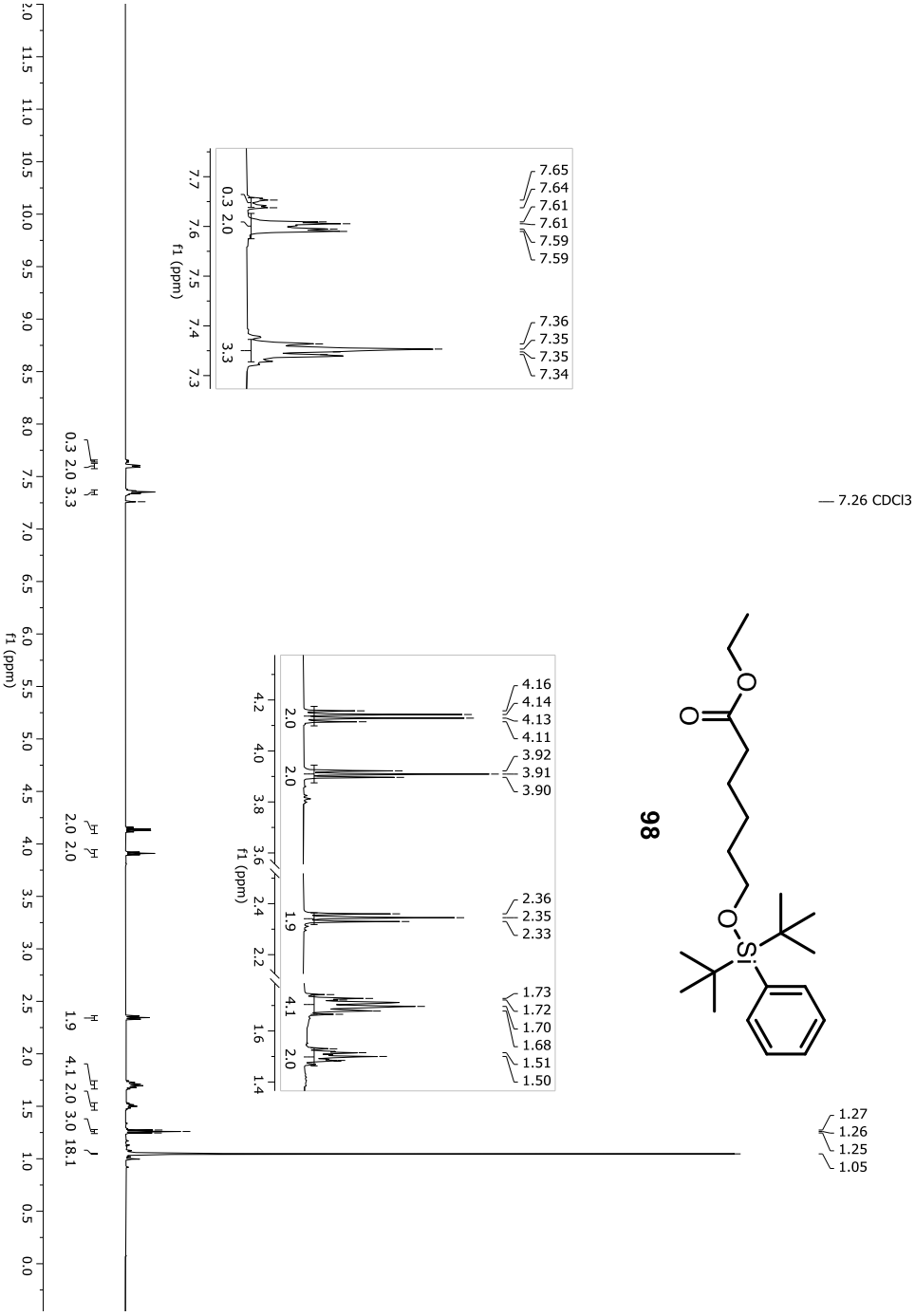

Figure A-148. ^{13}C-NMR spectrum of compound 98

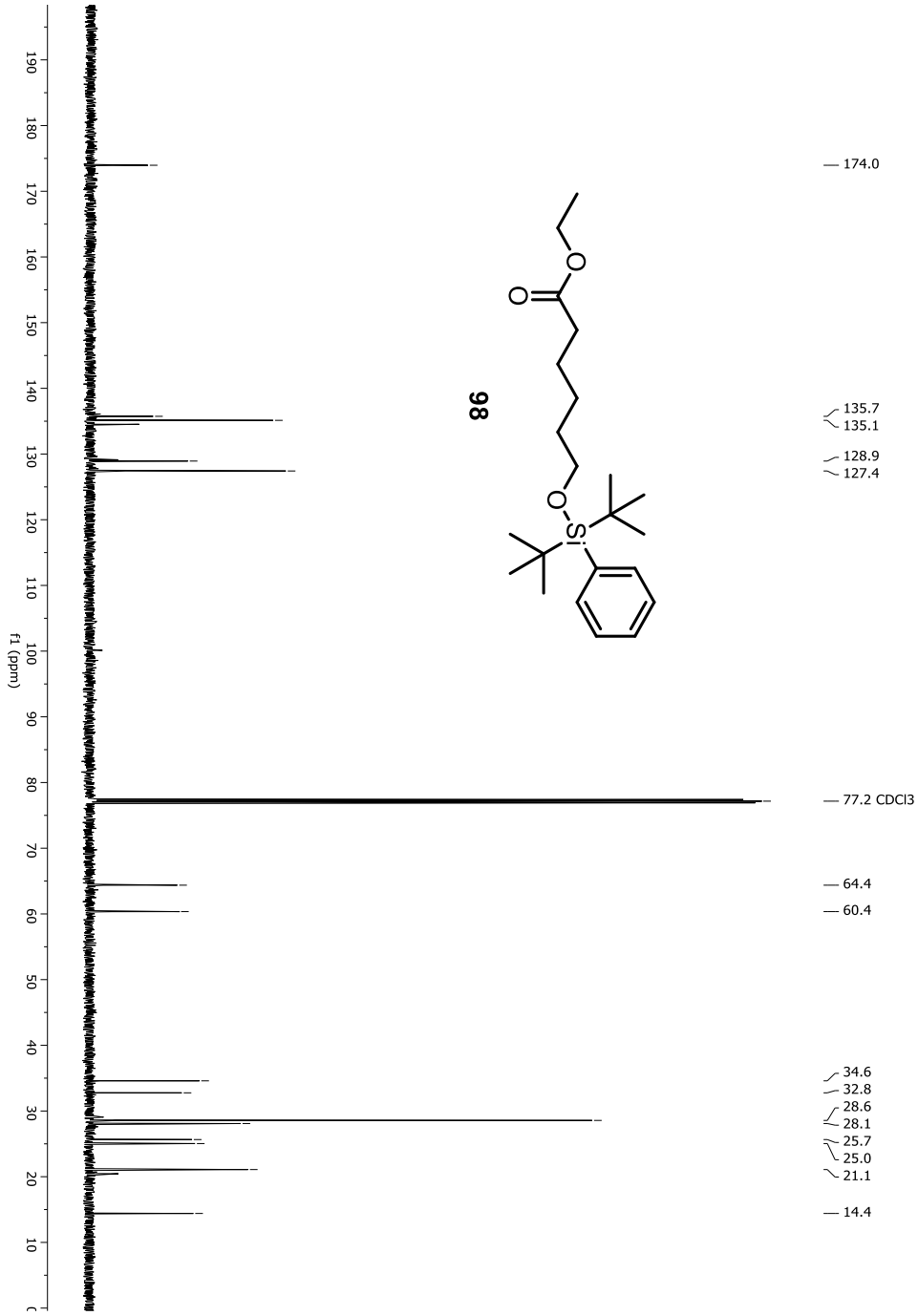

Figure A-149. HRMS spectrum of compound 98

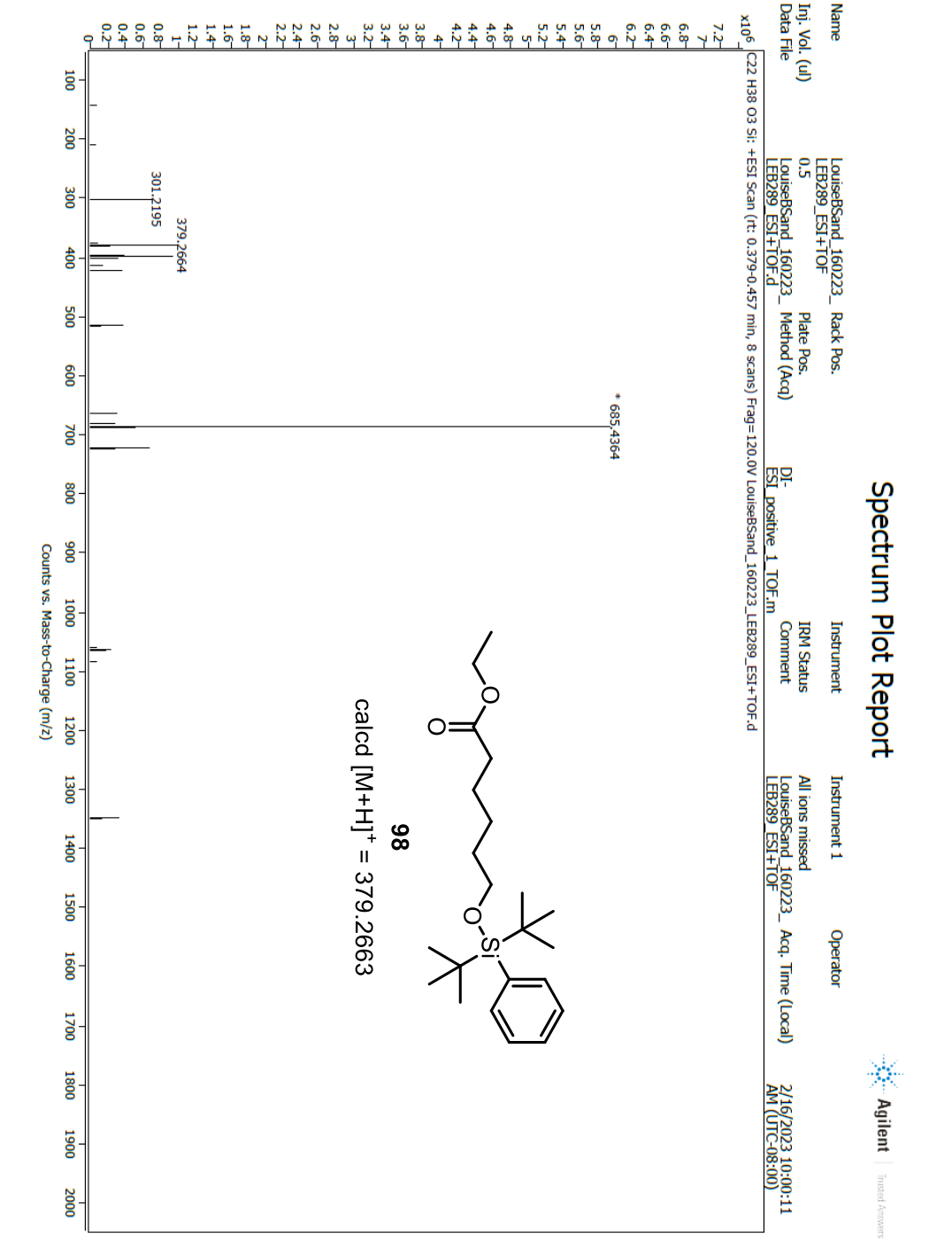

Figure A-150. ^{1}H-NMR spectrum of compound 99

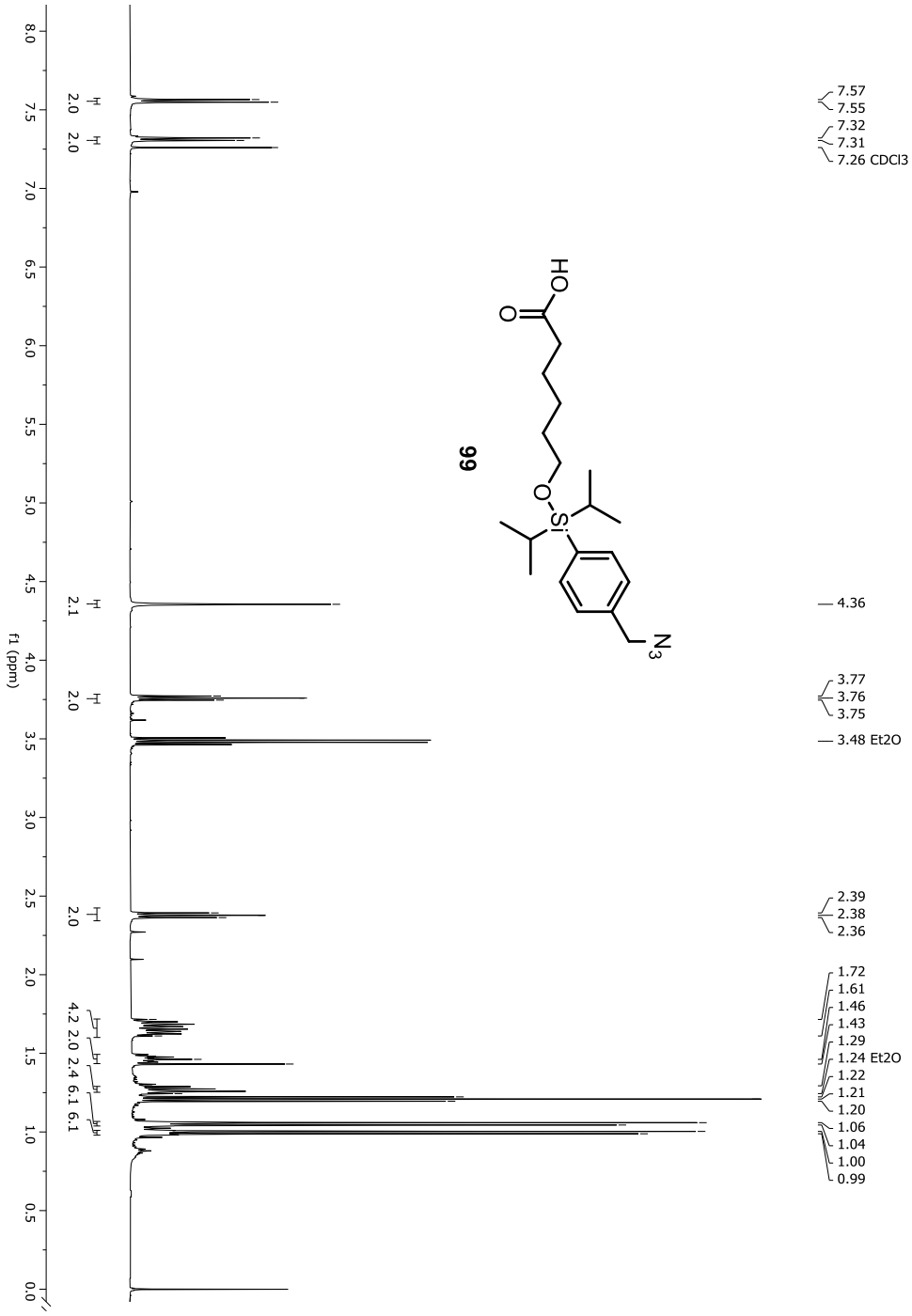

Figure A-151. ^{13}C-NMR spectrum of compound 99

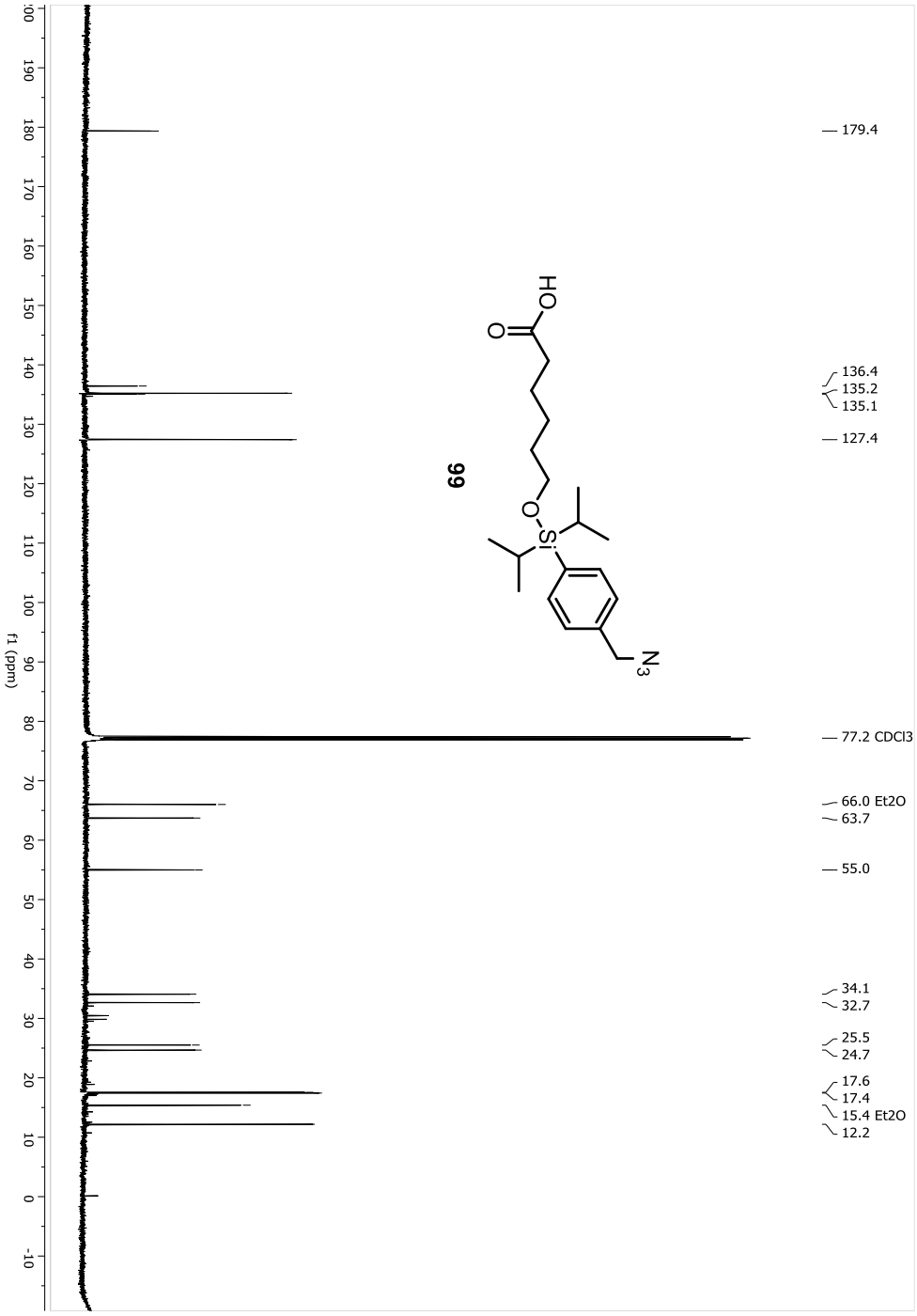

Figure A-152. HRMS spectrum of compound 99

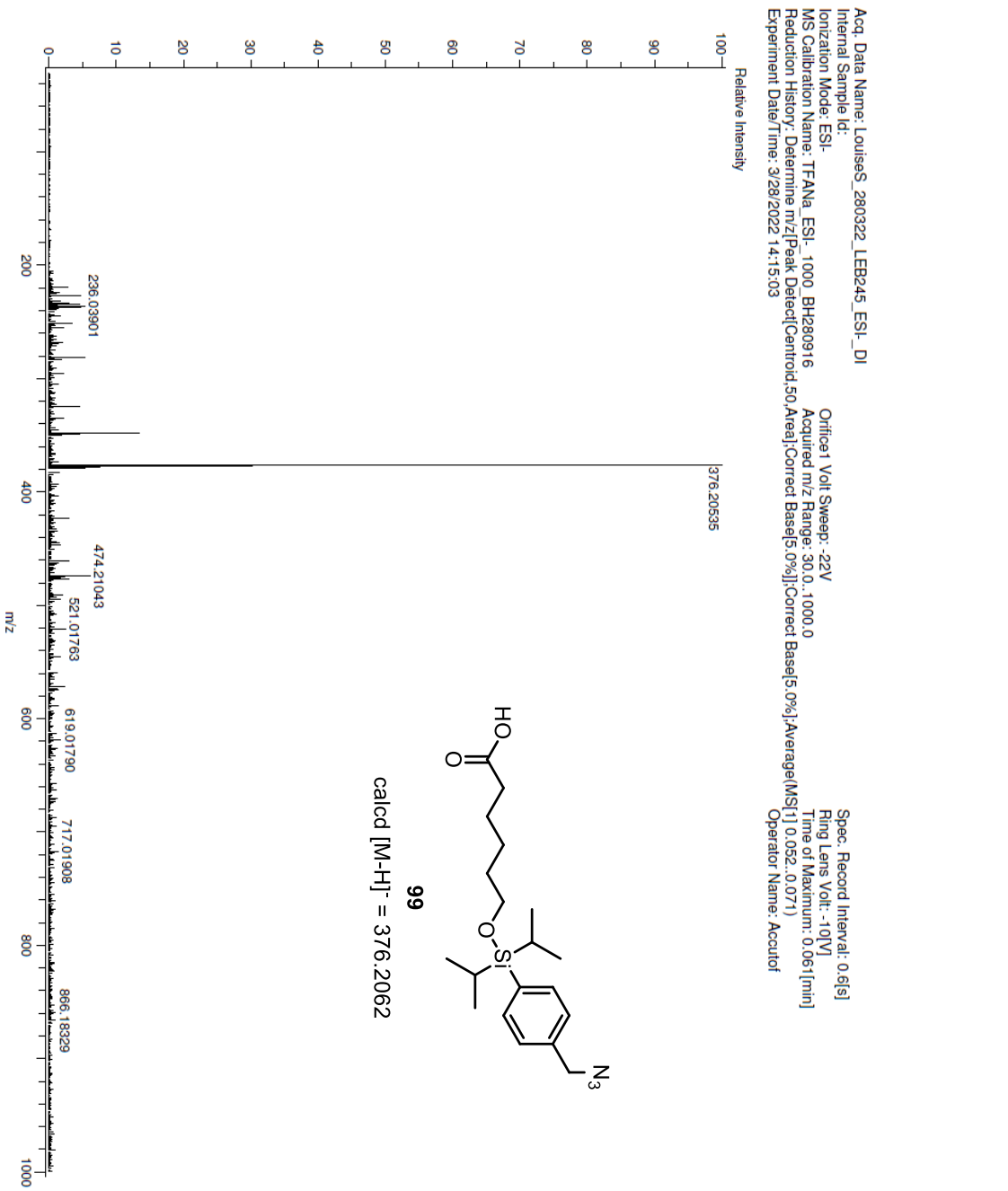

Figure A-153. ^{1}H-NMR spectrum of compound 101

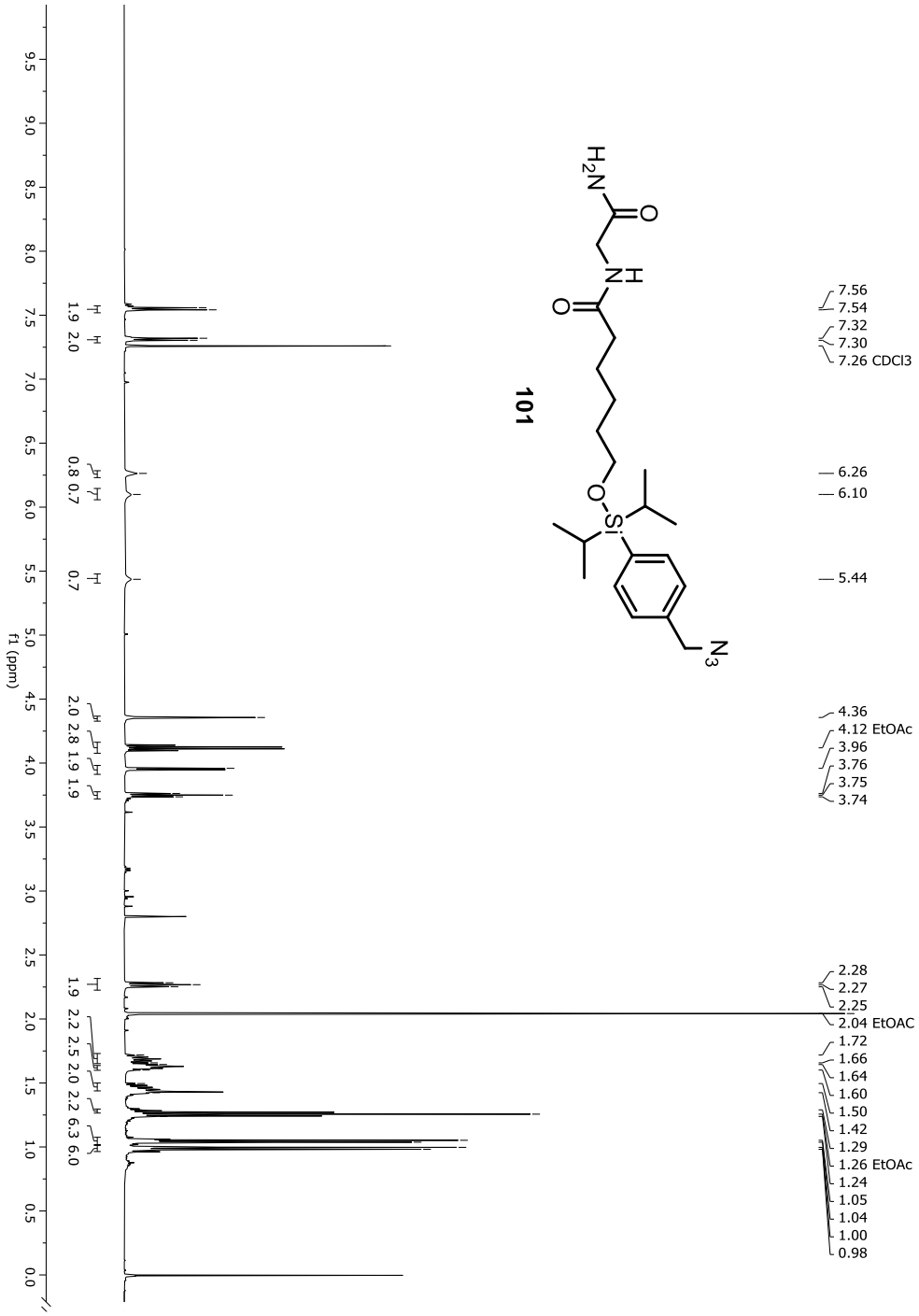

Figure A-154. ^{13}C-NMR spectrum of compound 101

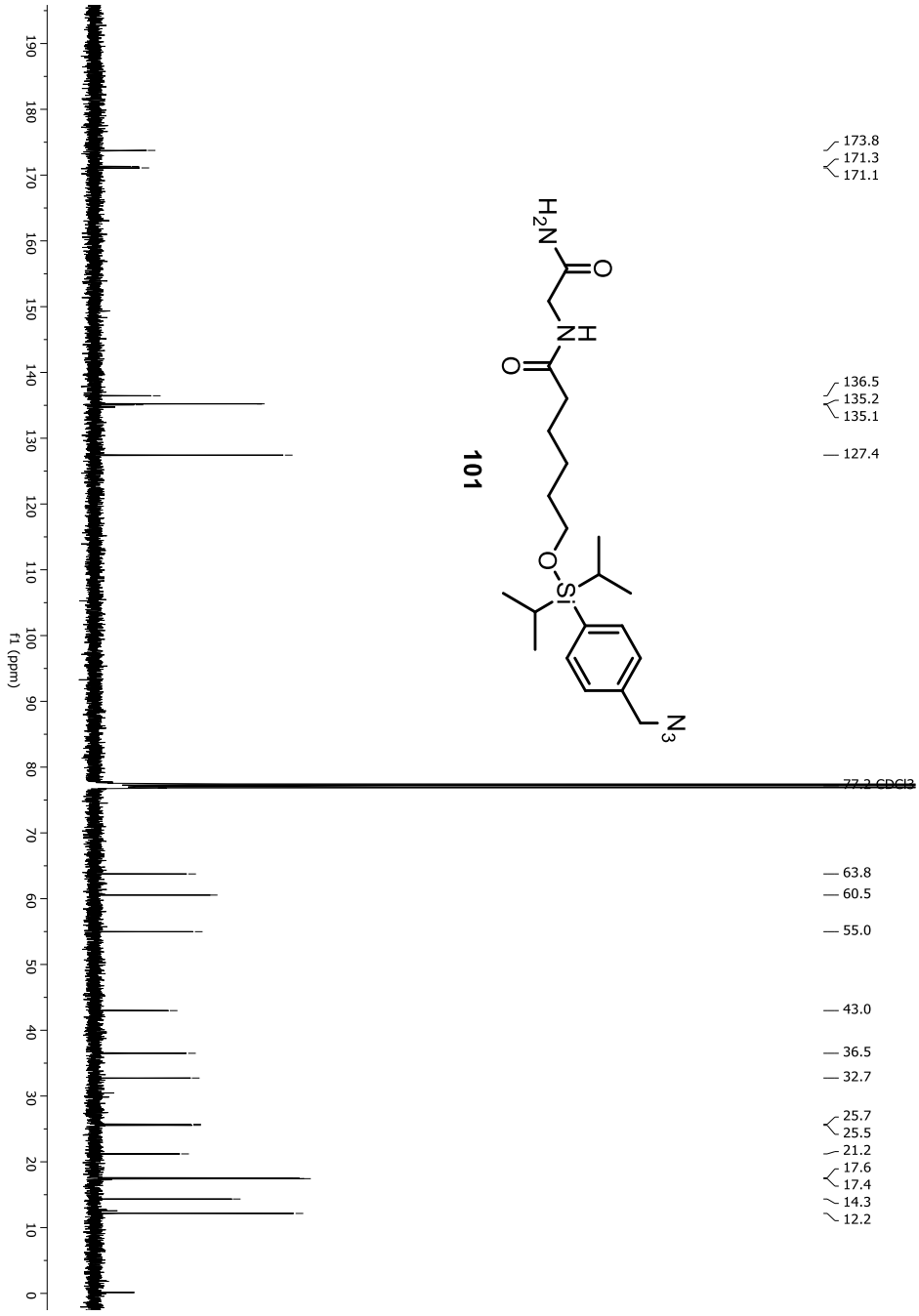

Figure A-155. ^{1}H-NMR spectrum of compound 103

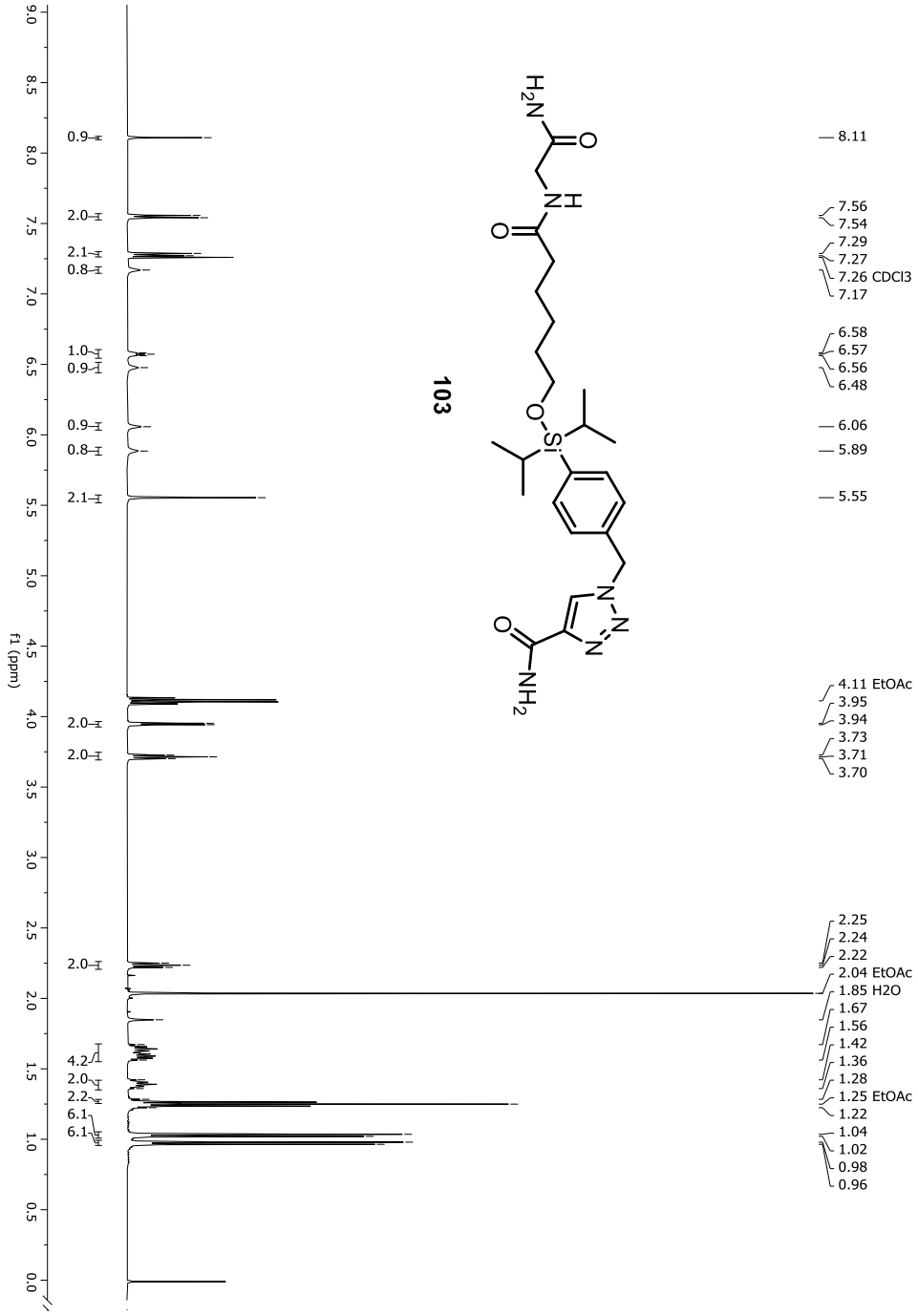

Figure A-156. ^{13}C-NMR spectrum of compound 103

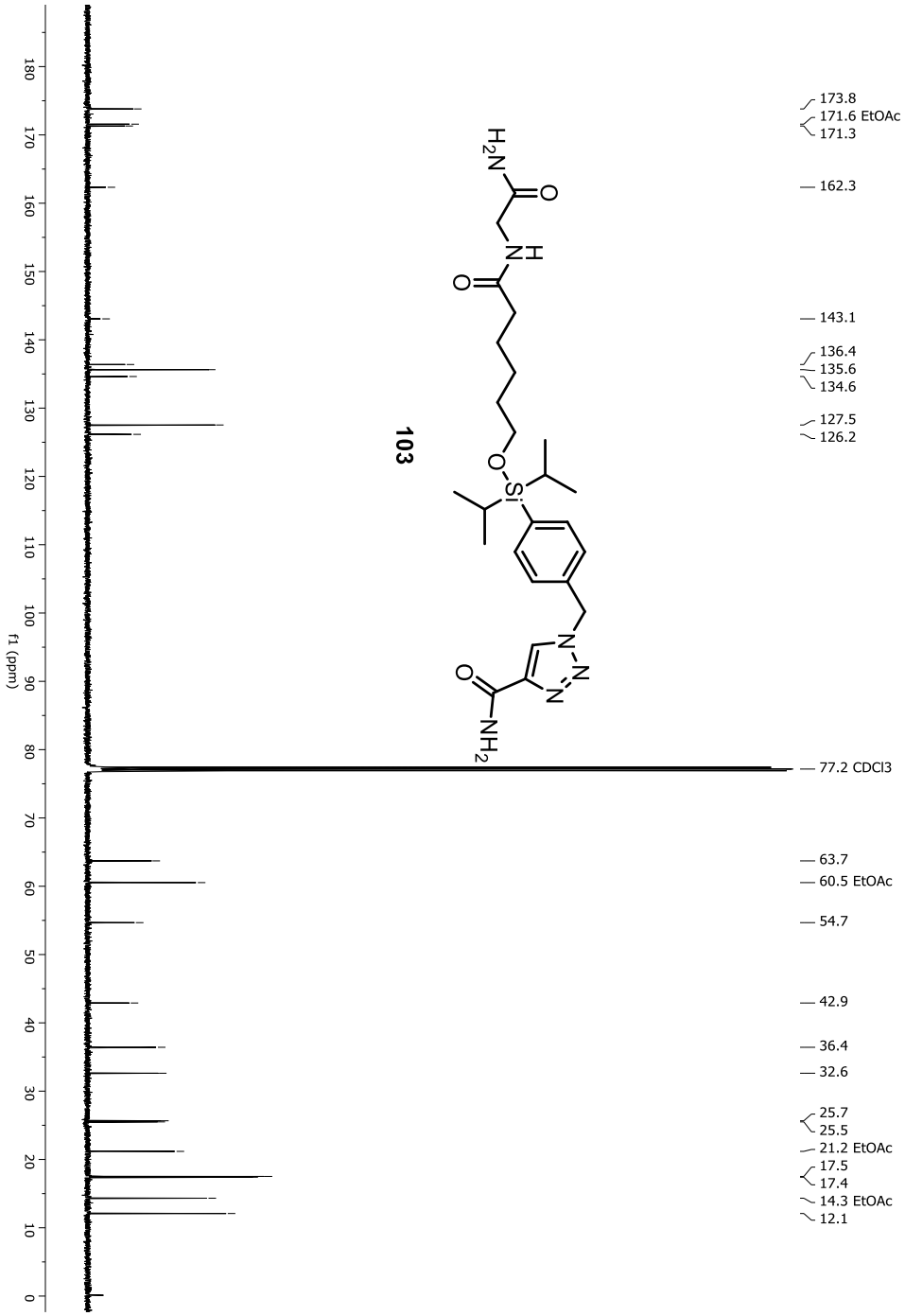

Figure A-157. ^{1}H-NMR spectrum of compound 108

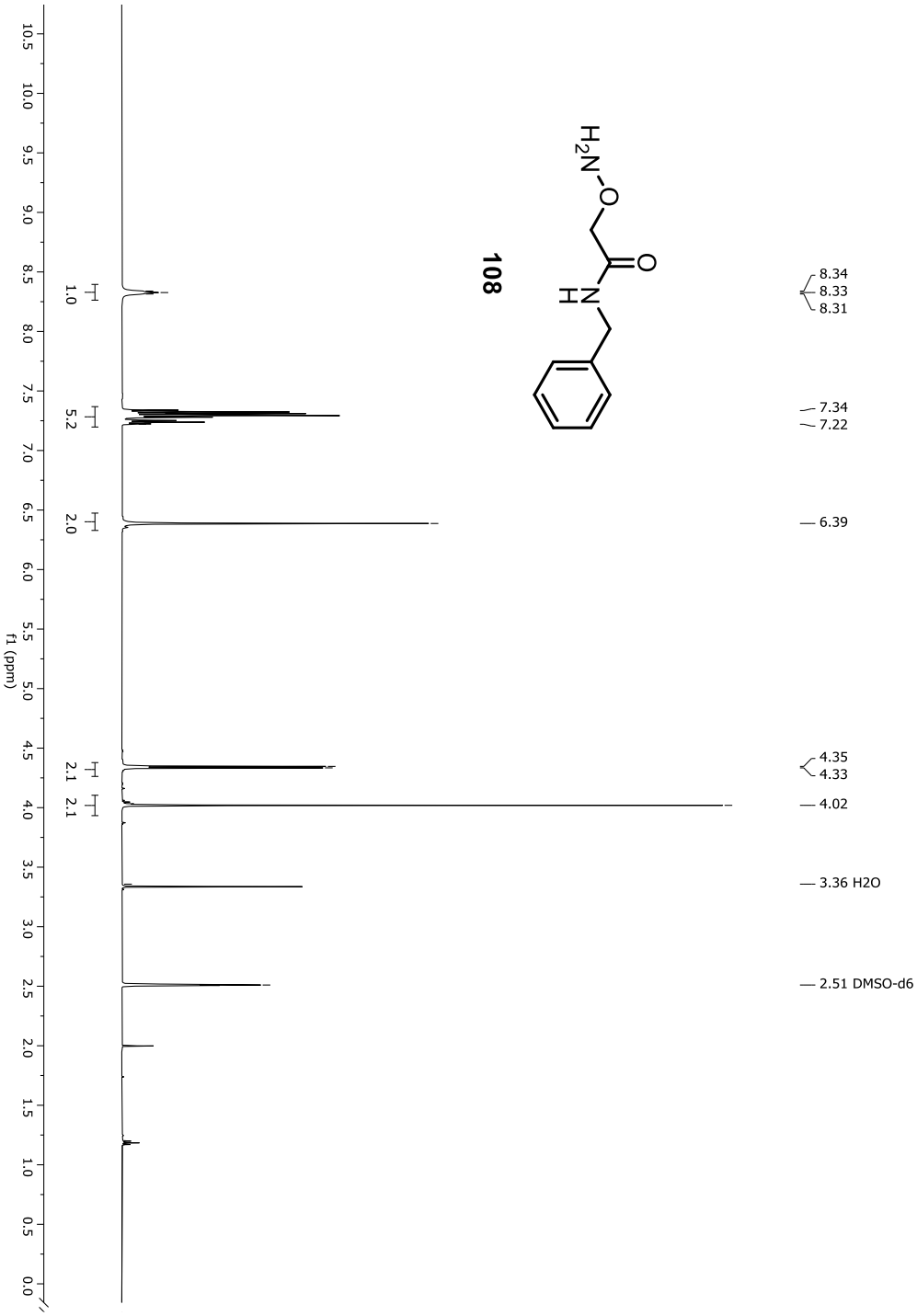

Figure A-158. ^{13}C-NMR spectrum of compound 108

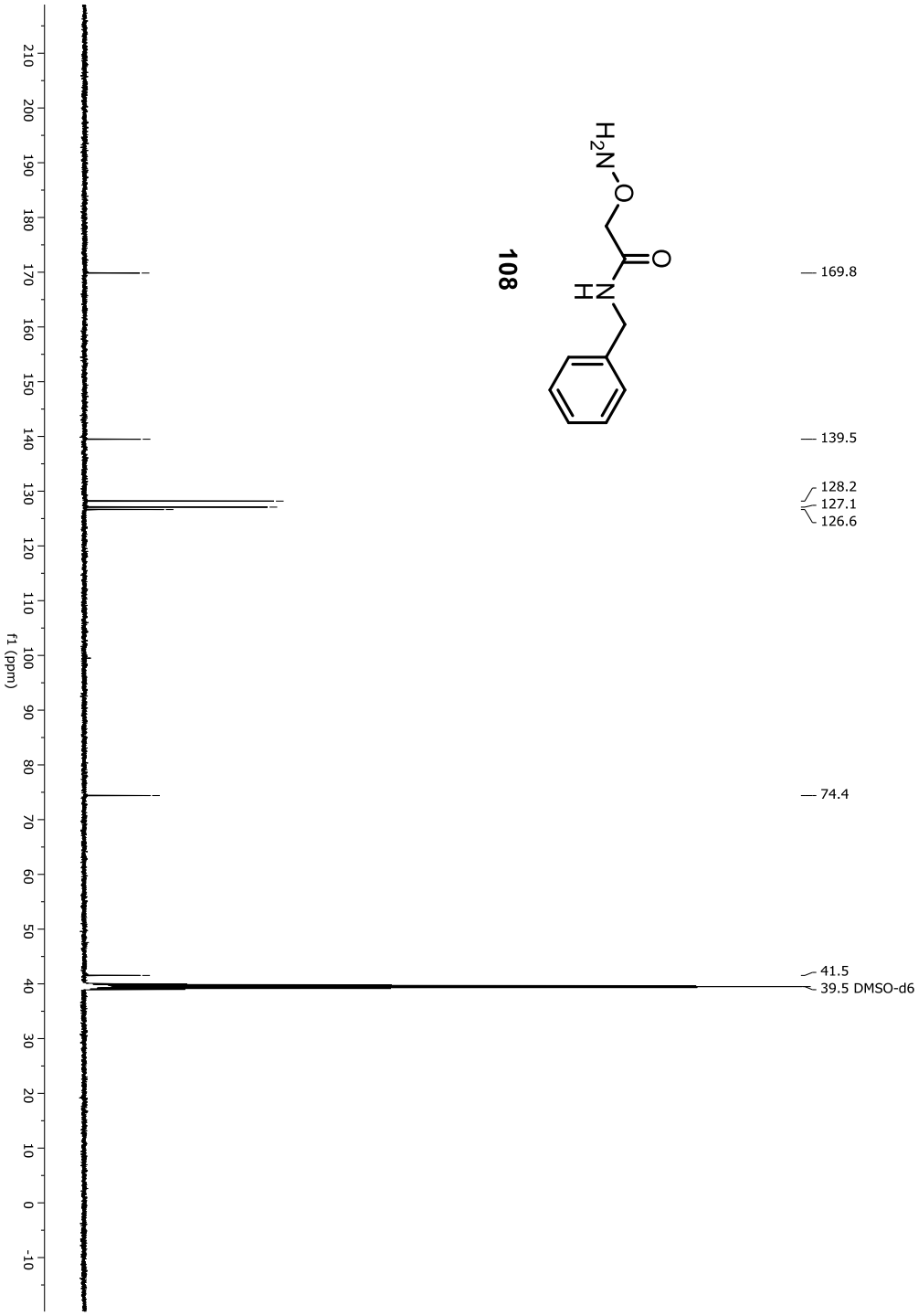

Figure A-159. HRMS spectrum of compound 108

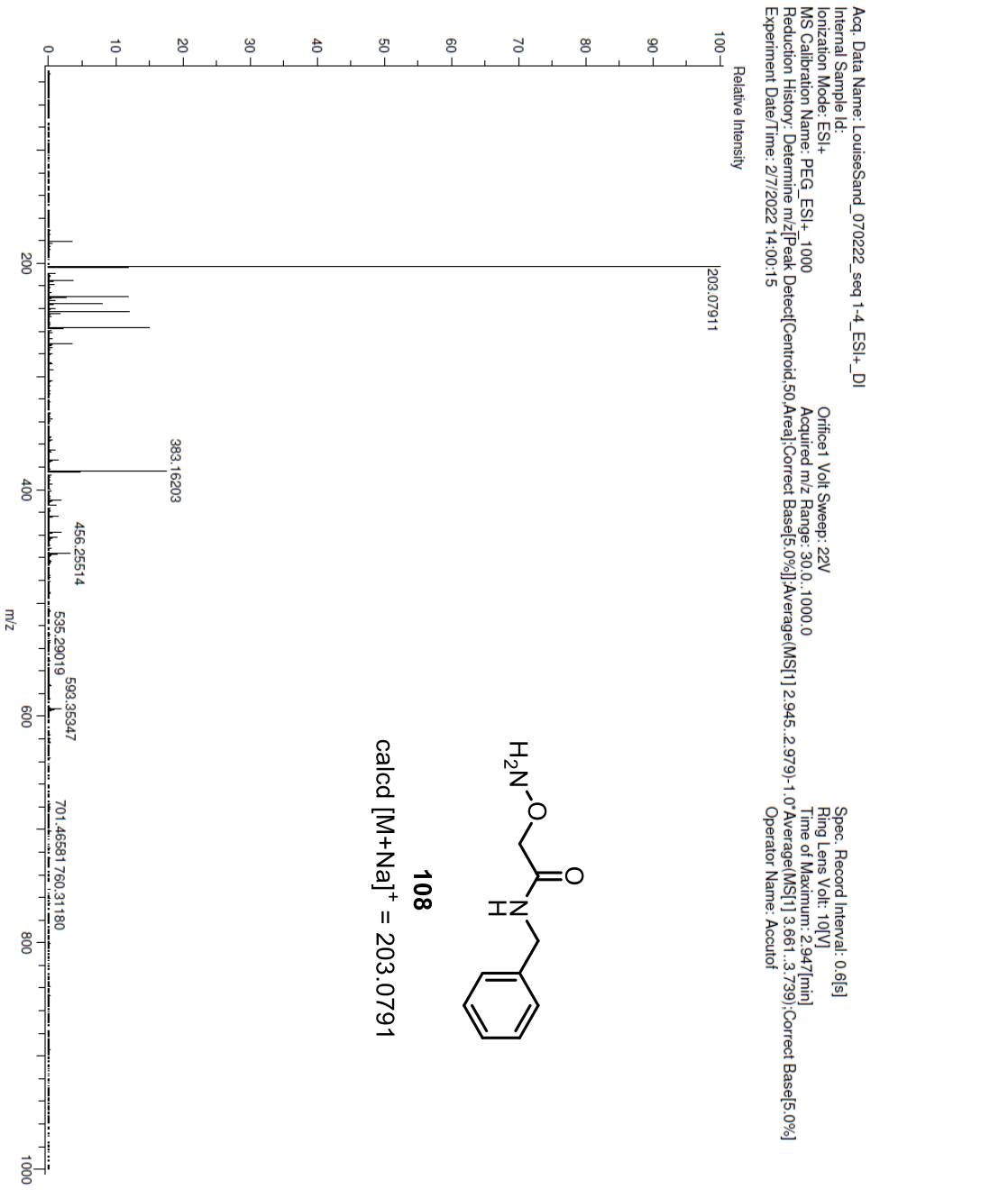

Figure A-160. ^{1}H-NMR spectrum of compound 109

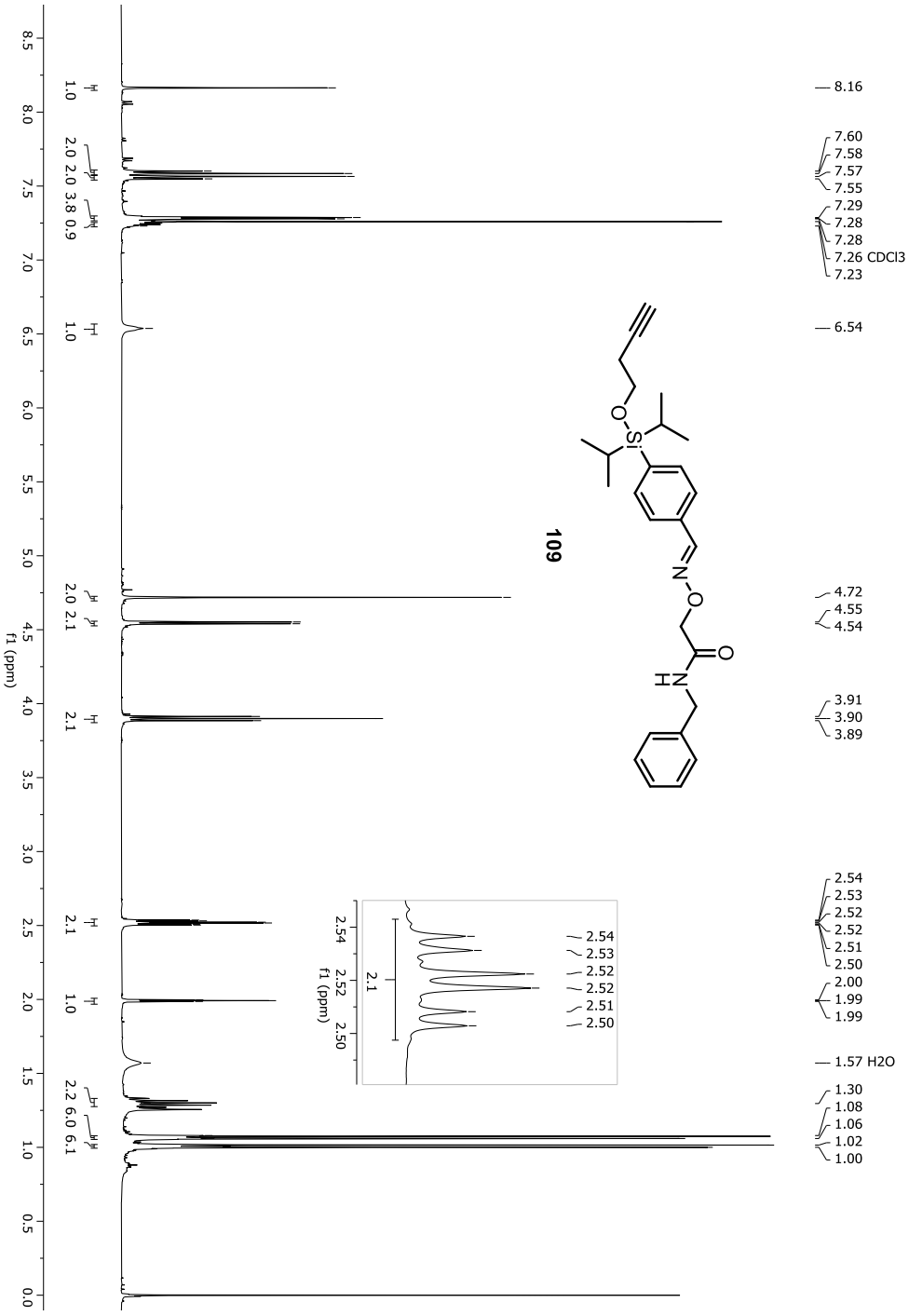

Figure A-161. ^{13}C-NMR spectrum of compound 109

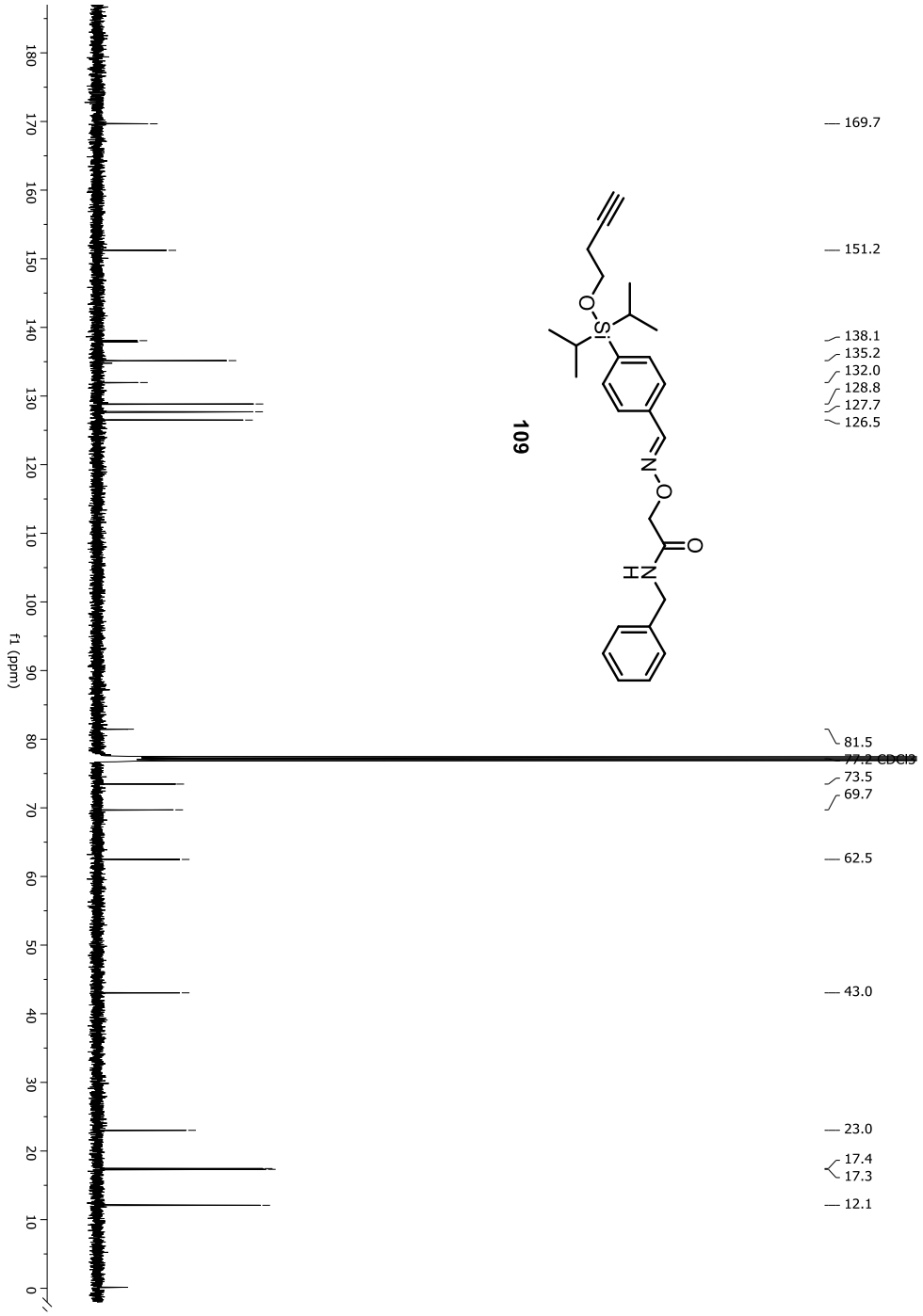

Figure A-162. HRMS spectrum of compound 109

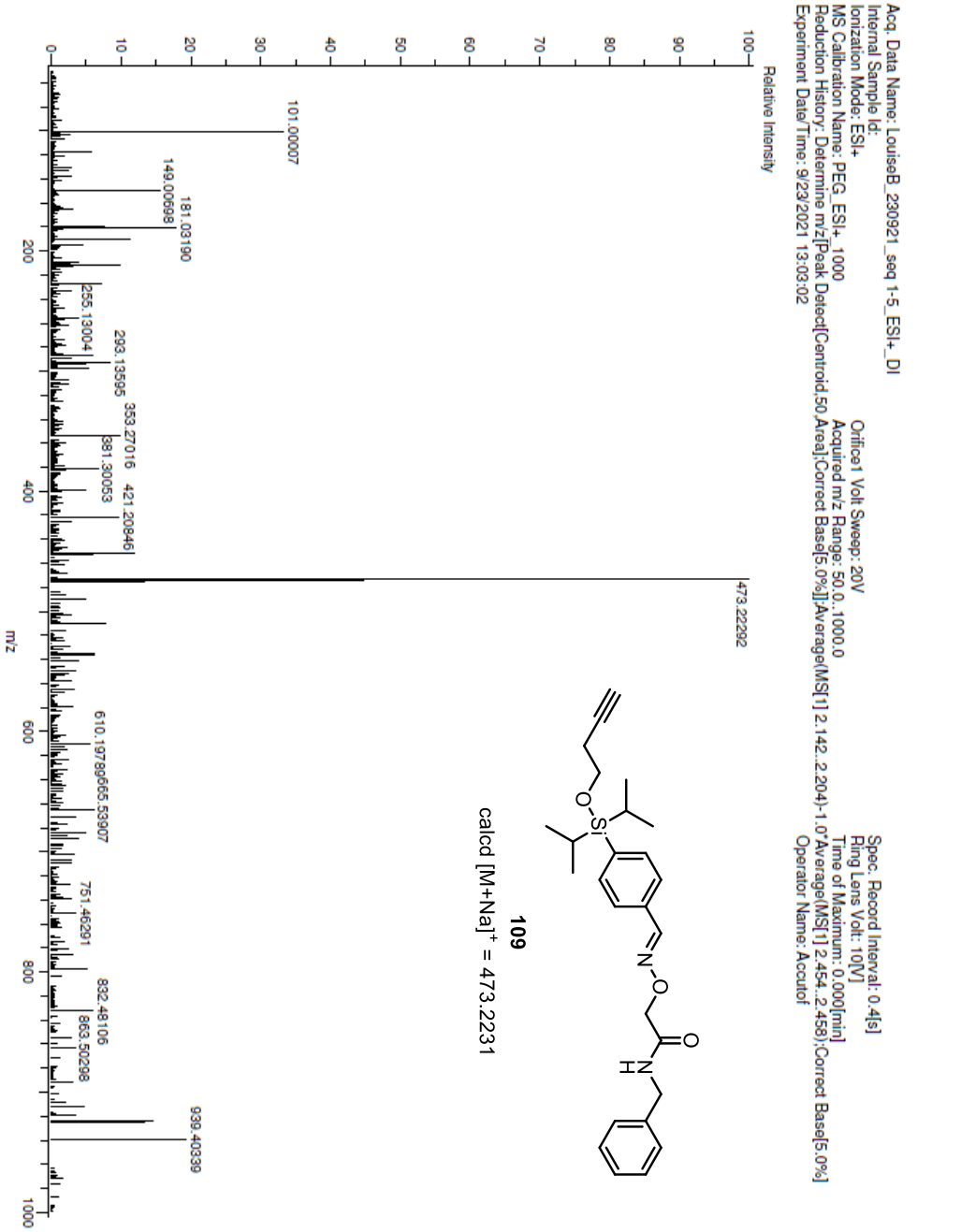

Figure A-163. ^{1}H-NMR spectrum of compound 111

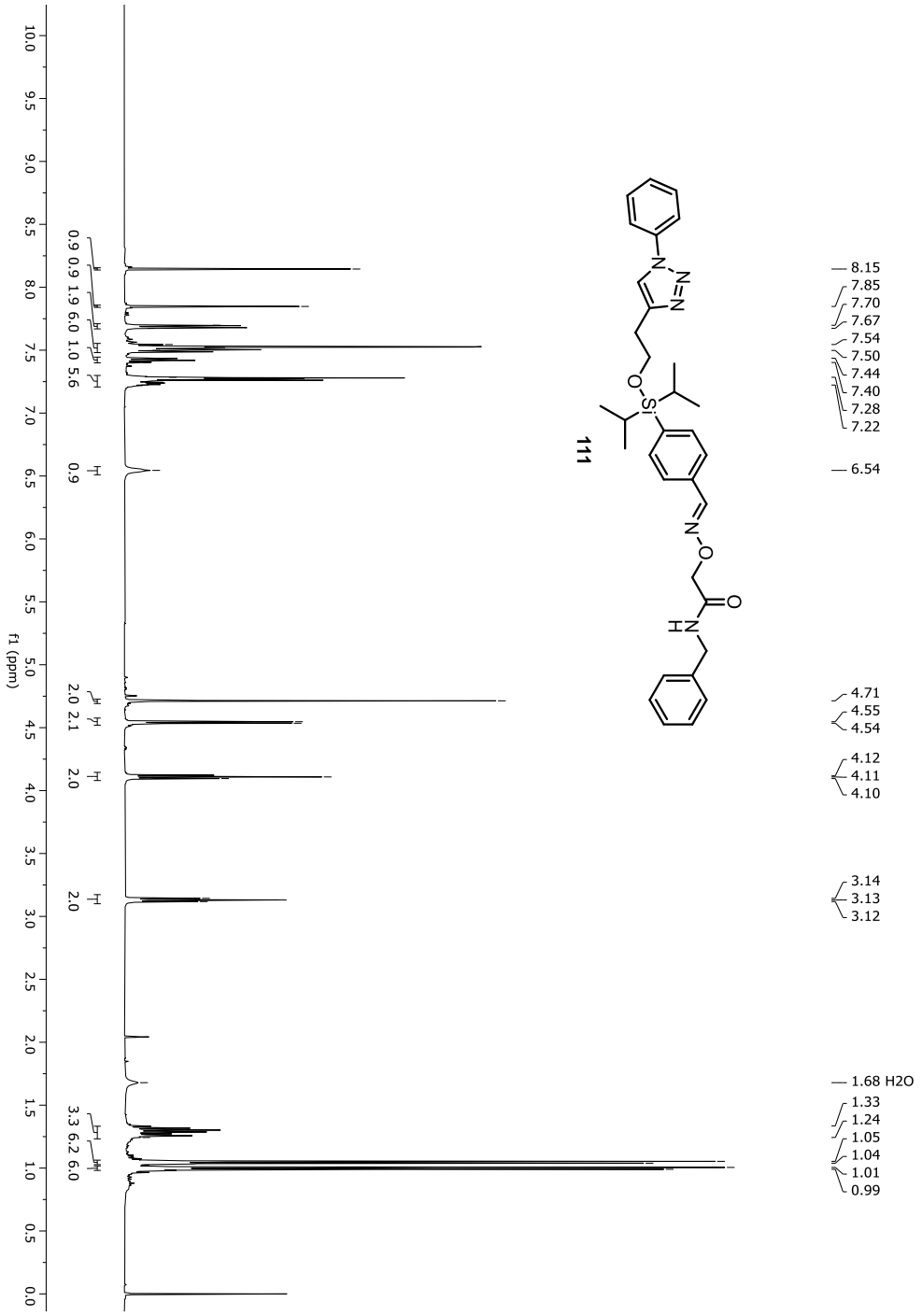

Figure A-164. ^{13}C-NMR spectrum of compound 111

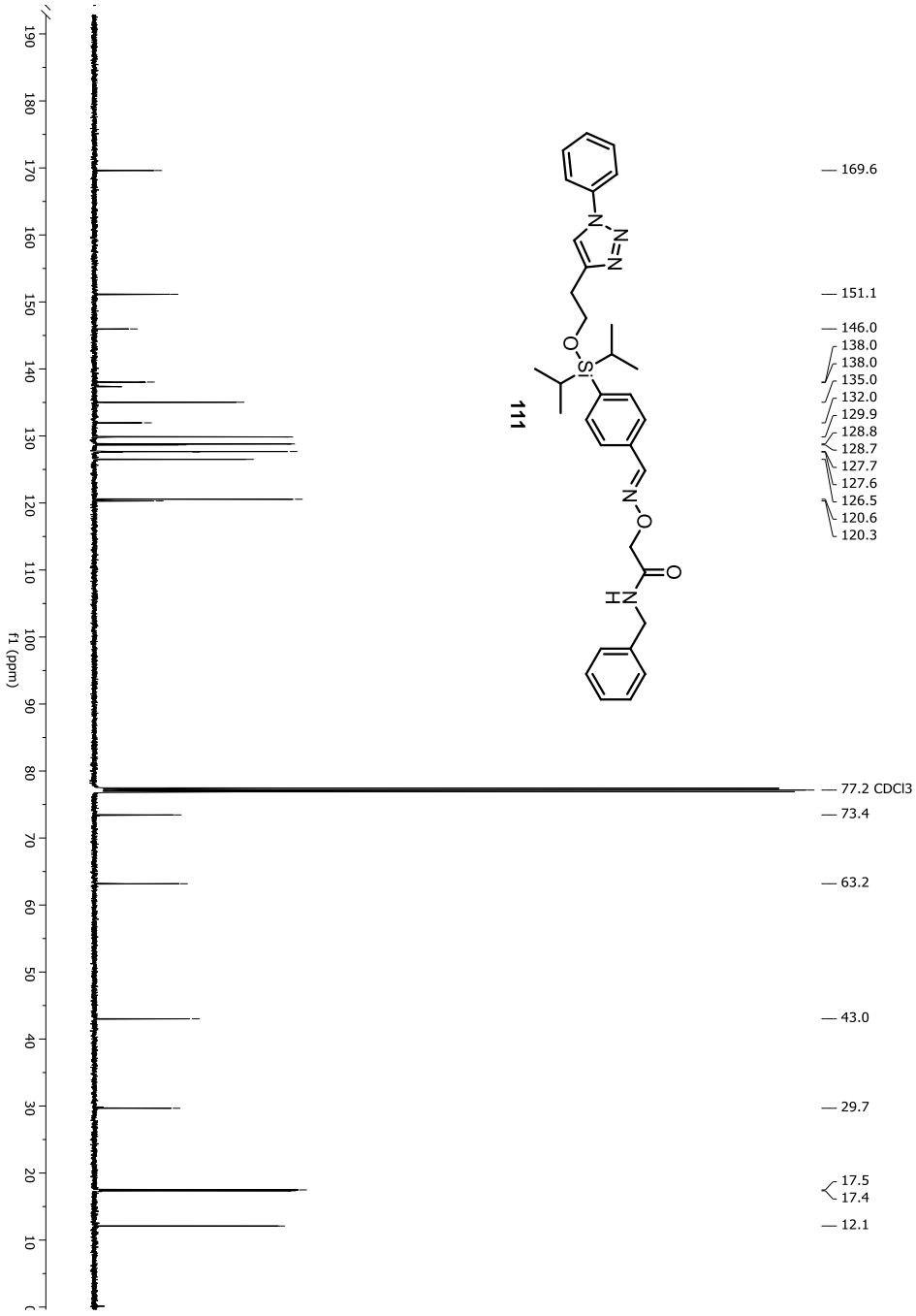

Figure A-165. HRMS spectrum of compound 111

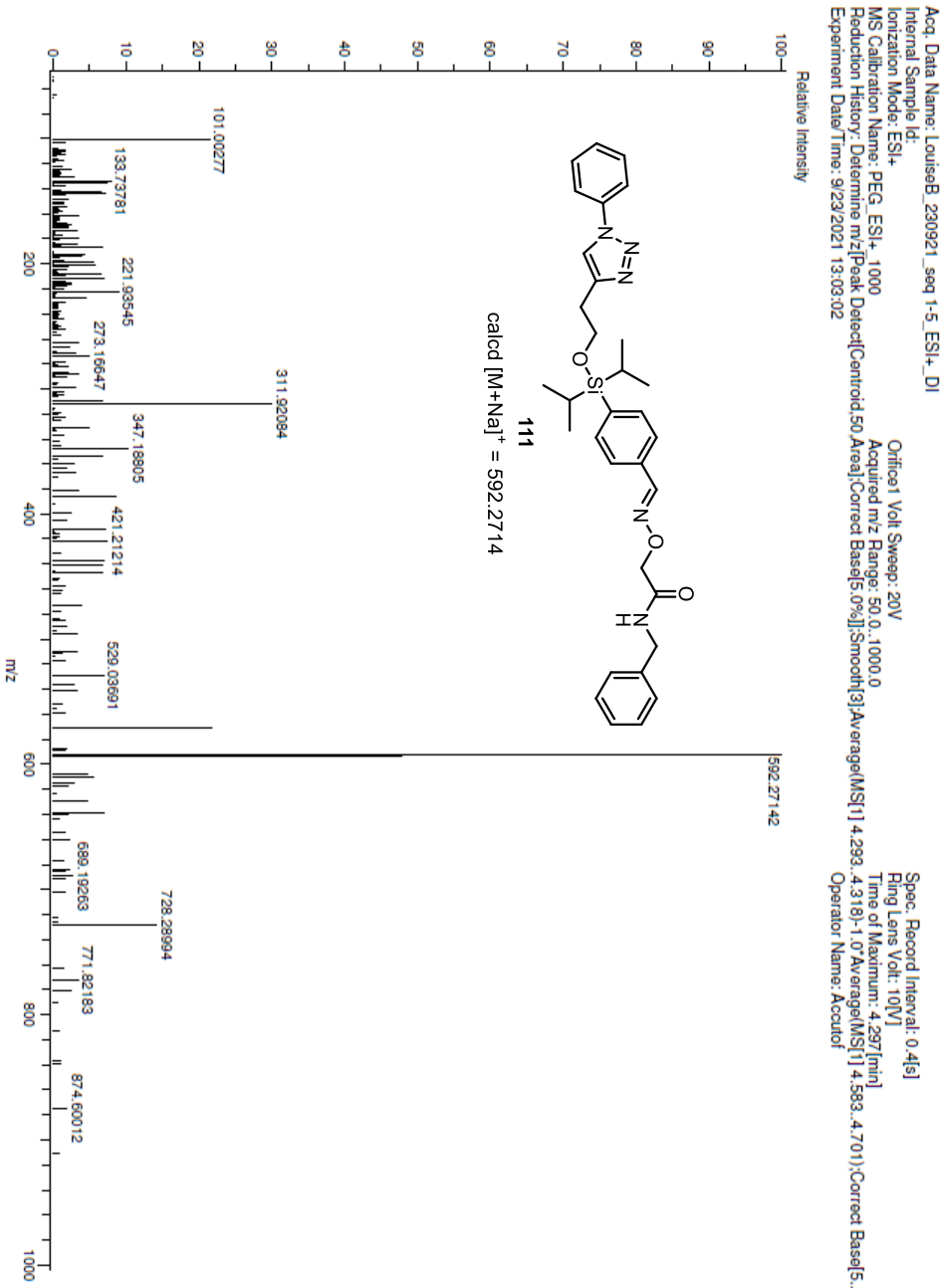

Figure A-166. ^{1}H-NMR spectrum of compound 114

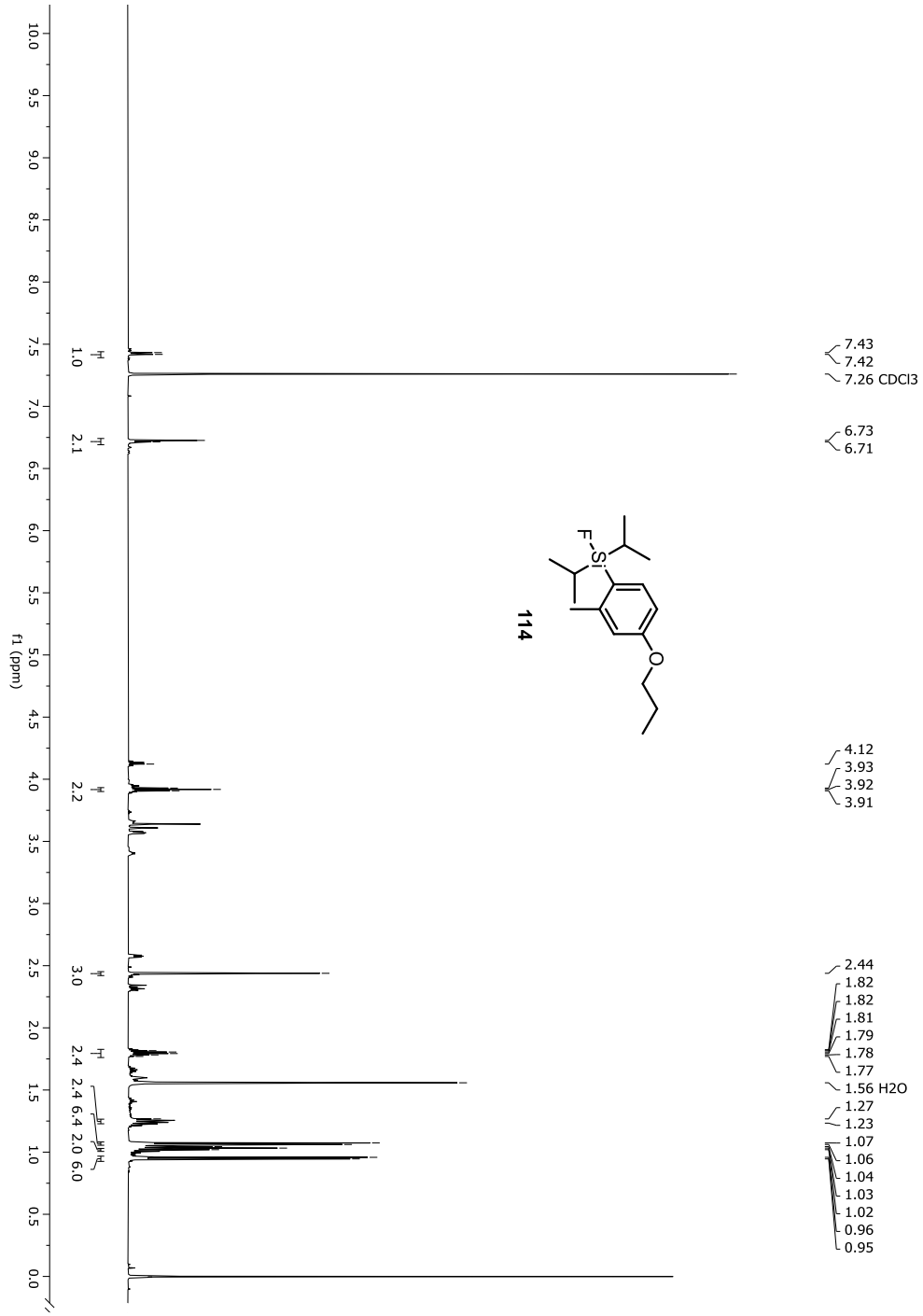

Figure A-167. ^{13}C-NMR spectrum of compound 114

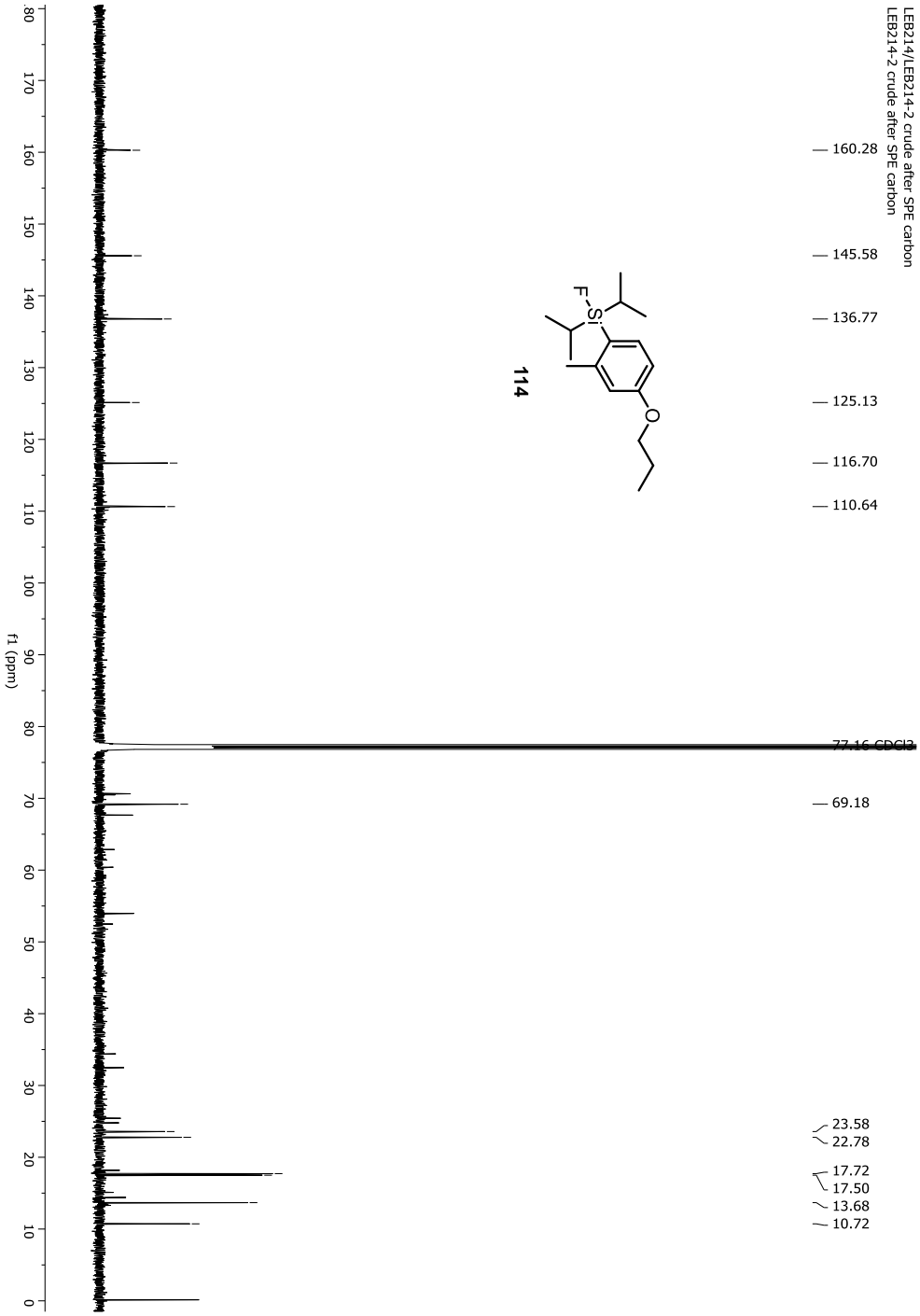

Figure A-168. GC-MS chromatogram of compound 114

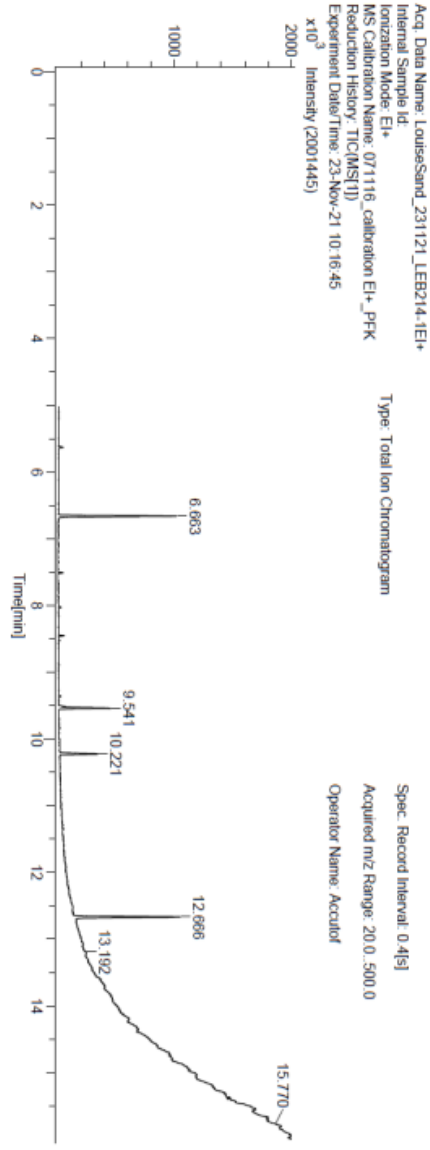

Figure A-169. HRMS spectrum of compound 114 (Rt = 10.221)

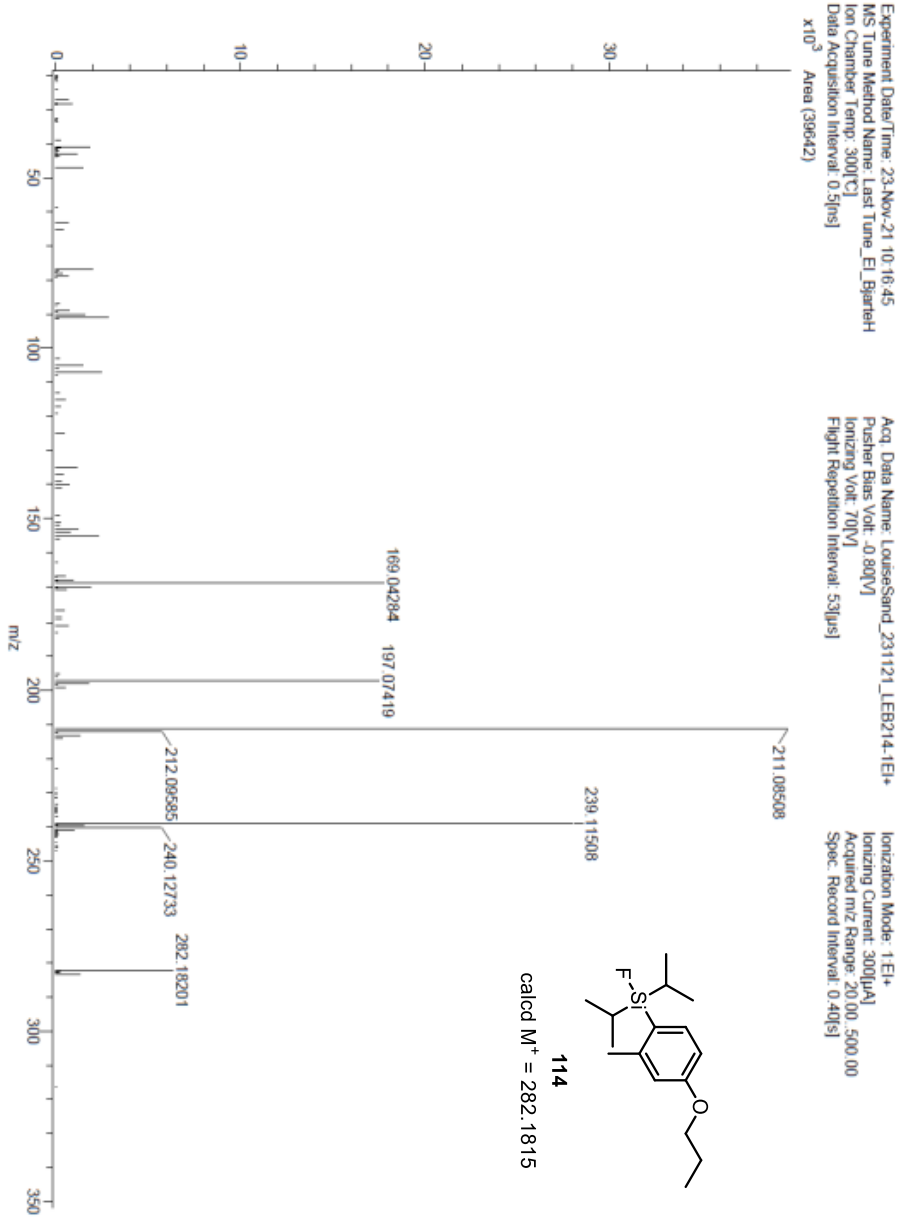

Figure A-170. ^{1}H-NMR spectrum of compound 114 (from solid-phase)

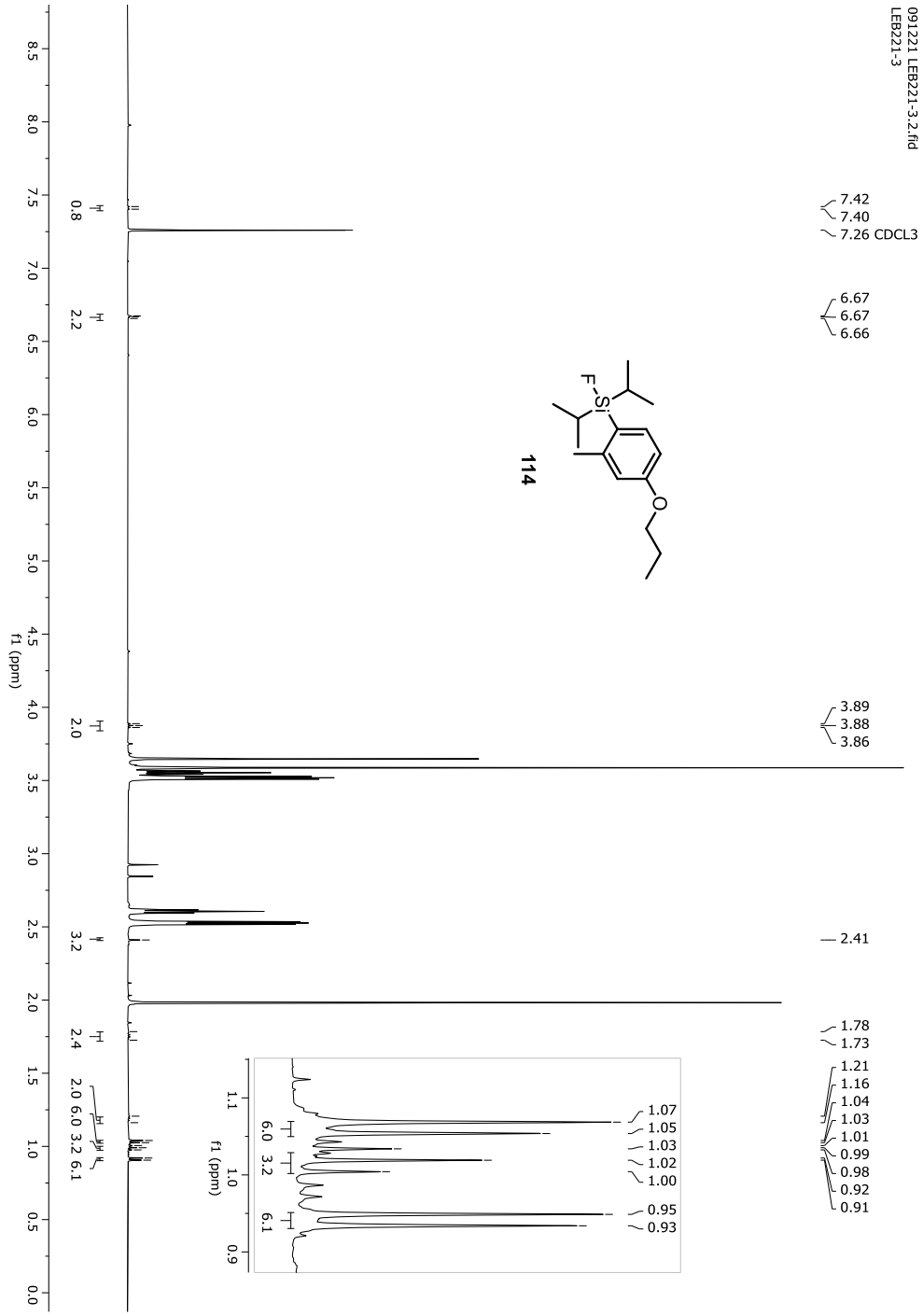

Figure A-171. GC-MS chromatogram of compound 114 (from solid-phase)

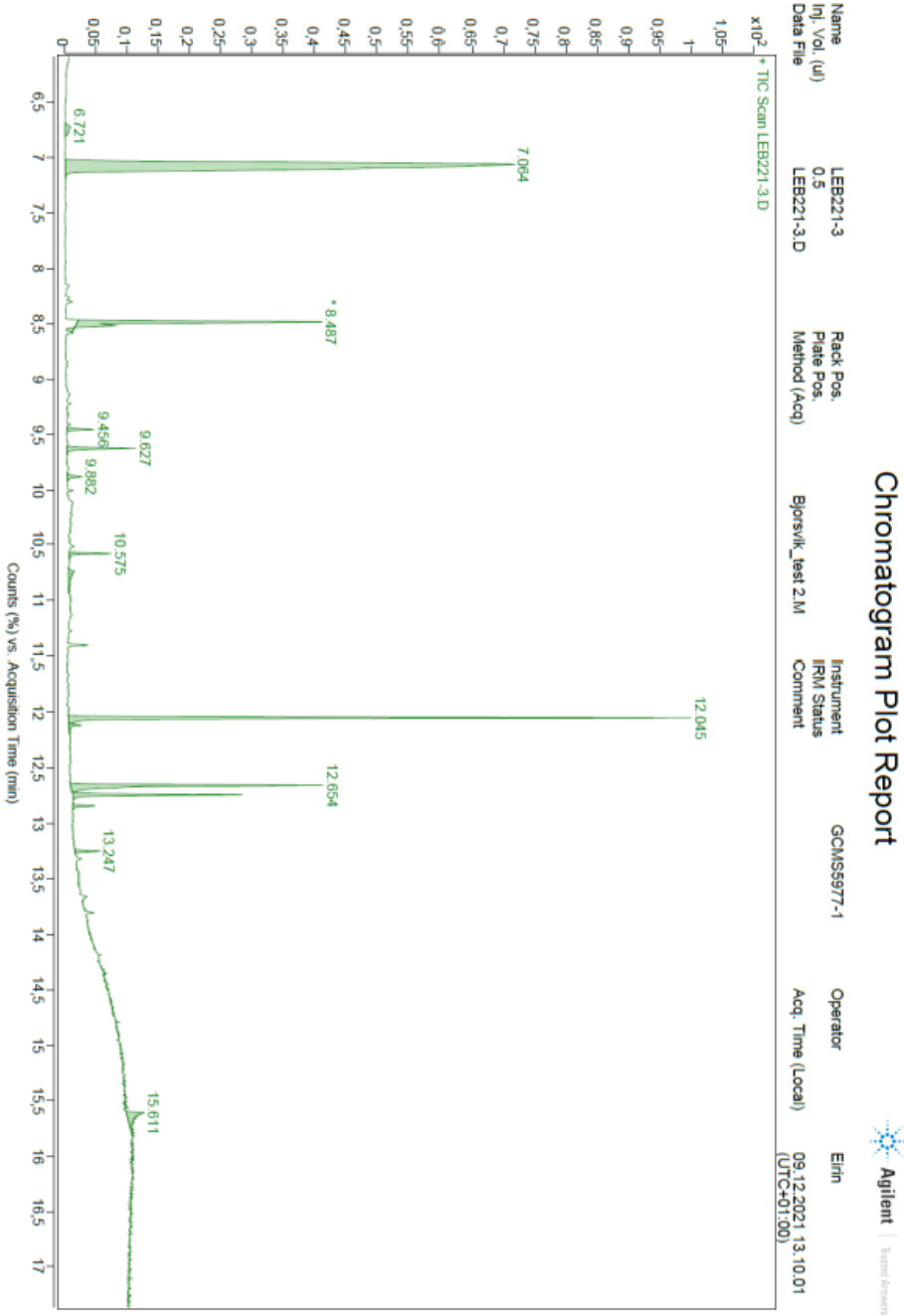

Figure A-172. GC-MS spectrum of compound 114 (Rt = 12.045)

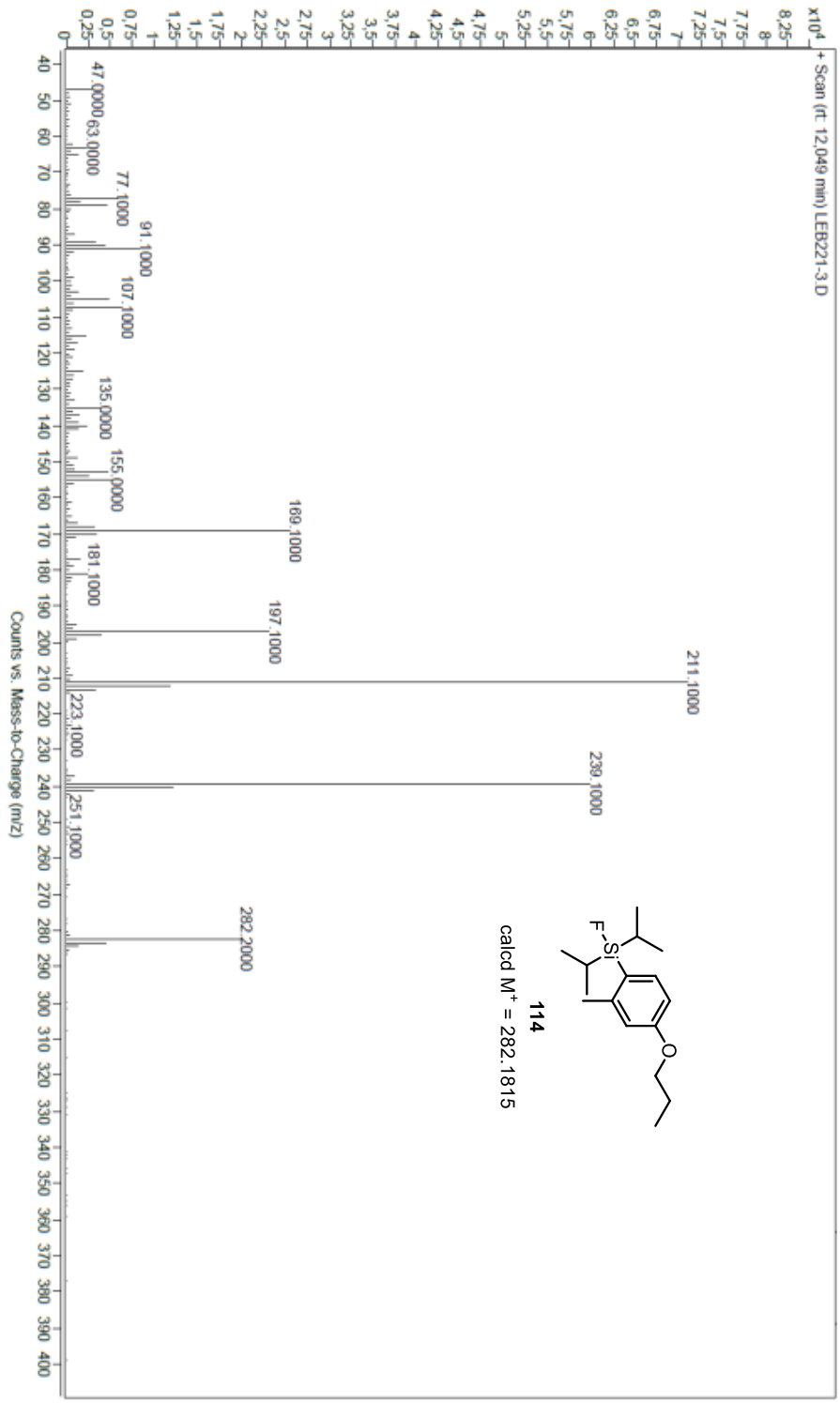

Figure A-173. ^{1}H-NMR spectrum of compound 118

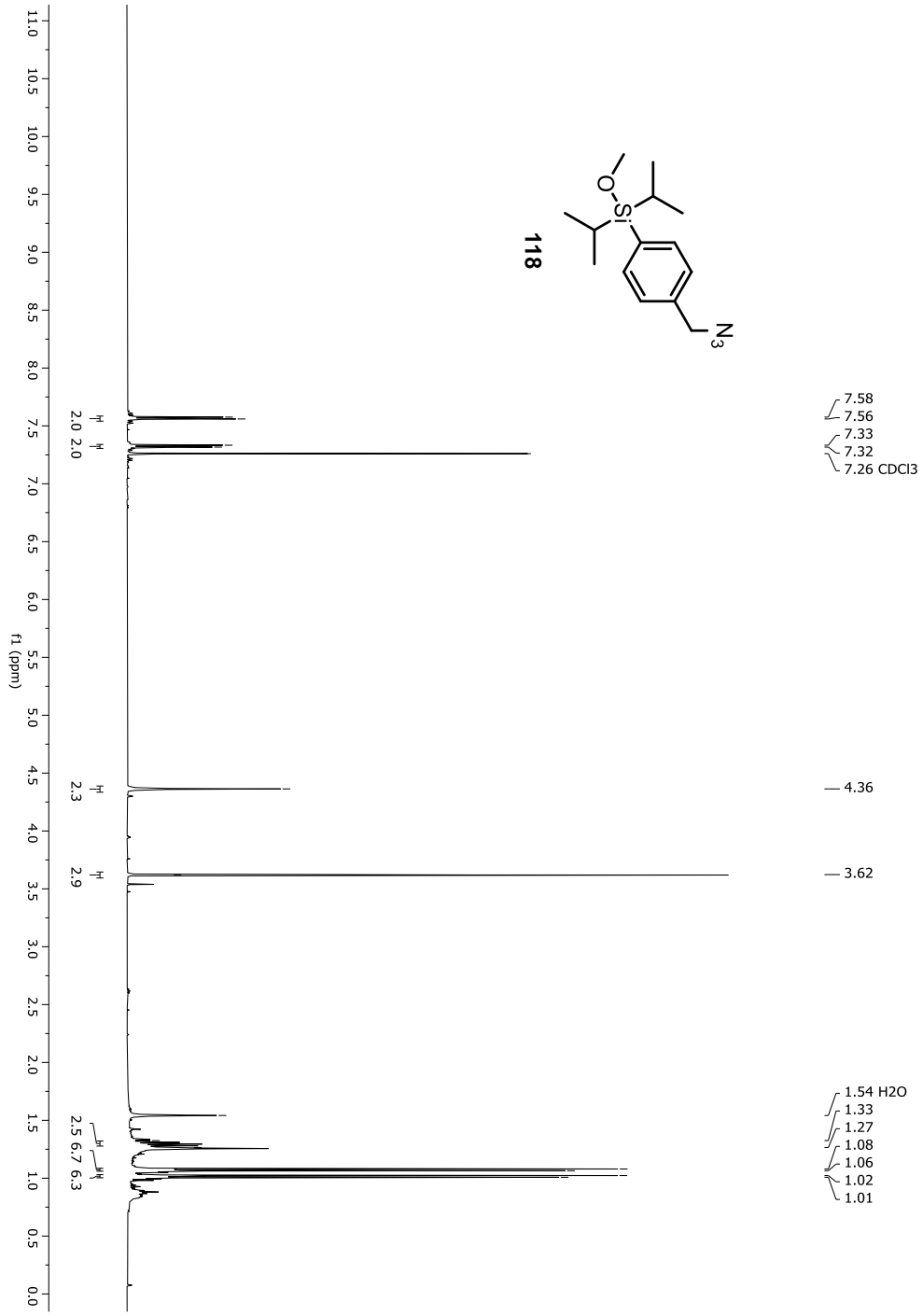

Figure A-174. ^{13}C-NMR spectrum of compound 118

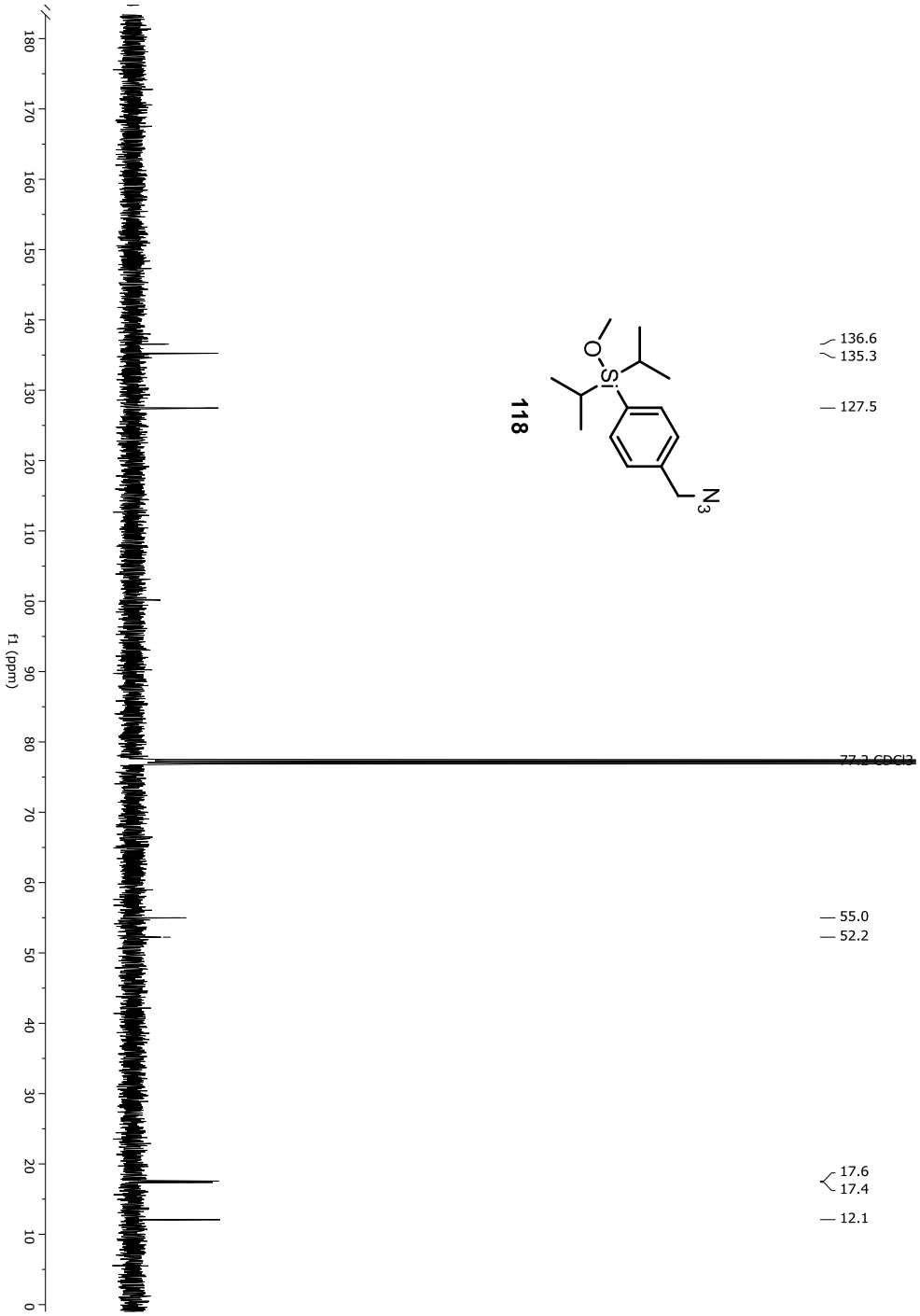

Figure A-175. ^{1}H-NMR spectrum of compound 119

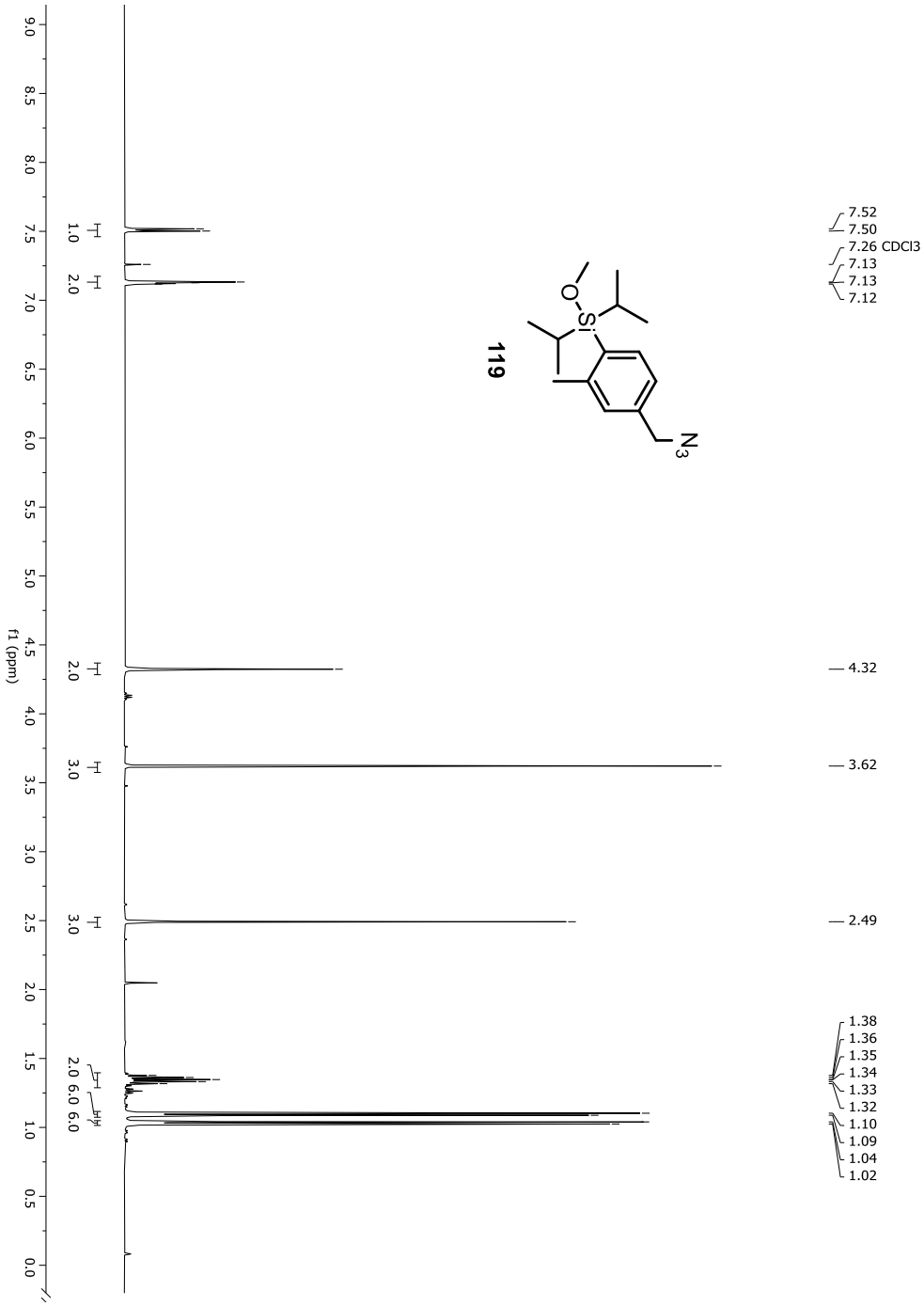

Figure A-176. ^{13}C-NMR spectrum of compound 119

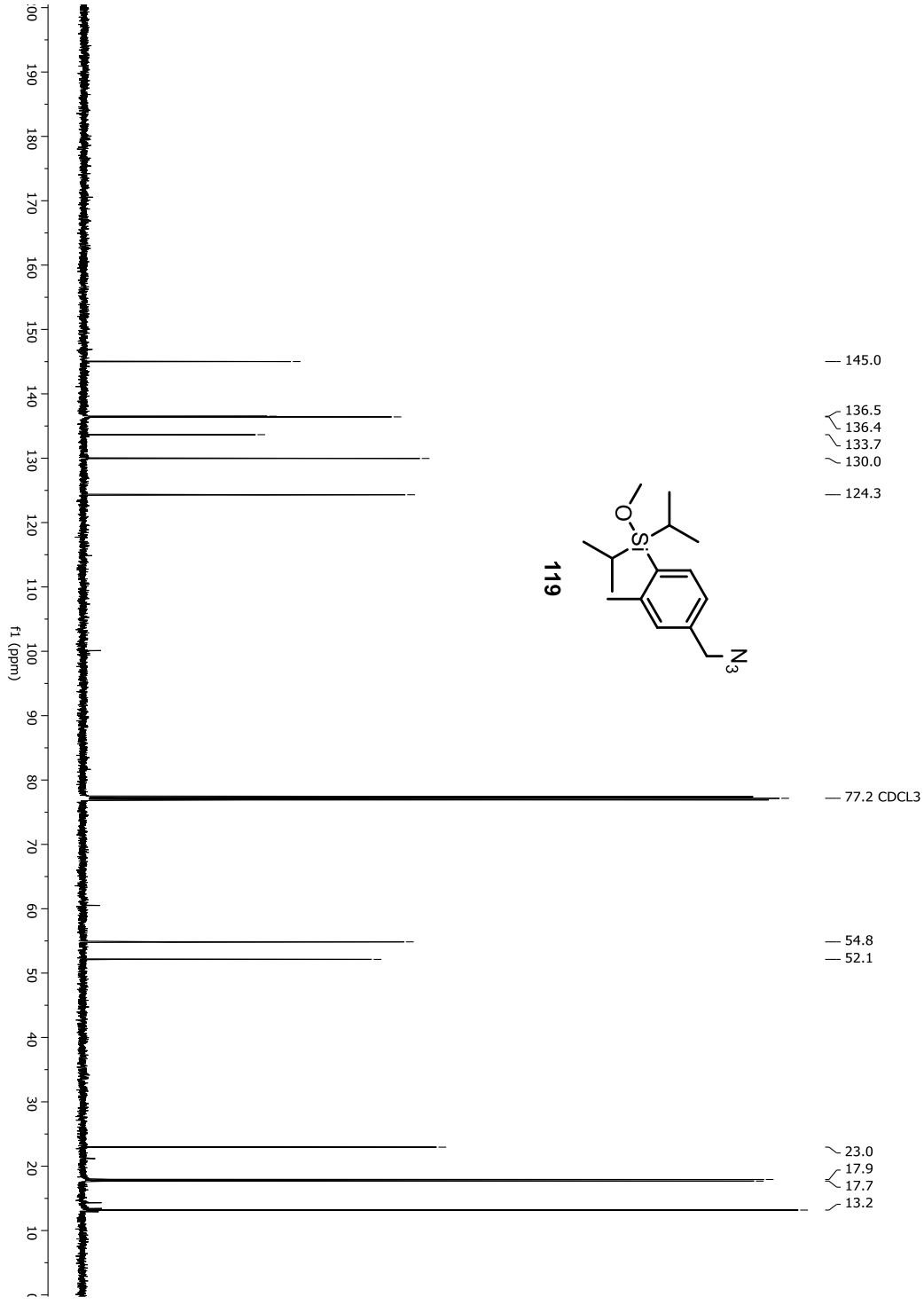

Figure A-177. HRMS spectrum of compound 119

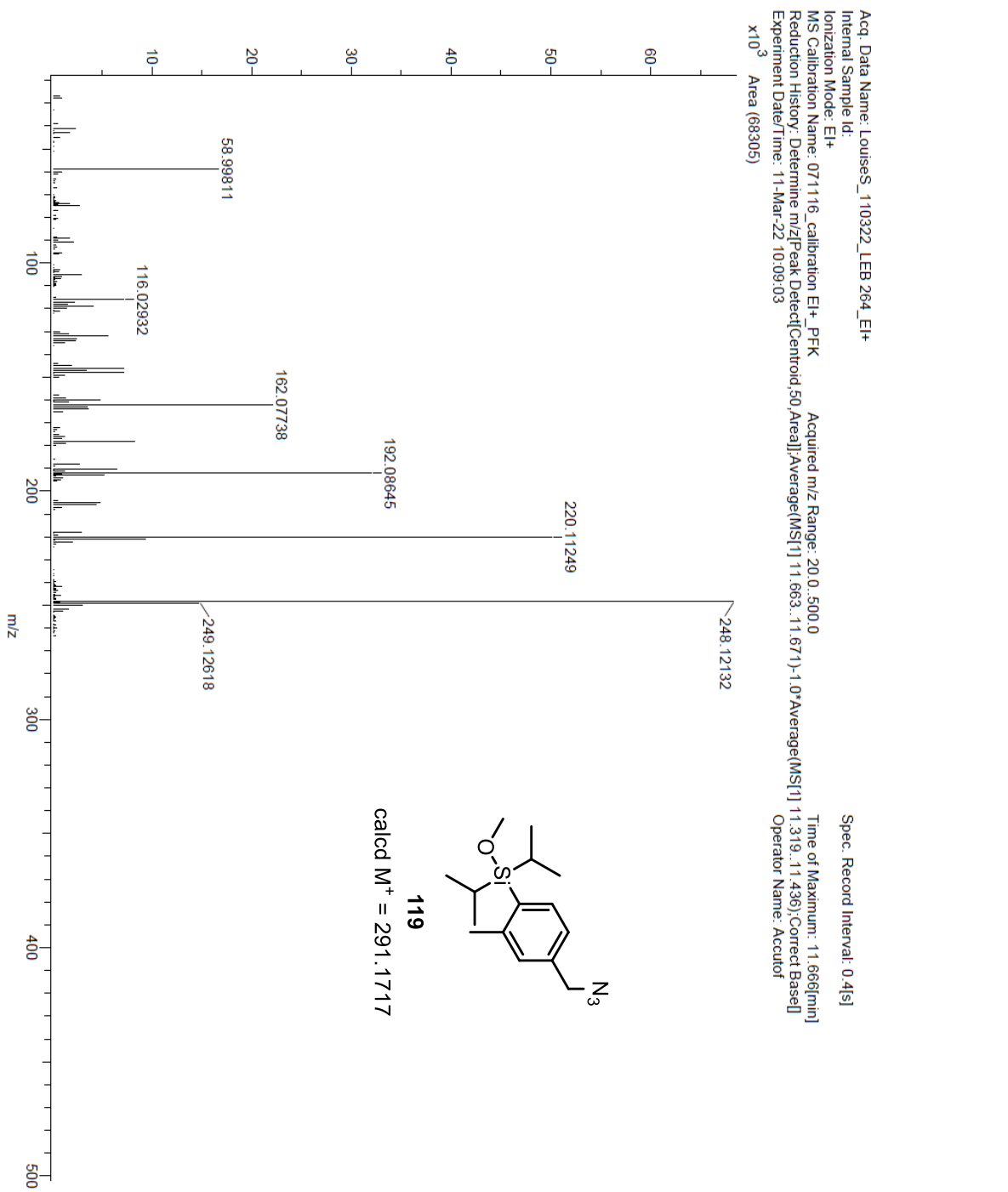

Figure A-178. ^{1}H-NMR spectrum of compound 120

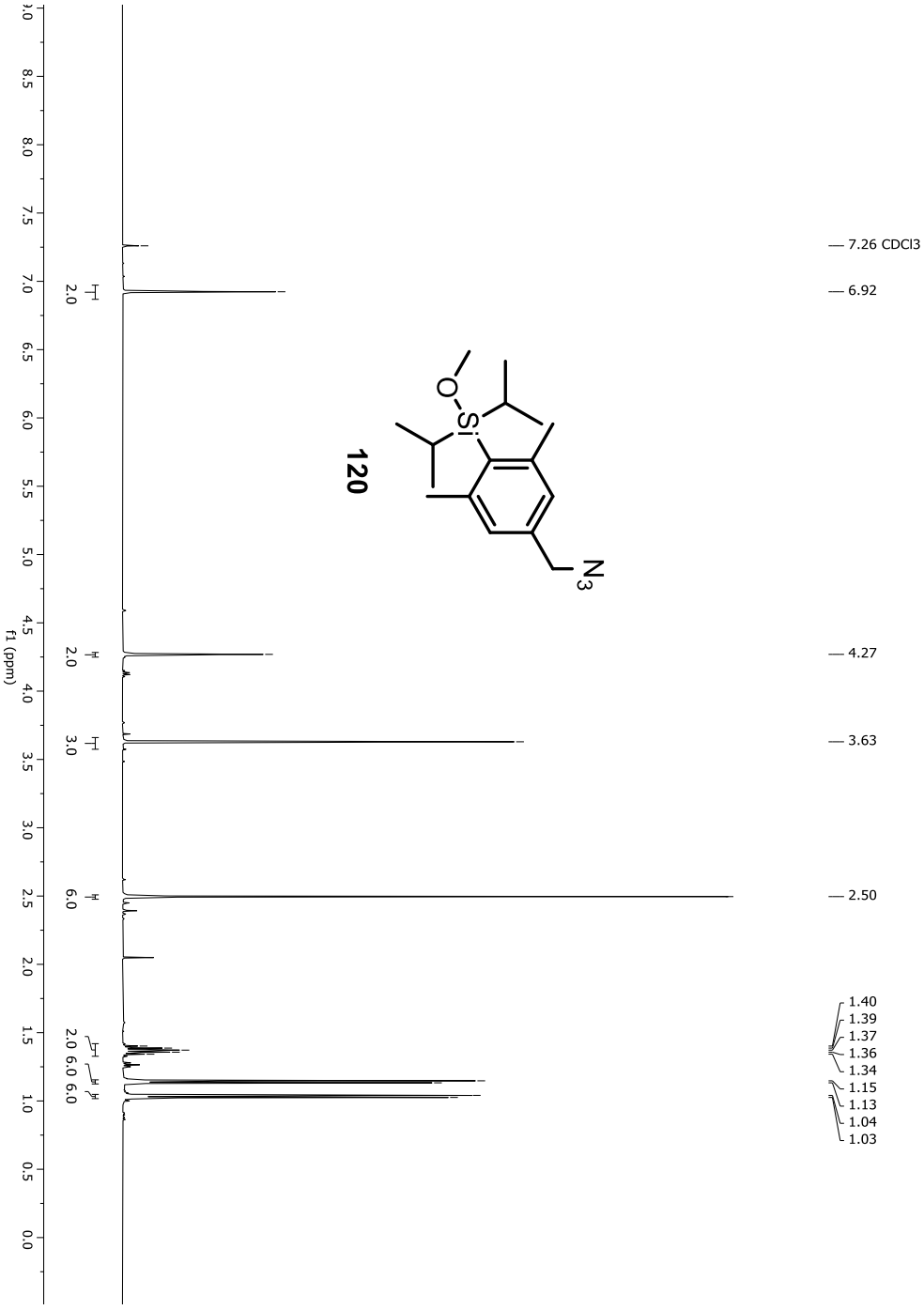

Figure A-179. ^{13}C-NMR spectrum of compound 120

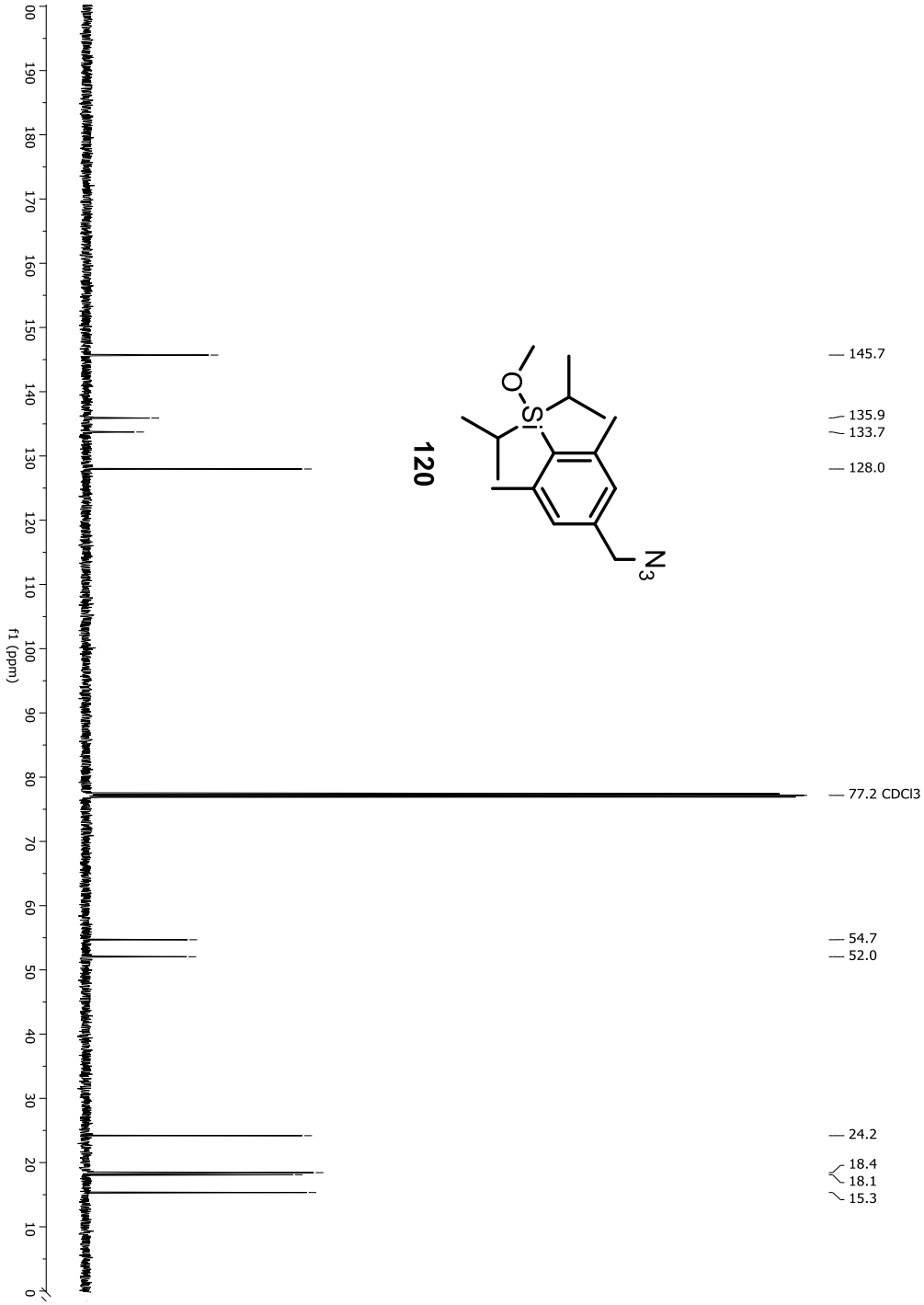

Figure A-180. HRMS spectrum of compound 120

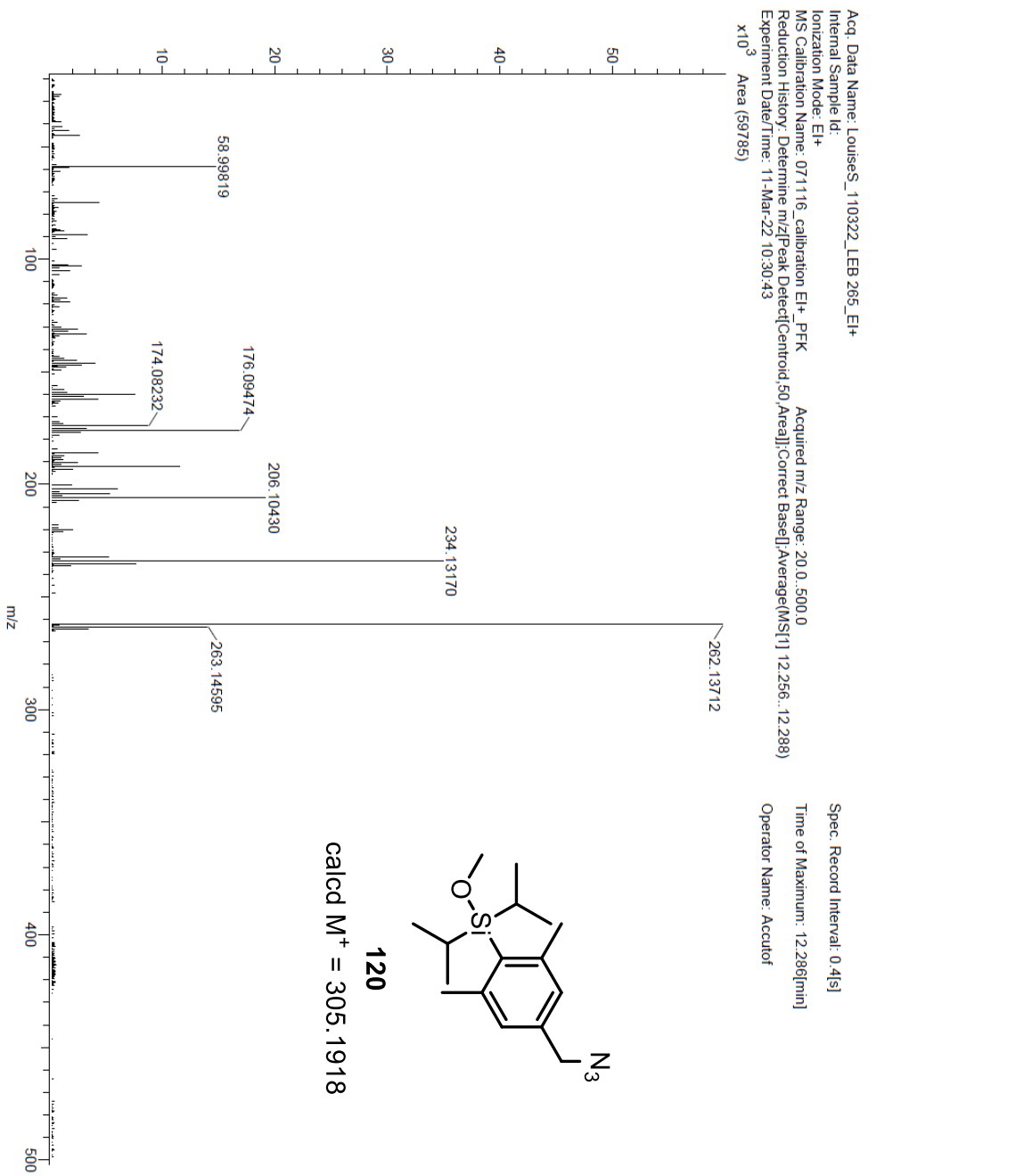

Figure A-181. ^{1}H-NMR spectrum of compound 121

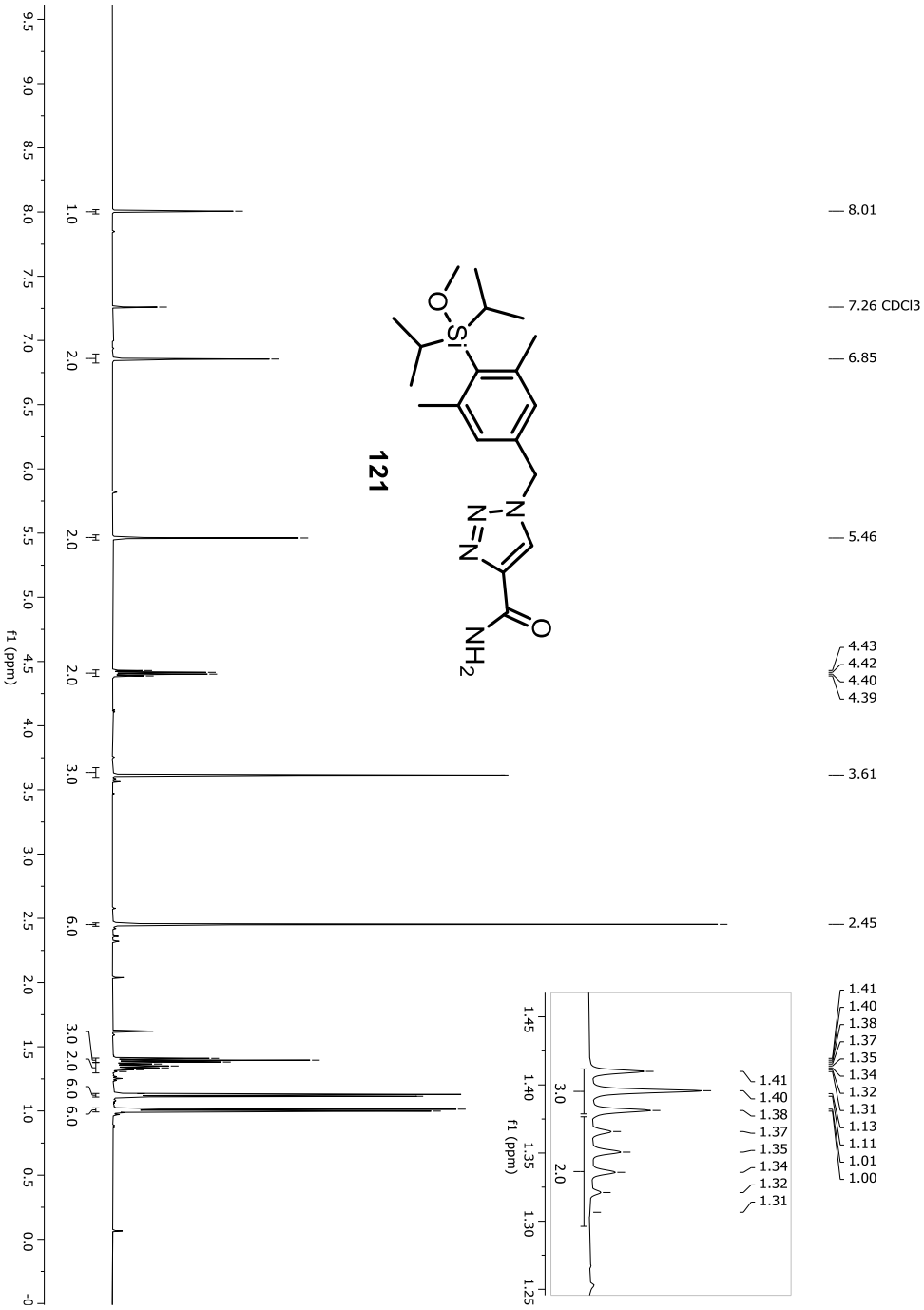

Figure A-182. ^{13}C-NMR spectrum of compound 121

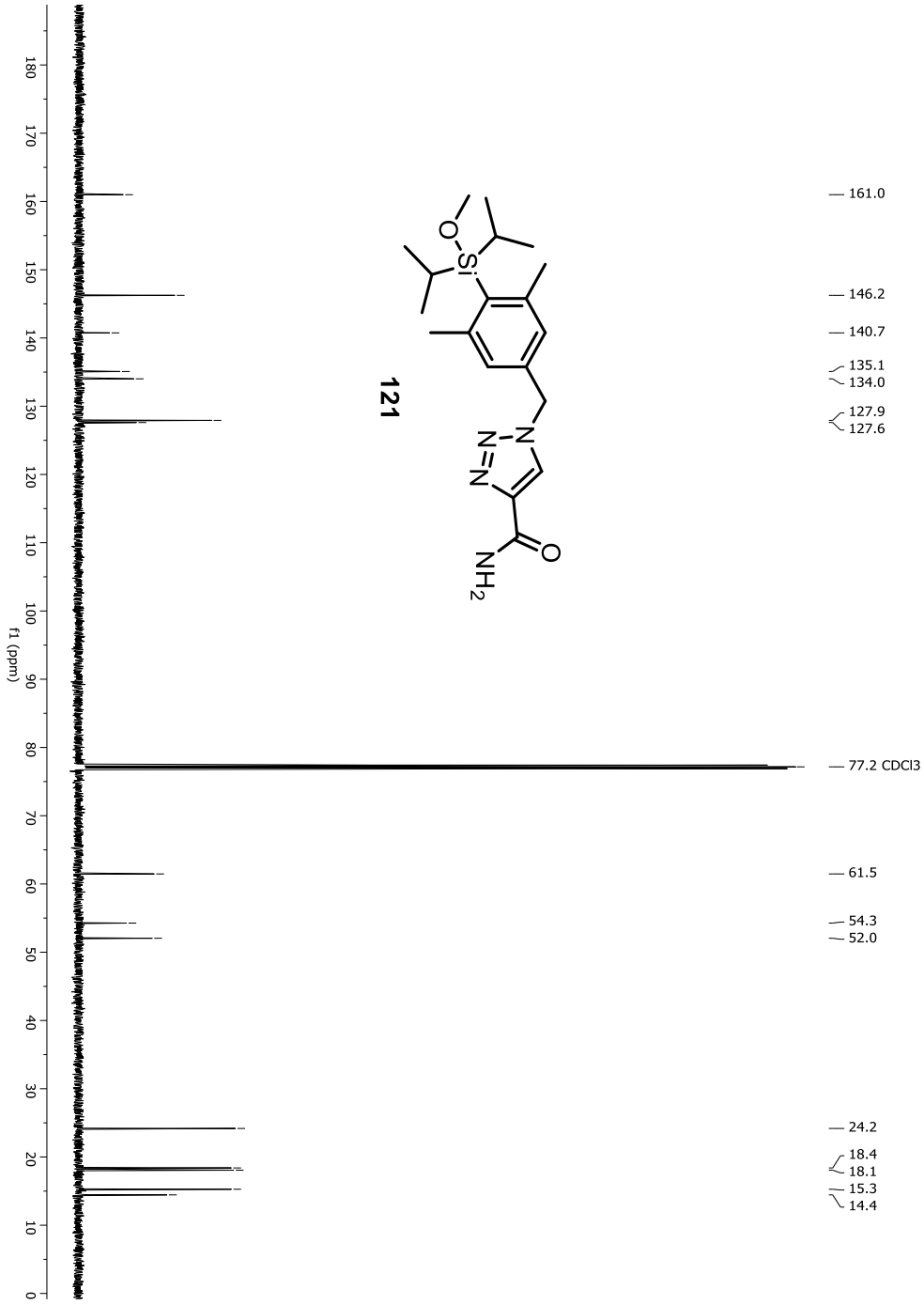

Figure A-183. ^{1}H-NMR spectrum of compound 130

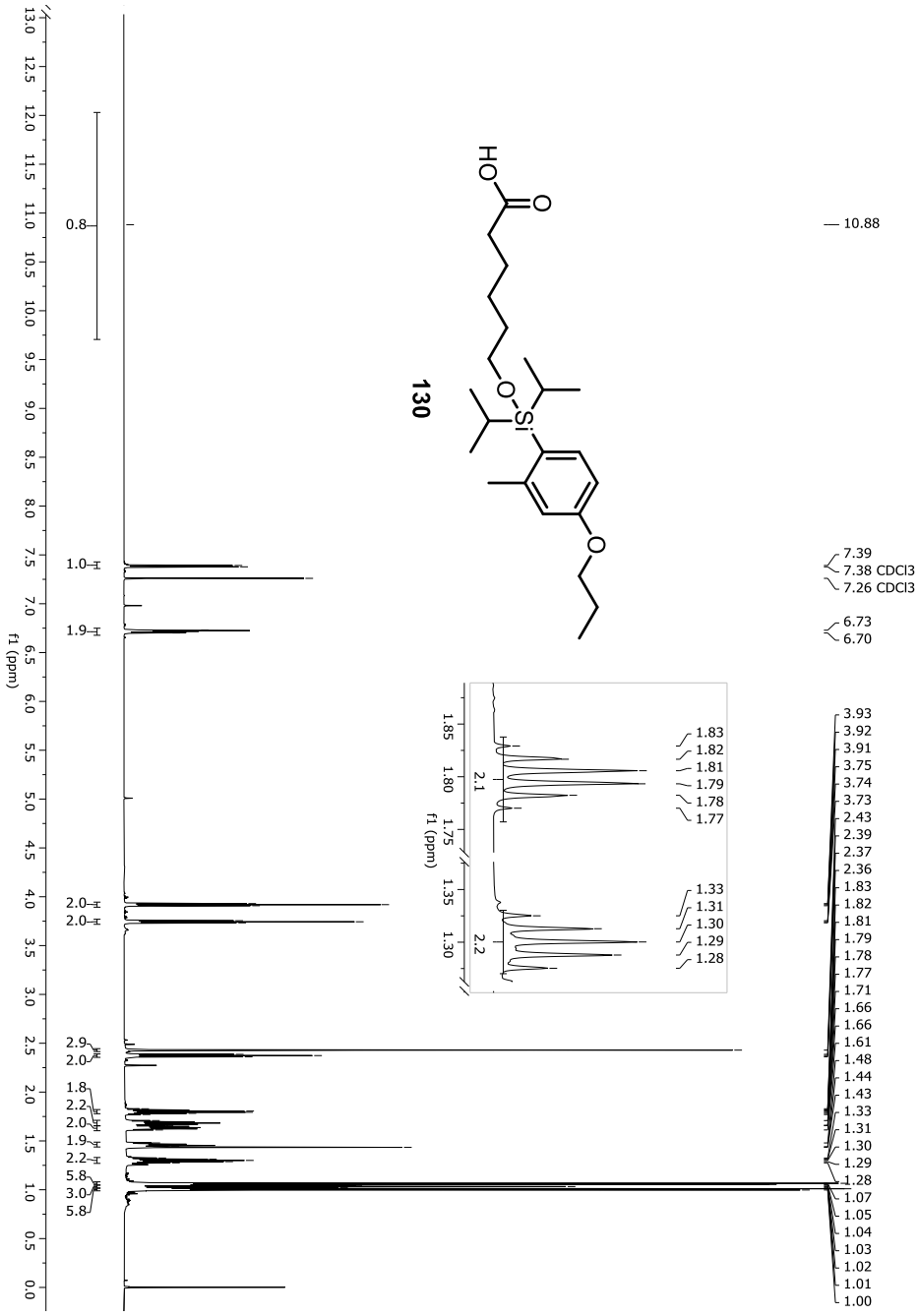

Figure A-184. ^{13}C-NMR spectrum of compound 130

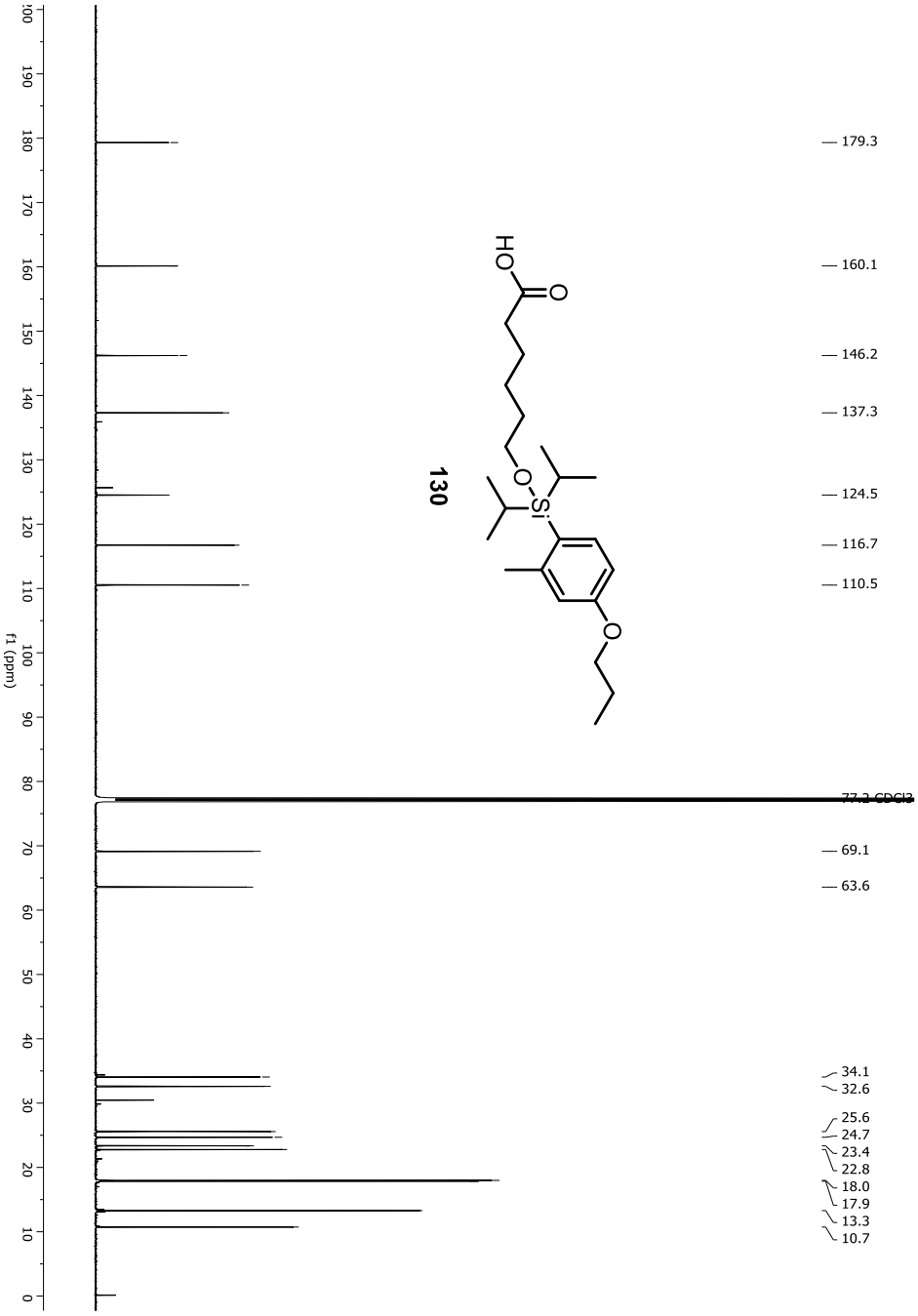

Figure A-185. HRMS spectrum of compound 130

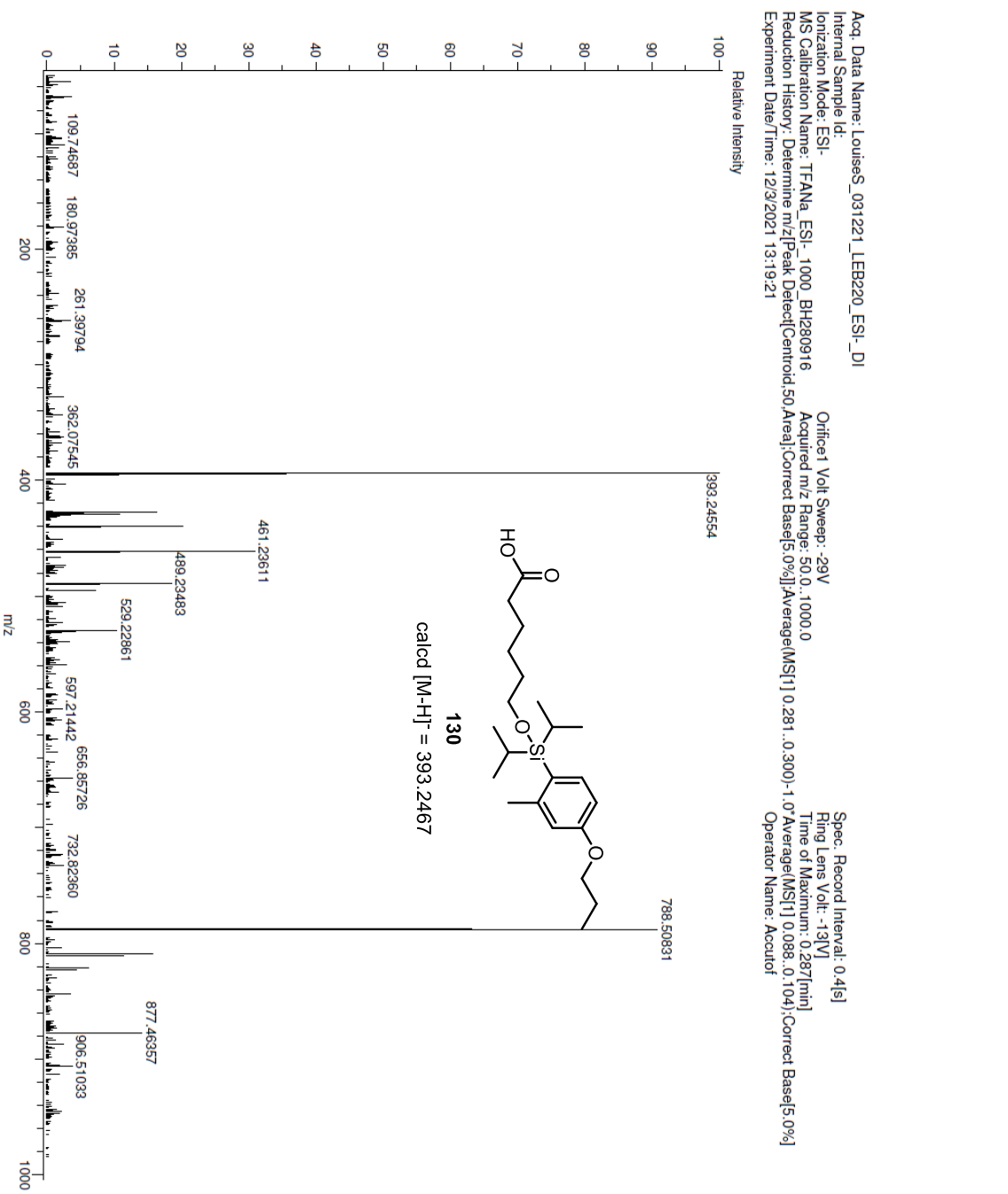

Figure A-186. ^{1}H-NMR spectrum of compound 132

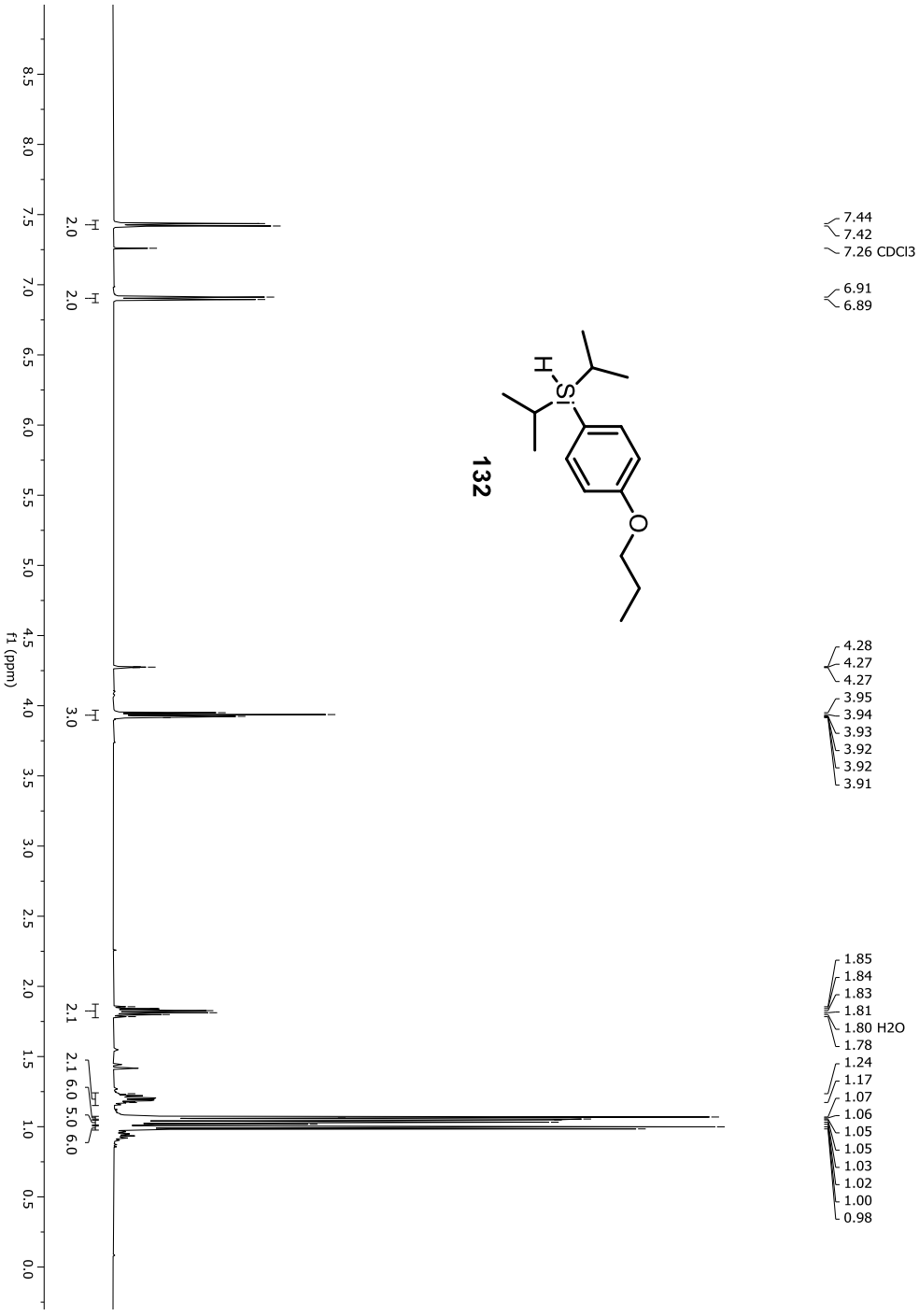

Figure A-187. ^{13}C-NMR spectrum of compound 132

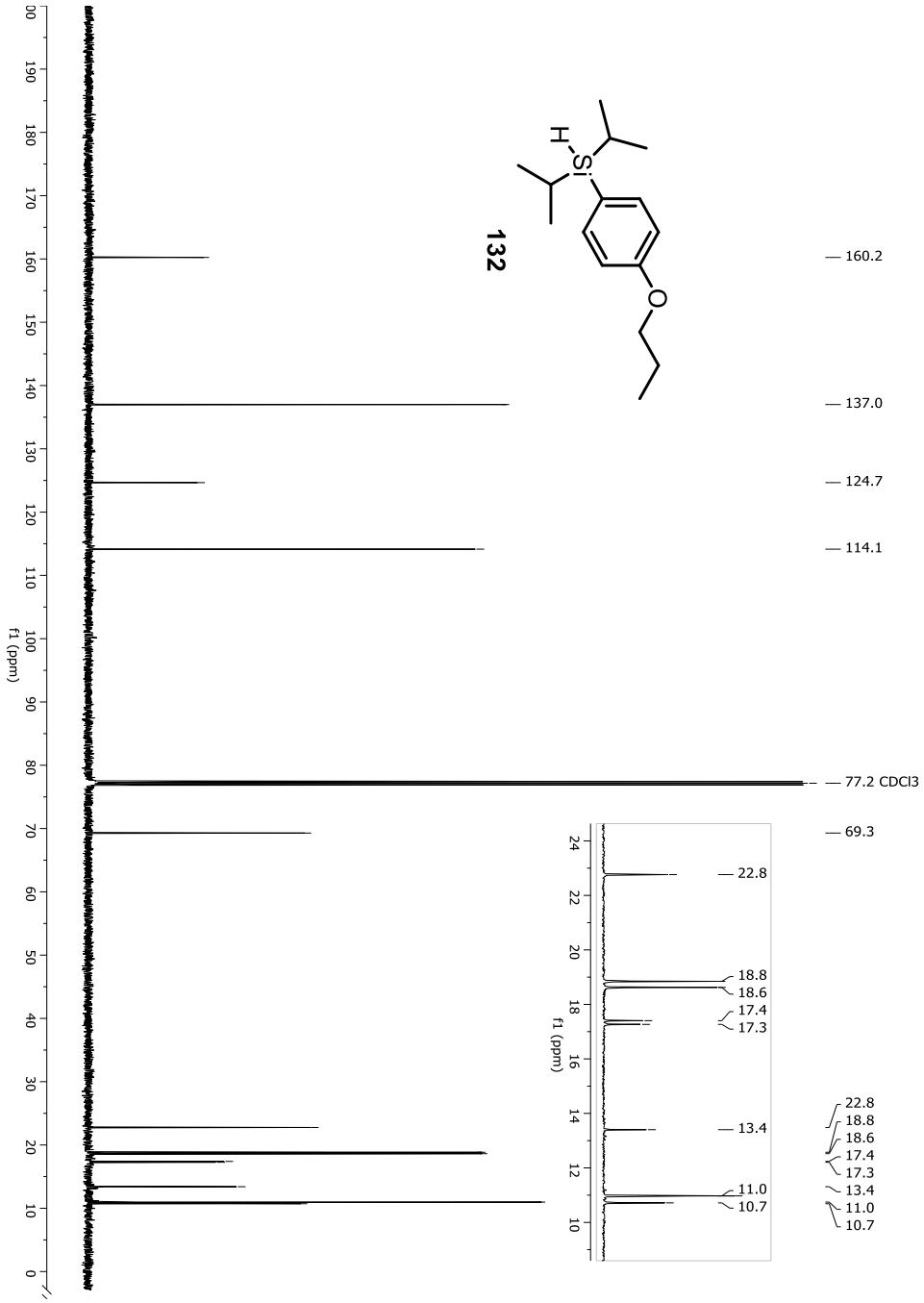

Figure A-188. ^{1}H-NMR spectrum of compound 133

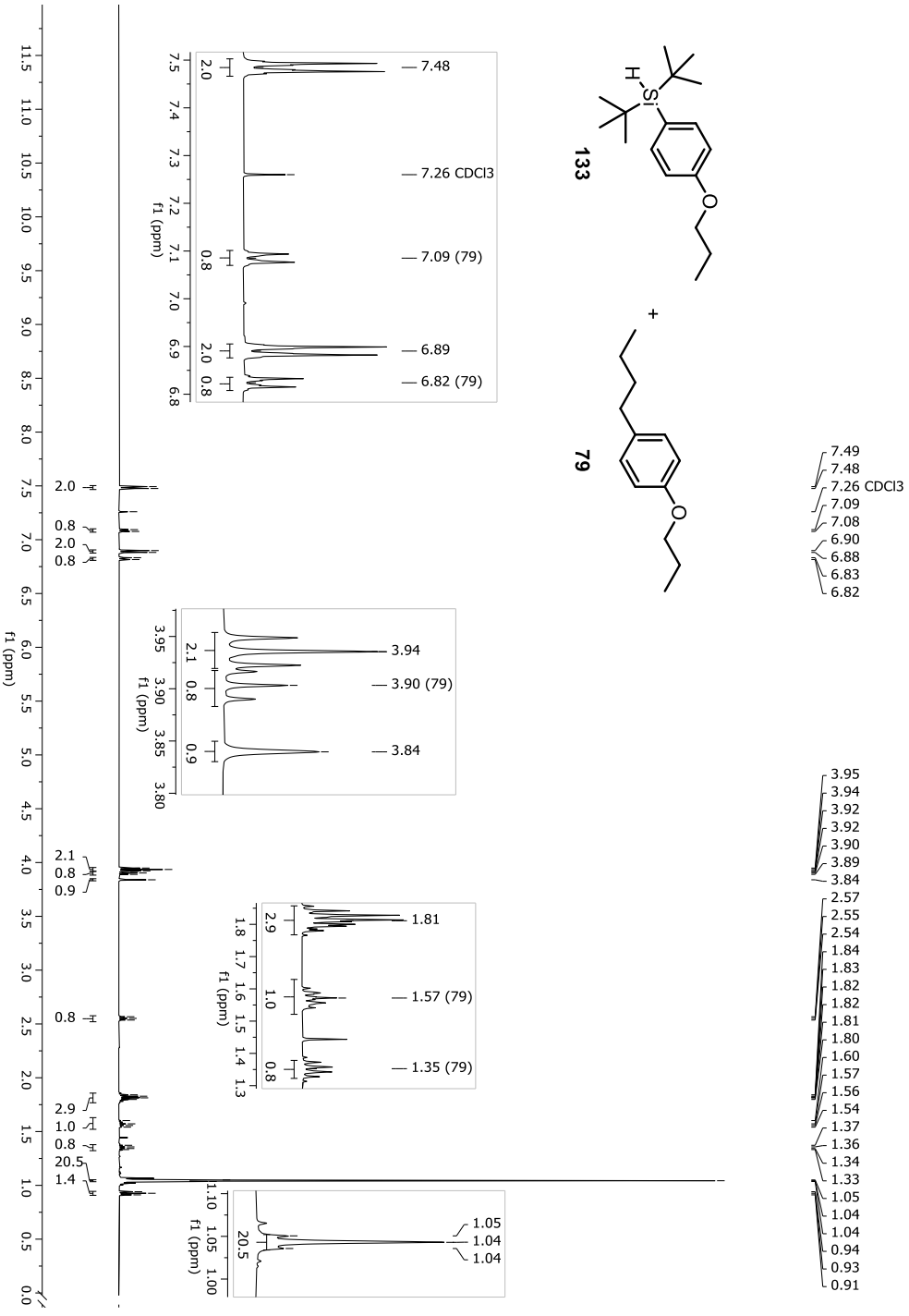

Figure A-189. ^{13}C-NMR spectrum of compound 133

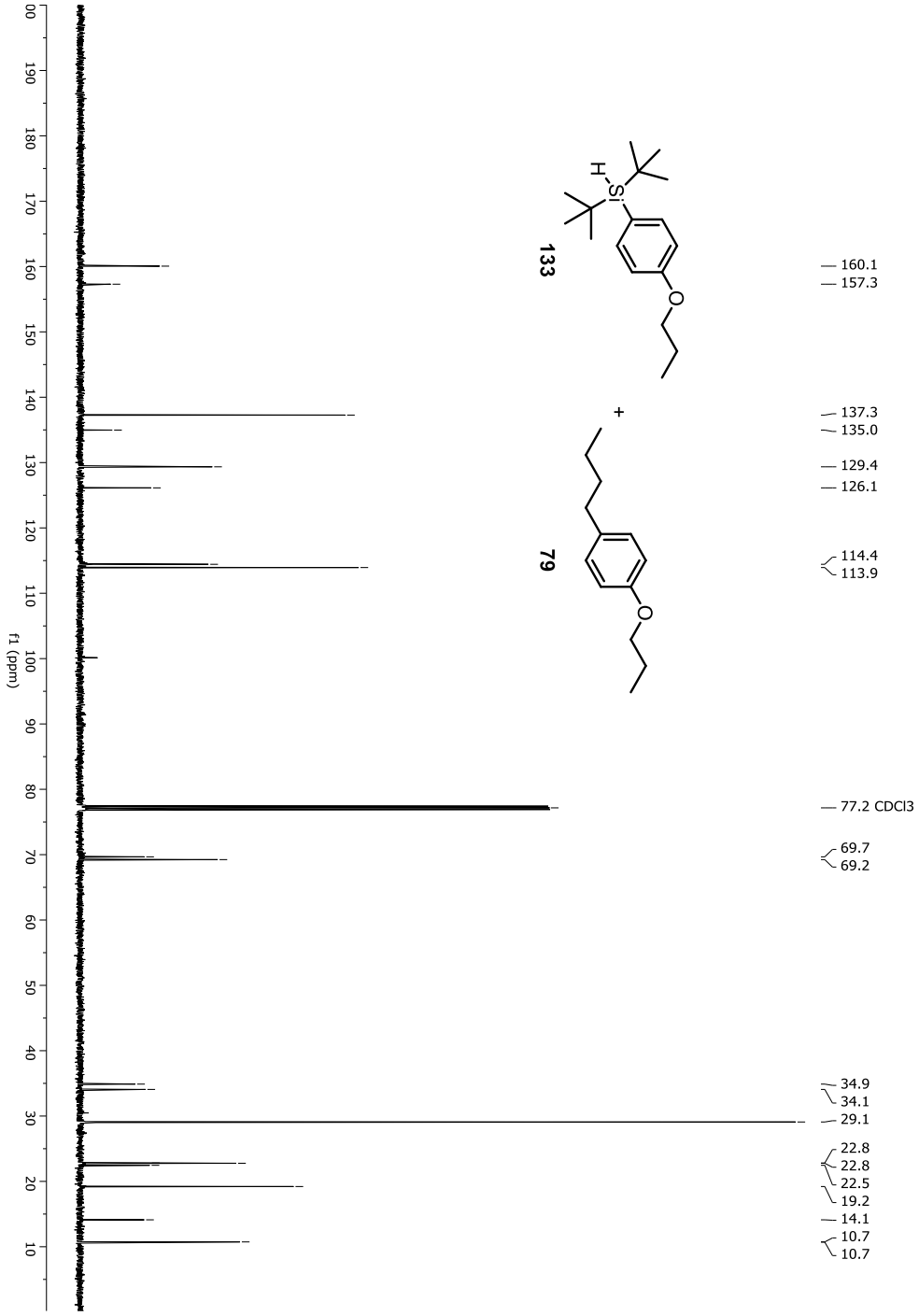

Figure A-190. ^{1}H-NMR spectrum of compound 134

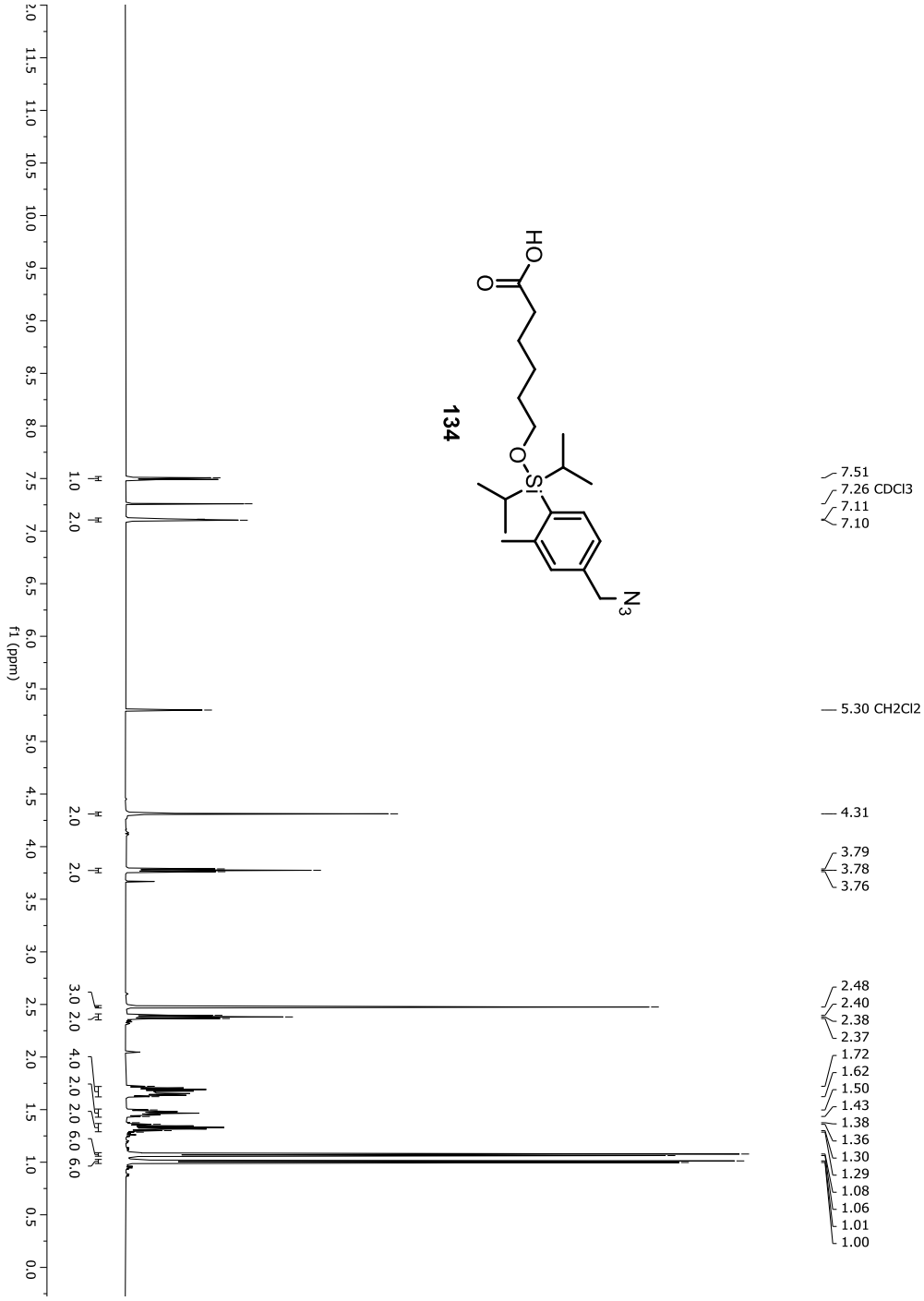

Figure A-191. ^{13}C-NMR spectrum of compound 134

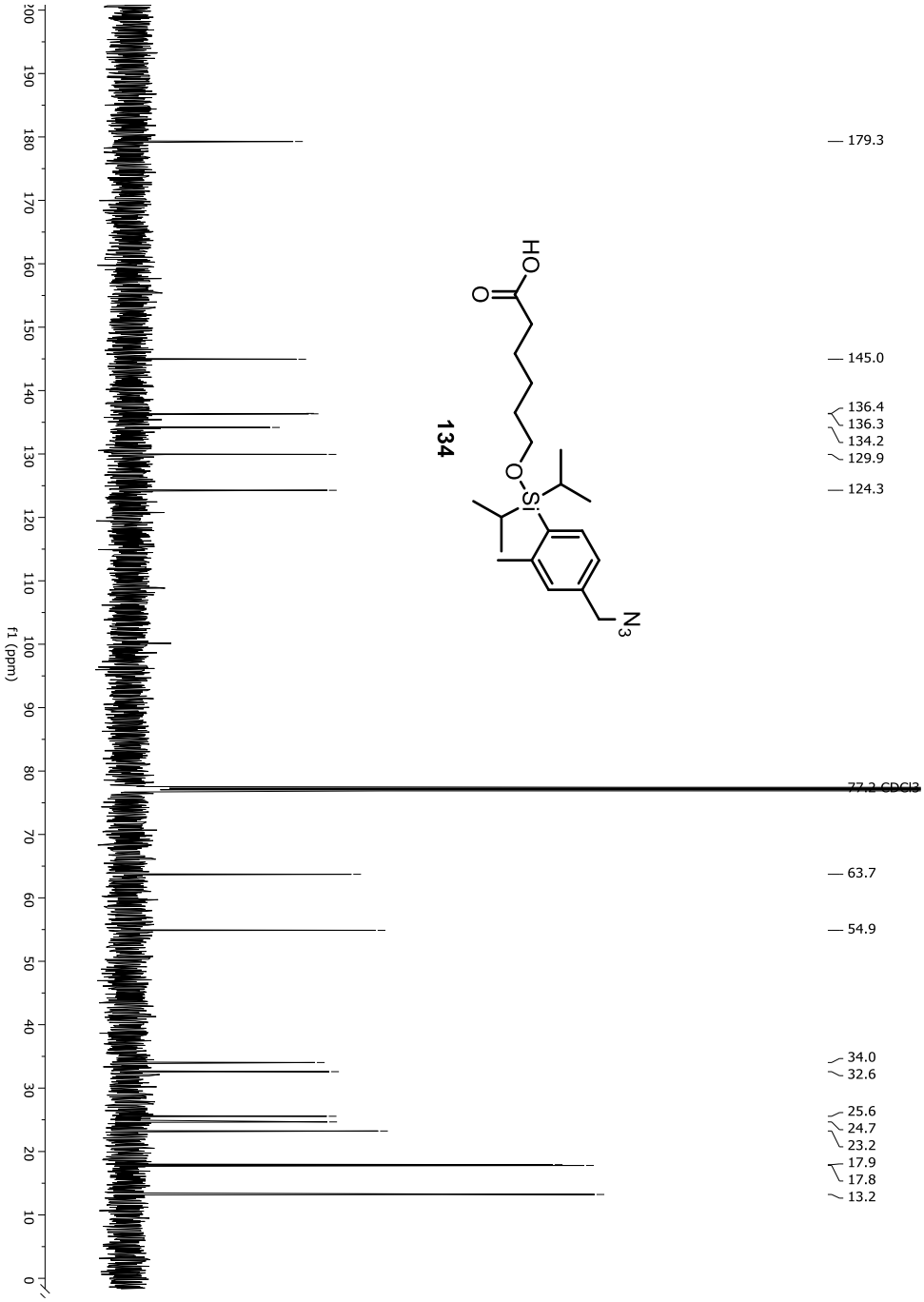

Figure A-192. HRMS spectrum of compound 134

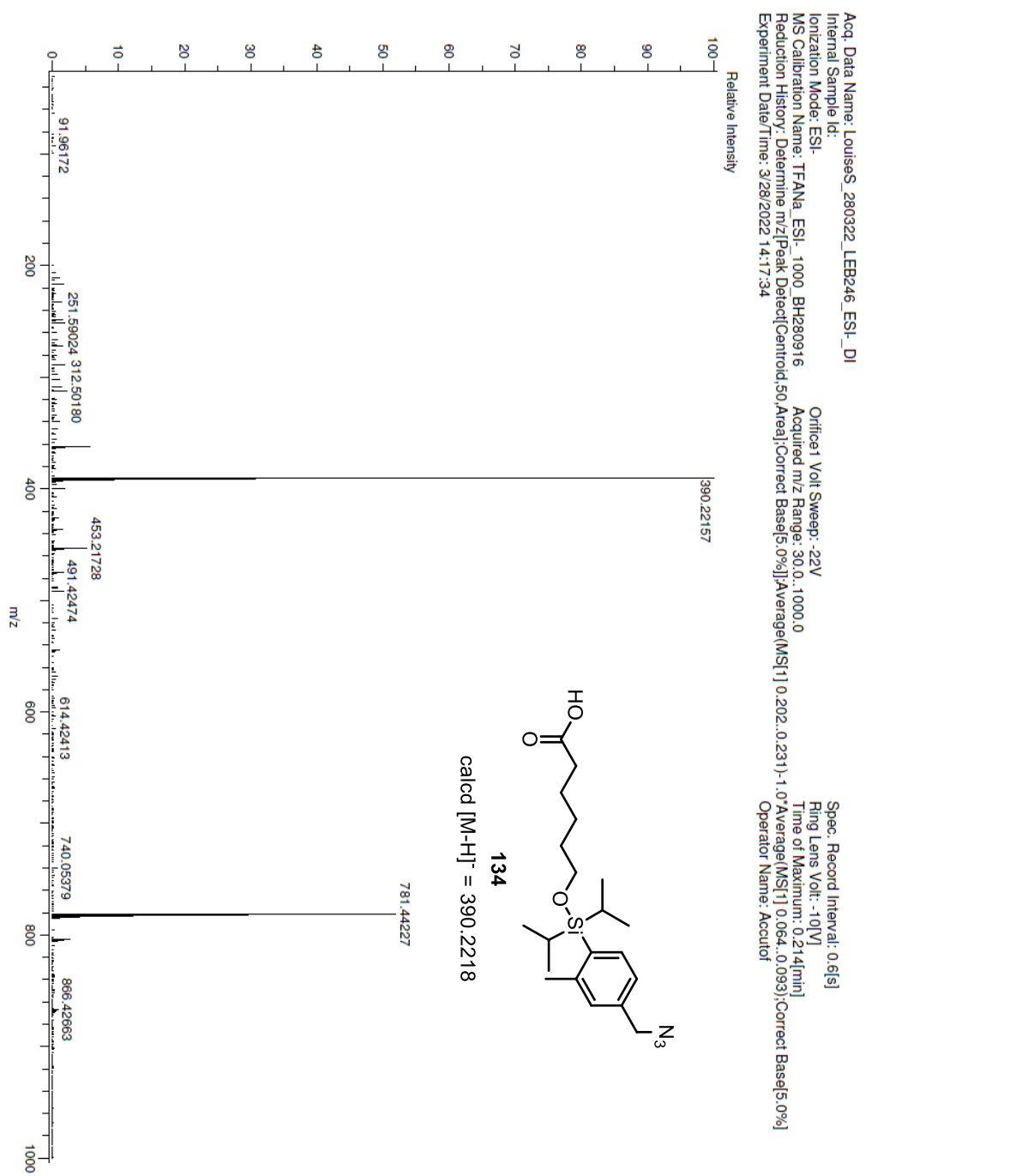

Figure A-193. ^{19}F-NMR spectrum of compound 127

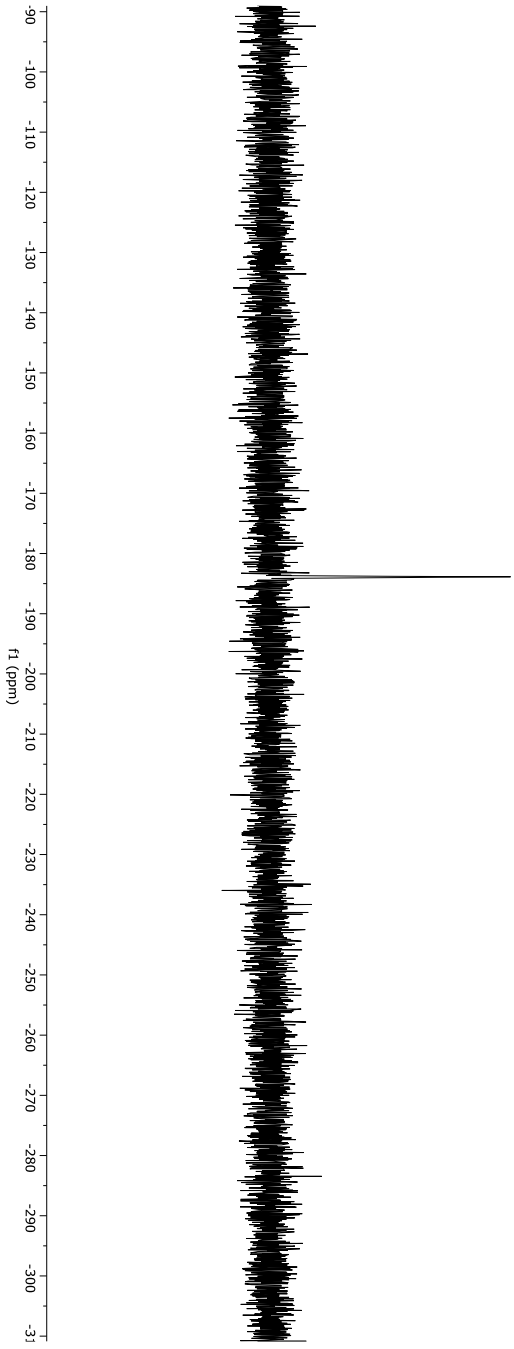

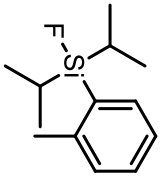

127

^{18}F-Fluorination: Radio-TLC (rt, 60 min)

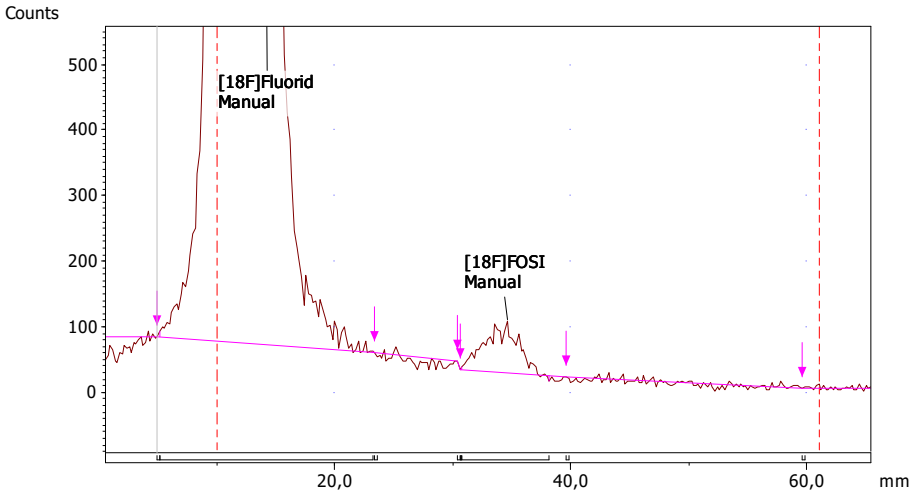

Figure A-194. *Radio-TLC of reaction mixture in the first ^{18}F-fluorination. Stirring at rt for 60 min, no filtering through alumina cartridge. One new radioactive peak is present (R_f = 0.48).*

Table A-1. Radio-TLC data

Name	Start (mm)	End (mm)	Retention (RF)	Area (Counts)	%ROI (%)	%Total (%)
BP 1	5,0	5,2	-0,098			
[^{18}F]Fluorid	5,2	23,2	0,051	99344,00	98,53	100,41
BP 2	23,4	23,6	0,263			
BP 3	30,4	30,6	0,400			
BP 4	30,6	30,8	0,404			
[^{18}F]FOSI	30,8	38,2	0,482	1478,00	1,47	1,49
BP 5	39,6	39,8	0,580			
BP 6	59,6	59,8	0,973			
2 Peaks				100822,00	100,00	101,91

Total Area: 98934,50 Counts
Average Background: 27 Counts

^{18}F-Fluorination: Radio-TLC (50 ºC, 30 min + 70 ºC, 30 min)

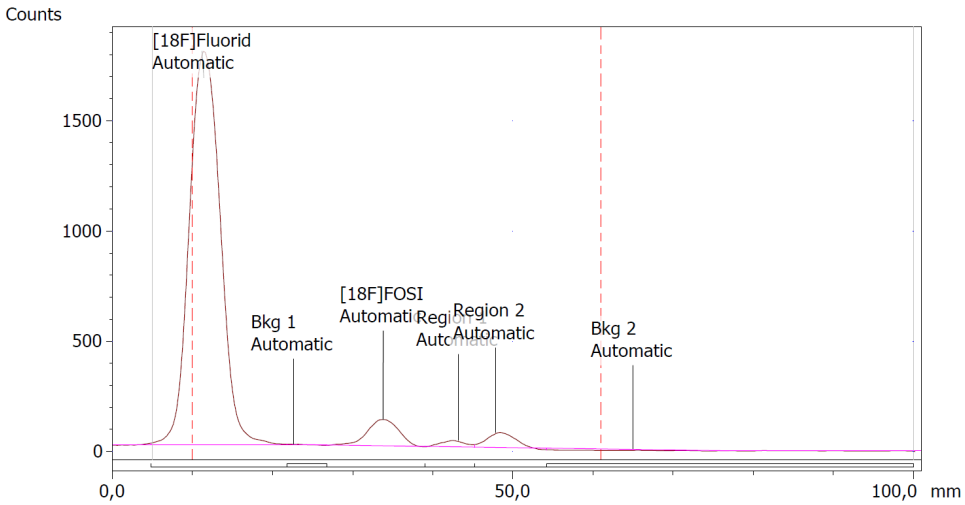

Figure A-195. *Radio-TLC of second experiment after stirring at 50 ºC for 30 min followed by 70 ºC for 30 min.*

Table A-2. Radio-TLC data: 50 ºC for 30 min followed by 70 ºC for 30 min.

Name	Start (mm)	End (mm)	Retention (RF)	Area (Counts)	%ROI (%)	%Total (%)
[18F]Fluorid	4,8	27,2	0,039	108521,71	94,58	96,12
Bkg 1	27,2	30,6	0,377			
[18F]FOSI	30,6	40,4	0,510	5319,66	4,64	4,71
Region 1	40,4	48,2	0,675	904,90	0,79	0,80
Reject 1	48,2	56,8	0,816			
Bkg 2	56,8	100,0	1,216			
3 Peaks				114746,27	100,00	101,64

Total Area: 112897,23 Counts
Average Background: 37 Counts

^{18}F-Fluorination: Radio-TLC (50 ºC, 30 min + 70 ºC, 30 min + filtering)

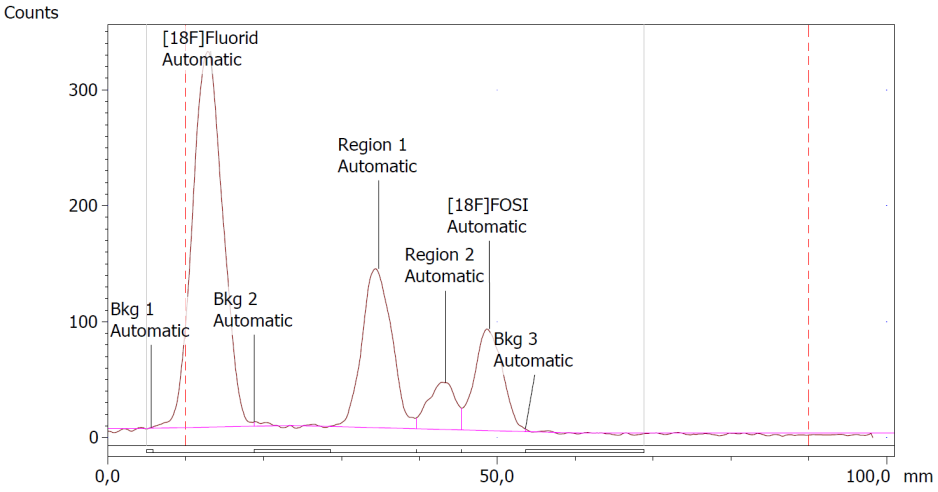

Figure A-196. *Radio-TLC after stirring at 50 ºC for 30 min followed by 70 ºC for 30 min, and filtering the mixture through an alumina cartridge after the reaction time.*

Table A-3. Radio-TLC after stirring at 50 ºC for 30 min followed by 70 ºC for 30 min and filtering the mixture through an alumina cartridge after the reaction time.

Name	Start (mm)	End (mm)	Retention (RF)	Area (Counts)	%ROI (%)	%Total (%)
Bkg 1	5,0	5,8	-0,055			
[18F]Fluorid	5,8	18,8	0,040	7417,77	56,54	56,55
Bkg 2	18,8	28,6	0,110			
Region 1	28,6	39,6	0,310	3035,85	23,14	23,15
Region 2	39,6	45,4	0,418	819,37	6,25	6,25
[18F]FOSI	45,4	53,6	0,488	1846,58	14,08	14,08
Bkg 3	53,6	68,8	0,545			
4 Peaks				13119,57	100,00	100,03

Total Area: 13116,16 Counts
Average Background: 7 Counts

^{18}F-Fluorination: Radio-TLC (50 ºC, 30 min)

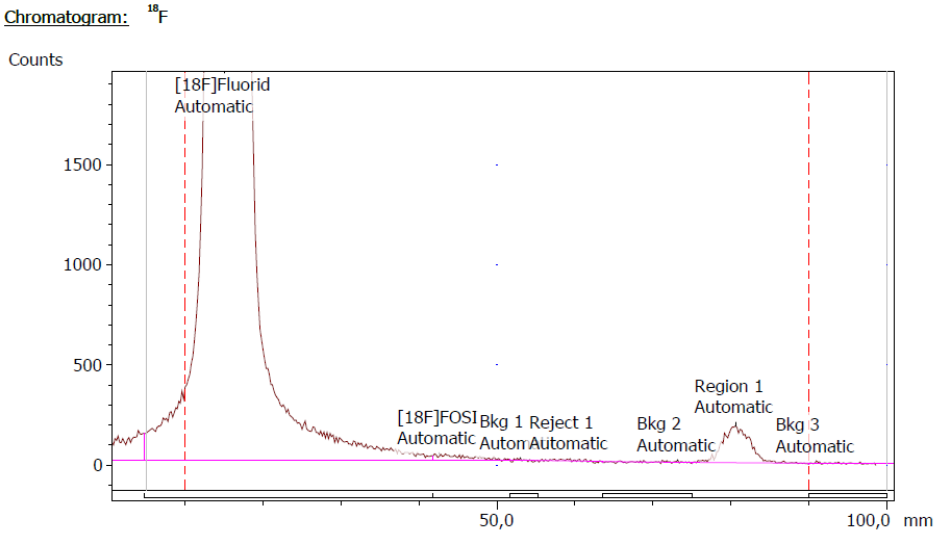

Figure A-197. *Repeated experiment: Radio-TLC stirring at 50 ºC for 30 min.*

Table A-4. Repeated experiment: Radio-TLC data stirring at 50 ºC for 30 min

Name	Start (mm)	End (mm)	Retention (RF)	Area (Counts)	%ROI (%)	%Total (%)
[18F]Fluorid	4,8	41,8	0,063	312647,00	98,63	98,68
[18F]FOSI	41,8	51,6	0,408	726,00	0,23	0,23
Bkg 1	51,6	55,2	0,538			
Reject 1	55,2	63,6	0,618			
Bkg 2	63,6	75,0	0,790			
Region 1	75,0	90,0	0,883	3621,08	1,14	1,14
Bkg 3	90,0	100,0	1,013			
3 Peaks				316994,08	100,00	100,05

Total Area: 316831,57 Counts
Average Background: 19 Counts

^{18}F-Fluorination: Radio-TLC (50 ºC, 60 min)

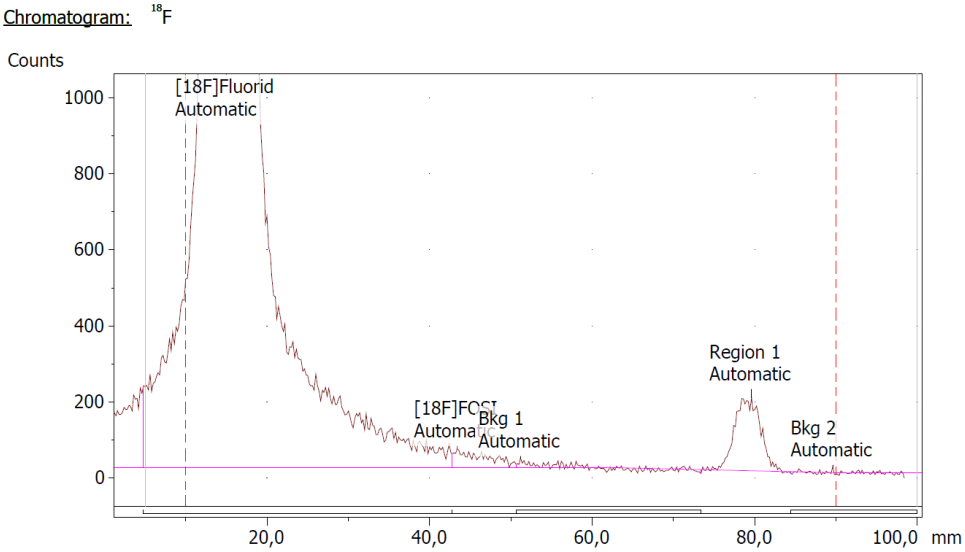

Figure A-198. *Repeated experiment: Radio-TLC stirring at 50 ºC for 60 min.*

Table A-5. Repeated experiment: Radio-TLC data stirring at 50 ºC for 60 min

Name	Start (mm)	End (mm)	Retention (RF)	Area (Counts)	%ROI (%)	%Total (%)
[18F]Fluorid	4,8	42,8	0,063	435532,00	98,96	99,02
[18F]FOSI	42,8	50,6	0,418	1072,42	0,24	0,24
Bkg 1	50,6	73,4	0,515			
Region 1	73,4	84,4	0,870	3505,15	0,80	0,80
Bkg 2	84,4	100,0	0,995			
3 Peaks				440109,57	100,00	100,06

Total Area:	439841,14 Counts
Average Background:	24 Counts

Graphic design: Communication Division, UiB / Print: Skipnes Kommunikasjon AS

uib.no

ISBN: 9788230847831 (print)
9788230855850 (PDF)